ROAD RUNOFF OVER THE SHOULDER DIFFUSE INFILTRATION. REAL-SCALE EXPERIMENTATION AND OPTIMIZATION

THÈSE N^{O} 3858 (2007)

PRÉSENTÉE LE 28 AOÛT 2007

À LA FACULTÉ DE L'ENVIRONNEMENT NATUREL, ARCHITECTURAL ET CONSTRUIT
LABORATOIRE DE GÉOLOGIE DE L'INGÉNIEUR ET DE L'ENVIRONNEMENT
PROGRAMME DOCTORAL EN ENVIRONNEMENT

ÉCOLE POLYTECHNIQUE FÉDÉRALE DE LAUSANNE

POUR L'OBTENTION DU GRADE DE DOCTEUR ÈS SCIENCES

PAR

Pascal PIGUET

diplômé en sciences de la terre, Université de Neuchâtel
de nationalité suisse et originaire du Chenit (VD)

acceptée sur proposition du jury:

Prof. M. Schuler, président du jury
Prof. A. Parriaux, Dr M. Bensimon, directeurs de thèse
Prof. A.-G. Dumont, rapporteur
Dr J.-F. Jaton, rapporteur
Dr M. Legret, rapporteur

ÉCOLE POLYTECHNIQUE
FÉDÉRALE DE LAUSANNE

Suisse
2007

ABSTRACT

A new concept of road runoff management, based on diffuse infiltration over the shoulder, was tested in a real-scale experimentation site located near Grandson, Switzerland. This new concept consists in diffusely infiltrating the road runoff in the infiltration slope adjoining the road shoulder; where road contaminants are retained. This presupposed that the road shoulder was as tightened as possible to effectively drive the road runoff to the slope, and that the infiltration slope effectively retains all road pollutants. Those two main postulates needed strong scientific verification. For this purpose, five different shoulder designs were tested in Grandson to assess which one presented the best hydraulic performance, i.e. which shoulder was the most impervious. Those designs were made of gravel mixed with humus (SGL), gravel mixed with clay (SGC), gravel seeded with lawn (SGL), a prolonged HMF road base (SH), and a bentonitic geotextile tightening (SB). Also, to verify the retention of pollutant, two infiltration slopes adjoining SGL (LW) and SH (LH) were set as lysimeter (basal geomembrane collecting road effluents); the third infiltration slope (LB) had a direct connection with the aquifer which was closely monitored (6 piezometers located up- and downstream from the road; influence of the road runoff was thus emphasized). Finally, to ensure that this new concept do not lower the road bearing capacity, deflectometers were placed in the road structure; 3 campaigns of levelling assessed the road settlement.

Hydraulic assessment of the shoulders, based on 112 natural precipitation as well as 3 artificial watering tests, showed strong discrepancies between all shoulders behaviours. They had to deal with potentially high amount of water. Lag times ranged from a few minutes to several hours. Results showed that lag times were only function of the precipitation mean intensity. The infiltration process could be assessed by a modified Green & Ampt equation. The moisturizing front was frank and linearly progressed downward. Shoulders vertical hydraulic conductivities ranged from $4.6 \cdot 10^{-6}$ (SGC) to $2.2 \cdot 10^{-5}$ $m \cdot s^{-1}$ (SGL). The exfiltration volume is function of the water volume available at the shoulder surface. The drought preceding the rain event has no influence on the stock variation or the exfiltration volume. Road runoff used two different infiltration paths: the macroporosity drives the water efficiently and rapidly, while the microporosity is less efficient and retains the moisture longer. Tracer tests (Brine) proved that the contamination first flush passed over the shoulders. This is also confirmed by the flux calculation. Runoff coefficients C_R ranged from 0.3 (SGL) to 0.9 (SB). This coefficient decreased rapidly once the shoulder is wet. Only SB really fulfilled its task, letting water through only in harsh hydraulic conditions (100 mm; 40mm/h). It is highly recommended for further road development: for new roads as well as old roads being refurbished. The shoulder SH proved to be inefficient for structural and material reasons. Other shoulders are comparatively ineffective. SGC must be enhanced; in that case it could offer a valuable alternative.

The bearing capacity of the road was very good. The road lifetime was evaluated to more than 20 years ($1 \cdot 10^9$ residual standard axle load). The Grandson experimental site could not conclusively demonstrate a worsening of the geotechnical behaviour of the road. This is due to the particularly good material and road pavement thickness used for this road. Infiltrations in shoulders are high enough and would have doubtless caused a loss of bearing capacity in case the road would have been more modestly dimensioned. It is therefore clear that the shoulder must be tightened.

Geochemical results concerned six families of contaminant: MTE, PAH, C_X, BTEX, MTBE, and PCB. Batch and column tests allowed calculating MTE and PAH distribution coefficient K_d in the Grandson soils, as well as in other typical Swiss soils. Results showed that mobile elements are B, Br, Mo, Ba, Sb, Zn, and V ($0 < K_d < 90$). Less mobile elements are Ni, Cd, Cr, and Rb ($200 < K_d < 300$). Elements with very low mobility are Pb, Mn, and Ti ($1500 < K_d < 3500$). PAH mobility was high for the light PAH (naphthalene, acenaphtene, fluorene, anthracene; $K_d < 75$). Heavy PAH had lower mobility ($K_d > 175$). Comparisons with other typical soils enlightened the predominant influence of the pH. Batch test performed with acidic soils (pH = 5.5) confirmed lower MTE K_d. MTE are thus more mobile in acidic soils. Other physicochemical parameters have a smaller influence. The column test performed with a synthetically loaded solution (MTE and PAH) infiltrating the Grandson soils showed that MTE are more mobile in

dynamic conditions. This is easily explained by the reduced contact time between the contaminant and the soil aggregates. PAH were not detected at the column outlet, thus showing a very good retention in the column soil. Soil layers analyses demonstrated that PAH were mostly retained in the surface layers. Also, MTE with low mobility show the same behaviour. Mobile elements showed no preferential retention layer.

Concerning the infiltration slope, lag times were usually greater than those encountered for the shoulders. Lag time were function of the rain mean intensity. The influence of the preceding drought was significant. Exfiltration volumes E_L were high in case of large event; it could be approximated by a simple equation function of the API and surface available water. Moisture redistribution processes occurred in the soils as long as there is a volumetric water content θ gradient. Fluxes strongly varied in magnitude and direction during a precipitation event: usually from about $1 \cdot 10^{-8}$ to $1 \cdot 10^{-5}$ $m \cdot s^{-1}$ and from up- to downward (evaporation to infiltration). The first flush effect was poor to medium. NaCl signal was highly buffered. The pH was also completely buffered by the soil high carbonate content. It thus shifted from 6.5 in the rainwater to 8 in the LW exfiltration water.

To especially emphasize the geochemical behaviour, an artificial precipitation test was created to control every aspect of the rainfall. It was judged very representative of a natural storm. MTE and PAH contaminants had two different behaviours: mobile elements moved mainly in solute and have concentration correlated with EC. Elements with low mobility had higher concentrations correlated with the turbidity peaks. They were transported sorbed to particles. Comparison between the particular and solute form concentrations confirmed that mobile elements are measured in similar concentrations whether the sample was filtered at 0.45 µm, at 1 µm, or not filtered at all prior to acidification. On the contrary, less mobile elements are easily sorbed to particles. The MTE concentrations under sorbed form range from 5% (Rb, Sb) to 98% (Pb) of the total concentration. They had strong first flush effects. B, V, Cr, Mn, Ni, CU, Zn, Br, Mo, Cd, Sb, and Pb were identified as road tracers. Fe and Al represented 80% of the road runoff. Overall, the total MTE concentration in the lysimeter first water collected decreased to $1/30^{th}$ of the road runoff first flush concentration. Mobile elements were less retained. The PAH total concentration in the lysimeter first collected water was about 1'000 times lower than in the road runoff first flush. The PAH concentration was mainly constituted by mobile PAH naphthalene and phenanthrene. C_X were well represented in the road runoff. However, only heavy species were commonly found. C_{32} was the most common specie. The triplet C_{16}-C_{18}-C_{20} was always present in high concentration in the lysimeter exfiltration water. This triple is a great road tracer. BTEX, while present in the road runoff, were not detected in the lysimeter exfiltration water.

The alluvial aquifer was also monitored. It is confined between the Arnon (north) and a basement till which shallows up southward. Eastern and western limit are less known but might coincide with the river. The aquifer is clearly linked to the river. This is proved by the piezometric level, EC and T follow-up. EC and temperature also emphasized the higher activity in downstream piezometer. The road runoff infiltration could not be emphasized by the NaCl tracer test. The infiltrated water concentration was possibly buffered by the aquifer volume. Also, the brine was heavier than the aquifer water: it could have plunged to the bottom of the aquifer.

All families of contaminant are presented in the aquifer. However, the provenance of those contaminants remains uncertain. The groundwater was indeed as concentrated upstream as downstream. Moreover, the river concentrations had similar, or even higher, values. The contamination provenance is thus either the aerial deposition (equally distributed up- and downstream), either the Arnon River infiltrating the aquifer. The contaminant behaviours in the aquifer could be described. It confirmed the contaminant mobility previously noted during the batch, column and test precipitation experiments. Mobile substances are seen in higher concentrations, whereas substances with low mobility are sparsely found.

This project thus demonstrated that the new "over the shoulder diffuse infiltration" concept is clearly implementable. Aquifer concentrations were compared to Swiss legal concentration limits. Except for Cr, the aquifer water was of drinkable quality. This proved that the concept is robust, environmental-friendly and conclusive.

RÉSUMÉ

Un nouveau concept de management du ruissellement routier, basé sur l'infiltration diffuse par-dessus les banquettes, a été testé en grandeur réelle sur un site expérimental près de Grandson, Suisse. Ce nouveau concept consiste à infiltrer le ruissellement routier de manière diffuse dans des talus d'infiltration bordant la banquette routière. Les contaminants seront retenus dans ces talus. Cela présuppose que la banquette soit complètement imperméable pour conduire le ruissellement routier au talus d'infiltration de manière effective; et que le talus d'infiltration retienne concrètement les polluants routiers. Ces deux principaux postulats devaient être vérifiés scientifiquement. A cette fin, cinq structures de banquette ont été testées à Grandson pour définir quelle solution est la meilleure; soit celle qui est la plus imperméable. Ces cinq structures étaient faites d'un mélange gravier et humus (SGH), de gravier et argile (SGC), de gravier engazonné (SGL), d'un HMF (enrobé bitumineux pour couche de base) prolongé sous la banquette (SH) et finalement d'un géotextile bentonitique (SB). Afin de vérifier la rétention des polluants dans les sols, deux talus d'infiltrations ont été construits sous forme de lysimètres, c'est-à-dire avec une membrane de collecte sous-jacente. Ils bordent SGL (LW) et SH (LH). Le troisième talus d'infiltration a une connexion directe avec la nappe souterraine. Cette dernière était équipée de six piézomètres ; trois en amont et trois en aval de la route. L'influence du ruissellement routier pouvait donc être vérifiée. Finalement, la portance de la route était constamment surveillée à l'aide de déflectomètres et de campagnes de nivellement.

L'évaluation du comportement hydraulique des banquettes, basée sur 112 précipitations naturelles ainsi que 3 événements artificiels, a démontré de grandes différences entre chaque banquette. Elles doivent potentiellement gérer de gros volume d'eau. Les temps de réponse se situent entre quelques minutes à quelques heures. Ceux-ci sont uniquement fonction de l'intensité moyenne de la pluie. L'infiltration dans les banquettes peut être facilement évaluée à l'aide des équations de Green & Ampt (1911) modifiées pour ce travail. Le front d'humidification est franc et progresse linéairement vers le bas. Les conductivités hydrauliques verticales des banquettes se situent entre $4 \cdot 10^{-6}$ (SGC) et $2.2 \cdot 10^{-5}$ $m \cdot s^{-1}$ (SGL). Le volume exfiltré est fonction du volume disponible en surface uniquement. La sécheresse précédant l'événement n'a pas d'influence sur la variation de stock ou le volume exfiltré. L'infiltration utilise deux cheminements différents: la macroporosité conduit l'eau rapidement et efficacement, tandis que la microporosité est moins efficace et retient l'eau plus longtemps. Les essais de traçage avec saumure ont prouvé que le « first flush » passe au-dessus des banquettes. Cela est également étayé par les calculs de flux. Les coefficients de ruissellement se situent entre 0.3 (SGL) et 0.9 (SB). Ils décroissent rapidement lorsque la banquette est humide. Seule la banquette SB a rempli les conditions précitées, c'est-à-dire être suffisamment imperméable pour conduire le ruissellement au talus d'infiltration. Cette banquette est recommandée pour toute nouvelle construction ou modification d'ancienne route. La banquette SH était inefficace pour des raisons structurelle et matérielle. Les autres banquettes étaient également inefficaces. SGC peut être utilisée si les modifications conseillées sont appliquées.

La capacité portante de la route n'a jamais été mise en danger. L'espérance de vie de la route est très haute ; elle est en tout cas de plus de 20 ans ($1 \cdot 10^9$ essieux standard résiduels). Ainsi, le site de Grandson n'a jamais pu mettre en exergue une péjoration des qualités géotechniques de la route. Cela est sans doute dû aux caractéristiques particulières de celle-ci: une très bonne grave de fondation et de remblai ainsi qu'une épaisseur significative de la couche d'enrobée HMF. Les infiltrations dans les banquettes étaient importantes; sans ce dimensionnement généreux, la route aurait sans doute montré une perte de portance: la banquette doit donc être imperméabilisée.

Les vérifications géochimiques concernent six familles de contaminants: ETM, HAP, C_X, BTEX, MTBE, and PCB. Les tests batch et en colonne ont permis de calculer les coefficients de distribution K_d des ETM et HAP; ce pour les sols de Grandson et d'autres sols typiques suisses. Les résultats ont montrés que B, Br, Mo, Ba, Sb, Zn, et V sont mobiles ($0 < K_d < 90$). Les éléments Ni, Cd, Cr, et Rb sont moins mobiles ($200 < K_d < 300$); tandis que Pb, Mn, et Ti sont très peu mobiles ($1500 < K_d < 3500$). La mobilité des HAP est haute pour les molécules légères (naphtalène, acenaphtène, fluorène, anthracène; $K_d < 75$), tandis que les composés lourds sont peu mobiles ($K_d > 175$). La

comparaison avec les autres sols typiques suisses ont mis en exergue l'influence prépondérante du pH. Les ETM sont nettement plus mobile dans des sols acides (ph = 5.5). Les autres paramètres physico-chimiques ont moins d'influence. Le test en colonne a été fait avec une solution dopée en ETM et en HAP sur les sols de Grandson; les ETM sont plus mobile dans cette expérience dynamique. Cela est causé par un temps de contact plus court entre la substance et le sol. Les HAP n'ont pas été détectés en sortie de colonne: la rétention était bonne et s'est faite en surface de sol, de même que les ETM peu mobiles. Les ETM très mobiles ne montrent pas de rétention particulière.

En ce qui concerne les talus d'infiltration, les temps de réponse étaient plus importants que ceux des banquettes. Ils sont fonction de l'intensité moyenne de la pluie. L'influence de la sécheresse précédant l'événement est significative. Les volumes exfiltrés étaient très importants en cas de forte pluie ; ils peuvent être approximés à l'aide d'une simple équation empirique fonction de l'indice de précipitation antécédente IPA et du volume disponible en surface. Les flux de redistribution d'humidité du sol sont importants; ils agissent en permanence tant qu'un gradient d'humidité existe. Les flux varient fortement en intensité et direction durant un événement: en général d'environ $1 \cdot 10^{-8}$ à $1 \cdot 10^{-5}$ $m \cdot s^{-1}$ et de la direction « haut » vers « bas ». L'effet « first flush » est faible à moyen: le signal du traceur NaCl était hautement tamponné. Le pH est aussi complètement tamponné par la teneur en carbonate du sol : il passe d'environ 6.5 dans le ruissellement routier à 8 dans l'eau exfiltrée des sols.

Pour particulièrement mettre en valeur le comportement géochimique, une précipitation artificielle a été créée pour contrôler tout les aspects de la pluie. Elle a été jugée très représentative d'une pluie naturelle. Les ETM et HAP se comportent de deux manières différentes: les substances mobiles sont principalement transportées en solution; leurs concentrations sont corrélable avec la conductivité électrique. Les substances peu mobiles sont plus concentrées et sont corrélées avec la turbidité. Ils sont transportés sorbés sur des particules. La comparaison entre les deux modes de transport a confirmé que les substances mobiles sont trouvées en concentration similaire quel que soit le filtrage utilisé. De manière contraire, les substances peu mobiles sont facilement sorbées. La concentration particulaire se situe entre 5% (Rb, Sb) et 98% (Pb) de la concentration totale. Elles montrent un effet « first flush » prononcé. B, V, Cr, Mn, Ni, CU, Zn, Br, Mo, Cd, Sb, et Pb ont été identifié comme traceurs routiers. Fe et Al représentent 80% du ruissellement routier. De manière globale, la concentration totale de MTE décroit à $1/30^{ème}$ de la concentration du ruissellement routier. Les éléments mobiles sont moins bien retenus. La concentration totale en HAP décroit à $1/1000^{ème}$ de la concentration du ruissellement routier. Celle-ci est essentiellement constituée des composés mobiles naphtalène and phénanthrène. Les aliphatiques sont présents dans le ruissellement routier, surtout les lourds. C_{32} est le plus communément rencontré. Le triple C_{16}-C_{18}-C_{20} est toujours présent dans l'eau d'exfiltration; ce triplet est un traceur routier idéal. BTEX ne sont plus détecté dans l'eau d'exfiltration.

L'aquifère alluvial est confiné entre l'Arnon et une moraine de base dont la profondeur décroit vers le sud. Les limites est et ouest sont inconnue mais coïncident également certainement avec l'Arnon. L'aquifère est clairement influencé par la rivière. Ceci a été démontré par les suivis piézométriques, de conductivité électrique, et de température. Ces deux derniers ont également démontré une activité supérieure dans les piézomètres avals. L'infiltration du ruissellement routier dans la nappe n'a pas pu être démontrée par traceur NaCl. Soit la concentration de NaCl a été tamponnée, soit elle n'a pu être détectée car elle a plongé au fond de l'aquifère (densité plus élevée).

Toute les familles de contaminant ont été détectées dans l'aquifère. Néanmoins, l'origine de ces contaminants est incertaine. En effet, les concentrations mesurées sont similaire en amont et aval de la route; l'effet du ruissellement routier n'est pas prouvé. De plus, la rivière contient des concentrations similaires, ou même plus forte. La contamination de l'aquifère peut donc être causée par la rivière ou par la déposition aérienne. Le comportement des substances dans l'aquifère est en tout point comparable au comportement dans les talus d'infiltration.

La bonne conduite de ce projet a ainsi pu démontrer que le concept " infiltration diffuse par dessus les banquettes" est clairement implémentable. Les concentrations mesurées dans l'aquifère, comparées aux normes de la législation suisse, ont montrés que les eaux souterraines sont pratiquement potable, exception faite du Cr. Cela prouve définitivement que ce concept est robuste et qu'il apporte une réelle amélioration environnementale.

TABLE OF CONTENT

ACRONYMS, ABBREVIATIONS AND VARIABLES

AB11s	Road wearing course
API	Antecedent precipitation index
A_W	Available water on the shoulder surface
b	Bertrand – Krajewski & Chebs pollutogram coefficient
BTEX	Benzene – Toluene – Ethylbenzene – Xylenes serie
B_W	Available water on the lysimeter surface
C	Concentration
C(t)	Concentration rate
C/N	Carbon/nitrogen ratio
C_e	Concentration of substance in the liquid at equilibrium state
CEC	Cation exchange capacity
C_G	Centre of gravity
C_R	Runoff coefficient
C_s	Concentration of substance in the solid at equilibrium state
C_T	Tracer coefficient, i.e. restitution fraction Є[0;1]
C_X	Aliphatic hydrocarbons
d	Drawdown
DL	Dispersion
DOC	Dissolved organic carbon
D_R	Road dissemination
E	Apparent elastic modulus
EAWAG	Swiss Federal Institute of Aquatic Science and Technology
EC	Electric conductivity
E_L	Exfiltration flow from the lysimeter
EP	Evaluation points used for the OFEV concept feasibility
EPA	US Environmental Protection Agency
EPFL	Swiss federal institute of technology, Lausanne
E_S	Exfiltration flow from the shoulder
ETP_L	Evapotranspiration from the lysimeter
ETP_S	Evapotranspiration from the shoulder
FOC	Fraction of organic carbon
FWD	Falling weight deflectometry
GEOLEP	Laboratory for Geological Engineering, Swiss Federal Institute of Technology
GEOWEB	3D-net use dot stabilize the infiltration slope LH
Grad	Gradient
H	Hydraulic head
HMF	Road base
HMT22s	Road base course
HPLC	High Pressure Liquid Chromatography
Hu	Humidity
i	Infiltration flux, as opposed to infiltration flow I
ICPMS-HR	Inductively Coupled Plasma Mass Spectrometer – High Resolution
IDF plot	Intensity – duration – frequency plot designed to assess the precipitation characteristics
I_L	Infiltration flow in the lysimeter
I_{max}	Maximum rain intensity
I_{mean}	Mean rain intensity
I_S	Infiltration flow in the shoulder
K(θ)	hydraulic conductivity in the unsaturated zone
K_{API}	Recession factor for API calculation
K_d	Distribution coefficient
K_H	Horizontal hydraulic conductivity
K_{OC}	Distribution coefficient normalized on FOC
K_S	Hydraulic conductivity at saturation
K_V	Vertical hydraulic conductivity
LAVOC	Traffic facilities laboratory, EPFL
LB	Infiltration slope associated with the shoulder tightened with bentonic geotextile
LH	Lysimeter associated with the shoulder tightened with HMF
LW	Lysimeter associated with SGL REF (20m) without geomembrane
MSDA	Manuel Suisse des Denrées Alimentaires (Swiss manual on foodstuff)
msl	Metres above sea level
MTBE	Methyl Tertiobutyl Ether

MTE	Mineral trace elements
NABO	National soil conservation service
NTU	Nephelometric turbidity unit
OEaux	Ordinance on water
OFEV	Swiss Federal office for the environment
OFROU	Swiss Federal Road Office
OM	Organic matter
OSEC	Ordinance on alien substances and compounds
OSite	Ordinance on contaminated sites
PAH	Polycyclic aromatic hydrocarbons
PCA	Principal components analysis
PCB	Polychlorobyphenyls
PE	Polyethylene
P_L	Precipitation on the lysimeter
POC	Particular organic carbon
P_R	Precipitation on the road
P_S	Precipitation on the shoulder
Q	Flow in litre per second
QFF	Atmospheric pressure
q_{xx}	Darcy's flux in metre per second that concerns xx (q_{RS}, for example, is the flux of the shoulder runoff)
R_L	Lysimeter runoff ≈ 0
Rn	Solar radiation
R_R	Road runoff
R_S	Shoulder runoff
R_S*	Initial shoulder runoff
RU	Useful reserve, corresponds to a specific water content
s	Compartment surface
S	Water stock
SB	Shoulder tightened with bentonitic geotextile
SESA	Vaud Cantonal water, soil and sanitation board
SGC	Shoulder with Gravel and Clay
SGH	Shoulder with Gravel and Humus
SGL	Shoulder with Gravel and Lawn
SGL REF	Shoulder with gravel and lawn, segment of 20m. It is the reference for geotechnical issues only
SH	Shoulder tightened with HMF
s_L	Surface of the lysimeter
SR	Regional Road Office, canton Vaud
s_R	Surface of the road
s_S	Surface of the shoulder
S_T	Storativity
T	Temperature
TDR	Time domain reflectometry
TDS	Total dissolved solid
Test n°1	Artificial watering test performed to assess the hydraulic behaviour of the compartments
Test n°2	Artificial watering test performed to assess the chemical behaviour of the infiltration slopes
Test n°3	Artificial watering test performed to assess the geotechnical behaviour of the compartments
TOC	Total organic carbon
T_R	Transmissivity
$T_{Student}$	Student-test T coefficient
T_{VOL}	Threshold volume, i.e. maximal precipitation volume inducing no exfiltration
U	Wind speed
UZ	Unsaturated zone
V_0	Dead volume of the column
V_{mean}	Mean speed of a tracer
V_{peak}	Peak speed of a tracer
VSA	Swiss water pollution control association
VSS	Road Professional Association
xD_R	Fraction of the water dissemination that settles on the shoulder
yD_R	Fraction of the water dissemination that settles on the lysimeter
z	Depth
α	Dispersivity
ΔS_L	Stock variation in the lysimeter
ΔS_S	Stock variation in the shoulder
θ	Volumetric water content (or soil moisture)
θ*	Reduced volumetric water content
θr	Residual volumetric water content
θ_S	Volumetric water content at saturation
θ_V	Volumetric water content once the macroporosity has drained
φ	Internal friction angle
∇K	Hydraulic conductivity tensor. The tensor has three components x, y, and z in 3D
Ψ(θ)	Matrix potential, also called suction, in the unsaturated zone

ROAD RUNOFF OVER THE SHOULDER DIFFUSE INFILTRATION.

REAL-SCALE EXPERIMENTATION AND OPTIMIZATION.

CHAPTER 1

INTRODUCTION

1.1 LEGITIMIZATION AND PRINCIPLES

Swiss law indicates that polluted water must be treated, whereas clear water must be infiltrated wherever it is possible. It also promotes the conservation "as natural as possible" of the water cycle.

Runoffs coming from road pavements, parking places and roofs have always been considered to be lightly to heavily polluted and thus have to be treated. The treatment of road runoff was therefore regulated by Swiss laws. Those are today considered obsoletes: until now on, runoffs were treated mechanically, running through sewers and collecting pipes to oil and particles separators, usually *in fine* directed to surface waters. Although efficient, those installations are expensive and invasive.

While these treatment installations are fully compliant with the law, the water cycle is perturbed. Moreover, in Switzerland, around 1 km^2 per year is asphalted or built-upon since the early 60's. This rate, while not constant over the time, should not decrease in the 21st century. Swiss legal texts are summarized in appendix I.

Concerned that road pollution is disseminated in surface water and that rainfalls participate less efficiently to aquifer recharge, the Swiss Federal Office for the Environment (OFEV) and the Swiss water pollution control association (VSA) edited a new Directive (Protection des eaux lors de l'évacuation des eaux des voies de communication, 2002, called Directive 2002 in the text below) that may radically change the road engineers' way of thinking. That directive indeed favours the infiltration of lightly polluted water wherever it is possible, thus considering the surrounding filtering soils as an integrant part of the road environment. The principal condition is that the water reaching the aquifer must not be polluted. The runoff evacuation system must also guarantee the security of the road and comfort for road users.

Local feasibility, legal factors and the principle of proportionality will be the determinant factors for the implementation of the new infiltration concept in the field. Local feasibility concerns road traffic and level of pollution as well as local aquifer characteristics and soil factors such as pH, clay contents, thickness and humus percentage. Legal factors concern field occupation and property, and water protection zones. The principle of proportionality is based on economical and human factors. Summary of the 2002 OFEV directive is shown in appendix II.

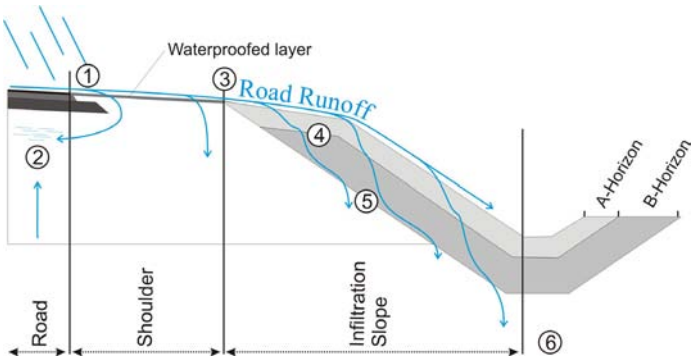

Fig. 1.1: 2D transect of an idealized road side segment. Runoff (blue arrows) must infiltrate the infiltration slope (A and B horizons) to be filtered before reaching the aquifer (6). Therefore the shoulder should be as waterproof as possible (1) to avoid early infiltration in the superstructure and creation of saturated zone under the road subgrade (2). The transition from the shoulder to the infiltration slope (3) is of upmost importance. A and B horizons are two exogenous soils with different physical and chemical characteristics. Water flow might be perturbed when reaching the A - B horizons (4) and B horizon - embankment (5) boundaries due to hydraulic conductivity contrast and matrix potential effects.

Assessing the feasibility, reliability and credibility of this new concept is not straight-forward. It needs scientific research, particularly real-scale experimentations. Thus, the Laboratory for Engineering and environmental geology, Swiss Federal Institute of Technology, Lausanne (GEOLEP) have been entrusted by the Swiss Federal Road Office (OFROU), the regional Road

Office (SR Canton de Vaud) and the Road Professional Association (VSS) to design and monitor an experimental station in Grandson (see paragraph 1.5 for location), composed by a modified 95 m road section. The construction phase was over in late 2003.

This study is fully based on the simplest case described by the 2002 Directive (appendix II), i.e. "over the shoulder diffuse infiltration". Neither artificial material nor installation is involved for the chemical retention. Artificial tightening layers are used for the shoulder design. The principle is to conduct the road runoff to infiltration slopes over a tighten shoulder (Fig. 1.1). The soil, composed by one A and one B pedological horizons will play the role of filters. Also, all the organic compound remediation (through phyto- and bioremediation) occurs in the soil (See §1.4). According to the Swiss legislation, the water reaching the aquifer must not alter the underground water quality (appendix I and II).

1.2 STUDY OBJECTIVES

1.2.1 PROBLEMATIC

The main objective of this study is to test the feasibility and efficiency of the new OFEV concept, using real-scale experimentations. Hydraulic, chemical and geotechnical behaviours are monitored. The OFEV concept relies on two main postulates:

1) the shoulder is impermeable, i.e. most/all of the road water runoff runs down to the infiltration slope
2) the A and B horizons are efficient filters and retain most of the pollutants (organic and inorganic)[1]

Although those two postulates are the basis of the OFEV concept, they must be scientifically verified:

Postulate 1) The constitutive material and design of the shoulder are the key to the water paths scheme. If the shoulder is not well designed, the runoff will not reach the infiltration slope. The conditions that the shoulder must fulfil are threefold:

- The shoulder must be users friendly and welcome all road appliances (traffic signs, crash barriers, emergency stop area, etc.). The shoulder design must be engineer friendly as well.
- The shoulder must satisfy the environmental and practical requirements under regional climatic conditions. Thus, it must be tightened enough to drive most of the runoff to the infiltration slope. This will predominantly depend of its constitutive materials and the presence or not of an artificial tightening layer.
- The road and foundation stability must not be reduced by infiltration through the shoulder

Postulate 2) The second postulate needs strong verifications. The geochemical behaviour must be monitored. The OFEV Directive (appendix II) constrains the soils, road traffic and aquifer vulnerability specificities and characteristics. Grandson site must be classified and fitted into the OFEV scheme. The infiltration feasibility assessment requires strong knowledge about the pollutants, soils, aquifer and all the interactions in-between:

- The road pollutants fate must be clarified. Despite the abundant literature about this subject, a more specific understanding is necessary regarding the Grandson experimental site. The road runoff must be thoroughly studied. Specific gasoline additives behaviours are not well known and must also be considered (MTBE).
- Infiltration slope soils must be characterized. Chemical and physical properties will be measured through various *in situ* and laboratory experiments.
- The aquifer and nearby river will also be monitored; theirs specificities will be enlightened and level of pollution measured. The aquifer indeed constitutes the reception body of the infiltration, while the Arnon River may strongly influence the aquifer chemical and dynamical behaviours.

[1] Moreover, organic pollutants might be removed through phyto- and/or bioremediation. Organic compounds remediation is not addressed in the present study.

- Soils and pollutants interaction will be measured. Column experiments with soils coming from the infiltration slope will enlighten pollutants behaviour, i.e. retention and releasing processes.

The goal of the present study is to scientifically verify those two postulates. Limitations, restrictions, and nuances of those two postulates must be identified and quantified.

1.2.2 MEANS AND IMPLEMENTATION

Five shoulder designs were tested. Three infiltration slopes adjoin three of those five shoulder types, and two of those infiltration slopes are lysimeter[2]. The hydraulic behaviour of the experimental station was investigated. Figure 1.1 shows the main points that are monitored:

- the shoulder impermeable capacity (1)
- the embankment water content and possible road weakening (2)
- transition from the shoulder to the soils (3)
- A-B horizons interactions (4)
- B horizon-embankment interaction, and finally the alluvial aquifer behaviour (5)
- the aquifer

Based on the hydraulic experimental results, the best shoulder design must be enlighten. Figure 1.2 shows the particular approach to design the most suitable shoulder. It will also emphasize possible problems arising with the transition of water from an impervious layer (road) to two permeable bodies (road foundation and infiltration slopes).

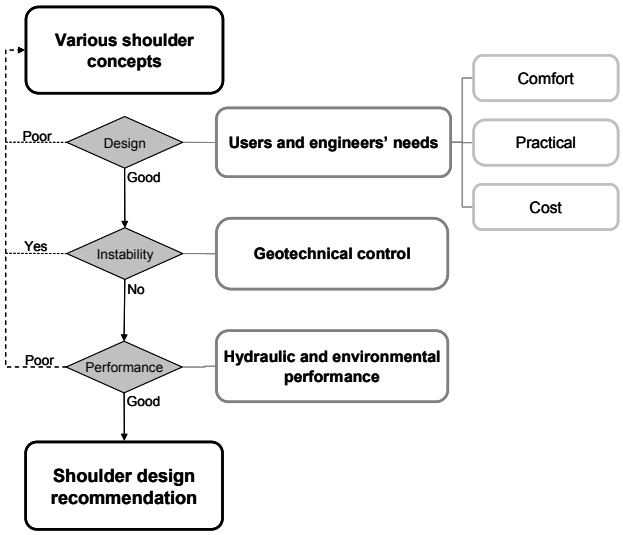

Figure 1.2: Evaluating the most suitable shoulder. Shoulders have been designed in collaboration with the VSS and SR to fulfil the users (stability, comfort) and engineers' needs (feasibility). Additional costs will be taken into consideration. Shoulders influence on the road stability must not be negative. Shoulder hydraulic performance will be the key to a good stability. Indeed, the less water infiltrates the shoulder, the more stable the road foundation will remain.

The geotechnical behaviour was evaluated. Deflection sensors have been put in the road superstructure, levelling and FWD campaigns were performed. Results were compared with infiltration conditions to weigh up the water infiltration influence.

The comparison of samples coming from the various sampling points (road runoff, bottom of the lysimeter, aquifer) were used to assess the substance retention in the infiltration slope and unsaturated zone. Combination with the hydraulic results gave the dynamic contaminant behaviour. Column and batch tests gave strong insight of the soil parameters and contaminant behaviours. Results were generalised to typical Swiss soil types.

1.3 WORK SPECIFICITIES

The present research was highly innovative and pioneering: its main remarkable innovations (regarding other similar studies) were:

- Surroundings soils were not contaminated by previous road traffic. The road segment was new and has been used for only a couple of months prior to the start of this study. Thus, the initial soil pollution was negligible.

[2] i.e. soil are overlaying a geomembrane which collects the infiltration water

A similar work has been conducted in the HES Burgdorf (federal report, Boller 2006). The road there has however been in use for 50 years. Moreover, sampling and mass balances were done on a monthly basis.

- Five shoulder designs were tested simultaneously and were equipped with instruments consequently. Thus, was possible to factually compare the shoulder performances.
- Two lysimeters with high soil volume permitted *in situ* infiltration experimentations. It included water and road contaminants mass balance calculations. Thus, the retention of contaminant could be calculated.
- The underlying aquifer was restricted to a small area and was thus easy to monitor. It allowed testing the complete infiltration cycle and imission measurements.
- The road segment was equipped with various instruments; numerous punctual levelling tests were performed. This allowed monitoring the road stability in various conditions.

1.4 STATE OF THE ART

1.4.1 FLOW PROCESSES

Most of the references used for hydrogeological formulation were found in Musy and Soutter (1991) and Mermoud (1999). Also, a fairly good introduction to unsaturated zone fluxes has been made by Lacas (PhD thesis, 2005).

1.4.1.1 Road runoff and first flush

Fractionation of the pollution on the road has been thoroughly studied by Sansalone and Buchberger (1996), Lindgren (1996) and Reinirkens (1996). Sansalone and Cristina (2004) studied the fractionation of heavy metals in snowmelt. Dean, Sansalone and Cartledgte (2005) made a significant effort to understand the metal speciation in the road runoff as function of the hydrometeorological conditions.

Concerning the first-flush effect, Bertrand and Krajewski (1995, 1998) have greatly improved the comprehension and, above all, the mathematical determination of the first flush. They postulated that 80% of the transported mass must be found in the first 30% of the road runoff volume. Other authors have different limit values, especially when concerned with reservoir dimensioning: 20% of the mass in the first 80% of road runoff (Stahre and Urbonas, 1990; Sansalone and Buchberger 1997) or 25% of the mass in the first 50% of the volume (Wanielista and Yousef 1993; Sansalone and Buchberger 1997). For simplification reasons, Helsel and Kim (1979) postulated that the first flush is apparent as soon as the M(V) curve is above the bissectrice (see § 3.3.1 for an example). In the present study, the equation of Bertrand and Krajewski is used.

Geiger (1987) and Saget and Chebbo (1995) studied the relationship between the drought preceding the precipitation. They observed that the first flush effect is remarkable when the precipitation is heavy and follows long deposition periods (i.e. long drought preceding the event).

1.4.1.2 Unsaturated zone

The unsaturated zone is the source of many different processes concerning flows as well as substance retention. It is evidently vein to try to establish an exhaustive list of all authors who have worked on this subject. However, in regard to the present study, significant work has been made by Labadia and Buttle (1996) who worked on the salt pathways and fate in soils and shoulders. Hansson (2005) considered the water transport in the road structures and embankment. Roseen, Thomas and Ballestero (2006) studied the porous asphalt as a mean of infiltrating, and even treating, the road water runoff. Cyr and Chiasson (1999) have modelled the subsoil drainage systems for urban roadways. They thus determined the foundation main characteristics (porosity, hydraulic conductivity anisotropy).

Some organisations have edited their own handbook concerning the runoff and infiltration processes: the EPA, EAWAG, USGS, CNRS, IRD and UN organisation like FAO, WHO or WMO.

1.4.1.3 Time Domain Reflectometry TDR

The use of TDR probe to assess the soil moisture is a new technique empirically developed by engineers using cable tester. The TDR probes and datalogger are now readily available for this specific purpose. Although the literature about this subject is rare, a few authors have interest in the subject. Chih-Ping Lin (2003) developed numerical modelling to assess the influence of the rod lengths, bandwidth, impedance and electrical conductivity on the calculation of the soil moisture. He also proved that the main influence on the measurement is the soil texture and density. On the other hand, Ofer Dahan et al. (2003) tried different probes (flexible probe included) and rods length to measure the soil moisture in the deep vadose zone. Finally, the most important breakthrough about this technology were made by Topp (1980, 1984), Ledieu (1986) and Roth (1992) who all developed a different calibration equations (which transform the soil dielectric constant ε into the soil moisture θ; it this thus the backbone of this method). The Topp equation is used in the present study.

1.4.2 ROAD ENVIRONMENT AS A SOURCE

Road contamination is relatively well known thanks to previous works carried out in Switzerland and abroad. In Switzerland, numerous publications come from the EAWAG (Swiss Federal Institute of Aquatic Science and Technology), OFEV and EPFL. For example the gasoline additive MTBE (Methyl Tertiobutyl Ether) was thoroughly studied (mandate SEA "Beobachtung des Stoffwechsel der Antroposphäre im Einzugsgebiet ausgewählter Abwasserreinigungsanlagen" OFEV) due to its high toxicity and mobility. It is also a top priority for the US environment office.

The HES Burgdorf (Boller et al. 2006) has conducted a similar project to the present study. Differences were that the road was old (over 50 years) and had a very heavy traffic (~25'000 vehicles per day). The surrounding soils were thus already contaminated. In a sister project, punctual infiltration (as opposed to diffuse infiltration) was tested in three different columns composed of various material layers.

1.4.2.1 Fuels and Oils

Schlaepfer et al. (1996) identified the sources of most of the road contaminants. He tested fuels, motor and gearbox oils, lubricating oils, exhaust gas, brake oils and particles, tyres, etc. He tested the road wearing course, paints and barriers as well.

Heavy Metals and their behaviours in soils and artificial substrates were studied by Parriaux et al. (1999, OFROU n°426). Most of the road contaminants (confirmed and new) were identified during this work. Especially, fuels and oils were analysed. Study results showed that aquifers were vulnerable to road pollutants. It was thus proposed the notion of aquifer "vulnerability to road pollution". Further research about the mobility and biodegrability of the toxic substance in the saturated and non saturated zones are nevertheless necessary.

1.4.2.2 Exhaust gas

Legret (2001) studied the exhaust pipe gas and pinpointed the great differences in concentration existing in various conditions (cold or hot engine, speed, road type, etc.). He also confirmed the high PAH and particles concentration in diesel fuel. Standard fuel has more BTEX and aliphatic hydrocarbons.

Acres (1991) and Rogge (1993) studied the unitary emission of vehicles, i.e. the quantity of PAH and aliphatic hydrocarbons emitted per vehicle per kilometre. Orders of magnitude for PAH were ranging from 0.1 (anthracene) to 1.7 (benzo(e)pyrene) $\mu g \cdot km^{-1}$ for tourism car, from 1.6 (anthracene) to 22.6 (pyrene) $\mu g \cdot km^{-1}$ for heavy truck. Concerning aliphatic hydrocarbons, values were ranging from 4.6 to 113.5 $\mu g \cdot km^{-1}$ (C32 and C25) for tourism car, and from 12.0 to 991.3 $\mu g \cdot km^{-1}$ (C_{32} and C_{20}).

1.4.2.3 Abrasive particles (brakes, tyres, wearing course)

Muschack (1990) estimated the wearing course might release up to 3.8 $mg \cdot km^{-1}$ per vehicle. It is composed of 95% particles and 5% bituminous mix. The latter is composed of mineral trace elements (MTE: Fe, Ni, Ca, Co, Cu, Na, Mg, Zn, etc.) and heavy aliphatic hydrocarbons C_{19} and heavier.

Hildeman (1991) estimated the PAH concentration in tyres to 200 $\mu g \cdot g^{-1}$. Legret (1995) added that tyres contain high concentration of Cu and Zn.

Pagotto (1999) calculated the mass of material resulting of the tyres abrasion. Results show that a car releases about 61mg per km gum dust. This quantity is multiplied by 5 for heavy trucks (305 $mg \cdot km^{-1}$). Brakes release 20 to 47 $mg \cdot km^{-1}$ of particles. He also states that galvanized barriers releases 440 $g \cdot y^{-1}$ of solid particles, 1045 $m \cdot y^{-1}$ of Zn, 2.1 $g \cdot y^{-1}$ of Pb, 0.23 $g \cdot y^{-1}$ of Cu and 0.16 $g \cdot y^{-1}$ of Cd.

Legret (2001), Stotz and Krauth (1994), Baladès et al. (1995), Ranchet (1995) or Berbee et al. (1999) studied the influence of the wearing course on the retention of pollutants. They showed that a draining wearing course (porous asphalt) is more efficient and acts as a filter, but it is also more subject to pollutant releases in case of bad conditions (acidic precipitation, etc.).

1.4.3 KNOWN ROAD SUBSTANCES AND THEIR BEHAVIOUR

This paragraph presents a brief reminder about the substances coming from the road, their origins and known behaviours. Also, substances that are dangerous for human or those which face legal regulation (OEaux, OSEC, MSDA, OSite; §6.7) are especially emphasized.

Many authors have concentrated on substances originating in the road environment. A brief insight, far from exhaustive, is proposed in appendix II (tab. II.1) and in table 1.1. Overall, substances come from the construction, material, maintenance and usage of the road. Concerning Swiss specificities, Parriaux et al. (1999) have contributed to analyse the provenance of road contaminant. They notably identified several road specific tracers (PAH phenanthrene, fluoranthene and pyrene). In the present study are only considered the substances carried by the road runoff; aerial deposits are not taken into consideration[3].

Origin	Substance
Carburant, gasoline	Lead, nickel, zinc, soot (particular), PAH, C_X, BTEX
Oils, lubricants et greases	Lead, zinc, nickel, PAH, C_X, BTEX, PCB
Exhaust gas	Brome, lead, nickel, PAH, C_X, BTEX, MTBE
Exhaust gas catalyser	Platinum, palladium, rhodium, PAH, C_X, BTEX, MTBE
Brake pad	Copper, chromium, nickel, manganese, lead, dirt
Tyres wearing	Rubber, soot, sulphur, zinc oxide with cadmium and lead traces
Wearing course	Particles and colloids: zinc, silicate, calcium, magnesium, PAH
Concrete	Dirt
Asphalt	Dirt, PAH
Tar	Organic compounds, PAH
Marking paints	Rutile
Railing, signalisation	Iron, zinc, chromium, nickel
Corrosion, wearing	Aluminium, copper, iron, cobalt, manganese
Maintenance services; road dep.	Sodium, calcium, chlorine, sulphate, herbicides, etc

Table 1.1: Origins of the different substances found in the road runoff environment (Modified from Schlaepfer et al., 1996).

[3] It is to say, they are not directly taken into account. They may of course settle down on the infiltration slope surface and infiltrate with the precipitation. They will therefore be measured in the exfiltration flow. The quantity of substance that travels aerially is unknown.

Literature is fairly abundant on the road contaminant subject. Nevertheless, huge differences exist either concerning the concentration, content or type of substance present in the road runoff. It thus needed a better understanding and speciation of the substances present in the road runoff. This is discussed in chapter 4.3. Substances are divided in two categories: inorganic and organic compounds. Inorganic compounds includes the MTE (mineral trace element) while organic compounds consist of PAH (polycyclic aromatic hydrocarbon), aliphatic hydrocarbon C_X, monoaromatic hydrocarbon BTEX (benzene – toluene – ethylbenzene – xylene). It also comprises the PCB (polychlorobyphenyls) although they are usually not considered as organic compounds. Finally, gasoline additives are also considered as organic (MTBE, Br compounds).

1.4.3.1 MTE (Mineral Trace Elements)

Mineral trace elements were formerly called heavy metals. Baize (2000) modified this terminology to take into account light metals (< 5 $g \cdot cm^{-3}$) and non-metallic elements (metalloids like As) often comprised in the "heavy metal" terminology. MTE list usually includes 68 elements of the Mandeleïev Table[4]. MTE considered in the frame of this study are listed in table 4.2. MTE also come from other anthropogenic or natural origin, but this study is concentrating on MTE originating in the road environment only.

Those specific substances are dangerous for human: the lead, chromium (especially the chromium VI), mercury, arsenic, cadmium, and, in a lesser way, the vanadium. Lead and chromium may cause specific well-known diseases. Mercury and arsenic are lethal in high concentration. Cadmium is toxic for plants and animals. On the other hand, many MTE are well-known nutrients (Cu for example). Swiss regulation concerns Sb, As, Pb, Cd, Cr, Co, Cu, Ni, Mg, Ag, Zn and Sn.

MTE are non-volatile and conservative; they do not naturally degrade. MTE stability is considered to be the duration needed to be definitively trapped by solid matter (adsorption). Some of them might even not be found in the road runoff because they are very light and transported aerially. MTE mobility is very variable. It highly depends on the state of the MTE (in solute or bonded to matter (complexation)). It is important to note that the MTE state depends on the pH and the oxidising-reductive potential. The latter is itself depending on the presence (or absence) of material offering strong electrical bonds: clay and humus. Overall, the higher the pH and the lower the humus and clay content are, the higher the MTE mobility is. On the contrary, if soils offer alkaline pH and high humus and clay content, MTE are highly likely to be trapped in the first few centimetres of soil (Mason et al. 1999).

Although the complexation states existing for MTE are very different, they are not distinguished in this study. For memory, the different complexation states are listed thereafter:

- The non-specific adsorption (cationic exchange). Cations are electrostatically linked to the solid matter. It depends on the cation exchange capacity CEC.
- The specific adsorption. It also depends on the CEC but has stronger liaisons. Covalent chemical bonds appear between the substance and the solid matter.
- The precipitation. MTE can (co-) precipitate with clays, iron and manganese hydroxides and calcite. When the pH is high, this process might be prevalent.

Non-specific and specific adsorption may occur with solid inorganic and organic material. In case organic matter OM is involved, complexation may form chelates (organo-metallic compounds) that are less toxic for the environment.

Although strongly depending on the soil properties, the MTE mobility are usually considered as an intrinsic property. The following MTE are considered as very mobile: Mo and B. Those have an average mobility: Fe, Zn, Cd and Ti. Finally, the Pb, Al, Cr, Cu and Ni are considered to have a low mobility.

[4] Discrimination is made on the relative concentration. Traces are considered to have mean concentration in the earth crust of less than 1‰.

1.4.3.2 PAH (Polycyclic Aromatic Hydrocarbon)

PAH may come from natural sources but are above all the result of the combustion of organic material and derivative (carburant, wood, etc.). They are non-soluble in water and electrically very stable; they react with difficulty and need special condition for their degradation. This evidently augments their persistence in the environment. They easily accumulate in the biologic mass. Once in the environment, they easily fix on solid matter. They might then be (bio-) degraded. The highest concentration of PAH is thus found in sediments.

Overall, all PAH are highly toxic. They do represent a high risk for the environment, particularly for the fauna (notably the aquatic life). They have mutagen properties; are carcinogenous for a few of them (benzo(a)pyrene is a well-known factor inducing cancers). The Swiss regulation imposes a surveillance for all of the PAH with low concentration limits. They also all are listed in the "Priority pollutants" list of the EPA (US Environmental Protection Agency).

PAH are hydrophobic and preferentially adsorb on the OM. Overall, the greater the molecular weight of the molecule is, the more hydrophobic it is. Heavy PAH are thus rapidly trapped. Clays have less potential to fix PAH. However, PAH link often to particles. Chiou (1985) also demonstrated that the soil humidity has a great impact on the clay capacity to adsorb PAH: dry clay-rich soils have a great adsorption capacity. Light PAH preferentially link to big particles, whereas heavy PAH bond to small particles. Hoffman and Mills (1984) postulated that the origin of the PAH were the wearing of asphalt, tyres and brake pad for bigger molecules, while smaller molecule come from the combustion. Moreover, it must be kept in mind that the precipitation itself has an impact on the PAH fractionation: heavy molecules are mobilized by heavy rainfall while lighter one would be mobilized, deposited, and mobilized again by successive small events. During this (re-) mobilization, HAP might volatilize (Krein 2000). Finally, the solubility of PAH can be augmented by other compounds like MTBE or ethanol (Li 1996).

Contact time between PAH and soil surface has also a big influence. The longer the contact time is, the better the adsorption is. The order of magnitude of the PAH half-life is 1 year (Wild et al. 1991).

Degradation of PAH molecules is inversely linked to their chemical formulae, their concentration and their physical-chemical properties (Cerniglia 1993). The presence of one PAH specie can inhibit the degradation of another PAH specie. The most preponderant factor for the PAH degradation is their accessibility. It thus depends on soils characteristics. See §4.1.7.1 for precisions.

1.4.3.3 C_X (Aliphatic Hydrocarbon)

As for PAH, C_X may come from the natural environment; but they are above all coming from the incomplete combustion of various oils, fuel and carburant. They are gases (up to C_4), volatile liquids (up to C_{16}) and viscous solids (beyond C_{16}). Simoneit (1986) edited a simple and handy calculation method to assess the provenance of the C_X; this is called the CPI method:

$$CPI = 2 * \frac{nC_{23} + nC_{25} + nC_{27} + nC_{29}}{nC_{22} + nC_{24} + nC_{26} + nC_{28} + nC_{30}} \qquad [\,-\,]$$

A CPI factor of less than 2 indicates a petroleum origin (0.93 gasoline; 1.02 diesel; 0.96 gasoil), whereas a number higher than 2 show a natural origin.

Aliphatic hydrocarbons are present in gases (C_1 to C_4), gasolines (C_6 to C_{11}), kerosene (C_{10} to C_{16}), lubricating oil (C_{16} to C_{22}) and, for heavier compounds, in asphalts. All are insoluble in water. Those compounds are very stable and react with difficulty.

Overall, all C_X present a risk for human health. At low concentration, they may cause skin diseases and eye problem, sometimes drowsiness, narcosis and vertigo. At higher concentration, C_X may cause cancers, mutation or death.

Octane is for example lethal at low concentration. Natural metabolites (under-products) are also highly toxic, like CCl_4 (causes coma and fibrillation). However, fatal doses are sufficiently high not to consider the risk as a priority (compared to PAH and BTEX for example). Biological effects are especially remarkable in the aquatic environment.

Note that there are many types of C_X: alcane, alcene, diene and alcyne. Because alcenes are highly reactive (and thus disappear by complexation) and dienes and alcynes are very rare, only alcanes are considered in the road environment.

Swiss regulations especially consider the lighter C_5 to C_{10}. OSEC consider all C_X but as a whole. No specific limit is established for a singular compound.

1.4.3.4 BTEX (Benzene – Toluene – Ethylbenzene – Xylenes)

BTEX constitute a large part of the carburant composition. BTEX are highly volatile and are lightly soluble in water (far more soluble than PAH, though). They have thus the tendency to stay in solute phase and be transported farther than PAH. If trapped in water they may be carried to the alluvial aquifer. This is generally not the case because they evaporate first. BTEX usually do not react without a catalyser.

BTEX sorption on soil surface is influenced by the OM presence. The influence of clays and/or iron hydroxides is only significant when OM is absent (Karickhoff 1984).

The benzene is extremely toxic and may provoke a respiratory failure. Its narcotic effect is powerful. It is also carcinogenous (benzolism is a common well-known disease in the pump attendant community). Xylenes cause skin diseases and respiratory problems. Swiss regulations impose a concentration limit on all BTEX compounds (very strict for the benzene: 10 $ng \cdot l^{-1}$).

1.4.3.5 PCB (PolyChloroBiphenyls)

PCB group is made of 209 compounds containing chlorine. All 209 compounds have the same chemical structure: they are made of a biphenyl core where hydrogen atoms are replaced by chlorine atoms. Their weights practically do not vary and are thus of no consequence on discrimination. Thus the 209 compounds are homologues. Usage of the common chemical nomenclature for PCB is far too complicated (it would give molecules like “2,2’,3,3’,4,4’,5,5’,6,6’ decachloro-biphenyl”. Ballschmitter and Zell (1980) introduced a numeration which is far easier: from 1 to 209. PCB are thus numerated from PCB1 to PCB209 (sometimes the prefix PCB is even neglected).

PCB were mainly found in hydraulic apparatus and electrical devices. They were used as lubricant and found in gearbox and motor oils. Also, they were used as plastic thickening agent in anticorrosive paints. They are now forbidden in most of the countries (forbidden since 1972 in Switzerland). They are nevertheless still found in the environment.

PCB are toxic for human and environment. They easily bio-accumulate and are very persistent. Under certain conditions, PCB may produce dioxins as by-products. It is suspected that they are also carcinogenous. PCB concentration in the environment is strictly limited by Swiss regulations.

1.4.3.6 Gasoline additives

The MTBE (Methyl Tertiary Butyl Ether) is easily produced by combining methanol and isobutene. It is oxygen-rich compound that is used as a retardant and catalyser in carburant. It is liquid, volatile and flammable. As it is very soluble (Höhener and Dakhel 2002), it has become in the last few years a major concern for many governments. Therefore, the European Union has placed this compound on the “priority list” for risk assessment in 1997. The EPA even classified it as the most mobile carburant component (Interagency Assessment of Oxygenated Fuels).

The MTBE is easily transported from the runoff to the aquifer. It is highly persistent and does not react without additive source of energy (sun). Its half-life ranges from a few days in the atmosphere to more than 10 years in the water. As for all organic compounds, its sorption is controlled by the OM content. However, the MTBE adsorption is very weak (8%) compared to benzene (40%) for example (Squillace and Pankow 1997).

The MTBE is detectable by its taste or its odour at very low concentration (20 ppb). Its carcinogenous effect has not be proven yet but is suspected (it is indeed carcinogenous for rat and mice). The EPA however demonstrated that MTBE is toxic (chronic headaches, nausea, and eyes irritation). The required doses for generating a massive poisoning are probably higher than the detection limit by human senses. MTBE is controlled by Swiss regulations (200 $ng \cdot l^{-1}$).

Many other additives are used in the carburant as catalyser. They are usually not considered as dangerous and are less persistent than the MTBE. They are the methanol, ethanol, tertiary butyl alcohol (TBA), di-isopropyl ether (DIPE), ethyl tertiary butyl ether (ETBE), tertiary amyl methyl ether (TAME).

1.4.4 LIMITATIONS

The section 4.1 intends to introduce the reader to the complexity of the road substance behaviours. It is not the goal of the present study to fully understand each of the substance's behaviour; but rather to assess the global substance retention in the experimental site soils. The retention of the substance is therefore understood as a global retention factor which is the operator between the input and output substance masses:

$$M_{input} \rightarrow \| retention \| \rightarrow M_{output}$$

Retention is definite as all processes that trap the substance in the soils. Those processes are not differentiated. Retention occurs in the soil volume between the surface and the exfiltration point (lysimeter) or aquifer; column tests and soil analyses are useful to pinpoint the retention exact localisation.

1.4.4.1 Complexation states

As explained in §4.1.1, MTE complexation can be due to many processes. Complexation in organic compounds are also numerous. The complexation state of an organic compound is important because it leads the (bio) degradation process: the sorption state determines the molecule accessibility. Indeed, PAH adsorbed on quartz aggregates are more easily biodegraded: they are more accessible. However, PAH have a tendency to preferentially adsorb on clay and silt (Amellal and Portal et al. 2001). Along the time, PAH are less and less (bio-) available; they fix on solid matter in a more permanent way. Nevertheless, the OM degradation may inverse the process and free PAH molecules (Amellal and Portal et al. 2001).

BTEX are readily available in the water. They are indeed more soluble than PAH. However, it also happens that they are trapped in soil matter; humic acids solubilise the BTEX that go back to solute state.

Overall, complexation state of organic compounds leads the degradation of the compound. At the end, organic compounds are often (bio-) degraded; it is only a matter of time. Half-lives range from a few days (28; toluene) to thousands of days (4280 days; benzo(k)fluoranthene) (Wiedemeier and Rifai et al. 1999). Baize (2001) and Duchaufour (2001) studied and definite the retention potential of the clay-humus complex (also called plasma) and well described the adsorption processes. Duchaufour (2001) also demonstrated that anions may well be retained by non-soluble minerals like oxy-hydroxide. Anions are usually considered hard to sorb.

This is not the case for MTE. MTE are not (bio-) degradable. Thus, the complexation state will not lead the degradation rate but more the storage and release rate. Indeed, MTE mobility is linked to the characteristics of the solid matter they are bonded to. For example, Pb and Zn are potentially very mobile when associated with carbonates:

carbonates can be dissolved and carried away. Carbonates thus constitute a bad reservoir for MTE. On the contrary, OM is very stable and has even a tendency to grow. MTE trapped in MO are unlikely to be released soon.

In road contaminated sites, MTE will accumulate until the soil sorption capacity is over. At that moment, MTE would not be retained anymore and would migrate (Lind Bo 1995). The soil sorption capacity is however enormous. Fifty years of heavy traffic proved to be insufficient to overtake the soil capacities surrounding a Swiss national road (Burgdorf project, Boller 2006).

The complexation state of inorganic compounds mainly leads the sorption – release process of the compound. It also of course depends on external factors previously mentioned (pH, residence time, etc.).

Complexation states are not considered in the present study. However, one must be aware that a good retention does not mean a permanent retention. Subsequent releasing processes may occur. This is even more evident considering an unstable constitutive material like carbonates. Moreover, external factors can also be very influent: if an acidic rainfall occurs, it is likely that the soils will release high concentration of MTE, for example.

1.4.4.2 Aerial dissemination

Aerial dissemination constitutes the main issue for most of the authors dealing with road pollution problems. Indeed, according to various authors, the fraction of substance being carried away by the wind may count from 1 up to 99% of the emitted mass. It is therefore hard to edit precise and fixed rules leading the substance behaviour. Butler (1984) and Boller and Haefliger (1996) postulated that only 5 to 20% of the road contaminants might be mobilized by the road runoff. The rest is usually dispersed by the wind and traffic.

PAH are for example disseminated very rapidly. According to Hewitt and Rashed (1990), only 1% of the light and 30% of heavy PAH stay in the road surroundings. Lygren et al. (1984) concur with those values. Hautala et al. (1995) demonstrated that some light PAH species are more abundant at 30m than at 10m form the road. Scetauroute Society (1992) enlightened the difficulties to interpret the PAH distribution across the road surroundings.

Germany has made special efforts to identify road pollutants, especially along highways. Drillholes have been dug for years. It proved the influence of the wind and traffic in the dispersion of the road pollutants. The high heavy metals concentration in surroundings soils was also highlighted.

Dissemination processes were studied by Alloway (1995). He separated the deposition process into wet and dry deposition paths. Dry deposition is essentially due to gravity and might be mobilized by the runoff. Specific weight of the substance plays a preponderant role in the mobility. Wet deposition is mobilized in the atmosphere and is thus already either in solution either adsorbed.

MTE dissemination is also a big issue. The speciation of the considered compound is essential. Parmentier and Garrec (1994) showed that the relative concentration is maximal in the immediate road vicinity and logarithmically decreases along the distance from the road. Main wind directions, traffic charge and the site topography greatly influence the dissemination process. Lygren et al. (1984) demonstrated that half of the lead only is contained in the road runoff. The rest is aerially disseminated and deposited mainly at less than 7 m from the road. Hewitt and Rashed (1990) calculated that only 8% of lead is in the road runoff, 6% deposit in the first 50 m from the road and 86% are aerially disseminated further away. Contat et al. (1991) proved that a relation exists between the aerial dissemination of lead and the temperature (lower in summer, higher in winter).

Aerial dissemination is not part of the present study. The input potential pollution is the one recorded in the road runoff. However, as infiltration slopes extend up to 8 metres from the road, all aerial deposits settling down in that particular area are taken into account. The calculated output mass is thus the addition of the input and aerial deposits, minus the retention mass. Comparing the input and output masses (or concentrations) may therefore underestimate the retention in soils.

1.4.4.3 Colloids

Many authors agree on the fact that the road runoff is a biphasic transport mean. Some substances will travel under its solute form while other will preferentially travel adsorbed to suspended matter, i.e. particles or colloids. Assessing the importance of solid transport in regard to solute transport is fundamental. If all the substances are already adsorbed to suspended matter, a mere particle filter would be enough to trap all substances. On the contrary, the solute substances are more difficult to retain. Transport processes are also not the same: Corapcioglu and Kim (1995) demonstrated that the association between substances and colloids favours the transport. Models only based on advection, diffusion and dispersion therefore underestimate the pollutant transport. McCarthy (1989) showed that if colloids are made of the same composition as the soil matrix, pollutant may indifferently adsorb on the colloids or on the matrix. Therefore, colloids may steadily keep pollutant adsorbed during transport. Wan and Wilson (1994) presented the water-air interface as a major factor in the colloid transport: this interface sorbs colloids. This can ultimately stop the colloid migration. The unsaturated zone thus plays a significant role in colloids transport.

It has also been demonstrated that the augmentation of the complexation capacity by OM or co-solvent increases the transport speed (Enfield, Bengtsson et al. 1989; Dunnivant et Jardine 1992). The speed might even exceed a tracer speed (Ryan and Gschwend 1990). The transport of pollutant might be preponderant for certain species (Grolimund et al. 1996). This has also been demonstrated in Switzerland (Boivin, work under progress).

Sansalone and Buchberger (1996) showed that Zn, Cd, Ni and Cu are transported in solute form, Pb and Cr are half solute, half adsorbed while Fe and Al are almost completely adsorbed to suspended matter. Stotz (1987) established that 14% of PAH only were found in solution. The rest was rapidly adsorbed onto particles < 60 µm in diameter. DeNovio, Saiers and Ryan (2004) published a survey on the colloidal modelling and mass transfer. For an introduction on those processes, see De Jonge, Kjaergaard and Moldrup (2004). Rousseau (2004) made experiments on soil column to assess the physicochemical effects on particles mobilisation.

For those reasons, colloids transport is preponderant and might constitute a significant percentage of the substance transport. Therefore, it has been decided to take the colloidal form into account in the frame of the present study. For practical reasons, the substance transport process is not differentiated: water samples are simply acidified prior to filtration. Thus, the measured substance concentration is the maximum potential substance concentration. Although the acidification is carried out with great care, ions might even come from the mineral structure itself. Overall, the free substance concentration is therefore overrated[5]. If acidification would have been made after the filtration, measured concentrations would have been much lower.

1.4.5 FURTHER REFERENCES

For this study, the Climax theory (Clément 1916) will be taken into account. It stands that the soil solid phase morphology and composition can be considered as constant. The soil fluid phases (gaseous and liquid) vary very rapidly spatially and temporally.

Docourt (2005, postgraduate diploma thesis) investigated batch and column tests on Grandson soils. Results are presented in paragraphs 4.2.

Further references about road runoff and road contaminants are Daub (1994), Hvitved-Jacobson et al. (1991), Legret et al. (1987, 1997), Muschack (1989), Spangberg et al. (1993), Strecker et al. (1987) et Xanthopoulos (1994). Other more specific studies about the pollutant content in road runoff and peak charge are Harrison and Johnston et al. (1985), Ball and Hamilton et al. (1991), Hewitt and Rashed (1992), Sansalone and Buchberger 1997, Smith and Sievers (2000).

[5] The free substance concentration refers to the concentration of the substance that is indeed coming from the road environment (road runoff) or can indeed cause problem to the environment (percolation water). As it has been explained in the previous paragraphs, substances adsorbed on colloids may travel but are easily retained by a mere filter.

1.5 SITE SELECTION, GEOLOGICAL AND HYDROGEOLOGICAL BACKGROUNDS

The road section RC263c was built in 2003 between Champagnes and Grandson (lieu-dit La Deude, commune de Grandson), directly north of the motorway A5 "Champagnes" exit (figure 1.3). The construction agenda coincided very well with the project agenda and thus was a strong argument for the selection. Preliminary inquiries have been conducted to confirm that the site suited the specific OFEV requirements.

The road section is 95 m long (km 400 to 495) and is roughly N-S, lightly turning to the right. Illustration is shown in figure 1.4. It is smoothly inclined (3% transversal slope) eastward for runoff evacuation purpose. The testing section ends shortly before the northern crossroad, 30 m south of the bridge over the Arnon. The testing section lies on an area classified as "other sector" in the water protection zones classification. Thus, no specific protection policy has to be set. Swiss protection classification is summarized in the appendix I.2.

The site is situated directly south of the Arnon River. The small alluvial aquifer is restricted in quaternary sediments showing a suite of recent alluviums and moraine deposits. The Chatian Molass (yellow marls with gypsum and sandstones) is underlying the alluvium and moraine alternation. It is essentially free of water.

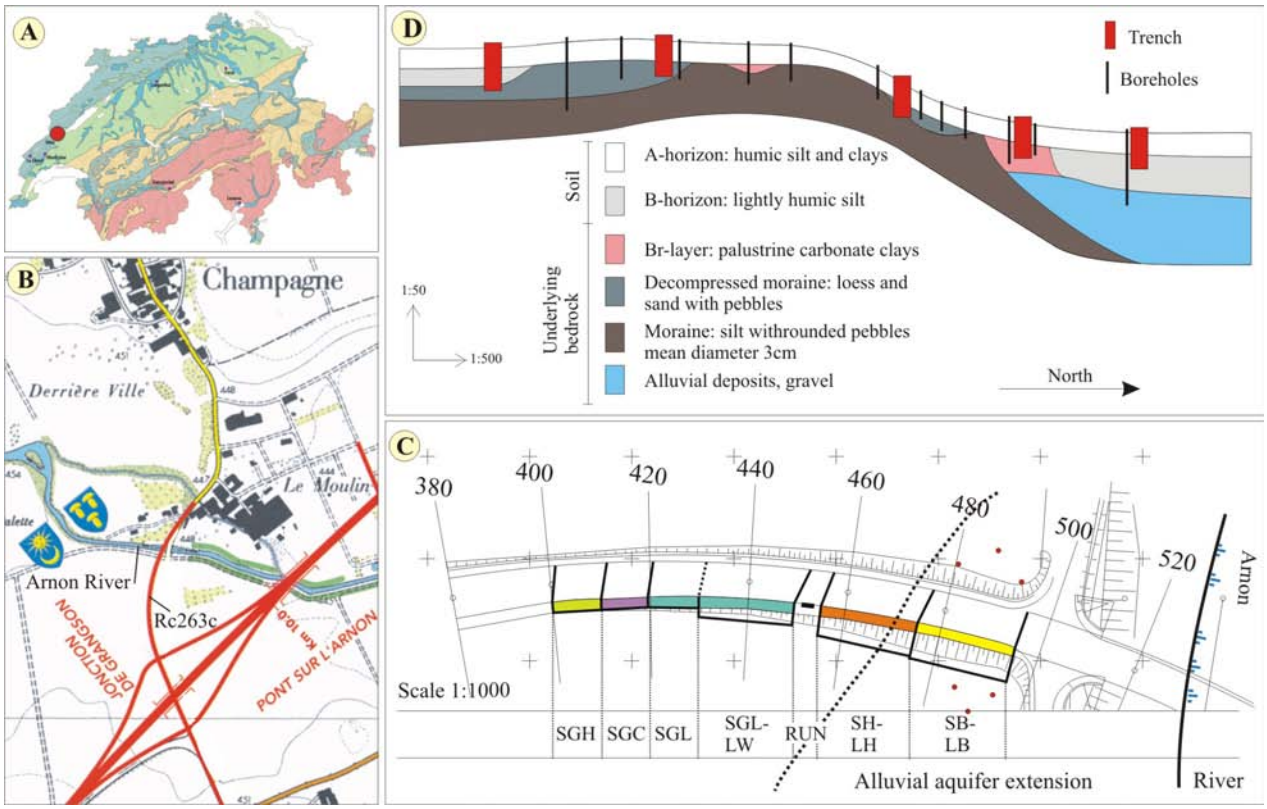

*Figure 1.3: **A)** Swiss map showing the specific soil spatial distribution in Switzerland with Jura type soils (blue), Plateau type soils (green), Prealpine type soils (orange) and Alpine type soils (red). Grandson soils belong to Jura type (blue). **B)** RC263c localisation. It is situated between the A5 motorway "Champagnes" exit and Arnon River. **C)** Plan showing the 95 m testing segment. Upper quotes are in meters. Special codification for the different compartments has been used for simplification purpose. See figure 2.2 for insights. The 2D plans also shows compartments extension (plain line), the aquifer extension (dashed line), the runoff collector (black box, km 455), and the Arnon River (far right). Red dots are piezometers. North is directed to the right. **D)** The underlying geology as extrapolated from the boreholes and trenches logs. The alluvial aquifer is restricted to the direct vicinity of the river. The moraine (lodgement till) is very impervious. Thus, only the northern compartment is suitable to study the connection between the road and the aquifer.*

Five trenches have been dug along the western profile of the road previous to the construction. The geological succession is composed of 5 main layers (out of which 1 and 2 are soil horizons):

1) The A horizon is less than 50 cm and is composed of fine alluvial carbonate silt.
2) The B horizon is composed of sandy silt, partially sealed.
3) The Br layer is composed of low carbonate grey clays with few pebbles and organic matter rests. This layer is highly impermeable. It corresponds to a palustrine edge in the alluvial context of the Arnon River.
4) The alluvial body (saturated and unsaturated zone) is composed of well sorted Jurassic carbonate pebbles in a sandy matrix. This horizon disappears when 50m away from the Arnon River. Thus, the alluvial aquifer is restrained in the vicinity of the river.
5) The basal layer throughout the profile is a highly impermeable moraine.

Six boreholes have been drilled east and west of the compartment 475-495 to monitor the alluvial aquifer. They have been equipped with piezometers. The drill logs confirm the presence of a highly impervious moraine between 3.5 (south) and 8.5 (north) meters depth, that limits the alluvial aquifer. The A and B horizon and Br layer are also present but more complicated when boreholes are close to the river. The alluvial body also contains more mixed-material lenses northward. Trenches and boreholes logs are shown in appendix III.2 and 3.

Nine infiltration tests (Porchet infiltrometer) have been conducted in various places east of the construction site (km 475 to 495). The overall infiltration rate was 10^{-6} to 10^{-7} $m \cdot s^{-1}$. The vertical hydraulic conductivity is considered low. The closer to the river, the higher is the hydraulic conductivity. Infiltration tests results are shown in appendix III.1.

The preliminary investigations showed that the Arnon River has a direct influence on the geological characteristics of the construction site. The alluvial aquifer exists only from km 465 (basal moraine, null flow limit) to km 515 (Arnon river, infiltration/exfiltration limit) with various thickness (0 to 6m). Western and eastern limits are not well knows. The regime is a free surface alluvial aquifer.

The alluvial aquifer is usually found at 1 m depth. Infiltration and aquifer contamination tests will be conducted only in the northern (km 475-495) compartment. The lodgement till is shallower southward.

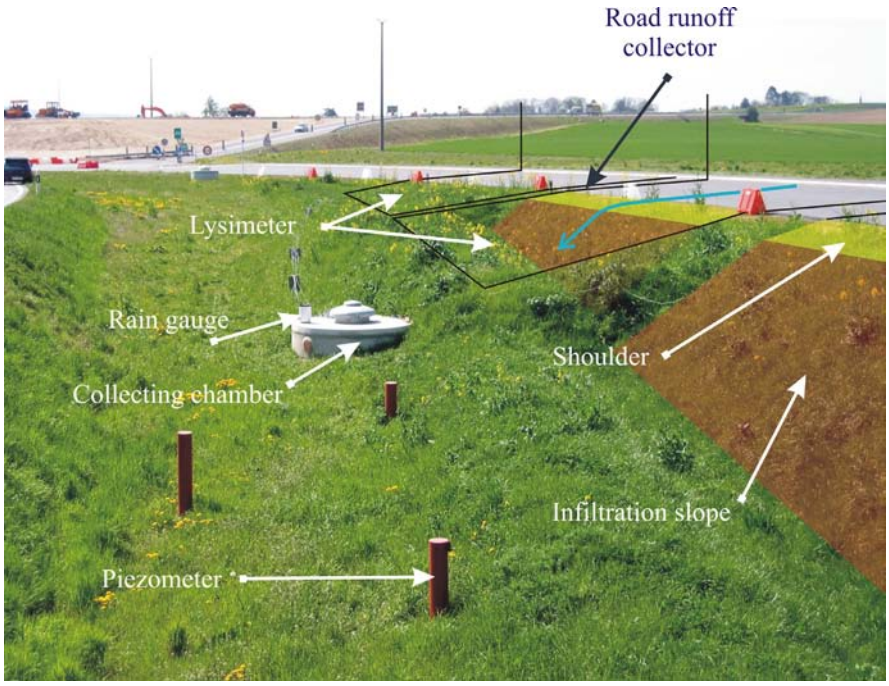

Figure 1.4: Picture of the experimental site, taken from the km 500 crossroad toward the south (see figure 1.3 for location). The two lysimeters, the infiltration slope connected to the aquifer, three piezometers and one collecting chamber are observable. The road runoff collector location is specified, although not visible.

CHAPTER 2

CONCEPTION AND CONSTRUCTION

2.1 1ST PHASE: CONCEPTION AND CONSTRUCTION

2.1.1 ROAD STRUCTURE

The road structure is a classical one for such kind of cantonal roads. However, two characteristics are uncommon:

- the road embankment and foundation are made of the same material: the superior quality gravel grave I
- the HMF (road base) is 14 cm thick, which is more commonly found in roads welcoming higher traffic and/or having a foundation and embankment of lower quality

The grave I (grave I SN 670 120d, figure 2.1) are made of Jurassic carbonate crushed stones coming from the Concise tunnels. The embankment is thicker northward. HMT22s (base course) and wearing course (AB11s, bituminous matrix ELF 50/70; Fezin refinery (F)) have the usual thickness (respectively 7 and 4cm).

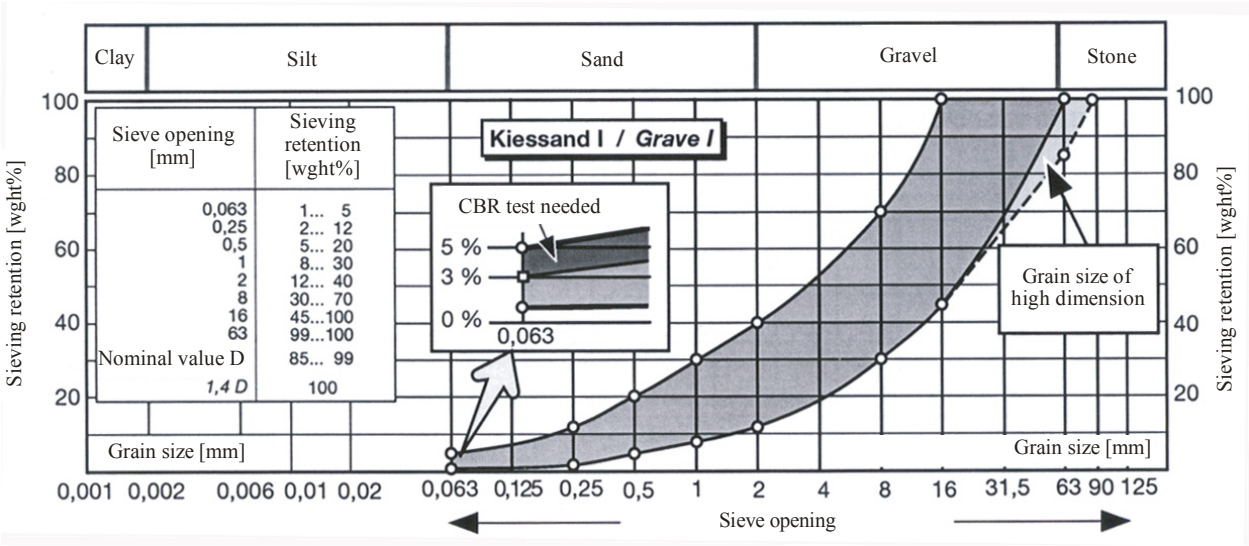

Figure 2.1: Granulometric curve of the grave I; the constitutive material of the road embankment, foundation and shoulder core. (from the Swiss norm SN 670 120).

2.1.2 SHOULDERS DESIGN AND CONSTRUCTION

During the conception phase, five shoulder designs have been selected and put into competition (figure 2.2). All shoulders respect the criteria described in the study objectives, i.e. as "stabilized shoulder". Moreover, let us remember that the shoulder main quality objective was to be as tight as possible; it was therefore designed accordingly. Pollutant retentive capacity of the shoulder was a mere verification in case the shoulder would not be perfectly impervious. The five shoulder designs are divided into 2 groups: with and without an artificial tightening layer. Shoulders are 1.5 m wide. The shoulder main components are:

1) the main body (gravel - grave I)
2) the specific tightening material (construction material mixture or solid layer)
3) the basal geomembrane

4) the collecting pipe

Number 3) and 4) are for testing purpose only and are not part of the basic design. They might actually disturb the road and shoulder behaviours[1]. For geotechnical comparison purpose, two shoulders made of grave I and lawn (SGL) have been built: one with an underlying collecting pipe and one without. The effect of the geomembrane (3) and collecting pipe (4) on the infiltration could also be assessed by comparison, as well as its impact on the road stability.

The 3 shoulders without artificial layer are made of:

- Gravel and Humus (SGH, km 400-410). As mentioned in figure 2.2, this compartment is only designed to ensure that the runoff fraction infiltrating the shoulder could be retained.
- Gravel and Clay (SGC, km 410-420). The SGC shoulder is designed to have a high impermeable potential.
- Gravel and Lawn (SGL, km 420-430). Its homogeneity guarantees a good stability. This is the reference shoulder; mostly because it is the simplest one and is already widely used in Switzerland. This shoulder is repeated twice: in the first compartment (10 m; km 420-430), the shoulder respects the mentioned construction method; in the second compartment (20 m; km 430-450), the shoulder has neither underlying geomembrane nor collecting pipe.

The two shoulders with an artificial tightening layer are made of (basic design are displayed in figure 2.2, complete profiles are in figure 2.3):

- a buried prolonged HMF (road base) coated with a bituminous mixture (SH km 450-470)
- a buried bentonitic geotextile (SB km 475-495)

The 7 compartments positions are shown in figure 1.3. Their lengths are 1x5 m, 3x10 m and 3x20 m respectively; they include the 5 shoulders types. The first short compartment of 5 m is the runoff collector (RUN km 450-455), bordered by a 1.8m colleting sink. It has a direct connection with the collecting chamber. The 3x10 m compartments are dedicated to the 3 shoulders with no artificial layer (SGH, SGC, and SGL (10 m)). The 3x20 m compartments are dedicated to SGL (20 m), SH and SB. All these compartments are physically separated by thick black stripes of road paint (Basler Lacke 43-9100-290, 4.5 mm) that prevent the runoff from crossing from one compartment to another. It allows constraining the rainfall catchments surface.

The shoulder thickness has been set by SR (Service des Routes vaudois) for stability reasons. The construction method is as follow (figure 2.4):

- The embankment is levelled and the geomembrane (Sarnafil, SaRi 303-083) and collecting pipe are placed (when applicable). The PE110 collecting pipe is embodied with a geotextile to prevent any obstruction with fine particles coming from the grave I leaching.
- The grave I is compacted up to HMF level (foundation level).
- The shoulder special tightening layer is either placed at that depth (artificial layer; -26cm) and then covered with 11 (SH) or 26cm (SB) of grave I, either placed on top of another 21cm of compacted grave I.

The surface mixture is 5 cm thick. It is composed of sorted gravel and 10% weight of A horizon rich soil (SN 640 673) for SGH. For SGC, it is composed of gravel (maximum diameter 20 mm) and 8% weight clay. The mixing is conducted under moist conditions; a particular attention is made to avoid clay aggregates. It is well homogenized. Finally, for SGL, the special mixture is composed of grave I seeded with lawn. For shoulders without bordering infiltration slope, the edge of the shoulder is covered with A horizon (30cm thick) with a 2:3 slope.

[1] The collecting pipe goals were to measure the water flow and to take samples. However, they also act like drain pipes, i.e. they favour the draining of soils and shoulders. They indeed constitute a local hydraulic head H minimum (inside of the pipe, H is equal to z only).

Shoulder with **G**ravel and **H**umus	**SGH**
Shoulder built with grave I and humus. Humus has been chosen for its contaminant retention potential. The grave I is simply mixed with 10% weight of humus-rich A-horizon. Thickness of the special layer is 5 cm.	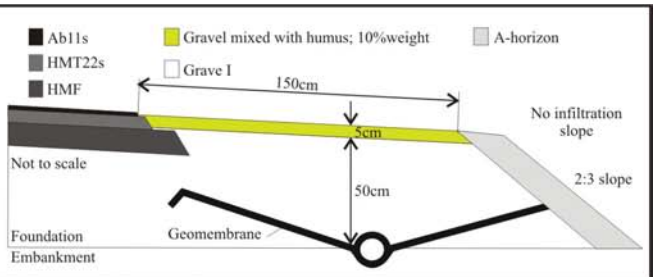
Shoulder with **G**ravel and **C**lay	**SGC**
Shoulder built with grave I and clay. Clay has been chosen for its tightening potential. The grave I is simply mixed with 8% weight of clay. The mix is conducted in wet conditions; a special attention was made to avoid aggregate formation. Thickness of the special layer is 5 cm.	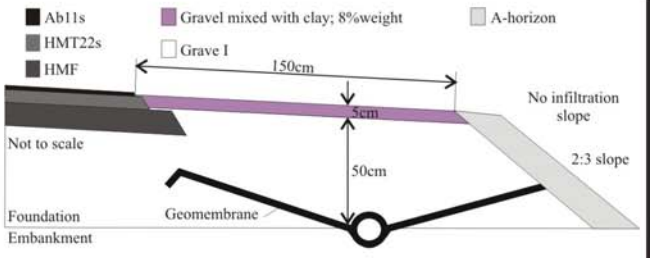
Shoulder with **G**ravel and **L**awn	**SGL** (10m)
Shoulder built with grave I and seeded with lawn. Lawn has been chosen for its stabilizing potential. The grave I is simply mixed with lawn seeds. Thickness of the special layer is 5 cm.	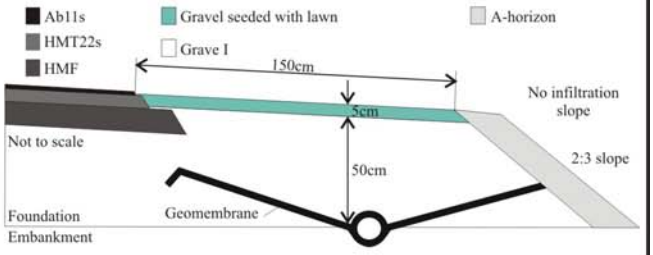
Shoulder with **G**ravel and **L**awn	**SGL** (20m)
Specificities of this shoulder are the same as SGL (10m). Only the geomembrane and collecting pipe are missing. This allowed testing the influence of the collecting pipe. Moreover, an infiltration slope borders the shoulder. See text for precision about the collecting pipe and geomembrane possible side-effects.	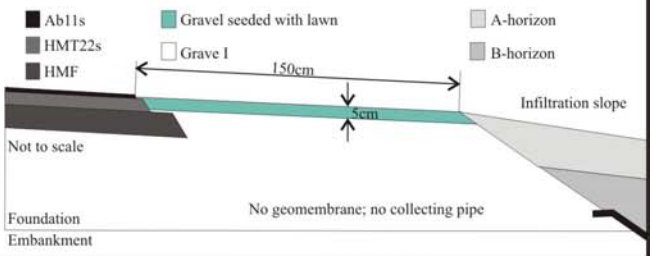
Shoulder with prolonged **H**MF	**SH**
Shoulder built with grave I underlying and overlaying a prolonged HMF. The latter has been coated with a bituminous mixture for tightening. Special effort has been made to coat the shoulder edge. Solution proposed by the road engineers for its easy construction technique.	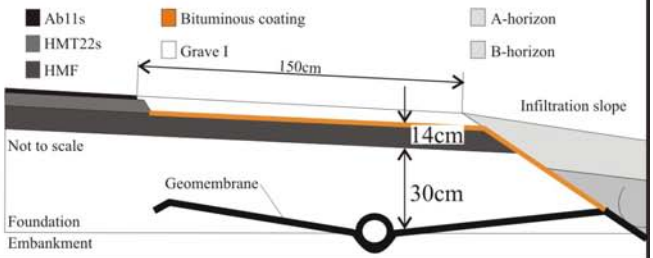
Shoulder with **B**entonitic geotextile	**SB**
Shoulder built with grave I underlying and overlaying a bentonitic geotextile sheet. A small piece of geomembrane is used to bond the geotextile and the HMF. The geotextile indeed cannot be sited under the HMF; the HMF laying temperature is too high. 2 cm of rounded gravel is put directly above the geotextile to avoid piercing. Solution proposed by the GEOLEP for its well-known impermeable	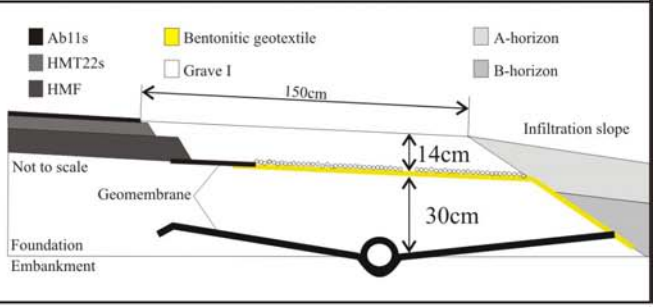

Figure 2.2: Sketches, brief description and nomenclature used for the five different shoulder designs. The nomenclature is used not only for the spatial situation (see fig. 2.4) but for the collecting pipes numeration as well. A distinction is made between SGL 10m and SGL 20m because no collecting pipe underlies SGL 20m. SGL will mean SGL 10m unless otherwise specified. Infiltration slopes border SGL 20m, SH and SB.

The artificial layer used for SH is a prolonged HMF (14 cm thick) underlying the grave I. A bituminous mixture coats the HMF and shoulder edge which are thus waterproofed. Special efforts have been made to perfectly seal the shoulder edge with the bituminous coating (figure 2.2 SH). In SB, the artificial layer is a 2 cm bentonitic geotextile (Volclay Voltex®) placed at HMF base level. This material has been chosen for its very impervious and self-healing properties (INSA, Institut National Supérieur Appliqué, Lyon). It is made of sodic bentonite trapped between 2 geotextiles. The Bentonitic geotextile cannot be sited directly under the HMF due to high temperature conditions (the HMF is posed at 160°C) and inflation risk in wet conditions. Therefore, a waterproofed geomembrane is used as a link between the HMF and the geotextile (see figure 2.2 SB). The Geotextile is thus sited a few cm away from the HMF. Ultimately, the shoulder is covered with 2 cm of rounded crushed stone (6-8 cm, to avoid piercing of the geotextile) and 24 cm of grave I.

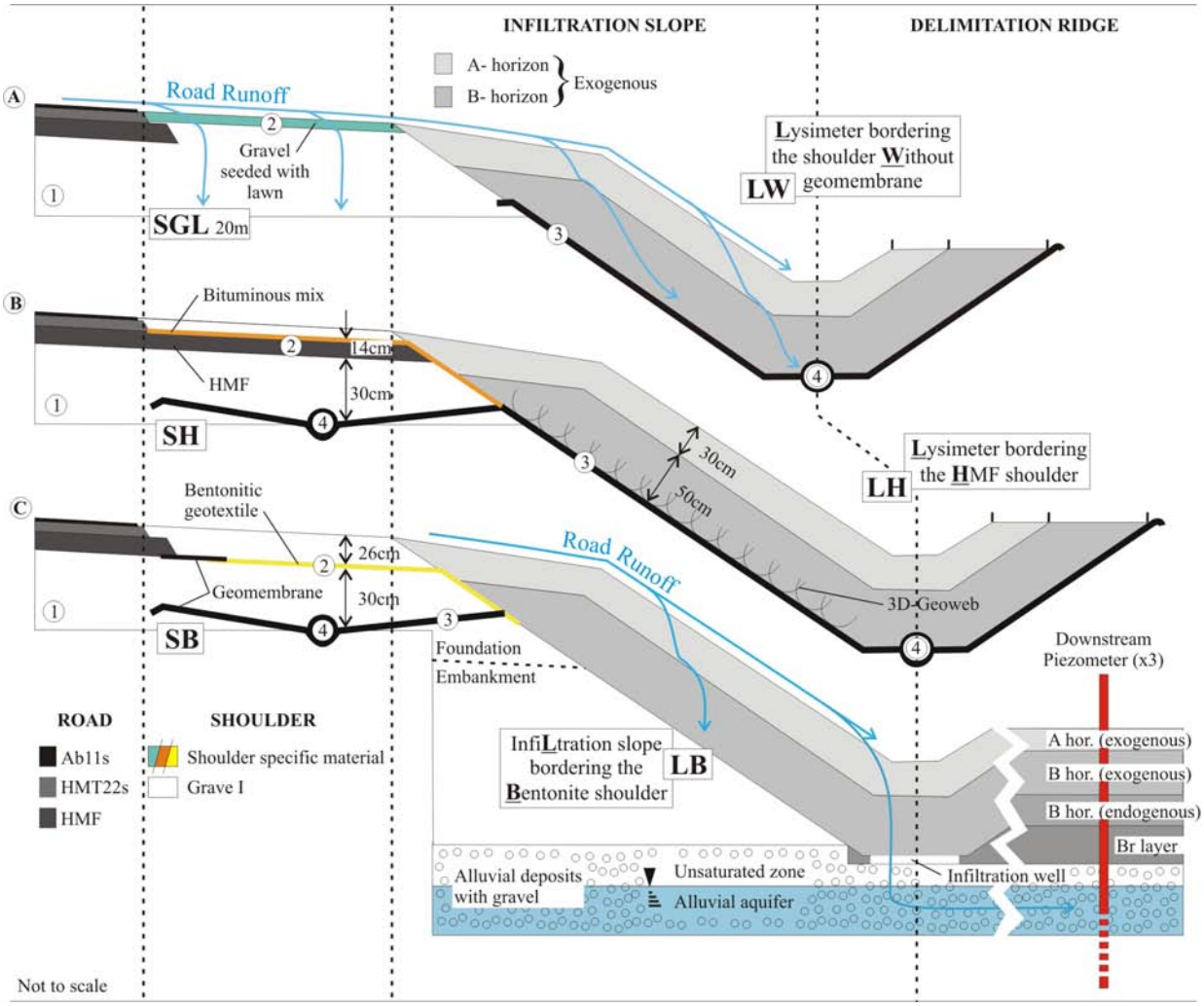

Figure 2.3: 2D sketches of the three complete SGL 20 m, SH-LH and SB-LB compartments. Profiles are W-E. Again, the basic material is grave I (1). (2) is the tightening material, (3) the geomembrane and (4) the collecting pipe. Nomenclature is shown in bold characters. Again, acronyms are used for spatial localisation (fig. 1.3) and collecting pipes (4) numeration as well. ***A)*** *SGL (20 m) and coupled lysimeter LW. This compartment represents the idealized road side (shoulder and infiltration slope) as it presently widely exists in Switzerland. The only experimental installation (3-4) is found under the A and B-horizons and thus no perturbation should occur prior to that point. Water streaming, infiltration, retention and releasing should not be perturbed by the experimental construction. It also allows comparing results with SGL 10m.* ***B)*** *SH and coupled lysimeter LH. Due to the low roughness of the basal geomembrane (3), a 3D net (Geoweb) was installed onto the geomembrane. See § 2.1.4 for side effects.* ***C)*** *SB and coupled infiltration slope LB. Neither geomembrane nor collecting pipe is sited under LB. No Geoweb was needed. Due to the presence of the low vertical hydraulic conductivity Br-layer, infiltration wells has been dug to allow water reaching the aquifer. Aquifer streaming direction is W-E. Three upstream piezometers (not apparent on this sketch, far left) allow comparing the underground water quality before and after road contamination.*

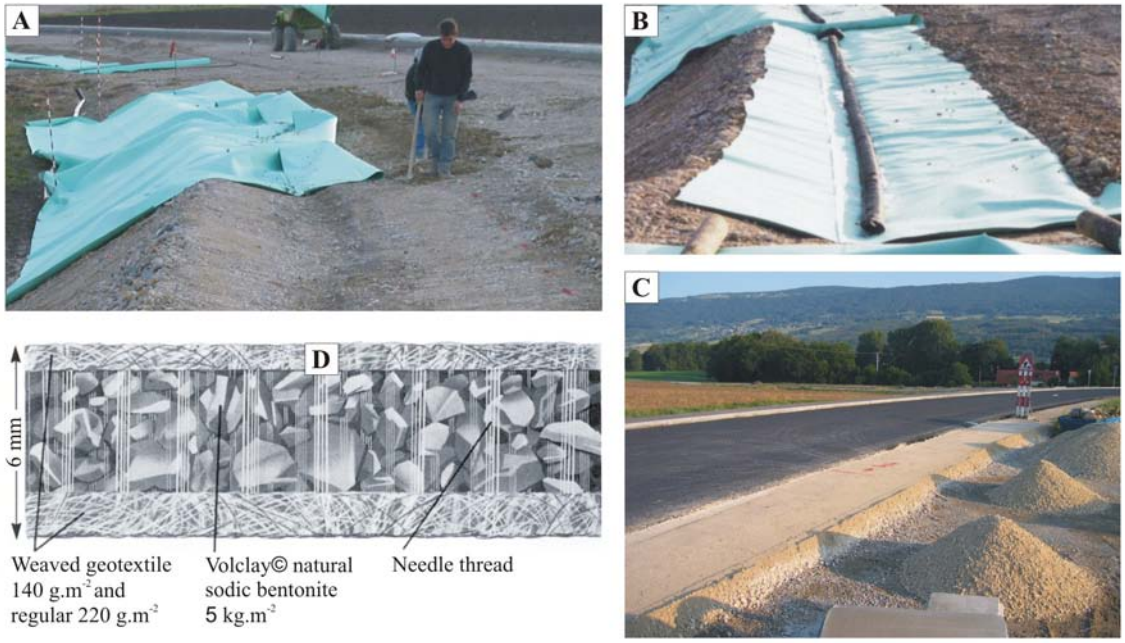

*Figure 2.4: Illustration of the shoulder construction. **A)** Levelling of the embankment top that will welcome the geomembrane. The geomembrane sheet is present at the back. **B)** Geomembrane fitted to the embankment. The collecting pipe is placed in the centre. The pipe has been coated with geotextile to avoid holes obstruction. **C)** Shoulders once the foundation has been levelled. Gravel piles nearby are the material that will be used shortly after to make the special 5 cm thick layer. **D)** Bentonitic geotextile profile.*

2.1.3 INFILTRATION SLOPES

Infiltration slopes have 2 designs. First, infiltration slopes with underlying waterproof geomembrane are considered as lysimeters. They allowed measuring water flows going through 30 cm of A and 50 cm of B horizons (exogenous soils, see §2.1.4) and to take samples. Second, infiltration slope with no geomembrane allow a direct connection between road runoff and the alluvial aquifer. Six piezometers are placed for monitoring and sampling purposes.

It is postulated that SH and SB will have the best hydraulic comportment (artificial waterproof layer) and are so eligible for the infiltration slope tests. They are equipped with infiltration slopes (lysimeter LH and infiltration trench LB). SGL (20 m), as the referential shoulder, is equipped as well with an infiltration slope (lysimeter LW). The Infiltration slopes are shown in figure 2.3.

The lysimeter profile is dug next to the shoulder and levelled. Particular caution is used for the levelling phase to avoid water concentration or reverse flow. The geomembrane is next fitted to tight the trench. The collecting pipe is placed at the bottom of the basin. Again, it is enveloped by geotextile and rounded gravel to avoid obstruction of the pores by fine particles. A (30 cm) and B (50 cm) horizons soils are then used to fill the basin. The infiltration slope LB has neither geomembrane nor Geoweb (see §2.1.4). The edge between the shoulder SB and the surrounding soil is made of bentonitic geotextile.

2.1.4 SPECIFIC CONSTRUCTION PROBLEMS

Three specific problems arose during the construction phase. First, the volume of soil on the site was not sufficient to build all the infiltration slopes. Thus, the totality of the soil was taken close to the nearby A5 motorway constructing site (A and B horizon similar to those found on the experimental site).

Particular problems happened for the LH construction. Slope stability models showed that the slope would be subject to landslides under wet conditions due to the presence of the geomembrane (low roughness preferential slide surface).

Therefore, a 3D-net (Geoweb) has to be used. This net is fixed with nails and cables (see figure 2.5B for illustrations). It stabilizes the slope and has holes to avoid disturbing water infiltration. Finally, 50cm of B horizon soil and 30cm of A horizon soil fill the lysimeter. This difficulty is only due to the geomembrane presence and will not exist in the practice of road construction (figure 2.5B).

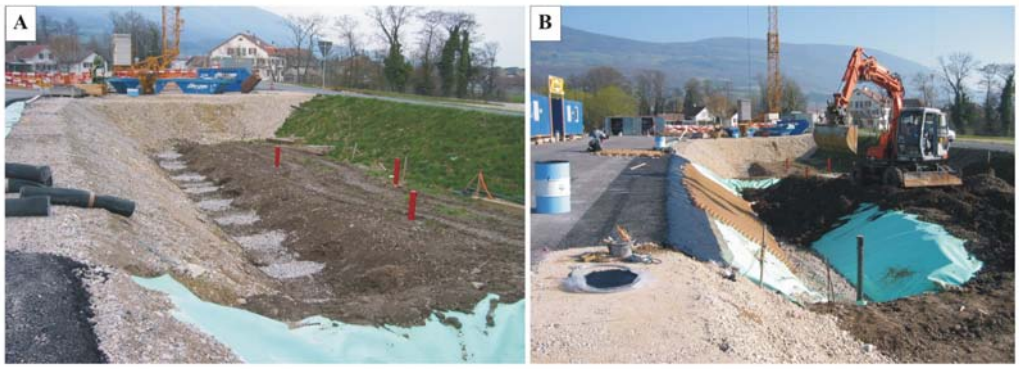

Figure 2.5: Illustrations of the problems encountered for LH and LB. ***A****) Nine infiltration wells have been dug at the bottom of the LB infiltration slope to by-pass the Br impervious layer.* ***B****) A 3D-net has been used to stabilize the LH infiltration slope. It is discernable in brown. Note the bituminous coating on the shoulder and shoulder edge; and the geomembrane as well. The collecting pipe was surrounded by gravel to avoid pipe holes obstruction*

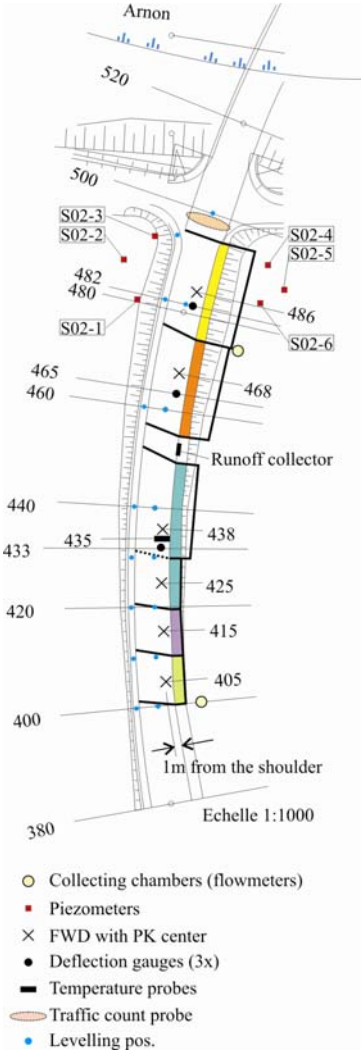

Figure 2.6: Road instrumentation localisation. Colours correspond to the figure 2.2. Piezometers positions and nomenclature, reference distances and compartment surfaces are also shown.

Finally, for SB - LB, the trench bottom did not reach Br geological layer base. In order to avoid this layer stopping the water infiltration, nine infiltration wells have been dug and filled with gravel (50 cm depth; 1 m Ø; figure 2.5A).

2.2 2ND PHASE: MONITORING DESIGN

2.2.1 ROAD INSTRUMENTATION

The road has been equipped with various instruments whose positions are shown in figure 2.6. Six PT100 temperature probes have been positioned during the construction along the km 435 profile at 6, 12 and 26 cm depths, right and left of the northbound traffic lane. They are at the bottom of the AB11s, HMT22s and HMF respectively.

Three deflectometers have been placed in the SGL (20m), SH and SB road profiles. Temperature and deflection gauges are linked to a datalogger sited in the km 475 collecting chamber. Acquiring time step for these instruments is 30 minutes.

Six points have been selected for the three Falling Weight Deflectometry (FWD) campaigns. All emplacements are 1 m away from the shoulders. The campaigns have been conducted in November 2004, April and September 2005. Levelling campaigns have been performed shortly after the FWD campaigns (1-3 days later). Sixteen control points are positioned on the western walking path and on the road axis. Road traffic is counted in both directions.

Inductive reels have been buried in the road pavement just south of the bridge over the Arnon. Datalogger records the traffic per hour.

2.2.2 HYDRAULIC MEASUREMENTS (figure 2.5)

The key part of the installation are the eight collecting pipes used to measure and sample the water flows getting through the shoulders and infiltration slopes (table 2.1). Figure 2.7 summarize the road runoff infiltration paths and the interception points, while figure 2.8 shows a 3D isometric view of the experimental station. It well recapitulates the overall architecture, shoulders and infiltration slopes designs, positions and nomenclature. Collecting pipes are underlying 5 different shoulder types and 2 lysimeters (figures 2.2 and 2.3). One more is used to collect road runoff. Pipes are made of PE110 (polyethylene) and are therefore inert. Collecting pipes (half screened pipe) are embodied with geotextile to avoid particle migration and obstruction. Special effort has been made to seal the basin formed by the geomembrane, especially where the collecting pipe penetrate the membrane. Several pieces of geomembrane have been thermo-welded to suture the area. All pipes are running (2% slope) to 2 collecting chambers (km 400 and 475). SGH, SGC and SGL pipes are directed to the first chamber (km 400) while others are directed to the second one (km 475). Both chambers are above the highest level reached by the Arnon to avoid back flooding. Water is then evacuated by a pipe downstream, far away from the station, to avoid influence on the aquifer. The evacuating pipe has no-return valves preventing back flows. Six piezometers form 2 triangles up- and downstream of the 475-495 compartment to monitor the alluvial aquifer. They are numbered clockwise from S02-1 to S02-6.

N°	Mean of measurement		
	What?	**How?**	**Where?** (see fig. 1.1)
1	Runoff	Special segment with pipe	Runoff collector RUN
2	Shoulder inf.	Geomembrane + collecting pipe	Shoulders with special geomaterial mixture SGH,SGC,SGL
3	Slope inf.	Lysimeter + Geom. + coll. Pipe piezometers (GW recharge)	2x Lysimeter LW,LH Groundwater infiltration LB
4	Overflow	No measurements, visual check	-
5	ETP	Estimat. API, Meteoswiss data	Station Mathod, Yverdon

Table 2.1: Measurement means. Instrumentation in the collecting chambers concerns essentially the flow measurement. Hydraulic behaviour is the key part to understand water paths and retention. Geochemical behaviour is related to sampling and laboratory measurements and experiments.

Eight V-shape thin-plate weirs and bubble flowmeters (hydrostatic probe) have been placed under all pipe ends to monitor the water flows coming through the various shoulders and lysimeters as well as from the road runoff compartment. Weirs and probes have been gauged in lab (appendix V). Flowmeters have dataloggers included with a 1 minute time step.

Rainfall is sampled and registered with a 0.1 mm tipping bucket ISCO rain gauge. Rain gauge signal is recorded by one flowmeter datalogger. The level of the river is recorded downstream (near the river delta) by the regional "Service des eaux, sols et assainissment" (SESA, regional water, soil, and rehabilitation board).

Infiltration through soil and unsaturated zone is generally measured with difficulties. Ten TDR (Time Domain Reflectometry) probes have been buried (spring 2005) along a perpendicular profile crossing the SGH-LW compartment. Probes are linked to an impulse generator and a datalogger. The probe positions as well as methods are shown in appendix VII. The repartition of these probes and delivered results gave information on infiltration processes, flows, stock variation and preferential water paths.

2.2.3 GEOCHEMICAL CONTINUOUS MEASUREMENTS

Turbidity, Total Organic Carbon TOC, electrical conductivity EC and temperature T have been recorded continuously in the road runoff. Turbidity and TOC have been recorded with a light enhanced fluorescent tracer sensor GGUN FL-22 (Schnegg and Costa 2003). Present studies demonstrated that light sensors detection works very well for turbidity and TOC (Savoy et al. work under progress). Turbidity is detected with a 660 nm wavelength IR light while TOC wavelength detection is UV 370 nm. EC and T were measured with a WTW LF 323 probe. All these instruments had their own built in dataloggers. Time step was 1 minute for all of them.

To avoid instruments taking measurements of a large mixed volume of water in the weirs, these instruments were placed in a funnel directly positioned under the pipe end. The funnel goal was to constrict the water flow, thus creating a small basin of continuously flowing water.

Due to the lack of place and the high costs of these probes, only the runoff collecting pipe has been equipped. During specific experimentation (artificial rainfall experiments, see §2.2.4), these instruments have been moved to the active collecting pipe; so all variables could be measured for each compartment.

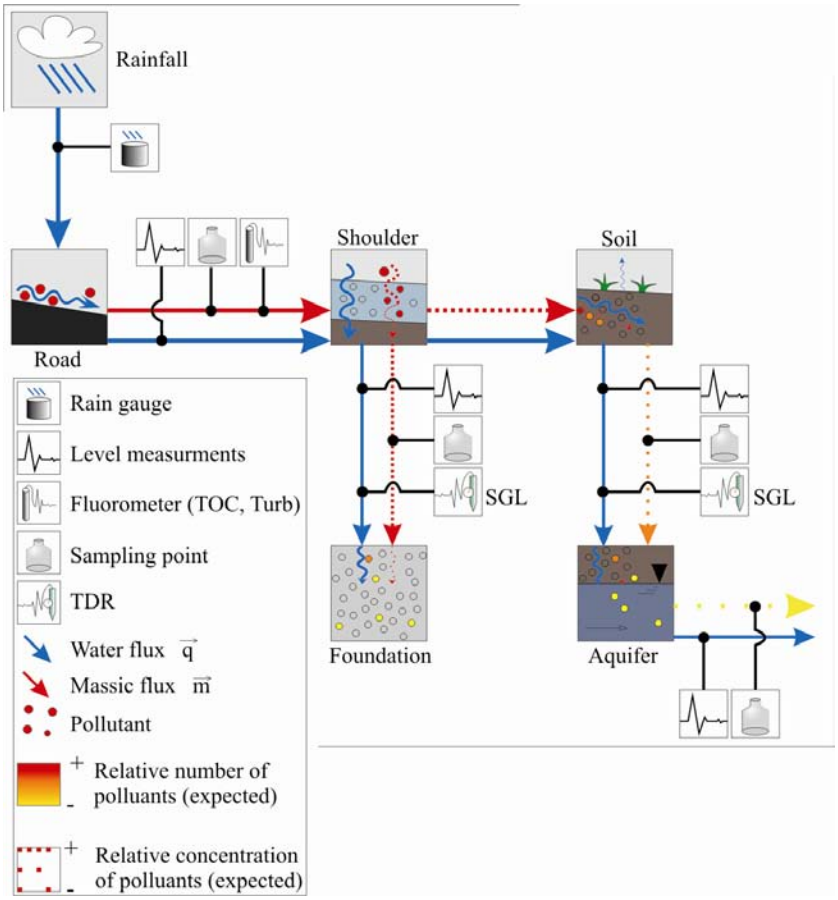

Figure 2.7: Instrumentation conception. All massic and water flux are monitored. Flux between the shoulder and the infiltration soils are recorded in particular experiments only. Road runoff has physicochemical sensors (TOC, Turbidity, temperature and electrical conductivity.
Contaminant relative number and concentration are expected to lower through the shoulder and soils. Aquifer is monitored as well and compared to the Arnon River.

2.2.4 SPECIFIC SAMPLING CAMPAIGNS AND EXPERIMENTS

When needed, specific instruments have been placed in the collecting chambers. It included automatic samplers (ISCO 6712), water detection probes and a WTW pH 323 pH-probe which were used in the runoff collector. Gutters have been dug along the SGH, SGC and SGL shoulder edge (§4.1.3). Those allowed taking samples and monitoring water volume flowing over the shoulders. They were used only during specific experiments; the monitoring and flow measurements were handmade.

Batch and Column tests have been conducted in laboratory with soils coming from the LH lysimeter (Docourt 2005). The goals of those tests were to calculate the specific sorption distribution coefficient K_d for the ETM and PAH substances (lixiviation; constant regime infiltration experiments with loaded water samples). See paragraphs 4.2 for methods, strategy and results.

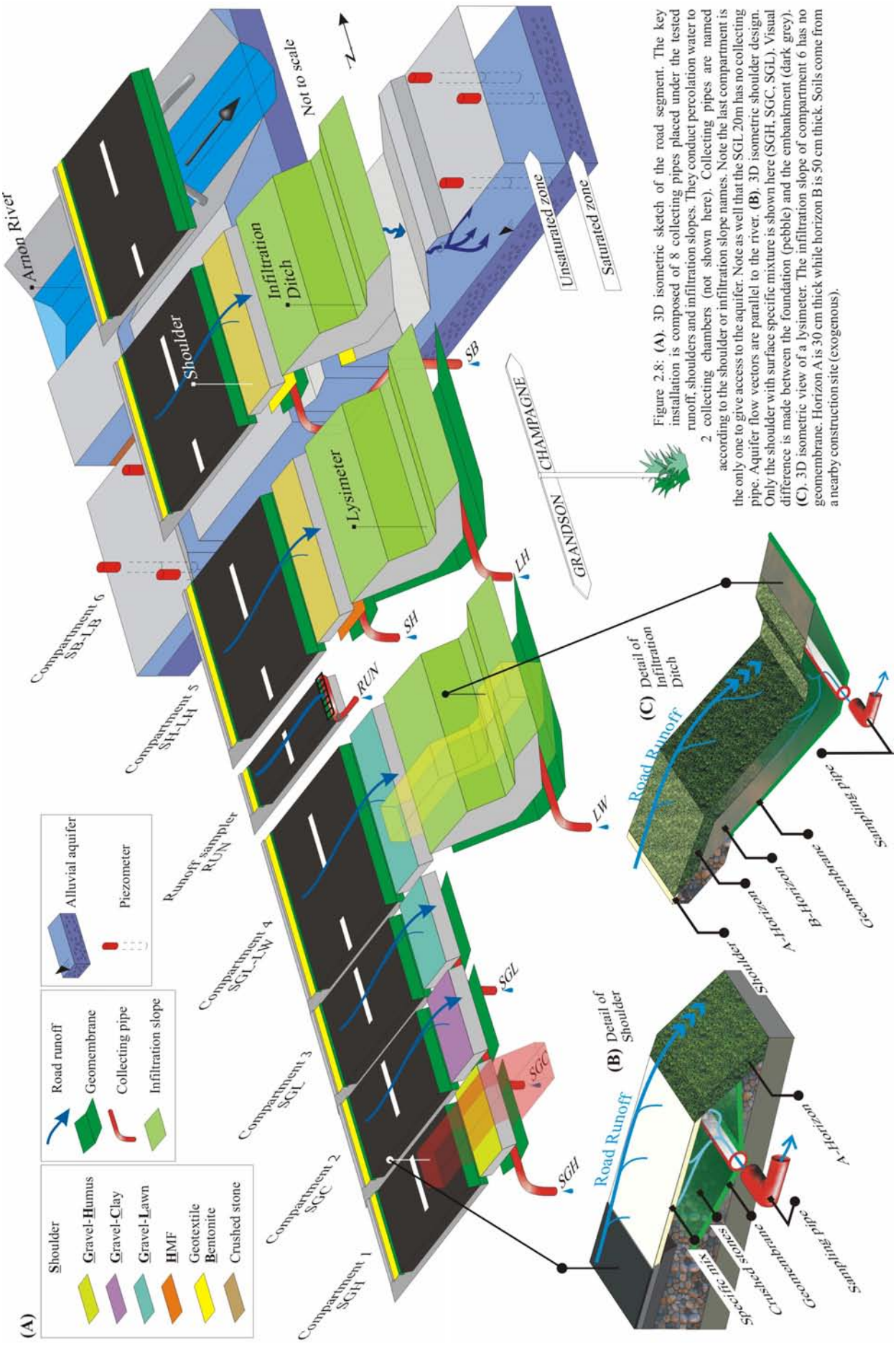

Figure 2.8: **(A)**. 3D isometric sketch of the road segment. The key installation is composed of 8 collecting pipes placed under the tested runoff, shoulders and infiltration slopes. They conduct percolation water to 2 collecting chambers (not shown here). Collecting pipes are named according to the shoulder or infiltration slope names. Note the last compartment is the only one to give access to the aquifer. Note as well that the SGL 20m has no collecting pipe. Aquifer flow vectors are parallel to the river. **(B)**. 3D isometric shoulder design. Only the shoulder with surface specific mixture is shown here (SGH, SGC, SGL). Visual difference is made between the foundation (pebble) and the embankment (dark grey). **(C)**. 3D isometric view of a lysimeter. The infiltration slope of compartment 6 has no geomembrane. Horizon A is 30 cm thick while horizon B is 50 cm thick. Soils come from a nearby construction site (exogenous).

2.3 3RD PHASE: CONSTRUCTION VERIFICATION AND CHARACTERISATION

Because few concessions had to be made during and after the construction phase[2], the site may have been altered in some ways. Therefore, investigations have been conducted on shoulders material, infiltration slopes physical and hydraulic properties and the alluvial aquifer. These tests have provided various intrinsic results that characterise the experimental site. They helped with the interpretation and resolution of numerous hydraulic and stability problems.

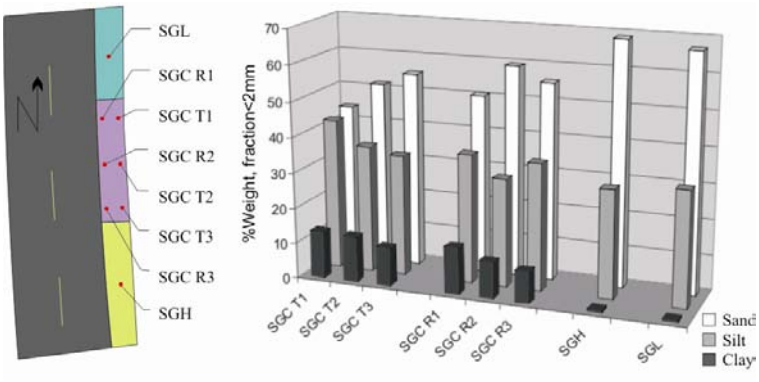

Figure 2.9: SGC material < 2 mm content. SGH and SGL are shown for comparison. SGC was the most likely shoulder to have loss of material due to clay migration. It in fact shows a slight migration of clay in depth (material was found in the weir) and down the light shoulder slope (eastward and southward). SGH and SGL granulometries fit the grave I requirements. Shoulder colours are related to fig. 1.3c: yellow SGH, purple SGC and green SGL. Samples nomenclature: R road side, T slope side.

2.3.1 SHOULDERS

Sixteen shoulders gravel samples have been taken in October 2004, one year after completion of the road construction, for granulometry analyses. Fraction < 2 mm was concentrated by sedimentation, the bigger fraction was sieved. SH and SB granulometries has been tested as well for comparison purpose and verification of the grave I granulometry. In that case, granulometry has no influence on infiltration processes. Results showed that the SGH and SGL granulometries respect the grave I requirements. SGC clay percentage is slightly below the wanted level with 8-13% weight of the < 2 mm fraction (2.5-3.5% of total mass) (figure 2.9). Geospatial analysis showed that the clay fraction has migrated along water stream from higher to lower grounds and through the shoulder (10-13% edge side, 8-13% road side; 13% in the north, 8-10% in the south). Southward slightly dipping slope in the southern part might explain the decrease in clay content in that area. Deep obstruction with clay particles is possible. Overall, the shoulders fit the conditions according to the design.

2.3.2 INFILTRATION SLOPES

Infiltration slopes material has been thoroughly studied. Granulometry, infiltrometry and retractometry tests have been performed in late 2003. Retractometry consists in continuously measuring the shrinkage curve (Massic volume V [$dm^3 \cdot kg^{-1}$] versus weight water content W [$kg \cdot kg^{-1}$]) of a soil sample. It is a reference method which allows measuring all physical parameters describing the soil structure (density, micro- and macroporosity, structure stability, matrix potential (also known as "suction")). For more information, see Braudeau 2002 and Wind 1968.

Twelve soil samples have been taken in the 2 horizons of each infiltration slope (top and bottom of the slope) in September 2003. These samples granulometries show high clay content (25-30% wght). No difference is visible between A and B horizon but concerning the fraction > 2 mm (28% in A and 45% weight in B horizon).

Ten suction and 3 double-ring infiltrometer tests have been done in various places of A and B horizons. Hydraulic conductivities in saturated conditions K_S extend from 3 to $6 \cdot 10^{-6}$ $m \cdot s^{-1}$ in A horizon, and from $5 \cdot 10^{-7}$ to $9 \cdot 10^{-6}$ $m \cdot s^{-1}$ in B horizon. These conductivities are considered as medium. Double-ring infiltrometry shows higher K_S ($6 \cdot 10^{-6}$ to $3 \cdot 10^{-4}$ $m \cdot s^{-1}$ for A horizon) because this method takes preferential flows into account, while suction infiltrometry does not.

[2] I.e. exogenous soils used, road opening retarded, weathering previous to the beginning of this study, etc.

Retractometry allows to measure density, porosity, the structure stability and the water retention potential of the soil. Density is clearly higher in B horizon at the bottom of the slope (1.59) than in B horizon, top of the slope, (1.50) and A horizon at the top of the slope (1.35). Similarly, the total porosity decreases with depth (A top 49.5; B top 44.1; B bottom 22.2). Finally, the soil stability is greater in B (bottom) than in B (top) and A horizons. Soils should be even more compacted today.

	A-horizon (2003)	*A-horizon (2004)*	*B-horizon (2003)*	*B-horizon (2004)*
Vertical hydraulic conductivity (saturated) K_S [ms^{-1}]	*Suction: $3\text{-}6 \cdot 10^{-6}$ Double-ring: $6 \cdot 10^{-6}$ to $3 \cdot 10^{-4}$*	*10^{-5}*	*$5 \cdot 10^{-7}$ to $9 \cdot 10^{-6}$*	*10^{-5}*
pH	*8.2*	*7.9*	*8.25*	*8*
TOC [%]	*1.7-2*	*2-2.2*	*1.5-1.7*	*1.9-2.2*
OM [%]	*2.9-3.5*	*3.5-3.8*	*2.6-2.9*	*3.3-3.8*
CEC [$cmol^+/kg$]	*5.2*	*5.2*	-	-
C/N [-]	*9-11*	*9-11*	-	-

Table 2.2: Summary of the different physical and geochemical soil properties.

Geochemical analyses (pH, TOC, Organic Matter OM, carbon/nitrogen ratio C/N and CEC Cation Exchange Capacity) have also been conducted. Mean pH of the samples is slightly superior to 8 (8.22). It reveals the presence of carbonates (also enlightened by HCl test). No difference exists between A and B horizons (8.19 and 8.25 respectively). Organic carbon contents are between 1.7 and 2% for A-horizon and 1.5 and 1.7% in the B-horizon. OM is obtained multiplying the TOC by 1.728 (Baize 2000). It is situated between 2.5 and 3.5%. It is logically lower in the B-horizon than in the A-horizon but is nevertheless pretty high in the B-horizon. C/N ratio allow estimating the level of degradation of the OM. C/N are comprised between 9 and 11 (no unit), showing that the OM is well degraded and evolved. CEC again shows no real difference between A and B-horizons with values around $5.2 cmol^+ \cdot kg^{-1}$.

Column tests conducted on the LH lysimeter soils have also revealed information. The soils were sampled one year after the first verification process, i.e. late 2004. A few differences occurred: pH measurements were a bit less alkaline (7.89 to 8.04) with the lower values at the surface (0-30 cm, 7.9-7.89). The difference is too low to be significant. TOC was measured between 2 and 2.2% (A-horizon) and between 1.9 and 2.2% (B-horizon), lightly more than previously. Also, OM was between 3.3 and 3.8%. Soils thus evolve in a normal way, gaining OM along its transformations. Infiltration tests have also been conducted but are highly irrelevant because column soils were sampled and put back together. Perturbation must be high. Vertical hydraulic conductivity is around 10^{-5} $m \cdot s^{-1}$, which is explicably higher than measurements made on the field. Summary of the different values is given in table 2.2.

To summarize, the A and B horizons are very similar. Clay and humus contents are especially alike with the A-horizon slightly depleted and the B-horizon slightly richer in humus, compared to OFEV recommendations.

2.3.3 TRAFFIC CHARGE

Traffic charge has been recorded for more than one year from January 2004 to end of September 2005. Missing data occurred due to maintenance. Figure 2.10 shows 2 specific weeks of 2004 and 2005. It appears that the road segment is essentially used one way. The average number of vehicles going to Grandson (southbound, western lane) is 280 per day and remains fairly constant, while the average number of vehicles going to Champagnes (northward, eastern lane) is 1800. It also is constant throughout 2004 and 2005. Weekends use is slightly lower with averages of 220 and 1000, depicting that roughly half of the traffic are commuters. On a larger scale, peaks of traffic appeared in June, July and October 2004 due to road maintenance on other road segments and opening of the A5 motorway. Peak traffic charge reached 5800 vehicles in one day (June 2004), 800 vehicles per hour at 08h00.

Field observations during this study show that the traffic was unfortunately very disparate. Construction sites in the area (A5 highway, Concise tunnels, demolition of the old Champagnes road segment, construction of a new bridge over the Arnon River in the vicinity, ground levelling in the field west to the experimental site, deposition, stocking and manipulation of gravel, sand, soils and grounds in the eastern field, etc.) brought a lot of different trucks, carriers, working machines of every types, etc. on the road in 2004. 2005 was much calmer because most of the constructions were terminated. Usual vehicles essentially concerns commuters and villagers private cars, a few trucks (no major industry in the vicinity) and agricultural machines.

Due to the traffic composition, a minor shift in the pollution type is expected: 2004 samples should show a big amount of colloidal particles, dust and fine mineral elements. These were observed in the weirs that were periodically cleaned. Cleaning of the weirs in 2005 was less necessary. It is also possible that the specific particular pollution in 2004 played a significant role in the soil pores obstruction. 2005 sample should essentially contain more common road pollutants. It is obvious that the shift between these two pollution types is faint.

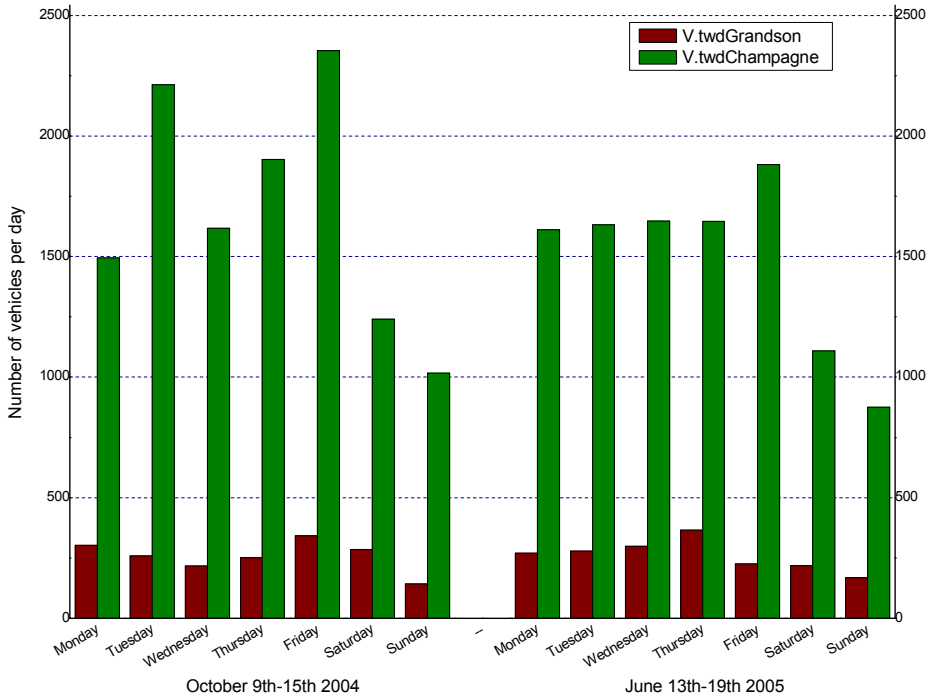

Figure 2.10: Traffic charge during 2 specific weeks. Traffic is essentially one way with roughly 10-15% of the traffic only headed to Grandson. No real difference exists between vehicle count averages in 2004 and 2005. On weekends traffic is 40% lower. Differences from one day to another in 2004 could be explained by the number of nearby construction sites and associated special traffic (machines, trucks, carriers etc.). Weekday traffic in 2005 is fairly constant. No more construction site is exploited in 2005.

2.3.4 POTENTIAL CONTAMINATION SOURCES

Potential contamination sources have been identified in 2004. This was necessary to assess the occasional bias in the chemical analyses made on the Arnon and alluvial aquifer samples. Aerial pollution is considered as low and uniform. No specific pollution occurred during the experimental monitoring, either in the river or the road.

No greater pollution source than the road itself exists in the direct vicinity. Industries in Champagnes are light polluters. Waste water is rejected in the Arnon River downstream of the experimental site. Fumes from the chimneys are of no concern because winds (main directions SW “Vent” and NE “Bise”) disperse pollutants away from the site.

Industries in Grandson or Yverdon-les-Bains are far away. They cannot be identified as specific sources, although aerosol pollutants might come from there (SW).

Diffuse and punctual contamination sources of the Arnon River and thus the alluvial aquifer have also been identified. SESA confirmed there was no source of concern in the catchment's basin of the Arnon River. Territory occupation map (Vaud canton) shows a few industrial zones, artisan and agricultural zones and public utility zones (water treatment plant, waste dump, etc.). Here is a list of potential polluters that might occasionally release pollutant upstream of the experimental site. Nevertheless, the high dilution factor throughout the catchment's basin of the Arnon River should buffer any peak contamination very rapidly and efficiently.

- Giez, southern slope of the Arnon catchment's basin: ancient communal sanitary landfill.
- Vugelles, northern slope: military firing range.
- La Mothe: Sawing facility in the village.
- Vuiteboeuf, eastern part of the village: water treatment plant with oxidizing basins.
- Vuiteboeuf, western part: communal waste dump and sanitary landfill.
- Ste-Croix: water treatment plant

Pollutant charges, types and mobility are unknown for all those sites.

2.3.5 RUNOFF INFILTRATION ADMISSIBILITY

In the directive 2002 (main frame in annexe II), OFEV specified the conditions the infiltration site must fulfil. It includes the level of pollution emitted, the soil and unsaturated zone properties:

- Level of pollution and traffic charges: the level of pollution is assessed using evaluation points (EP). Methods are shown in appendix II table II.2. It takes into account the daily traffic, the traffic part heavier than 2.5 tons, the road segment slope and the road maintenance. EP < 5 is considered to be a low pollution level, 5-14 is average while > 14 is a high pollution level.
- Soils (appendix II table II.3): A horizon must be ≥ 30 cm thick and B horizon must be ≥ 70 cm thick. A horizon pH must be ≥ 6.5 Humus content in the A horizon must be ≥ 4%, while it must be ≥ 1 in the B horizon. Clay content must be between 10 and 35% for both horizons. Percentages are in mass. See appendix II for average and minimal requirements. Insufficient conditions are those fitting below the minimal requirements.
- Unsaturated zone (appendix II table II.4): For an optimal requirement, the unsaturated zone must be ≥1m thick and have high absorption and infiltration capacities. Composition must be an unstable rock material with fine granulometry like clays, silts or silty sands. Again, see appendix II for average and minimal requirements.

Respecting the preceding order, the conditions found on the experimental site in Grandson are listed below:

- The traffic charge is 2100 per working day (EP = 2.1). The amount of vehicles heavier than 2.5 tons is unknown but can be evaluated, due to nearby field cropping and industries, to be higher than 8%. (EP = 2). The road segment slope is well under 8% (EP = 0). The number of mechanical cleaning per month is zero (EP = 0). The level of pollution is therefore evaluated to be low (EP = 4.1).
- The A and B horizons are 30 and 70 cm thick respectively. A horizon pH is slightly superior to 8. Humus content in A and B horizon increased from 2.9 and 2.6% respectively (2003) to 3.5 and 3.3% (2004). Clay content is between 25 and 30%. Soils parameters are therefore average (due to the lack of humus which is critical for organic compounds retention).
- The unsaturated zone is composed of recent alluvium and moraines deposits. It includes well sorted Jurassic carbonate pebbles in a sandy matrix. It also has a fair amount of clay. It is a b type unsaturated zone.

The runoff infiltration admissibility (appendix II table II.5) can therefore be assessed. The level of pollution is low. The soil quality is average as well as the unsaturated zone quality. The underground water vulnerability is average. Therefore, the runoff infiltration is admissible in this particular area (other sector classification, see appendix I).

2.4 EXPERIMENTAL MONITORING STRATEGY

This project strongly depends on rain event occurrences. Unlike in usual hydraulic or hydrogeological projects, continuous measurements were not possible and thus a specific monitoring and sampling strategy had to be edited. This strategy is based on rainfall events occurrence. No measurements were taken during dry periods.

2.4.1 EVENTS

As infiltration and retention processes throughout the shoulder strongly influence the output hydrograms, the notion of "rainfall event" itself needs to be clarified. Each event is distinguished from the preceding and following by a steady-state null output flow (recorded by the flowmeters). In case multiple rainfall events occurred in a short time but have only one continuous output hydrogram (multiple peaks but no interruption), it has been considered to be only one event, even if the rain gauge shows 2 separated rainfalls. Event is thus defined by the flowmeter output hydrogram and not by the rain gauge hyetogram.

Two kinds of hydraulic data have been collected: natural and artificial rainfall data. First, 112 natural rainfall events have been recorded through rain gauge (tipping-bucket 0.1 mm, time step 1 min.) and flowmeters (placed at the end of shoulders and lysimeters exfiltration pipes, see appendix V). Data recorded are the time, mean and maximum intensity, duration and the output hydrogram for each collecting pipe. Physicochemical data (TOC, turbidity, temperature, electrical conductivity) are recorded in the road runoff R_R. Example of the data provided during a natural rainfall event is shown in figure 2.11.

As weather conditions might greatly vary, all the parameters are not fully known. Therefore artificial rainfall events have been performed. Water was either pumped from the Arnon, either collected on a PE waterproofed roof. The latter was for chemical experiences purpose. Artificial rainfall use allows controlling every aspects of the event, from the input volume to the rain intensity. Weather and time, antecedent precipitation index (API), preceding droughts, etc. are also under tight control. Three specific experiments have been performed:

- test n°1: constant regime, average intensity, long duration rainfall
- test n°2: transitory regime, high-intensity, short duration (rainstorm)
- test n°3: constant regime, very high intensity, average duration

The first experiment with a constant regime (test n°1) helped to qualify the shoulders hydraulic parameters, while the second with a constant regime (test n°3) was designed to monitor the road structure behaviour under very wet conditions. For the test n°1, three cubic meters are watered onto each compartment in 1 hour, representing approximately 30-40 mm/h. The high volume tends to saturate the shoulders and thus give information about the vertical hydraulic conductivity K_S. For the test n°3, the same amount of water was watered on the road in about half the time; this represents rain intensities of about 100-110 mm/h. It permitted to estimate the road stability (FWD tests, levelling) in the worst hydraulic conditions. See chapter 5 for further explanations. The transitory regime experiment (test n°2) mimics a summer typical rainfall (15 min, 20 mm/h). Rain intensity variations respect a pre-established rainfall hyetogram and are made with a flowmeter coupled to the pump. This experiment was designed for chemical analysis.

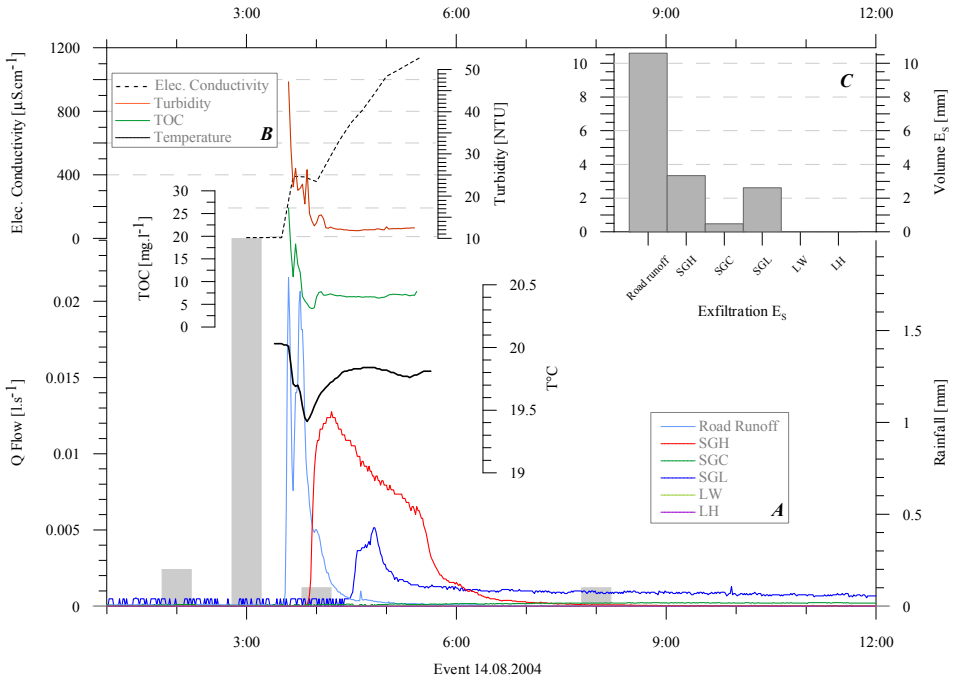

Figure 2.11: Example of a natural rainfall event (August 14th, 2004). 112 natural and 3 artificial events have been monitored. ***A)*** *Outgoing flows exfiltrating the shoulders and lysimeters. Raw data recorded by the flowmeters are water heights; Flows are calculated with the kindsvater-Shen equation. Note the lognormal trend of each curve. The general behaviour of SGH, SGC and SGL is well represented by this graphic. Precipitation is also plotted (grey bar chart).* ***B)*** *Physicochemical parameters recorded in the road runoff collector. Instruments were placed in a funnel (flow reduction) to avoid measuring mixed totalized water (weir). Note that the TOC, turbidity, temperature and electrical conductivity probes did not record anything when out of the water. A strong correlation exists between the road runoff flow peak and the physical-chemical parameters. For insight about those correlations, see chapter 4.* ***C)*** *Exfiltration volume E_S [mm] of the shoulders and lysimeters. The lysimeters had no response. The volume E_S is calculated by integrating the flow Q over the time then divided by the surface of the compartment considered. See text for equations.*

2.4.2 SAMPLING STRATEGY

As continuous measurements are not possible, sampling is also a major issue. The sampling strategy must allow efficient and economical assessment of the particularities of each event while optimizing the number of analysed samples. It also must use the adequate methods. Sampling strategy is based on dynamic conditions with sampling during rainfall events.

Figure 2.12 illustrates the strategy followed during the sampling campaign. Q, TOC and EC value curves were used to assess if the sample taken (star on the upper figure) was worth analysing or not. Samples could be “critical” (for example the first flush), “important” (for example the peak flow Q), “normal” (for example in-between samples) and “discarded” (samples that are of no use, i.e. taken at a wrong time). Note that this sampling timing is only an example: real sampling and sample discrimination might have a completely different display.

The wide range of pollutants being analysed also imposed two types of bottle, thus making the sampling more difficult. During very low exfiltration flow Q, it was hardly possible to fill both bottles at the same time. Filling the 1 litre bottle took sometimes up to 10 minutes.

Sampling time step was highly depending on the rainfall type (short time step for thunderstorm, longer for winter type rainfall, usually comprised between 2 and 10 minutes). Time step is also increasing from the beginning to the end of the event. Time step were also influenced by the flow. Very small amount of water during small rainfall were

barely sufficient to fill in 1.5 l.; the samples could thus be considered as totalized samples (the totality of output water is contained in one sample).

Sample importance	*Analyses*
Critical	All MTE Anions PAH BTEX PCBs Aliphatic C_x MTBE, Br-additives
Important	All MTE PAH Aliphatic C_x
Normal	Major MTE
- Discarded -	No analysis

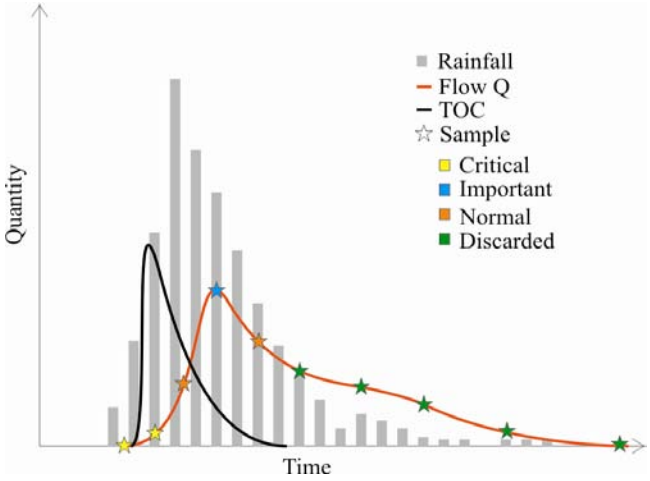

Figure 2.12: Samples discrimination. ***Right****: The discrimination is based on the Q and TOC (and electrical conductivity EC, not shown here) data. Preliminary tests showed that TOC and EC were representative of the organic compound and MTE contents respectively. In this particular example, 5 samples out of 10 would be discarded. The first sample is considered critical in all events (first flush). The second critical sample coincides with the TOC peak. The important sample coincides with the flow peak. Phenomenon might happen here because of the changing flow regime. Normal samples coincide with the decreasing TOC curves. It might also be the increasing TOC curve. Note that this discrimination method was not rigid: it was made on a case-to-case basis.* ***Left****: Description of the critical, important, normal and discarded sample ranking. (MTE: mineral trace element; Anions: chlorine, sulphates, nitrates; PAH: polycyclic aromatic hydrocarbon; BTEX: benzene, toluene, ethylene, xylene series; Aliphatic hydrocarbon from C_2 to C_{22}; Gasoline additives: MTBE and Br-based products).*

2.4.3 SAMPLES CONDITIONING

Usually, more samples than needed were taken. Specific samples to analyse were then chosen; for this purpose was used *a posteriori* turbidity, electrical conductivity, TOC and linked hydrograms data curves. This strategy proved to be efficient: it lowered the number of samples to be analysed. The resulting costs were thus lowered as well. TOC and electrical conductivity were considered to be representative of, respectively, the organic compounds and MTE.

To successfully carry out this method, particular mean of conservation were used to preserve the samples. Samples designated for MTE analysis were acidified and put into fridges. Acidification will be extensively discussed in the paragraph 4.1. Samples designated for organic compounds analysis were frozen in aluminium caskets. Volatiles were analysed immediately on the same day; they cannot be stored.

2.4.4 SAMPLES ANALYSES

Based on the same discrimination method described above (Q, TOC and electrical conductivity EC discrimination), samples were extensively analysed (all selected pollutants) when critical. Only TME, PAH and aliphatic hydrocarbons were analysed in important samples, while in non critical (or normal) samples were only measured major TME. Other samples were discarded.

CHAPTER 3

HYDRAULIC BEHAVIOUR

In this chapter, the hydraulic behaviour of all shoulders, lysimeters, unsaturated and saturated zone is studied:

1) The basic volume balance is explained. It mostly concerns the mathematical basis needed to understand the flow patterns (§3.1). Insight of data processing is presented.

2) The main processes during a rainfall event are described, using examples of artificial infiltration tests. Those key paragraphs are very important to understand the ongoing processes that take place during the flow and infiltration of the runoff. This part concerns the dynamic behaviour of the water runoff (analytic mechanist model, §§3.3.1; 3.4.2; 3.5.2).

3) The different elements composing the water balance are described, from the precipitation to the aquifer, following the natural water path (road – shoulder – infiltration slope – unsaturated zone – aquifer). A special attention is given on the shoulder paragraph (because it is one of the key element for the present study):

   Three empirical, conceptual and deterministic models, based on statistical analysis of the natural events, are developed. They evolve from the simplest to the most complicated. Empirical models compare the input and output values (water volumes that have transited in the shoulder) to assess the hydraulic behaviour of the shoulder.

4) Finally, a synthesis of all remarkable observations is made. It summarizes the key points that have to be kept in mind when analysing the chemical behaviour in chapter 4.

3.1 WATER BALANCE

Equations of the water balance can be expressed in two different units: litres or millimetres. The unit [litre] is more convenient for calculation purposes but does not allow a direct comparison between the different compartment behaviours. Because the final goal of this study is to assess the different behaviour of the shoulders and to select which one behaves optimally, the unit [mm] has been chosen as a reference. This choice, although logical and pertinent, implies that a flow quitting a surface s_i must be corrected when entering the surface s_j. For example, if 1 mm falls on the road (s_R = 80 m^2), the equivalent volume for the shoulder (s_S = 20 m^2) will be as much as four times greater ($s_R/s_S \cdot R_R$ = 4 mm). Considering the precipitation on the shoulder (still 1 mm), the total amount of water available on the shoulder is 5 mm[1].

Figure 3.1 shows the basic principle for the hydraulic balance of the shoulders and lysimeters. Road dissemination D_R is deducted by difference between rainfall P_R and road runoff R_R:

Equ. 3.1) $$R_R = P_R - D_R \quad \text{[mm]}$$

Road dissemination is not significant but may explain the difference between the calculated road runoff volume and the precipitation volume. The shoulder has three different incoming flows: the road runoff R_R, the precipitation that fall over the shoulder P_S and a fraction x of the previously described dissemination D_R. The shoulder water balance is:

[1] This example considers that 100% of the rainfall participates to the road runoff. Calculated surfaces are given in appendix V.

Equ. 3.2a)

$$\frac{s_R}{s_S} R_R + P_S + xD_R = I_S + ETP_S + R_S \quad \text{[mm]}$$

(s_R/s_S: surface ratio [-]; P_S: precipitation on the shoulder [mm]; xD_R: fraction of the dissemination that falls on the shoulder [mm]; I_S: infiltration in the shoulder [mm]; ETP_S: evapotranspiration on the shoulder [mm]; R_S: shoulder runoff [mm])

With *equ. 3.2b)*

$$I_S = E_S \pm \Delta S_S \quad \text{[mm]}$$

(E_S: exfiltration volume [mm]; ΔS_S: stock variation in the shoulder [mm])

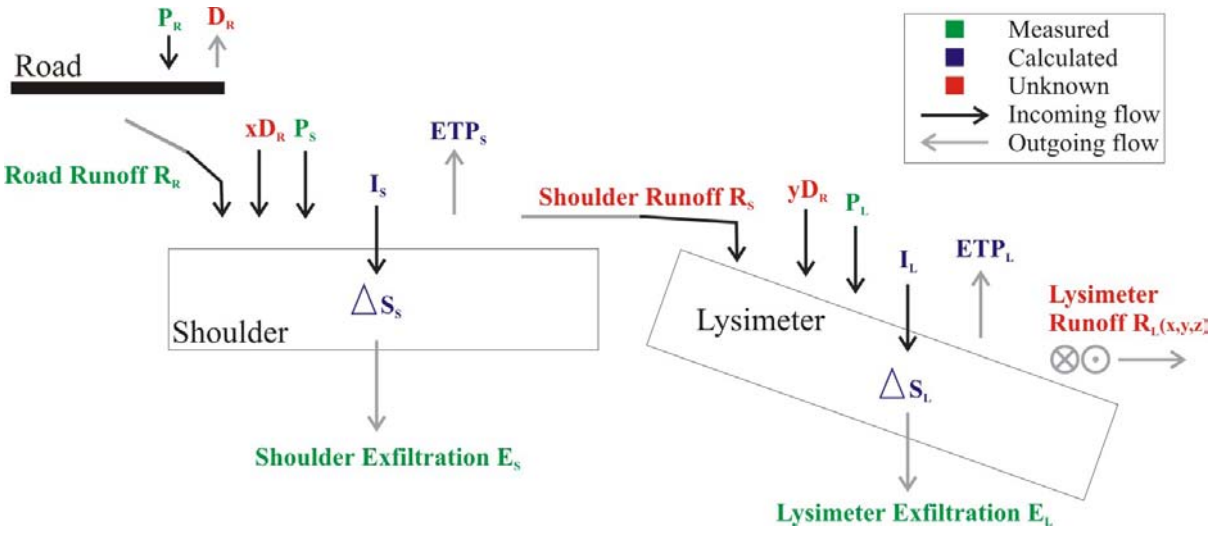

Figure 3.1: Water volume balance. Green labels are measured variables, blue one are calculated using external data (for example meteorological data), red one are unknown variables. Black arrows are incoming flows; grey arrows are outgoing flows. Road runoff R_R and shoulder runoff R_S are both. Boxes represent the shoulder and lysimeter physical bodies. Indices R, S and L respectively stand for road, shoulder and lysimeter.

The expression of the lysimeter water balance is similar:

Equ. 3.3a)

$$\frac{s_L}{s_{R+S}} R_S + P_L + yD_R = I_L + ETP_L \pm R_L \quad \text{[mm]}$$

(s_L/s_{R+S}: surface ratio [-]; P_L: precipitation on the lysimeter [mm]; yD_R: fraction of the dissemination that falls on the shoulder [mm]; I_L: infiltration in the lysimeter [mm]; ETP_L: evapotranspiration on the lysimeter [mm]; R_L: lateral lysimeter runoff [mm])

With *equ. 3.3b)*

$$I_L = E_L \pm \Delta S_L \quad \text{[mm]}$$

Note that the dissemination D_R do not fall entirely on the shoulder and lysimeter: $x + y \leq 1$. Due to the particular design of the lysimeters (physical boundaries separating them from the surrounding field), the lateral lysimeter runoff R_L has no escape; it is equal to zero (field observation).

The variables P_R, P_S and P_L are equal to the precipitation P [mm]. The indices only geographically situate the compartment that is considered. The precipitation P is directly measured (§3.1.1). The variables R_R, E_S and E_L are indirectly measured: on the basis of the recorded water heights, the water flows are calculated and integrated over the time (see §3.1.1 for development). The variables ETP_S and ETP_L are calculated using the Penmann-Monteigh Food

and Agriculture Organisation equation (PMFAO, appendix VI). The stock variations ΔS_S and ΔS_L are indirectly measured using the TDR probes (see §3.1.1), although the calculation proved to be difficult. The stock variations can also be determined employing the Antecedent Precipitation Index API (decaying factor K_{API} is a function of ETP and soil properties, appendix VI).

The variable R_S and fractions x and y are unknown and need to be determined:

Equ. 3.4a) $$R_S = A_W - (I_S + ETP_S)$$ [mm]

(A_W: available water reaching the shoulder [mm])

With *Equ. 3.4b)* $$A_W = \frac{s_R}{s_S} R_R + P_S + xD_R$$ [mm]

The variable A_W represents the volume of all the water arriving at the surface of the shoulder. The use of this variable simplifies the comparison between what enters the shoulder and what gets out; it symbolises the *Available water* for the shoulder. The same way, the available water reaching the lysimeter is noted B_W:

Equ. 3.5) $$B_W = \frac{s_{R+S}}{s_L} R_S + P_L + yD_R$$ [mm]

Fractions x and y are empirically assessed.

3.1.1 DATA PROCESSING

3.1.1.1 Exfiltration volume R_R, E_S, E_L

The record of the precipitations is automatic. For specific purposes (depending on the duration of the studied period), precipitation data recorded each minute are integrated to achieve a time step of one hour or one day. Thus the rainfall per minute / per hour / per day are available.

Calculation of output flows from shoulder, lysimeter and runoff collector requires 3 steps:

2) Data acquisition: the water level is recorded by flowmeters in a weir directly out of the pipe end. Time step for level measurements is 1 minute. Instrumental precision is 0.1 mm.

3) The water level is then converted into flow Q [$l.s^{-1}$] using the Kindersvater-Shen equation (international norm ISO 1438/1-1980, Equation 2.1). Weirs and flowmeter have been pre-calibrated in laboratory. See appendix V for calibration curves.

4) The flow is finally converted into a normalized volume. Compartments surfaces are clearly delimited and have been measured (precision is 5 cm on the road, 20 cm in the field). Systematic error on surface calculation is thus between 1.3 (RUN) and 11% (SGL-LW). Surfaces and volumes errors are listed in table V.1, appendix V. The flow is integrated along the time to give the total volume [litre]. Result is then divided by the surface s for direct comparison with rainfall measurements:

Equ. 3.6) $$Volume_{normalized} = \frac{\int_{t_0}^{t_{end}} Q dt}{s}$$ [mm]

($Volume_{normalized}$: total water volume exfiltrating the considered shoulder/lysimeter [mm]; Q: water flow exfiltrating the considered shoulder/lysimeter [$l.s^{-1}$]; s: surface of the considered shoulder/lysimeter [m^2])

T_0 and T_{end} represent the beginning and end of the rainfall event. The surface s is the surface of the considered catchment surface. $Volume_{normalised}$ is the output volume per unit of surface ([l·m^{-2}] = [mm]). It can immediately be compared to the precipitation [mm]. Steps 1 to 3 are thoroughly described in annexe V.

3.1.1.2 Soil moisture using TDR probes (see appendix VII for calculation details)

The TDR probes give soil water content results (θ [m^3.m^{-3}] or [%]). The principle is to measure the time needed for an electromagnetic wave to propagate through the soil. The time needed is proportional to the dielectric constant of the material the wave is travelling in, which is itself proportional to the volumetric water content. It thus needs some calculation to obtain the stock volume. Probes have been calibrated in laboratory, using the Topp et al. Equation (1984). The hardware has been bought from Campbell Scientific. Software routine has been modified from the native one delivered by the factory to achieve a time step of 1 minute and to immediately deliver the soil moisture θ. The volume of the water stock S is equal to the total volume of the shoulder/lysimeter multiplied by θ and divided by the surface s (to achieve mm equivalent):

Equ. 3.7)
$$S = \frac{\theta \cdot V_{tot}}{s} \cdot 1000 \quad \text{[mm]}$$

(S: stock [mm]; θ: volumetric water content [m^3.m^{-3}]; V_{tot}: total volume of the shoulder/lysimeter considered [m^3]; s: surface of the shoulder/lysimeter considered [m^2])

The stock variation between time 1 and time 2, between the surface and the depth z_1 is:

Equ. 3.8)
$$\Delta S_{t_1;t_2} = \int_0^{z_1} \Delta\theta dz \quad \text{[mm]}$$

Shoulder and lysimeter volumes are calculated using the surface and depths measurements (appendix V). Note that this method designated to assess the soil water content, while accurate, is complicated to use. It indeed gives θ values over the time; it is thus far more efficiently used when analysing a single event (dynamic behaviour). When comparing many events (statistical behaviour, §3.4.3; §3.5.3), the soil moisture is calculated using the API.

3.1.1.3 Soil moisture using ETP and API

Evaporation and transpiration (ETP) are important processes. The higher ETP is, the lower the infiltration will be. High ETP values indeed increase the soil suction and diminish the vertical flows intensity. Thus, the chemical substances stay longer in contact with the soil grains (longer adsorption time). Many authors (Gardner 1958, Mermoud 1989, Brooks and Corey 1966) formulated evaporation equations based on the Darcy law. They all postulate that the evaporated water comes from the underlying aquifer (capillarity and suction). In this project, the understanding of the processes taking place at the surface, before the infiltration, is more fundamental. Moreover, all the compartments do not have a direct vertical access to the aquifer. Therefore, the ETP equation used in this project is based on the meteorological factors rather than on the soil properties.

The empirical PMFAO equation (appendix VI) depends on the various meteorological parameters supplied by Meteoswiss (Mathod meteorological station; 10 km from the Grandson site,). These parameters can indeed easily be considered as regional factors (mean temperature, air humidity, atmospheric pressure, sunning, solar heat flux and wind); they were recorded on a daily basis. By convention, the result of the PMFAO equation stands for a surface of reference covered with lawn; it is thus very convenient for this project (all lysimeters and shoulders but SGC are covered with lawn). The development of the equations governing the ETP and API is described in appendix VI.

The API represents the maximum potential stock of water contained in the soil (or shoulder). It is based on the assumption of a lognormal decay of the soil moisture along the time. The equation used in this project is function of the ETP:

Equ. 3.9) $$API = API_0 * K_{API} + P$$ [mm]

(API: antecedent precipitation index [mm]; API_0: API on day d-1 [mm]; K_{API}: recession constant function of ETP [no unit]; P: precipitation [mm])

The stock variation ΔS has been calibrated using the TDR results. Indeed, the water content decreasing rate is logically correlated with the API recession constant K_{API}. The more it rains, the slower θ decreases. The initial moisture in the shoulder is resulting from the decrease of the precedent event θ_V (which is the resulting water content once the macroporosity has drained). Δθ is thus:

Equ. 3.10) $$\Delta\theta_{t_1;t_2} = \theta_V - \theta_V \cdot K_{API}$$ [$m_3 \cdot m_{-3}$]

(θ_V: water content once the macroporosity has drained; K_{API}: recession constant of the shoulder considered)

ΔS is then calculated using the equation 3.8. This method has been used because the TDR probes where not available before 2005. Moreover, only one probe is buried in the SGL, other shoulders have no TDR. As those must have different behaviour (different recession constant K_{API}), ΔS is calculated for each shoulder using the equation 3.10. Concerning lysimeters, TDR probes are sufficient because soils are the same in both.

Knowing the exact ETP concerning only the water precipitated and not the soil moisture due to antecedent precipitation is nearly impossible. For simplification purpose, the ETP will simply be subtracted from the available water value A_W (equ. 3.4a). The effect of the ETP lasts indeed long after the rainfall event finishes and thus mobilizes water even if the precipitation has stopped. Using the ETP value as the real evaporation and transpiration value is therefore a good assumption.

Various models of API have been calculated using different values of K_{API} (recession factor, see appendix VI) for the different shoulders. Because only the five first centimetres of the shoulders have different composition, the API values have only 1-2% variance. Thus, only one value of K_{API} has been used for all shoulders.

3.1.2 ARTIFICIAL PRECIPITATION TESTS

In September 2004 and November 2005, two artificial precipitation tests were conducted. The artificial test (referred as test n°1 and test n°3[2]) goals were:

- To assess the dynamic processes leading the infiltration I and shoulder runoff flux q_{RS} [$m \cdot s^{-1}$]
- To calculate remarkable values like the vertical hydraulic conductivity K_S [$m \cdot s^{-1}$].
- The test n°3 was designed to put the road under constraining hydraulic conditions. Compartments were extensively watered.

3.1.2.1 Artificial test n°1

The first test was especially designed to assess the infiltration processes through the shoulders and infiltration slopes. The watering flow Q was constant (3 m^3 were pumped from the Arnon onto each compartment, totalizing a Q = 35-

[2] The artificial test n°2 is discussed in chapter 4.

45 litres per minute[3]. This represents a normalized volume of 30 to 40 mm. Only the road was watered while the shoulders and infiltration slopes were left dry. The water detected on and under them was therefore the result of the runoff. Moreover, in order to determine the paths and behaviours of the substances carried by the runoff, one kilograms of NaCl was dissolved in 5 litres of water and poured onto the road. Recorded data were the exfiltrating flow Q (calculated with equation 3.6, see also appendix V), the total organic carbon TOC, the turbidity NTU, the temperature T and the electrical conductivity EC (calibrated at 20°C). Cl^- concentrations were analysed in laboratory. API were 15 and 80 mm for the shoulders and lysimeters respectively.

3.1.2.2 Artificial test n°3

During that artificial event, the watering was even more intense. Three cubic metres were watered on the road in 26 minutes. This represents a rainfall of 30 mm; 110 mm/h on the road, 150 mm, 500 mm/h on the shoulder. The lag times were far shorter (SGH: only 6 minutes against 14 minutes during the test n°1). As the rainfall volume was the same as in the artificial test n°1, the lag time is then supposed to be a function of the rain intensity and not of the rain volume. This is confirmed with the natural rainfall analysis (§3.4.3.4). Hydraulic results are highly concordant with the artificial test n°1: no difference (but lag times) occurred. Precision about this test are exposed in the chapter 5.

3.2 PRECIPITATIONS P [mm]

From the 1st of February 2004 to the 30th of November 2005, 112 rainfall events have been recorded (54 events in 2004, 58 in 2005). Precipitation P was recorded with a tipping-bucket Rain gauge (0.1 mm, time step 1 min.) located on the top of the collect chamber n°1. Definition of a rainfall event is an event with no significant interruption (interruption of a few minutes might occur).

Those events have precipitation volumes ranging from 0.4 to 78 mm, mean intensities ranging from 0.07 to 48 mm/h (calculated) and duration ranging from 6 minutes to 72 hours. See table VI.1, appendix VI for events main characteristics. Precipitations during those 2 years are also shown in figure 3.12. Only volumes, duration, mean and maximum intensities and the preceding drought duration were recorded (or calculated) on the Grandson site. For other meteorological factors, see 3.1.1.

The IDF plot (intensity – duration – frequency, figure 3.2) shows the 2004 and 2005 events distribution. Logically, events having a return period greater than one year have a low intensity – long duration profile. This is due to the regional meteorology conditions inherent to the Swiss Plateau and, in general, to all similar climatic regions. All in all, 95% of the recorded precipitations have a short return period (T_{Ret} < 1 year). IDF plots are compared to the return period calculated by the VSS for the SN 640 350 “Intensité des pluies” that concerns the road dimensioning.

For comparison purpose, artificial precipitation data are also plotted in the IDF graphic (green crosses). Tests n°1 ($3m^3$ spread over the road in 1 hour) and n°3 ($3m^3$ in 25 minutes) are well beyond the longer return period (T_{Ret} = 20 years). On the contrary, Test n°2 plot is well within the shorter return period T_{Ret} = 1 year. It has nevertheless the second higher mean intensity that is recorded. This fact validates the affirmation that test n°2 is very representative of a summer rainstorm (high intensity, short duration).

[3] The flows depended on the watering hose length: the flow Q was smaller for the compartment which was the farthest from the river.

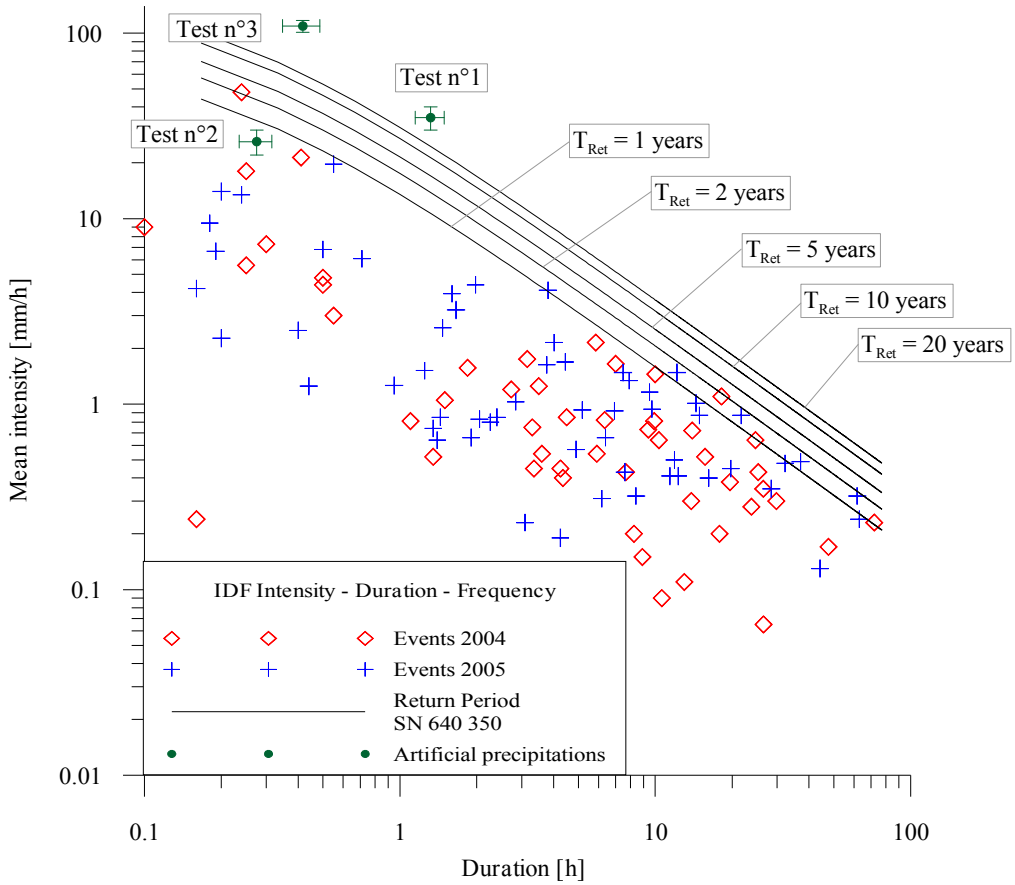

Figure 3.2: IDF curve for the 2004 (red) and 2005 (blue) precipitations. Black solid curves are return periods of 1, 2, 5, 10 and 20 years (SN 640 350 "Evacuation des eaux de chaussée") calculated by the VSS for the western Swiss Plateau. Most of the plots have a short return period. All those having a return period longer than 1 year have important durations (> 10 hours). This is due to the specificities of the Grandson site climatic region. Artificial tests data are also plotted (green crosses). Error bars show the intensity and duration small variations between compartments.

3.3 ROAD RUNOFF

3.3.1 ANALYTICAL APPROACH

To assess the road runoff buffering during its transit on the road, the compartment RUN was also watered, although no NaCl was added on the road[4]. The figure 3.3 shows a neat "box-shaped" runoff flow. There is no significant flow buffering on the road: the road has a runoff coefficient C_R (see §3.4.1 for C_R definition) of nearly 1. This is also shown by the cumulative volume curve which is practically a straight line. Runoff flow fluctuations are due to the formation of "waves" on the surface of the road. The watering itself is the cause: during the first artificial rainfall test, the watering was made using a garden hose. The method, while practical, was not very efficient to homogeneously distribute the water on the road. The water moved more rapidly in area already wet, while dry areas slowed the water flow. It then formed waves that are visible on the road runoff flow. The watering process was sensibly improved for the artificial test 2 and 3. During natural events, the road is regularly moisturized; it is consequently expected that the road runoff is only a function of the form of the precipitation P.

[4] NB: to assess the background concentration caused by the road traffic.

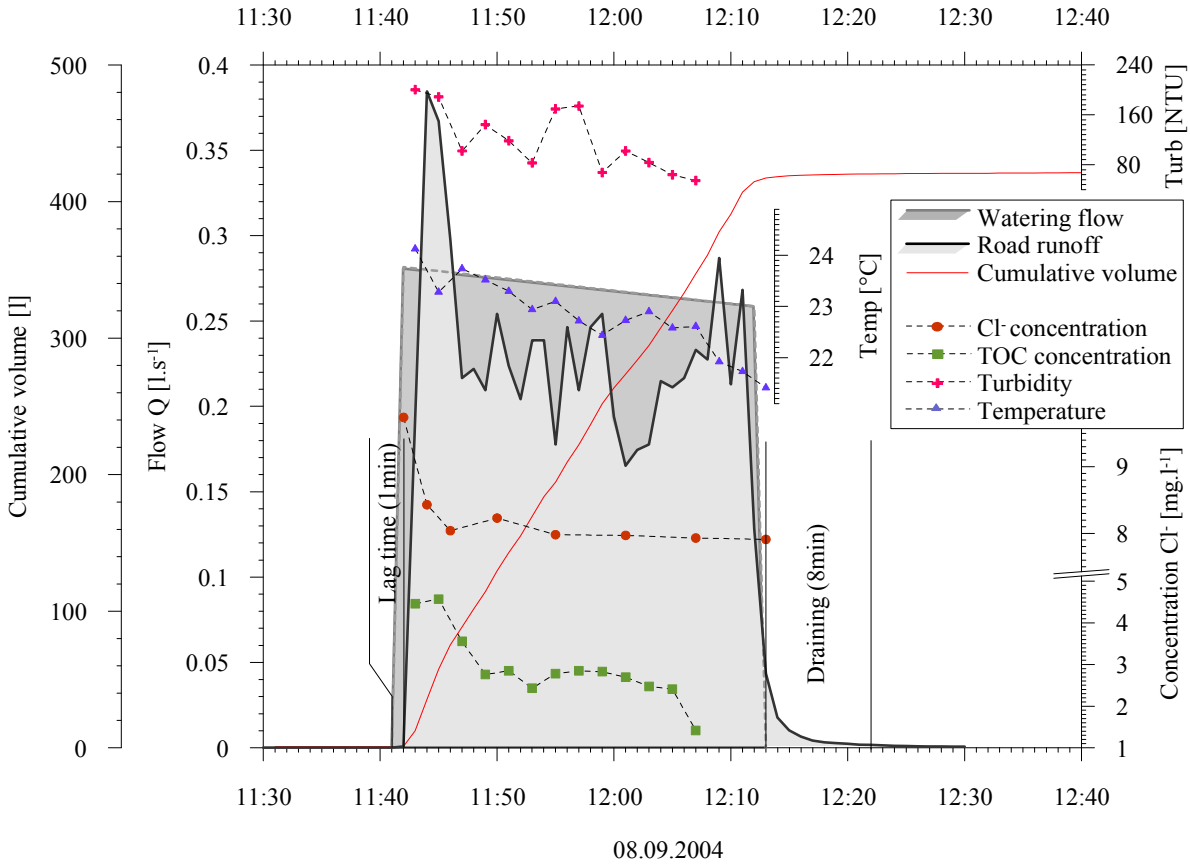

Figure 3.3: Road runoff flow during the artificial watering test n°1. The watering flow (50 l·min^{-1}, 540 l., 35 mm) and resulting road runoff flow are almost equal. The time shifts between the watering and the resulting runoff flows are called the lag time (beginning) and the draining (at the end). See text for definition. The physicochemical parameters have also been plotted. All of them have a significant decrease between the beginning and the end of the event. Cl$^-$ shows a second peak, which is thoroughly discussed later.

The road runoff flow shows an appreciable time shift. The lag time is definite as the time needed for the rainfall to moisten the road, flow to the runoff collector and along the collecting pipe. The lag time is therefore the time difference between the beginning of the rain and the detection of water rising in the weirs. The lag time monitored for the road runoff is always subtracted from the lag time recorded for the shoulder: the shoulder lag time is then only the time needed for the water to percolate through the shoulder. It does not comprehend the moisturizing time and flowing time (in the pipes) any more. The same way, a time shift exists at the end of the event that is called the draining. It is the time needed for the collecting pipes to empty. As it is shown in figure 3.3, the draining concerns a negligible volume in the case of the road runoff. As the draining has an important signification in the case of the shoulder/soils, it is discussed later in due paragraphs. Observation of the physicochemical parameters demonstrates the presence of a first-flush effect (See next page for definition). Particularly, the evolution of the Cl$^-$ concentration is very typical: an intense peak in the first water coming in the weir, followed by a second late smaller peak. This behaviour is found for all the shoulders and lysimeter in a wide range of rain conditions. The figure 3.4 presents the resulting Cl$^-$ pollutogram (see next page for definition). The TOC, turbidity and temperature also have their maximum values in the early water, which is logical. The flow acceleration indeed exists uniquely at the very beginning of the event and thus mobilizes particles only during a brief instant. Behaviours of the physicochemical parameters are discussed in chapter 4 “geochemical behaviour”.

First flush and pollutogram definition

One of the numerous first-flush definitions has been made by Bertrand-Krajewski & Chebs, 1995, 1998. They postulated that there is a first-flush effect when 80% of the substance mass is accounted for in the first 30% of the water volume ($b \leq 0.185$, see figure 3.4 for equation). This definition has been preferred for its convenience and simplicity, although the b limit was not considered, only the general pollutogram trend.

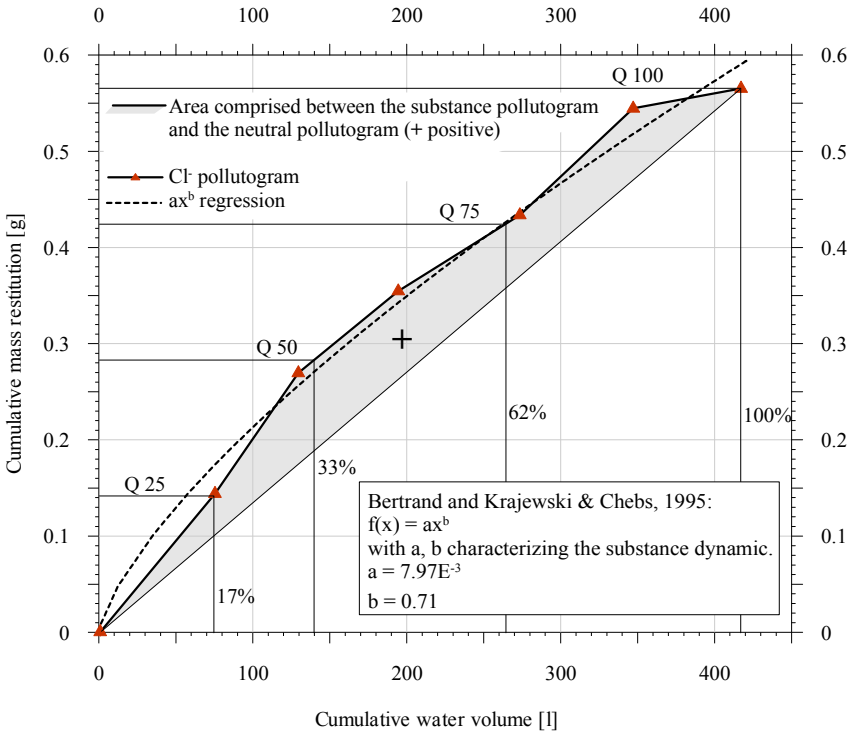

Figure 3.4: Cl⁻ pollutogram from the road runoff. Although the Cl⁻ does not show a strong first flush effect (b = 0.71; here roughly 50% of the mass in the first 30% of volume), the relative substance charge is always greater than the relative water volume (b=1). Q are quartiles.

Pollutograms express the cumulative mass restitution as a function of the cumulative water volume restitution M(V). The form of the curve is function of the substance behaviour. Note that the pollutogram must not be confused with the evolution of the concentration. The concentration may be higher in the first water coming out of the pipe, but as the flow at that time is really low, the massic flow [$g \cdot s^{-1}$] coming out of the pipe is also low (massic flow = flow x concentration). On the other hand, a sample with low concentration that has been taken later, during the flow peak, will have a significant massic flow. The concentration would therefore decrease along the time, but the resulting pollutogram would be negative, i.e. most of the contaminant mass is retarded and do not come at the beginning of the event. The limit between the first flush effect and retardation effect is b = 1. Coefficient b < 1 implies a first flush effect (the lower b, the stronger the effect).

3.3.2 Road runoff R_R and Dissemination D_R [mm] – statistical approach

Many authors (see §1.4.3.2 "Aerial dissemination") have demonstrated that the precipitated water volume not only participate to the road runoff R_R but is also disseminated and evaporated (sum = D_R). Particular examination of these phenomena has been made in the similar research "Bankette bestehender Strassen" (which concerns shoulders of an ancient road, Burgdorf, Boller 2006).

The general equation 3.1 links the precipitation P_R, the road runoff R_R and the dissemination D_R. The precipitation P is measured, the road runoff R_R is calculated (equ. 3.6, s = 13.6 m^2 ± 3.2%). The dissemination D_R includes the following processes:

- Capillary suction wetting the road pavement.
- Water being retained in small holes, basins and in every singularities of the wearing course profile.
- Evaporation may be especially high, particularly in summer when the road pavement is very hot. It may indeed retain a lot of calorific energy.

The estimated loss of water through these three ways is roughly 20% (Boller 2006). Moreover, precipitated water is also splashed away and proximally and distally dispersed:

- Splashing (< 5 m distant from road) depends on the traffic density and speed and local particularities like pavement roughness, pavement slope, dominant wind directions, etc.

- Proximal (< 25 m) and distal disseminations (> 25 m) depend on the same factors as splashing but spread water further.

Splashing, proximal and distal dissemination may represent up to 40% of the total precipitated volume in the Burgdorf conditions (high traffic density, high speed limit, etc.). Thus, road runoff may be reduced to 40% of the total precipitated volume P. Water lost during all those five processes is put under the D_R term in the water balance figure 3.1. Specific percentages due to the cited processes are not individualized.

On the Grandson site, in order to assess the volume of water lost through those particular processes, the calculated road runoff volume R_R [mm] is compared to the precipitation P_R [mm]. Figure 3.5 shows the correlation between the precipitation and the road runoff. The Result validates the calculation method of R_R, keeping in mind that the error on the flow calculation is function of the flow value. The linear regression fit passes through the origin and has a slope of almost 1. Thus, the road runoff and precipitations could be considered of equal values ($R_R \approx P$); percentages calculated in Burgdorf (op.cit.) are therefore not used. Consequently, the dissemination D_R has only been calculated for event that has been thoroughly and individually studied. In the cases where D_R was negative, it has been neglected. Values of D_R will be specified in the appropriate paragraphs.

Also, note that Hassan & White (1996) calculated a vertical hydraulic conductivity K_v for asphalt material of $1 \cdot 10^{-6}$ $m \cdot s^{-1}$. Draining wearing courses may have K_v up to $9.8 \cdot 10^{-2}$ $m \cdot s^{-1}$.

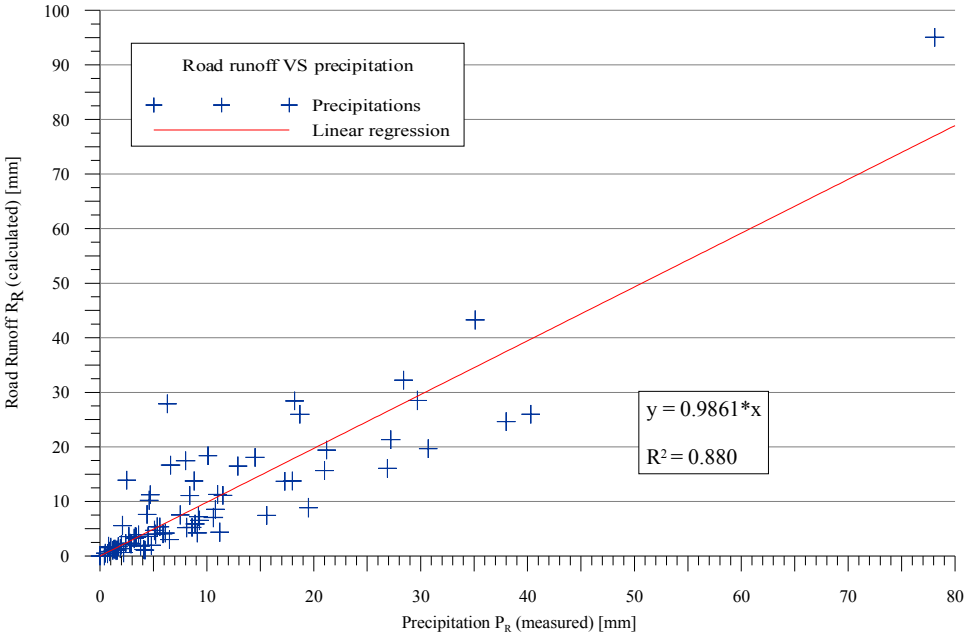

Figure 3.5: Road runoff R_R versus rainfall P_R. Fit reports a linear regression passing through the origin with a slope of nearly 1. D_R represents only 1.2% of the precipitation P_R and is therefore neglected. $R^2 = 0.88$.

Reasons why the D_R term is almost null are:

- The traffic conditions on the Grandson site are more favourable than those encountered in Burgdorf (traffic density and speed are far lower; traffic is not symmetric; etc.). Thus, the water is less splashed away.
- The road specificities are different. The water is more rapidly evacuated due to the steeper pavement slope. Combined to a low traffic, it assures that the greatest part of the precipitation flows away.
- The variance might be affected by an underestimation of the catchment surface s (the surface calculation has an error of 4% but transversal flows (parallel to the road direction) may have occurred, draining a larger area). Small precipitations inducing very large road runoffs are hardly explainable.

Note that the R_R flow and volume calculation error cannot be the main source of error: the error is distributed along the linear fit. For statistic and large scale calculations, the P value was used as road runoff value ($P = R_R$). The P data indeed contains a smaller error than R_R (measurement instead of calculation).

3.4 SHOULDER

3.4.1 SHOULDER FLUXES BALANCE

For reminder, the shoulder is made essentially of coarse material that is usually considered as very permeable. For this project, five different shoulders have been designed to make them less permeable. Material used for this end were humus (SGH), clay (SGC), lawn (SGL), road base HMF (SH) and a special bentonitic layer (SB). To reach one of the goal of this project, i.e. to assess which shoulder has the best capacity to drive the water to the infiltration slope, the shoulder runoff R_S must be assessed. For this purpose a runoff coefficient C_R is introduced:

Equ. 3.11)
$$C_R = \frac{R_S}{A_W} \qquad [\,-\,]$$

(R_S: shoulder runoff; A_W: available water on the shoulder)

The higher this coefficient is, the better the shoulder drives the water to the infiltration slope.

The water balance shown in the paragraph 3.1 is a conceptual model. It considers only input and output values without any consideration for the physical processes occurring in the shoulder. The water balance is therefore hereby modified to take into account the physical behaviour of the infiltration. The basic laws needed to express the shoulder runoff are the Darcy's and the Continuity Laws (modified for uni-dimensional vertical transfer, appendix IV):

Combining and integrating the cited equations (Mermoud 1999), the quantified water flux equation is (considering the shoulder material is homogenous and isotropic):

Equ. 3.12)
$$\frac{\delta S_{0-z_1}}{\delta t} = q_0 - q_{z_1} \qquad [\mathrm{m \cdot s^{-1}}]$$

(q_{z1} and q_0: water fluxes through the section at depths z_1 and surface; $\delta S_{0\text{-}z1}$: stock variation between the depths z_1 and surface)

The figure 3.6 shows the water fluxes entering and leaving the shoulder. The analytical solution is therefore (flux balance):

Equ. 3.13a)
$$q_{RS} = q_{RR} + q_{PS} - i_S \qquad [\mathrm{m \cdot s^{-1}}]$$

With the equation:

Equ. 3.13b)
$$i_S = q_{ES} + \frac{\delta S_{0-z_1}}{\delta t} - e_S \qquad [\mathrm{m \cdot s^{-1}}]$$

(q_{ES}: q_{Z2}; evaporation e_S is null when $i > 0$; the stock variation is an average value)

The shoulder runoff flux q_{RS} is therefore a function of the infiltration flux i which is itself a function of the operators hydraulic conductivity $K(\theta)$ and matrix potential $\Psi(\theta)$[5]. Those two operators can only be empirically assessed. The rate of infiltration is indeed only measurable using an infiltrometer. The TDR probe placed in the shoulder measures only the θ mean value, which is not sufficient to calculate those operators. Values have been taken from

[5] The infiltration i is supposed to decrease along the time following the general formulation of Richards (1931). This equation is highly non-linear and has partial derivatives. It has generally no analytical solution.

"Modelisation du drainage souterrain des routes municipals", Cyr & Chiasson 2000. As it is demonstrated in the §3.4.2, the infiltration in the shoulder can be empirically assessed using a modified semi-empirical Green & Ampt (1911) equation.

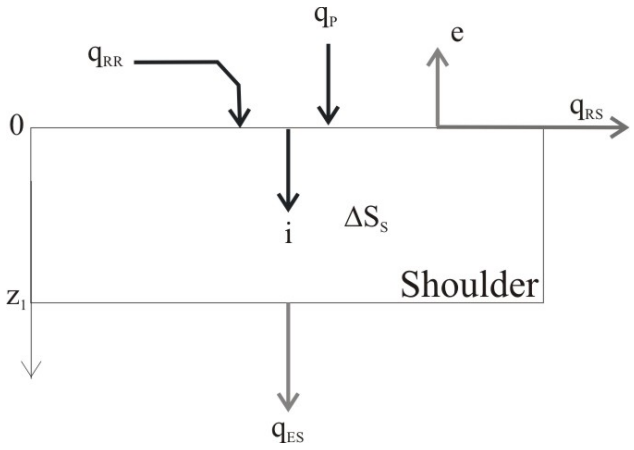

Figure 3.6: Flux balance. Outgoing flux are represented in grey, incoming fluxes are in black (q_{RR}: road runoff flux; q_P: precipitation intensity; e: evaporation; q_{RS}: shoulder runoff flux; i: infiltration; q_{ES}: exfiltration flux; all fluxes are in $m \cdot s^{-1}$)

Remarkable values:

Insight of the equations 3.13a and b demonstrates that the infiltration i is equal to:

- $i = K(\theta) = K_S$ if the shoulder is saturated. Indeed, the gradient $\delta H(\theta)/\delta z$ is then null. Only the gravitation drives the water flow.
- $i = \Delta S$ if the outgoing flux q_{ES} is null.
- i = a constant if the flux q first derivative is a constant. Indeed, the stock variation is then linearly varying (see §3.4.2 for insight).

3.4.2 ANALYTICAL APPROACH – example of SGH

To illustrate the shoulder behaviours, the example of the SGH is hereby presented. Figures concerning the other shoulders are in appendix IV. Processes are indeed very well discernable in the SGH. Infiltration processes are explained analysing the SGH exfiltration flow (light grey area, figure 3.7).

During the road watering, the pump had a short failure which stopped the incoming flow during 5 minutes. It seems that there was no consequence on the SGH outgoing flow. The incoming volume was almost 3 m^3 watered during 1h27. The equivalent precipitation is 145 mm[6]. Electrical conductivity of the Arnon river was 346 $\mu S \cdot cm^{-1}$; Cl^-

3.4.2.1 General assumptions

The shoulder is considered as homogeneous and isotropic. Initial soil moisture θ_r is assessed to be constant along z. In the transmission zone, the shoulder is saturated (verified with TDR), the hydraulic conductivity $K(\theta)$ is then the saturated hydraulic conductivity K_S. The pressure head at the moisturizing front is constant. Stock and stock variation calculations (when available) or assessments have been made using the equation 3.12 with $q_0 = i$; q_1 = SGH q_{ES}; z_1 = geomembrane depth. Remember that the stock variation ΔS is linked to the water content θ by the equation 3.8.

The shoulder is thus considered as a simplified elementary soil volume. As it is explained thereafter, this assumption is very well founded. Values provided concern the SGH.

[6] 41 mm on the road ($s \approx 80\ m^2$), the equivalent for the shoulder ($s \approx 20\ m^2$) is almost four times greater (2900 litres on 20 m^2).

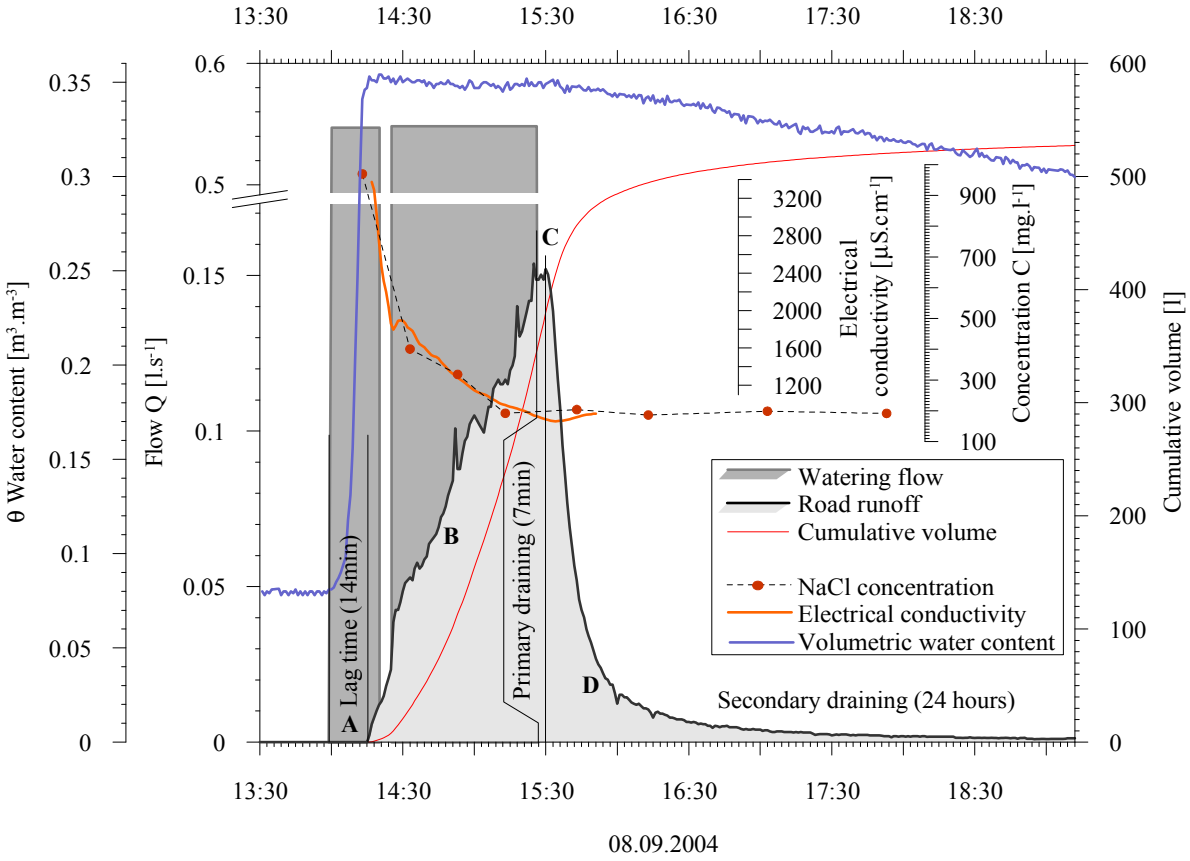

*Figure 3.7: SGH compartment, artificial test n°1. The watered volume (dark grey, 36 l·min^{-1}, 2900 l, 42 mm, 5 minutes break of flow due to a pump failure) is far greater than the SGH output volume (light grey, 570 l, 8.2 mm). Note that the Q axis has a break. SGH outgoing flow Q is composed of four parts: **A**) the flow is null, **B**) the flow constantly increase (cumulative volume also shows a linear increase), **C**) the flow is constant and **D**) the flow exponentially decrease. Note that the flux q=Q*s. The lag time is 14 minutes. Two kinds of draining time appear: the primary draining corresponds to the emptying of the macro-porosity (7min, when the suction plays no role), while the secondary draining is the queuing emptying of the macroporosity (maybe 1 hours) and microporosity. The transition from one to another is impossible to pinpoint. The drying and emptying of the microporosity may take days. Blue curve represent the volumetric water content θ (NB: the data comes from artificial test n°3: the probes were not installed in 2004. Hydraulic results from tests n°1 and 3 are very similar: the blue curve is thus indicative. The maximum θ is measured in a sand socket; grave I has normally a maximum θ of 0.17 (Cyr&Chiasson, 2000).). The electrical conductivity and Cl^- concentration match almost perfectly. The second peak in the Cl^- concentration is present, though it might be caused by the reactivation of the watering. See text for discussion.*

3.4.2.2 Hydraulic processes

The SGH outgoing flow q_{ES} presents four different steps (A – D) with two limits (A', B') (figures 3.7 and 3.8):

A1) As soon as the water reaches the shoulder, the water moisturizes the surface and propagates downwards. The infiltration rate during this time is unknown: it follows the formulation of Richards (1931). Nevertheless, the moisture θ augments. According to the equation 3.13, the stock variation augments linearly and the stock itself has a positive second derivative.

A2) The surface is saturated (θ_S). The moisturizing front progresses downward at a constant rhythm. Indeed, the TDR probe placed at mid-depth of the shoulder shows a linear augmentation of θ (from 0.08 to 0.35 m^3·m^{-3} along the time[7]

[7] Note that the TDR probe is placed in a socket full of Fontainebleau sand to assure a good contact between the two rods and the shoulder material. The recorded porosity is therefore the sand porosity. The grave I efficient porosity is supposed to be lower (17%, Cyr and Chiasson, 2000). See appendix VII.

(figure 3.7, blue curve, increase of $4.33 \cdot 10^{-4}$ $m^3 \cdot m^{-3} \cdot s^{-1}$). This means, from now on, that the stock variation is constant (ΔS = 0.15mm) and the stock itself grows linearly (with slope = ΔS). The linear, almost vertical, θ curve is significant: the function Ψ is nearly inefficient; only the gravity drives the water in the shoulder. The Continuity Law postulates that the variation of the water content θ over the time is equal to the spatial variation of the fluxes q. The spatial variation of q is subsequently a constant. Therefore, the moisturizing front can be imagined as a tilted surface regularly progressing downward over the time. At a depth z, θ augments linearly as soon as the moisturizing front reaches that depth. θ augments until θ_S. The tilted surface makes an angle α with the vertical. The bigger α is, the more rapidly θ is augmenting. The Green & Ampt (1911) semi-empirical infiltration model has α = 90°.

Note that A1) and A2) are represented only by A) on the figure 3.7. The exfiltrating flux q_{ES} is still zero. Equation 3.13 shows that the mean i flux during this period is $1.83 \cdot 10^{-4}$ $m \cdot s^{-1}$, with a stock augmentation of 150 mm.

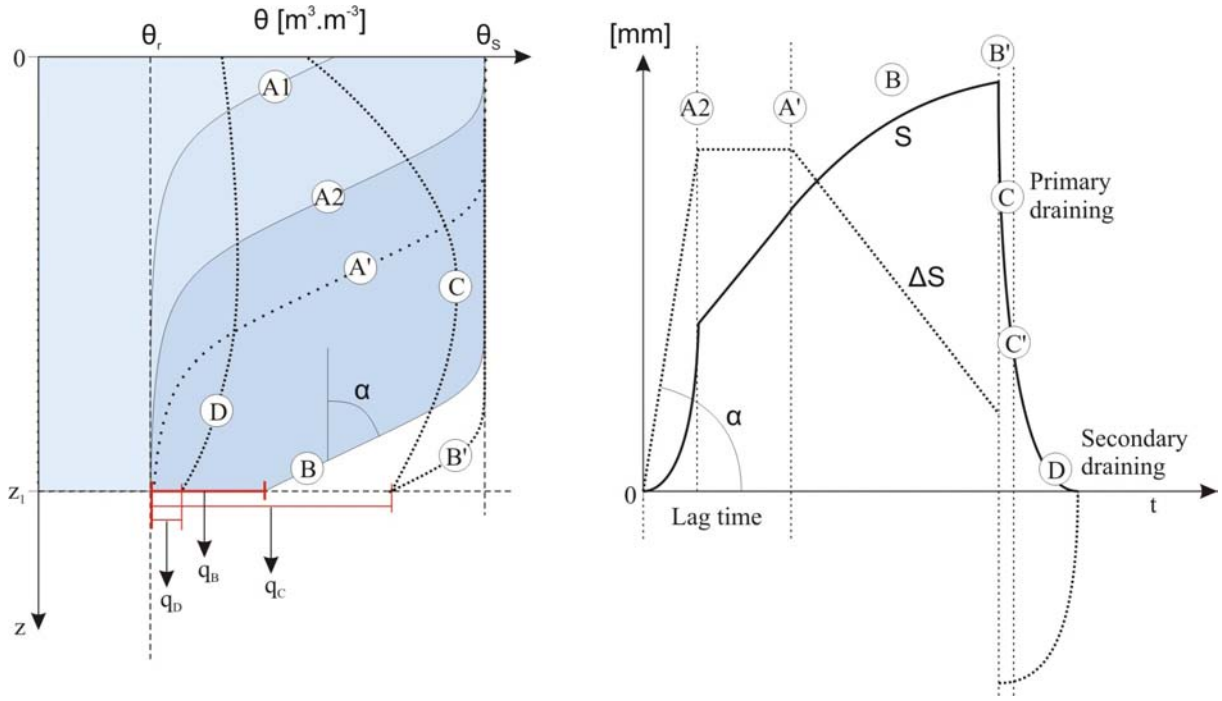

*Figure 3.8: **Left**: Evolution of the moisturizing front. **Right**: evolution of the stock during the interval (X). Letters correspond to the figure 3.7. A1) surface is moisturized. It is still not saturated but the front nevertheless goes down. A2) the surface is saturated. From now on, the stock linearly augments while the stock variation is null. A') first detection of water in the weirs. The stock variation decreases from this point, the stock itself still augments. B) The moisturizing front progresses downward. The shoulder is almost completely moisturized. B') Alimentation is cut off. The stock drops. Stock variation is highly negative. C) Primary draining: the macro-porosity empties. D) Secondary draining: the micro-porosity empties. See text for discussion. θ_r: residual water content; θ_S: saturated water content; q_X: outgoing flux during the period (X).*

A') The moisturizing front reaches the depth z_1, where the geomembrane lies. The flux q_{ES} starts to rise. Still, the conditions of the moisturizing front above z_1 are the same as for A2. The lag time is 14 minutes. Integrating the Green & Ampt equation, the lag time is:

Equ. 3.14)
$$t = \frac{\theta_S - \theta_r}{K_S}\left[z_1 + hf \cdot \ln(1 - \frac{z_1}{hf})\right] \quad \text{[second]}$$

The lag time is thus a function of the depth z, K_S, θ and the pressure head at the moisturizing front hf. Generally, hf values ranging from -0.01 to -0.05m are observed in coarse material. This allows calculating K_S = $2 \cdot 10^{-4}$ $m \cdot s^{-1}$.

Remember that the pressure head is assumed to be constant in the Green & Ampt formulation, as well as the difference in moisture θ. K_S is then an approximation based on simplifications.

B) As the water exits the system, the stock variation decreases linearly. The stock S slows its augmentation with a negative second derivative. The exfiltration q_{ES} rises linearly ($q'=3.3\cdot10^{-8}$ $m\cdot s^{-2}$). As the stock variation also behaves linearly, the infiltration i is a linear function of t. Considering the Darcy's Law, the strait linear trend of q demonstrates that the influence of the suction is very small. Thus, the flux q depends essentially on the gravitational head.

B') The road watering ceases abruptly. The exfiltration flux q has reached its maximum value. In the case of SGL (not shown here), the maximum q value has been reached before the end of the watering. In that particular case, the q value reached is equal to $K_S = 7\cdot10^{-6}$ $m\cdot s^{-1}$. The stock variation jumps from a positive but decreasing value to an increasing but negative value. As there is no refill flux, the stock variation will stay negative. The stock itself decreases rapidly from this moment on.

C) The flux q_{ES} is constant. As the infiltration i is null, the stock decreases rapidly. The stock variation is strongly negative. The slope of ΔS is quadratic. The cause of the constant exfiltrating flux is that the macroporosity empties with no retention effect. Indeed, the porosity in coarse material is big enough to empty rapidly. The macroporosity can well be compared to a pipe net. The figure 3.9A shows the Ψ(θ) curve for coarse material, while figure 3.9B explains why the emptying of the pores is so different from the filling.

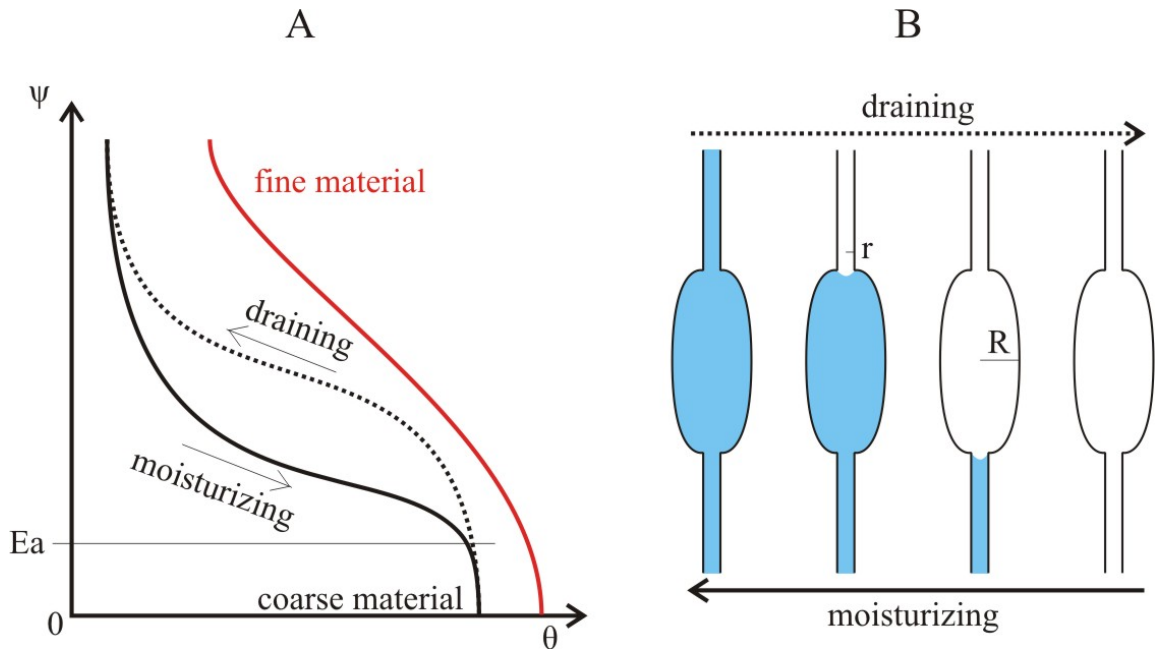

*Figure 3.9: **A)** Example of three Ψ(θ) curves. The trend is highly non-linear. The curve shape depends on the material considered. The hysteresis between the pores moisturizing and draining is emphasised. The example of the shoulder is presented in black, the case of a soil in red. (Ea: air entry suction: suction needed to begin the draining of the water). **B)** The hysteresis is caused by the difference between the radius of the macro- and microporosity (Jurin Law): Ψdrain = a·r, while Ψmoist = a·R. Thus, Ψdrain > Ψmoist. Modified from Musy and Soutter 1991.*

C') Although impossible to pinpoint in time, the limit between the primary and secondary draining is important. The secondary draining indeed symbolizes the emptying of the microporosity. The frontier in suction between the macro- and microporosity is often accepted to be 1 bar. When the macroporosity is empty, the exfiltrating flux drops very rapidly.

D) The flux q_{ES} still decreases but less rapidly. The cause is that the microporosity is not driven by capillarity but by water adsorption. The suction augments rapidly when the draining begins (figure 3.9A). The flux q_{ES} tends to an asymptotic null value. It may take days for the flux to be zero.

The draining process (C-D) is not the same as the filling process. This is due to the strong hysteresis that exists between the moisturizing and draining suction function. While the filling of the pores depends on the radius of the macroporosity R, the emptying depends on the radius r of the microporosity (Jurin Law, R>r). Thus, the suction is greater during the draining than during the filling.

Regressive analyses of the exfiltration flux and water content behaviour validates the employ of the Green & Ampt semi-empirical formulation. Indeed, the SGH linear q_{ES} and θ augmentations, regarding the Continuity Law, are function of time and space. This shoulder can be imagined as a unitary gravel volume which is rapidly wet when an event occurs. The air saturation[8] plays a little role because it can escape downward. Surface processes have little influence (effect of plants, "battage"[9], and evaporation). The moisturizing front propagates using the soil cracks, macro and microporosity. Literature gives little information about the interaction between the different porosities; they are supposed to be important. Once wet, the shoulder conducts the water downwards at a constant rate. If the rainfall event lasts long enough, the exfiltration q_{ES} will be equal to K_S. Also, the lag time allows calculating an approximation of K_S using the Green & Ampt equation. As soon as the infiltration stops, the macroporosity empties very rapidly. The hysteresis between the filling and emptying processes of the porosity is due to the pores radius ratio. Once the macroporosity is empty, the micro porosity drains down during a long time. This is due to the augmentation of the suction along θ: the further the shoulder dries, the higher the suction rises. The remaining water is the stock (θ = 0.05 to 0.08 $m^3 \cdot m^{-3}$ in the shoulders, which represent a volume of 0.5 to 0.8 m^3).

Note that the "air entry suction", i.e. the suction needed to empty the pores and let the air fill the porosity is almost null in the case there is a collecting pipe under the shoulder. The air can indeed come from the surface (normal case) or from the bottom (pipe case).

The total volume exfiltrated E_S is 580 l. The runoff coefficient C_R is R_S/A_W = 0.8.

3.4.2.3 Conservative tracer test NaCl

One kg of NaCl was mixed to 5 litres of water. The brine was poured on the road previous to the watering. Cl^- concentrations of all samples were analysed in laboratory. The electrical conductivity shows a perfect match with the Cl^- concentration (figure 3.7). The first sample analysed, as well as the first water detected by the EC probe show the highest concentration ($\approx$ 1 $g \cdot l^{-1}$). The concentration then decreases exponentially and stabilizes around 200 $mg \cdot l^{-1}$. As in the case of the road runoff, a second Cl^- peak is discernable, although it is not clear. It is more like a rupture in the logarithmic decreasing curve. The hypothesis is there is a second (lognormal) distribution superposed to the first. Reasons for this second peak are unknown. As the two peaks are visible even in the road runoff, this means the two peaks (or two superposed curves) are not only due to the water transition in the shoulder, but also to a fractionation in surface of the road. Four hypotheses arise:

1. The substance is heterogeneously distributed on the surface of the road. This could be due to the traffic redistributing the substance while passing. The substance would thus be concentrated in undisturbed places and depleted on the traffic lanes. Peaks would be function of the distance of the substance from the runoff collector.
2. The substance itself fractionates during its transport. This, however, it scarcely possible because it does not respond to the convection, diffusion (Fick) and dispersion Laws.

[8] The air saturation plays usually a significant role in keeping the soils dry: "air piston" effect. It needs a certain amount of water to begin the infiltration, see Musy and Soutter, 1991.
[9] The "battage" is the soil hardening due to the beating of rain drops; it makes the soil more impermeable.

3. The substance fractionates as a function of the transport path used. Water moving more rapidly in the first case and slower in the second. This postulate that there are only two distinctly different paths: the inter-aggregates pores (or macroporosity) and intra-aggregates pores (or microporosity). This hypothesis has been thoroughly studied by Van Genuchten & Wierenga (1976) and Simunek et al. (2003). Figure 3.11 illustrates the difference.
4. A piston effect, while possible and even probable, cannot explain the two peaks. Indeed, in case of a strong piston effect pushing a pre-existing loaded stock, the first peak would have been the smaller and the second peak would have been the bigger. This is not the case.

The hypothesis about the substance distribution on the road hardly concerns the shoulders because the tracer was poured only in one place. Shoulders nevertheless show two peaks. As it has been illustrated by the hydraulic analysis of SGH, the two porosities are well distinct. The two Cl^- peaks are therefore in agreement with the hydraulic behaviour.

The restitution amount is 125g. The rest of the substance is transported beyond the shoulder, carried by the shoulder runoff. The fraction of tracer belonging to R_S is $C_T = 0.875$, which is close to the runoff coefficient $C_R = 0.8$. It is supposed that the 7.5% missing are trapped in the pores, which means that 220 litres are stocked in the shoulder (0.075*2900 l.). This is not concordant with the θ calculation (500 to 800 l.). This means that not only most of the watered volume passes over the shoulder, but also that the runoff coefficient C_R is higher at the beginning of the event. Therefore, the first flush passes essentially over the shoulder; the water exfiltrated is comes from later in the event. The figure 3.10 shows the pollutogram for SGH, Cl^-. The first flush effect, while bigger than in the road runoff, is still below the Bertrand–Krajewski & Chebbs requirements (b = 0.42). Only 60% of the mass of Cl^- arrive in the first 30% of the cumulative water volume.

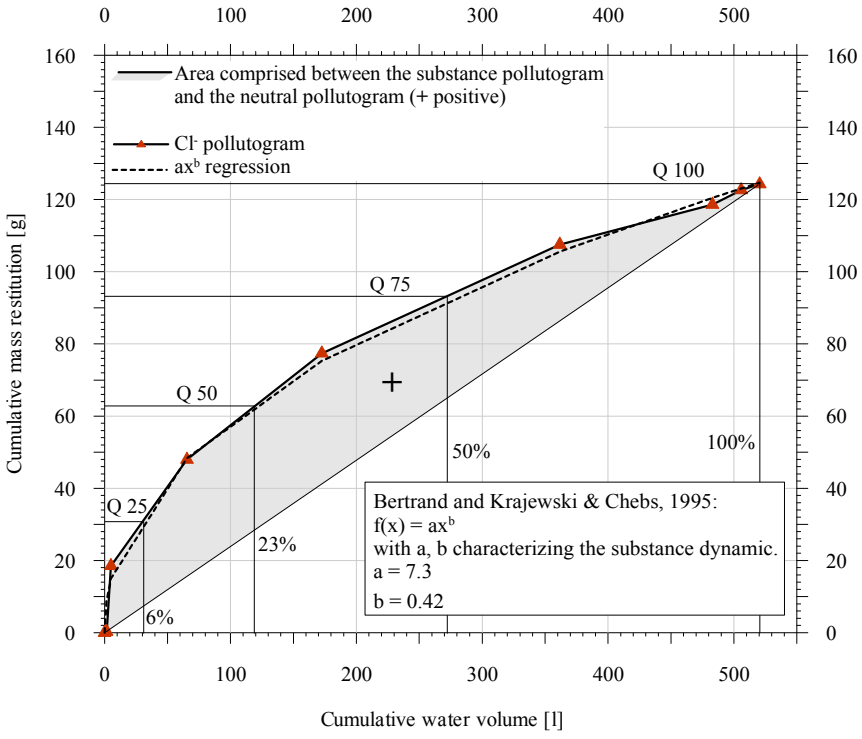

Figure 3.10: SGH pollutogram concerning Cl^-. The first flush effect is more contrasted than for the road runoff because the repartition on the road was punctual. Also, the amount of NaCl was far greater.

3.4.2.4 Comparison between shoulders (figures are in appendix IV)

The analysis presented in the previous paragraph concerns the shoulder SGH during the experimental test n°1 only. Hereby are presented the results concerning the other shoulders. In order to avoid overwhelming and painful repetitions, other shoulder behaviours are compared to the description of SGH.

SGC: Overall, the SGC behaves the same way as SGH. Differences occurring are only a matter of descriptive values. Those, however, are significant. For clarity, the following letters are linked to figures 3.7 and 3.8:

- A) Lag time (29 minutes): Knowing the properties of clay, it is well probable that the K_S is lower. Moreover, the clay minerals filling the pores, the macroporosity must have a lower radius R. This results in longer moisturizing time and therefore transit duration.
- B) The linear q slope ($q' = 7.5 \cdot 10^{-8}$ m·s^{-2}): The Green & Ampt model needs further change. As the linear exfiltrating slope is smaller than the one in SGH, the angle α is smaller as well. The moisturizing front presents thus a sharper edge and descends slower. The resulting q is thus also linear but increases slower. The maximum flow Q value reached is the smaller of all shoulders (0.07 l·s^{-1}).
- C) The duration of the macroporosity emptying (10 minutes): the presence of clay changes the Ψ(θ) curve shape and limits (figure 3.9A, red curve). The water content in the shoulder is higher when saturated and also when drained. The suction is overall higher than in shoulders without clay. The result is the macro and microporosities take more time to empty.
- D) The shape of the decreasing q: the shape of the decreasing q curve, while still logarithmic is far less pronounced than for SGH. The slope q' at that moment is almost equal to q' during the interval A).This means that the hysteresis between the moisturizing and draining is smaller: R is not so different from r. This is concordant with A): the macroporosity is less developed in a shoulder built with clay.
- The Cl^- restitution mass: the calculated Cl^- restitution is 40g. Most of the tracer passes over the shoulder. The curve still shows two peaks.
- The pollutogram: The pollutogram shows a coefficient b of only 0.72. The first flush effect is nearly inexistent because all the first flush has passed over the shoulder (80% of mass in the first 70% of the cumulate volume). The restitution mass is one third of the one observed in SGH.

Overall, the SGC may contain more water than other shoulders. Nevertheless, it takes more time to fill and drain. This results in a longer lag time and a greater runoff coefficient ($C_R = 0.91$). The exfiltrated volume is only 280 l. Moreover, the first flush fraction C_T (= 0.96) is also bigger. Finally, the C_T at the beginning of the event must be nearly 1 (because the shoulder is so difficult to infiltrate). The cumulative water volume curve is smoother (less steep during B, less flat during C, D). Note that the less pronounced hysteresis between the moisturizing and draining could also be due to the clay swelling: the clay swells in contact with water and obstructs the pores.

Considering that only five centimetres of different material at the surface of the shoulder induce such differences in the behaviour of SGC, it would be interesting to evaluate the impact of an increase of the thickness of the mixed gravel-clay layer. This matter is discussed in chapter 6.

SGL: Again, the shoulder SGL behaves the same way as SGH does. The differences are smaller than those concerning SGC:

- A) Lag time is 20 minutes. It is between the lag times of SGH and SGC.
- B) The linear slope q' of the exfiltrating flux q is sensibly the same as SGH: $2.7 \cdot 10^{-7}$ m·s^{-1}. The maximum Q value is reached before the end of the watering on the road, thus giving the K_S value[10]: $7 \cdot 10^{-6}$ m·s^{-1}. Note that during the artificial test n°3, the saturation was also achieved but the recorded K_S was higher: $2.2 \cdot 10^{-5}$ m·s^{-1}.
- C) The duration of the primary draining is six minutes; it is similar to the duration recorded for SGH.
- D) The shape of the decreasing q curve is also similar to the one observed in SGH.
- The Cl^- restitution mass was 60g which is half of the mass recorded for SGH. As the infiltration processes are little different, this must be due to a bigger part of the tracer transported in the shoulder runoff. This is also emphasised by the longer lag time. The curve has the strongest second peak recorded.

[10] Note that this is the vertical hydraulic conductivity. If is seems a little low for a gravel, it is because K builds an ellipsoid due to the artificial compaction during the construction.

- The pollutogram shows a nearly linear curve. The b factor is 0.8. The first flush effect is nearly inexistent (80% of the mass are found in the first 70% of the cumulate volume).

Overall, the shoulder SGL behaves exactly the same way the shoulder SGH does. The fact that the vertical hydraulic conductivity was reached during the test does not prove that K_S of SGL is the lowest: indeed, the very long lag time in SGC prevented the flux q to augment further; the test was stopped too soon. The runoff coefficient was 0.81 (total exfiltrated volume: 540 l.). The C_T was 0.94, almost similar to the value recorded for SGC.

Concerning **SH**, differences are caused by the presence of the HMF situated at mid-depth of the shoulder. Although it might be hard to consider the HMF layer as water conductive, Hassan & White (1996) calculated that the hydraulic conductivity K of an asphalt layer may be as high as $1 \cdot 10^{-6}$ m·s^{-1}.

- A) The lag time is 17 minutes. The presence of the HMF layer does not prevent the water percolating the shoulder. This could be due to by-pass paths difficult to localize or deformity in the HMF or, more presumably, in the bituminous coating. The water is without doubt infiltrating laterally from the infiltration slope (figure 3.11). The shoulder material under the HMF layer is of course dryer than the watered part[11]: the suction is thus a bit higher there; water is lightly attracted, though, due to the gravel material that cannot induce high matrix potential. Once wet, the shoulder behaves as the SGH.
- B) The outgoing flux q is measured only with a pot (sampling bottles) and a chronometer. This is because at that time, no flowmeter was available. The curve is consequently less trustful. The shape is more soften. The linear increase could be due to the exfiltrating flux itself or to the discreet interval between each sample. The maximal Q value reached is $2.0 \cdot 10^{-6}$ m·s^{-1}. The progress of the water being presumably complex, it is hard to arrive at any conclusion concerning this particular test. Nevertheless, the cumulative water volume shows a curve similar to SGC.
- C) and D) The q curve decreases shows a shape similar to those observed in the SGC. The decrease is nevertheless a bit faster. No constant flux is discernable.

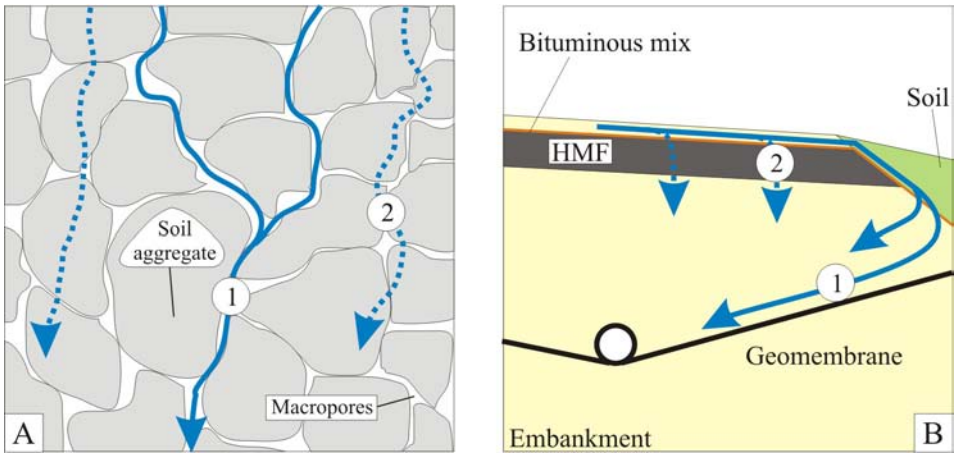

Figure *3.11: **A)** Illustration of the two possible water paths. The path n°1 uses the macroporosity and moves fast. This is presumably the main water path in the shoulder. Note that K_h is 10 times higher than K_v and thus helps the water flux. The paths n°2 uses the microporosity and "jumps" from aggregate to aggregate (grey surface are not grains but soil aggregate). It is slower but represents a higher volume. **B)** Illustration of the possible water path in the SH. The faster path (1) is through the soil before coming back toward the shoulder, infiltrating the bituminous coating which is useless. A second, slower path (2) is through the HMF itself. As it is the first flush that filled the cracks and imperfection of the surface of the HMF, it is this very second path that transports much of the substance. Thus, the second peak recorded is higher than the first.*

[11] It is even dryer than if there were no collecting pipe.

- The Cl^- restitution mass was 80g. Postulating that the water comes from the shoulder - infiltration slope boundary, it nevertheless means that most of the tracer finds its way to the infiltration slope itself. The curve, while showing the two usual peaks, also presents a strong increase at the end of the event. This last peak is even far greater than the first one. This could mean the flux transporting the greatest part of the substance has been overtaken by a flux using a faster path. See figure 3.11 for precision.
- The SH pollutogram is strait with a coefficient b of 1. The substance invariably comes along with the water with no acceleration or retardation.

The processes occurring in the SH are rather difficult to assess. The water infiltrates the shoulder supposedly using a path around the HMF layer. It is also helped by the high horizontal hydraulic conductivity (ten times higher than the vertical one). The bituminous coating effect is negligible. The path n°1 is indeed essentially horizontal. The runoff coefficient is nevertheless high, while smaller than for the SGC (C_R=0.89). The exfiltrated volume is 360 l. The Cl^- concentration varies awkwardly. Preferential flow paths are to be found. The C_T is 0.92, but presumably smaller (the end of the Cl^- concentration curve is not recorded).

SB: Results are not comparable to those provided by SGH.

- A) The lag time is 37 minutes. It is the longest lat time recorded. This means the geotextile takes a long time to become a little bit permeable.
- B) The q curve is similar to the one presented by SH. There is no real linear increase of q. The maximum value reached is $q=2.0 \cdot 10^{-6}$.
- C) and D) The curve decreased in a way similar to SH.
- The restitution mass is the lowest observed: 15g. The Cl^- concentration curve shows one peak only but is composed of no more than 4 values. Note that the main peak does not coincide with the first sample taken. The resulting mass flux is buffered; to the contrary of the shoulders SGH, SGC and SGL whose mass fluxes are sharp.
- The resulting pollutogram shows a coefficient b of 1.

The shoulder SB has the longest lag time and smallest restitution volume. It also presents a neutral pollutogram based on the smallest total restitution mass. It is indeed the least permeable shoulder.

	Hydraulic flux					Intrinsic char.		Tracer test			Bertrand - Krajewski
	Lag time	Max. Q	q'	Volume	C_R	K_S [1]	K_S [2]	Max. C	Rest. Mass	C_T	b
	[min]	[$l.s^{-1}$]	[$m.s^2$]	[l]	[-]	[$m.s^{-1}$]	[$m.s^{-1}$]	[$mg.l^{-1}$]	[g]	[-]	[-]
SGH	14	0.15	$3.3 \cdot 10^{-8}$	580	0.8	$2 \cdot 10^{-5}$	$6.5 \cdot 10^{-4}$	1000	125	0.87	0.42
SGC	29	0.07	$7.5 \cdot 10^{-8}$	280	0.91	$4.5 \cdot 10^{-6}$	$3.2 \cdot 10^{-4}$	450	40	0.96	0.72
SGL	20	0.14	$2.7 \cdot 10^{-7}$	540	0.81	$2.2 \cdot 10^{-5}$*	$4.6 \cdot 10^{-4}$	350	60	0.94	0.80
SH	17	0.10	-	370	0.89	$6.6 \cdot 10^{-6}$	$5.4 \cdot 10^{-4}$	350	80	0.92	1
SB	37	0.07	-	150	0.94	$1.5 \cdot 10^{-5}$	$2.5 \cdot 10^{-4}$	130	15	0.98	1

*Table 3.1: Summary of the main characteristics concerning the dynamic behaviour of the five shoulders (q: flux; q': slope of flux q; Volume: total volume exfiltrated; C_R: runoff coefficient; K_S: vertical saturated hydraulic conductivity; C: concentration; Rest. Mass: restitution mass; C_T: Tracer coefficient; b: Bertrand–Krawjeski regression factor (< 0.18 = first-flush)). [1] K_S read on the q curve. The full saturation of all shoulders (but SGL) has not been reached: those are therefore minimum values. Those are the maximum values ever recorded in Grandson; they come from the artificial test n°3. [2] K_S calculated with the lag time and distance ratio. They are indicative but overrated because assumption is made that the shoulder is saturated. *K_S value registered at saturation.*

3.4.2.5 Discussion

This paragraph exposes a general discussion about the infiltration processes in the shoulders. For conclusions about the precise behaviours of the shoulders, see chapter 6 “synthesis”. As it is very hard to separate the shoulder behaviour from the surrounding soil behaviour, the infiltration dynamic described by the TDR probe buried in the SGL 20m shoulder is conjointly described with the soil infiltration dynamic in the §§3.5.2.1.

Generally speaking, the shoulder runoff was not only directed toward the infiltration slope but also laterally along the road. Indeed, the transition road – shoulder shows a small depression running along the road. During the watering of compartment (SGC for example), the compartment lying just downward (the road climbs to the bridge over the Arnon, i.e. SGH in this example) had also shown exfiltration fluxes. The fluxes are higher if the considered compartment (SGC) is less permeable. The volume exfiltrating a neighbour compartment has been taken into account for the volume calculation. This fact is inherent to the shoulder separation and has no influence when considering a shoulder running along the road for kilometres. Nevertheless, a special attention must be made on the shoulder inclination.

The lag time is representative of the time needed for the road runoff to moisturize the shoulder along z. It is thus an indirect measurement of the hydraulic conductivity. The calculated K_S indeed are proportional to the lag times (mean Darcy’s velocity). Exogenous impermeable layers (HMF, Bentonite) distort the calculation because it is not possible to assume that the shoulder is homogenous anymore. Nevertheless, an average K_S is calculated for comparison purpose (table 3.1). Real K_S values must be between the K_S^1 and K_S^2 values and must also respect the relative ranking of the lag times. They are concordant with K_S given for “coarse sand” or “sand with gravel”. The SB K_S is the smaller (very fine sand, coarse silts).

The substance transport is influenced by the time needed to moisturize the shoulder and to begin the infiltration itself. As long as it has not begun, the substance is carried away by the shoulder runoff. The tracer test showed that roughly 90% of the tracer ran to the infiltration slope. The first flush is indeed driven to the infiltration slope.

The propagation of the moisturizing front and substance transport highly depend on the presence or not of an exogenous layer in the shoulder. In the case there is none (SGH, SGC, SGL), the water propagates linearly in time and space along z. The moisturizing front is clearly distinguishable: the volumetric water content rises linearly and very fast. The speed at which the shoulder moisturizes dictates the rate at which the exfiltrating flux increases (q’).

Water paths are twofold: in the macroporosity where the water runs fast and transports most of the substances, and in the microporosity where the water runs slowly and also transports substances but in lower concentration. It is not clear if the initial concentration was different or the same for both paths. Indeed, the lower concentration noted in the supposed microporosity path might be due to a higher retention factor (intra-aggregate porosity has a far bigger exchange surface). The presence of clay diminishes the difference between the micro and macroporosity (either by filling the pores, either by swelling, more presumably by both). It is therefore more impermeable. The usage of two progress paths results in two chemically distinct water qualities. The first water arriving is the most concentrated flux, followed by the second less concentrated flux. The time needed for draining the macroporosity is clearly discernable.

In the case of SH, the presence of the HMF layer disturbs the flows. It is nevertheless possible to specify the probable water paths using tracer test results. The water is laterally infiltrating from the infiltration slope to the foundation. The HMF is however not impermeable and also shows a percolation. Water getting around the HMF is faster than the one penetrating the HMF.

In the case of SB, the shoulder is a bi-layers model: the grave I (above and below the bentonitic layer) behaves as in SGH, while the bentonitic layer has a far lower K_S. It is extremely impermeable. The hydraulic as well as pollutive dynamics show strong buffering.

Cl^- Pollutograms for all shoulders can be described by a unique coefficient b ($b \in [0;1]$). The higher b is, the more neutral the pollutive dynamic is. To the contrary, a low b coefficient shows a strong first-flush effect. Shoulders with

no exogenous layer have a first flush effect, although not very pronounced, while SH and SB have neutral pollutograms. The exogenous layer thus acts like a retardant: the substance concentrates at the interface grave I - layer and is continuously carried away by the infiltrating water. It is possible that those layers also constitute semi-permeable membranes that augment the so far negligible osmotic pressure head.

3.4.3 STATISTICAL APPROACH – MULTIPLE COMPARISONS – NATURAL EVENTS

Different methods have been used to assess the runoff coefficient C_R of all shoulders, based on all recorded events:

- A graphical analysis which allows taking into account the variance of the exfiltration volumes E_S. This solution permits to estimate the exfiltration volume for all sorts of precipitation. Hydrometeorological factors are taken into account. As it is a graphical analysis, the data graphical dispersion is used to estimate the global variation that occurs. It is thus close to a stochastic C_R resolution.
- A simple and practical calculation of the runoff coefficient C_R. This coefficient is calculated using the equation of the water balance (fig. 3.1). All terms of the equations are calculated separately. The only unknown variable is the shoulder runoff R_S. Once deduced, the runoff coefficient C_R can be calculated.
- The building of an empirical equation deduced from the water balance resolution. The empirical equation is calibrated using the 2004 events data and tested using the 2005 events data. It is therefore more reliable and solid. This equation can be used to calculate high-quality estimation of every terms of the mass balance (concerning the shoulders). This empirical equation is deterministic.
- As the previously described empirical solutions are varying only in one dimension (uni-variance, opposed to multi-variance) because only the precipitation volume is used, a more complicated empirical solution has been developed. It includes the statistical analysis of the parameters that might influence the infiltration, and the building of 3D plots.

The general equations governing the shoulder water balance are 3.2a and b (figure 3.1). For reminder, the available water on the shoulder A_W is the sum of the corrected road runoff R_R, the precipitation P_S and the fraction x of the road dissemination D_R. Figure 3.12 summarizes those parameter as function of the time, during the studied period. For comparison purpose, data concerning lysimeters are also shown.

Values R_R and E_S are calculated with the general equation 3.6, §3.1.1. Surfaces s are respectively s = 13.6 m^2 for R_R and s = s_S (18 m^2 ± 2) for E_S (surface depends of the compartment that is considered, see appendix V table V.1 for exact values). The precipitation P is measured. The stock variation ΔS and the evapotranspiration ETP_S are calculated (appendix VI). The shoulder runoff R_S is deducted by subtraction. It is the only unknown variable.

3.4.3.1 Graphical analysis – 2D-1 parameter plots (A_W) – univariance

This solution allows estimating the shoulder runoff R_S for every precipitation P_R (≈ road runoff R_R) value. It also comprises a variance estimation (which depends on the weather conditions, principally API). The variance estimation can be compared to a stochastic solution because it gives a relative confidence index ε. Finally, it permits to estimate the shoulder runoff before and after the shoulder is fully humid. The C_R indeed varies over time during one precipitation: C_R is higher when the shoulder is dry and lower when wet. Because many small events occurred (P < 5 mm), the precipitation sometimes stopped before the shoulder is fully wet. This is observable in the figure 3.13. The specific processes inducing this C_R variation are discussed in §3.3.

For this empirical approximation of the C_R coefficient, the exfiltration volume E_S [mm] has simply been plotted against the road runoff volume R_R [mm]. The needed R_S is deduced from the slope of the linear regression fit. Figure 3.13 shows the results for the shoulders SGL. Graphical resolutions for other shoulders are in appendix V.

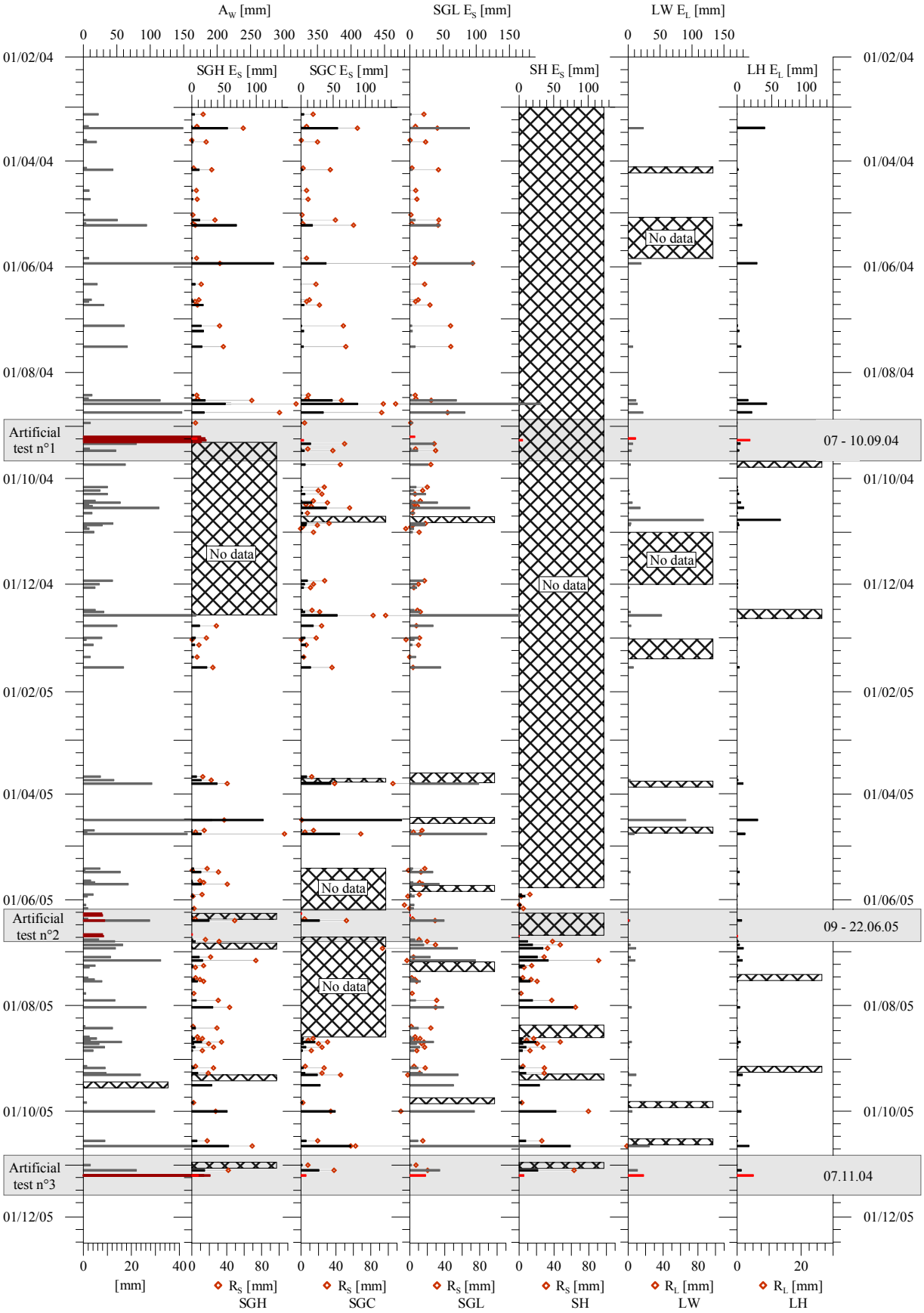

Figure 3.12: A_W, E_S and E_L values for all the shoulders and lysimeters. Artificial events are also shown in red bars for comparison purpose. Red lozenges represent the R_S values. Runoff values do not exist for the lysimeters. All plots are on the same scale. Missing data are highlighted with a grid pattern. See text for discussion.

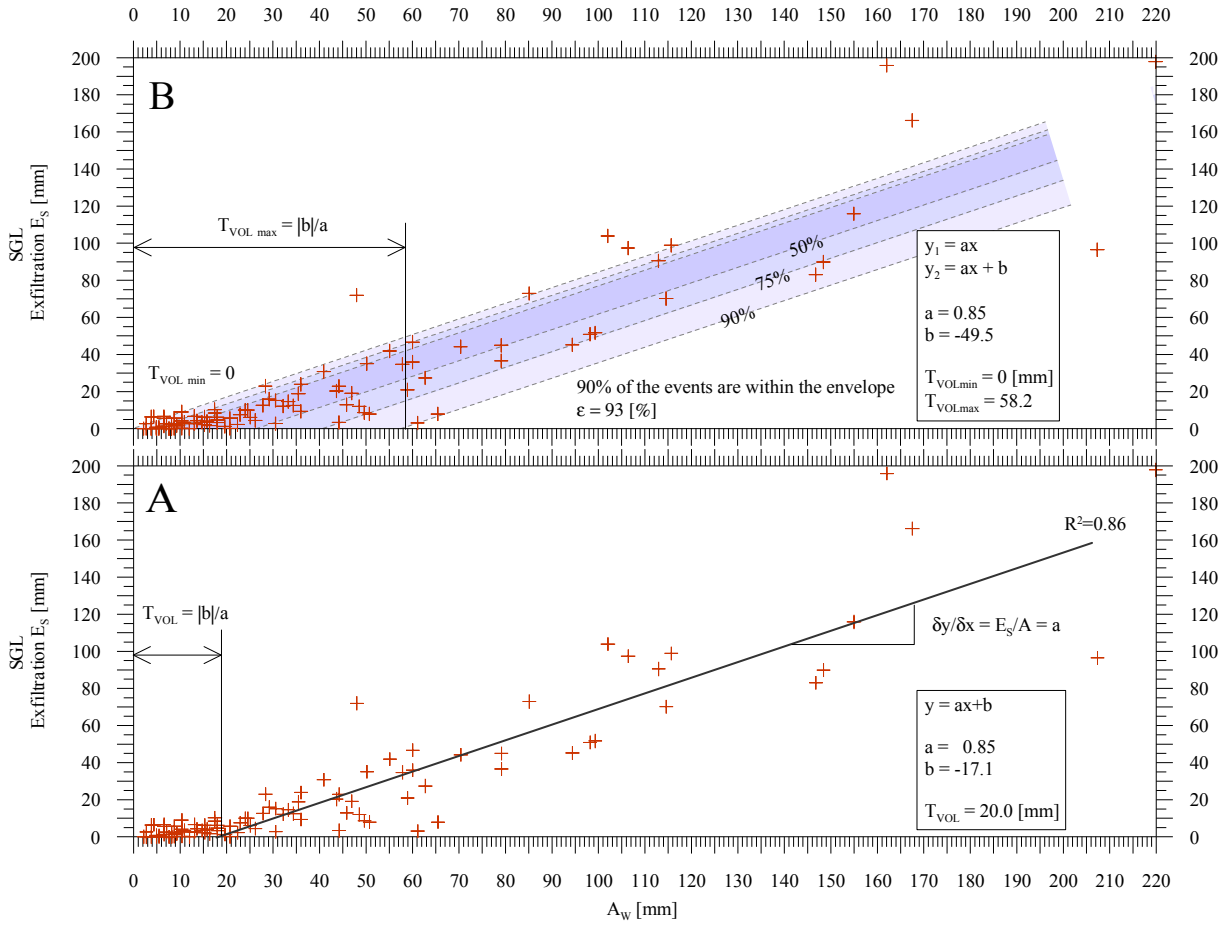

*Figure 3.13: Shoulder exfiltration E_S as function of A_W. Example of SGL. **A)** Linear regression fit. The fit shows 2 components: a part where $E_S = 0$ and a part where it is linearly linked to A_W. The slope of the linear fit represents the ratio E_S/A_W. R_S is then deduced using the equation 3.4. See text for discussion. **B)** The same plot allows estimating the variance both parts of the linear fit. The boundaries are determined by the threshold values $T_{VOL\ max}$ and $T_{VOL\ min}$. The confidence index ε traduces the probability the E_S value will be in a given range. The higher the confidence index is, the wider the range is. Confidence index areas are shown in light blue. They have been bordered counting the events that belong or not to the area.*

The calculation of exfiltration volumes E_S was the key process (equation 3.6). Values of the weirs and compartments main characteristics are available in appendix V, as well as error estimations. Values of calculated E_S are shown in appendix V, while figure 3.12 illustrates the correspondence between A_W and E_S for all shoulders (SB does not appear because no exfiltration was observed for the natural precipitation). For comparison purpose, the artificial events have also been plotted in that figure. Note that the scales are the same for all plots to emphasize the comparisons between shoulders. E_S values strongly depend on the shoulder considered. They increase linearly with the precipitation volume (see §3.4.3.2). E_S values range from zero for low rainfalls to nearly 200 mm in case the rainfall is very heavy. Overall, the E_S values are greater for SGL and smaller for SGC. This means SGC releases less water than other shoulders.

The example of SGL clearly shows a dual trend. At low A_W values (< 20 mm), E_S is null. At higher values of A_W, E_S is increasing more or less linearly. The linear regressive fit has thus two components: 1) a volume threshold (noted T_{VOL}) where no exfiltration value E_S is recorded and 2) a linear increase of E_S linked to A_W by the equation:

Equ. 3.15) $$E_S = a \cdot A_W + b$$ [mm]

(a; b: regression fitting factors [-])

In this example, a = 0.85 and b = -17.1. The slope, a, has a strong physical meaning. It represents the road runoff fraction that is infiltrated. A slope of 1 means that all the incoming water is infiltrated. A slope of zero means that all the water is flowing over the shoulder (C_R = 1-a). The threshold T_{VOL} is calculated:

Equ. 3.16) $$T_{VOL} = \frac{|b|}{a} = R_{S*} + ETP_S + \Delta S$$ [mm]

(R_{S*}: initial shoulder runoff < R_S: shoulder runoff, see below for further explanation)

And its value is, for SGL, T_{VOL} = 20mm. Each event has a different threshold. T_{VOL} represent the average threshold for the shoulder. The Threshold is empirically calculated but has also a strong physical and practical meaning. It indeed includes:

- the water volume that is trapped in the shoulder (stock variation ΔS)
- the water volume that is evaporated and transpired by plants (ETP_S)
- the water volume that is flowing over the shoulder before moisturization (initial shoulder runoff R_{S*})

The initial shoulder runoff R_{S*} is the shoulder runoff that occurs in case the shoulder is dry (see §3.4.2 for explanation about the processes). The initial runoff R_{S*} is proportionally greater than the shoulder runoff R_S:

Equ. 3.17) $$\frac{R_{S*}}{A_W} \geq \frac{R_S}{A_W}$$ [-]

The meaning of the initial shoulder runoff R_{S*} is important because it carries the first flush.

Equation 3.16 shows that the greater T_{VOL}, the more tightened and/or water retentive the shoulder is. The figure 3.13b also shows T_{VOL} maximum and minimum values (noted $T_{VOL\ max}$ and $T_{VOL\ min}$; $T_{VOL\ min}$= 0). These values of T_{VOL} have physical significations as well: $T_{VOL\ max}$ is the threshold when the weather is hot and windy; and when the shoulder is dry. $T_{VOL\ min}$ is the threshold when the shoulder is wet and the weather is cold and rainy. Both $T_{VOL\ min}$ and $T_{VOL\ max}$ build an envelope that comprises ε [%] of all events (ε = 93% of the events for SGL). The distance from the linear regression fit represents the interval of confidence[12]. This envelope constructs an empirical stochastic model that can be used to assess the response of any type of rainfall. Note that because ETP and ΔS values should be more or less equal for all the shoulders (same meteorological conditions during a specific event), the threshold T_{VOL} is proportional to R_{S*}: comparison of different T_{VOL} gives information on the runoff behaviour.

Based on the preceding observations, the following rules were established to calculate the shoulder runoff R_S:

Equ. 3.18a) $$If\ A_W < T_{VOL}\quad then\quad R_S \leq T_{VOL}$$ *[mm]*

Equ. 3.18b) $$If\ A_W > T_{VOL}\quad then\quad R_S = A_W - E_S$$ *[mm]*

As no indication about the ETP or the ΔS is available from the graphical analysis, they are unknown: the shoulder runoff R_S is smaller or equal to T_{VOL} (equation 3.18a). Because the first assumption is that $A_W < T_{VOL}$, all the road runoff is nevertheless not infiltrating the road structure[13]. The low R_S has thus no consequence. At higher values of A_W, it is assumed that the ETP and stock variation are proportionally less participating. In the equation 3.16, the ETP and ΔS have been considered null. C_R is then calculated using the equation:

[12] The confidence index ε traduces the probability that the E_S value will be in a given range. The wider the range is, the higher the confidence index is.

[13] The road runoff is either stocked in the shoulder, either evaporated, and either driven to the infiltration slope.

Equ. 3.19) $$C_R = 1 - \frac{E_S}{A_W}$$ *[mm]*

The graphical analysis of all events permitted to assess the following factors for all the shoulders: a, b, T_{VOL}, $T_{VOL\ max}$, $T_{VOL\ min}$, and C_R (R^2 for each linear fit is also specified). Figures concerning SGH, SGC, SH and SB[14] are in appendix V. Table 3.2 summarizes those values for each shoulder.

	a	b	T_{VOL}	$T_{VOL\ max}$	$T_{VOL\ min}$	C_R
SGH	0.40	-3.70	11.0	40.00	0.00	0.60
SGC	0.42	-5.64	14.9	58.00	0.00	0.58
SGL	0.85	17.10	20.0	58.20	0.00	0.15
SH	0.51	-2.04	5.0	28.50	0.00	0.49
SB	0.00	0.00				1.00

Table 3.2: Summary of values deduced by graphical analysis. T_{VOL} and C_R are the most important data. SGL showed the highest threshold but also the lowest runoff coefficient.

General behaviours can thus be sorted out:

- SGH has a pretty high C_R but a low T_{VOL}. This means small events will immediately have a consequence: the shoulder is early permeable. Once wet, the shoulder drives most of the water to the infiltration slope (the vertical hydraulic conductivity k must be low). Note that there are less numerous measurements than for other shoulders (see figure 3.12 or table V.2, appendix V).
- SGC also has a high C_R but has a higher T_{VOL} than SGH. This shoulder drives most of the water to the infiltration slope and it takes a larger volume to moisture the shoulder. This is certainly due to its bare clay surface layer.
- SGL has the highest T_{VOL} value but the lowest C_R. It almost infiltrates all the available water A_W but it takes up to 20 mm to moisture the shoulder. This is certainly due to the presence of vegetation which intercepts the road runoff, consumes large amount of water, and favours the infiltration along its roots.
- SH has a very low $_{TVOL}$ value and an average $_{CR}$. The shoulder can retain only 5 mm and drives only 50% of the road runoff to the infiltration slope. The low $_{TVOL}$ is not a surprise because its volume is half occupied by the HMF. On the other hand, this complicated and expensive shoulder design shows one of the worst $_{CR}$.
- With no E_S value recorded, the shoulder SB has of course a C_R of 1[15]. T_{VOL} is not calculated (separation between the two domains does not exist).

It is interesting to see that, although E_S volumes in figure 3.13 come from different events, it also represents the evolution of E_S as a function of A_W during one single event (evolution of volumes). E_S indeed is the integral of Q_S; A_W the integral of Q_R (Q_S and Q_A being the flows exfiltrating the shoulder and arriving on the shoulder respectively). Therefore, the behaviours of the shoulders can be assessed dynamically: the increase of the exfiltrating volume ES as a function of the available water A_W. Then, T_{VOL} is the volume needed to moisturize the shoulder and C_R the runoff coefficient leading the volume fractionation.

3.4.3.2 Mathematical solution – Empirical solving - univariance

This solution allows inter- or extrapolation but is deterministic. It only gives R_S results for the data provided (R_R, P_S, E_S, ETP_S, ΔS) responding to the equation 3.2. As it has been explained in §3.3.2, the fraction x of the factor D_R is considered null (all the water precipitated on the road is included in R_R).

[14] The shoulder SB has shown no exfiltration E_S values.
[15] Remember that ETP and ΔS are neglected and that the C_R concerns uniquely the second part of the linear fit ($A_W > T_{VOL}$).

E_S and R_R values were previously calculated in the preceding §3.4.3.1. The stock variation ΔS and evapotranspiration ETP assessment use empirical equations. Results must not be considered as computing but good approximations. For this reason, no error calculations were made. The use of the meteorological factors to build the PMFAO is shown in detail in appendix VI. As anticipated, results (figure 3.14C) show a sinusoidal curve strongly bound up with seasons. Values range from nearly zero (December – January) to 2 – 2.5 mm in July – August (appendix VI).

API Values range from 0 to 120 mm in the shoulders and from 25 to 190 mm in the soils. Values are concordant with the examples found in the literature (Mermoud 1999) but are a bit lower. This can be explained considering the low RU constant (appendix VI), itself due to the low depth reached by the roots. The stock variation is calculated using the API estimations. Figure 3.14 shows the results. Values are ranging from -12 to 70 mm for the shoulders and from -4 to 80mm for the lysimeters. The effect of the precipitations on the API is clearly visible. The effect of the ETP on the stock variation, while existing, is far less important than the effect of the precipitation.

The values of R_S for the different shoulders are given by the equation 3.4. R_S values are shown in the figure 3.15. The average runoff coefficients C_R are given by the equation 3.11. Average C_R coefficients are listed in the table 3.3.

The SB runoff coefficient has been calculated subtracting only the stock variation ΔS and ETP to the available water A_W. As it is not based on field measurements, the number of available data is greater.

Figure 3.15 illustrates the fractionation of the available water A_W into the 4 identified water fluxes (R_S, E_S, ETP, ΔS) for all the shoulders. Altogether, the following comments can be made:

- Overall, all the shoulders behaved similarly. SB Showed no E_S.
- For low value of A_W, the ETP and ΔS have significant importance. ETP can count up to 50% of A_W, while ΔS can represent 80% of A_W.
- For higher values of A_W (A_W > 15-20mm), the sum of ETP and ΔS represent a maximum of 20%. The rest of A_W is divided between the R_S and E_S.
- Proportionally (left-hand diagrams), the shoulder runoff R_S reach maximum values at the same point where the ETP and ΔS reach their lowest percentages (i.e. $A_W \approx$ 15-20 mm). Below the A_W limit that separates these two different behaviours, R_S is greater than after this limit. This confirm the existence of the initial shoulder runoff R_{S*}.
- For higher values of A_W, R_S decreases again. This decreasing trend corresponds to the augmentation of the vertical hydraulic conductivity k in the shoulder (see §3.4.2 for insight). E_S percentage rises.
- Average R_S values are approximations. R_S percentages vary as a function of A_W.
- A few events have negative balances. This means that ETP + ΔS + I_S is greater than A_W. This is especially observed for low A_W values. This is mostly due to the calculation error, greater for the low volumes.

Table 3.3: Average C_R coefficients. SGL has the lowest coefficient, while SB has the highest. See text for discussion. The 2004 average C_R have been used to calibrate the empirical equation linking C_R and A. See §3.4.3.3.

	SGH	SGC	SGL	SH	SB
Nb of events	80	81	102	31	109
C_R [-]	0.57	0.61	0.36	0.63	0.89
C_R [-] 2004	0.52	0.64	0.45	-	0.87

Having a closer look on the different shoulders, the following remarks stand:

- SGH (80 events recorded): this shoulder has a moderate R_S average (57%). The influence of ETP and ΔS is variable (10 to 95%) for low A_W values and is stable (ETP + ΔS = 21%) for higher values of A_W. The limit is A_W = 10 mm. R_S does not decrease rapidly after that limit (from R_S average ≈ 76 to 48%).
- SGC (81 events recorded): S_R average is 62%. The influence of ETP and ΔS is appreciable (8 to 93%) until A_W = 12 mm. It then stabilizes (ETP + ΔS = 19%) for higher values of A_W. As for SGH, R_S does not decrease rapidly after the A_W limit (from R_S average ≈ 80 to 48%).

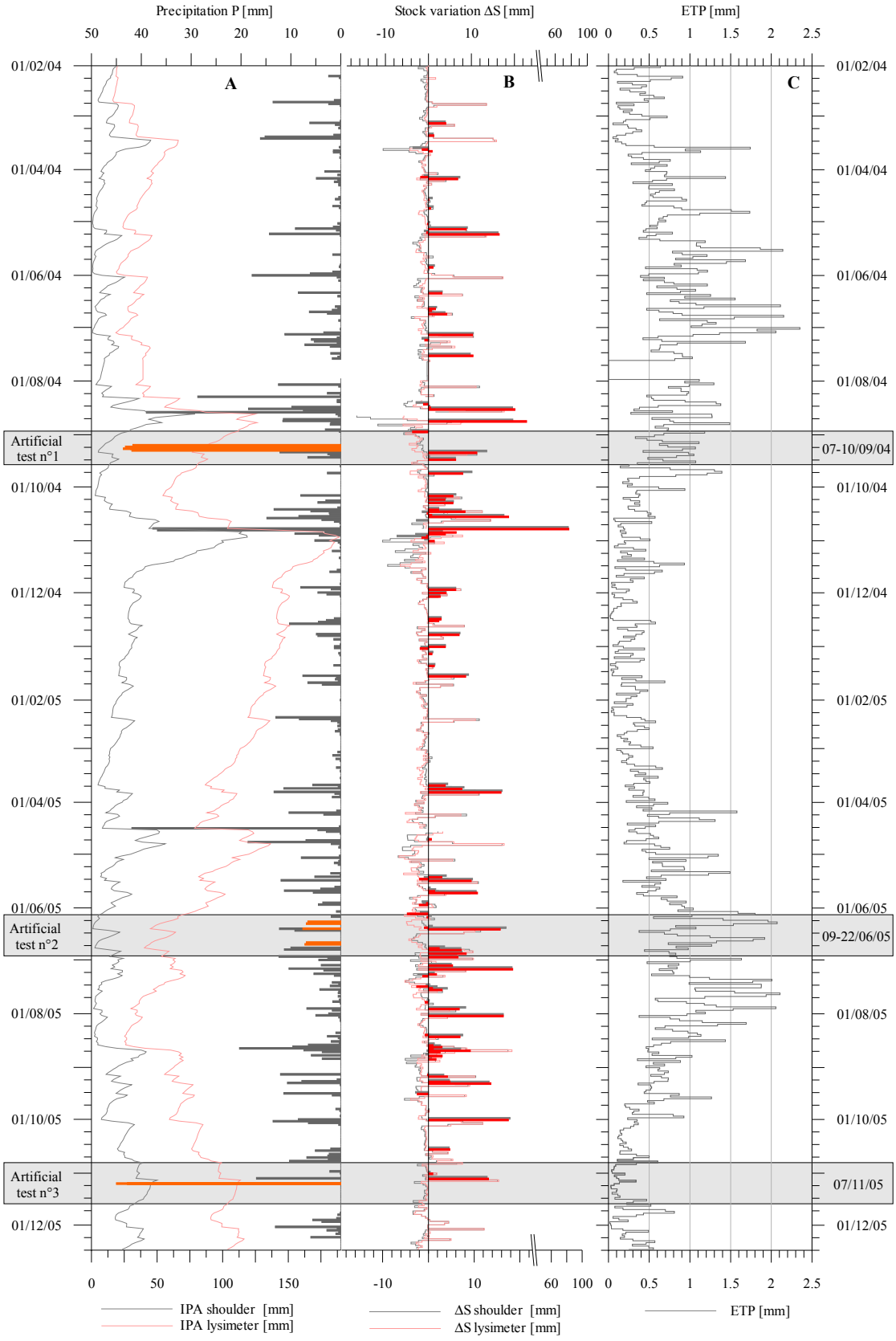

*The Figure 3.14: **A)** Precipitation (bar diagram) and API from shoulder and lysimeter (lines). The shoulder API is lower due to a high K_{API} and low RU (see appendix VI): the shoulder cannot retain water due to its permeability. Note the high correlation between P and API. **B)** Stock variations ΔS for the shoulder (grey) and for the lysimeter (red). Highlighted boxes show the ΔS for the specific events that have been recorded. Practically all events have a positive stock variation; it means a refill of the stock S. **C)** ETP curve. The curve is correlated to the seasons and thus shows a sinusoidal trend.*

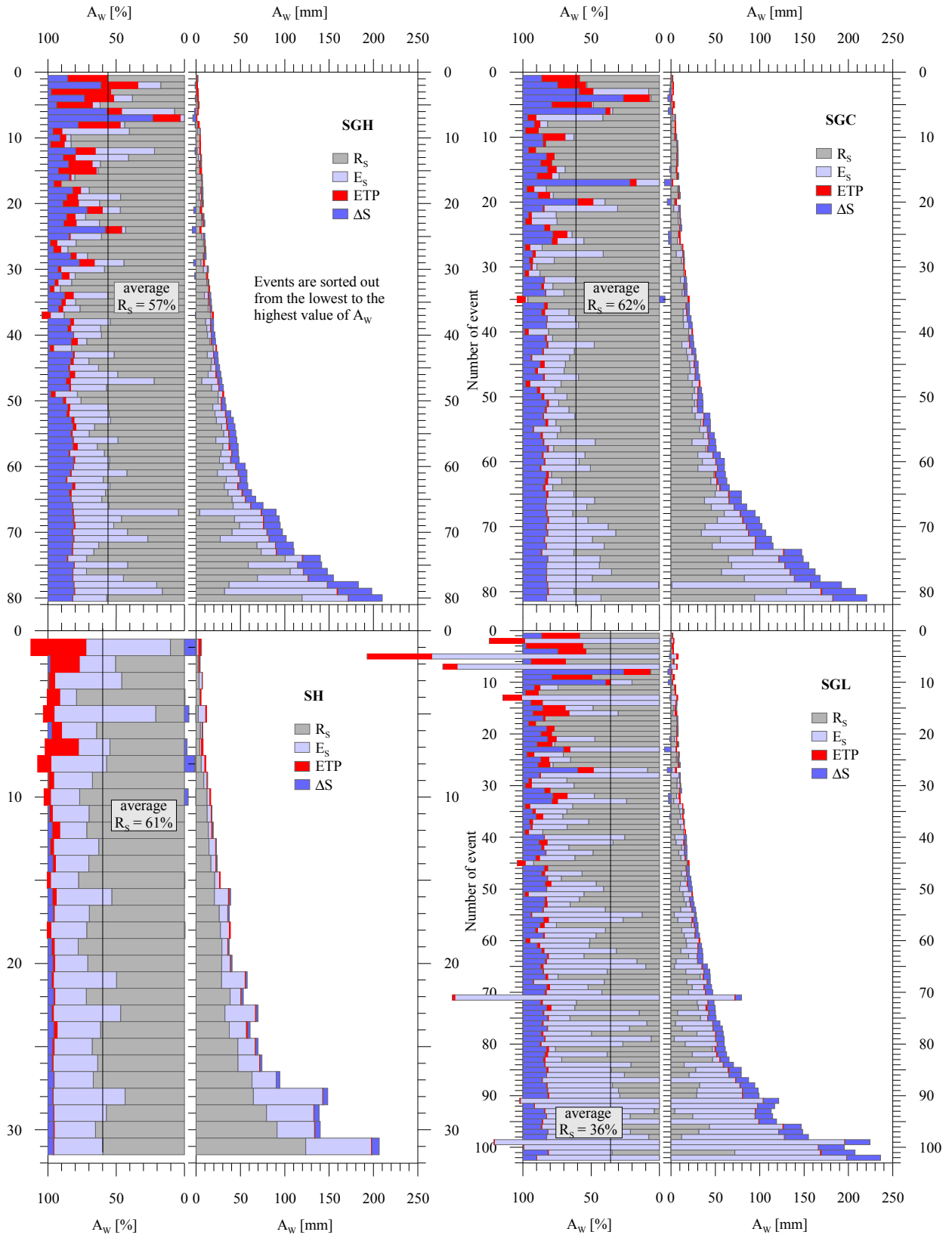

Figure 3.15: Global fractionation of the available water in all the shoulders. For each shoulder, the right-hand side bar diagrams are in absolute value [mm], left-hand side bar diagrams are in relative value [%].The relative importance of ETP and ΔS is bigger for small events (small A_W). For larger event, the ETP is insignificant while the stock variation seems to stabilize to a specific value. R_S and E_S vary as function of external factors (meteorology, etc.). The average shoulder runoff R_S is specified. Negative values are due to error on exfiltration E_S calculation (as specified in appendix V, the smaller E_S is, the grater the error is. See text for discussion.

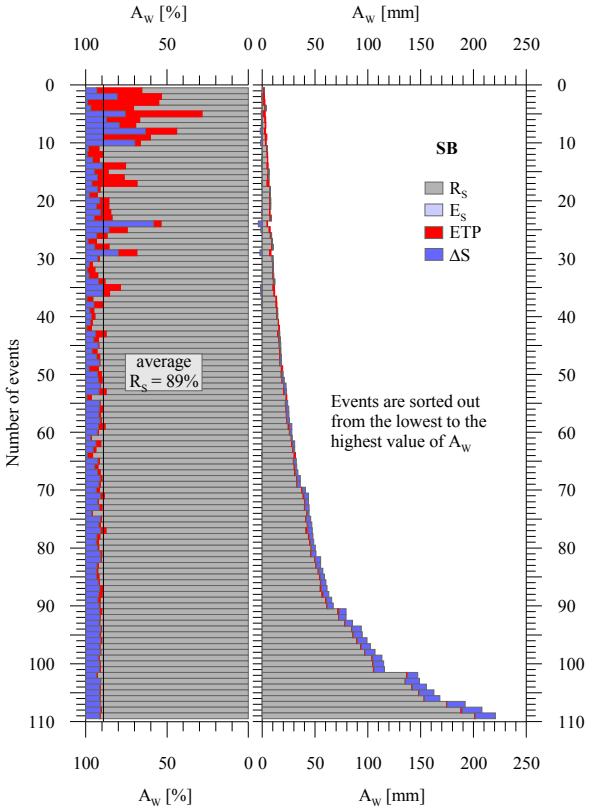

Figure 3.16: Global runoff fractionation for the SB shoulder. Remarks of figure 3.15 are applicable. See text for discussion.

- SGL (103 events recorded): S_R average is 36%. The influence of ETP and ΔS is far greater than for the other shoulders. The negative balances are mainly seen for this shoulder. The limit A_W = 11 mm separates the domain where ETP + ΔS varies (5 to 92%) from the domain where it stabilizes (ETP + ΔS = 19%). R_S average decreases more drastically than for the other shoulder (from R_S average ≈ 60 to 20%).
- SH (31 events recorded): R_S average is 61%. The influence of ETP and ΔS is less remarkable than for the other shoulders (this could be due to the smaller event population). Few negative balances occur in this shoulder. The influence of ETP and ΔS is variable (5 to 50%) but less important than in the other shoulder. This is because the potential stock is far lower than in the other shoulders (half of the shoulder thickness is used by the HMF with S = 0). The limit A_W = 13 mm separates the domain where ETP + ΔS varies and the domain where it is stable (ETP + ΔS = 8%). R_S average decreasing trend is nearly invisible.
- SB (110 events recorded): R_S average is 89%. No E_S values have ever been recorded from this shoulder. The influence of ETP and ΔS is appreciable (8 to 72%) until A_W = 16 mm. It then stabilizes (ETP + ΔS = 10%) for higher values of A_W. R_S represents the whole fraction that is not ETP or ΔS. It never decreases.

Processes that affect the E_S and R_S percentages are discussed in §3.3.1. It is evident that the runoff coefficient C_R is not a constant but a function of A_W. A comparison between the present results and results coming from the graphical analysis brings up these remarks:

- The threshold T_{VOL} is sensibly the same as the limit value where ETP and ΔS influences disappear. This value ranges from A_W = 5 to 20 mm. Extreme values are found in the graphical analysis. This is surely due to the imprecision of the method. In the numerical method, values range from 10 to 16 mm.
- Runoff coefficients range from 0.15 to 1. Again, the graphical analysis gives the wider range. Values for the numerical analysis fall between 0.36 and 0.89. Correspondences between the graphical and numerical analyses are very good.

	T_{VOL} [mm]		C_R [-]		**ETP + ΔS** [%]	
	Graphical	Numerical	Graphical	Numerical	Graphical	Numerical
SGH	13.0	10.0	0.60	0.57	cst	21
SGC	14.9	12.0	0.58	0.61	cst	19
SGL	20.0	11.0	0.15	0.36	cst	19
SH	5.0	13.0	0.49	0.63	cst	8
SB	-	16.0	1.00	0.89	cst	10

Table 3.4: Comparison between results coming from the graphical and numerical analyses (cst = constant with no determined value).

- The numerical analysis confirms that the initial shoulder runoff R_{S*} is proportionally greater than R_S. It is highlighted by the high R_S values for small events ($A_W < T_{VOL}$) and smaller R_S for large events ($A_W > T_{VOL}$). The R_S decreases when the shoulder is wet.

- In the graphical analysis, it is a good assumption to suppose that ETP and ΔS are constants for large events ($A_W > T_{VOL}$). They indeed conserve a constant proportion (5-20%) in the numerical analysis.

3.4.3.3 Assessment of an empirical relationship between A_W and C_R

Note that despite the fact that the previous figures (3.15 and to 3.16) show all measurements obtained during the present study, the data used to create and calibrate the following empirical equations come from 2004 only. Thus, the 2005 data have been used to test and validate the equations. The following paragraphs are therefore divided in three parts: editing, calibrating and testing the equation.

Equations edition

As for the graphical analysis, the equation has two different expressions. It depends if the input value A_W is greater or smaller than T_{VOL}:

Equ. 3.20a) *If* $A_W < T_{VOL}$ *then* $$C_R = a - \frac{b}{A_W}$$ *[mm]*

Equ. 3.20b) *If* $A_W > T_{VOL}$ *then* $$C_R = c - \frac{d}{A_W}$$ *[mm]*

(a, b, c and d are fitting factors. a; c Є[0;1], b < d. See "calibration" for explanation)

Has A_W could be difficult to assess, the following simplification can be made: $A_W \approx 5 \cdot P$[16] The equation 3.21 has been modified from equation 3.4:

Equ. 3.21a) $$R_S = A_W - E_S - ETP_S - \Delta S)$$ *[mm]*

(the stock variation is positive. Only few events have shown a negative variation)

Equ. 3.21b) $$R_S = (1 - x - y) \cdot A_W - ETP$$ *[mm]*

(E_S and ΔS are considered to be linear functions of A_W. This assumption is highly probable and has been suggested by the graphical and the numerical analyses: x is the ES fraction of A_W, y is the ΔS fraction of A_W)

Equ. 3.22a) $$C_R = (1 - x - y) - \frac{ETP}{A_W}$$ *[mm]*

(a = 1-x-y; a Є[0;1]; ETP = b; remind that as it is an empirical equation, ETP is a variable that is supposed to be unknown)

The same way, C_R for $A_W > T_{VOL}$ is calculated:

Equ. 3.22b) $$C_R = (1 - x) - \frac{ETP + \Delta S}{A_W}$$ *[mm]*

(c = 1-x; c Є[0;1]; ETP + ΔS = d; the same remark goes: ΔS is a variable that is supposed to be unknown)

[16] In case the road or shoulders have different surfaces from those found in Grandson, the factor s_R/s_S must be calculated.

ETP value is considered to always be a constant. E_S and ΔS vary if $A_W < T_{VOL}$. If $A_W > T_{VOL}$ then only E_S varies; ΔS is a constant (because the shoulder is nearly saturated). Figure 3.17 show the evolution of the different terms as function of the volume A_W.

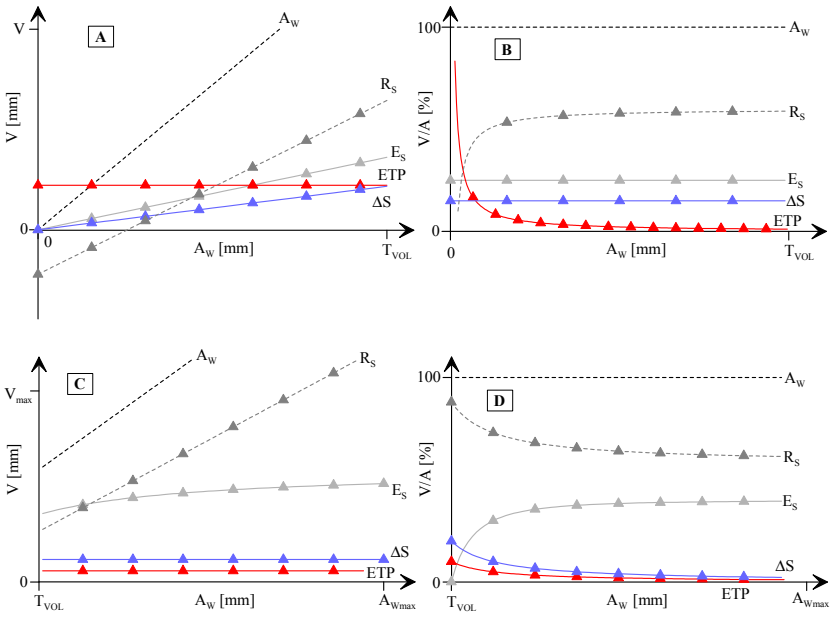

*Figure 3.17: **A)** Evolution of the volume as a function of A_W for $A_W < T_{VOL}$. Note that this graphic is empirical and do not reflect the physical reality (R_S cannot be negative). **B)** Same plot expressed in percent. R_S has then a 1/x trend. **C)** Evolution of the volume for $A_W > T_{VOL}$. ΔS is now considered as a constant because the shoulder is saturated (or nearly so). **D)** Same plot expressed in percent. R_S has a -1/x trend but the increase is very small.*

Calibration

Data from the 2004 have been used for the calibration. Table 3.5 shows a, b, c and d values for each shoulder. Calibrations have been made using a fitting software (Datafit 8.2 from Oakdale).

What is not really surprising in the results provided is that all d factors are negative. This means that the R_S value indeed decreases after the peak recorded at $A_W = T_{VOL}$. The explanation could be that the exfiltration volume E_S has a -1/x trend.

Verification

The figure 3.18 illustrates the C_R values for all shoulders. Red crosses represent the 2005 data. The 2005 data verify for each shoulder the good fits. It has also been plotted the C_R for 2005 for comparison purpose. It appears that each shoulder presents a significant C_R increase around the peak $A_W = T_{VOL}$. To the contrary, the C_R is slightly lower for high A_W values. Because all trends change similarly, it is postulated that the causes are meteorological factors and not aging. Aging would indeed have changed the behaviour of one or two shoulders, probably in different ways (see §3.4.3.5 for insight). This figure really emphasizes the good behaviour of the SB shoulder.

		Fit fact.	SGH	SGC	SGL	SH	SB
2004	$A_W < T_{VOL}$	a	0.65	0.70	0.51	-	0.91
		b	0.57	0.65	0.08	-	0.87
	$A_W > T_{VOL}$	c	0.50	0.58	0.26	-	0.91
		d	-2.20	-2.77	-5.36	-	-0.10
2005	$A_W < T_{VOL}$	a	0.77	0.85	0.66	0.90	1.03
		b	1.18	1.75	2.81	1.62	1.39
	$A_W > T_{VOL}$	c	0.46	0.38	-0.01	0.79	0.91
		d	-4.73	-5.95	-11.31	-0.84	-0.22

Table 3.5: fitting factors for each shoulder. 2004 data have been used for calibration whereas 2005 data have been used for verification. As there is a slight difference between the two set of fitting factors, the 2005 data fits have also been plotted in figure 3.18. The rise might be due to the aging.

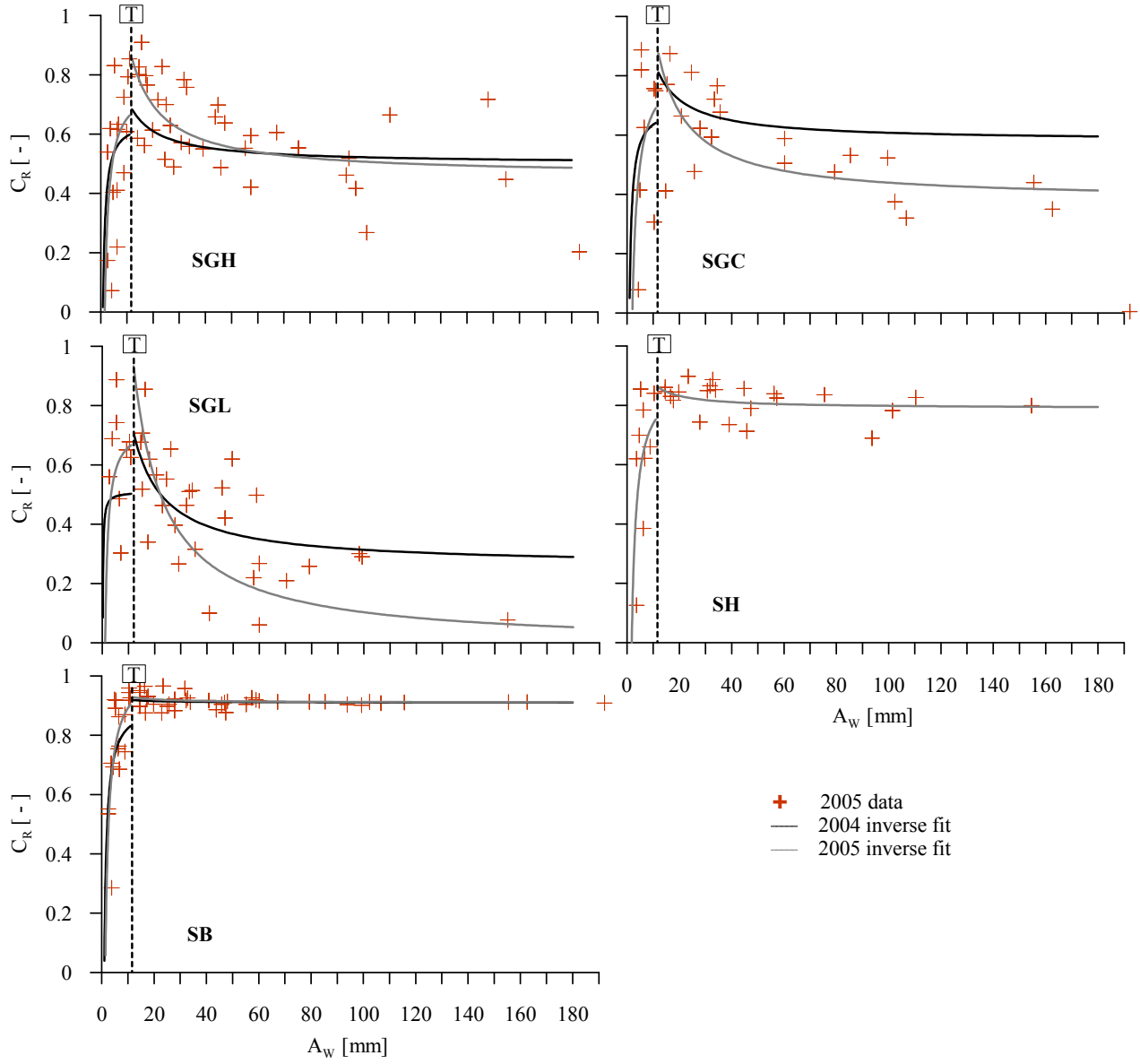

Figure 3.18: C_R factors for each shoulder. The 2 components equation 3.20a and b create a step at $A_W = T_{VOL}$. Black lines are regressive fits from 2004 data. Red crosses are 2005 data. Fits of SH and SB are excellent; fits of SGH and SGC are average; SGL fit is not convincing. For further interest, regression fits from 2005 data have also been plotted (grey lines). The C_R show a significant rise at $A_W = T_{VOL}$ and a fall at higher values (for SGC and SGL only). SH has no 2004 data.

Verification done, the equations 3.20a and b can be used to assess the runoff coefficient C_R for each shoulder with a good level of confidence. Particularly, the C_R for SB and SH can indeed be calculated with the empirical equations with a very high level of confidence. Moreover, results for those two shoulders validate the method and the equation form (a-b/x). The empirical equations can also be used for SGH and SGC but results will have a lower level of confidence. Concerning SGL, results could doubtfully be used to obtain more than a mere approximation.

Nevertheless, it must be kept in mind that all assessment results would only be empirical estimations. They indeed are function of A_W only. The various other parameters are not taken into account (like API, rain intensity, etc). The many variations of C_R that are not fully understood yet are doubtless governed by those very parameters.

3.4.3.4 Empirical solution – 3D-three parameter plots (R_R, Mean intensity, API) – multivariance - PCA

Because the previous empirical solutions were only varying along one axis (precipitation), they are not perfect. Even if results presented in the previous solution are good, construction of an empirical solution needs stronger determination. The solution presented here is therefore more complex. It includes statistical parameter assessment (linear and multi-variance), parameter descriptive assessment and 3D plots. The effect of each parameter on the infiltration and runoff processes are studied.

Parameter assessment

Many parameters are supposed to influence the runoff infiltration. Meteorological factors are the mean temperature (T), humidity (Hu), atmospheric pressure (QFF), wind speed (U) and solar radiation (Rn). These factors[17] are grouped into the API factor and are thus forcibly correlated to API (however complicated the existing correlation might be). Rainfall factors are the volume P, duration d, maximum and mean intensities I_{max} and I_{mean}, and finally the surface hardening due to the rain drops (*battage*) which cannot be numerically assessed: it is indistinctly comprised in the mean or maximum intensity. Seasonal factor is the date (season is hard to assess; days are transformed into numerical values, excel). Intrinsic factors represent the migration of fine particles, pores obstruction (with fine particles or pollutants), biologic perforation and traffic damage. Intrinsic factors cannot be measured but evaluated. Intrinsic and seasonal factors are referred to using the term “aging”. They indeed evolve with time. Values for the intrinsic factors are unknown. Only the date is used.

Therefore, 6 parameters (API, rainfall, duration, mean intensity, maximum intensity and date) influence to a certain extent the water infiltration through the shoulders. Statistical methods have been used to weigh up the possible interactions between them. These methods are linear correlation (parameter 1 versus parameter 2) and PCA (principal components analysis, multi-parameters). For description of these two methods, see “Introduction à la statistique”, Stephan Morgenthaler (1997); or any other statistic book. Brief explanations are made in annexe VIII.

The direct confrontation consists in finding any linear relationships between two parameters. The results are shown in appendix VIII. What is interesting is that the precipitations are correlated with the maximum intensities ($R = 0.6$) but not with the mean intensities. Thus, in case of a multi-parameter plot where rainfall is the main parameter, the mean intensity would be chosen over the maximum intensity to represent one of the axes. The resulting variance would indeed be greater. There is no other significant correlation observed: all other high correlation coefficient R^2 concern meteorological factors that are logically correlated (temperature and sunning; temperature and solar heat flux; humidity and sunning; humidity and solar heat flux; sunning and solar heat flux). All the meteorological parameters are grouped in the API factor and will not be considered further. API has no significant correlation with any of the other parameters (API with humidity $R^2 = 0.11$). Therefore, knowing that the rainfall and the maximum intensity are linearly linked, only 5 principal components might lead the infiltration process (API, rainfall, duration, mean intensity and date).

Remaining five parameters have been analysed using the macro XLStat software for Excel. For comparison purpose, all parameters have been plotted including the parameters already discarded (see appendix VIII). The figure 3.19 shows the PCA results. Surprisingly, the PCA shows that all parameters are regrouped in 4 main directions: The directions governed by the rainfall, the API, the mean intensity and the atmospheric pressure. The difference between this analysis and the one made for the direct correlation is that this one considers all parameters at the same time. It then standardizes the values using a standard matrix: values are standardized in regard of all other parameters and not only one. Therefore, new correlations appear that were invisible in the correlation matrix build for the previous statistical analysis.

[17] ETP is not used because it has a strong seasonal correlation which tends to disappear in the API. Moreover, API better reflects the shoulder tendency to have a high or low vertical hydraulic conductivity.

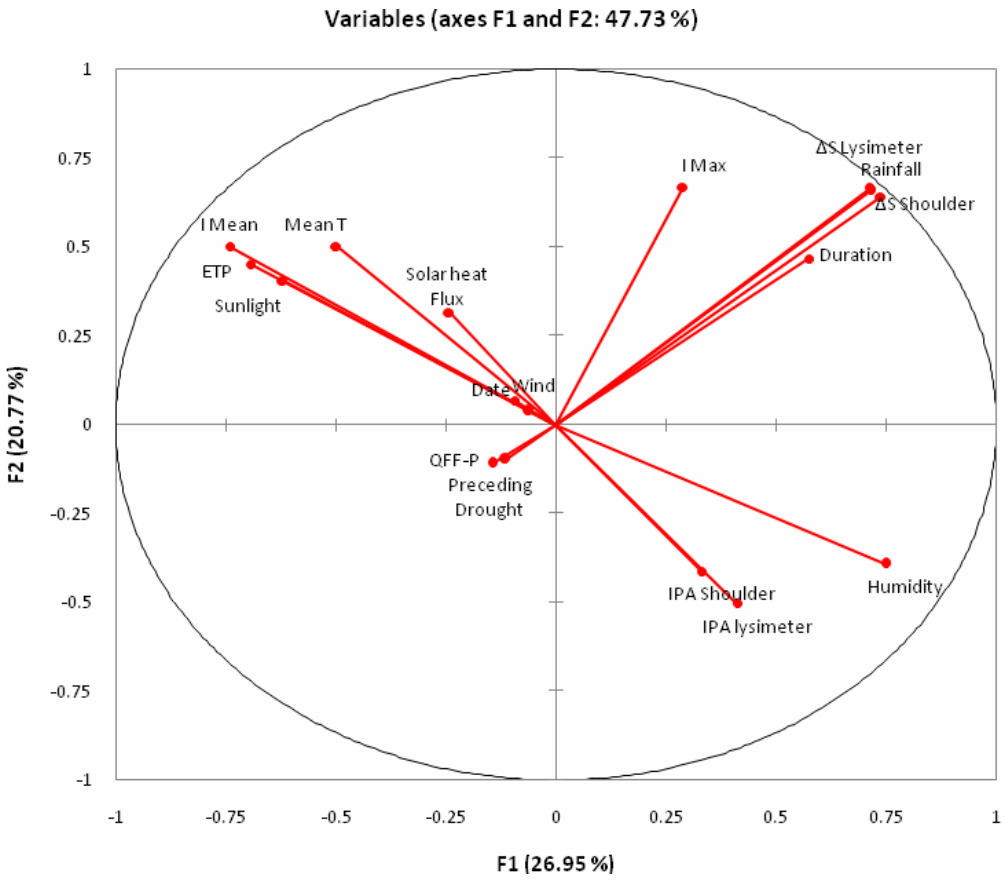

Figure 3.19: PCA plot. 112 data. Four main directions are remarkable: Rainfall P, API, mean intensity I_{mean} and atmospheric pressure QFF. Humidity and the maximum intensity I_{max} are slightly varying but nevertheless correlated to two other main directions.

Because the preceding drought is an observation measurement that is highly questionable[18] and the QFF is included in the API, the fourth axis can be discarded (A4, lower left, figure 3.19). Three main axes remain. For the present study, the parameters P, I_{mean} and API have been chosen.

The precipitation P has the lowest measurement error among the variables that belong to the first axis (A1, upper right). As it has been discussed in the previous §3.4.3.2, the stock variation is highly correlated with the precipitation P. I_{max} is indeed correlated with P. The duration is correlated as well, which is logical and instinctively sensed. As it has been explained before, $A_W \approx 5 \cdot P$ is used instead of P. It is more representative of the reality.

The second leading axis A2 (upper left) regroups all the meteorological factors (but humidity and QFF), the aging (date) and the mean intensity. The mean intensity has been chosen for two reasons: 1) the meteorological factors are all included in the API calculation and 2) the mean intensity assesses the rain hyetogram form (skewness, etc.). The aging vector has the same direction but its weight is far too low.

Finally, the third axis A3 (lower right) is essentially composed of the API. The humidity seems to also be a good candidate for this axis: it is predictably correlated with API. The API has been chosen because it includes all meteorological factors.

[18] Observation were made counting the number of day without rain preceding the concerned event; as rainfall were not all recorded, the count is not outstandingly precise.

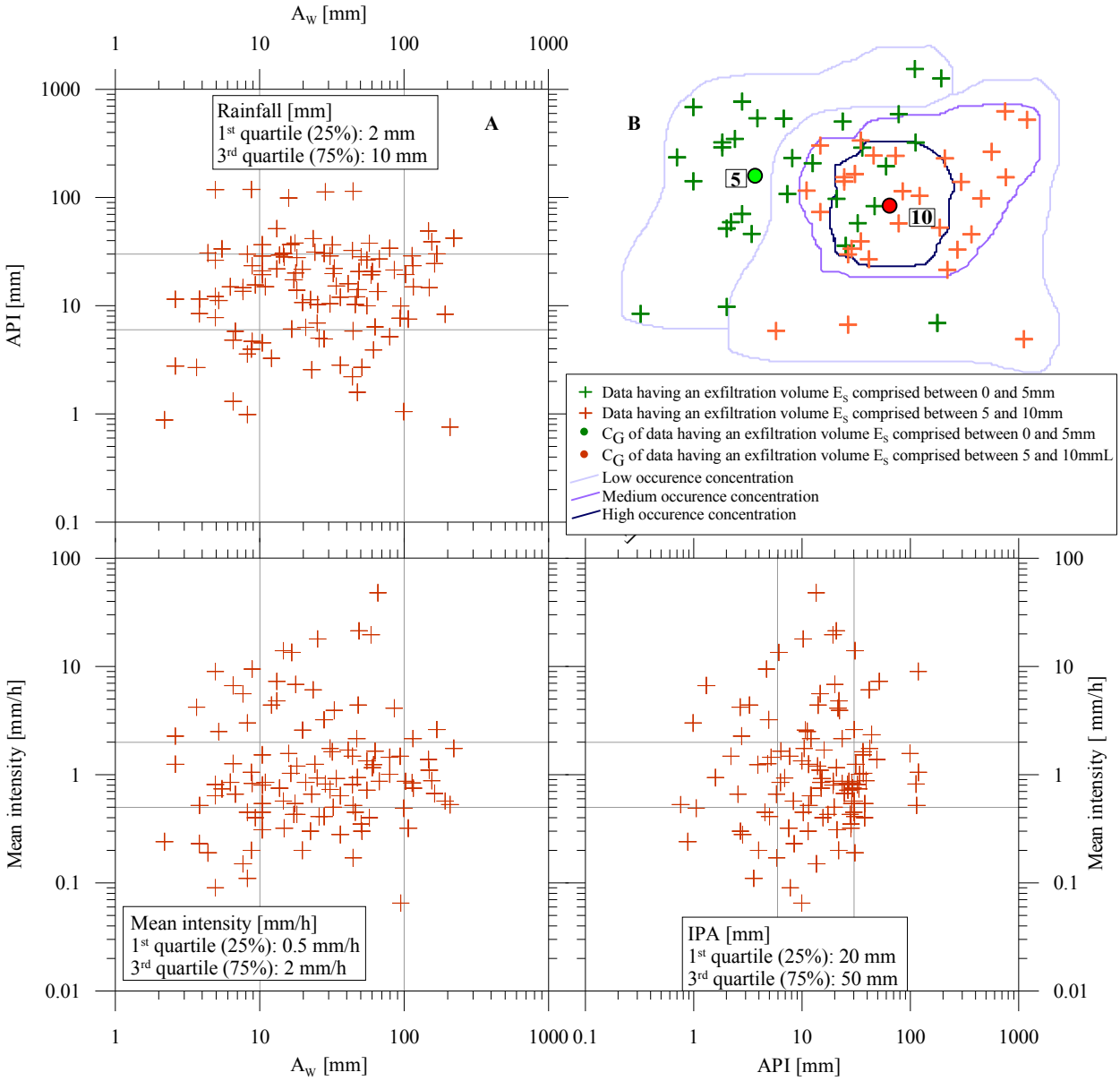

Figure 3.20: ***A)*** *2D projections of the 3D plot. All events are comprised within the domain built by only three parameters out of thirteen (see PCA). Axes are on the log10 scale. The data cloud is well distributed and confirms the axes and scale choices. 25 and 75% quartile separations build 27 different small cubes that have significant physical meanings: they separate the thunderstorm-type event from the winter-type, for example. Fifty percent quartile does not appear on the figure. Axes values corresponding to the quartiles are also shown in the legend boxes.* ***B)*** *Procedure employed to calculate the centres of gravity C_G for a given interval. For example, the interval "exfiltration of 0 to 5 mm" is represented by a boxed "5". The interval 5-10 is represented by a boxed "10" and so on. C_G are weighted centres of gravity and not geometric averages, i.e. centres of the occurrence concentration contours.*

Therefore, the 3D empirical model has the axes A_W, I_{mean} and API. The statistical analysis of those three parameters shows that events are log-normally distributed (asymmetric Gaussian). The axes scales are therefore not linear but log10 (figure VIII.2, appendix VIII). As all events must be comprised within the domain definite by the three axes A1 to A3, there must be extreme events, i.e. events that are placed at ends of the axes. A thunderstorm is for example placed at the far end of the I_{mean} axis with small A_W and API values. To the contrary, a long winter event will have high A_W and API values, and low I_{mean} value. Description of the lognormal distribution thus permits to give significant physical meaning to the 3D plots. Separations within the domain constructed by the three A1 to A3 axes

would therefore represent separations between real natural event types. The separation placements are calculated using the lognormal distribution (see appendix VIII). Separations are placed at 25, 50 and 75% quartiles.

The figure 3.20A shows the resulting 3D plot. For visualisation purpose, it is projected into three 2D plots. Results show a well distributed cloud of data centred on the 50% quartile of each axis. The data cloud is thus spherical.

Gravity centres C_G are the weighted[19] centres of gravity of a surface defined by data bracketed in a given interval. For example, the C_G "5" is the weighted C_G of the surface delimited by all data having an E_S of 0 to 5 mm. Method is graphically illustrated in figure 3.20B. Gravity centres of each surface area have been calculated using Surfer 8 (Golden Software). The principle is to count the number of points included in a definite radius around each data point. Thus, a percentage value can be attributed to each point. Surfaces are then automatically contoured. C_G are helpful to see the global evolution trend of exfiltration volumes E_S and E_L but also lag times (same principle, the boxed number represent the lag time interval) and seasons.

Projections of all events on the three 2D graphics can be discriminated using different type of data set (R_S, E_S, date, lag time). The discrimination consists in sorting out the data in different discreet sets of value (for example: set1 E_S Є (0;10) [mm]; set2 E_S Є (10;20); etc.). Plotting the different sets one after another in the 3D diagram shows the evolution of E_S (for example) as a function of A_W, API and I_{mean}. In a larger sense, this allows understanding the behaviour of the considered data set as a function of the three selected parameters. The most pertinent data set would be R_S. Unfortunately, as the API and available water A_W values are used to calculate R_S but not I_{mean}, results would be wrongly affected (A_W and API are axes of the 3D diagram). Note that the present empirical solution is independent from the two presented before (graphical and mathematical analyses); the results provided by the other empirical solutions can therefore not be used. The chosen data set are those that are not correlated with the axes nor calculated using one of the axes label:

- The seasonal change can be assessed separating the data in 4 different discreet season sets for each year (creating 8 new data sets) and compared. The weather change between 2004 and 2005 can thus be assessed.
- The exfiltration E_S is measured using the weirs. It is not linked to the API or A_W by calculation. R_S can be calculated afterward.
- The lag time, i.e. the time needed for the precipitated water to reach the exfiltration point under the shoulder, was also measured. Because lag time should not have any effect on the water balance, specific processes are discussed in §3.4.2.2 which concerns the dynamic of the infiltration.

Only final results are shown here; 3D diagrams needed to build the final figure are shown in appendix VIII.

3.4.3.5 Seasonal discrimination

Seasonal discrimination is rather hard to assess. It indeed depends on the transformation of lists of data into discreet sets of data. For simplicity, equinoxes dates have been used as discreet set limits (21th of March, June, September and December). Results are provided in figure 3.23. Each coloured increment represents a season. Note that the seasons of 2004 and 2005 are plotted together in the coloured areas. Only centres of gravity, noted C_G, represent discriminated seasons and years.

Evolutions of A_W, I_{mean} and API as function of season are clearly visible. For example, in the $A_W - I_{mean}$ face, winter is confined to the lower left quartile while summer is represented in the upper centre quartile. Spring and autumn are in-between. Yellow and green dots are the gravity centres of the 2004 and respectively 2005 events.

The shift between the 2004 and 2005 weather is somewhat important. It must not be forgotten that the scales are logarithmic. Overall, the year 2005 was appreciably rainier than 2004: higher volume A_W and API. Summer, to the contrary, has a lower A_W in 2005 than in 2004. It nevertheless was wetter in 2005. Concerning the I_{mean}, summer and

[19] And not the geometrical centre of gravity which is the centre of the surface.

winter show higher values in 2005 while autumn and spring have higher values in 2004. It is thus not surprising that the runoff coefficient C_R had varied between 2004 and 2005 (§3.4.3.3). As the year 2005 was wetter, it is perfectly normal to see a lower mean C_R coefficient.

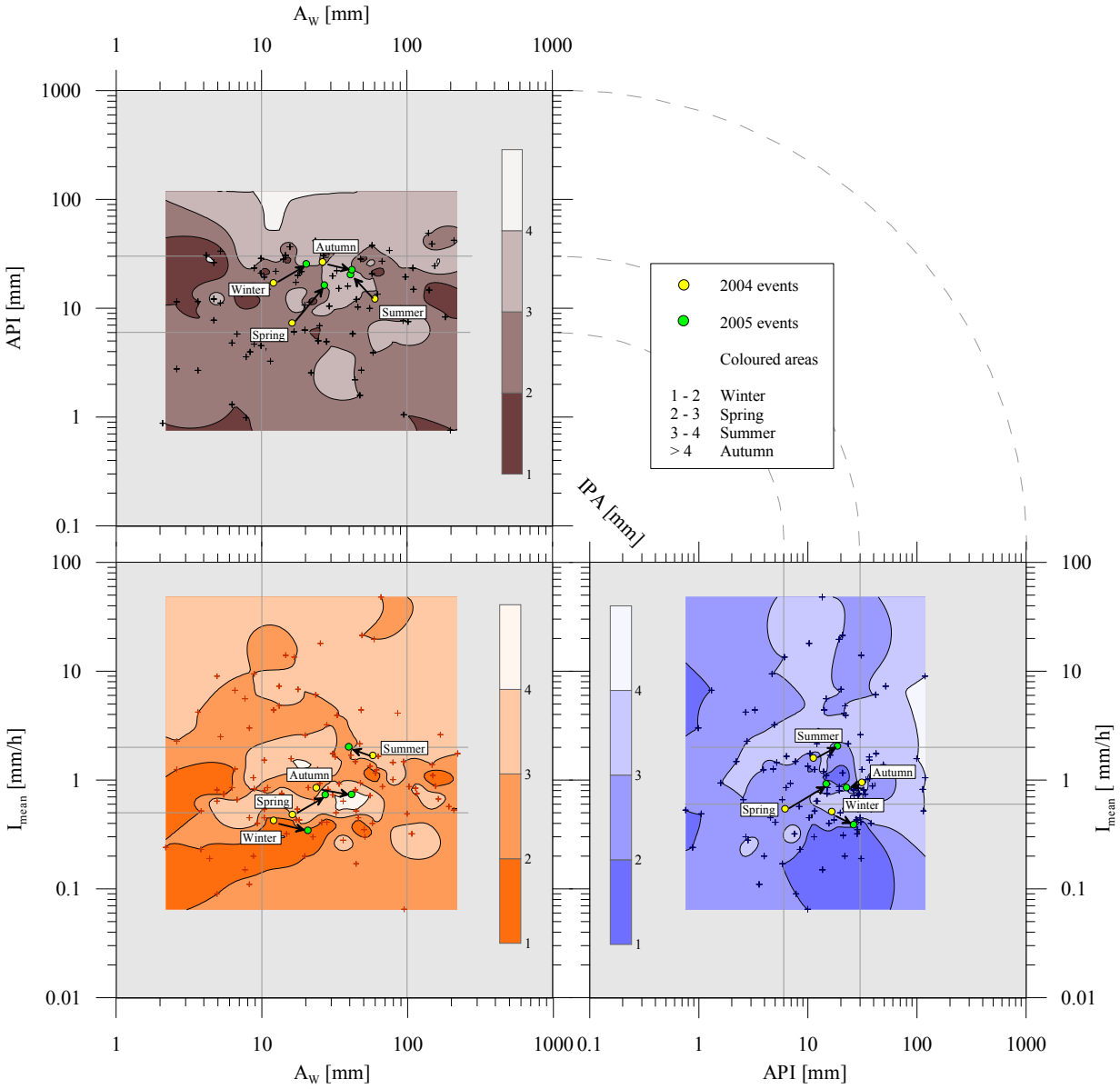

Figure 3.21: Seasonal discrimination. Evolutions of A_W, I_{mean} and API as function of the season are evident and logical. Moreover, the four seasons show a slight difference between 2004 and 2005. The year 2005 was overall more rainy than 2004. Only summer presents a dryer weather. API says that the soils were also wetter in 2005.

3.4.3.6 Discrimination based on the exfiltration values

The exfiltration discrimination is based on the discreet sorting of the event using the E_S data. The intervals are 10 mm increments (0;10) (10;20) (20;30) etc.. Thus the evolution of E_S can be assessed as a function of A_W, API and I_{mean}. The figures 3.22 show the results for SGH. To avoid repetition and tedious readings, the results concerning SGC, SGL and SH are extensively exposed in appendix VIII. SB cannot be represented in the 3D diagram because no E_S value was recorded. Coloured areas include events which E_S correspond to the discreet interval specified. For

example, the coloured area (0;10) regroups all the events with exfiltration values E_S comprised between zero and ten mm. Concerning the results, the following remarks stand (example of SGH):

- SGH: the C_G of the first interval (0; 5mm) is pretty much on the 25% A_W and 50% I_{mean} quartiles, and between the 25 and 50% API quartile. The C_G of the last interval (70; 130 mm) is well beyond the 75% A_W quartile, nearly on the 25% I_{mean} quartile and below the 25% API quartile. The C_G of value E_S evolves, not surprisingly, from lower toward higher values of A_W (from 10 to 130 mm). In other term, the more it rains, the higher the exfiltration volume is. The evolution is neat and undisputable. E_S show some variation along API: there is an important rise of E_S along API. This means that if the shoulder is wet, it let pass more water through. The last interval C_G might be due to erratic values because the E_S upward trend is significant. Finally, the evolution of E_S along the I_{mean} axis is more erratic. It seems that, although I_{mean} composes the third PCA main direction, it has no influence on E_S. Still, a small E_S shift is observable from higher to lower values of I_{mean}. Remember that high I_{mean} value is synonym with thunderstorm and low value represents longer, winter-like events. SGH is thus more retentive during thunderstorm. Concerning the coloured surface areas, the shift along A_W is clearly visible as well as the small shift along I_{mean} (lower right of the orange XY plan). To the contrary, the YZ blue plan shows no particular trend.

Considering the general behaviour of SGH, it is more retentive when the rainfall event is small, thunderstorm-like and when the shoulder is dry. On the contrary, its behaviour is worse when the rainfall event is large, last longer and when the shoulder is wet. This is a typical behaviour.

In general, the behaviour of SGC is the same as SGH (see appendix VIII). Small discrepancies are the API influence (SGC is practically not influenced) and the absolute E_S values observed. C_G are placed at higher values of A_W, meaning that the exfiltration only begins when the available water on the shoulder is greater than the amount needed for SGH. This amount of water is the threshold T_{VOL}. SGL behaves more like SGH than SGC. It is indeed lightly influenced by the API and the C_G positioning is pretty much the same. Finally, SH shoulder behaves the same way the other shoulders do. It is nevertheless more dependent on the API variations. This might be due to the presence of the HMF layer.

Overall, all shoulders have the same comportments (based on the exfiltration volume assessment): The exfiltration augments in relation with A_W: they are more water retentive when the rainfall event is small (i.e. the A_W volume is small). Also, shoulders are more retentive when the shoulder is dry. However, the advantages of the dry shoulder quickly disappear. The effect of the rain mean intensity is almost zero.

Parameters that have an influence (or supposedly so) on the runoff fractionation, i.e. on the fraction of the available water A_W that exfiltrates the shoulder, have been analysed. Most of them have been discarded using statistical analysis. It remained only three different directions of variance that are A_W, API and I_{mean}. 3D-plot projections showed that, although the three selected axes are not correlated one with another and supposedly lead the shoulder behaviours, only the available water A_W really has some influence on the exfiltration volume E_S. E_S can thus be expressed as a function of A_W. ETP is a function of the meteorological factors and is thus independent of A_W. The stock variation is supposedly linked to A_W, but nothing in the present 3D assessment proves or denies this fact.

Therefore, the equations designed in §3.4.3.3 are still valid. No further modification is suggested by the 3D multi-variances analysis. The most pertinent result of this empirical solution is that the exfiltration values depend only on the available water at the surface of the shoulder A_W. Moreover, this method helped to collect precious information that are discussed in §3.4.3.5.

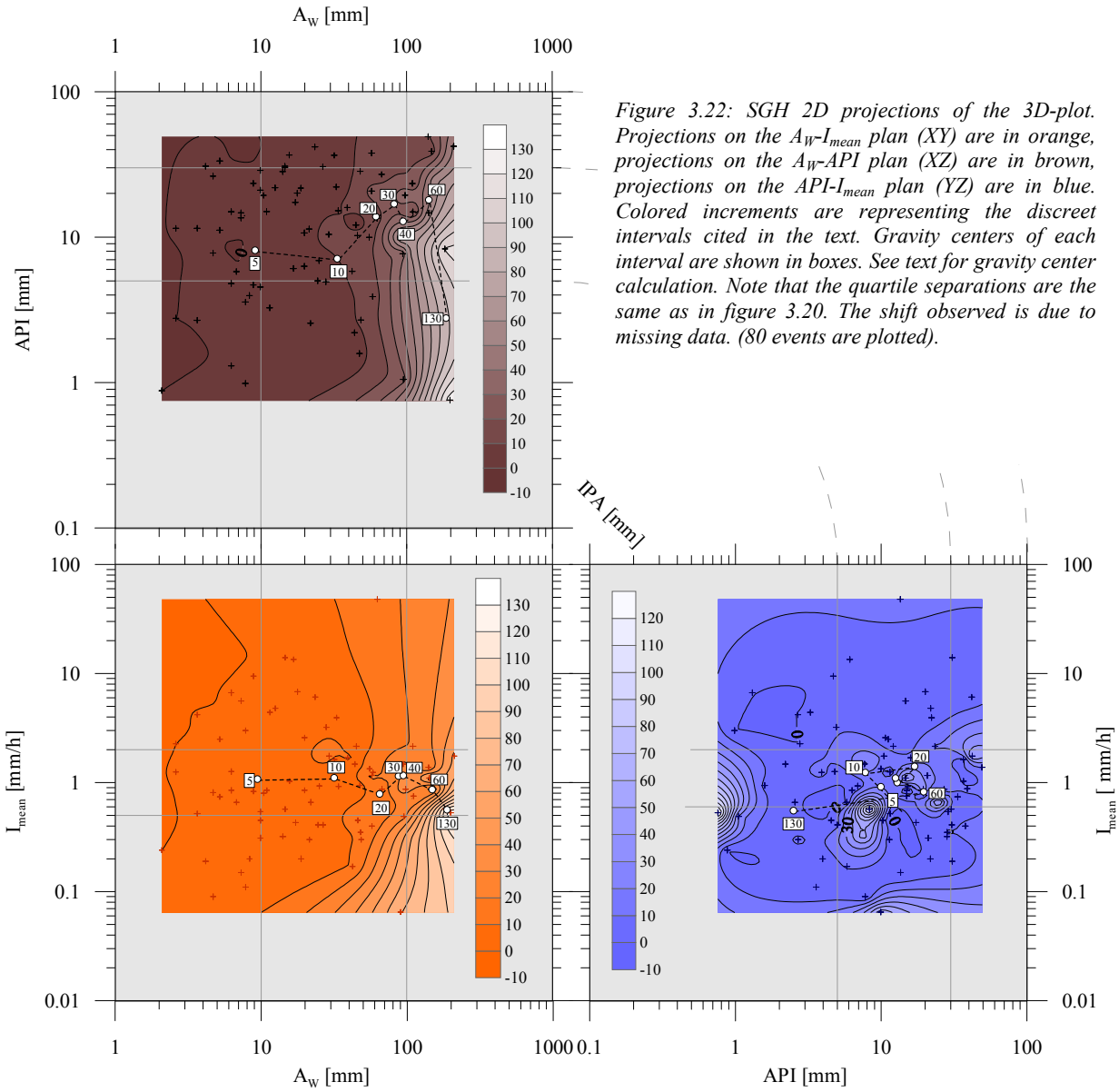

Figure 3.22: SGH 2D projections of the 3D-plot. Projections on the A_W-I_{mean} plan (XY) are in orange, projections on the A_W-API plan (XZ) are in brown, projections on the API-I_{mean} plan (YZ) are in blue. Colored increments are representing the discreet intervals cited in the text. Gravity centers of each interval are shown in boxes. See text for gravity center calculation. Note that the quartile separations are the same as in figure 3.20. The shift observed is due to missing data. (80 events are plotted).

3.4.3.7 Lag time discrimination

The same way, the lag times have been studied. Values have been corrected to take into account the runoff travel duration over the road and in the pipes. The correction consists in subtracting the lag time recorded for the road runoff (R_R). Thus, lag time values give only the transit duration during which the water goes through the shoulder. Because the lag time discrimination is not part of the water balance, only the results are discussed here. Precision about the lag time are made in chapter §3.4.2 which concerns the dynamic of the processes. Figures are in appendix VIII.

Results concerning the shoulder SGL present a strong correlation between the lag time and the precipitation mean intensity (figure 3.23B). For a precipitation which intensity is less than 0.2 $mm \cdot h^{-1}$, a lag time greater than 10 hours is expected, while for precipitation which intensity is greater than 5 $mm \cdot h^{-1}$, the expected lag time is below 30 minutes (see for example the artificial rainfall n°1). The maximum recorded lag time concerning SGL is 580 minutes. As the precipitation intensity is connected to the event type, it is now well determined that a thunderstorm runoff (high intensity) might infiltrate much faster than a long, winter-looking event. Thunderstorms are thus jeopardizing the road bearing capacity in a worse way than longer event. Moreover, the amount of substances carried by the

thunderstorm runoff is expected to be higher: longer deposition time with no rain, faster acceleration of the runoff, first-flush effect, etc. Those facts are presented in detail in chapter 4.

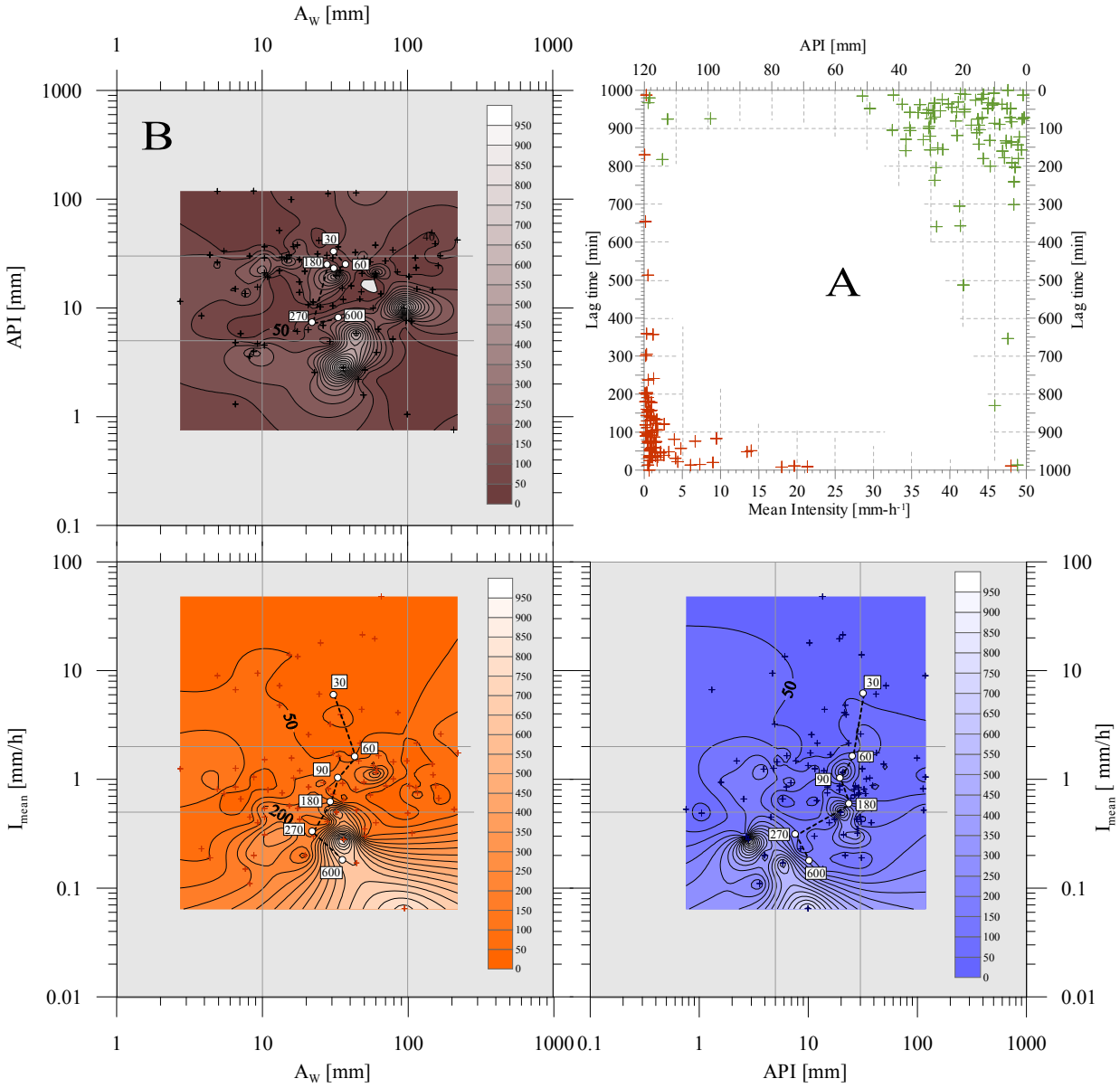

*Figure 3.23: Lag time evolution in the SGL. **A)** 2D-plot of lag times as function of the mean intensity and API. In both cases, data are confined in an envelope having a first order inverse polynomial trend. See text for discussion. **B)** The lag time is strongly correlated with the precipitation intensity. The higher the intensity of the precipitation is, the shorter the lag time lasts. For a rainfall intensity greater than 5 mm·h^{-1}, the lag time is systematically shorter than 30 minutes. On the other hand, the lag time seems to be also influenced by the API, although it is less clear than for the intensity. Lag times nevertheless augments if the API is low. Boxes with number represent the gravity centre of the considered lag times ([90] is for example the gravity centre of the 60 – 90 minutes lag times). Isograds are calculated using the kriging (linear) method, Surfer (Golden Software).*

In a modest way, also API is influencing lag times. This influence is of course obvious: the dryer the shoulder is, the longer it takes to moisturize the shoulder. Nevertheless, 3D-plots show that the influence of API is at the same time less evident and less efficient that the rainfall intensity. This is symptomatic of a material having poor retention capacity (low suction, see §3.5.2.2). Indeed, in the case shoulders had higher stock capacities, it is well clear that the API would have a greater influence.

Plotting lag times against API or I_{mean} (figure 3.23A), data seem to be confined within an envelope respecting a first order inverse polynomial[20]. Computation of the return period of lag times needs a more exhaustive database with many years of study. At best it could be expected that return periods are the same for precipitations and lag times but this assumption requires verification.

Overall, all shoulders present the same behaviour (appendix VIII): a strong correlation between lag times and the precipitation intensity and a somewhat less pertinent correlation between lag times and API. The stronger the rainfall is, the shorter the lag time is. The dryer the shoulder is, the longer the lag time is.

3.5 INFILTRATION SLOPE

For reminder, the infiltration slope is composed of 2 horizons A and B. Description of those 2 horizons are available in chapter 2. Three compartments (SGL-LW; SH-LH and SB-LB) have an infiltration slope bordering the shoulder. The two first compartments have lysimeters, i.e. infiltration slope overlaying a geomembrane designed to collect the exfiltrating water. The last compartment has an infiltration slope conducting directly to the aquifer. It is commonly called the unsaturated zone UZ.

3.5.1 LYSIMETER FLUXES BALANCE (fig. 3.24)

The lysimeter flux balance is practically the same as the shoulder flux balance. The difference is that the fluxes cannot be considered as vertical only. The Darcy's Law has to be taken in its full version as well as the Continuity Law (appendix IV). Moreover, the presences of two layers (horizon A and B) and the impermeable geomembrane (case of the lysimeters) or the embankment (case of the UZ) make the assessment even more complicated. This can only be solved with numerical applications.

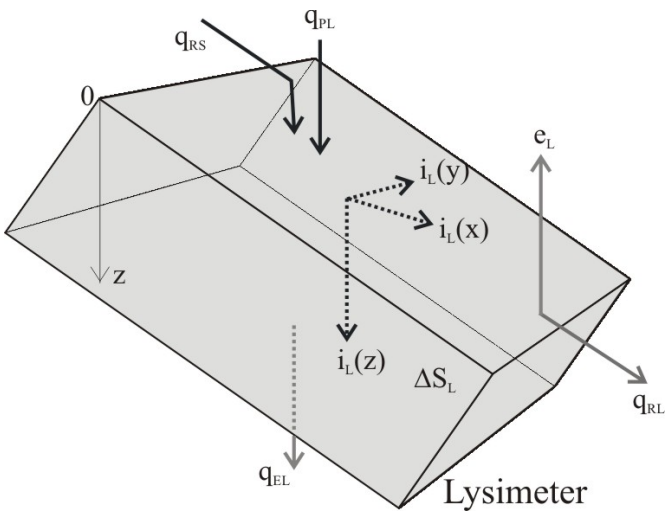

Figure 3.24: Lysimeter fluxes balance. The infiltration component is three-dimensional. The flux q_{RL} is supposed to be zero, but this has to be verified. Incoming fluxes are in black, outgoing fluxes are in grey.

3.5.2 ANALYTICAL APPROACH

3.5.2.1 Lysimeter LW

Two lysimeters border the shoulders SGL and SH, named respectively LW and LH. In the present paragraph, only results concerning the lysimeter LW are presented because TDR probes were installed in that lysimeter. As previously mentioned in the paragraph 3.4 "Shoulders", fluxes presentation and interpretation also include the fluxes in the shoulder. Indeed, it is impossible to separately treat fluxes existing in the shoulder and soils. SGL Results concerning the LH are shown in appendix IV. First, global processes are explained in regard to the artificial infiltration test n°1. Second, fluxes are described using the example of a natural event (4th of November 2005) and therefore take into account the natural rainfall falling directly over the lysimeter.

Figure 3.25 presents the main response of LW during the artificial test n°1. The description of the processes follows the same points A-D as in the shoulder paragraph:

[20] y=a+b/x: which is also the formulation of the return periods, IDF plots, §3.2 "Precipitations".

A) The lag time is 39 minutes. This time is needed for the water to run over the shoulder, moisturize the soil surface and propagate downward. The propagation of the moisturizing front is illustrated and explained using the example of the natural event of November, the 4th 2005 (§3.5.2.2). When the lysimeter begins to exfiltrate, already 1870 litres have been poured onto the road.

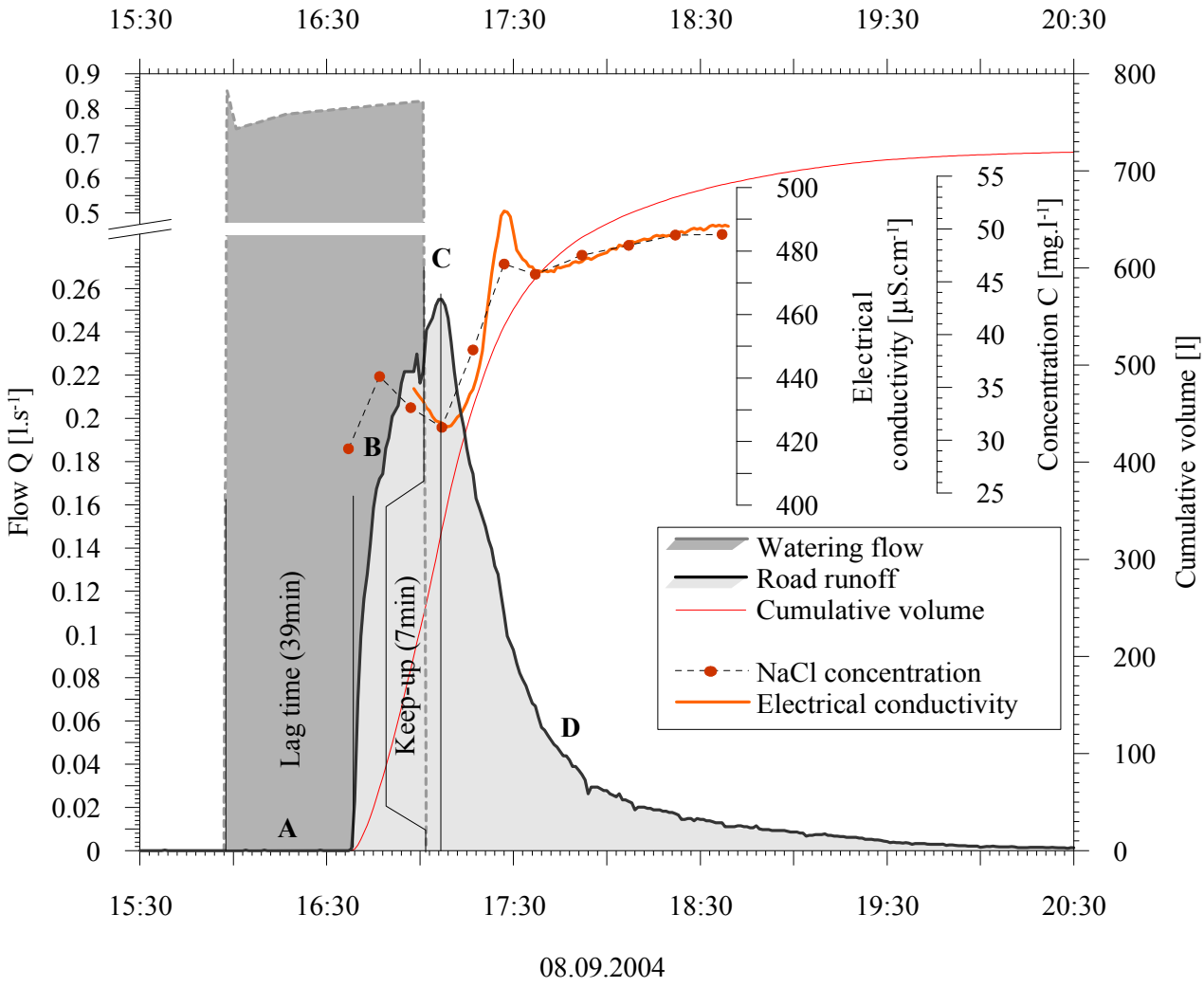

*Figure 3.25: Illustration of the lysimeter LW. **A)** The lag time is logically much greater than for a shoulder. This is the time needed for the road runoff to flow over the shoulder and infiltrate the lysimeter. **B)** The flow increases not linearly. This is due to strong suction. **C)** The keep-up interval (time during the flow Q still increases) is due to a piston effect. The keep-up is the time between the end of the watering and the beginning of the flow decrease. During this time, the flow continues to increase. **D)** The decrease is logically logarithmic. The more the lysimeter dries, the higher the suction is. The Cl^- concentration curve shows 3 distinct peaks, correlated with the EC. The first peak is due to a strong piston effect. This peak is indeed not the highest concentration recorded during this artificial event.*

B) The augmentation of Q along the time is clearly not linear: it presents a very steep slope which flattens progressively. The progression of Q strongly suggests that 1) a strong piston effect exists and 2) the suction has a great influence. Indeed, the slope q' at the beginning of the event is so steep it is almost impossible to consider it as a progressive increase: the water comes at once. The piston hypothesis is strongly supported by the Cl^- concentration curve which shows a first peak at that moment. The progression is very regular (but for an indentation). The maximum flow reached is 0.26 litres per second. The inverse logarithmic shape of the Q curve implies a diminution of the hydraulic head gradient compensating and overtaking the augmentation of K(θ) along the time. The indentation which breaks the curve perfect shape has little interpretation. It is

possibly the transition between the water already stocked in the soils and the water coming from the shoulder runoff. It indeed almost coincides with the minimum peak of Cl^-. The indentation has also been noted in the LH Q flow, just previous to the end of the watering.

C) The exfiltration flow still increases for a while after the end of the watering. This is due to the water still moisturizing the soil and progressing. It indeed keeps a high hydraulic head gradient and an increasing K(θ). This is called the keep-up and lasts 7 minutes. It stops abruptly and causes a rapid decrease of the flow. The flow peak coincides with the chlorine minimum value.

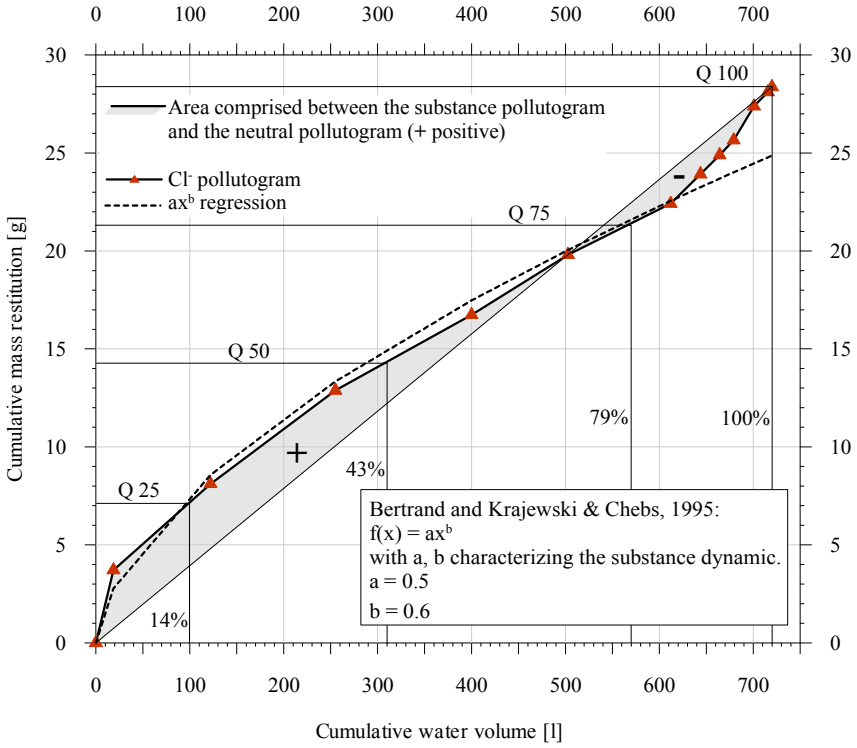

Figure 3.26: LW pollutogram. The first flush effect is modest, inversing at the end of the event. This positive - negative trend is symptomatic of a chlorine depletion between 35 and 84% of the water cumulated volume.

D) In comparison with the shoulder processes, the flow decreases less rapidly. The suction indeed has a stronger influence in the soils than in the gravel composing the shoulders. The water is thus better retained in the porosity. It is also highly probable that the difference between the macro and microporosity is smaller than in the gravel composing the shoulders; maybe comparable to the SGC. During this decrease, the chlorine concentration rises two times. First, immediately after the flow peak it rises to 47 $mg \cdot l^{-1}$ and secondly, after a break, to 50 $mg \cdot l^{-1}$. Those two peaks are likely due to the draining of the primary and secondary porosities. As the concentrations are almost the same in both cases, it is expected that the chlorine fractionation between those two porosities is even. The shape of those peaks indicates that the buffer effect is nearly null in the macroporosity and high in the microporosity.

The resulting pollutogram (figure 3.26) is showing a small first flush effect followed by a chlorine depletion, and finally a new increase at the end of the event. The change in pollutive dynamic is due to the different flowing paths followed by the infiltrating water.

The soils have a higher available stock than the shoulder, relatively to their volumes. Once watered upon, the soil infiltrate the fresh water which pushes the old water downward (piston effect) with its content (substances not adsorbed yet). The hydraulic conductivity augments exponentially along with the moisture θ. The presence of the stock facilitates the water transmission along the depth. The strong suction is rapidly reduced while K(θ) augments. The hydraulic head also diminishes rapidly along the time, and so does Q. The water uses two porosities like for the shoulders but their mean radiuses R and r are far less different. The macroporosity path is faster and has little buffering. To the contrary, the microporosity path is slow but has a strong buffer effect. The resulting exfiltration volume is 820 litres.

3.5.2.2 Darcy's fluxes distribution

To understand the behaviour of the fluxes in the shoulder and lysimeters, 8 TDR probes have been installed in the LW lysimeter (profile 440). TDR probes measures the volumetric water content with a fairly good precision. A particular attention has been directed to the calibration because different methods might be more or less influenced by salt concentration in solute. Topp et al. Equation is widely known and recognized as little influenced by solute content (Mermoud 1999). See paragraph 3.1.1.2 and appendix VII for precision on TDR method and calculation.

Because TDR measurements are very dynamic and thus provide a lot of data, it is impossible to present a complete study of all different behaviours observed in the various meteorological conditions. Therefore, one single example of a representative natural event has been thoroughly studied. It is a moderate precipitation with moderate duration that occurred on the 4th of November 2005. Volumetric water contents θ in the shoulder and lysimeter had highly representative behaviours during this particular event, i.e. they can be considered as the average behaviours of θ (31 events recorded). Besides, the precipitation hyetogram is usual and easy to interpret. The following paragraphs present the results.

Natural event

The chosen natural event of November the 4th, 2005 had a precipitation of 14.5mm and lasted 14 hours and 26 minutes. The mean intensity was 1 mm·h^{-1} and maximum intensity was 2.7 mm·h^{-1} (recorded at 18h00). The period without precipitation preceding the event was 3.3 days long. Figure 3.27 presents the exfiltrating flows Q and precipitation hyetogram. As previously demonstrated in the paragraph "Shoulders", the shoulder responses are well

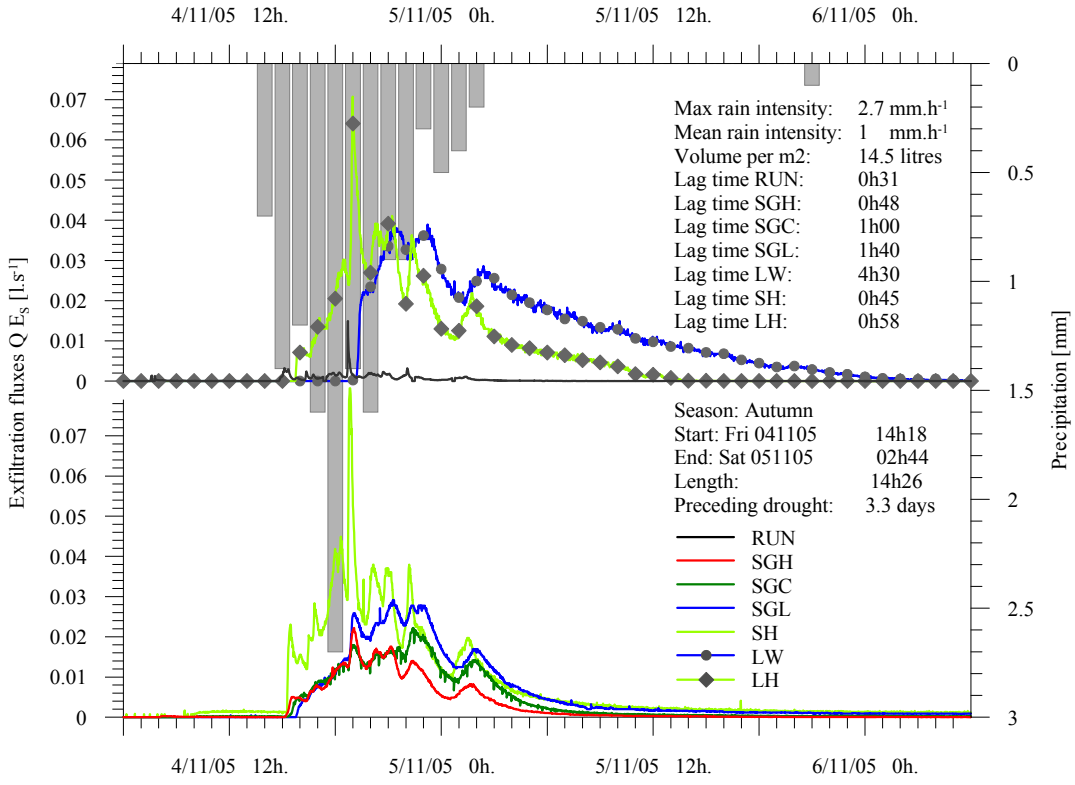

Figure 3.27: Event of November the 4th, 2005. The hyetogram is very usual and highly representative. Shoulder SH shows a higher exfiltration flow Q E_S because it drains 40 m^2 while other drains only 20 m^2. It nevertheless directly responds to the rainfall variation while other shoulders have a buffered behaviour (at least at the beginning of the event). In the upper pan are displayed the runoff flow (14.3 m^2) and lysimeter E_L. Colours correspond to the associated shoulder.

correlated with the hyetogram. Peaks in the hyetogram always have a consequence on the flow curves. This is more evident at the end of the event because the soil/shoulder is already wet and thus conducts the infiltrating water more efficiently. At the beginning of the event, the response is buffered because the soil/shoulder is dry; the infiltrating water is at that time moisturizing the soil/shoulder material. The exception is the shoulder SH which has a strong response to the precipitation very soon after the event beginning. It confirms that the SH is not suitable as an impermeable layer. It might infiltrate the first flush. Note that all flows Q are displayed as raw data, i.e. SH shows a bigger flow also because it drains 40 m^2 instead of 20 m^2 (other shoulders). Nevertheless, the direct influence of the rainfall hyetogram on the SH flow curve is undeniable.

TDR measurements

TDR positions and signal computation are given in appendix VII. The TDR measurements give the volumetric water content θ. It therefore needs some calculation and modelling to obtain the Darcy's fluxes $\vec{q}$ (figure 3.28):

Equ. 3.23) $$\vec{q} = -K(\theta) \cdot \vec{grad}(z + \Psi(\theta))$$ [m·s^{-1}]

($\vec{q}$: Darcy's flux; K(θ): hydraulic conductivity as a function of θ; z: elevation; Ψ(θ): matrix potential as a function of θ, also called the suction. It is a negative value)

Note that $\vec{q}$ is a vector and thus has two components: the magnitude (length of the vector) and dip (direction of the vector). The magnitude represents the Darcy's flux q. The dip is the angle between the horizontal and the vector, directed to the right (0° is a horizontal arrow directed to the right, hence from the road to the shoulder). Positive angles (0; 180°) are directed downward; they represent infiltration fluxes (90° represent a vertical infiltration flux). Negative angles (0; -180°) are directed upward and represent evaporation and/or redistribution fluxes. The $\vec{q}$ angle is the same as the hydraulic head gradient and is therefore calculated from the 2D representation of H=Ψ(θ)+z. It is postulated that $\vec{q}$ is always perpendicular to the equipotential lines[21].

The point where the vector is applied is placed in an ortho-normalized grid XY. X and Y [cm] reference levels (where X; Y = 0) are for X: the downstream edge of the wearing course, near the transition to the shoulder. For Y, it is the regional base level: Lake Neuchâtel. The coordinates of the point at the edge of the wearing course is therefore P{0; 48888.1}. X and Y coordinates are used to compute the elevation z.

Mathematical models (Surfer 8, Golden Software) use the krigging 2D interpolation method (linear for θ and H; logarithmic for K and q). Boundary conditions (surface of the shoulder/soil and bottom of the shoulder) are given in figure legends because they are different for each case.

Operators Ψ(θ) and K(θ) are calculated in laboratory (retractometry, see 2.6.2). Results give about 30 suction Ψ and water content θ couples of values. Those values are linked by a regressive non-linear equation developed by Van Genuchten (1980) which is widely used and recognized:

Equ. 3.24) $$\Psi(\theta) = \frac{\left[\theta^{*-1/m} - 1\right]^{1/n}}{\alpha}$$ [m]

(Ψ: matrix potential; θ: reduced water content; m, n, α: fitting factors, also known as intrinsic soil properties. Is widely accepted: m=1-1/n (Mualem 1976)*

[21] This is not always the case. The anisotropic tensor ∇K which describes the hydraulic conductivity into the three directions X, Y, Z is unknown for the soils. In the shoulder, the vertical K is assessed to be 10 times lower than the horizontal K (Cyr & Chiasson 2000).

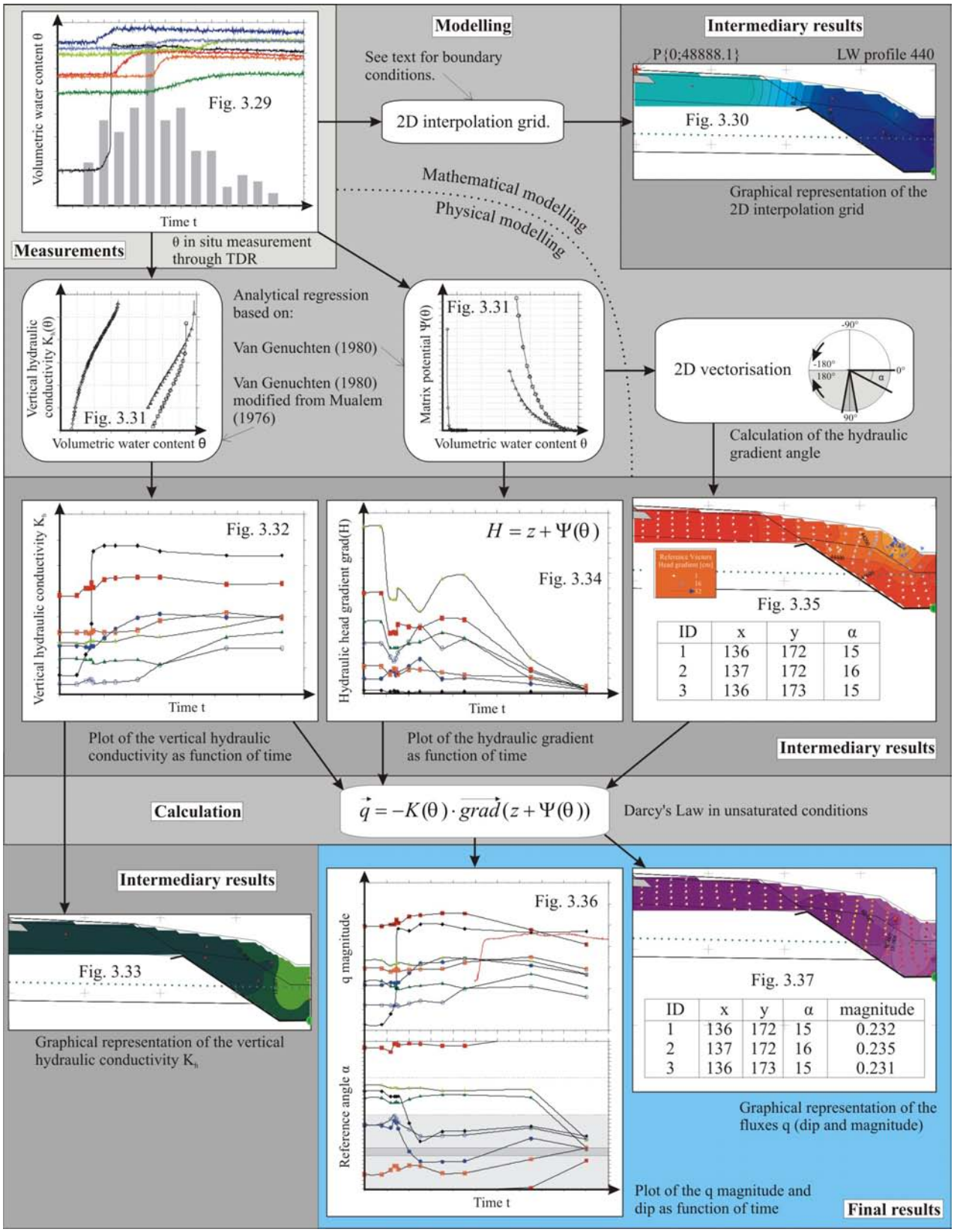

Figure 3.28: Insight of the procedure leading from θ to $\vec{q}$. Physical modelling (Ψ(θ) and K(θ) curves) are based on intrinsic soil properties analysed in laboratory, while mathematical modelling is based on graphical interpolation between the points of measurement. Each Darcy's Law component is calculated separately and is plotted in the ortho-normalized XY grid. Figure numbers are specified in the sketch boxes to allow easy access to full information. Final results are the fluxes angle and magnitude plotted over the time, as well as a 2D flux representation in the XY grid. See text for precision.

Equ. 3.24a)

$$\theta^* = \frac{\theta - \theta_r}{\theta_s - \theta_r} \qquad [m^3 \cdot m^{-3}]$$

(θ^*: reduced water content; θ: measured volumetric water content; θ_r: residual water content; θ_s: water content at saturation)

Van Genuchten described the fitting parameters n, m and α as soil intrinsic factors. They are inherent to the studied soil and can therefore be used for other relationship like (Van Genuchten 1980, based on Mualem (1976):

Equ. 3.25)

$$K(\theta) = K_S \cdot \theta^{*k} \left[1 - (\theta^{*1/m})^m\right]^2 \qquad [m \cdot s^{-1}]$$

(K: hydraulic conductivity; K_S: hydraulic conductivity at saturation; θ^*: reduced water content; k, m: fitting factors, respectively k=0.5 and m=1-1/n (Mualem 1976)

Once operators K and Ψ are calculated, as well as the dip angle, the vector $\vec{q}$ is easily calculated. Results are then plotted in the 2D 440 LW profile. Results are provided in two forms. The first represents the temporal evolution of the Darcy's equation parameters, while the second shows the spatial distribution of those parameters (2D 440 LW profile).

Volumetric water content θ

The TDR raw measurements are shown in figure 3.29. Raw measurements are directly expressed in θ [$m^3 \cdot m^{-3}$]. Observations are the following:

- The TDR 2 placed in the shoulder (solid black line) had a strong response. θ raised very rapidly to its maximum.

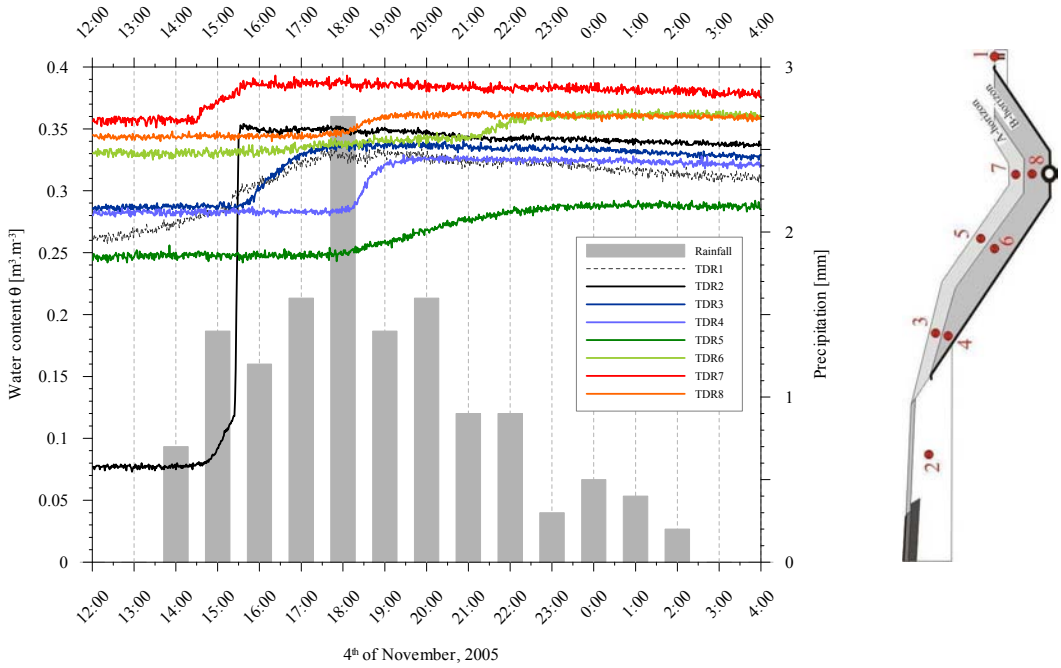

Figure 3.29: Raw TDR measurements and precipitation hyetogram. On the right is proposed a sketch map showing the TDR probes positions. Depths and distances are available in appendix VII. Colour code represents the proximity to the road: blue is proximal, green is in-between and red is distal. Dark colours are surface probes while light colours are deep one. Note the TDR 2 (shoulder, solid black) had a very strong response to the precipitation. It recorded the water content of the Fontainebleau sand the probe was lying in (0.35). The maximum grave I water content is 0.17 $m^3 \cdot m^{-3}$ (Cyr & Chiasson 2000).

- The other TDR having a fast answer is the n°7 located in the trench (red). Its response was as fast as for TDR 2, but the amplitude of θ was far smaller. The soil was indeed pretty wet before the event began. Soon after was reacting the TDR 3.
- All TDR couples (blue, green, red) clearly demonstrate that the surface probe was contacted by the moisturizing front before the deeper one, which is logical.
- Proximal (blue) TDR couples had almost the same θ water content previous to the rainfall. This also true for distal (red) probes. The green couple had a huge difference. The probe installed in the middle of the slope, near the surface, was the driest point of the lysimeter.
- Prior to the rainfall, distal TDR had higher water content than any other point. This is surely due to the redistribution of moisture concentrating the water in the trench, at the end of the previous event. This might be a consequence of the presence of the drain pipe.
- All signals decrease very softly after having reached its maximum.

Overall, all signals showed clear inflexion in the curve when contacted by the moisturizing front. This is less true for the TDR 5. This could be explained by a strong runoff coefficient in the middle of the slope. This would indeed prevent the water from infiltrating there. The probe signal would therefore be uniquely due to infiltration by suction and hence buffered. This would also explain why the TDR 7 at the bottom of the trench is responding so fast: the water runs over the slope to the bottom of the trench.

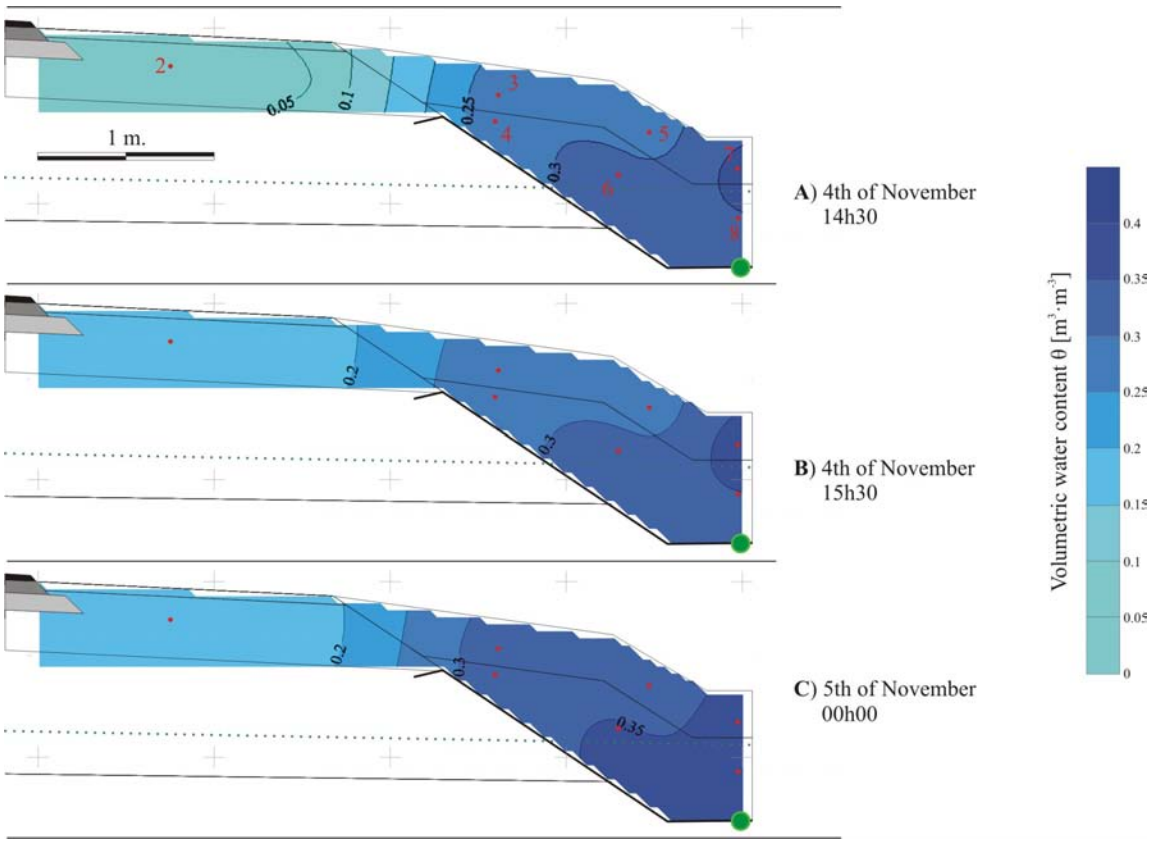

*Figure 3.30: θ distribution; LW 440 profile. **A)** State previous to the rainfall start. The distribution is quasi linear between the shoulder and the lysimeter bottom. **B)** One hour after the rainfall began; the shoulder has reached its maximum water content. The θ difference is less important between the shoulder and the soil. **C)** At midnight, the θ difference in the bottom of the lysimeter is also attenuated. During all the precipitation duration, the zone directly over the geomembrane is wetter than the overlaying soil. Boundary conditions for the 2D krigging are: 2m under the shoulder θ = 0.05; geomembrane is a cutting edge (i.e. has no influence on the θ equivalence lines); surface of the shoulder θ = 0.05 for A, θ = 0.17 for B and C; surface of the soil, θ = TDR1; exfiltration point (thick green dot) θ = TDR8; left and right boundaries have no influence at all on the interpolation (it is not extrapolation).*

Three different times have been chosen for displaying the 2D profiles. The first is obviously prior to the rainfall start, at 14h30. The second is one hour later (15h30), once the shoulder is almost saturated (maximum θ). The last one is arbitrarily at midnight, when all probes have reached their maximum θ value. Those times are used for all 2D cross sections.

During the rainfall (figure 3.30 B and C), the shoulder became almost fully saturated. θ reached 0.17 $m^3 \cdot m^{-3}$. The volumetric water content θ also rose in the lysimeter and reached 0.3 to 0.39 $m^3 \cdot m^{-3}$. The 0.3 limit reached the shoulder/lysimeter boundary.

Prior to the event start, the θ distribution from the shoulder to the bottom of the lysimeter is quasi linear (figure 3.30A). Note that in this 2D profiles, the shoulder water content has been corrected[22] (to fulfil the condition $\theta_S = 0.17$ $m^3 \cdot m^{-3}$). The θ is increasing toward the lysimeter and toward the bottom. Exception is the point TDR 7 which has a slightly higher θ than TDR 8. θ is thus higher along the geomembrane.

Operators K(θ) and Ψ(θ)

Those operators have great consequences on the infiltration process. Indeed, at low θ, the hydraulic conductivity K is almost null (orders of value are from $1 \cdot 10^{-10}$ to $1 \cdot 10^{-4}$ $m \cdot s^{-1}$). At the same θ, the suction might be great (from 0 to 20 metres). As those operators are uniquely depending on the volumetric water content θ, it is fairly easy to calculate their variation along the time, as well as their spatial distribution.

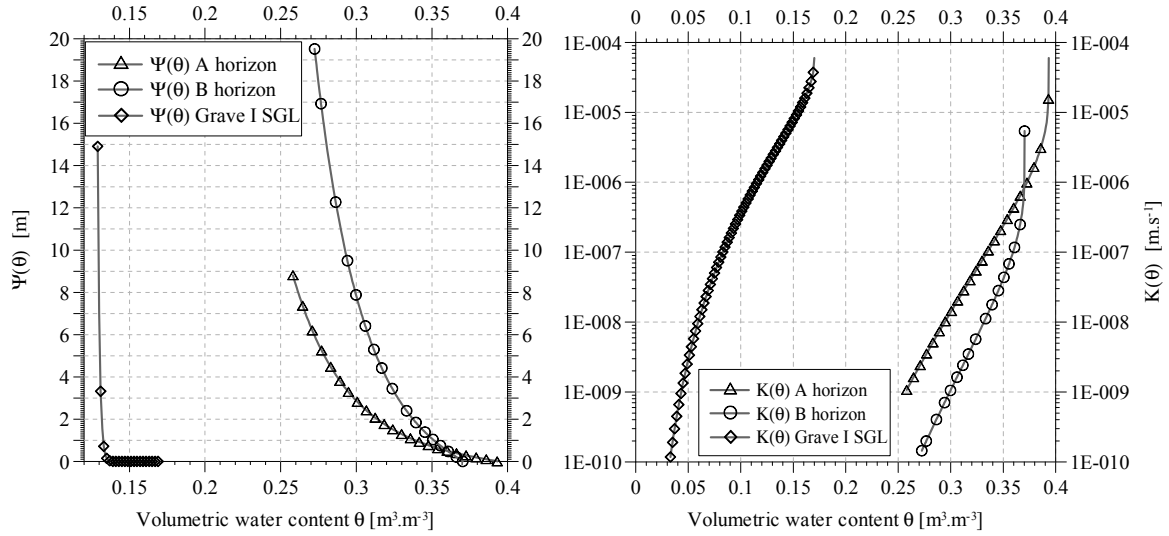

Figure 3.31: Operators Ψ(θ) and K(θ). Those curves have been computed using the Van Genuchten (1980) and Van Genuchten (1980) modified from Mualem (1976) equations. Raw data to fit were measured in laboratory. ***Left****: Ψ(θ). Note that the shoulder suction is almost null for most of θ values. A and B horizon curves are very similar.* ***Right****: K(θ). For the shoulder, K represents the vertical hydraulic conductivity. The horizontal hydraulic conductivity is supposed to be 10 times higher. For A and B horizons, K represents the average hydraulic conductivity in every direction.*

[22] The correction is linear, i.e. the saturated volumetric water content θ_S measured (0.35 $m^3 \cdot m^{-3}$) correspond to 0.17 $m^3 \cdot m^{-3}$ in the corrected scale, and 0 stays 0. This simplification is made for easier handling. It fairly corresponds to the reality in rapid moisturizing conditions. During the draining conditions, hysteresis might be great because the Fontainebleau sand retains the water while the shoulder grave I is emptying rapidly.

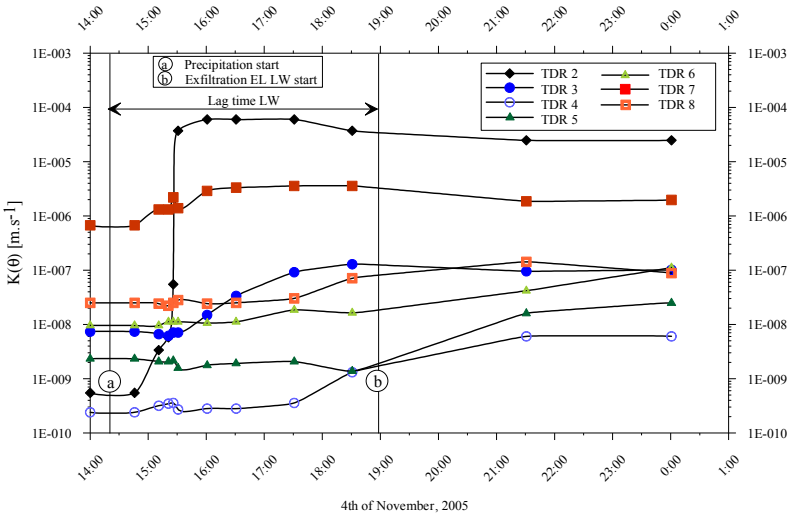

Figure 3.32: Time variation of K(θ). Colour code is the same as in figure 3.29. Note that the trends of the different curves are sensibly the same as for θ. This is because K(θ) operators are almost linear.

Variations of K along the time (figure 3.32) show the same trends as θ. This is because the operator K(θ) is not so strongly non-linear. The TDR 2 hydraulic conductivity variation ranges from $1 \cdot 10^{-10}$ to $1 \cdot 10^{-4}$ $m \cdot s^{-1}$. TDR 3 presents the second higher K variation (from $1 \cdot 10^{-8}$ to $1 \cdot 10^{-7}$ $m \cdot s^{-1}$), which is only a factor 10 order of magnitude. The smallest hydraulic conductivity is recorded by the TDR 4. Although the water content is not the smallest for that particular probe, K is smaller because the B-horizon K(θ) function has lower K value than the A-horizon function for the same θ. Final hydraulic conductivities range from $1 \cdot 10^{-8}$ to $5 \cdot 10^{-5}$ $m \cdot s^{-1}$, which is not very conductive.

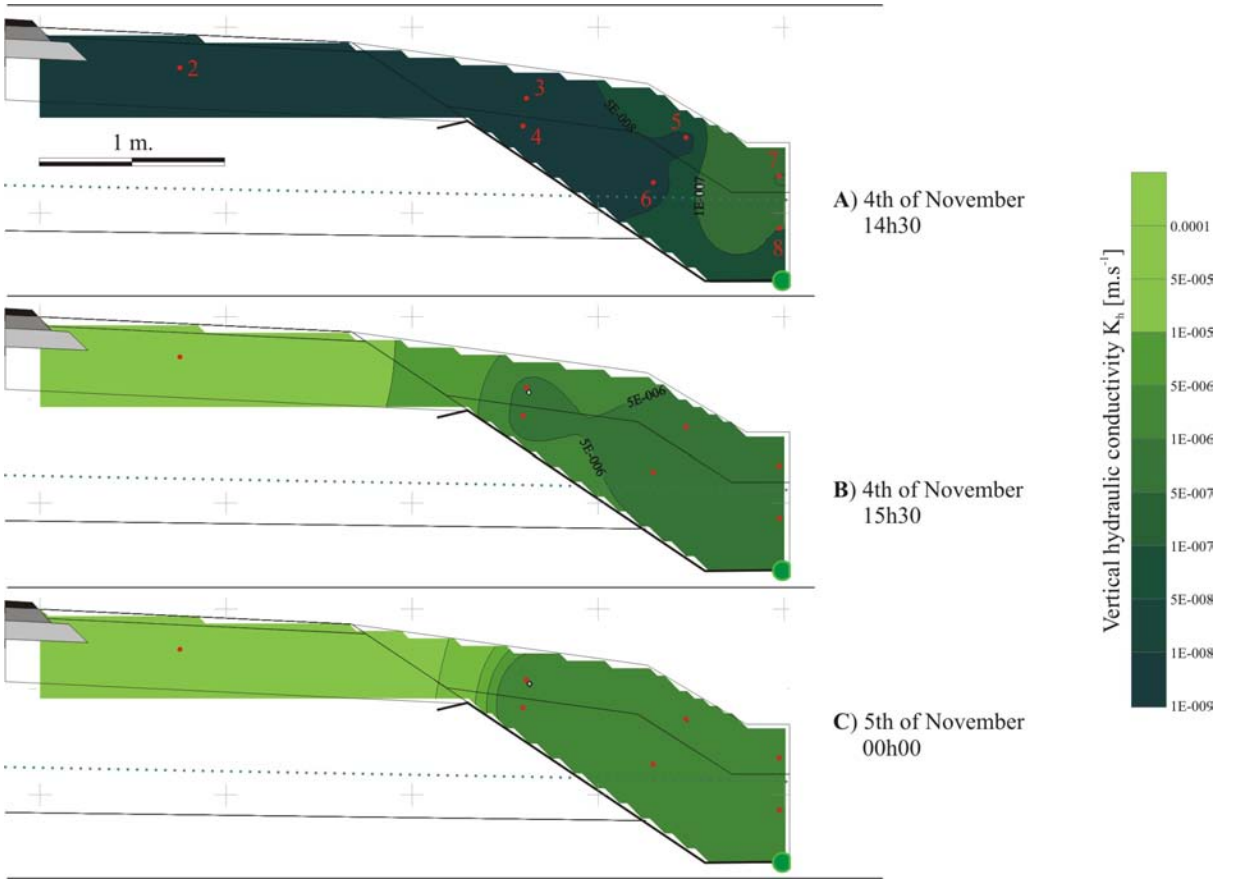

*Figure 3.33: K distribution; LW 440 profile. **A)** State previous to the rainfall start. The distribution is logically reverse compared with the θ distribution. The hydraulic conductivity is very small in the shoulder and higher in the wet soils. **B)** One hour after the rainfall began; the shoulder has reached its maximum water content and thus its maximum vertical hydraulic conductivity ($1 \cdot 10^{-4}$ $m \cdot s^{-1}$). In the soils, the hydraulic conductivity has also raised (from $1 \cdot 10^{-7}$ to $5 \cdot 10^{-6}$ $m \cdot s^{-1}$). **C)** At midnight, the K difference in the bottom of the lysimeter is almost inexistent. Boundary conditions for the 2D krigging are the same as for figure 3.30 but transformed into K using the K(θ) operator.*

Spatial distributions of the hydraulic conductivities prior to the precipitation (figure 3.33A) are more or less the reverse compared to the θ spatial distribution. K are far lower in the shoulder and in the upper part of the lysimeter than in the lower lysimeter. This situation is favourable because it prevents the first flush to directly infiltrate the shoulder. The road runoff is thus infiltrating the soils near the bottom of the trench. To the contrary, once the shoulder is fully wet (figure 3.33B and C), K is far greater in the shoulder than in the nearby soils. The hydraulic conductivities K tend to increase in the soils independently of the A and B horizon separation. Even if the first flush has already passed over the shoulder, this may jeopardize the road structure. Indeed, large amount of water may infiltrate the shoulder and road superstructure, especially if the rainfall event has a long duration.

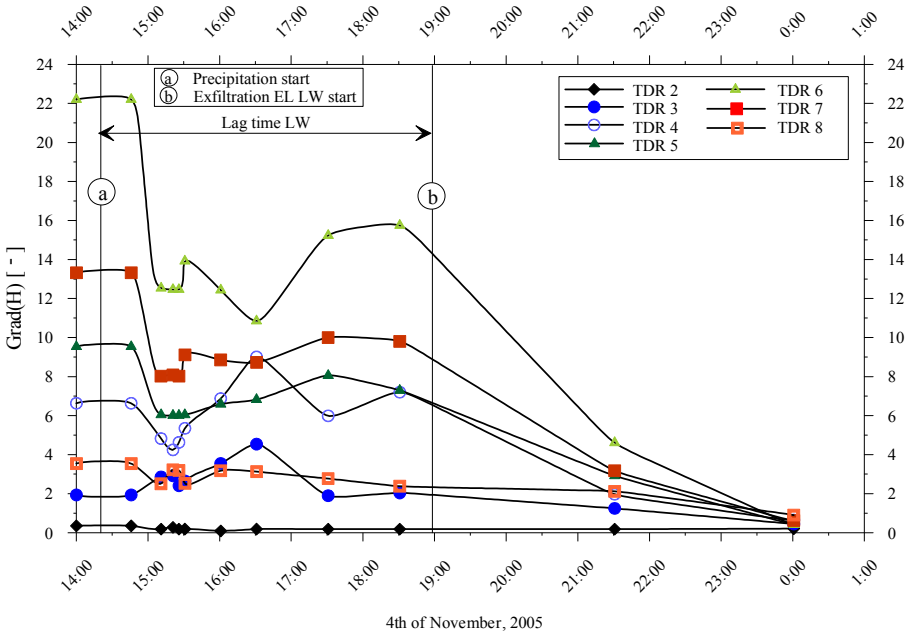

Figure 3.34: Time evolution of the hydraulic head gradient Grad(H). The gradient of H is GradH=(Ψ+z)/l, with l=distance between the two point of measurement of Ψ and z. Reminder: colour code is the same as in the previous figures, i.e. it represents the proximity to the road: blue is proximal, green is in-between and red is distal. Dark colours are surface probes while light colours are deep one. The gradient is of course strongly dependant of Ψ which is non-linear. The two first points for all curves are not yet influenced by the rainfall. All trends show a significant decrease once the moisturizing front is reaching the probes. They also show a slight increase shortly after that due to the water redistribution (while the rainfall temporarily diminishes). Note that the gradient in the shoulder (black) stays very low, while it strongly varies in TDR6 (light green). Overall, the gradient is spectacularly decreasing to reach a value of around 1.

The hydraulic head gradient variation along the time is presented in figure 3.34. Note that the two first points of each curve represent the grad(H) before the moisturizing front reached the TDR probes. Once the water reached the probes, the suction Ψ decreased drastically, thus increasing H. The gradient is a relative value: it does describe the hydraulic potential of one point relatively to its neighbour points[23]. If the grad(H) decreases at one point, it means that the neighbour points got a similar H than the considered point, i.e. the moisturizing front progresses. Strong grad(H) drop therefore illustrates a rapid moisturizing of the material. The propagation of the water front in such a case is postulated to be through the macroporosity. TDR 6 signal is a good example of such case.

To the contrary, when the surface becomes saturated, the head gradient of surface probes might raise. This is because the difference of the hydraulic head H between the surface and the bottom of the lysimeter is greater than previously. This is illustrated by the TDR 3 signal.

[23] Mathematically, it represents the slope of the 3D XYZ diagram. More basically, it is the normalized distance between the hydraulic equipotential lines.

There is no evident relationship between all TDR signals because the moisturizing front progresses at the same time downward and laterally, from the shoulder to the lysimeter. Evident negative correlation between TDR 4 and 6 between 15h30 and 17h30 are due to the preferential flow path, parallel to the geomembrane, toward the bottom of the lysimeter.

2D cross sections present two different parameters (figure 3.35). Coloured contours are the equipotential lines (equivalent hydraulic head H), while vectors show the hydraulic head gradient (length = gradient value). Note that the measurements are made in centimetres.

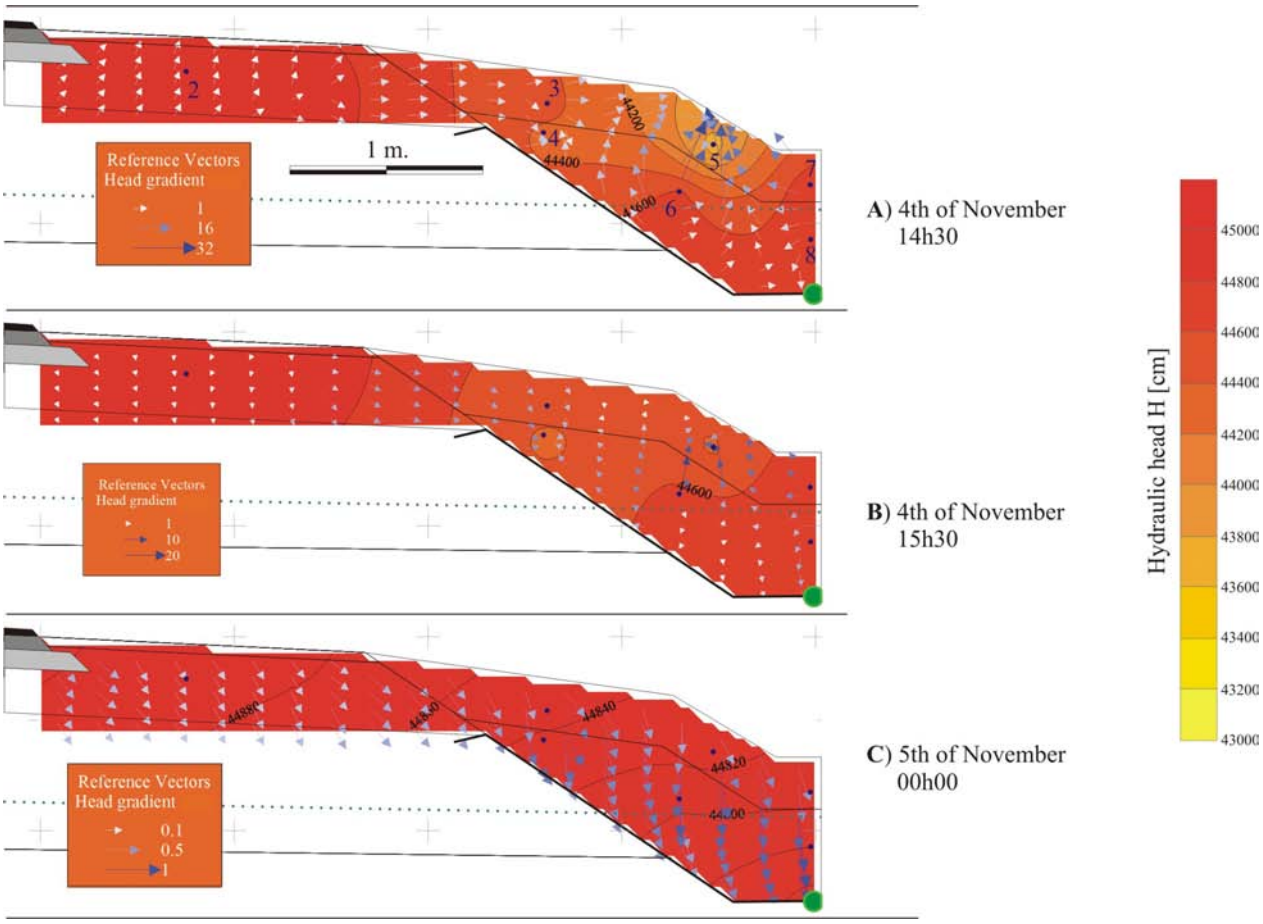

Figure 3.35: Hydraulic head H (red coloured scale) and hydraulic head gradient (white to blue arrows) distribution. Note that the arrows length and colour scale is not the same for the three case A, B and C. Scales are specified for each 2D profile. ***A)*** *Situation prior to the rainfall. Although having a slightly higher suction than the lysimeter, the shoulder has the greater hydraulic head H because its elevation is higher. The lowest H is met around the TDR 5. This is because its θ value is far smaller than in other places. Gradient are directed upward is most places, involving evaporation (shoulder) and redistribution (around TDR 5).* ***B)*** *Situation one hour after the rains began. Minimal H values are located in the lysimeter slope, while maximum values are distributed in the shoulder and in the bottom of the lysimeter. The differences between the highest and lowest values of H are less important than in case A. Thus, the gradient grad(H) are also lower. The gradients in the shoulder are no longer directed upward but downward. There is still a strong distribution effect around the TDR 5. Remind that the exfiltration E_L has not yet begun (will do at 18h42).* ***D)*** *Situation at midnight. The H differences due to the suction Ψ are now negligible. Only the elevation z is efficiently constraining H. Gradients are now at their lowest value (0.1 to 1). They are all directed downward, almost vertically. Boundary conditions for the 2D krigging are: 2 m under the shoulder H = 44600 cm (estimated suction of 88.1 cm); geomembrane is a cutting edge (i.e. has no influence on the H equipotential lines); surface of the shoulder H = 44400 cm for A (488.1cm of suction), H = 44888.1 cm for B and C (no suction); surface of the soil, H = Ψ (θ from TDR 1); exfiltration point (thick green dot) H = z (44751.1 cm); left and right boundaries have no influence at all on the interpolation (it is not extrapolation).*

Prior to the precipitation (figure 3.35A), the hydraulic head is at its maximum in the shoulder and minimal around TDR 5. While the suction has little effect in the shoulder, it has a great importance for the TDR 5. The hydraulic head is also greater at the bottom of the lysimeter. This is due to its lower suction (high water content). This situation leads to a strong gradient around the TDR 5, while it is very weak in the shoulder or at the bottom of the lysimeter. Gradient directions are mostly directed upward: the evaporation and redistribution process are predominant.

Once the shoulder is almost saturated (figure 3.35B), the maximal H values are located in the shoulder and also at the bottom of the lysimeter. The amplitude of variation of H along the profile tends to diminish. TDR 5 has no longer a strong suction (redistribution and rainfall were effective). It nevertheless still influences the gradient direction. Grad(H) vectors are now directed downward in the shoulder. The direction of q is therefore infiltration there. In the lysimeter, vectors are still showing some redistribution. This illustrate why shoulders exfiltration always starts before lysimeter exfiltration.

Finally, at midnight (figure 3.35C), when all TDR signals have reached their maximum water content value, the hydraulic head distribution is practically only influenced by the elevation z. The suction Ψ has no longer any strong effect on H. Grad(H) are now at their lowest value because the difference between the maximum and minimum H are very low (100cm at maximum between the shoulder and the bottom of the lysimeter). All gradient vectors are directed downward.

Fluxes q

Fluxes are calculated using the equation 3.23. The first remarkable impression given by the q values (figure 3.36A) is that the curve trends are very similar to those of the water content (figure 3.29) or K(θ). This means that the operator Ψ(θ) is not very effective to modify the q trend, especially when the water content θ stays in a given interval (Ψ is especially non-linear at high and low values of θ). Fluxes q are thus mostly influenced by K(θ). Again, the biggest amplitude is seen in the shoulder (TDR 2), increasing from $2 \cdot 10^{-10}$ to $1 \cdot 10^{-5}$ $m \cdot s^{-1}$. This represents a 100'000 time augmentation. Also, TDR 3 and 4 show the second and third amplitude variation (roughly from $2 \cdot 10^{-8}$ to $3 \cdot 10^{-7}$ $m \cdot s^{-1}$ and, respectively, from $2 \cdot 10^{-9}$ to $1 \cdot 10^{-8}$ $m \cdot s^{-1}$). Those variations are only a 10 times factor. Other points of measurements all show smaller q magnitude variation. The lowest variation is recorded in TDR 6 (about from $1 \cdot 10^{-7}$ to $2 \cdot 10^{-7}$ $m \cdot s^{-1}$). It only doubles. The highest flux q is recorded in the TDR 7 ($5 \cdot 10^{-5}$ $m \cdot s^{-1}$). This means that the shoulder runoff indeed runs over the surface of the slope directly to the bottom of the trench; it infiltrates there. Also, water coming from the opposite side (counter slope) is directed to the bottom of the trench. Because TDR 8 does present a flux of only about $1\text{-}5 \cdot 10^{-5}$ $m \cdot s^{-1}$, it can be assessed that most of the water infiltrating in the bottom of the trench is redistributed in the soils. It does not infiltrate further downward. The exfiltrating curve q E_L LW is also shown for comparison purpose. The flux q [$m \cdot s^{-1}$] is calculated from the LW E_L flow Q [$m^3 \cdot s^{-1}$]: q = Q/10. The number 10 represents the estimation of the surface of exfiltration along the 20 m length drain pipe. The curve shows a rapid increase soon after its beginning[24] and stabilizes at $5 \cdot 10^{-6}$ $m \cdot s^{-1}$. At a certain point, q E_L LW overtakes the q value recorded in TDR 8. From that moment on, most of the water exfiltrating is coming from alongside the geomembrane. Indeed, TDR 8 shows only a small infiltration q.

As previously mentioned, the dipping angle of the flux $\vec{q}$ in the shoulder varies from -60° (evaporation) to 60° (infiltration) (figure 3.36B). The inflexion point of the angle curve coincides with the q magnitude augmentation, soon after the rains began. The curve trend is very similar for TDR 3 and 4, although in a lesser extent for TDR 4. This illustrates the strong road runoff arrival on the shoulder and lysimeter first part (where TDR 3 and 4 lies). Indeed, as soon as the water has come to those places, it infiltrated and thus modified the dip angle. TDR 5 and 6 $\vec{q}$ angles stay negative for a long time, finally turning to infiltration at around 22h00. This illustrates the strong moisture redistribution effect already mentioned. During this time, the shoulder runoff does not affect TDR 5 and 6. The

[24] The curve originates at q = 0. The first value recorded is about $1 \cdot 10^{-8}$ $m \cdot s^{-1}$. This is the detection limit of the flowmeter. At lower value, the flux in undetectable (it flows drop by drop...).

shoulder runoff principally runs at the surface of the slope, or at the bottom, confined to a few cm above the geomembrane. TDR 7 has a horizontal right-to-left angle. This also confirms a strong redistribution. It turns to 90° vertical infiltration at a later time. It is believed that the TDR 8 signal is strongly affected by the exfiltration point (drain pipe, constant H = 447.511 m). It nevertheless never spreads far from the vertical infiltration angle. Exception made of TDR 2 and 3, angle trends strongly vary only after a long while (after 21h30). Overall, all TDR signals tend to the vertical infiltration angle (90°).

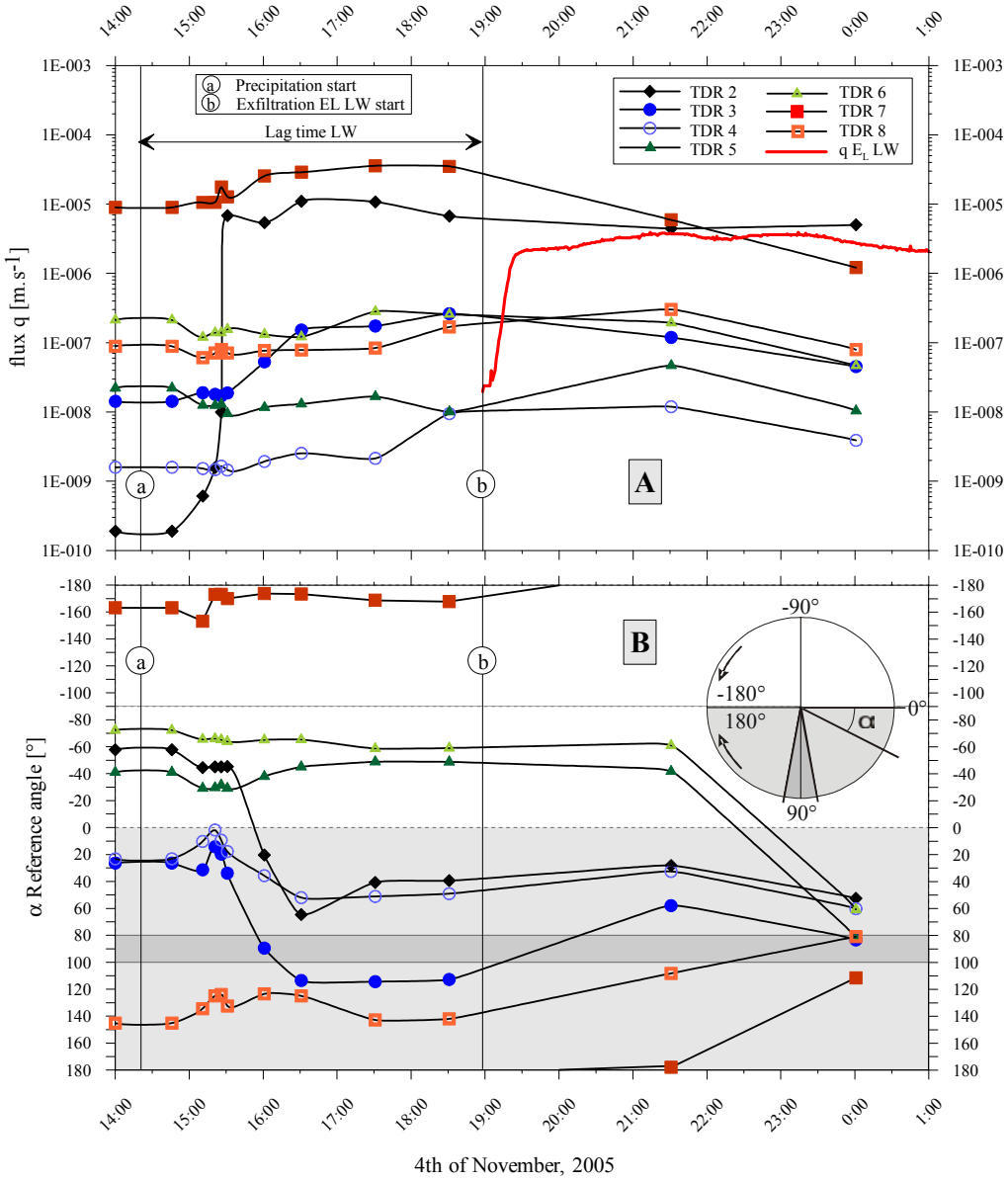

*Figure 3.36: Fluxes q magnitude (A) and dip (B). **A)** q magnitude. The variation of flux is great in the shoulder (TDR 2) and very small in the lysimeter slope (TDR 5, 6). The highest flux is recorded in the TDR 7, at the bottom of the lysimeter. It demonstrates that the shoulder runoff effectively runs over the shoulder and infiltrate in the trench bottom. In red is displayed the exfiltration flux q E_L of the lysimeter LW. It grows very rapidly and stabilizes at a fixed q (see text for calculation). It becomes the second greater flux recorded after the TDR 2 at the end of the recorded period. **B)** $\vec{q}$ dip angles. Positive angles are directed downward (infiltration), negative angles are directed upward (evaporation, redistribution). 0° is directed to the right (from shoulder to lysimeter). Grey zones are positive angles. Dark grey zone is vertical angle directed downward (90±10°). $\vec{q}$ angles in the shoulder (black lozenge) vary from -60° to 60° (from evaporation to infiltration). This behaviour is mimicked by TDR 3 and, in a lesser way, TDR 4. TDR 5 and 6 have a very late angle inversion. All curves tend to the vertical infiltration angle (dark grey zone, 90°).*

While it has been postulated that the flux q are parallel to the hydraulic head gradient, it is only an approximation. This is especially true in the shoulder where the hydraulic conductivity K is anisotropic: the hydraulic conductivity is a tensor ∇K which has at least 2 different values: the vertical K_v and horizontal K_h. It is postulated that $K_h = 10 \cdot K_v$ (Cyr & Chiasson 2000). The implications are that the shoulder q vectors shown in the figure 3.36 and 3.37 should be more horizontal than displayed. The ∇K for A and B horizons are unknown.

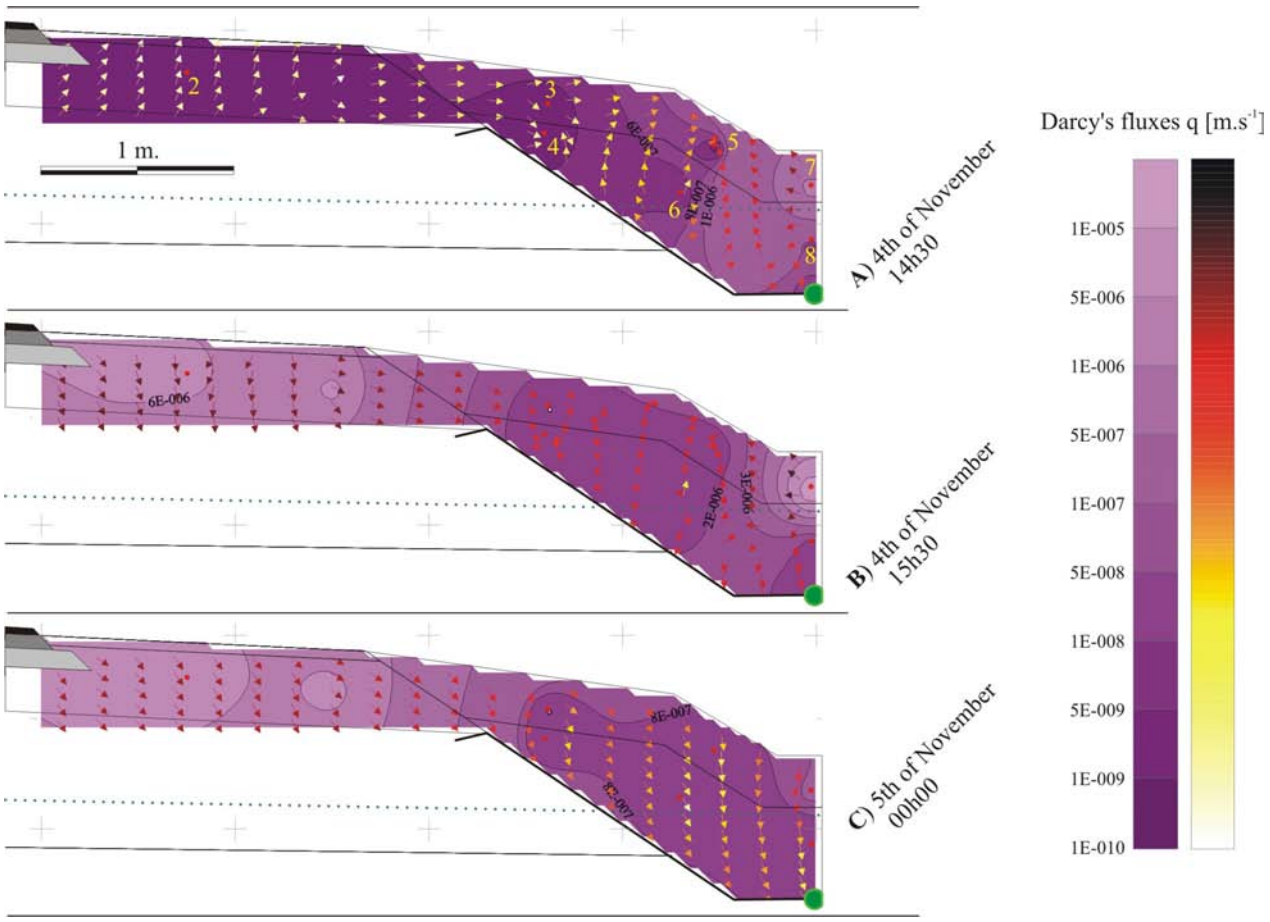

Figure 3.37: Fluxes spatial distribution. Purple scale illustrates the flux magnitude distribution while the white to black scale represents the q vector magnitude. ***A)*** *Situation prior to the rainfall. Strong moisture redistribution occurs in the lysimeter soils while evaporation is taking place in the shoulder. Overall, all fluxes are more or less directed upward. Only the exfiltration point (thick green dot) bends the q vectors downward in its direct vicinity.* ***B)*** *Situation 1 hour after the rains started. Redistribution is still important in the lysimeter. Vector directions are still more or less upward there. In the shoulder, a strong infiltration process has begun. Fluxes are directed downward. At the shoulder – lysimeter boundary, fluxes are still directed toward the soils. From that moment on, infiltration in the shoulder might jeopardize the road structure stability.* ***C)*** *Situation at midnight. All vectors are directed downward. Shoulder and lysimeter infiltrate at different rate: the shoulder fluxes are 100 times higher than those in the lysimeter. Redistribution in the soils has ended. Suction is no more an efficient process, water mainly flows by gravity. Boundary conditions for the 2D krigging are the same as in the hydraulic head distribution figure 3.35. All interpolation points have simply been multiplied by the distributed hydraulic conductivity K (figure 3.33).*

Spatial distribution of the fluxes $\bar{q}$ before the rain began (figure 3.37A) illustrates the strong moisture redistribution in the soils. The q magnitude is indeed far greater around TDR 5 and 7 than in other places. Globally, the fluxes are directed toward the steepest slope (TDR 5). This concurs with the small volumetric water content recorded around that probe. Note the influence of the exfiltration point (thick green dot): it attracts or bends the fluxes toward 90°. In the shoulder, fluxes are overall directed upward. This is due to evaporation. Flux magnitudes there are very small though ($5 \cdot 10^{-10}$ to $5 \cdot 10^{-8}$ $m \cdot s^{-1}$). The transition limit between the shoulder and the soils shows horizontal fluxes

directed to the soils. This is because the suction in the shoulder is far smaller than the suction in the soils. This is also demonstrated by the $\Psi(\theta)$ curves (figure 3.31 left). Overall, the situation prior to the rainfall is a redistribution and evaporation situation: fluxes redistribute moisture to achieve an equilibrium state[25]. During this particular event, the equilibrium was not achieved yet.

One hour after the rain has begun (figure 3.37B), the moisture redistribution is still occurring in the lysimeter. As the surface, the trench bottom and the shoulder have been widely watered, the fluxes are even greater (higher K). Fluxes around TDR 7 are the highest. Distribution of the q magnitude shows that q is greater in the trench bottom and in the shoulder, smaller along the lysimeter slope. The shoulder presents now a strong infiltration process. All q vectors are directed downward. Magnitudes of q are pretty high ($1 \cdot 10^{-5}$ m·s^{-1}). In case the road superstructure is dry and has a strong suction component, the moisture might be attracted there. It is very unfavourable for the road stability.

Finally, at midnight, the q magnitude distribution is more linear: from higher value in the shoulder ($5 \cdot 10^{-6}$ m·s^{-1}) to lower value at the bottom of the lysimeter ($1 \cdot 10^{-7}$ m·s^{-1}). The influence of the road runoff is then clearly visible. All fluxes are infiltrating, i.e. are directed downward. Suction is no more an issue; moisture propagates essentially by gravity.

Summary

Intrinsic characteristics of the shoulder and soils (A and B horizons) clearly lead the infiltration processes. Indeed, the operator $K(\theta)$ has a great influence on the fluxes magnitude. The suction does not strongly influence the flux magnitude but defines the flux direction. They both depend on the volumetric water content.

Previous to any rainfall, the soils are in a redistribution state, i.e. the suction (and therefore fluxes) tends to lower the differences in water content that exist between different locations. Redistribution has not been observed in the shoulder[26]. Fluxes are directed from the higher to the lower volumetric water content θ. It also seems that the moisture remaining at the end of an event is concentrating in the bottom of the lysimeter and along the geomembrane. This might be due to the presence of the drain pipe which attracts the moisture downward (the hydraulic head there is equal to the elevation only).

Once watered upon, the shoulder first drives the road runoff to the infiltration slope. This is because the hydraulic conductivity is almost inexistent. Then, once the shoulder begins to be wet, fluxes rapidly turn from evaporation to infiltration. The vertical hydraulic conductivity augments drastically and becomes 100’000 times higher. The infiltration rate thus augments rapidly and may endanger the road stability. It also continues to drive the exceeding water to the infiltration slope. Remember that the horizontal hydraulic conductivity K_h is 10 times greater than K_v.

The soils in the infiltration slopes continue to redistribute the moisture. Water at the surface and in the bottom of the trench augments the hydraulic head gradient and thus increases the fluxes magnitude. The part where the infiltration slope is steeper infiltrates water at a lower rate than the parts at the top and bottom of the lysimeter. The shoulder runoff therefore:

- either infiltrates at the top of the lysimeter and runs along the geomembrane
- either runs over the surface of the steep slope and infiltrate preferentially at the bottom of the trench

Whichever of those two paths is used, this forces the fluxes to turn toward the zone where the water content stays low, i.e. the middle of the steeper slope. The redistribution goes on until all the soils have similar water content.

[25] Even approaching an equilibrium state, evaporation still occurs. An equilibrium state is thus very hard to reach. Equilibrium is achieved when fluxes are null, therefore when θ is the residual θ everywhere.

[26] It is nevertheless highly probable that redistribution processes exist in the shoulder; they are not detected because only one probe is installed in the shoulder.

When the redistribution stops (either because redistribution has been effective, either because the rainfall provides enough water to almost saturate the soils), all fluxes turn downward to an infiltration state. The infiltration is not always more efficient in the shoulder than in the lysimeter. Some events that have been studied show a stronger infiltration in the lysimeter. This was because the soils where wetter or the rain heavier. Overall, the exfiltration through the shoulder always begins before the exfiltration through the soils. The influence of the drain pipe and geomembrane are not fully understood yet. The drain pipe nevertheless promotes the infiltration. The geomembrane confines the infiltration in the soil structure, preventing the water to reach the embankment.

3.5.2.3 Lysimeter LH

The lysimeter LH, adjoining the shoulder SH, presents evident differences from LW during the artificial test n°1 (appendix IV):

- the lag time is far smaller (22 minutes), which is only five minutes more than the lag time recorded for the associated shoulder SH
- the maximum Q is as high as twice the Q recorded for LW (0.5 $l \cdot s^{-1}$)
- the Q decreasing trend is more pronounced
- the resulting exfiltration volume is 1300 litres
- the concentration of Cl^- shows only two peaks, the first one being at 80 $mg \cdot l^{-1}$
- the pollutogram is always positive and has a stronger first-flush effect (b = 0.38)

The fact that the water runs so rapidly to the bottom of the lysimeter and that the obtained flow Q is so great can be explained by some preferential flow paths. Remember that this lysimeter is bigger than LW: the distance from the shoulder to the collecting pipe situated at the bottom of the lysimeter is 1.6 times the same distance in LW. It consequently should be the contrary: LW showing longer lag time and larger exfiltration volume than LH[27]. Moreover, the flow Q decreases faster and more uniformly than for LW. This means the participating macroporosity has a bigger role in the infiltration than for LW. Two chlorine peaks, the first being the bigger, are observed. This could mean the role of the stock is almost null in this lysimeter. Finally, the pollutogram looks more like the one calculated for SGH than the one of LW: it is strongly positive and shows a massive arrival of chlorine at the beginning of the exfiltration.

All these remarks suggest that not only there are preferential paths allowing the infiltrated water to run faster but also that the stock is not pushed downward (no indication of a piston effect, first arrival of chlorine is the biggest). As the two lysimeter have been built the same way and with the same material, this strange behaviour cannot be due to the soil itself. The reason has to be found elsewhere, most likely at the transition between the shoulder and the lysimeter. In the §3.4.2.4, it has been postulated that the road runoff infiltrates the shoulder laterally, from the soil. This presupposes that, to the contrary of the LW lysimeter, the shoulder runoff does not flow on the surface of the lysimeter at all. Once the water reaches the bituminous coating, the fractionation between the water flowing laterally to the shoulder and the water percolating down the lysimeter is made as function of the bituminous coating hydraulic conductivity. The water percolating down the lysimeter concentrates along the impermeable geomembrane and runs along it to the collecting pipe. The soil therefore merely participates to the infiltration process, and thus is relatively inefficient to adsorb the substances. An unknown fraction of the water flowing along the geomembrane is sucked upward by capillarity but certainly not high enough to make the A-horizon participate. The effect of the Geoweb[28], although having small holes to allow the water circulation, is unknown. It very likely accelerates the downward flow: soil is less compacted in the Geoweb alveolus; it is even probable that alveolus were partially filled during the soil installation. The lag time without the Geoweb would be higher.

[27] Larger volume is also due to the different behaviours of the associated shoulder. Nevertheless, only 150 litres separate the SGL from the SH. Moreover, the SGL without colleting pipe and geomembrane should be even less permeable than the SGL studied in the previous chapter.

[28] Remember the Geoweb net was deployed to avoid landslides.

The lysimeter LH shows strong evidences of dysfunction: it does not fulfil the task assigned. It concentrates the shoulder runoff along the impermeable geomembrane (at the bottom of the lysimeter) and thus prevents the A and B-horizons to accomplish their task, i.e. to adsorb the substances carried by the runoff. In the case there was no geomembrane, the runoff would simply infiltrate the embankment[29].

Note that another hypothesis causing this preferential flow along the geomembrane could be a superior growth of cracks, fissures and joint at the slope inflexion, near the shoulder – lysimeter transition. Those cracks would be caused by the soil surface reptation. However, neither trace nor indication of reptation has been observed in the field. Reptation might however exist but would be very slow and light.

3.5.2.4 Infiltration slope LB

Concerning the infiltration slope associated to SB (bentonitic shoulder), the only valuable source of information on the infiltration flow is the aquifer chlorine concentration. The possible impact of 3 cubic metres on the aquifer is in all considerations impossible to measure. It should be negligible but for its substance content. For information about the aquifer behaviour and results, see §3.6, and chapter 4.

3.5.3 STATISTICAL APPROACH

Empirical assessment of the water volume exfiltrating the 2 lysimeters has been made. Water balance for the lysimeters is given by the equations 3.3a and b). The water that is available for infiltration on the surface is called B_W. The exfiltration volume E_L, ETP and the API are calculated the same way as in §3.2. Results are shown in tables V.2, appendix V, and VI.1, appendix VI. The water balance diagram (figure 3.1) assumes that the only unknown variable is the stock variation ΔS.

3.5.3.1 Mathematical solution – Empirical solving - univariance

Results of the calculated ΔS are presented in figure 3.38. The ETP is emphasized for comparison. It is evident that the variation of the stock ΔS is intimately linked to the API and, forcibly, to the ETP. To the contrary of the shoulders, the infiltration slope soils are thus heavily depending on the drought: the dryer the soils are, the more water they retain. The addition of the API and ΔS for each event show that LW may retain around 160-200 mm at maximum[30]. This means the soil maximum water content after primary draining is roughly 25% (14 m^3). The ΔS recorded for the lysimeter LH is a little bit higher than for LW (200-220 mm) but concordant. Anyway, the maximum amount of water that can be stored in the lysimeter LH is 28% (26 m^3). This maximum water content is relatively small in regard to values found in the literature: this is surely due to the presence of the collecting pipes which act like drains. They indeed favour the percolation inducing an artificial break in the hydraulic head profile.

Extrapolating those results for SB, the water volume that can be retained in the infiltration slope is 30 m^3 at minimum. The infiltration slope SB must indeed have a higher water content value than the lysimeters (no collecting pipes).

Also, the TDR probes should allow calculating the stock variation. Nevertheless, as it has been demonstrated in previous paragraphs, lysimeters cannot, to the contrary of shoulders, be compared to unitary soil volumes. As six probes have been installed at different places and different depths, it is impossible to calculate a global stock variation without resorting to numerical methods. The dynamic analysis of the propagation of the moisturizing front is made at §3.5.2.2.

[29] It of course respects the hydraulic conductivity ratio between the soil and grave I: in case the soil hydraulic conductivity K is smaller than the grave I K, perched groundwater may form or soil may render infiltration difficult.
[30] This does not relate the maximum stock when soils are saturated but when they are gravitationally drained.

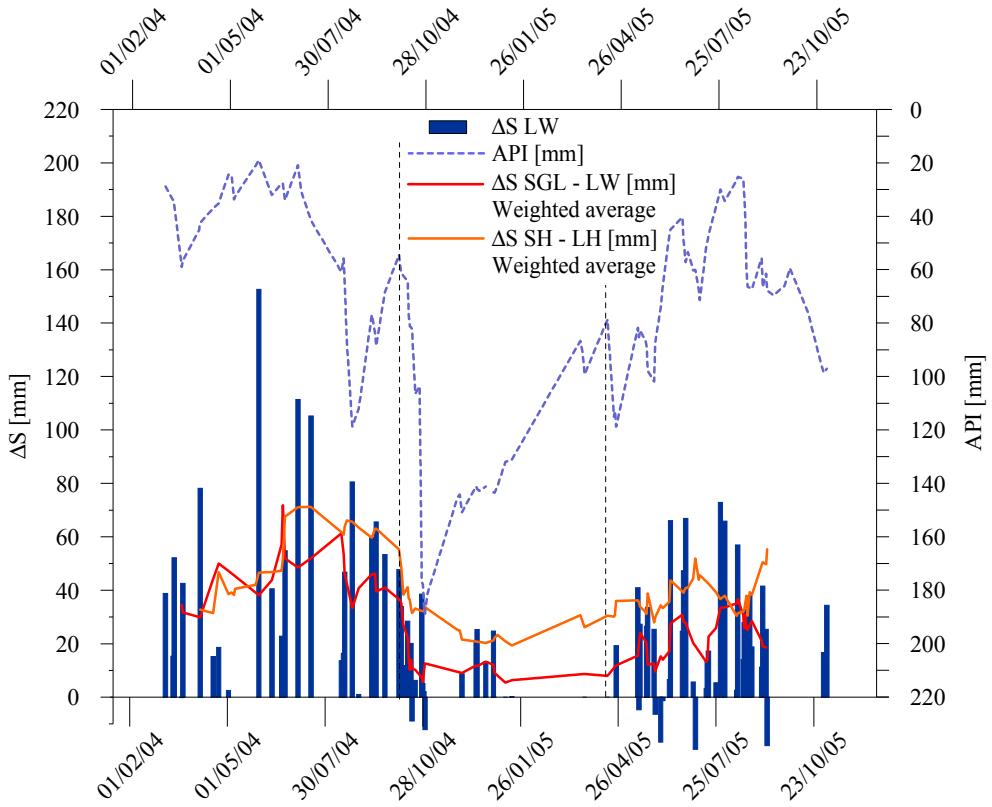

Figure 3.38: ΔS for each event. Blue bars represent the ΔS of LW. For simplification, only the weighted average has been plotted for LH. Both lysimeter show a strong correlation between ΔS and the API. The higher the API, the lower the soil water retention is. Differences between winter and summer are highly marked. Sum of API and ΔS gives an indication on the maximum volume that might be retained by the lysimeter.

3.5.3.2 *Empirical solution – 3D-three parameter plots (B_W, I_{mean}, API) – multivariance*

The exfiltration volumes E_L from both lysimeters have also been plotted in the 3D diagram. Results concerning the lysimeter LW are presented in the figure 3.39. First, not only the joint influences of the available water B_W and the API are clearly visible but also the logarithmic trend they present. Indeed, separation distances between the centres of gravity are logarithmically decreasing, as well as the value gap between the centres of gravity. The influence of the rain and API could therefore be linearly linked to the exfiltration volumes E_L[31]. The influence of the rainfall intensity is negligible. The empirical resulting formulation has therefore the form:

Equ. 3.23) $$E_L = a + b \cdot B_W + c \cdot API \qquad [mm]$$

This model is highly simplified but allows estimating the exfiltration volume E_L as function of the rainfall (and thus the available water B_W using the equations 3.18a and b) and the API. Coefficients a, b and c for LW and LH are presented in table 3.6. Required API values might be calculated using more simple equation than the one used in this project. In the case of LH, the calculated coefficients (linear 3D regression) present a very small dependence to the API, which confirm the preferential flow hypothesis. The infiltrated water indeed runs along the geomembrane. Whether the soil is dry or not has almost no influence at all on the resulting exfiltration volume. The threshold value under which no exfiltration is recorded is set with limit condition $E_L \leq 0$. It therefore gives a couple of values B_W and API. Examples of T_{VOL} value are also shown in table 3.6.

[31] Remember the scales are logarithmic. This is a postulate.

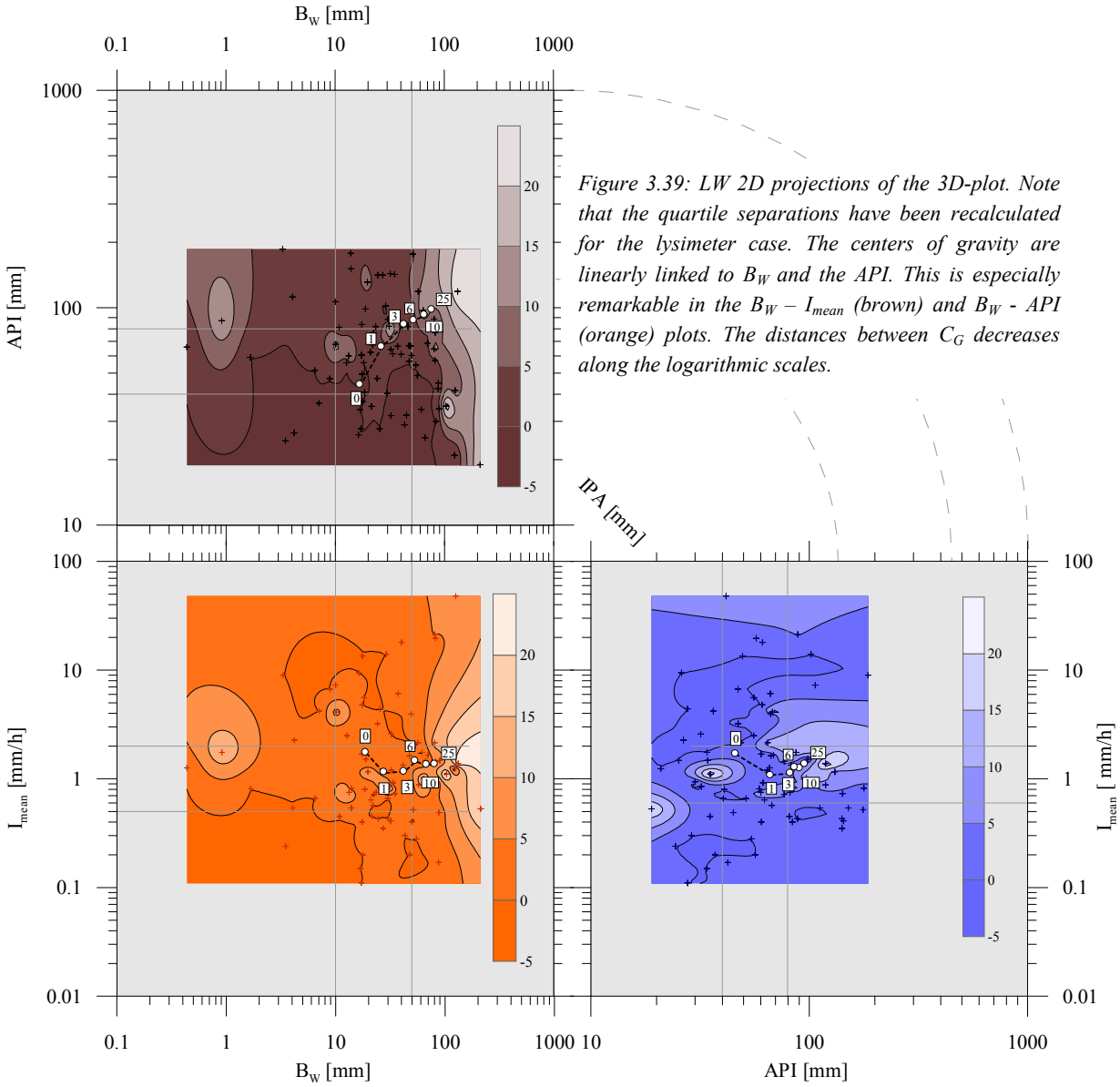

Figure 3.39: LW 2D projections of the 3D-plot. Note that the quartile separations have been recalculated for the lysimeter case. The centers of gravity are linearly linked to B_W and the API. This is especially remarkable in the B_W – I_{mean} (brown) and B_W - API (orange) plots. The distances between C_G decreases along the logarithmic scales.

Again, the threshold T_{VOL} function confirms that LH exfiltration E_L does not depend on the API, thus on the soil moisture.

	a	*b*	*c*	T_{VOL}
LW	-2.61	0.084	0.035	B_W=50;API=18/ B_W=20; API=45
LH	-2.62	0.78	-9E-4	B_W=50; API=75/ B_W=20; API=180

Table 3.6: Calculated coefficients in 3D linear numerical regression. The lysimeter LH shows a nearly inexistent API dependence ($c \approx 0$).

3.5.3.3 Lag time discrimination

As in the shoulder analysis, the lag time of the exfiltration response have been plotted versus the mean intensity, the available water B_W and the API (example of LW, figure 3.40). The figure shows that the lag time is not easily correlated with any of those variables. It can nevertheless be assessed that, like for the shoulders, the mean intensity is the principal component leading the lag time behaviour. Lag times indeed decreases with higher mean intensities. For rainfall which intensities are over 7 mm·h^{-1}, the lag time is presumably less than one hour. To the contrary, lag

times of more than ten hours might happen if the rain intensity is less than 0.4 mm·h^{-1}. Overall, the API does not seem to have a serious or even regular influence on lag times.

Note that the "zero" centre of gravity represents all events that had not given any exfiltration volume; it is thus hard to interpret the position of this C_G because it could also be interpreted as an "infinity lag time" C_G. It would then be at the other end of the bold dotted trend line. However, the position of this C_G is logical: If there is very small amount of water available on the surface of the lysimeter, it is highly probable that no water at all would reach the bottom of the lysimeter. The "zero" lag time represents thus all the infiltration that have aborted.

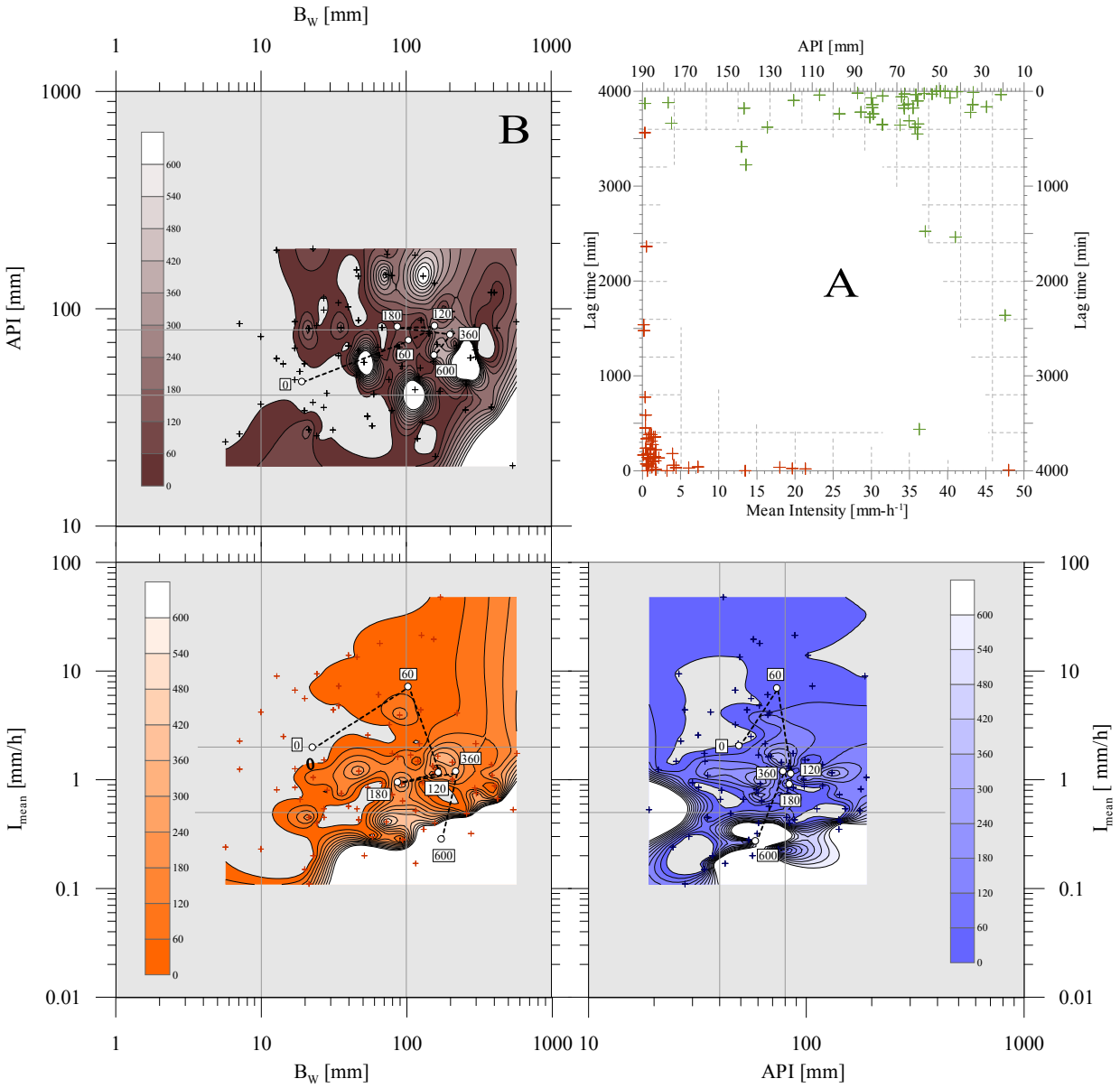

*Figure 3.40: Lag times in the lysimeter LW. **A)** Lag times as function of the Imean or the API. If the correlation with the I_{mean} is clearly established, the API influence is more confuse. **B)** 2D projections of the lag times repartition. Influence of the available water B_W is obvious for the cases where no exfiltration water was observed. When water was seen in the exfiltration pipe, lag times were correlated to the mean intensities.*

Lag times concerning the lysimeter LH are far shorter than those recorded for LW. Averages are 130 and 185 minutes for LH and LW respectively. The general trend is nevertheless exactly the same. Lag times in the infiltration slopes

are very important because it constraints the time for substances adsorption and exchange. The shorter the lag time, the less the substances are expected to be adsorbed. Unfortunately, as it has been already demonstrated in previous paragraphs, the precipitations with high mean intensities, which also have the shorter lag times, are more likely to mobilize substances from the road surface. Therefore, events that must closely be watched upon are the thunderstorms. For this reason, the test n°2 (geochemical assessment) mimics a thunderstorm.

3.6 ALLUVIAL AQUIFER

3.6.1 GEOGRAPHICAL AND HYDROGEOLOGICAL LIMITS

The accumulation basin of the Arnon is 75 km^2. It spreads from the plain regions of Onnens - Champagnes – Fiez – Novalles and the northern zone of Grandson. Limits are the first Jura crest to the north-west, the lake to the south-east (regional basal level) and the moraine ridge to the south-west. The north-eastern limit is harder to localize; probably coinciding with the hills between Corcelles and Onnens.

In the northern part of the Arnon hillslope, the karstic underground flows are heavily constraints by the argovian impermeable layer. The first anticline crest of the Jura Mountains, where the Argovian is at its uppermost level, is therefore the hydrogeological northern limit of the Arnon accumulation basin (Fiez/Novalles report, GEOLEP, 1989). Other hydrogeological limits coincide with the geographical limits described above.

The accumulation basin is composed of two main blocks which influence the transfer of water from the Jura to the Lake, essentially though the Arnon. The first block is in the upper part of the basin. It is essentially made of Jurassic and Cretaceous limestone dipping southward. Underground water is confined in the upper layers. Flows are mostly in the karst and run fast (50 $m \cdot h^{-1}$). It is therefore only little purified. Flow directions are constrained by the Argovian aquitard. It causes the water to meet the surface at the Mothe, Diaz and Covatanne springs. The second block is mainly composed of the Arnon plain overlaying the molasse. The plain is made of porous media - quaternary river deposits – that are confined in the topographic depressions.

The alluvial aquifer below the experimental site is composed of porous material. Their description is thoroughly made in the chapter 1. The extension of the aquifer is limited to the north by the Arnon and to the south by an impermeable moraine layer which comes closer to the surface southward. The western and eastern limits are not well known. The western limit is assumed to be the Arnon infiltrating the aquifer. It is not completely excluded that the eastern limit spreads far from the testing site. Therefore, the aquifer is only confined to the alluvial deposit overlaying the basal till running along the south edge of the Arnon. The aquifer lateral wall is only 40 metres from the Arnon. Overall, the aquifer is an unconfined one[32].

3.6.2 HYDROGEOLOGICAL PARAMETERS

Various tests have been conducted on the alluvial aquifer to determine the hydraulic conductivity K, storativity coefficient S_T[33] and transmissivity T_R[34]. These are salt infiltration test (piezometer), slug test (essai Lefranc), pump test and local tracer test. See appendix IX for calculation methods.

[32] Locally, the palustrine gleys near the surface might set the aquifer into a semi-confined state. This has no effect on the overall aquifer behaviour because the extension of such semi-confined state is negligible.

[33] The storativity coefficient S_T is the water quantity liberated for a given head loss; it equals the efficient porosity n_e in unconfined porous media. The efficient porosity is the porosity which contains mobile water, as opposed to the "confined" or "dead" porosity which is not linked to the porosity network. The efficient and confined porosities together constitute the total porosity.

[34] The transmissivity T_R is the capacity of an aquifer to mobilize its water. It is $T_R = K \cdot e$ (e = aquifer thickness).

3.6.2.1 NaCl test

Salt infiltration (brine) tests have been conducted in 6 piezometers of the km 475-495 compartment (10/03/2004). The goal was to roughly determine the aquifer water flow and to assess vertical repartition of possibly different flows[35]. Practically, the saline solute was homogenized in the piezometer (artificial convection with an underwater micro-pump); the electrical conductivity EC was monitored (calib. 20°C). The decrease of the EC along the time was then recorded.

Initially, the salt solute tended to sink to the bottom of the piezometer (higher density). Figure 3.41 illustrates the piezometer behaviours three days after the injection. Dead volume could be found at the bottom of the piezometers S02_1, 2, 5 and 6. The 2 piezometers closest to the Arnon (S02_3 and 4) were active all along theirs lengths. The temperature and EC transition coincided with the screening-to-plain transition of the piezometers (see borehole logs, appendix III). All screened zones (active zone) showed active interval; the brine was not trapped. This demonstrates that all the places where the aquifer is in contact with the piezometers have significant flows. EC values in the screened parts of the piezometers have returned to values previously measured within less than three days. To the contrary, the bottom parts of the piezometers have concentrated the brine; the EC thus raised a little.

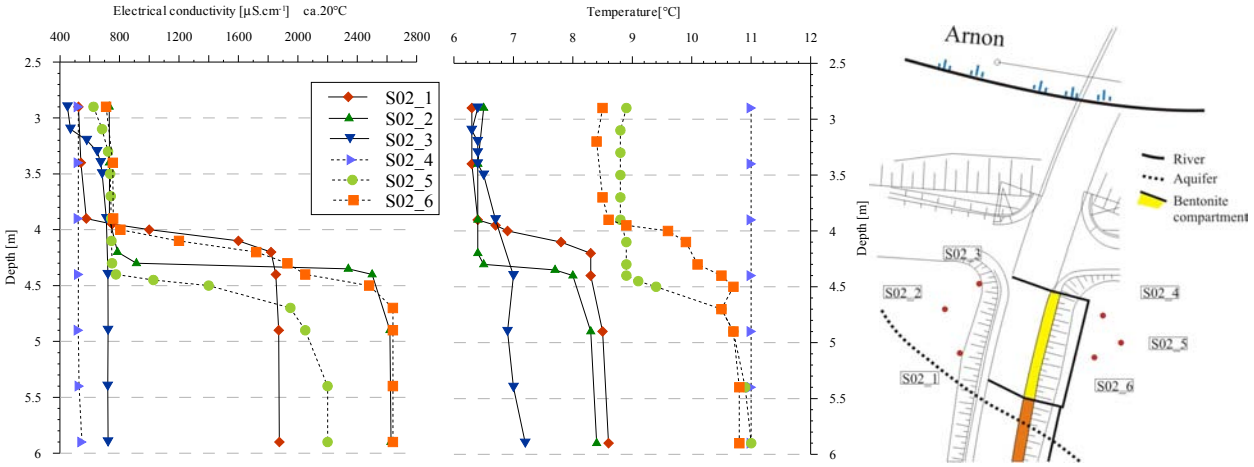

Figure 3.41: EC and T°C recorded in the six piezometers three days after the brine injection. The initial EC in all piezometers was roughly 2200-2400 µS·cm^{-1}. Augmentations at the bottom of some piezometers are due to the primary settling of the brine. Temperatures were roughly 6.5°C upstream, 8.5-9.5°C downstream. Piezometers standing far from the Arnon had brutal EC and temperature transitions within very small depth intervals (few cm to 20cm at max.). Transitions coincided with tube screenings. Bluish colours are used for piezometers close to the Arnon (S02_3 and 4) while reddish colours are used for distal piezometers (1 and 6). Greenish colours are used for piezometers in-between (2 and 5). Downstream piezometers are in light colours and dotted lines, upstream piezometers are in dark colours and plain line.

3.6.2.2 Slug test

Slug tests are used to determine the hydraulic conductivity K directly around the piezometers. This method usually works only with low hydraulic conductivity, which is not the case of the grandson aquifer. The principle is to remove (or add) water in a piezometer at once[36]. Regarding the slug test carried out all piezometers in Grandson, the assumption is made that K is bigger than 10^{-5} to 10^{-4} m·s^{-1}. Pumping test gives better results.

[35] In general, heterogeneous alluvial aquifers have great horizontal flow differences along the piezometer. This is due to the contrast of hydraulic conductivity in the different layers. The NaCl method is easy and fast to implement and allows selecting the best piezometer to use for future tracer tests.

[36] Using a tube sealed at its base for example. This method differs from the pumping test because it is not a continuous test. The water volume is removed in a few seconds.

3.6.2.3 Pumping test

A short term pump test has been performed in S02_5 to confirm this assumption (17/06/2004). It lasted 4h25 and the water level recovering has been monitored for 40 minutes. Pumping flow was 48 l·min^{-1}. The drawdown d has been monitored in each piezometer. Time step for measurement was short at the beginning and progressively increased. Figure 3.42 presents the drawdown in the piezometer S02_5. The drawdown did not level after a while but, to the contrary, increased its rate at the end of the test. The aquifer wall has been reached and thus the aquifer was not able to sustain the pumped flow. Nevertheless, the drawdown complies with the Jacob hypothesis during a significant time (from t = 2500 to t = 12000 seconds); it was therefore possible to calculate the transmissivity T_R, the storativity coefficient S_T and the hydraulic conductivity K.

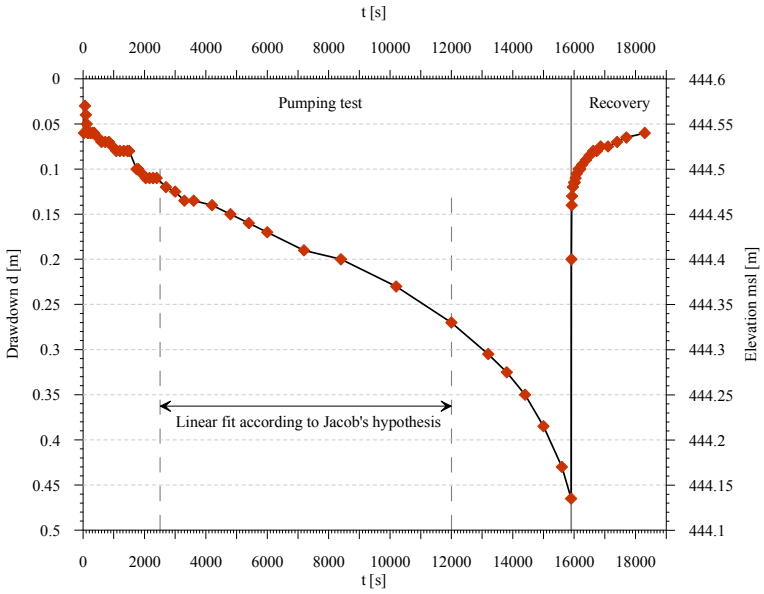

Figure 3.42: Drawdown and recovery (start at t = 15900s (4h25)) curves recorded in the piezometer S02_5. To the contrary of a common pumping test in a porous aquifer, the water table did not level when t augmented but decreases even faster; the aquifer wall has been reached (most likely the basal till which shallows up southward). Jacob's equilibrium regime occurs between t = 2500 and t = 12000s.

Calculations were made according to Jacob and Theis transitory regime equations. Results confirm an average K of $8.7 \cdot 10^{-4}$ m·s^{-1} in accordance with the geological settings. It also emphasises multiples heterogeneities (K ranges from $1.18 \cdot 10^{-3}$ to $6.72 \cdot 10^{-4}$ m·s^{-1}). Storativity coefficient S_T varies from 13 to 22% (S_T=0.132 to 0.223), still in agreement with geological background. The transmissivity T_R ranges from $1.18 \cdot 10^{-3}$ to $8.7 \cdot 10^{-4}$ m^2·s^{-1}. Upstream piezometers have shown a small late[37] non-significant drawdown. After 3h20 the water level decreased faster. This highlighted the presence of a highly impervious boundary. Calculations situated it in a radius of 14m from S02_5. This coincides very well with assumptions made during early geological investigations. Results are shown in table 3.7.

Piezometer		Jacob (transitory regime)		Theis (transitory regime)	
		T_R [m^2·s^{-1}]	**K [m·s^{-1}]**	**T_R [m^2·s^{-1}]**	**K [m·s^{-1}]**
S02-5	E = 1.3	$8.7 \cdot 10^{-4}$	$6.7 \cdot 10^{-4}$	$4.8 \cdot 10^{-3}$	$3.7 \cdot 10^{-3}$
S02-4	E = 3.0	$1.9 \cdot 10^{-3}$	$6.3 \cdot 10^{-4}$	-	-
S02-6	E = 0.9	$1.2 \cdot 10^{-3}$	$1.3 \cdot 10^{-3}$	-	-

Table 3.7: Summary of the different hydraulic conductivity calculated with the pump test data. E is the saturated thickness observed in the borehole logs. All results are in agreement with geological settings.

[37] From one hour in the S02_3 to 3 hours in the S02_1.

3.6.2.4 Tracer test

Punctual tracer test was performed (conservative Borax $Na_2B_4O_7*10H_2O$, 700 g in 5 l. water) from September 7th to 17th, 2004. Borax was injected in S02_2 (upstream) at once. Other piezometers were monitored during 10 days (2 samples per day were analysed with ICPMS-HR during the first 5 days, then 1 sample per day).

Piezometer	V_{pic} [m·d^{-1}]	V_{mean} [m·d^{-1}]	Dispersivity α [m]	Dispersion DL [m^2·d^{-1}]	K_{mean} [m·s^{-1}]
S02_1	55.7	16.0	0.76	12.2	3.94E-03
S02_3	9.7	4.8	1.29	6.2	9.42E-04
S02_4	220.5	54.2	4.09	221.7	1.20E-02
S02_5	250.8	63.5	4.33	275.2	1.45E-02
S02_6	237.7	56.9	4.24	241.1	8.11E-03
average	236.3	58.2	4.2	246.0	1.2E-02

Table 3.8: Aquifer parameters determined by the borax tracer test. Averages are given for the downstream piezometers; upstream piezometers values are given for information only. Flow direction is from W to E, parallel to the Arnon. Transit speed is very high (240 m·d^{-1}). According to the scale of this aquifer, the dispersive and diffusive processes must be as important as the advection process.

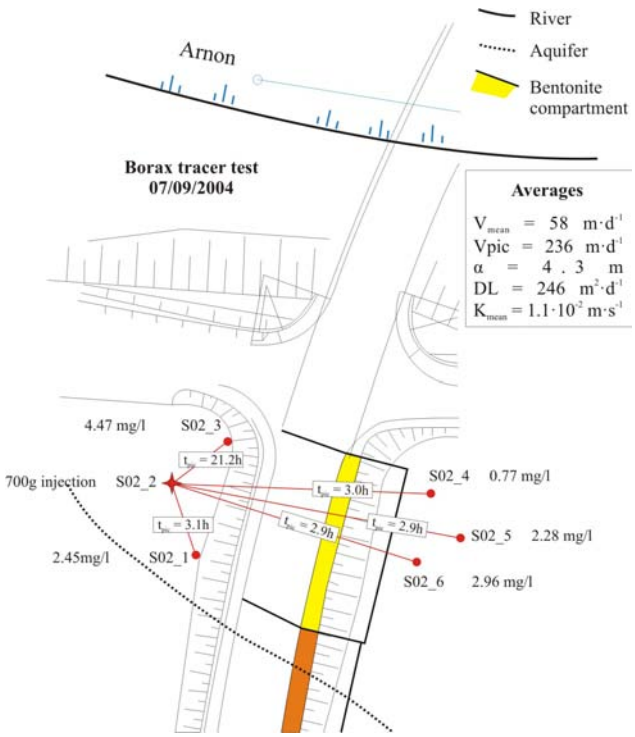

Figure 3.43: Schematic map of the tracer propagation. Borax took roughly 3 hours to go from S02_2 to all other piezometers but S02_3 (21 hours). This means the fluxes are from W to E. Piezometer S02_3 is "upstream" and only dispersivity and dispersion lead borax in that piezometer. Those two processes are as efficient as advection in such a small aquifer. The aquifer wall was deducted from the geological borehole and trench logs; distance was calculated using the pumping test results.

The hydraulic connection between up- and downstream piezometers is clearly established. Flow direction is from W to E[38]. Coefficients determination (table 3.8) has been made by fitting a model curve to the restitution curve (OFEV 2002 *"Utilisation des traceurs artificiels en hydrogeologie"*; Maloszewski 1985). Transit speeds are very high (peak speed $V_{pic} \approx 240$ m·d^{-1}, average real speed $V_{moy} \approx 58$ m·d^{-1}). Dispersion DL and dispersivity α are also very high (246 m^2·d^{-1} and 4.2 m respectively). Darcy's Law shows an average K of $1.1 \cdot 10^{-2}$ for the considered aquifer. It does not take heterogeneities into account. According to the considered scale, K ranges thus between $1.2 \cdot 10^{-2}$ and $9 \cdot 10^{-4}$ m·s^{-1}.

The hydraulic connection between the up- and downstream piezometers is hence clearly demonstrated (figure 3.43). Dispersivity and dispersion are very large but concordant with an aquifer of such a small volume. Those processes are postulated to be as important as the advection process. This is demonstrated by the very late but strong response of S02_3 placed "upstream" of the injection point. The effective speed V_{pic} does not really represent the solute speed; indeed, part of the injected mass stay trapped in the piezometer and is released punctually when conditions are favourable (flood, etc.). This is illustrated by the restitution curves given in appendix IX (multiple peaks). V_{mean} values are therefore preferred to assess the water fluxes in the aquifer (moreover, V_{mean} take into account the heterogeneity of the aquifer).

[38] Regarding the water table behaviour explained further, the tracer test was conducted in low water condition.

3.6.3 AQUIFER BEHAVIOUR

3.6.3.1 Water Table follow-up

Long term campaign of water table level measurements in the piezometers clearly shows seasonal variations of about 80 cm (March to end of September) uniformly distributed over the aquifer (figure 3.45). Rainfalls influence the aquifer water table mostly in spring and autumn, when the ground and soils are cold and saturated. The aquifer response is less visible in mid-summer; precipitations do not participate as efficiently as in winter to recharge the aquifer because the ETP is high and the soils are dry. For example, the heavy rainfall period recorded in late October 2004, after a long rainy period, induced a fast 1 m elevation of the water table. The aquifer highest level was recorded 1 day after the precipitation. To the contrary, the fairly high precipitation recorded in the first week of July 2004 did neither influence the water table nor the river at all. This confirms that the aquifer mostly respond to the river flow and merely directly to the rainfall in drought period.

Figure 3.44 also emphasizes the connection between the aquifer and the Arnon. A raise in the Arnon flow systematically induce a synchronous raise of the aquifer water table. Only the event of June the 1st and 2nd, 2004, demonstrates that the aquifer also reacts to precipitations in some circumstances. Indeed, this event caused a rather big elevation of the water table while the river did not exceed 4 $m^3 \cdot s^{-1}$, which is comparable to previous events (07/05/04 or 17/12/04 for example). Overall, the river caused the major fluctuations of the water table while precipitations only influenced it in rare occasions.

During low water periods (mid-summer) recorded in the aquifer, the underwater flow is clearly directed from the up- to the downstream piezometers (figure 3.46B). Fluxes run parallel to the postulated aquifer wall (see borehole and trench logs, appendix III). Piezometers S02_4 and 5 always gave elevation values close to each other, while S02_6 always had the lowest ones. It also presents a strong gradient in its surroundings, maybe caused by a local more impermeable layer. During low water period, the Arnon River clearly supplies the aquifer.

In flooding periods (like mid-March or late October), the water table distribution in the aquifer has sometimes a tendency to reverse in the upstream piezometers (figure 3.46A). Therefore, the fluxes are coming more from the W and not from the NW. This is always the case when the water table exceeds 445.3 msl. The aquifer recharge during high water is no as clearly linked to the river as in low water; it is very possible that the water comes from further west or from high infiltration along the basement till (south) deepening under the aquifer northward.

Overall, in both water table conditions, the average gradient is roughly 0.013, (1.3%) which is considerable. One could suppose that this high gradient is a consequence of the river bed configuration. Indeed, a few metres after crossing the bridge, the river passes over a step, creating a 70 cm fall. This fall is of course absent in the aquifer which may increase its head gradient locally due to stronger infiltration coming from the river (figure 3.44).

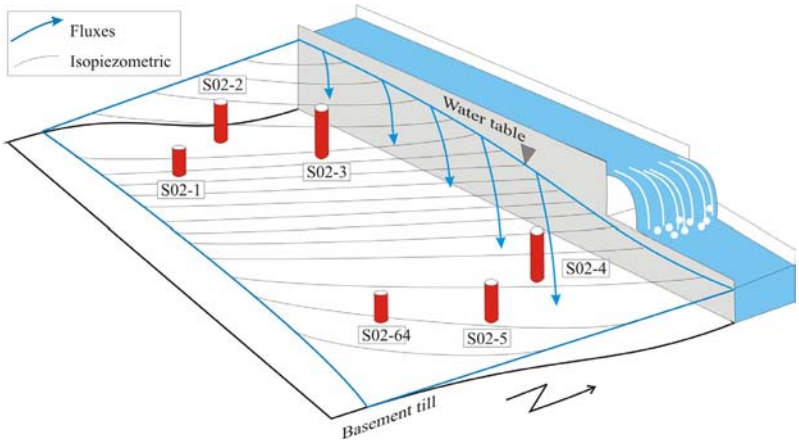

Figure 3.44: Illustration of the water table being affected by the river bed configuration. Note the gradient increases near the fall. Fluxes are therefore also greater. This would also explain why S02_4 is very active.

3.6.3.2 Electrical conductivity EC

EC was measured punctually using a WTW probe calibrated at 20°C. Measurements were conducted about 50 cm to 1 m below the surface. Results (figure 3.45B) demonstrated a strong link between the river EC and the aquifer. The EC indeed depicted a gradient from the river (≈ 300 $\mu S \cdot cm^{-1}$) to inland piezometers (≈ 600 to 900

$\mu S \cdot cm^{-1}$). A slightly smaller EC drop between up- and downstream piezometers (650-700 to 500-600 $\mu S \cdot cm^{-1}$) also exists. Considering the piezometers close to the river, S02_4 showed no fluctuation at all while S02_3 had remarkable EC peaks after considerable precipitations; it was fairly rapidly returning to its basal EC. The river or infiltrated precipitation strongly influenced those piezometers. Other piezometers reacted only modestly to precipitations or river rises.

Strong perturbations at the end of the year were due to heavy duty field work carried out in the upstream area. Excavators and trucks have filled and levelled the plain with exogenous material (agricultural soils) that have been leached for weeks by precipitations. It is therefore not surprising to see high EC during long periods in all piezometers. Interpretations do not take those values into account.

Altogether, the EC were pretty stable along the first half of the year. No seasonal variation was visible. EC coming from piezometers other than S02_3 and 4 did not seem to be particularly linked to the river or the precipitation. Water table rises indiscriminately induced sometimes dilution and fall of the EC, sometimes high substance content and higher EC.

3.6.3.3 Temperature

Strangely, temperature measurements (figure 3.45C) in the piezometers close to the river were fairly stable while the river temperature fluctuated seasonally. Indeed, S02_4 had almost the same temperature throughout the year; other piezometers had values more affected by the season. This is explained by a different rate of renewing of the water volume in that piezometer. This has also been shown in the brine injection test[39]. Rises of temperature in the piezometers are therefore due to temperature conduction and exchange in the soils and aquifer material. All piezometers nevertheless reacted to infiltration of precipitation or river water, showing slight temperature adjustments. Downstream piezometers are less influenced by the seasonal temperature changes, while upstream piezometers are strongly influenced by those changes. This means that there is a greater water renewal rate in downstream piezometer. This is in agreement with conclusions based on EC, water table follow-up and various hydrogeological tests.

3.6.4 CONNECTION BETWEEN THE AQUIFER AND THE ROAD RUNOFF

During the watering test n°1, NaCl brine was deposited on the road – SB shoulder boundary to note the connection between the road runoff and the aquifer. NaCl thus infiltrated the LB infiltration slope. As mineral trace elements (MTE) were also measured during this particular test, results are presented in §4.6.1. The connection between the road runoff and aquifer could not be emphasized. The chorine plume was either missed, either completely buffered by the aquifer volume. In case it was missed, there was no tailing: the peak would have been very low. It is also possible that the brine plunged to the bottom of the aquifer. Despite the early sampling (first sample taken 1 hour after the injection) and the homogenisation of the piezometer volume, the Cl^- concentration stayed around 11 $mg \cdot l^{-1}$ in S02_4 and 16 $mg \cdot l^{-1}$ in S02_5. The river was 7.7 $mg \cdot l^{-1}$. This of course does not mean that there is no connection. The road runoff inevitably infiltrates the aquifer.

[39] During the brine test, S02_4 kept the same temperature all along its profile, showing no temperature gradient at all. Other piezometers had strong temperature and EC transitions levels, although the transition in S02_3 was not so marked. See figure 3.41.

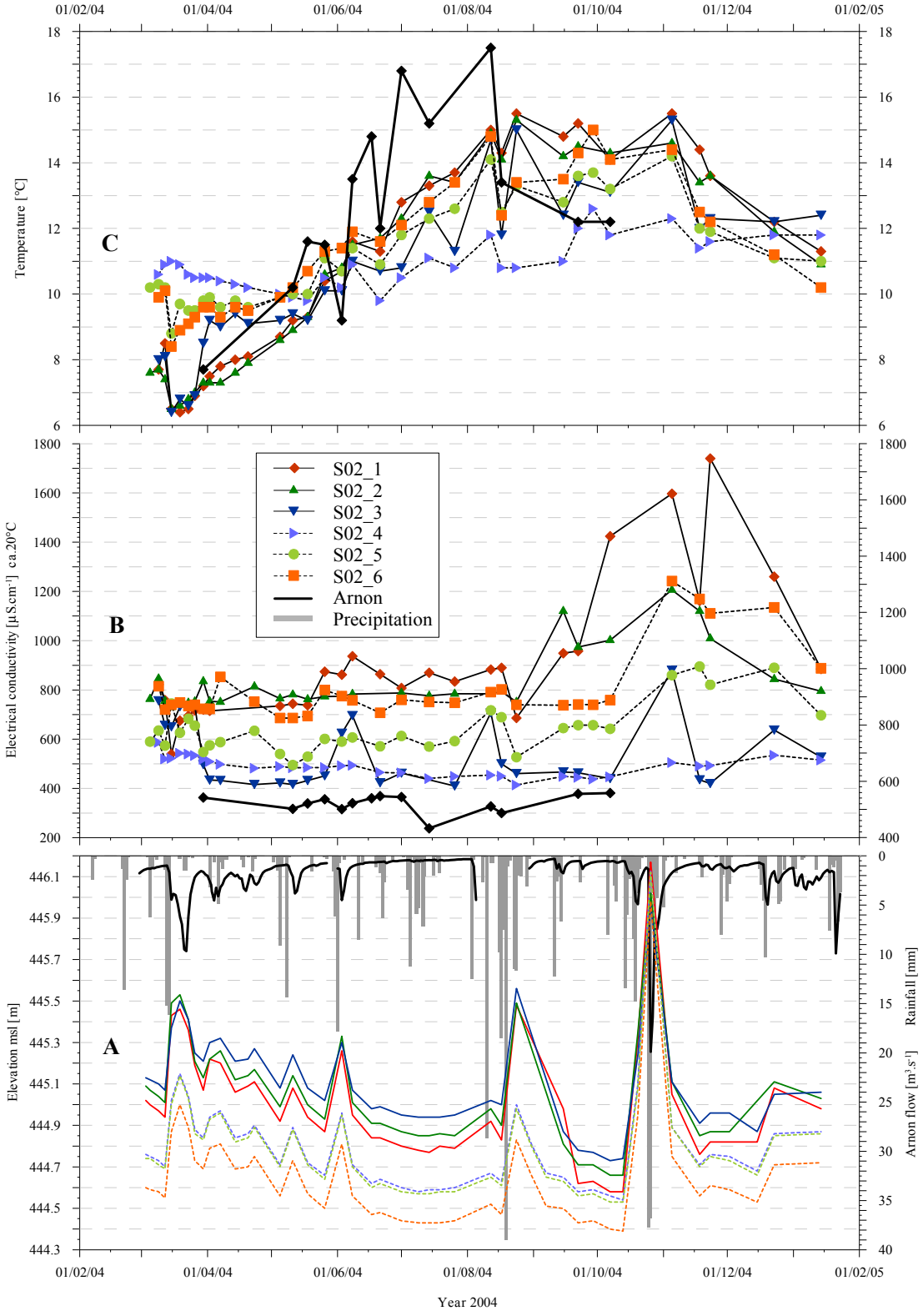

Figure 3.45: Annual behaviour of the 6 piezometers implemented in the experimental Grandson site. ***A)*** *Water table elevation in year 2004. The water table response is clearly linked to the Arnon flow and to the precipitation. In a few cases, the hydraulic gradient and thus the flow reverse (March, the 14th and 15th in the upstream piezometers for example). Overall, the water table is linked to seasonal changes.* ***B)*** *Electrical conductivity in the six piezometers. The EC in the river is fairly stable (320 µS·cm^{-1}). Piezometers close to the Arnon (blue) have also the lowest EC. The upstream piezometer (dark blue) responded to rainfall events while the downstream piezometer (light blue) did not.* ***C)*** *Temperature in the piezometers. Piezometers close to the river have the lowest amplitude difference (10 to 12°C for S02_4) while the piezometers far away have a larger amplitude (6.5 to 15.5°C for S02_1). Differences also exist between up- and downstream piezometers. The Arnon River has an average seasonal trend.*

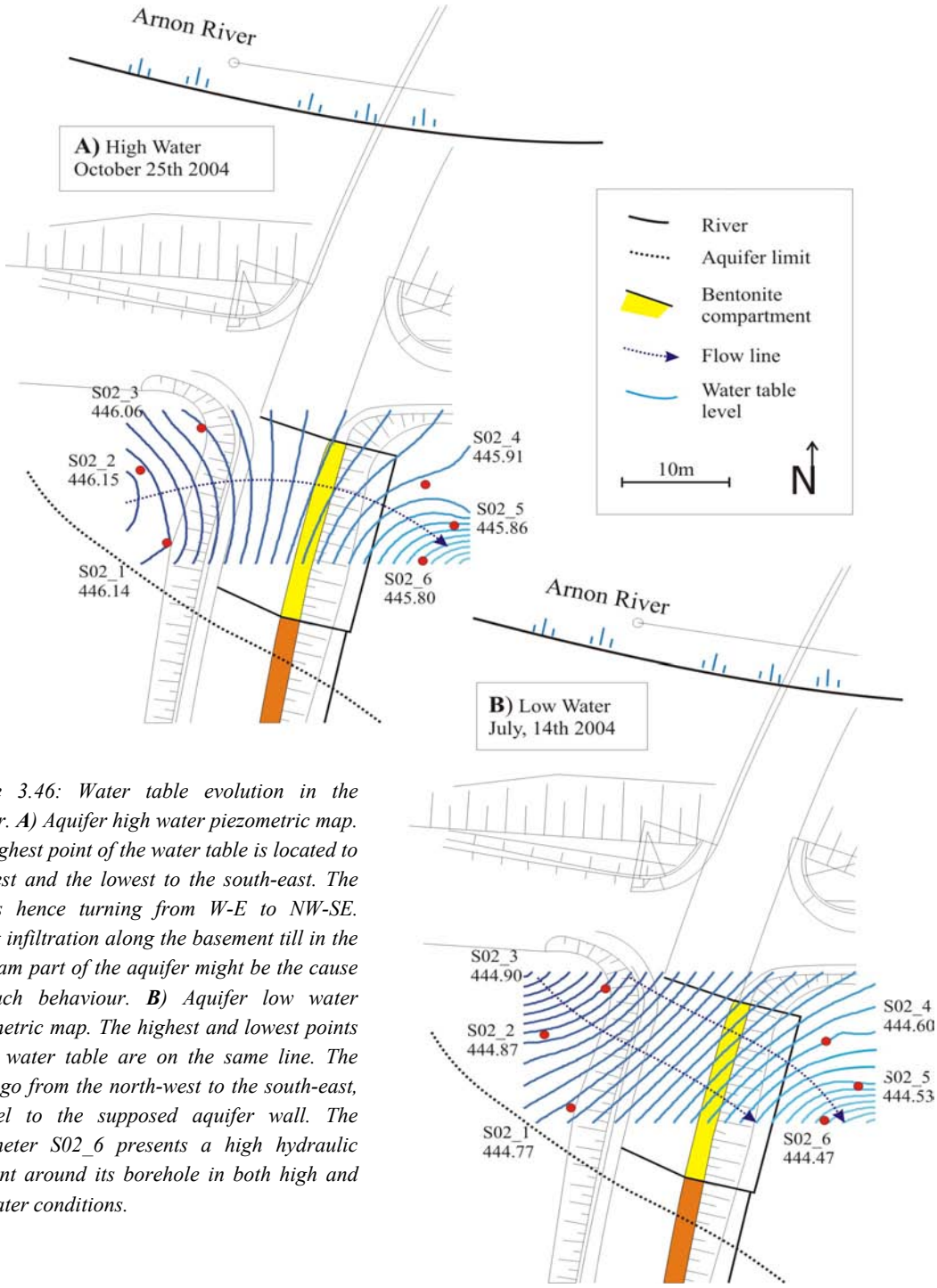

*Figure 3.46: Water table evolution in the aquifer. **A)** Aquifer high water piezometric map. The highest point of the water table is located to the west and the lowest to the south-east. The flux is hence turning from W-E to NW-SE. Strong infiltration along the basement till in the upstream part of the aquifer might be the cause for such behaviour. **B)** Aquifer low water piezometric map. The highest and lowest points of the water table are on the same line. The fluxes go from the north-west to the south-east, parallel to the supposed aquifer wall. The piezometer S02_6 presents a high hydraulic gradient around its borehole in both high and low water conditions.*

3.6.5 SUMMARY

The aquifer underlying the experimental site has a high hydraulic conductivity K (average K of $1 \cdot 10^{-3}$ m·s^{-1}) and a low volume (efficient porosity n_e = 13-22%, thickness e = 1 to 3 m). The average transmissivity T_R is $1.5 \cdot 10^{-3}$ m^2·s^{-1}. The aquifer is located in alluvial material, laid there by an ancient river bed. Alluvial material overlies a basement till which is highly impermeable. The basement till shallows up southward and thus constitutes the southern aquifer wall. It is situated only 14 m south from S02_5.

Water fluxes within the aquifer are clearly NW-SE in low water, W-E in high water conditions. This is confirmed with the tracer test. Due to its small size, the dispersion and diffusion processes are postulated to be as important as advection. Values are indeed very high. The fluxes real speed are around 60 m·d^{-1}, which is quite high. The head

gradient is 0.013, surely augmented by the river bed configuration. Exfiltration limit is unknown but might coincide further downstream with the Arnon River; it is also possible that the aquifer widen in the plain eastward.

Downstream piezometers are much more active than upstream ones. Their water content is renewed at a faster rate than those upstream. This means a higher rate of infiltration coming from the river, due to a higher gradient (see figure 3.33). Every piezometer but S02_4 has a "dead" volume situated at its bottom; old water may be trapped there. This dead volume is hard to remobilize; only time allows a good dilution.

The aquifer is clearly linked to the nearby Arnon River which alters the water table and water physical properties quickly (1-2 days). The river is the principal source of alimentation; this is even clearer in summer when the soil and unsaturated zone are dry. In that case only the river aliments the aquifer. Also, the aquifer water table follows the seasonal cycle the river water flow. In term of volume, the influence of precipitations directly infiltrating the aquifer could not be clearly enlightened but surely exists. Substances infiltrating the aquifer are discussed in chapter 4.

3.7 SUMMARY

In this chapter has been analysed the hydraulic behaviour of the road – shoulder – infiltration slope – alluvial aquifer profile. For this purpose, numerous methods and instrumentation have been used. Key data were the exfiltration flows, the precipitation and the climatic parameters. TDR method proved to be useful to measure the soil moisture and calculate Darcy's fluxes q. The number of natural precipitation events analysed was 112. All of them caused a road runoff. Natural rainfall events were not sufficient to understand the infiltration processes taking place in the shoulders and soils. For that reason, three artificial infiltration tests were conducted. Artificial test n°1 and 3 greatly helped to understand and illustrate the flow pattern. Those two tests had large infiltration volume, far beyond the return period of 20 years.

3.7.1 The ROAD

- The road runoff coefficient C_R is 1. The road runoff hydrogram thus mimics the rainfall hyetogram.
- The water dissemination caused by vehicles is almost inexistent. This is because the road has a very low traffic which circulates at low speed. Also, the steep slope favours the fast evacuation of water from the road.
- Road runoff always has a first flush effect, it is widely discussed in chapter 4.

3.7.2 SHOULDERS

- It has been illustrated that the shoulder has to handle potentially large volume of water running from the road. This is even truer in the case of the Grandson experimental site where all the road runoff is directed to one side of the road. The road surface in Grandson corresponds to one side of a motorway, in case the road runoff is evacuated to both sides.
- During the infiltration process, the infiltration function i can be assessed with the modified semi-empirical Green & Ampt equation (1911). It describes a moisturizing front linearly advancing downward.
- Once wet, the shoulder is permeable and infiltrate large amount of water. Infiltration fluxes can be as high as $1 \cdot 10^{-5}$ m·s^{-1}.
- Vertical hydraulic conductivities range from $4.6 \cdot 10^{-6}$ (SGC) to $2.2 \cdot 10^{-5}$ m·s^{-1} (SGL).
- Lag times are shorter than those recorded in the lysimeters. They range from a few minutes to 1 hour. The lag time is a function of the mean intensity.
- As demonstrated by the statistical analysis, the exfiltration volume E_S is essentially a function of the available water A_W; it can be easily calculated by simple empirical equations. All shoulders have their own fitting equation factors.
- Tracer test (NaCl) demonstrated the presence of two flow paths: the macroporosity drives the water efficiently and rapidly, while the microporosity is less efficient and retains the moisture longer.

- Tracer test proved that most of the first flush passed over the shoulder. This is also confirmed by the fluxes q computation. The shoulder is highly impermeable at the beginning of a precipitation.
- Runoff coefficients C_R range from 0.3 (SGL) to 0.9 (SB). This coefficient decreases rapidly once the shoulder is wet (unless for SB which never exfiltrated any water in natural conditions).
- Considering the shoulders *raison d'être*, i.e. to drive the water to the infiltration slope, the best behaviour is met in the SB. It indeed never showed any exfiltration during natural event. The shoulder SH proved to be inefficient for structural and material reasons. Other shoulders are comparatively ineffective.

3.7.3 UNSATURATED ZONE

- Lag times are usually greater than those encountered for the shoulders. Exfiltration volumes E_L are high in case of large event.
- Lag time are function of the mean intensity. The influence of API exists but is hard to illustrate.
- As it has been demonstrated by the statistical analysis, the exfiltration volume E_L can be approximated by a simple equation. Indeed, the E_L is only function of the API and available water B_W.
- Fluxes in the soils are dependant of the hydraulic conductivity (modify the q magnitude) and suction (modify the q direction).
- Moisture redistribution processes occur in the soils as long as there is a volumetric water content θ gradient. As evaporation occurs all the time, redistribution is unlikely to cease. Only when θ is equal to the residual θ_r will no longer be flux.
- Fluxes strongly vary in magnitude and direction during a precipitation: usually from about $1 \cdot 10^{-8}$ to $1 \cdot 10^{-5}$ $m \cdot s^{-1}$ and from up- to downward.
- Water infiltrates at the top of the lysimeter. It then runs over the geomembrane and over the slope surface. The place where the slope is the steepest does not infiltrate much.
- The first flush effect is poor to medium. NaCl signal is highly buffered.
- The LH lysimeter showed many clues of dysfunction. It indeed had shorter lag time, higher exfiltration volume and higher tracer restitution. It finally had a strong first flush effect. Remember that this lysimeter has almost twice the volume of LW and should therefore have shown the reverse trend. Solving the empirical equation linking E_L to API and B_W confirms the bad behaviour of LH: it is not function of API.

3.7.4 SATURATED ZONE

- The alluvial aquifer is narrow (50 m); it is confined between the Arnon (north) and a basement till which shallows up southward. Eastern and western limit are less known but might coincide with the river.
- Different tests and studies have been conducted to assess the aquifer parameters: NaCl tracer test, slug test, pumping test, borax tracer test, piezometric level follow-up, and physicochemical recordings.
- The aquifer has the following properties: the mean horizontal hydraulic conductivity is $1 \cdot 10^{-3}$ $m \cdot s^{-1}$. The transmissivity is $2 \cdot 10^{-3}$ $m^2 \cdot s^{-1}$ (mean thickness e is only 2 m). The real average speed is 60 $m \cdot d^{-1}$. Dispersivity and dispersion are very high but concordant with such a small aquifer. It is postulated that half of the water movements are due to those processes, and half to advection.
- The pumping test demonstrated the presence of an aquifer wall. It is postulated that it is the basement till, south of the experimental site. The calculated position coincided well with the geological interpretation.
- The aquifer has a strong gradient which is caused by the step profile of the river bed. This also augments the water fluxes in the downstream piezometers.
- The aquifer is clearly linked to the river. This is proved by the piezometric level, EC and T follow-up. EC and temperature also emphasize the higher activity in downstream piezometer, especially S02_4.
- The road runoff infiltration could not be emphasized by the NaCl tracer test. The infiltrated water concentration was possibly buffered by the aquifer volume. Also, the brine was heavier than the aquifer water: it could have plunged to the bottom of the aquifer.

CHAPTER 4

CHEMICAL BEHAVIOUR

Once the road runoff successfully ran over the shoulder and infiltrated the infiltration slope, contaminants are in contact with the soils material. Some processes may then occur that trap the contaminant in the soil (sorption, (co-) precipitation, etc., those are discussed later). However, as efficient as they are, those processes hardly completely retain contaminants: it is just a matter of time until the contaminant migrates downward. Complete and irreversible fixation/elimination may exist (ion complexation, absorption, phyto- and bioremediation for organic compounds, etc.) but needs a lot of time. Therefore, the more retarded is the contaminant, the more unlikely the contaminant will ever reach the aquifer.

In this chapter is therefore discussed the geochemical behaviour of road substances[1] when infiltrating one A and one B soil horizons. The retention (through adsorption, absorption, (co-)precipitation) of substances is assessed comparing the road runoff dynamic with the infiltration dynamic. This chapter is divided in five main parts:

1) Analytical considerations are presented. They include soil and water sample treatments, methods and calculations. A small reminder of the sampling strategy is also showed.

2) Results of the batch tests are provided. Those tests allow calculating the distribution coefficient K_d in a static environment. Interpretation of the coefficients gives strong insight of the contaminants behaviours in the Grandson soils. K_d is generalised for other typical Swiss soils. Batch tests have been performed on Grandson soil by Martine Docourt, in a postgraduate diploma thesis integrally carried out in the frame of the present project ("Mobilité des pollutants routiers dans les sol. Exemple des HAP et des ETM", GEOLEP, 2005). Also, generalisation to Swiss soils have been done with the help of two trainees (P. Kerhervé and M. Fouquet), from the ENGEES (Ecole national du génie de l'eau et de l'environnement de Strasbourg).

3) Results concerning the column tests are presented. Those tests were made to assess and simulate the infiltration of MTE (mineral trace elements) and PAH (polycyclic aromatic hydrocarbon) into the Grandson soils. Calculation of dynamic distribution coefficients K_d are also displayed, as well as comparisons between K_d coming from the batch and column tests. Column tests have been performed by Docourt (2005) in the frame of her postgraduate diploma thesis.

4) The illustration of the substance behaviour, retention, and releasing in the in situ Grandson soils is provided using the single example of the artificial infiltration test n°2. This test was made with rainwater collected on PE (polyethylene) sheet covering roofs at the EPFL site. This constitutes the key paragraph of this chapter.

5) Chemical behaviour is generalised, taking all studied natural events into account. Mass balances are assessed for particular substances. Generalisation also assesses the potential substance retention in other particular Swiss soils (Jura, Plateau, Alpine soils).

4.1 ANALYTICAL CONSIDERATIONS

In this specific paragraph, insight of the methodology and strategy used for sampling and analyses are presented. Soils have been sampled to assess the substance concentration that has been retained in soils during the infiltration; while exfiltration flows and aquifer were sampled to assess the concentration of substances that were mobile. The Arnon River was sampled to assess the background pollution level.

[1] The word « substance » includes contaminants, pollutants and geogenic elements indistinctly.

As it has been explained in paragraph 1.4.3.3, the strategy was designed to take into account the different transportation means, i.e. solute and particular (and colloidal) transports. All samples were acidified prior to filtration. This forcibly allows all particles to release its sorbed substances. The measured concentration is thus the maximal potential concentration[2]. Therefore, the substance concentration measured in soil samples includes all those concentrations:

- the concentration of substances that were sorbed to the soil matrix
- the concentration of substances that were sorbed to trapped particles and colloids
- the concentration of substances that were trapped in the retention water (permanent water film around soil grains)
- the concentration of substances that have precipitated

Sample treatment may also liberate substances that were part of the matrix composition (clay often contains a wide range of elements, more or less free). Differentiation of all those concentrations is not made in the present study.

The substance concentrations analysed in water samples include:

- the solute concentration
- the concentration of substance sorbed to colloids and particles liberated by the acidification

As particles and colloids may travel as fast, or even faster, than a dye tracer (Ryan and Gschwend 1990), it is of course indispensable to intercept the colloids and its possible substance load. Acidifying prior to filtration ensure that all the potential substance mass is taken into account.

Substances analysed were largely concurring with the previous study of Parriaux et al. (1999). Indeed, strong determination (ACP, linear correlation) of all studied road substances has been made in that study. It thus did not need further determination. MTBE and PCB were added. Table 4.1 lists the substances that were considered during this study.

4.1.1 WATER SAMPLES

Overall, more than 300 water samples were collected from the different collecting points. Collecting points were the exfiltration drain pipes (8 of them), piezometers (6 of them) and the river (figure 2.4, 2.5). Samples have also been taken in the water tanks prior to artificial precipitation tests, to assess the background level of the rainwater. Different sampling methods have been tested (automatic sampler, first flush sampler) but the most efficient proved to be hand sampling. The latter has been used whenever it was possible. Not all events were sampled. Hand sampling permits evidently all types of sampling. It is nevertheless very constraining due to the specificity of this study, i.e. event based strategy. It thus needed extended logistic and manpower.

Automatic samplers (ISCO 6712) were difficult to trigger. Water detection was not always satisfying but the major problem was to take sample directly in the reception funnel[3] (to avoid sampling a large totalized volume of water directly in the weirs, thus not directly related to the current event). Indeed, when the sampler sucked up all the available water in the funnel, it defused. Therefore, the volume of water collected was generally insufficient. Also, samplers could not accommodate the 2 types of bottles.

The wide range of pollutants being analysed also imposed two types of bottles, thus making the sampling more difficult. PE bottles (0.5 litre) were for the trace mineral elements (MTE), while the glass bottles (1 litre) were for the volatile and organic compounds. The latter needed to be filled up to the top to avoid volatile compounds release.

[2] This is true for soil *and* water samples.
[3] The reception funnel is the funnel located directly under the collecting pipe arrival, in the collecting chamber. Water flowing in the pipe first arrives in the funnel.

Organic compounds					Inorganic compounds	
C_X	BTEX	PAH	PCB	Additive	MTE	Anions
C10	*benzene*	*Naphthalene*	28	*MTBE*	Al	Cl
C11	*toluene*	*Acenaphtene*	52		B	NO_3
C12	*ethylbenzene*	*Fluorene*	101		Ba	SO_4
C14	*p+m xylene*	*Phenanthrene*	149		Br	
C16	*o xylene*	*Anthracene*	118		Cd	
C18	*isopropylbenzene*	*Fluoranthene*	153		Co	
C20		*Pyrene*	105		Cr	
C24		*Benzo(a)anthracene*	138		Cu	
C28		*Chrysene*	128		Fe	
C32		*Benzo(e)pyrene*	156		Mn	
C36		*Benzo(b)fluoranthene*	180		Mo	
C40		*Benzo(k)fluoranthene*	170		Ni	
		Benzo(a)pyrene			Pb	
		Dibenz(a,h)anthracene			Rb	
		Benzo(g,h,i)perylene			Sb	
		Indeno(1,2,3c,d)pyrene			Sc	
					Ti	
					U	
					V	
					Zn	

Table 4.1: Exhaustive list of all substances analysed in this project. Note that all substances were not analysed in all samples. See paragraph 2.7 for discrimination process.

A special installation was designed to take the first sample during the first flush event. First flush sampling consisted in one glass bottle and one plastic bottle linked to the reception funnel with a hose (1 cm internal Ø). Smaller hoses (1 mm internal Ø) directed upward permitted the air to go out when the water comes in. Bottles were sealed. When the bottles are full, water fills the 1 cm hose and makes the funnel spill out. This sampling method was especially interesting to collect the first flush and first amount of water getting through the shoulders and lysimeter.

Samples in the aquifer and Arnon River were taken with a stainless steel cylinder. The cylinder was thoroughly cleaned with the water to be collected between each sample. Between each sampling campaign, the cylinder was cleaned with HNO_3 5% to avoid contamination by prior samplings.

4.1.1.1 Inorganic compounds

Samples were taken into new 5 dl PE bottles. Bottles were previously rinsed with water to be collected. Samples were acidified with HNO_3 (65% Merck) soon after returning from the field. Acidification ensures that the MTE compounds do not (co-) precipitate (Taylor 1989) or bond to the bottle material. They were then stored in fridges (4°C, Bensimon and Parriaux 1990; Bensimon et al. 1991) until decision was made to analyse or discard the sample (see paragraph 2.7.2). Anyway, all samples were kept in the fridge to ensure later access. Acidified samples may stay in fridges for long period until analyses. Once the decision to analyse the sample was made, the sample was filtered on 0.45 µm filters (see appendix IX for complete methodology).

The sample MTE were then analysed by ICPMS-HR (Inductively Coupled Plasma Mass Spectrometer – High Resolution) at the GEOLEP (Bradshaw et al. 1989; Bensimon et al. 1994). Trace element analyses of runoff samples were performed with Inductively Coupled Plasma Sector Field Mass spectrometer (ICP-SFMS). The Inductively Coupled Plasma Mass spectrometry (ICP-MS) is well-known to be an extraordinarily sensitive analytical technique because of the much lower background signals and higher ion transmission. The ICP- SFMS instrument used in this work was the Finnigan™ Element2 High Performance High Resolution ICP-MS, which consists of a double focusing reverse geometry mass spectrometer.

Results were provided in concentration [$\mu g \cdot l^{-1}$]. MTE analysed are listed in table 4.1. Detection limits were less than 0.2 $ng \cdot l^{-1}$ for all elements.

Anions (chlorine, nitrides, sulphides, bromines) were measured using HPLC (High Pressure Liquid Chromatography; Dogan and Haerdi 1981). In chromatography (liquid or gaseous), a mobile phase is running through a static phase. The mobile phase is pumped (constant pressure and flow). The sample to analyse is added to the mobile phase. Substances in the mobile phase are not equivalently retained by the static phase. It depends of the considered substance. Substances are thus separated. Their passage durations qualitatively characterize the substance, while the intensity of the chromatogram quantitatively characterizes the substance.

4.1.1.2 Organic compounds (Kelly et al. 2000, modified by CECOTOX)

Water samples were taken into brownish glass bottles to avoid light reaction. Screw caps had inside membrane to ensure that no air bubbles remain atop of the liquid. Samples were poured into aluminium caskets as soon as returning from the field. Caskets were then covered and put into freezer for conservation. Concerning volatile compounds (BTEX), they were immediately analysed as soon as back from the field. See appendix IX for complete methodology.

PAH and C_X were detected using HPLC-FLD (High Pressure Liquid Chromatography coupled to Fluorescence Light Detection), System HP1050, column Vydac 201TP54 (25cm x 4.6mm), $1ml \cdot min^{-1}$, 50:50 % ACN:eau, ACN gradient at 100% in 20 minutes, total time 40 min.

Results are provided either in $ng \cdot l^{-1}$ (PAH, PCB, BTEX, MTBE), either in $\mu g \cdot l^{-1}$ (Aliphatic hydrocarbons C_X).

4.1.1.3 Physicochemical parameters

Electrical conductivity EC: The EC is a global parameter measuring the global mineralisation of water. The EC corresponds to the conductance of the water volume located between the cathode and the anode, each of them having a surface of $1cm^2$ and separated by 1cm. Many empirical approximations exist to calculate the total dissolved solids TDS from EC: $TDS = 0.67 \cdot EC$ [$mg \cdot l^{-1}$] is widely used (the factor ranges from 0.5 to 0.9). Knowing the TDS is important to assess the water load. MTE content is associated with TDS (Tyagi et al. 2003). The EC was continuously measured in the road runoff and punctually measured in other samples. The exception is for artificial precipitation tests where EC were continuously measured in all exfiltration flows, as well as in column tests. The probe was a WTW LF 323.

The pH: the pH is not easily measured. The probe needs a lot of care and calibration is frequently necessary. It is nevertheless an important parameter because it really strongly affects the substance behaviours. The more acidic the soil (or rain) is, the less the MTE is likely to be sorbed. On the contrary, an alkaline soil is more apt to retain MTE. As it is demonstrated in paragraph 4.2.2.3, the pH is the key parameter describing the soil retention capacity. The pH was punctually measured in the exfiltration flows (in situ and column tests). The exception is concerning the artificial precipitation tests where pH was continuously measured. The probe was a WTW pH 323.

The turbidity: the turbidity is an empirical measurement describing the water ability to absorb the incident light. This property is caused by all kinds of suspension particles (colloids, detritic particles, OM, living material, etc.). Those particle sizes range from the nm to the mm. This parameter is of upmost importance because particles offer large surfaces for interaction with contaminants. Particles also have specific transport behaviours: they can travel as fast (Enfield, Bengtsson et al. 1989; Dunnivant et Jardine 1992) or even faster (Ryan and Gschwend 1990) than a conservative tracer. It is therefore very important to keep records on the turbidity behaviour. In the frame of the present study, the turbidity is also a good indicator of the dry deposition on the road between rain events. It induces the first flush effect. Turbidity measurements were carried out with a fluorometer GGUN FL-22; 660nm wavelength IR led. Turbidity was always measured along with EC.

TOC (total organic carbon): The TOC is the addition of the DOC (dissolved organic carbon) and POC (particular organic carbon). The DOC includes all organic carbon elements smaller than 0.45 µm (hydrophilic or humic acids for example), while the POC includes the bigger particles. Generally, natural water POC content is negligible and hence the TOC = DOC. As this project does not deal with natural water, the TOC is kept. If there is a straight correlation between the TOC and PAH or Aliphatic hydrocarbon content is unclear. While some authors (Petruzzelli et al. 2002, Wang et al. 2005) demonstrated that a high correlation exists between PAH and TOC, some other (Fredrickson 2003 for example) denied this relationship. However, the present work shows that a correlation, although not perfect, exists between TOC and organic compounds in the road environment. The TOC was measured with a fluorometer GGUN FL-22; 254 nm wavelength UV led. TOC was always measured along with EC and turbidity. The specific wavelength of the led is accorded to the specific light absorption of TOC (Savoy et al. work under progress).

4.1.2 SOIL SAMPLES

Here is described the soil sampling method. It concerns soil sampling in the experimental site of Grandson and in other Swiss locations as well (Vallorbe, Vevey, Villard). Soil samplings in Grandson were made three times in 4 years to observe the substances concentration evolution. Soil samples (A and B horizons) were also taken near Vevey, Vallorbe and Villard (see localisation in paragraph 4.2.2.3). Batch tests have been carried out on those samples to assess the possible generalisation of the Grandson results to all Switzerland. Substance extraction was carried out to create solutes; those could be analysed the same way as the water samples. No sample was taken from the shoulder to avoid destroying them.

However, this paragraph 4.1.2 only concerns the substance extraction (lixiviation) and not the batch tests methodology. That is described in paragraph 4.2.2.

In grandson, the first sampling campaign was carried out during the infiltration slope construction, in early 2003. The second sampling was made in preparation for column tests (September 2004). Soils were then reconstituted in the PE column. Column tests are thoroughly described in paragraph 4.2.3. The third sampling campaign was carried out in early December 2006. Samples in other Swiss location were taken in summer 2005.

Soil sampling was carried out with a cleaned auger and a small spade. Auger and spade were cleaned with fresh water prior to each sampling campaign. Samples localization and depths were thoroughly noted. Samples were then put in plastic bags (inert food freezing bags). Once back from the field, samples were stored in PE Tupperware for air drying in a clean place.

For inorganic elements, soil samples have been dried at 105°C for 24 hours. They were then sieved at 2 mm. Ten grams of soil were put in an Erlenmeyer with precisely 100ml of HNO_3 2M. The Erlenmeyer is then covered with a glass dish and plunged in a 100°C water bath. After one hour, the suspension is filtered (hot filtration) in a 100 ml PE bottle. Filtrate is then diluted and analysed with ICPMS-HR (paragraph 4.1.1.1).

The solid – liquid extraction of organic compounds only concerns the PAH. Indeed, BTEX and MTBE are postulated to be far too soluble to be sorbed. Aliphatic hydrocarbons were not measured in soils. Specific methodology is shown in appendix IX.

4.1.3 ARTIFICIAL PRECIPITATION TEST N°2

As mentioned in chapter 3, the thunderstorm-like event is the more likely to infiltrate rapidly and efficiently huge amount of water. Consequently, thunderstorms also are more prone to create first-flush effect, and to mobilize all

sorts of contaminant from the surface of the road[4]. The follow-up of all natural rainfall events confirms that the higher contaminant concentrations were met shortly after a storm. Subsequently, in order to obtain complete and controlled measurements of the contaminant transportation, an artificial precipitation test was designed. The artificial test n°2 allowed testing the first flush effect and contaminant transportation while controlling every aspect of the road watering. Also, because all compartments were watered one after another (in June 2005), instruments were moved from one exfiltration point to the other. The following parameters were measured in all exfiltration flows: flow Q, EC, T°C, pH, O_2, Turbidity, and TOC. About eight samples per exfiltration point were taken and analysed for all contaminant (table 4.1).

The experimentation protocol was as follow:

- Rainfall water was collected on PE sheets covering a building roof at the EPFL site. Two closed tanks of 1 m^3 each were filled. Gutter and funnel were made of PE; tanks were in fibreglass. One sample was taken in each tank for analysis after homogenisation.
- To precise the shoulder runoff, three PE gutters were installed at the SGH, SGC and SGL edges (figure 4.1). The shoulder runoff flows were therefore measured. Gutters trench were made impermeable by mixing the excavated material with bentonite. A special effort was made to especially tighten the upstream side of the gutters. Samples were also taken there. The presence of gutters allows measuring the variable R_S directly; thus the only unknown variable was the stock variation ΔS_S[5].

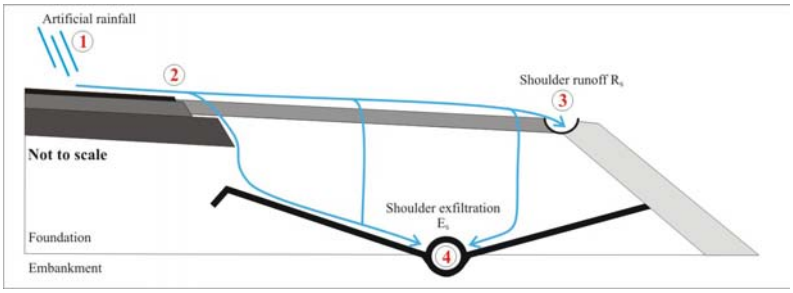

Figure 4.1: Location of the water measurement points in SGH, SGC and SGL. The precipitation (1) was measured at the watering hose outlet, while the shoulder runoff (3) was measured in the gutter outgoing flow. The road runoff (2) and shoulder exfiltration (4) were measured in the exfiltration pipes.

- The pumping and watering hoses were abundantly rinsed with fresh river water, emptied and then rinsed again with rainwater in close circuit. The watering method was improved since the artificial test n°1. Watering was more diffuse and thus more rainfall-like.
- The precipitation hyetogram was designed to simulate a thunderstorm-like rainfall. The rainfall volume was about 7 mm; the mean rainfall intensity was 23 $mm \cdot h^{-1}$. Figure 4.2 shows the watering hyetogram. During the watering, the flow was constantly measured with a flowmeter coupled to the hose. Tests were performed after a long dry period of nine days at minimum. The duration of the dry period indeed controls the contaminant concentration on the road (Hermann 1981).
- Samples were taken directly out of the exfiltration pipe. The first flush effect was sampled by taking the first water coming out of the exfiltration pipe. Six to nine samples, depending on the exfiltration volume, were taken; this allowed understanding the dynamic of the contaminant transportation and to estimate the distribution coefficient K_d for the lysimeters (see §§4.2.2 and 4.2.3).

[4] Remind that the mobilization of particles and colloids is function of the speed of the water flowing over the road. Particles and colloids will then move by saltation until the flow speed drops. When the speed is not fast enough, the particles and colloids are not moved. The particles and colloids are mobilized as function of the flow speed and particle size (Stokes Law).

[5] This is only valid for the three shoulders SGH, SGC and SGL. Shoulders with adjoining lysimeters were of course not modified with gutters.

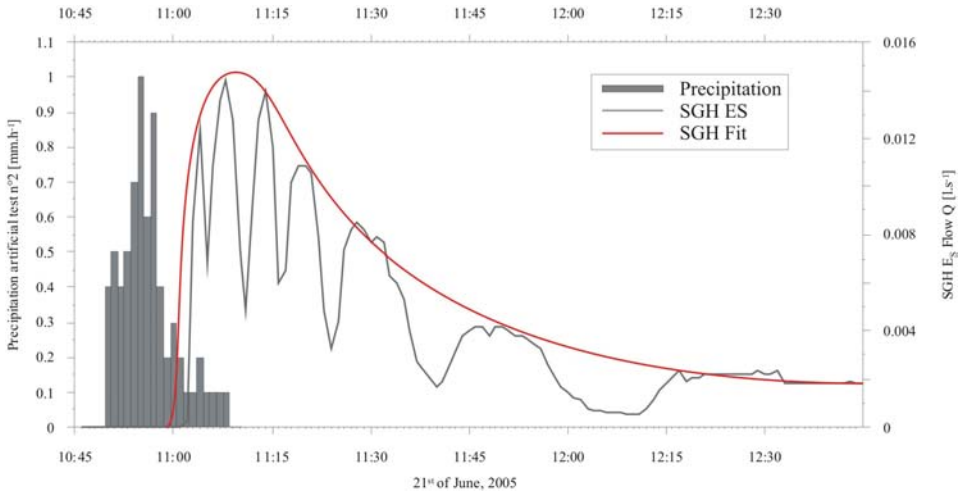

Figure 4.2: Artificial precipitation n°2 hyetogram. The precipitation mimics a thunderstorm-like event. The grey curve represents, as an example, the exfiltration flow E_S from SGH. Indentations are due to the sampling. Each indentation represents 1.5 litres. Note that the higher the flow, the shorter the time needed for taking the samples is. The red curve is the SGH response with corrections.

4.2 BATCH AND COLUMN TESTS

4.2.1 SOIL CONTAMINANT CONTENT

4.2.1.1 Soil contaminated by the ancient road

Prior to the full column test, Docourt (2005) investigated the soil surrounding the experimental site, i.e. soils that have been contaminated by the previous road (which was used for dozens of years). Therefore, the two first column tests were conducted with contaminated soils in a glass column of 65 cm in height and 9.3 cm internal diameter. Soils were sampled with a sampler which has a slightly lower internal diameter. During the first column test, it was however impossible to infiltrate the sampled soils afterward; the sampler had compacted the soils far too much (Docourt 2005). The sampling method was therefore adapted: other soil samples were taken with a spade and auger. During the second column test, a synthetic loaded solution[6] with PAH only was infiltrated in the column (loaded solution was 2 $\mu g \cdot l^{-1}$, Docourt 2005).

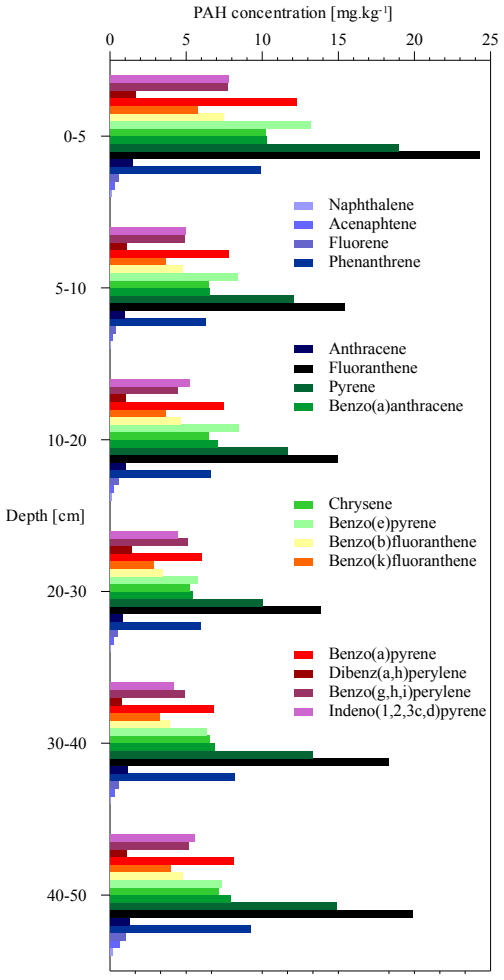

Figure 4.3: PAH concentration in the soils surrounding the experimental site. Phenanthrene, fluoranthene and pyrene presence and concentration prove that the previous contamination was due to the ancient road (Parriaux et al. 1999). Those soils were not used for the experimentation because the contaminant content was much too high. This high concentration validates the choice to import other "clean" soils. It also shows how much contaminant soils may retain. Modified from Docourt 2005.

[6] The loaded solution is a solution were particular contaminants have been added. The final concentration of the loaded solution is calculated based on real observations (Parriaux et al. 1999; Piguet, present work) and the amount of soil. It is further be referenced to "loaded solution" only.

The figure 4.3 shows the results of PAH extraction coming from the soil of the second glass column. Of course, the very high PAH content prevent the loaded solution to influence in any way the soil contaminant content. The phenanthrene, fluoranthene and pyrene are three road tracers (Parriaux et al. 1999). Present results enlighten the need to install "fresh" uncontaminated soils; it thus validates the choice to import exogenous A and B-horizons. Also, the very high concentrations demonstrate that soils have a great capacity to retain and stock contaminants.

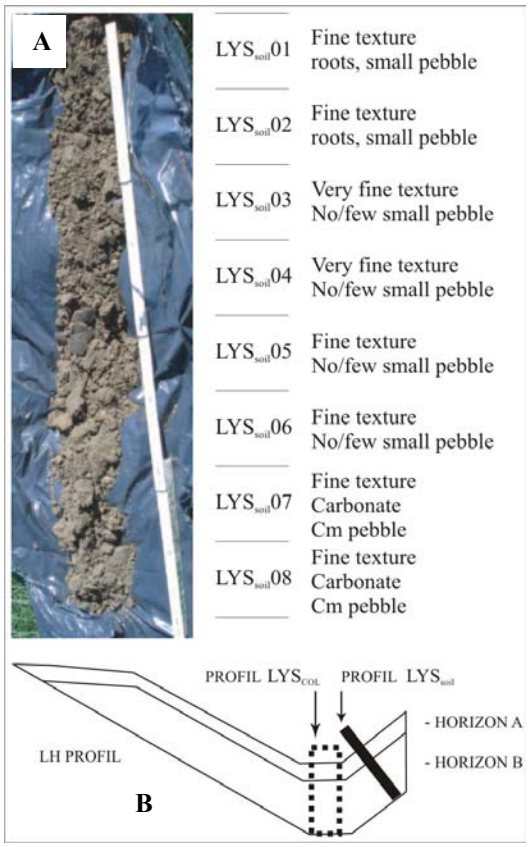

*Figure 4.4: Auger drill description (**A**) and location (**B**). **A**) Description of the drilled soil log. **B** The drill has been performed on the lysimeter LH far side to avoid strong disturbance on the natural flow path. In dashed line is located the PE column drilling and sampling site (LYS_{Col} samples). To the contrary of the LYS_{Soil}, LYS_{Col} samples must have been taken in the trench bottom: the large volume needed would have caused collapses if drilled in the slope.) Modified from Docourt 2005.*

4.2.1.2 Soil newly installed in the infiltration slopes

Soils have been drilled with an auger and reconstituted horizontally at the surface. A sample has then been taken every 10 cm along the 80 cm soil log (named from $LYS_{Soil}01$ to $LYS_{Soil}08$) (figure 4.4). The mean pH is 7.95. No real difference is notable between the A and B horizons (Docourt 2005). The organic carbon content ranges from 1.9 to 2.2%. The average is 2% (2 is used for K_{OC} calculation). High values are met at the surface and at the bottom of the soil log (Docourt 2005). Organic matter OM thus ranges from 3.25 to 3.8% (OM = 1.723·TOC, Baize 2000).

Figure 4.5B presents the concentration of PAH in the lysimeter LH soil log. Generally, every soil sample gives a similar response (ratio between PAH are the same), although PAH concentrations are not exactly the same in all samples. Higher concentrations are found in surface (~1.7 $mg \cdot kg^{-1}$; 0-20 cm) and in sample 30-40 cm (> 2.5 $mg \cdot kg^{-1}$) (Docourt 2005). Concentrations of PAH in the soils indicate that the lysimeter soils were lightly influenced by road contamination prior to the lysimeter construction. Those concentrations could indeed not be reached in only one year of functioning of the newly built RC263. Contamination was aerial (soils were taken far from the ancient road). PAH concentrations were however 100 times lower than in soil contaminated by the ancient road (§4.2.1.1).

Concerning MTE (figure 4.5A), the soil contamination was low. All values are below or approaching the OSol legal limits. Only the lead overtakes those limit values (Docourt 2005). Overall, the distribution of MTE along the soil log is well distributed; no particular retention layer appears. The homogeneity of the MTE distribution suggests that the soil were previously contaminated, before its installation in the infiltration slopes.

Analyses performed in 2003 by LPE (laboratory of pedology, EPFL), using ICP-AES[7], revealed that the MTE content was always lower than the OSol legal limit. Cu was for example between 60 and 150 $\mu g \cdot kg^{-1}$. Legal limit is 400 $\mu g \cdot kg^{-1}$. It therefore seems that the MTE content slightly increased during the year 2003-2004.

[7] Detection limits: Cd: 5$\mu g \cdot l^{-1}$, Cu: 5$\mu g \cdot l^{-1}$, Ni: 20 $\mu g \cdot l^{-1}$, Pb: 100 $\mu g \cdot l^{-1}$, Zn: 10 $\mu g \cdot l^{-1}$, Cr: 20 $\mu g \cdot l^{-1}$

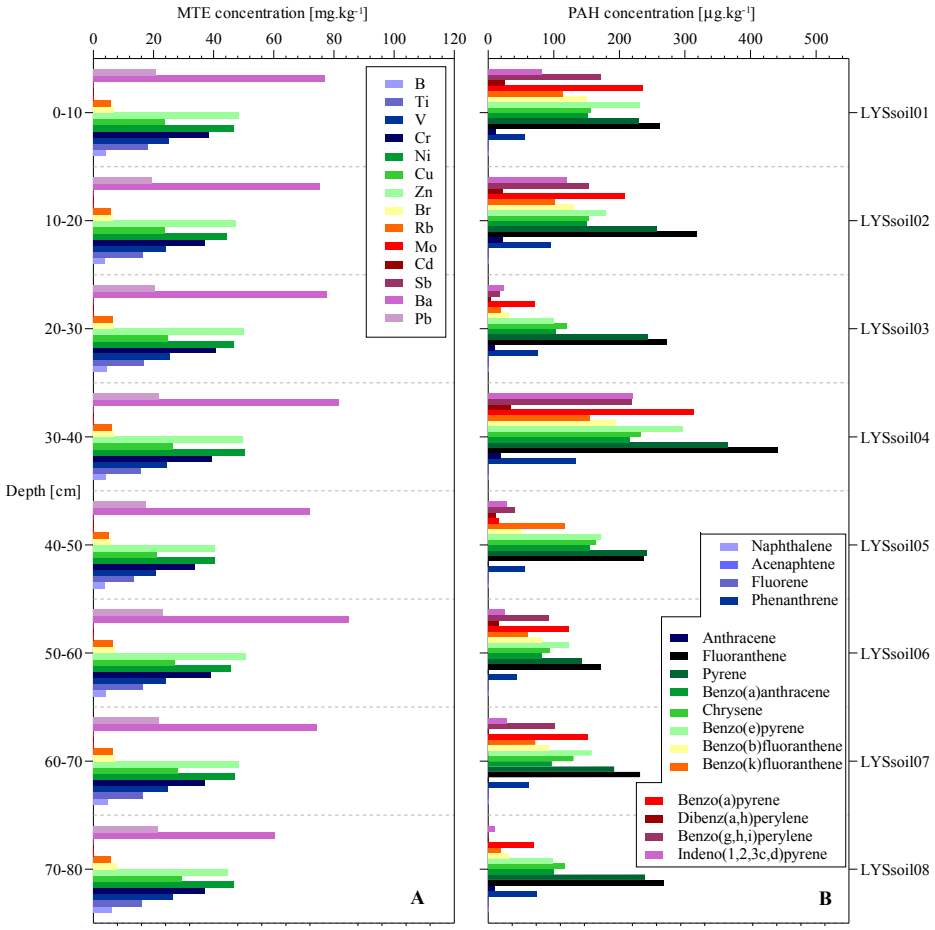

*Figure 4.5: PAH and MTE concentration in the LH lysimeter soil, September 2004. **A)** MTE concentration in the LH soils. All horizons have roughly the same concentrations. This also stands for Al, Fe and Mn which are not represented here (concentrations of 10'000, 12'000, and 800 mg·kg^{-1}). No difference is visible between the A and B horizons. **B)** Fluoranthene and Pyrene have the highest concentrations in the whole soil log. As mentioned in Parriaux et al. 1999, those two PAH are strong road contamination indicators. Other heavier PAH also show significant concentrations. Light PAH are absent. Overall, no specific discrimination of PAH retention along the profile is noted. The higher concentration of LYS05 (surface of the B horizon) suggest that this horizon was once at the soil surface, prior to its installation in the lysimeters.*

4.2.2 BATCH TESTS

Those tests have been conducted to specifically assess the behaviour of contaminant in the Grandson soils. Batch tests allow specifying the fractionation of any contaminant between the sorbed and solute part. The batch and column tests are based on the following principle: a loaded solution is added to the soil sample (batch) or to the water volume intended to infiltrate the soil column. Specification of the loaded solution are presented in due paragraphs.

Because batch tests multiply the number of samples to analyse, it has not been possible to test all substance considered in the present study. Only PAH and MTE were tested (Docourt 2005). See table 4.1 for tested PAH and MTE. Batch tests were made on the Grandson soil profile (8 samples along the 80cm of A and B-horizons) and in three different places in Switzerland (Vallorbe, Vevey, Villard, each time 1 sample in the A and 1sample in the B horizons).

4.2.2.1 Specific methodology

The batch test protocol was modified by Docourt (2005) from OECD (Organisation for Economic Co-operation and Development 1981-2000). The principle is to put a known soil mass in contact with loaded solutions which

concentration and volume are also known. 300g of soil were taken from the 10 cm horizons, 450 g from the 15 cm horizons. See table 4.6 for soil samples thicknesses and depths. Samples were then homogeneously mixed together and air dried. The resulting totalized soil is representative of the whole column soils.

Twenty grams (organic batch tests, PAH) or 18 g (inorganic batch tests, MTE) of air dried soil samples were put in a centrifugal tube (PAH) or in a PE flask (MTE). 100 ml (PAH) or 90 ml (MTE) of loaded solution was added. Sample was then agitated for 16 hours. The equilibrium solution was recuperated after centrifugation (PAH) of filtration (MTE). PAH were then extracted and analysed by HPLC (§4.1.1.2). MTE were analysed by ICPMS-HR (4.1.1.1). Concerning the PAH, the operation was repeated twice to obtain 200 ml of solution for analysis.

The concentrations of the loaded solutions were chosen in respect to known road runoff concentration. Concerning the MTE, the reference concentration was the one observed in the Grandson site, while for PAH it was the study of Parriaux et al. 1999. Concentrations of PAH and MTE in loaded solution are shown in table 4.2. A blank sample (only purified water) was carried out first. This allowed determining the background by measuring the contaminant release concentration.

[µg·l^{-1}]	Test 1	Test 2	Test 3	Test 4	Test 5	Test 6	Test 7
∑ PAH	4	40	200	400	1000	2000	4000
Each MTE (Cd; Pb)	10 (1)	50 (5)	100 (10)	250 (25)	500 (50)	1000 (100)	

Table 4.2: Synthetic loaded solution concentrations for the seven rows of batch tests. Concentration for PAH are the total concentrations, whereas concentrations for MTE are for each element. Numbers between brackets are the concentrations for Cd and Pb. Modified from Docourt (2005).

Thanks to the batch tests, the distribution coefficient K_d can be determined for each of the studied contaminant (OECD 1981; Dzombak and Luthy 1984; Hasset and Banwart 1989; Kanazawa 1989; Wood et al. 1990; Kördel et al. 1993; Tebaay 1994). Note that the K_d distribution coefficient of the batch tests are static K_d, while K_d coefficient of column tests are dynamic K_d. K_d calculated from batch tests and from column tests can then be compared (Wagner et al. 1994):

Equ. 4.1)

$$K_d = \frac{C_s}{C_e} = \frac{m_{cont} / m_{soil}}{C_e} \qquad [l \cdot kg^{-1}]$$

(K_d: distribution coefficient [$l \cdot kg^{-1}$]; m_{cont}: mass of contaminant [µg]; m_{soil}: mass of dried soil [kg]; C_e: concentration of the contaminant in the liquid at equilibrium state; C_e: concentration of the contaminant in the soil at equilibrium state)

The K_d is depending on the soil properties and the considered contaminant. Note that, concerning PAH, many publication use the K_{OC}, which is the K_d normalized on the fraction of organic carbon FOC. The use of the K_{OC} is nearly independent of the soil investigated (OECD 1981; Hasset and Banwart 1989; Kanazawa 1989; Weber and Miller 1989; Kördel et al. 1993; Tebaay 1994; Winkler 1995). The isotherm is definite as the curve linking C_s to C_e. In case it is linear, K_d is simply the curve slope. If the curve is non-linear (logarithmic), the curve must be approximate by the Freundlich model (K_{fr}):

Equ. 4.2)

$$C_s = K_{fr} \cdot C_e^{\,n} \rightarrow \log C_s = \log K_{fr} + \log C_e \qquad [\mu g \cdot kg^{-1}]$$

Interpretation of the K_d gives strong insight of the substance behaviour in soils.

4.2.2.2 Results

The blank tests were designed to assess the basic releasing capacity of soils. Note that the concentration in the equilibrium solution after 16 hours of agitation does not reflect the concentration of the contaminant in soils. On the other hand, concentration in the equilibrium solution does not reflect the substance mobility either. Only calculated K_d are representative of the substance mobility. The blank sample test gave the following results (Docourt 2005) concerning the PAH:

- Benzo(g,h,i)perylene has the highest concentration while it is also highly hydrophobic (multiple benzene cores). Note that it is found only in moderate concentration in soils (§4.2.1). It must be very mobile.
- Benzo(a)pyrene, benzo(e)pyrene, naphthalene and benzo(b)fluoranthene also have high concentrations in the equilibrium solution: they are widely present in the soil (although naphthalene was no found in the soils LYS_{Soil}, §4.2.1).
- Pyrene and fluoranthene are found with lower concentrations, although they have the highest concentration in all soil samples $LYS_{Soil}01$ to $LYS_{Soil}08$. It depicts a good soil retention.
- Other PAH (benzo(k)fluoranthene, chrysene, benzo(a)anthracene, phenanthrene and dibenz(a,h)anthracene) have low concentration, while having fairly high concentrations in soils. This demonstrates a good soil retention.

Regarding the MTE, the preponderant releasing concentrations concern the Al and Fe. Br and B follow with half the concentration. Those 4 MTE are not significantly linked to the road environment. They are easily released. Other MTE have lower releasing concentration.

Concerning batch tests with loaded solution, C_s versus C_e plots were made (Docourt 2005) for each PAH and MTE. Examples of the three identified PAH road tracers are presented in the figure 4.6. Overall, plots have similar trends: curves have an inflexion points at the 5th test. This is due to the background soil releasing (Docourt 2005). Releasing is even greater than sorption in some cases. Benzo(g,h,i)perylene shows the highest releasing concentration. This is not surprising regarding the blank test. K_d have been calculated using the Freundlich model. Results are presented in table 4.3A.

Orders of magnitude of K_{OC} are lower than those found in the literature. Docourt (2005) postulated that the reasons are 1) the previous soil contamination and 2) the fact that all PAH are tested simultaneously. Cerniglia (1993) indeed demonstrated that the presence of one PAH specie influence the other PAH behaviours. Fluoranthene and pyrene have the highest calculated K_d. As those PAH also have the highest recorded concentrations in road runoff (Parriaux et al. 1999), it is not surprising that they also have the greatest concentrations in soils. Similarly, the general PAH concentration in soils follows the K_d trend: the higher the K_d, the higher the concentration in soils.

*Table 4.3: **A)** MTE K_d calculated from the MTE isotherms. Br, B and Mo have very low K_d; Ba, Sb, Zn and V have low K_d; Ni, Cd, Cr and Rb have average K_d; Pb, Mn and Ti have high K_d. Br is used like an ideal conservative tracer in column experiments ($K_d \approx 0$). **B)** PAH K_d, and KOC. Overall, distribution coefficients K_{OC} of all PAH are lower than those found in the literature (Docourt 2005). Docourt (2005) postulated that the lower value encountered are due to the previous contamination and to the fact that all PAH were tested at the same time.*

(A) MTE	K_d	(B) PAH	K_d	Koc (foc = 0.02)
Br	0.01	Naphthalene	19.8	990
B	1.4	Acenaphtene	39.3	1965
Mo	5.4	Fluorene	65.6	3280
Ba	39.2	Phenanthrene	175.8	8790
Sb	66.1	Anthracene	57.7	2885
Zn	73.8	Fluoranthene	247.2	12360
V	88.6	Pyrene	256.4	12820
Ni	214.8	Benzo(a)anthracene	177.8	8890
Cd	285	Chrysene	193.6	9680
Cr	298.7	Benzo(e)pyrene	187.9	9395
Rb	271.4	Benzo(b)fluoranthene	199.5	9975
Pb	1561.1	Benzo(k)fluoranthene	114	5700
Mn	1616.1	Benzo(a)pyrene	181.1	9055
Ti	3642.7	Dibenz(a,h)anthracene	73.3	3665
Cu	?	Benzo(g,h,i)perylene	238.8	11940
Al	?	Indeno(1,2,3c,d)pyrene	?	?
Fe	?			

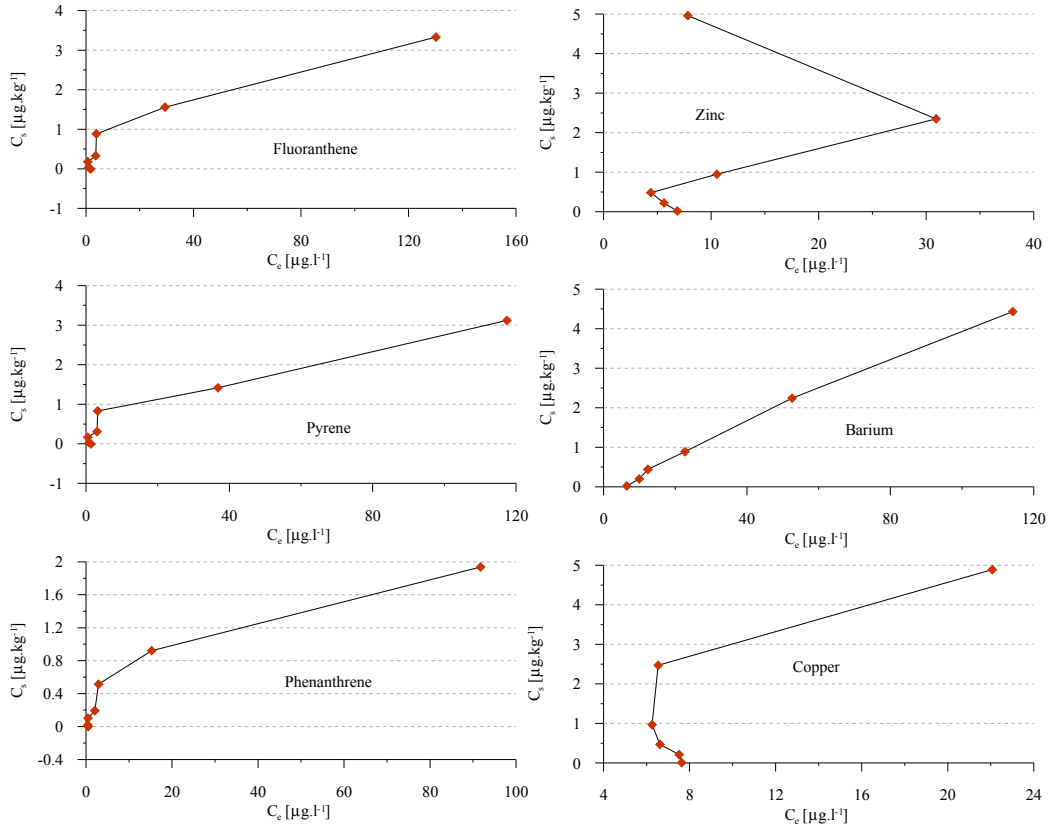

Figure 4.6: C_s versus C_e plots of road tracers. Phenanthrene, pyrene and fluoranthene are displayed on the left, while Zn, Ba, and Cu are shown on the right. The PAH were declared road specific tracers by Parriaux et al. 1999. For PAH, loaded solution concentrations for test 1 to 4 are not sufficient to inhibit the soil PAH releasing. The releasing is however lower than the sorption. For MTE, different behaviours are seen as function of the soil release and element mobility. Ba curve is typical for a very mobile MTE, while Cu has a strong release at low concentration o the loaded solution. See text for precision concerning their behaviours.

Regarding the MTE, batch tests results are regrouped according to their behaviours (Docourt 2005):

- The first group is made of Rb, Mo, V, Sb, Ba, B and Br. Their isotherms are clearly linear: the concentration of MTE in the loaded solution does not affect the sorption of the substance. B, Br and Mo are highly mobile, while Rb, V, Sb and Ba have low mobility. Ba, Br and B have been identified as specific road tracers (Parriaux et al. 1999). Mo and V as well in a lower extent (due to lower concentration in the road runoff). Cd and Pb also belong to that group, although their concentration in the loaded solution were 10 times lower than for other MTE. Pb is of course a strong road contaminant (still widely found in soils although forbidden in fuels).
- The second group is made of Zn and Cr. Their linear isotherms are aborted in the last test. This may be due to (co-) precipitation. Zn has a strong release concentration in the first 3 tests. Zn is a road tracer, while Cr is less likely to indicate road contamination (Parriaux et al. 1999).
- The third group is made of Ti, Mn, Ni and Cu. Their isotherms are showing a strong background release. Only the last test shows a linear increase of the C_s. The releasing is less important than the sorption (no negative value). Cu and Mn are directly linked to the road (Parriaux et al. 1999). Ti and Ni are found in lower concentration in the road runoff and thus are weakly related to the road environment.
- The fourth group is made of Al and Fe. Their releasing is very high in the first 3-4 tests. Negative values indicate a higher releasing rate than the sorption rate.

The resulting K_d have been calculated (Docourt 2005). K_d for Fe, Al and Cu were not calculated due to their strong releasing behaviours. Br, B, Ba and Mo have the lowest K_d (table 4.3B). Overall, orders of magnitude of the

distribution coefficients K_d for all MTE concur with the literature. Differences concern B and Cd: B should be less mobile but might be mobilized by the oxidant conditions of the batch test (Förstner 1985); Cd should be more mobile (Alloway 1995) but may be trapped by the soil high carbonate content (Perrono 1999).

4.2.2.3 Generalisation to other typical Swiss soils

In summer 2005, soil samples have been collected in three different representative Swiss locations (figure 4.7). Note that those locations were arbitrarily chosen while wandering. Sampling has been made with an auger and spade at 15 and 45cm depth. For each location, three different points spaced from each other by a few metres have been drilled. Samples of the same depth have then been homogeneously mixed to augment the representativeness[8] of the sample. Characteristics of the soils are (table 4.4):

- Vallorbe: it is representative of the Jura alkaline soils. Soils there have high carbonate content (HCl reaction) and are fairly alkaline.
- Villard: it is representative of the Swiss Plateau. The OM is fairly high, as well as the coarse material content. No HCl reaction.
- Vevey: it is representative of the Prealps and Alps. Soils are acidic and OM content is very low. No HCl reaction.

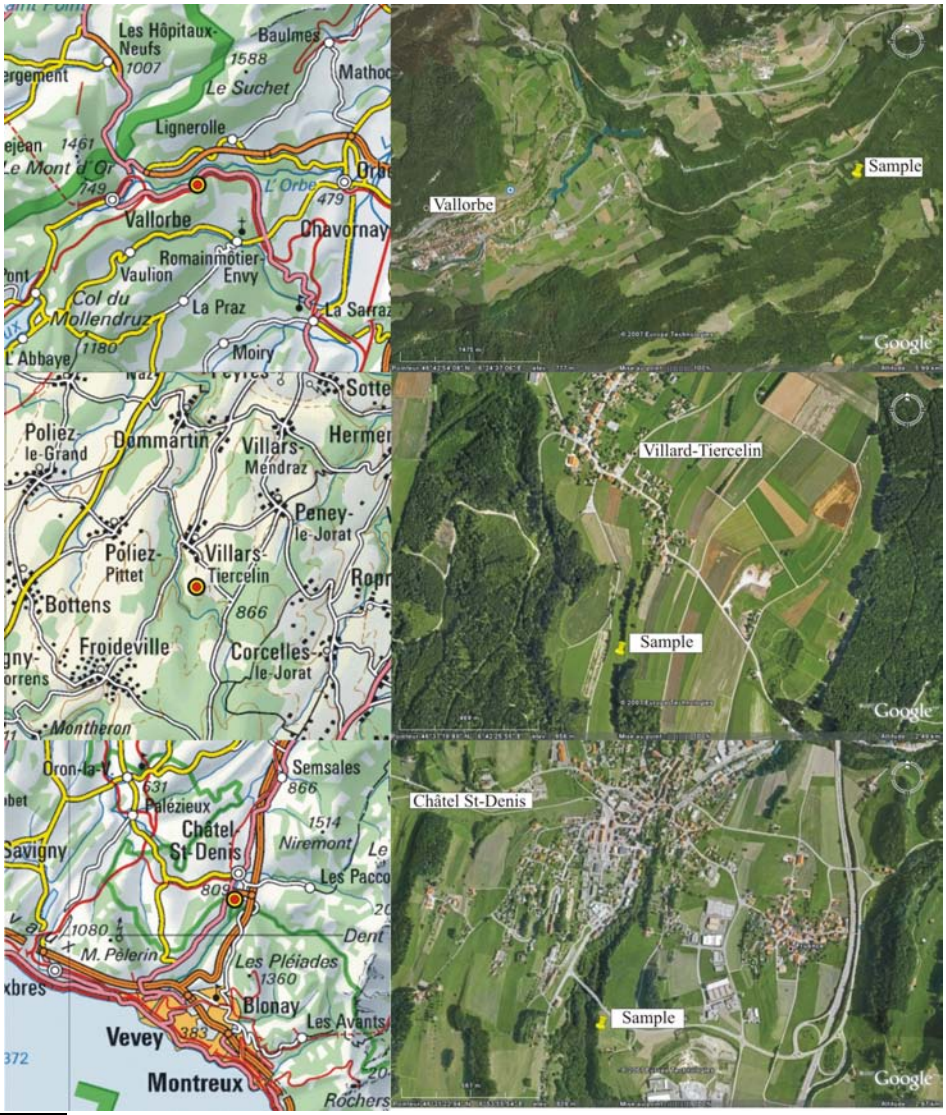

Figure 4.7: Location of the other studied representative Swiss soils. Those three soils are respectively representative of the Jura Mountain alkaline soil, of the Plateau humus-rich soil and of the Alps acidic, humus-poor soils.

Coordinates are for:

Vallorbe:
46°43'3.28"N; 6°25'53.73"E.

Villard:
46°37'8.45"N; 6°42'19.14"E.

Vevey:
46°31'4.80"N; 6°53'52.45"E.

(Sources, left-hand maps: Swissgeo.ch; right-hand maps: Google earth)

[8] For example, in the case stones would have been present and disturb the granulometry measurement; or if the soil was more polluted in a specific place.

	Jura Mountain				Plateau		Prealps	
	Grandson		Vallorbe		Villard		Vevey	
	Horizons		Horizons		Horizons		Horizons	
	A	B	A	B	A	B	A	B
pH	8.2	8.2	7.4	7.7	6.2	6.7	5.3	5.4
TOC [%]	2.1	2.0	3.3	1.8	5.4	3.24	1.0	0.7
OM [%]	3.5	3.4	5.7	3.1	9.3	5.6	1.7	1.2
Clay content [%]	28	25	12	10	9	9	20	18
Silt content [%]	32	32	26	17	18	18	38	32

Table 4.4: Summary of the principal soil characteristics in Grandson (reference experimental site), Vallorbe, Villard and Vevey. As anticipated, soils are more alkaline in the Jura Mountains and more acidic in the Prealps. pH is always slightly higher in the B-horizon. OM is higher in the Plateau region and low in the Prealps. As anticipated, B-horizons have much lower OM values than A-horizons. The granulometry showed very fine material in Prealps. Clays are more present in A-horizons.

Batch tests have been conducted on the soil samples. Only MTE were tested as indicators of a specific behaviour. Results are as follow:

- Vallorbe: batch tests revealed results very similar to the Grandson results. Four main behaviour groups are distinct.
  - The first group comprehends MTE which isotherms are linear (Mo, Ba, Sb, V, B, Br, Cd). The linear isotherm means that the loaded solution concentration does not affect the MTE adsorption. Note that those MTE are the same as in Grandson. Only Pb is missing.
  - The second group is made of Zn, Cr and Ni. They show a linear isotherm which is ended by an inflexion point. Behaviours of those MTE are clearly different at higher loaded solution concentrations. (co-) precipitation may have occurred (Docourt 2005).
  - The third group is made of Mn alone. The background release is important. Only the last test shows a linear increase.
  - The fourth group is made of aluminium and iron. Like in Grandson, they have a very high background release. Releasing is greater than sorption in the first 3 tests.

- Villard: batch tests revealed that no MTE linear isotherm exists in the Villard soils.
  - The first group is made of MTE which isotherms are unclear. It nevertheless shows an inflexion point and can be brought close to the second group of Vallorbe and Grandson. MTE a here are Sb and Mo. A presupposed precipitation might be the cause of the inflexion point.
  - The second group is made of MTE which isotherms are clearly linear only for the last 2-3 tests. MTE are Cu, Ba, Cr, Zn and Ni.
  - The third group is made of Fe and Al, which behaviours are the same as in the other locations.

- Vevey: batch tests showed similar results as in Villard. No MTE linear isotherm behaviour is visible.
  - The first group contains Cu, SB and Mo. They have an inflexion point at the end of a linear behaviour.
  - The second group has Zn, Cr, Ni and Ba. They show a slight background release.
  - The third group is made of Al and Fe which isotherm is the same as in the other soils.

At first sight, the soil analyses and batch tests confirm the NABO (Swiss soil conservation service) survey (2001). During that study, pH, OM and clay content were analysed. Results showed that the soil alkalinity decreases from northern to southern Switzerland. Also, the MTE adsorption capacity is higher in the Jura soils, diminishes in the Plateau and is minimal in the Alps. MTE retention is therefore mainly function of the pH. No interaction between the OM and clay content were enlightened[9].

Analyses of the three different soils, added to those coming from Grandson, concur with the NABO survey (2001). Soils are more alkaline in Grandson and Vallorbe, a bit acidic in Villard and frankly acidic in Vevey. Distribution coefficients K_d demonstrate that the overall mobility of MTE is higher in Vevey or Villard than in Grandson (table

[9] Although they surely exists, those interactions are less influent that the pH. Their effect on the soil retention is thus invisible.

4.5). A direct influence of the pH is thus noted. The MTE K_d for all considered locations gives the following information (sorted from the most to the least mobile MTE, in Grandson):

- Br and B are highly mobile in every soil. No retention is noted anywhere (K_d = 0 to 2)
- Mo (K_d = 5 to 500) is clearly mobile in alkaline soils and slightly mobile in acidic soils. This confirms the Förstner conclusions (1985)
- Ba (K_d = 40 to 110) is fairly mobile. Its mobility is weakly influenced by pH. OM may have a buffer influence
- Sb (K_d = 65 to 190) mobility is higher in Jura soils than in Alps soils. Overall it is mobile
- Zn is more mobile (K_d = 80) in Grandson than in any other place (K_d = 220). The sorption capacity of Zn is however the highest in Vallorbe, another alkaline soil
- V (K_d = 90) is fairly mobile in alkaline soils. Analytic problems caused no result for acidic soils
- Ni is more mobile in acidic condition (K_d = 120) than in alkaline condition (K_d = 270). This is also the case for Cd (K_d = 360 alkaline; K_d = 70 acidic). For Cd, the presence of carbonate in the Grandson and Vallorbe soils may have played a significant role (Perrono 1999)
- On the contrary, Cr is fairly mobile in alkaline soils (K_d = 300) but practically immobile in acidic condition (K_d = 3000)
- Rb has an average mobility in Grandson (K_d = 270). No K_d values could be calculated for other soils
- Pb, Mn and Ti are very little mobile. Pb seems to be even less mobile in acidic condition (K_d = 1560 alkaline; K_d = 4840 acidic). No K_d values could be calculated for Mn and Ti elsewhere than in the Jura

	Grandson	Vallorbe	Villard	Vevey	Mobility F(acid)
	K_d [l·kg^{-1}]				
Br	0.01	0	0	2	→
B	1	1	0	3	→
Mo	5	7	176	476	↓
Ba	39.2	53	110	26	→
Sb	66	39	189	190	↓
Zn	74	263	214	209	→
V	89	100	-	-	-
Ni	215	270	235	132	↑
Cd	285	355	81	71	↑
Cr	299	278	1287	2981	↓
Rb	271	-	-	-	-
Pb	1561	-	1541	4837	↓
Mn	1616	992	77	12	↑
Ti	3642	-	-	51	↑

Table 4.5: K_d of all analysed MTE in the four representative Swiss locations. Cu, Al and Fe K_d values could not be calculated due to high releasing. Values were nevertheless higher in the equilibrium solution in Vevey soils; this confirms the influence of acidic soils. Mobility trends as function of acidity is also shown (mobility = F(acid)). While the decrease of mobility for Mo and Sb has been described by NABO (2001) and Förstner (1985), the Cr and Pb decrease of mobility is more surprising.

Acidic soils have overall lesser potential to adsorb MTE. Only 4 MTE species have shown a higher retention in acidic conditions: Mo and Sb behaviours were described in the literature, while Pb and Cr behaviours are more surprising. The previous contamination of the Grandson soils (lysimeter soil Pb and Cr contents are pretty high; §4.2.1) is probably the cause of the low K_d recorded in Grandson (equilibrium concentration C_e is higher).

The experimental Grandson site has very alkaline soils. The physicochemical properties of those soils are therefore very favourable for retention. Retention potential of acidic Swiss soils (Plateau, Alps) is supposed to be lower. However, two of the most dangerous MTE species (lead and chromium) appear to be less mobile in acidic soils. This would demand confirmation in further studies. The fact is that the acidity of soils strongly influences the potential MTE retention. This has to be taken into account when assessing the potentiality of the "over the shoulder diffuse infiltration" feasibility.

The potential PAH retention in different Swiss soils could not be assessed. However, based on the literature, the soils of the Swiss Plateau seem to be the more able to retain the PAH. Indeed, they have the highest OM content.

4.2.3 COLUMN TESTS

Column tests allowed testing the infiltration of heavily polluted water. It also permitted to experiment the substance release (blank lixiviation test) and to locate the soil volume that mostly retains the pollutants.

Three column tests have been performed (Docourt 2005). The two first one were made on soils that come from outside of the newly installed infiltration slopes. Those tests were made to precise the method, to optimize the lixiviation conditions and sampling procedure as well as to measure the soil contaminant content that were caused by the ancient road (see §4.2.1.1). Newly installed soil (infiltration slope) could not be dug for those purposes; it would have compromised their integrity and structure. Because only soils belonging to the infiltration slopes are interesting for this project, only the third PE column test is discussed here. The third test is called PE column test because it has been conducted in a polyethylene PE column, as opposed to the two first tests that were performed in a glass column. PE was chosen for its inert behaviour regarding MTE.

4.2.3.1 Specific methodology

The third test (PE column test) was performed on soil coming from the 80 cm thick LH lysimeter. A special attention to lesser disrupt the soil structure during the particular PE column sampling was made. It was especially taken care not to destroy the soil aggregates. It was decided to use a PE column specially designed and constructed for this study (e-Pond, Vevey, CH). The column had a 30 cm internal diameter and was 1.1 m in height. Its internal volume was thus far greater than the glass column. This was decided to avoid the great influence of preferential flow along the column wall. As the contained soil volume is greater, it also allow using larger mass of contaminant. Overall, a bigger column is more representative of the natural soil infiltration. Sampling was carried out on the most distal side of the lysimeter LH to avoid disturbance in the natural infiltration path (figure 4.4). The samples, called $LYS_{Col}01$ to $LYS_{Col}07$, were 10 or 15 cm thick (table 4.6). Filling of the column respected the soil thickness and order (Docourt 2005). The density and mass of soils were recorded during the column filling[10]. The density was 1.16 $g \cdot cm^{-3}$. The column was filled by 56'549 cm^3, for a total weight of 65.6 kg (Docourt 2005). Soil characteristics are described in table 4.4 (Grandson) and paragraph 2.6.2.

Sample	Depth [cm]	Sample	Depth [cm]
$LYS_{Col}01$	0-10	$COL_{Soil}01$	0-5
$LYS_{Col}02$	10-20	$COL_{Soil}02$	5-10
$LYS_{Col}03$	20-30	$COL_{Soil}03$	10-15
$LYS_{Col}04$	30-40	$COL_{Soil}04$	15-20
$LYS_{Col}05$	40-50	$COL_{Soil}05$	20-25
$LYS_{Col}06$	50-60	$COL_{Soil}06$	25-30
$LYS_{Col}07$	60-70		

Table 4.6: Thickness and depth of the samples for the third column test. LYS_{Col} samples were taken during the soil sampling in Grandson, while COL_{Soil} were taken after the column test, in the column. COL_{Soil} samples were less thick because the soil column packed down during the sampling (ratio ~ ½).

The water alimentation for PE column test 3 was made with a peristaltic pump. Water was pumped to a pierced basin standing over the column surface. Infiltration was vertical; the flow going from the top to the bottom by gravity. It thus simulates a precipitation. A blank lixiviation (with deionised water) was carried out to assess the substances mobilized during the infiltration. Samples were periodically taken at the column outlet. The calculated vertical hydraulic conductivity was $1 \cdot 10^{-5}$ $m \cdot s^{-1}$ (during the lixiviation test, Docourt 2005); it concurs with values found in situ for the infiltration slopes (chapter 3).

A tracer test (boron, lowest K_d) was made to assess the dynamic behaviour of conservative tracer in that column (Docourt 2005). Indeed, results of the column test provide restitution curves for all contaminant. The ideal behaviour must therefore be known. The restitution curve of the boron gives the following information: the storage volume, the

[10] It was postulated that the soil layer would settle down during the test. That is why those values were recorded at that moment and not when taking sample for further analysis. It was also needed to design the loaded concentration.

restitution curve without dispersion and the mean transit speed. It also allows calculating the column dead volume V_0 (see below).

After having injected the loaded solution in the first place (pulse infiltration), the column was washed for days. The pulse solution was preferred because it simulates the first flush effect and avoids substance dispersion. The loaded solution concentration was decided according to the results of batch tests (Docourt 2005). The loaded solution concentration was adapted to the higher soil mass contained in the column. The infiltration was therefore carried out with concentration 1000 (MTE) or 2000 (PAH) times higher than those observed in a "natural" road runoff (current work; Parriaux et al. 1999).

At the beginning of the test, the sampling time step at the column outlet was one sample at each exfiltrated litre[11]; it then spaced out. Sample volumes are presented in figure 4.9. The EC was measured in each sample to assess the concentration of the total dissolved solid TDS. Moreover, the pH and Reduction - oxidation potential were measured in a few samples. Samples were then treated as described in paragraph 4.1.

Soil samples were taken at the end of the column test to assess the difference of contaminant content in the soils. Those concentrations were compared to the concentration of contaminant found prior to the column test, during the soil sampling. Samples were taken with a small tube vertically inserted in the soil column. As the soil column packed down to half of the original height when the tube was inserted, the thicknesses of the soil samples were lower than 10 cm; they were 5 cm (Docourt 2005). Six samples were taken from the bottom to the top of the column. Thickness has been corrected according to the packing.

The distribution coefficient K_d is extracted from the following equation (Wagner et al. 1994; Walter et al. 2000):

Equ. 4.3a)
$$R = 1 + d\frac{1-n_e}{n_e}\cdot K_d \qquad [\,-\,]$$

Equ. 4.3b)
$$R = \frac{E_{col}}{V_0}; d = \frac{m_{soil}}{V_{col}}; n_e = \frac{V_0}{V_{col}}$$

(R: retardation factor [-]; d: soil dry density [g·ml^{-1}]; n_e: efficient porosity [ml·ml^{-1}]; K_d: distribution coefficient of the column [l·kg^{-1}]; E_{col}: exfiltration volume at the column outlet [ml]; V_0: dead volume of the column [ml]; m_{soil}: mass of dried soil [g]; V_{col}: geometrical volume of the soil column [ml])

4.2.3.2 Results - Lixiviation test

A simple lixiviation test has been performed. Twelve litres of deionised water have been diffusively infiltrated in the column; six litres have been collected at the column outlet. The water sample was homogenized and analysed for PAH and MTE content.

Regarding PAH, results show lower concentrations than in blank batch tests (figure 4.8A). This is easily explained by the shorter contact time between soils and infiltrating water (Docourt 2005). Also, more contaminant species were seen in the blank batch test. It is surprising to see that the PAH that were predominantly released were neither those with the highest soil concentration nor those with the lowest K_d: they were the heavier one (benzo(a)pyrene, benzo(b)fluoranthene and benzo(k)fluoranthene). The PAH with the higher mobility is only in the fourth position (naphthalene), while PAH with the highest recorded soil concentrations are in sixth and seventh positions (fluoranthene and pyrene). However, concentrations are low in regard to the blank batch test.

[11] For this particular column test, the exfiltration rate is counted in volume (litre) and not in time. Therefore, all graphical illustrations of the column behaviour have the unit "litre" in abscise.

Concerning MTE, measured concentrations were of the same order than concentration recorded in the blank batch test (figure 4.8B) (Docourt 2005). According to the calculated batch test K_d, mobile MTE are predominantly found in the exfiltrated water, while immobile MTE are found only in low concentrations. MTE natural release when infiltrated with clean water thus behaves like expected. Concentration in the soil also plays a role: Mo, for example, is highly mobile but found only in low concentration in the exfiltrated water. This is because its concentration in the column soil is negligible. Iron and aluminium are less released in the column test than in the blank batch test. The dynamic behaviour of K_d may here be of significant importance.

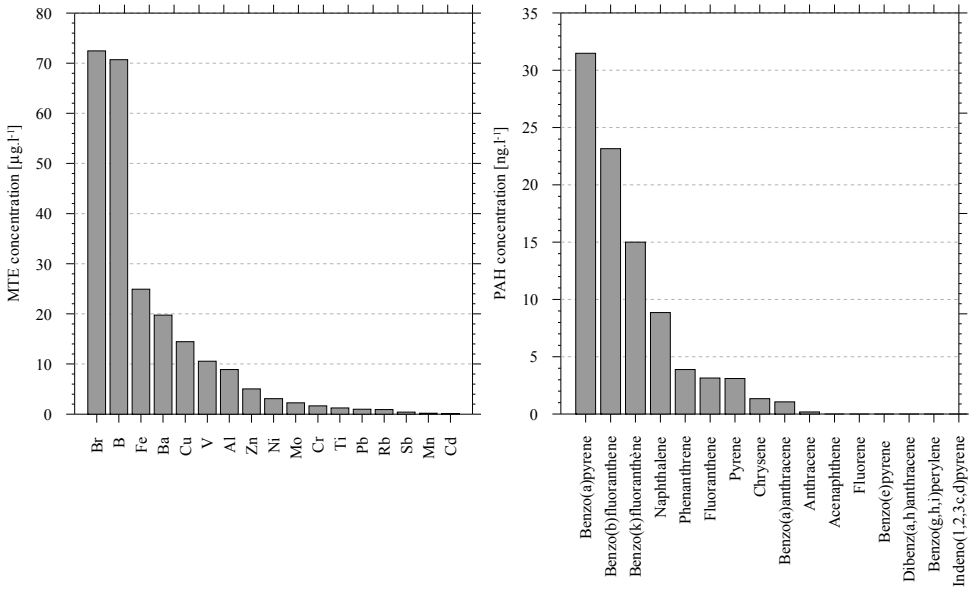

*Figure 4.8: **A)** PAH concentration in the leaching water. Highest concentrations are found for the heavy PAH. PAH with high mobility or high soil content are only found with average concentration. Strong differences between K_d from batch and column tests may be enlightened by the column test. Overall concentrations are very low. **B)** MTE concentration in the leaching water. Not surprisingly, mobile MTE are predominantly found in the solution. Immobile MTE have low concentration in the leaching water. Aluminium and iron concentration are fairly low in the solute although they show the greatest concentration in the column soil.*

4.2.3.3 PE Column test – physicochemical parameters

pH measurements in the exfiltration volume showed a fairly stable alkaline water. pH was around 8 (Docourt 2005). Oxidation-reduction measurements presented a decrease in oxidation potential between the surface (270mV) and the exfiltration water (100mV). This demonstrated that the oxidation condition within the column was less evident. Locally, reductive condition may have occurred (Docourt 2005). Electrical conductivity EC measurements were made in each collected sample. The linked TDS is only caused by MTE; the infiltration water was indeed deionised (Millipore). The resulting curve is presented in figure 4.9. Results present an ideal restitution curve considering that it was a punctual infiltration test with loaded solution. The maximal EC reached was around 1200 $\mu S \cdot cm^{-1}$ (TDS = 800 $\mu g \cdot l^{-1}$).

4.2.3.4 PE Column test – Br tracer test

As previously mentioned, the Br has been used as a conservative tracer test. The restitution curve (figure 4.9) has a very small dispersion. The restitution rate was 98%. The Br peak concentration represents the dead volume (Docourt 2005).

4.2.3.5 PAH restitution

All samples have been analysed for PAH content. No PAH were detected at all in any sample, although PAH concentrations in the loaded solution were much higher than in a basic road runoff (Parriaux et al. 1999). Nevertheless, PAH identification (but not quantification) could be made reading interferences in the background (Docourt 2005). Benzo(a)anthracene, chrysene, benzo(e)pyrene, benzo(b)fluoranthene, dibenz(a,h)anthracene, and benzo(g,h,i)perylene do not come out of the column.

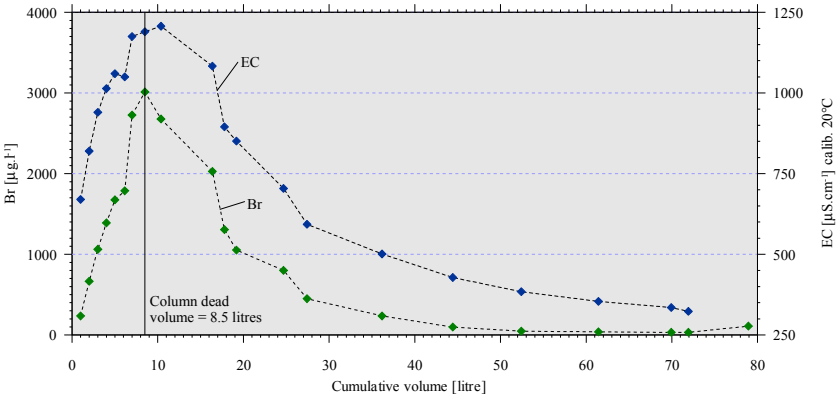

Figure 4.9: EC and Br tracer restitution curves. Both curves show similar trends. Their peaks are clearly visible. The tracer curve is ideal. The dead volume V_0 is considered to be the volume where the Br peak appeared (Docourt 2005).

Considering PAH, the retention potential of the column soil is great. It has of course not been possible to compute K_d for PAH.

4.2.3.6 MTE restitution

MTE, on the contrary, have fairly distinct specie restitution trends (Docourt 2005); their behaviours are therefore distinguishable. Examples of the three main behaviour classes are presented in figure 4.10. The three main classes are:

- The first class is made of MTE showing a normal restitution curve, i.e. the concentration increases, reaches a peak and then logarithmically decreases (figure 4.10A). This behaviour is showed by the example of the tracer Br. Also, B, Mn, Ba, Fe, Sb, and Mo behave likewise. The B and Mn have the highest restitution rate (not considering Br) recorded in the column test, i.e. 42 and 90%. Mn has also a shorter retardation R factor. Calculated K_d are B = 0.4 and Mn = 0.1 [$l \cdot kg^{-1}$]. Overall, K_d calculated with the column test are similar to K_d calculated with batch tests. Docourt (2005) postulated that the short retardation R for Mn was due to a localised reductive soil layer (Förstner 1985). However, this would not explain the very high restitution factor of nearly 90% (MTE loaded solution was 1000 times more concentrated than in a basic road runoff (§4.3). Ba has a very low restitution rate (< 1%) but a high K_d = 0.1 [$l \cdot kg^{-1}$]. Because most of the contaminant has been trapped in the surface layer (see § 4.2.4), it is highly probable that the measured peak is only the pores water being pushed (piston effect, see below). Fe, Sb and Mo also have restitution rates lower than 2%. K_d of Fe = 1, Sb = 1.2, Mo = 1.5 [$l \cdot kg^{-1}$]. Overall, all those MTE have a small piston effect mobilizing more concentrated water. This is called the primary releasing. The primary releasing trend is due to a piston effect draining the porosity. The higher concentration is due to a long exchange time. Note that the end of the primary concentration peak is always around E_{col}/V_0 =1.

- The second class is constituted by MTE only showing the primary releasing, i.e. the restitution curve has its maximal value at the beginning of the curve (figure 4.10B). The highest measured concentrations are therefore seen before the dead volume was reached. This class is made of Al, Cu, Zn, Rb, Pb, and Ti. Unfortunately, according to the distribution coefficients K_d of those components, the volume needed (E_{col}, equation 4.3a and b) to see the concentration peak would have been much too high (for example, to see a K_d of 70, which correspond to the K_d of Zn, the infiltration volume should have been 4000 litres at minimum to emphasize the concentration peak, which was impracticable). For that reason, K_d could not be calculated for those MTE. The primary releasing is highly marked. The difference between the pores and infiltration waters is indeed clearly

visible. This also demonstrates that the infiltration water has lost most of its MTE content: the mobility of those MTE species is low; their K_d are high.

- The third class is similar to the second but show only a very weak primary releasing (figure 4.10C). The concentration curve is then almost not varying. Their highest concentrations are nevertheless recorded in the first few litres. This class is made of V, Ni, Cd, and Cr. As in the second class, the coefficient K_d could not be calculated, the infiltration volume needed would have been too important. The difference between the pores water (pushed by the piston effect) and the infiltration loaded solution is negligible; this means that the mobility of those MTE is sufficient to keep a fairly high concentration in the infiltrating solution. Their K_d are thus average.

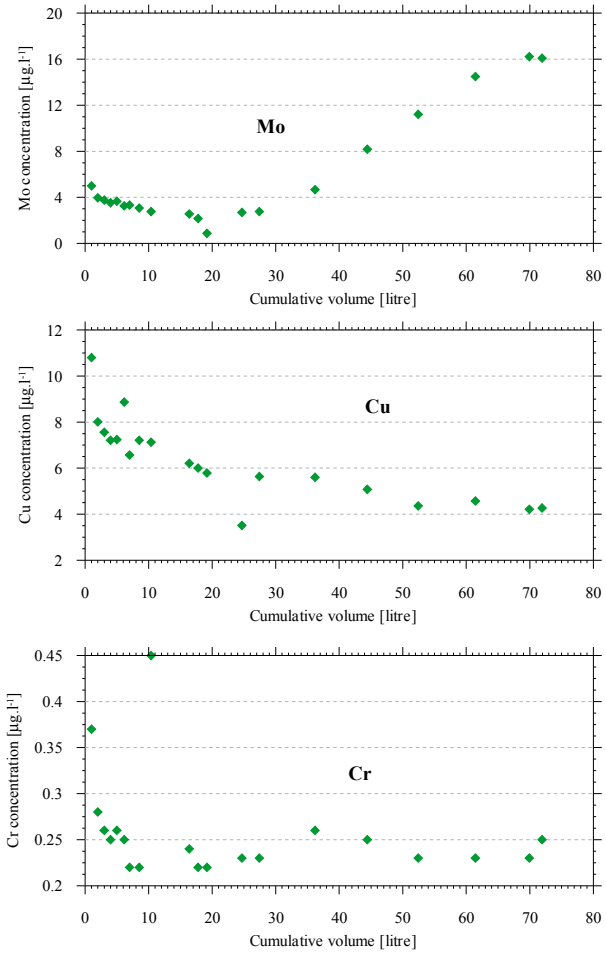

*Figure 4.10: **A)** Mo normal restitution curve. The retardation R is 8. Note the small decrease at the beginning, between E_{col}/V_0 = 0 to 1. This is due to the piston effect. **B)** Cu restitution curve with only the primary releasing. This releasing is due to the leaching occurring in the pores. Once the infiltrated solution reached the column outlet, the concentration stabilized. The real peak due to the infiltrated loaded solute is invisible. **C)** Cr restitution curve. The primary releasing concentration is very low; the concentration of the solute is almost the same and stays steady.*

Overall, all MTE have lower K_d values (or estimation) in the column tests than in batch tests; they have thus higher mobility. This is not surprising knowing that the contact time between the column soil and loaded solution is much shorter. The soil aggregates are also less accessible to the loaded solution because flows preferentially take the macroporosity path. Only K_d of the MTE Br, B, Mn, Mo and Sb could be calculated. Retention for other MTE could only be supposed. Retention is also assessed seeing the concentration augmentation in the column soils (§4.2.4).

4.2.4 SOIL CONTAMINANT CONTENT AFTER THE PE COLUMN TEST

The soil samples COL_{Soil} 1 to 6 were analysed to assess the soil contaminant content after the infiltration test with the loaded solute. Results presented in figure 4.11 demonstrate that the surface layer retained most of the PAH, as described by Butler (1984). This is especially emphasized by the three road tracers phenanthrene, fluoranthene and pyrene (Docourt 2005). Indeed, they constituted a significant part of the loaded solution concentration. Other samples have lower contaminant content (Docourt 2005). No specific difference could be enlightened between the soil analyses before and after the column test: the soil concentrations are too high.

MTE are also retained in the surface layer. Only very mobile MTE do not concentrate on the surface (B, Br, Mo). Ba, Cr, Cu, Zn, Cd, Pb and Ni show some significant concentration augmentation in the surface layers. Fe and Al have high concentrations before and after the column test; no specific interpretation can be made. Mn shows an increase of concentration at the surface and also a depletion in the bottom layers. The depletion concurs with the hypothesis of reductive conditions at the bottom of the column (Docourt 2005). Sb is only lightly concentrated in the surface layers (Docourt 2005). It is indeed mobile.

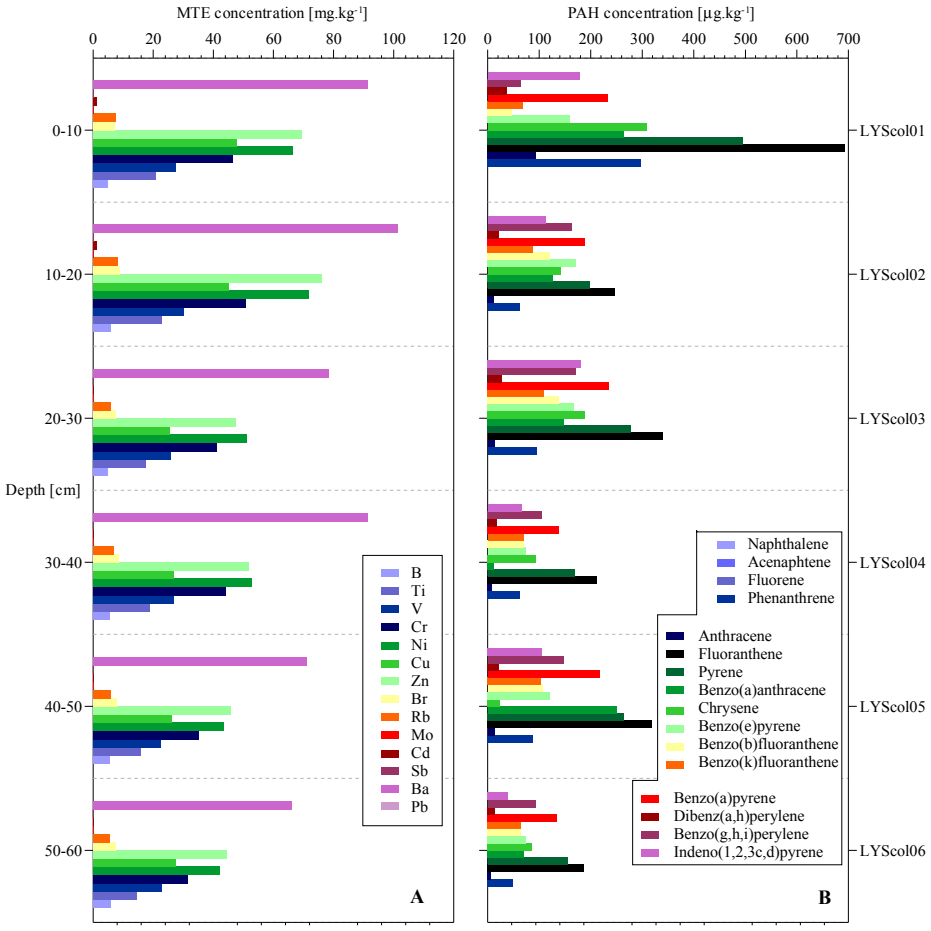

*Figure 4.11: PAH and MTE concentration in the LH lysimeter soil, situation after the PE column test. **A)** MTE concentration in the LH soils. No significant different is visible between the various layers. However, concentrations are slightly decreasing from the surface to the bottom of the column. The ratio between all MTE stays the same in all samples. **B)** Fluoranthene and Pyrene have the highest concentrations in the whole soil log. Their concentrations are especially high in the surface sample. Other heavier PAH also show significant concentrations. The surface layer has retained most of the PAH, while concentrations in the following horizons are roughly the same.*

4.3 ROAD RUNOFF CONTENT

This paragraph describes the contaminant content measured in the road runoff. The specific artificial test n°2 indeed gave strong insight of the road pollution dynamic. Also, the natural events road runoff content is presented. Finally, to assess the influence of the chosen methodology, i.e. acidifying before filtration, two samples were analysed in different ways. Indeed, in April 2007, one road runoff sample was divided in two samples (R_{R_acid} and R_{R_filtr}) and prepared differently: the first one was acidified then filtrated (i.e. the method used for the present project; R_{R_acid}), and one sample was filtrated and then acidified (R_{R_filtr}). This allows estimating the fractionation of contaminant between the solute phase and the colloidal and particular phase.

4.3.1 SOLUTE VERSUS COLLOIDAL AND PARTICULAR TRANSPORT

Because the colloidal and particular sorption has a big influence on the contaminant propagation, it was necessary to assess the distribution of MTE in solute, colloidal and particular transports. One first flush sample was thus taken during the thunderstorm event of the 26th of April, 2007. It did not rain for 23 days prior to the precipitation. MTE concentrations were concurring with all other events recorded and sampled[12]. Results are shown in figure 4.12. Not surprisingly, the mobile elements (B, Br, Mo) show no fractionation at all, while less mobile elements are sorbed to particles to different extents. Pb, for example, is nearly completely transported under sorbed form (98%), whereas Cu

[12] Note that the turbidity first peak also includes the particle deposition of the previous event in the collecting pipe. The quantification of what comes from the road and what comes from the collecting pipe is unknown. It is however unimportant to make the difference because the global contaminant mass balance is similar: what was deposited in the collecting pipe during the previous event is equal to what is deposited in that very pipe during the current event. Moreover, the particle deposition along the road and the collecting pipe must be homogenous: the particles are remobilized continuously by the runoff. As the runoff water front is slower and the runoff tail faster[12], the particles are concentrated in the first water coming out from the road runoff collecting pipe.

or Cr are 50% in solute, 50% sorbed to particles. No distinction could be emphasized between the colloidal and particular transport. They are not distinguished one from another further below.

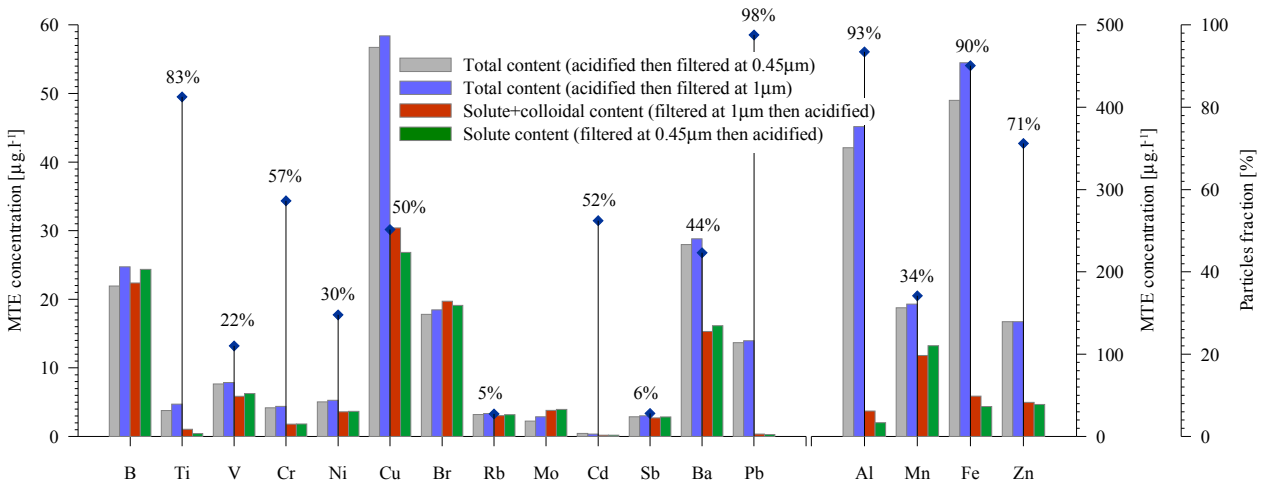

Figure 4.12: MTE fractionation in the road runoff. Comparison between the total content (solute + colloidal + particular content; grey and blue), the solute + colloidal content (red), and the solute content (green). The total content was measured twice to assess the effect of the late filtration. The grey bar chart was analysed like for every sample of this study (i.e. acidification and filtration at 0.45 µm), whereas the blue chart was filtered at 1 µm. The difference is minimal: no influence is noted about the filtration when is occurred after the acidification. The red bars represent the solute + colloidal content (filtration at 1 µm prior to the acidification). For every MTE, the difference between the filtration at 1 or 0.45 µm is insignificant. On the other hand, the difference between the total concentration and the solute concentration is significant for MTE with low mobility (Cu, Al, Fe, Zn, Pb). This confirms the great importance of the contaminant mobility in the road runoff and, in extenso, in all water fluxes. Mobile elements (B, Mo, Br) have similar concentrations in both analyses. Blue lozenges represent the particle percentage [%] of each MTE. Pb has the highest particle percentage, and also a very low mobility. Al and Fe are also practically totally under sorbed form. Note that the four MTE at the right hand side have a different scale.

4.3.2 ROAD RUNOFF CONTENT DURING TEST N°2

4.3.2.1 Hyetogram, exfiltration flow and physicochemical parameters

Figure 4.13 shows the artificial precipitation hyetogram, as well as all recorded physicochemical parameters. The flow Q and turbidity were measured continuously; EC and pH were measured manually in the water samples. Time step between samples was around 4 minutes.

The artificial rainfall hyetogram respects the intended trend. It has a volume of 7mm (96 litres). The calculated resulting exfiltration volume is 83 litres, to which 9.5 litres of samples must be added. The final volume is 93 litres (97% of the watering volume). The trend of the exfiltration curve is very similar to the watering hyetogram. This confirms the direct influence of the precipitation form on the road runoff exfiltration flow (§3.3.1).

The electrical conductivity EC has a strong peak measured in the first sample, i.e. in the first collected water. The maximal EC is 200 $\mu S \cdot cm^{-1}$; the equivalent total dissolved solid TDS is roughly 130 $mg \cdot l^{-1}$ (§4.1.1.3). This concentration is quite low as an absolute value (porous aquifer EC is between 50 and 200 $\mu S \cdot cm^{-1}$, river or lakes have EC of about 300 $\mu S \cdot cm^{-1}$). The EC decreases rapidly and shows a second peak arriving later. This second peak coincides with a later flow and turbidity augmentation. This fact links the EC with the reactivation of the flow. The calculated TDS pollutogram b coefficient is 0.82. This means that the TDS pollutogram is slightly positive, i.e. the TDS has a small first flush effect but overall is a function of the flow Q. Although EC was greater in the first sample, the TDS massic flux has its peak coinciding with the flow peak. It then decreased in the following samples. See figure 4.15 for examples of pollutogram.

The turbidity was not measured since the beginning of the exfiltration flow. This is due to the probe size: the funnel was full only on a later time. It however clearly shows a significant turbidity peak and a fast decreasing tail. The turbidity value during the first flush is presumably even greater[13]. This is not surprising at all because turbidity empirically represents the "concentration" of particles and colloids on the road pavement. Since no rainfall occurred in the 9 previous days, the deposition was significant. The turbidity shows a second augmentation coinciding with the flow and EC second peaks. Turbidity is thus increasing when the water flow augments: it confirms the particles behave according to the flow acceleration (Stokes Law). Remind that as the turbidity is an empirical measurement, it is not a concentration. The massic flux thus cannot be determined; neither can be computed the turbidity pollutogram. However, as indicative as it is, a "pollutogram" and coefficient b can be mathematically calculated. This gives an idea of "how the turbidity curve is linked to the flow curve"; it is nevertheless impossible to compare the first flush effect of the turbidity with, say for example, the first flush effect of MTE. The b coefficient of the turbidity during the artificial precipitation test n°2 is b = 0.65. The first flush, although present, is not heavily pronounced.

The pH is fairly constant along the artificial test. It has its maximal value coinciding with the peak Q value (pH = 7.6). The pH is then decreasing to slightly acidic value (pH = 6.6). Contaminants highly influenced by the pH will therefore be mobilized rather at the beginning and end of the event.

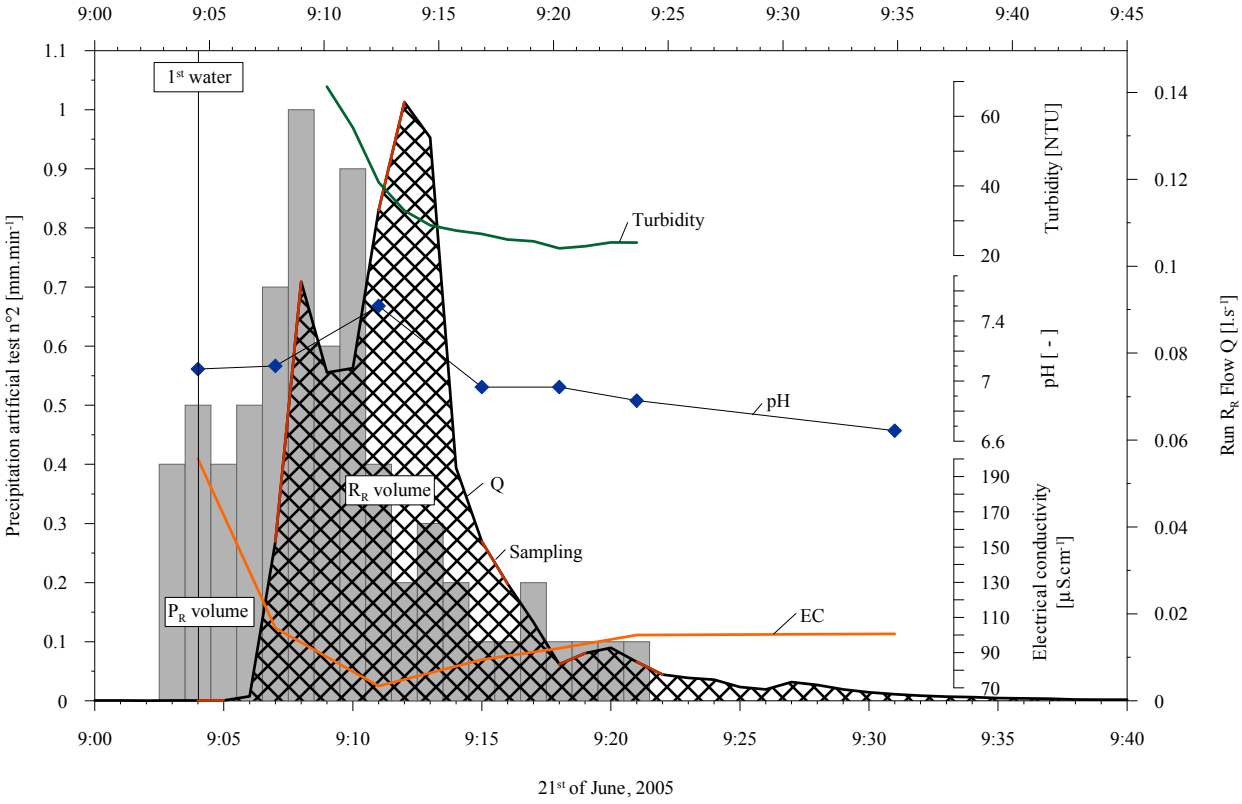

Figure 4.13: Precipitation, exfiltration and physicochemical parameters during the artificial watering of the road runoff compartment. TOC and O_2 were not recorded. Note that as the road runoff compartment is s = 13.6m², the volume of the watered and exfiltrated water are on the same scale and can therefore be directly compared. Remind that the seven taken samples (1.5·7 = 9.5 litres) have to be added. Red segments superposed to the black Q curve symbolize the samples. The Q flow resulting from the road watering has a trend similar to the rainfall hyetogram. The EC shows a first peak coinciding with the first collected water. It demonstrates the presence of the first flush. A second later peak is measureable. The pH is fairly constant but becomes a bit acidic at the end of the watering. The turbidity is fairly high, which is not surprising. It however decreases rapidly. This also enlightens the presence of the first flush.

[13] This is confirmed by other turbidity curves during natural events: the peak of turbidity coincides with the first flush. Examples are provided in §4.3.3.

4.3.2.2 MTE content

MTE listed in table 4.1 were analysed in 7 samples. Figure 4.14 shows the MTE content in the road runoff during the artificial test n°2. The reference sample has been taken in the rainwater tank prior to the road watering. Although all the watering material was abundantly rinsed with tap water many times, it did contain some MTE. This is presumably due to tank contamination. Indeed, the tank was a closed type tank which cannot be mechanically cleaned by rubbing. However, the low total MTE concentration (252 $\mu g \cdot l^{-1}$) was 100 times lower than in the first flush. It also displayed a MTE distribution different from the road runoff; this suggests that the rainwater contamination may not be due to road runoff pollution.

The first flush is remarkable (figure 4.14A). The total MTE concentration is 26'870 $\mu g \cdot l^{-1}$. It coincides with the EC peak and, certainly, with the non-appearing turbidity peak. A second MTE peak is discernable; is coincides with a flow reactivation and with the highest pH. Its total concentration is 5 times lower than the first flush. This second peak is surely the consequence of the hyetogram peak. Indeed, even if a strong first flush effect is noted, it was not caused by the highest precipitation intensity, which came five minutes later. Therefore, the first flush effect is caused by the road runoff first water (as far as the runoff is sufficiently strong to mobilize the contaminant), while secondary contaminant peaks are due to acceleration of the road runoff, i.e. to higher rain intensity.

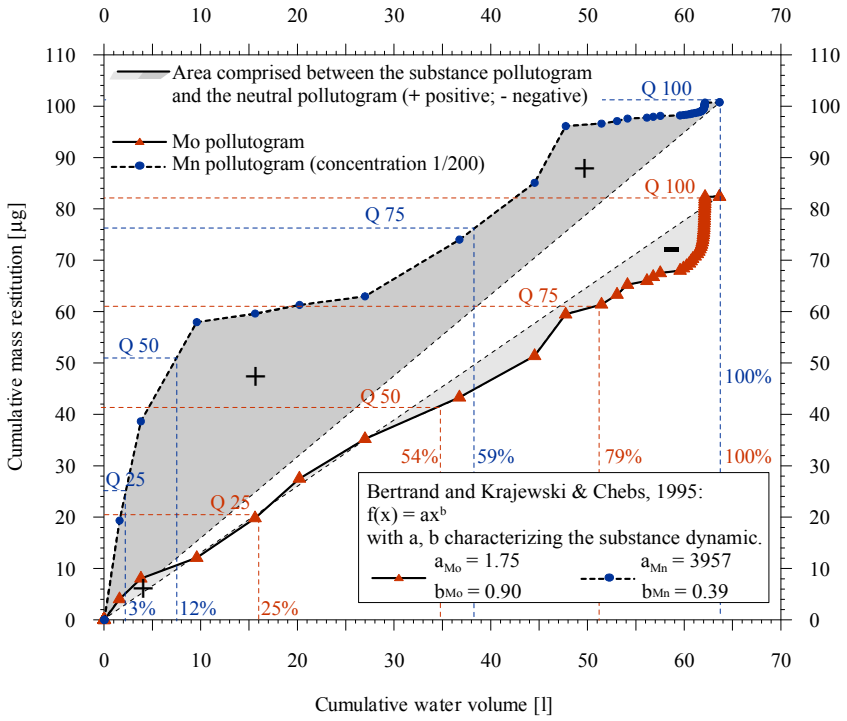

MTE	b Coefficient
Ti	1.18
Mo	0.90
B	0.86
Br	0.75
Rb	0.68
Zn	0.66
Cd	0.64
Pb	0.60
Sb	0.53
Cu	0.52
Ni	0.51
V	0.49
Al	0.48
Cr	0.47
Ba	0.46
Mn	0.39

*Figure 4.15: **Left**: Example of pollutograms. In red colour is represented the Mo pollutogram, an highly mobile element. Its pollutogram is neutral (b = 0.90); 50% of the mass was carried in the first 54% of the volume. It is even a bit depleted at the end of the event. In blue colour is represented the pollutogram of Mn, a far less mobile element. Its pollutogram is strongly positive (b = 0.4); 50% of the Ba mass arrived in the first 20% of the volume. Note that Ba cumulative mass has been divided by 5 for comparison purpose. **Right**: b coefficients for all MTE, sorted from the highest to the lowest. Note that mobile MTE identified during the batch and column tests (low K_d) also have the highest b coefficients (except for Ti, which has a b > 1; i.e. strongly negative pollutogram. This could indicate that Ti is more mobile than in dynamic experiment). MTE with low mobility (high K_d) have a strong first flush effect; this implies that the first flush effect would be preferentially due to colloids and particles. B, Br, Mo have pollutogram trends similar to the EC pollutogram (b = 0.82).*

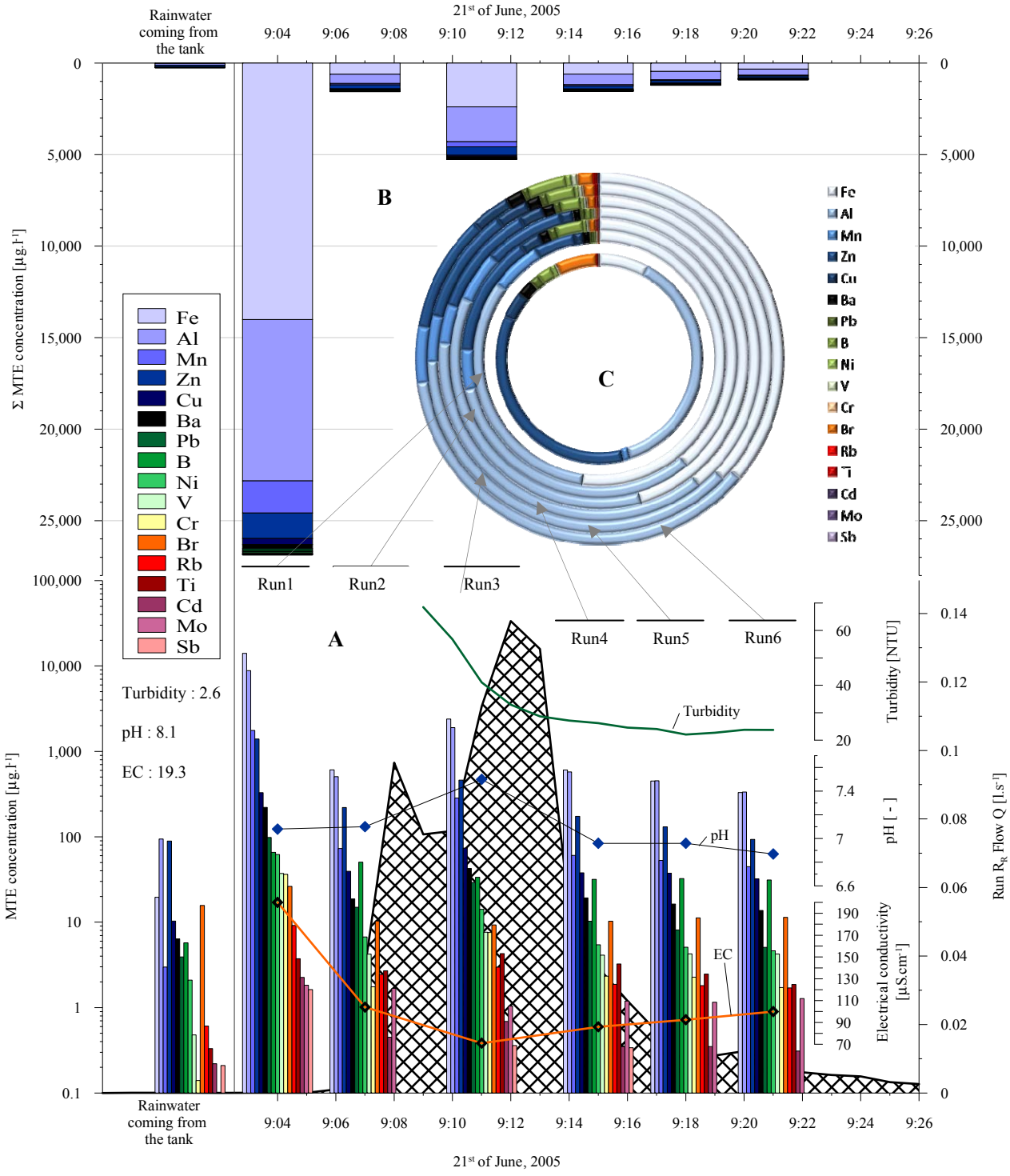

*Figure 4.14: Evolution of MTE concentration in the road runoff. **A)** MTE concentration in the 6 samples. Note the logarithmic scale. The sample on the left hand is the reference sample (rainwater). All MTE species are represented. MTE species are sorted out from their highest to their lowest concentration in the first flush. The proportionality of all MTE stays roughly constant in all six samples. MTE elements which are more concentrated at the end of the event are Zn, B, Br, Ti and Sb. They indeed make recognizable peaks. **B)** Sum of all MTE concentrations. This bar chart shows that Fe, Al, Mn, Zn and Cu constitute the fundamental part of the road runoff MTE content. A second peak of MTE is discernable, coinciding with the flow peak and highest pH. It strangely also coincides with the EC minimal value. The rainwater has a low total concentration of 252 µg·l^{-1}. **C)** MTE fractionation rings. The inner ring represents the rainwater sample. Outer circles represent the six road runoff samples, from the first flush (inside) to the last sample (outside). The fractionation is nearly inexistent. Note that the rainwater sample does not have the same MTE repartition; this implies that the contamination may not be due to the road pollution.*

The species Fe, Al, Mn, Zn and Cu represent nearly 100% of the road runoff content in all samples (figure 4.14B). Other species have concentration not overtaking 100 $\mu g \cdot l^{-1}$ (Pb). Even if the lead has been forbidden and is not used in fuels anymore, it had a fairly high concentration in the road runoff (25 times higher than in the rainwater). Lead decreased at the end of the event. Chromium is found in similar concentrations; it was almost absent in the rainwater. Only the antimony is not found in every sample. Mo was absent from the rainwater but is widely found in the road runoff. Its concentration did not decrease significantly. Overall, MTE which concentration did not decrease during the artificial precipitation were those labelled as highly mobile during batch and column tests (B, Br, Mo, Mn). This implies that the first flush effect is essentially caused by particular and colloidal contaminant transport; solute transport (containing the most mobile elements) would therefore not decrease along the time. This is confirmed by the pollutogram of figure 4.15. The most mobile element, Br, has an almost flat pollutogram with b coefficient of 0.90, while a strongly immobile element, Ba, shows a strong first flush effect with b coefficient of 0.46. See § 3.3.1 for reminder of the Bertrand-Krajewski definitions. See appendix X for all MTE pollutograms.

Fractionation of the MTE elements during the event is weak (figure 4.14C). The relative proportion of all MTE elements remained the same during the whole precipitation. The second peak relative proportions are similar to the first flush proportions, while other samples showed sample richer in B, Br, Rb, and Ti. This implies that MTE species did not behave all the same. Some are more likely to be mobilized during first flush and flow reactivation (RUN 1 and 3: Fe, Al, Mn, Pb), while some other are proportionally more concentrated in samples when the precipitation is decreasing (RUN 2, 4, 5, and 6: Zn, B, Br, Mo, Ti).

To summarize, the MTE dynamic behaviour depends on the transportation means. Mobile elements (low distribution coefficient K_d) are transported in solute, regardless of the precipitation intensity. Their concentration did not vary much during the event. Elements with low mobility (high K_d) are preferentially transported during high flow Q. It suggests a strong dependency on the flow Q intensity. Immobile elements would preferentially move sorbed to particles and colloids. The highest concentrations are however not coinciding with the highest precipitation intensity. The mobilized particles are thus smaller at that time. As presented by Grottker (1987), smaller particles and colloids indeed transport much more contaminants than bigger ones.

4.3.2.3 PAH content

PAH have been analysed in all samples, including the reference rainwater sample. Figure 4.16A (p.129) shows the PAH concentration in the seven samples. Again, low concentrations of contaminant have been found in the rainwater sample, for the same reasons given in §4.3.1.2. The Naphthalene, acenaphtene and dibenz(a,h)anthracene constitute the greatest part of the sample composition. All have low K_d.

Overall, all PAH are represented in the other samples. The first flush is well recognizable; its total concentration is 9838 $ng \cdot l^{-1}$, which is significantly higher than values found in the literature (Krauth and Klein (1982): 2500-2700 $ng \cdot l^{-1}$, Stotz (1987): 2500-2900 $ng \cdot l^{-1}$, Schlaepfer et al. (1996): 3000 $ng \cdot l^{-1}$, Lygren et al. (1984): 1400-4000 $ng \cdot l^{-1}$). This could be due to the fact that the aerial dissemination in Grandson is much lower than in other sites: Stotz demonstrated that only 14% of the PAH are found in the road runoff; this percentage is certainly greater in Grandson (§3.3.2). Concentrations are rather similar from benzo(e)pyrene (light blue) to benzo(k)fluoranthene (light green). The phenanthrene has intermediate concentration and separate the PAH with high concentrations from those with low concentrations (from dibenz(a,h)anthracene to fluorene). The difference fades out in the last samples (Run 4, 5, 6). The PAH identified as road tracers by Parriaux et al. (1999) are not emphasized in the first flush but only in the last samples. Indeed, Phenanthrene, fluoranthene, and pyrene have concentrations similar to other PAH (Run 1). Naphthalene, which is highly mobile (Docourt 2005), has the same concentration in every sample. Its concentration is also the same in the rainwater; its road affiliation is thus uncertain. PAH mobility (K_d) has a strong correlation with the PAH transportation mean: the more mobile (low K_d), the higher its concentration in the first flush (high b coefficient) (figure 4.16C). The lower its mobility (high K_d), the more constant its concentration stays in all samples ($b \approx 1$). This is enlightened by the K_d versus b coefficient table (table 4.7). The exception is the acenaphtene, which is

highly mobile but has a low b coefficient. Note that K_d were calculated on soil sample and not on road dust. The K_d limit which determines the behaviour of the PAH seems to be $K_d = 100$, which corresponds to b = 0.67.

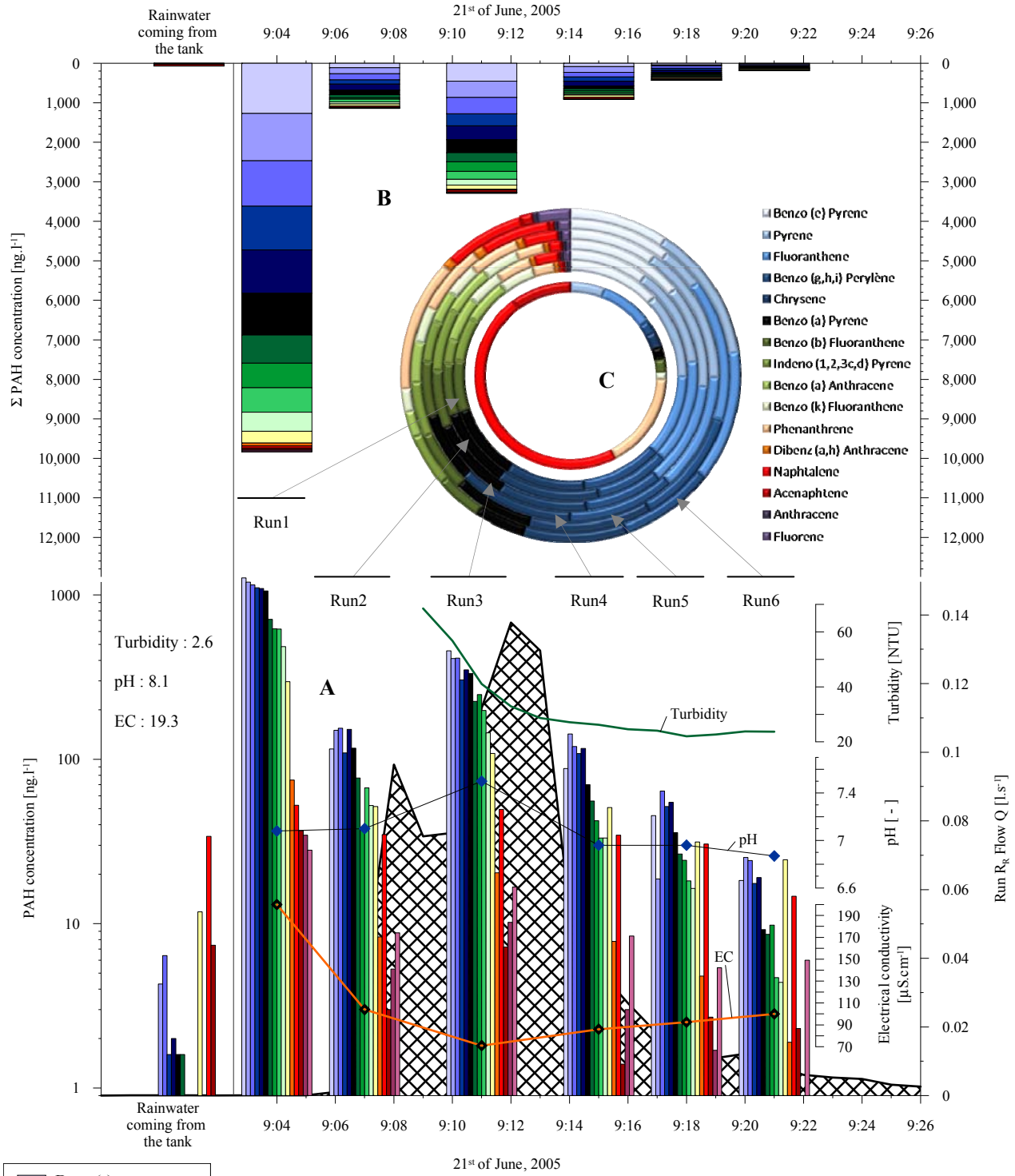

*Figure 4.16: Evolution of PAH concentration in the road runoff. **A)** PAH concentration in the 6 samples. Note the logarithmic scale. The sample on the left hand-side is the reference sample (rainwater). PAH species are sorted out from their highest to their lowest concentration in the first flush. The proportionality of all PAH stays roughly constant in all six samples. PAH species which are more concentrated at the end of the event are phenanthrene, naphthalene and fluorene. They indeed make recognizable peaks. **B)** Again, the first flush is remarkable. It is 150 times more loaded than the rainwater. A second PAH peak is noted, coinciding with the second MTE peak. All PAH species are represented in the runoff samples, only a few in the rainwater. **C)** PAH fractionation in the seven samples. The rainwater (inner circle) essentially contains naphthalene, acenaphtene and dibenz(a,h)anthracene. Road runoff samples roughly conserve the same PAH proportions. Phenanthrene to fluorene concentrations (yellow to violet) proportionally increase along the time.*

To summarize, PAH behaves like MTE do: mobile compounds stay in the solute form and only participate lightly to the first flush content; while compounds with low mobility easily complex to colloids and particles and thus participate greatly to the first flush content. This concurs with previous work treating the PAH transport in road runoff (Stotz 1987). It is interesting to note that the mobile PAH coincide mostly with light PAH, while heavy PAH are less mobile.

PAH	b coefficient	K_d
Naphthalene	0.92	19.8
Fluorene	0.82	65.6
Indeno(1,2,3,d,d)pyrene	0.71	-
Anthracene	0.67	57.7
Dibenz(a,h)anthracene	0.67	73.3
Phenanthrene	0.67	175.8
Fluoranthene	0.66	247.2
Pyrene	0.65	256.4
Chrysene	0.62	193.6
Benzo(a)anthracene	0.61	177.8
Benzo(e)pyrene	0.61	187.9
Benzo(b)fluoranthene	0.61	199.5
Benzo(a)pyrene	0.61	181.1
Benzo(k)fluoranthene	0.59	114.0
Benzo(g,h,i)perylene	0.58	238.8
Acenaphtene	0.46	39.3

Table 4.7: PAH mobility (K_d) and first flush behaviour (Bertrand-Krajewski & Chebs b coefficient). The higher the mobility (low K_d), the more neutral the resulting pollutogram is (b ≈ 1). If the mobility is low (high K_d), the resulting pollutogram shows a significant first flush effect (b ≈ 0.5). The exception to this rule is acenaphtene which is highly mobile but also presents a strong first flush effect.

4.3.2.4 Aliphatic hydrocarbons C_X content

C_{11} to C_{20} aliphatic hydrocarbons were present in the rainwater with concentrations of about 1 $\mu g \cdot l^{-1}$. However, those C_X were found in all samples with the same concentrations. C_{10} was not found in any sample. Heavier aliphatic hydrocarbons are present in the road runoff. Their concentrations range from 0 to 10 $\mu g \cdot l^{-1}$. Heavy species from C_{28} to C_{40} represent up to 85% of the first flush (Run 1) and flow peak samples (Run 3). In other samples (Run 2, 4, 5, 6), they represent 2/3 of the total content. C_{32} is abundant in all samples but the last one.

The first flush effect is not so evident as for MTE and PAH, although it exists. Other samples have total concentrations which are high comparing to the first flush. This suggests that the aliphatic hydrocarbons do not behave according to the transportation mean (solute versus particular) but to their weights. This is clearly confirmed by the b coefficients calculated for all C_X species (table 4.8): all coefficients are clearly around 1, which correspond to a fully neutral pollutogram. The C_X concentration depends only on the flow Q, and in a lesser extent, to their weights. Indeed, lighter C_X have b coefficients slightly under 1, while heavier CX have b coefficients a bit higher. Heavy C_X are thus weakly retarded. C_X pollutograms and dynamic concentrations are shown in appendix X.

C_X	b coefficient	BTEX	b coefficient	PCB species	b coefficient
C10	-	Benzene	0.64	PCB 105	0.75
C11	0.92	Toluene	0.73	PCB 128	0.80
C12	0.94	Ethylbenzene	0.91	PCB 118	0.83
C14	0.95	p+m Xylene	0.89	PCB 138	0.86
C16	0.92	o Xylene	0.92	PCB 156	0.87
C18	0.87	Isopropylbenzene	0.89	PCB 28	0.89
C20	1.04			PCB 52	0.89
C24	1.22	**MTBE**	0.51	PCB 153	0.89
C28	0.99			PCB 180	0.89
C32	0.93			PCB 149	0.92
C36	1.25			PCB 101	0.99
C40	0.95			PCB 170	1.09

*Table 4.8: Bertrand-Krajewski & Chebs b coefficients for C_X, BTEX, MTBE and PCB. **C_X**: Overall, b coefficients are all close to 1. Lighter C_X have however smaller b coefficient, while heavier C_X have b coefficient of 1 or above. This implies that C_X concentration in the road runoff is function of the flow Q and, to a lesser extent, a function of their weights. Heavier C_X are lightly retarded. **BTEX and MTBE**: Low b coefficients, describing a first flush effect, are found for benzene and toluene. Other BTEX have b coefficient of 0.9, symbolizing a nearly neutral pollutogram behaviour. The MTBE b coefficient depicts a moderate first flush effect. **PCB**: PCB species are sorted out as function of the b coefficient. Overall, all PCB have neutral or nearly neutral pollutograms. Their concentration is function of the precipitation intensity. PCB170 is slightly retarded.*

4.3.2.5 BTEX content

BTEX were widely present in the road runoff. Unfortunately, BTEX were also all present in high concentration in the rainwater that served for the watering ($\sum$ BTEX = 5350 ng·l^{-1}). The contamination provenance was unknown. However, the benzene high content, which is usually not found in road runoff[14], suggests a contamination coming from other source like unburned fuels (Chiron 1990). Concerning BTEX, the artificial test n°2 can be seen as a contaminant tracer test. Results are given in appendix X. The most important fact is that most of the BTEX evaporated rapidly from the road and were not found any more in high concentration in the road runoff. Indeed, only one fifth of the rainwater BTEX total concentration is found in the first flush. Four fifths of the BTEX thus evaporate during watering. BTEX concentrations in the road runoff concur with values found by Parriaux et al. (1999), although rainwater concentrations were so high.

Benzene was especially depleted (only 1/12th of rainwater benzene is found in the first flush); it also showed the lowest b coefficient (table 4.8). Benzene thus had the most pronounced first flush effect of all BTEX. Toluene is the only BTEX which concentration is higher in the first flush than in the rainwater sample. Toluene is thus present on the road pavement. Other BTEX have b coefficient of about 0.9, thus presenting an almost neutral pollutogram: BTEX concentrations in the road runoff depend on the flow Q. This concurs with the BTEX solubility described in the general literature.

However, the BTEX concentration in the road runoff samples varied along the time the same way as MTE and PAH did (two peaks in samples Run1 and 3). Considering that the BTEX source is the rainwater (i.e. it mimics a "continuous tracer injection"), the BTEX concentration should have stayed constant. Indeed, no interception but evaporation occurred between the injection and sampling points. Thus concentrations should have stayed the same regardless of the flow Q. This behaviour suggests that other processes have occurred on the road. One hypothesis is that the resulting BTEX road runoff content indeed comes from the road; the BTEX content in rainwater having completely evaporated from the road[15]. The resulting decreasing BTEX concentration is then explainable: it is simply a function of the flow Q.

4.3.2.6 MTBE content

Sample	MTBE [ng·l^{-1}]
Rainwater	19.1
Run 1	128.9
Run 2	26.4
Run 3	24.2
Run 4	26
Run 5	34.7
Run 6	24.6

Although forbidden, MTBE was found in the road runoff. It however stayed under the Swiss regulation limit of 200 ng·l^{-1}. The first flush is strongly marked with a concentration of 128.9 ng·l^{-1}. It then decreased to values around 30 ng·l^{-1} (Run 2) and stayed fairly constant. As the MTBE concentration in rainwater was 19.1 ng·l^{-1}, the resulting MTBE concentration in all samples (Run 1 to 6) forcibly came from the road pavement. Note that the first flush effect (b = 0.5, table 4.8) is lightly underestimated due to the initial rainwater concentration. Its first flush behaviour was caused by its very high solubility (Höhener and Dakhel 2002). MTBE pollutogram and concentration values are presented in appendix X.

4.3.2.7 PCB content

PCB are present in the road runoff only in trace concentrations. Indeed, the first flush total PCB content is only 20.5 ng·l^{-1} for the 209 PCB species[16], mainly due to the rainwater initial concentration (9.1 ng·l^{-1}). As for BTEX, the road runoff concentration shows two peaks mainly caused by the flow Q. PCB have light first flush effects. This is confirmed by the b coefficients calculated for PCB (table 4.8). PCB 105 has the lowest b coefficient but is all the same not presenting a strong first flush effect. Other PCB have coefficient around 0.8 – 0.9. This means that PCB indeed are mainly function of the flow Q. See appendix X for PCB concentrations and pollutograms.

[14] Benzene and toluene were never found in the road runoff during natural events.
[15] For example, the emulsion and strong brewing in the pump suction chamber or/and in the water spurt may have separated the water from the BTEX. BTEX then would have evaporated directly out of the watering hose.
[16] The twelve measured PCB represent 40% of the total PCB concentration (Source: CECOTOX , analytical protocol).

4.3.3 ROAD RUNOFF DURING NATURAL EVENTS

To validate the chemical behaviour of the road runoff, comparisons have been performed between the artificial test n°2 and four (out of 112) selected representative natural events. Recorded data were the hyetogram, the resulting road runoff flow Q, the turbidity, TOC and EC. During natural events, EC was continuously measured (time step 10 min) in a funnel.

4.3.3.1 Precipitation of August, the 16th, 2004 – very small event.

This event had minimal road leaching (figure 4.17A). It did not have a sufficient volume (0.5 mm; 1.2 $mm \cdot h^{-1}$) to create exfiltration from shoulders or lysimeters. Lag time was 7 minutes. The volume restitution was 98%. The bimodal road runoff flow curve is correlated to the hyetogram. The EC (and thus TDS) b coefficient is 0.99, thus showing a completely neutral behaviour: the EC was function of the flow. This coefficient is lower than the one calculated for the artificial test n°2. TOC presents a peak at the beginning of the event. Its pollutogram b coefficient is 0.35, thus representing a strong first flush effect. Its second visible peak is due to the biphasic[17] behaviour of TOC (DOC < 0.45 μm; POC > 0.45 μm). The turbidity presents a similar significant peak at the beginning of the event. The mathematical turbidity b coefficient would be 0.73.

4.3.3.2 Precipitation of July, the 17th, 2004 – thunderstorm.

This precipitation was a thunderstorm with 5.3 mm volume (48 $mm \cdot h^{-1}$). It thus resembles the artificial test n°2 very much. The lag time was 1 ½ minutes. It did induce exfiltration from shoulders and lysimeters. The road runoff flow has only one peak which is correlated with the hyetogram (figure 4.17B). The restitution volume was 102%. The EC has a coefficient b of 1.13, which is a bit higher than the coefficient calculated in the artificial test n°2. The TOC has a peak coinciding with the flow peak. Its coefficient b is 0.48. The first flush effect is thus really marked. A second peak is also apparent but is aborted; the probe got out of the water too soon. The mathematical b coefficient of the turbidity is 0.30. The turbidity has thus a higher first flush behaviour than in the test n°2.

4.3.3.3 Precipitation of August, the 19th, 2004 – Winter-like rainfall

This rainfall is representative of long, winter like events (figure 4.17C). Its duration was 24 hours with a total volume of 26 mm (1.15 $mm \cdot h^{-1}$). The lag time was 13 minutes. The precipitation had many peaks, each of them correlated to the road runoff flow. Coefficients b were calculated on the global trend curve and not on each peak. The EC overall b coefficient is 1.05, thus showing a small retardation of the TDS. TOC again shows the most pronounced first flush effect with a b coefficient of 0.18 (80% of the mass is in the first 25% of the road runoff volume). This low coefficient is mostly due to the fact that TOC stays around 0 to 1 during the whole event but in the first water. Not surprisingly, the turbidity shows its peaks during flow peaks. The correlation is undeniable. The general trend was increasing until 6 pm and then decreased.

4.3.3.4 Precipitation of September, the 14th, 2004 – small winter-like event

The short duration (4h20), winter-like event of September, the 14th, 2004 had a total precipitation volume of 1.3 mm (0.7 $mm \cdot h^{-1}$). The lag time was seven minutes. Its hyetogram had many peaks, each of them correlated with the road runoff flow (figure 4.17D). The general behaviour of the EC is similar to the other natural event described above. It had no first flush component (neutral pollutogram b = 0.95). The TOC has multiple peaks coinciding with the flow peaks. It general trends is however unclear. Its b coefficient is 0.4. It also reacted like in other natural event. The turbidity peaks are easily correlated with the flow peaks. The calculated b coefficient would be 0.42.

[17] The particles transport is one of the phases, the second is the solute part.

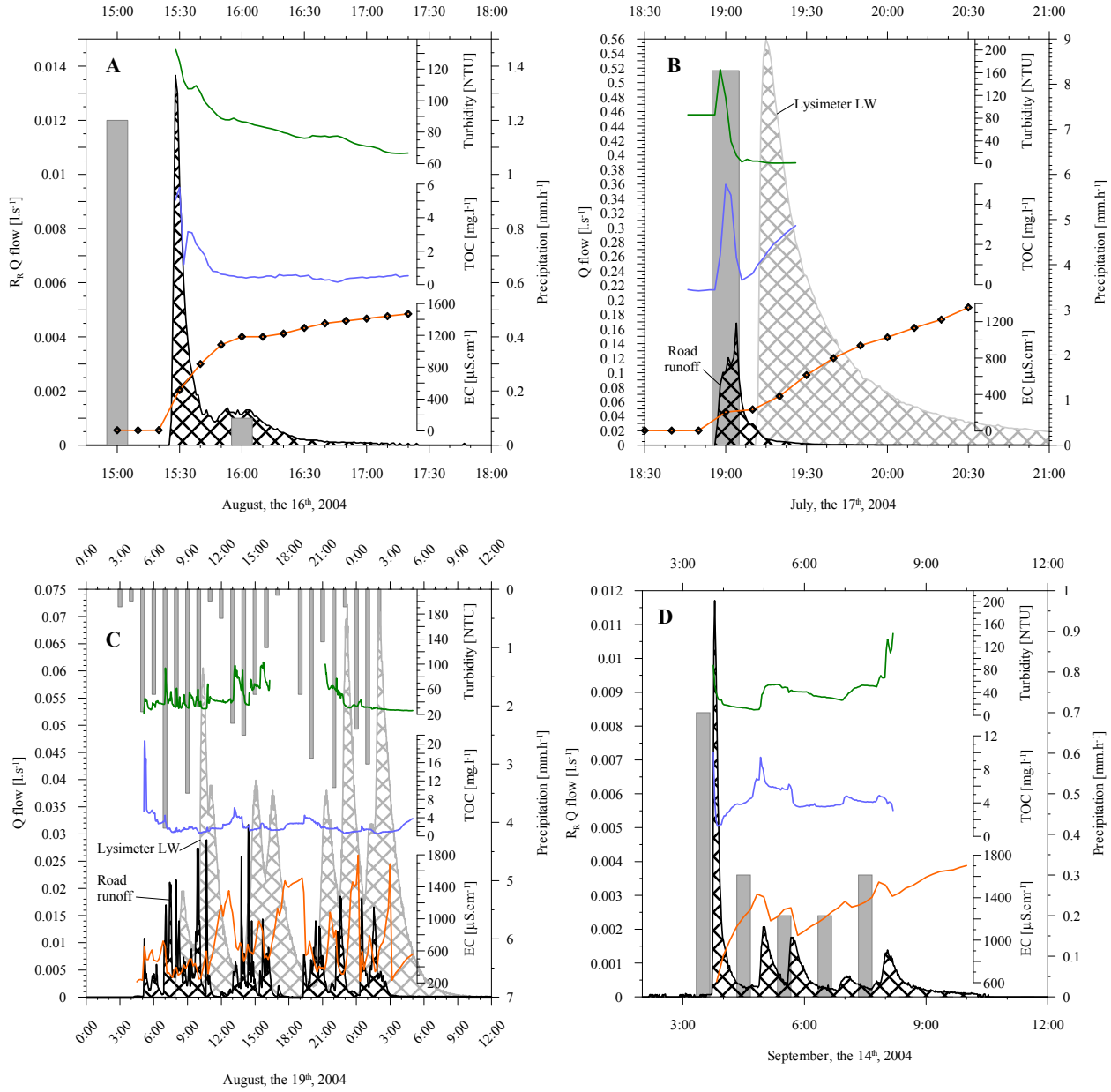

*Figure 4.17: **A)** Event of June, the 16th, 2004. This event did not induce exfiltration from the shoulders or lysimeters because the rain volume was too low. The road runoff flow is clearly correlated with the rain hyetogram. The EC augments with the cumulated volume R_R; this is shown by a coefficient b of 1. The TOC and turbidity have a first flush component clearly marked (resp. B = 0.35 and b = 0.73). **B)** Event of July, the 17th, 2004. This event is a thunderstorm that did induce exfiltration from shoulders and lysimeters (LW Q is presented; remind that the catchment surface is 300 m², against 13.6 for the road runoff). The EC cumulated curve shows a strongly negative pollutogram with b = 1.4. The TDS are remarkably retarded. TOC and turbidity curves present high values in the first water. Coefficients b are TOC b = 0.48 and Turb. b = 0.30. **C)** Event of August, the 19th, 2004. This event lasted for nearly 24 hours. Precipitation peaks always induced a road runoff flow reactivation. The physicochemical parameter behaviours are difficult to assess. EC curve must be separated in multiple events to be understood. EC peaks are greater and greater along the time; this indicates a normal accumulation (overall b is 1.05, not considering the irregularities). TOC has a very strong first flush effect; b = 0.18. Turbidity had a complex curve; it nevertheless was correlated with the road runoff flow. Its general trend however increased and reached a maximum during the longer rain interruption (18:00). It then decreased. **D)** Event of September, the 14th, 2004. This event particularly well demonstrated the correlation between the precipitation and the road runoff flow. Each precipitation peak induced a road runoff peak. Only shoulders showed exfiltration. The EC showed a multiple peak curve with a high b coefficient of 0.95. The TOC also had several peaks, all coinciding with turbidity and EC peaks. TOC b coefficient was 0.4. The turbidity peaks coincided with the flow peaks.*

4.3.4 GENERALISATION AND SUMMARY

The study of all natural events as well as the artificial precipitation test n°2 allows generalizing the physicochemical parameters behaviours. The contaminant content of the road runoff can also be generalised, thanks to analyses of natural event road runoff.

4.3.4.1 Electrical conductivity EC - TDS

The TDS pollutogram is more or less neutral in every situation (table 4.11). In some cases the TDS pollutogram is slightly positive (Artificial test n°1 and 2, minimal event) and sometimes slightly negative (natural storm). It however does not show any strong first flush or strong retardation. The minimal value was found in difficult conditions (massive flooding) and should thus not be considered[18]. The almost neutral pollutogram for TDS depicts the behaviour of solute transport. It is indeed function of the flow. It can be compared to a continuous tracer being leached by the road runoff. No punctual effect is noted. It is certain that the deposition time also has a certain influence, although not quantifiable. Moreover, the multiple reactivation of the rainfall (hyetogram peaks) strongly alters the pollutogram which then shows multiple convex (or concave) trends. The noted b coefficient is only describing the first of these curve "bulges". To really assess the TDS behaviour as function of the rainfall intensity would need many events with one precipitation peak only. Finally, the solute formation on the road is somewhat complicated; it depends on factors that are hardly quantifiable (meteorology, deposition rate, ion complexation, etc.). Note that the EC (and thus TDS) pollutogram behaviour is only representative for the dissolved content of the road runoff which is electrically loaded. It does not include the particular or colloidal contents, or electrically neutral elements.

Event	Event type	Rainfall volume [mm]	Event intensity [mm·h^{-1}]	EC b coef.	TOC b coef.	Turbidity b coef.
Artificial test n°1	Massive flooding	40	150	0.71	0.25	0.87
Artificial test n°2	Storm simulation	7	23	0.82	-	0.68
16th of June 2004	Minimal event	0.5	1.2	0.99	0.35	0.73
17th of July 2004	Storm	5.3	48	1.13	0.48	0.30
19th of August 2004	Long winter-like	26	1.2	1.05	0.18	-
14th of September 2004	Short winter-like	1.3	0.7	0.95	0.4	0.42

Table 4.11: Summary of the EC, TOC and turbidity b coefficients for the 6 studied events. See text for discussion.

4.3.4.2 Total organic carbon TOC

The TOC showed, in every condition, a strong first flush effect. It however does not seem to have any well-defined relation with the precipitation volume or intensity. The accumulation rate on the road has certainly also an influence. TOC has a coefficient b ranging from 0.18 to 0.48. It depicts the first flush behaviour of the particular component (POC > 0.45 µm) of the TOC. Strong TOC peaks are always correlated with the first road runoff flow peak. It then decreases and has a secondary augmentation (DOC < 0.45 µm). The DOC seems to behave exactly like TDS, i.e. strongly retarded when the rain intensity is high; neutral behaviour when the I_{mean} is low. This affirmation is based on the curve trend and not on b coefficients. Indeed, DOC b coefficients could not be computed; it does not make sense to compute b coefficient based on partial curve[19]. The secondary DOC peak is often cut off by a new POC peak, mobilized by an increase of the runoff flow. The particular and colloidal transport is indeed function of the acceleration (and not the speed) of the water on the road.

[18] Indeed, the watering of the road surface was not homogenous. It is not representative of a natural precipitation.
[19] Even if POC and DOC peaks are well defined and separated, they are including both components. The proportion of DOC and POC for each peak is unknown.

4.3.4.3 Turbidity

The turbidity represents the particular and colloidal content (*lato sensu*) of the runoff. It thus complements the TDS pollutogram behaviour[20]. The turbidity showed, like TOC, a significant first flush effect. The turbidity b coefficients range from 0.3 to 0.73 (not considering the artificial test n°1). It is however a bit weaker than for TOC. Strong indications of relationship between turbidity and I_{mean} exist. Like for TOC, this is surely due to very local negative or positive acceleration of the flow (runoff waves, car passing on the road, differences of transport modes like saltation and bed load inducing deposition and remobilization, etc.). It therefore strongly reacts to precipitation peaks. Second peaks of turbidity are due to the reactivation of the runoff flow. When the precipitation has only one peak (figure 4.17B), no second peak has never been observed. This is radically different from the TOC.

4.3.4.4 Contaminants

MTE identified as road tracers by Parriaux et al. (1999) are found in all road runoff samples, regardless of the considered precipitation event. Concentrations are however very different from one event to another. In figure 4.18A are displayed the concentration ranges for all MTE. Note that those concentrations are the maximum concentration recorded during all events; it is the concentration of the first flush. Many events have indeed provided samples with concentrations lower than the detection limits; their MTE content is thus not plotted.

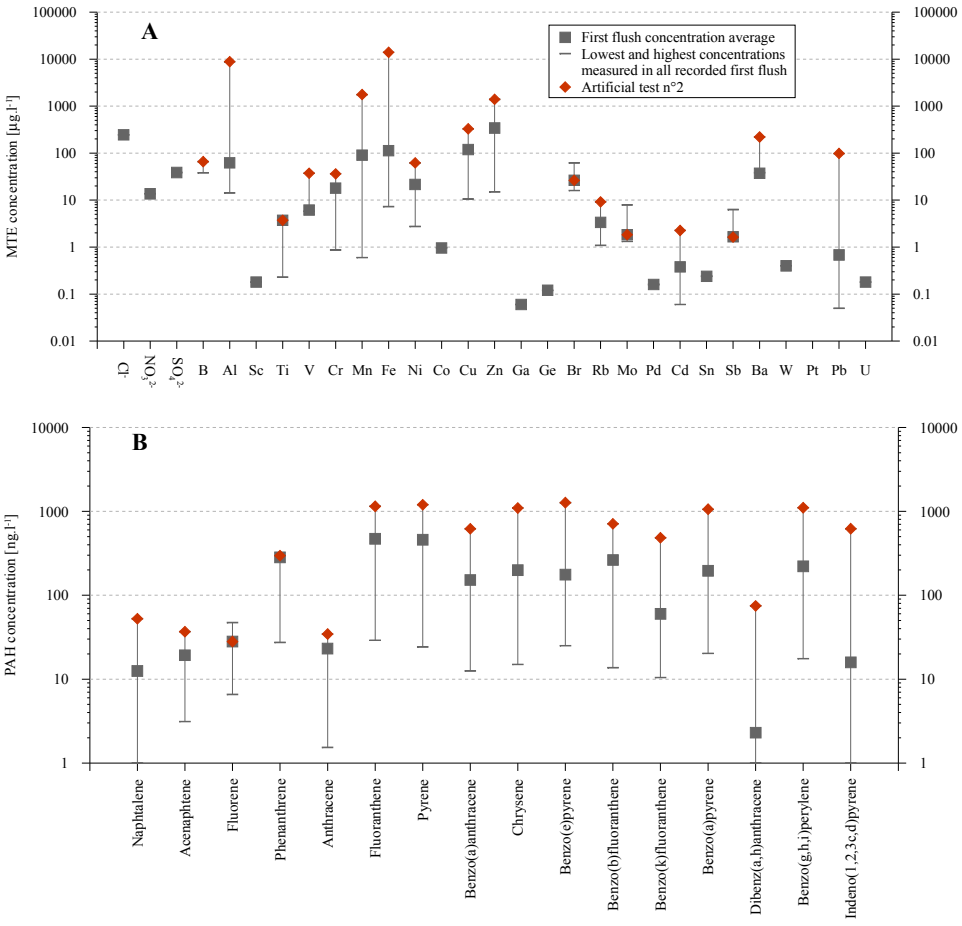

*Figure 4.18: MTE and PAH concentration in the road runoff. Squares represent the arithmetic averages of the first flush (6 of them), while error bars represent the maximum and minimum values recorded in the first flush. Artificial test n°2 values are noted in red. Note that the first flush concentrations recorded during the artificial test n°2 coincide nearly in every case with the maximal values. This means that interpretations based on the artificial test n°2 concern a highly contaminated road runoff. It thus validates the utilisation of the test n°2 as main example. Note that some elements have only one square: they have been analysed only once. **A)** MTE are sorted out according to their atomic weights. **B)** PAH are sorted out according to their molecular weights.*

[20] Note that, as the turbidity is an empirical measurement, the fraction < 0.45 µm is also counted in the turbidity as long as the particle refracts the light. The fraction > 0.45 µm is however assumed to be greater.

The proportionality of all MTE in samples, regardless of the event considered, is in most cases respected. This allows using some well identified MTE elements as road tracers. Most conclusive elements are B, V, Cr, Mn, Ni, CU, Zn, Br, Mo, Cd, Sb, and Pb. Those concur with the identified elements proposed by Parriaux et al. 1999).

MTE are mainly transported sorbed to particles. Only the most mobile elements are transported in solute and thus show pollutogram similar to TDS pollutograms (B, Br, Mo).

PAH are present is fairly constant and high concentration in the road runoff (figure 4.18B). The test n°2 relative concentration is very representative of a natural road runoff. All analysed first flush showed PAH in rather similar concentrations. Naphthalene, Dibenz(a,h)anthracene and Indeno(1,2,3c,d)pyrene were not always detected. Lighter PAH have the lowest concentrations, while heavier PAH (from fluoranthene) have higher concentrations. As demonstrated by batch and column tests, as well as test n°2 pollutograms, the heavier PAH have low mobility and strong first flush effect. This explains the lower concentrations met for light PAH. This weight limit (fluoranthene) confirms the b = 0.66 (K_d = 100) limit separating the mobile from the immobile PAH.

C_X are represented in the road runoff from C_{16} (appendix X). C_{32} is the most commonly found specie. Overall, concentrations are comparable with the values found in the literature (Parriaux et al. 1999). C_X b coefficients are ≈ 1. This illustrates a behaviour only function of the road runoff flow. Measured concentrations are thus function of the C_X deposition time on the road. Relative concentrations are, like for PAH and MTE, well defined. The artificial test n°2 relative concentrations are well representative. All road runoff contents have the same trend (two peaks around C_{18} and C_{32}). This confirms that the fractionation of C_X is constant; it is not function of the rainfall characteristics.

All BTEX are present in the road runoff except the ethylbenzene (appendix X). Concentrations are however very low (concentrations < 140 $ng \cdot l^{-1}$). The proportions are kept in all samples, regardless of the rain conditions. The specie o xylene is the most abundant. Benzene and toluene have low b coefficients, while others have b ≈ 1.

MTBE is widely found in the road runoff. It also shows a strong first flush behaviour (b = 0.5).

PCB have very low concentrations in all samples. The maximum value met is 1.4 $ng \cdot l^{-1}$ (PCB138). Overall, the proportion of all PCB is respected regardless of the event studied. The relative concentrations for the test n°2 are also well representative, even if PCB were found in the rainwater used for watering.

4.4 SHOULDER EXFILTRATION AND SHOULDER RUNOFF CONTENT

In this paragraph is discussed the contamination of the water percolating through shoulders (E_S) as well as running over them (R_S). However, shoulders were not specifically designed to retain contaminants. This is the role of the infiltration slope. Therefore, only main results about the shoulder retention capacities are discussed here. For insight of all results, see appendix X.

4.4.1 SHOULDER EXFILTRATION E_S CONTENT

The shoulders were watered with 310 litres of rainwater. The hyetogram is similar to the one displayed for the road runoff (figure 4.13; example of SGH in figure 4.2). Restitution volumes are specified in the figures Shoulders exfiltration flow curves are presented in appendix X.

The exfiltration water showed significant amount of contaminant whichever shoulder is considered. Note that, regarding the exfiltration content, the retention capacity of shoulders is exaggerated. Indeed, most of the contaminants are included in the first flush which runs over the shoulder (see chapter 3); the water which infiltrates the shoulders is already depleted. It is therefore useless to quantitatively compare the road runoff and the exfiltrated water. Figure 4.19 (MTE and PAH; other contaminants are presented in appendix X) shows the contaminant concentrations for relative comparison between shoulders only. The road runoff concentration is displayed for information. More information, particularly about the evolution of the b coefficients, is given in appendix X.

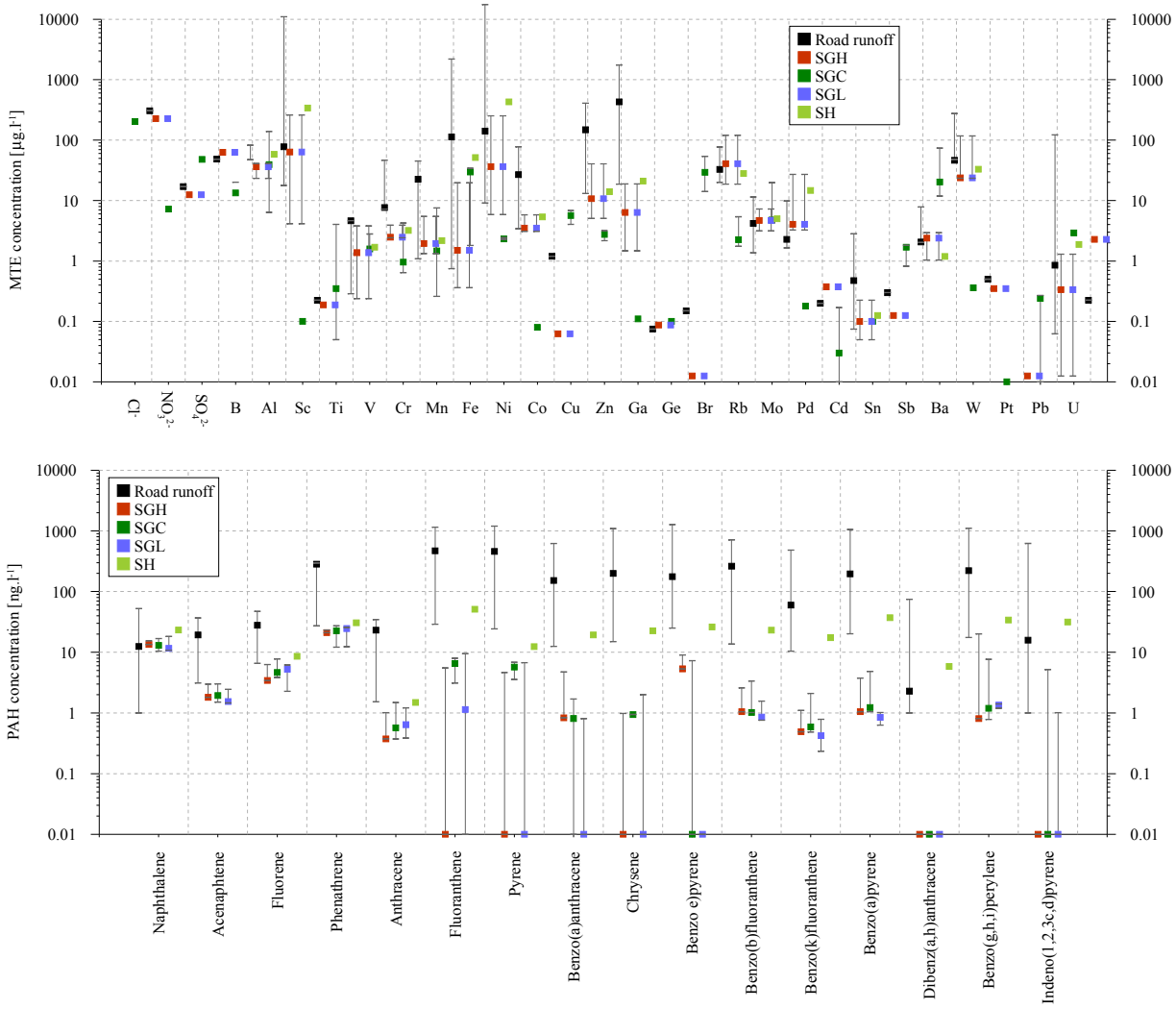

Figure 4.19: MTE and PAH concentrations in the first flush of shoulders exfiltration waters. Squares represent the average of the first flush concentrations; minima and maxima are the extreme first flush concentration values. ***A)*** *MTE and anions concentration in the road runoff and shoulder exfiltration. Anions are not retained at all. ETM elements which are easily sorbed are retained. For example, Mn (K_d = 0.39) has average concentration in the road runoff 100 times higher than those found in the exfiltration water. Other retained MTE are rather 5 to 10 times less concentrated in the exfiltration water. Overall, MTE are badly retained by shoulders; MTE concentration in exfiltration water is as concentrated as the road runoff (Al, Ga, Ge, Br, Mo, Pd, Sb, Ba, W). Note the ineffectiveness of the SGH, especially designed to retain pollutants. SH retention capacity is particularly not convincing.* ***B)*** *PAH concentration in the road runoff and shoulder exfiltration. Only naphthalene is not retained at all by all shoulders. Other PAH show concentration in the shoulder exfiltration 5 to 1000 times lower. SGH and SGL have greater capacities to retain PAH due to their humus content. SH clearly has the worst retention capacity; this is caused by its material which itself release PAH when leached by the road runoff.*

Assuming that the shoulders have a certain capacity to retain the particles and colloids, three different behaviours may occur in the exfiltration water E_S:

- Neutral pollutogram: the road runoff first flush passes over the shoulder; only the solute part is infiltrating the shoulders. As in the road runoff, the exfiltrating water first flush is driven by the flow. The higher the flow, the higher the massic flux [$g \cdot s^{-1}$]. This is the overall behaviour of SGC.
- Positive pollutogram: the exfiltration water shows a first flush (intensity from very strong (b = 0.1) to light (b = 0.9). The first flush in the shoulder exfiltration is due to:
  - the direct infiltration of the road water first flush
  - and/or to the infiltration of the road runoff first flush followed by large amount of "clean" water

  - and/or to contaminant release due to the infiltrating water leaching

  SH, for example, combines the direct infiltration with contaminant release (the HMF contains many MTE and PAH).
- Negative pollutograms: the contaminant are lightly retarded (b = 1.1) to very strongly retarded (b = 5). The retardation indicates a significant retention potential decreasing the contaminant mobility (K_d). This is for example the case for PAH in the SGL.

Those are general behaviours and are not representative of the complexity of the contaminant fractionation in the shoulder. Notably, the influence of one contaminant on the others, the sorption – releasing cycles and the biological interactions of organic compounds do alter the contaminant progress in the material. Contaminants are also influenced by their intrinsic properties. Aliphatic hydrocarbons, for example, have behaviours according to their molecular weights. Note that pollutograms are also strongly affected by the exfiltration flow curve. It indeed controls the abscissa of the M(V) plot (see §3.3.1 "first flush). The table 4.12 summarizes the behaviour of all groups of contaminants according to the considered shoulder.

The shoulder **SGH** (restitution volume ca. 65 litres), which was designed to retain contaminant, does not fulfil its task. Indeed, although organic compounds are found in low absolute concentration in the exfiltration water, the difference regarding other shoulder, particularly SGL, is negligible. Moreover, PAH are still widely found in the exfiltration water. MTE are found in the exfiltration water from all shoulders in same concentrations. The acidic pH found in the exfiltration water, certainly caused by humic acids, prevented the good retention. Aliphatic hydrocarbons behave the same way in each shoulder.

SGC (restitution volume ca. 65 litres), which high clay content would have suggested that it could well retain MTE, was also not very efficient; its first flush concentrations were the same as in the other shoulders. Not surprisingly PAH retention was lower than for SGH and SGL. PCB concentration in the SGC exfiltration water is almost as loaded as in the road runoff. Pollutograms for every type of contaminant are buffered: they are around 1 (neutral behaviour). However, fluoranthene, benzo(a)anthracene and benzo(e)pyrene have strong first flush b=0.3.

Overall, **SGL** (restitution volume ca. 45 litres) shows the lowest contaminant concentration. SGL retained PAH the same way as SGH, i.e. not very efficiently, but presents the lowest PAH concentration of all shoulder. The shoulder SGL practically let all the BTEX through, while other shoulders have better retention potential.

Overall, **SH** (restitution volume ca. 50 litres) presents the lowest retention potential. MTE, as well as PAH, easily percolated through the shoulder. This is surely due to leaching of the HMF layer which has a lot of PAH and MTE. C_X, BTEX, MTBE and PCB have concentrations similar as in the other shoulders. Pollutogram trends are equivalent as those encountered in the road runoff; this especially enlightens the poor retention and fractionation capacity of this shoulder.

4.4.2 SHOULDER RUNOFF R_S CONTENT

More importantly, the shoulder runoff did contain some large amount of pollutant. As the sampling required manpower and could not be automated, the shoulder runoff was only sampled during the artificial test n°2. However, as mentioned in the paragraph 4.3, the artificial test n°2 is very representative of the worst case scenario, i.e. a large thunderstorm occurring after a long dry period. No measurements were made in the shoulder runoff of SH and SB because no interception mean existed.

Surprisingly, relative concentrations found in the first water collected from the shoulder runoff are not similar to the road runoff concentrations. They are more like the shoulder exfiltration water concentration (appendix X). It thus seems that the postulated filtration and retention effect in the shoulder also exists on the shoulder surface. A small part of the particles would have already been settled. However, if the concentrations trends are similar, the absolute concentrations are logically higher than in the shoulder exfiltration.

Contaminant groups. Groups are sorted out according to the fraction of R_R found in the exfiltration water. 1/10 means that 1/10 of the R_R content was found in the E_S.	SGH				SGC				SGL				SH			
	fraction of R_R	b coef	Pollu-gram type	EC pH	fraction of R_R	b coef	Pollu-gram type	EC pH	fraction of R_R	b coef	Pollu-gram type	EC trend	fraction of R_R	b coef	Pollu-gram type	EC trend
Mn, Zn	1/100	0.7	Light FF	EC is increasing from 230 to 330 µS·cm^{-1}. No peak significant peak appeared, although the first measurement is slightly higher. pH is acidic and became neutral at the end of the event (from 6.77 to 6.9). This is caused by the humic acid.	1/100	0.95	± neutral	EC is increasing from 350 to 450 µS·cm^{-1}. This high TDS can be caused by leaching of the abundant clay material. It also materializes the retardation of solute. pH stayed between 7 and 8.	1/100	0.7	Light FF	EC is decreasing from 450 to 350 µS·cm^{-1}. pH is also decreasing from 8 to 7. The carbonate grave I explains this efficient pH buffering at the beginning of the event.	1/2 to 1/10	0.4	Strong FF	EC in the first water was 360 µS·cm^{-1}. It then showed a minimum (200 µS·cm^{-1}) and a second increase to 360 µS·cm^{-1} again. The by-pass between the surface and the exfiltration point strongly altered the natural EC behaviour. Indeed, pH stayed around 6.4 which was the rain pH.
Ti, V, Cr, Fe, Ni, Co, Cu, Cd, Pb	1/2 to 1/10	0.8	Light FF		1/2 to 1/10	1	neutral		1/2 to 1/10	0.8	Light FF		1/1 to 1/10	0.5	Strong FF	
C, N, S, B, Al, Sc, Ga, Ge, Br, Rb, Mo, Pd, Sn, Sb, Ba, W, Pt, U	1/1	1	neutral		1/1	1.15	Light retard.		1/1	1.20	Light retard.		1/1	0.62	FF	
Fluoranthene, pyrene, benzo(a)anthracene, chrysene, benzo(e)pyrene, dibenz(a,h)anthracene, indeno(1,2,3c,d)pyrene	1/100 to 1/10'000	1.35	Light retard.		1/100	0.4	Strong FF		1/100 to 1/10'000	5.2	Very strong retard.		1/10	0.25	Very strong FF	
Benzo(b)fluranthene, benzo(k)fluoranthene, benzo(a)pyrene, benzo(g,h,i)pery]ene	1/100	0.55	FF		1/100	0.75	Light FF		1/100	2.40	Strong retard.		1/10	0.25	Very strong FF	
Acenaphtene, fluorene, phenanthrene, anthracene	1/10 to 1/15	0.65	FF		1/10 to 1/15	1	neutral		1/10 to 1/15	2.20	Strong retard.		1/10	0.60	FF	
Naphthalene	1/1	0.85	Light FF		1/1	1	neutral		1/1	1.30	Light retard.		1/1	0.65	FF	
C_{24} to C_{40}	1/2 to 1/6	0.1	Very strong FF		1/2 to 1/6	0.95	± neutral		1/2 to 1/6	3	Very strong retard.		1/2 to 1/6	2.3	Strong retard.	
C_{16}, C_{18}, C_{20}	1/1	0.85	Light FF		1/1	1.5	Light retard.		1/1	1.10	Light retard.		1/1	0.35	Strong FF	
C_{10}, C_{11}, C_{12}, C_{14}	1/1	1.45	Light retard.		1/1	0.75	Light FF		1/1	1.10	Light retard.		1/1	0.65	FF	
BTEX	1/1 to 1/10	0.60	FF		1/1 to 1/10	*			1/1 to 1/2	*			1/5 to 1/10	0.5	Strong FF	
MTBE	1/5	0.7	Light FF		1/6	0.35	Strong FF		1/10	*			1/6	0.6	FF	
PCB	1/4 to 1/5	0.7	Light FF		1/1 to 1/2	0.85	Light FF		1/4 to 1/5	0.95	± neutral		*	0.6	FF	

Table 4.12: Summary of the contaminant behaviours in the shoulders. A (*) sign indicates a lack of data; i.e. either no contaminant was found in the exfiltration water, either only one or two samples showed contaminants (FF=first-flush).

The EC measured in the first R_S water collected confirms what have been exposed in the chapter 3 (table 4.13). Indeed, the road runoff EC decreased along the time. EC measured in the shoulder runoff allowed estimating which part of the road runoff first arrived to the edge of the shoulder. In the case of SGC, the measured EC corresponded to the road runoff EC peak; it thus means that the water ran over the shoulder first and infiltrated later. In the case of SGH, the measured EC corresponded to the road runoff tailing EC (EC at the end of the watering). This means that the road runoff first infiltrated the shoulder, then ran over the shoulder and reached the shoulder edge. SGL showed an intermediary behaviour.

The pH also confirmed the buffering effect of the rainwater in contact with carbonate material. Indeed, while pH of the rainfall was 6.5, the recorded pH in the shoulder runoff was roughly 7.5. It emphasizes the reactions between the road runoff and the shoulder material already happening on the shoulder surface.

	EC [µS·cm^{-1}]	pH [-]	R_S [litres]
SGH	95	7.44	45
SGC	280	7.65	90
SGL	200	7.68	65

Table 4.13: Physicochemical parameters of the shoulder runoff, measured in the first water collected. The EC is a good mean to assess the road runoff first flush behaviour. The SGC shoulder runoff has the highest EC, which is correlated with the road runoff first flush EC (figure 4.13, 9h05). On the other hand, the SGH road runoff EC is correlated with the road runoff tailing EC (figure 4.13, 9h30). The pH measurements confirmed that the rainwater (pH = 6.5) was rapidly buffered by the shoulder material. R_S volume once again emphasized the good impervious property of SGC.

No pollutogram was computed concerning the shoulder runoff because flows Q were measured by hand (pot and chronometer); they were thus presenting a “step plot” shape, ineffective to calculate b coefficients which are sensitive to the flow pattern.

4.5 INFILTRATION SLOPE EXFILTRATION CONTENT

4.5.1 INFILTRATION SLOPE EXFILTRATION DURING THE ARTIFICIAL TEST N°2

4.5.1.1 Hyetogram, exfiltration flow and physicochemical parameters

Due to the bad hydraulic performance of the LH lysimeter (see chapter 3), the assessment of the chemical behaviour in the infiltration slopes is made interpreting data coming from the lysimeter LW. Data concerning LH are provided for comparison purpose in boxed text.

The watering of the SGL-LW compartment, although occurring on different days, was conducted exactly as during the road runoff test (4.3.1.1). It therefore displays a very similar hyetogram (figure 4.20). The resulting simulated precipitation was 7.5 mm (16 mm·h^{-1}). The restitution volume was ca. 260 litres, with a lag time of 1h43. The curve trend of the exfiltrated water is highly representative of the LW behaviour (chapter 3). Note that the second peak is an artefact caused by the weir opening. When the flow reaches a minimal limit value, the water accumulates in the weir without overflow. This is due to the water superficial tension. Once the water height has enough increased, the water flows out again.

The LH lysimeter was watered in the same conditions. The restitution volume was ca. 50 litres with a lag time of 26 minutes only. This volume is lower than for LW but considering that almost 150 litres came out of the SH exfiltration pipe, this is not surprising. The LH exfiltration flow curve has a strong peak followed by a rapid decrease. The flow was less buffered by the soil than for LW.

During this test, the EC and pH were measured manually. The EC presented a strong increase immediately after the first water arrival. It reached its maximal value exactly at the same time as the flow peak (313 µS·cm^{-1}; TDS = 200 mg·l^{-1}; 9h22). It then kept this value along the whole event (three times higher than the road runoff EC). This

conductivity is slightly higher than EC recorded in the road runoff, also slightly higher than the one recorded in the SGL shoulder runoff (similar shoulder to the one adjoining LW). This demonstrates that solutes also got more loaded in the infiltration slope itself. The interpretation of this behaviour has to be related to chapter 3. Indeed, it has been demonstrated in that chapter that the first water coming out of the collecting pipe is the stock water ΔS. Only the first sample showed EC lower than 300 µS·cm^{-1}. This corresponds to the stock water which had time to equilibrate its TDS concentration. Then, EC stayed around 320 µS·cm^{-1} during all the exfiltration time. The solute residence time in the infiltration slope was not long enough to reduce the TDS concentration. The limit between the stock water and infiltrating water is therefore between samples LW1 and LW2. The process of TDS transport is thus as follow: as long as runoffs (R_R, R_S) and infiltrating water move, the solute got richer: they leach the road, shoulder surface and soil. If the water stays immobile, its TDS concentration decreases. Dissolved solids are absorbed, adsorbed or diffused in the permanent water[21] by osmosis (batch and column tests proved that the contact time is important: the longer the contact time, the lower the mobility). The TDS pollutogram is very lightly negative (b = 1.07). The solute thus continuously arrived in the collecting pipe as function of the exfiltration flow. The greater the flow, the heavier is the massic flux. The influence of the stock water EC is tiny because it is not strongly different from the infiltration water EC.

The EC measured out of the LH lysimeter decreased from 410 to 300 µS·cm^{-1}. It thus showed a first flush effect. This is likely due to the preferential flow paths; the road runoff rapidly and efficiently got through the soil without being buffered.

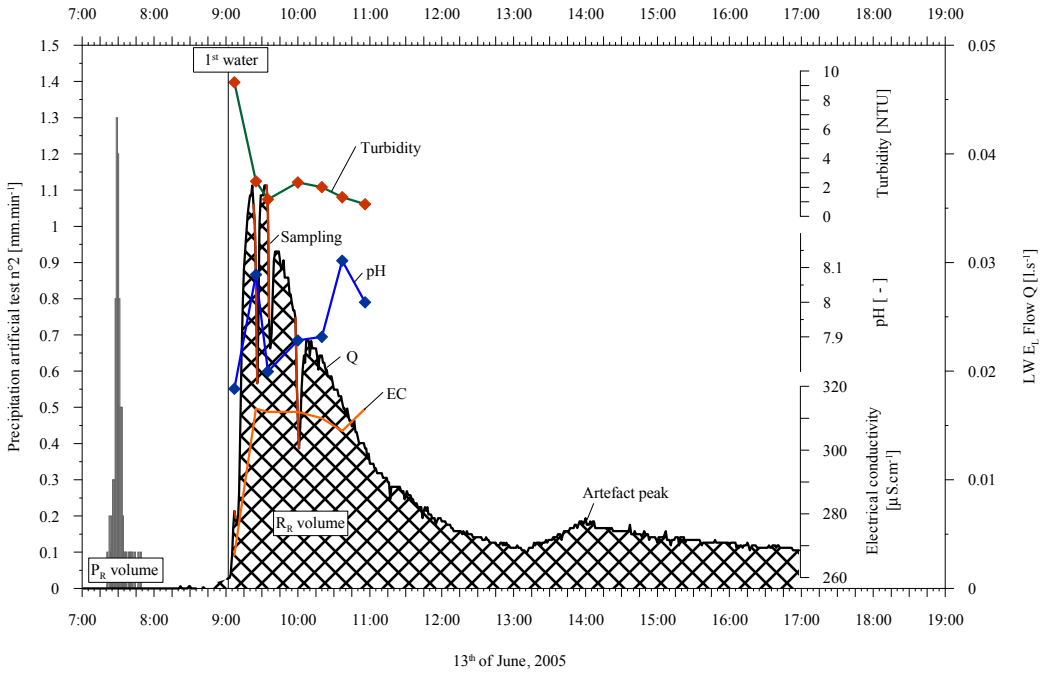

Figure 4.20: Precipitation, exfiltration and physicochemical parameters during the artificial watering of the SGL - LW compartment. Note that the rainfall and exfiltration flow are plotted on completely different scales and therefore cannot be compared. Red segments superposed to the black Q curve symbolize the samples. Resulting indentations are clearly visible. The Q flow presents a very commonly found trend: the peak arises shortly after the beginning of the exfiltration, followed by a long tailing. See text for explanation about the artefact peak. The EC shows its maximum coinciding with the flow peak and not with the first arrival of water (note, however, that the scale is only ranging from 260 to 320 µS·cm^{-1}; it is not a great difference). The EC then stayed constant. The EC behaviour demonstrates the lack of first flush effect. The pH is fairly constant but becomes a bit more alkaline at the end of the watering. This is due to the carbonate leaching. The turbidity is fairly low. Its general trend is however increasing at the beginning; it stabilizes afterward. The sampling altered the curve.

[21] The permanent water is the part of the water that stays indefinitely in the soil, sorbed to grains by its superficial tension.

The turbidity was also measured manually. The probe malfunctioned during the artificial test. After being put in order again, the probe was put in each sample that was previously homogenized. The turbidity curve is roughly similar to the one recorded in the road runoff but shows a second peak (coinciding with LW4). It decreases along the time, from 10 NTU to 1 NTU. Those values are very much lower than those encountered in the road runoff. 0.1 NTU is about the turbidity of the tap water (drinking water limit is often considered to be 1 NTU). This especially emphasizes the good capacity of the soils to filter particles. The decreasing curve enlightens the strong first flush of the turbidity. The turbidity first peak is certainly due to the remobilization of particles trapped in the soil and in the collecting pipe. They are carried down by the increasing infiltrating flow. The second peak, on the other hand, is certainly caused by small particles having percolated through the lysimeter from the road; they were not remobilized because the flow acceleration was negative at that time. Considering the flow limit between the stock water and infiltrating water (between LW1 and 2), the turbidity second peak due to the road turbidity is strongly retarded. The turbidity curve is negatively correlated with the EC curve, which was not the case for the road runoff.

The recorded turbidity in the first LH sample was 33, decreasing to 17 NTU. The curve thus showed a curve similar to the road runoff and to LW. Again, the preferential flow paths explain the difference in turbidity content. The curve, however, is highly irregular.

The pH was fairly constant. It stayed between 7.9 and 8.1. Again, the soil high carbonate content explains this high pH values, 1.5 pH unit higher than the road runoff pH.

The pH recorded out of the LH was constant with pH = 6.15. This value is comparable with road runoff; it was not buffered at all by the carbonate soils.

4.5.1.2 MTE concentrations

MTE concentration have been analysed in four samples (LW1 to LW4) presented in figure 4.21A. The road runoff first flush content is also presented for comparison purpose. The first peak is due to the stock remobilization (§4.5.2.1). MTE concentrations measured in the four samples are very similar from LW1 to LW4. The fractionation of MTE during the LW exfiltration is weak but recognizable. The following behaviours are noted:

- Very mobile elements (B, Br, Mo, $K_d < 5$) have very recognizable peaks; their concentrations remain the same from the road runoff to the lysimeter exfiltration water. This is also emphasized by the ring chart (fig. 4.21C). Zn, V, and Ba are also mobile elements ($K_d < 90$). Ti shows, like in the first flush, a behaviour that let suppose that it is more mobile than what was calculated in batch tests. Those seven elements show that their concentration peak is either coinciding with the first peak (very mobile elements Br, B) or is lightly retarded (in the second sample, other five elements). This confirms the mobility of those elements. For B and Br, the distinction between the stock water and the infiltrating water is impossible: they are mobile in the stock and present in the first water coming from the surface. All those MTE have neutral to slightly negative pollutograms, thus keeping the pollutogram trends acquired on the road (mobile elements had neutral pollutograms; they were continuously leached from the road).

- On the other hand, elements with low mobility ($200 < K_d < 300$) are relatively less concentrated: they have been retained in the soils. Those are Fe, Al, Mn, Cu, Ni, Cr, Rb, Cd, and Sb. They have two concentration peaks. The first peak is recorded in the first sample, whereas the second one is measured in the last sample. Those two peaks coincide with the turbidity peaks: this enlightens the fact that elements with low mobility are transported sorbed to particles. Pollutograms of those elements are very lightly positive ($0.9 < b < 1$), except for Fe and Al which have great concentrations ($0.8 < b < 0.9$).

- Elements with extremely low mobility, Mn and Pb, did not show a second peak. It is however very probably occurring later after LW4. Theirs pollutogram trends are thus not representative.

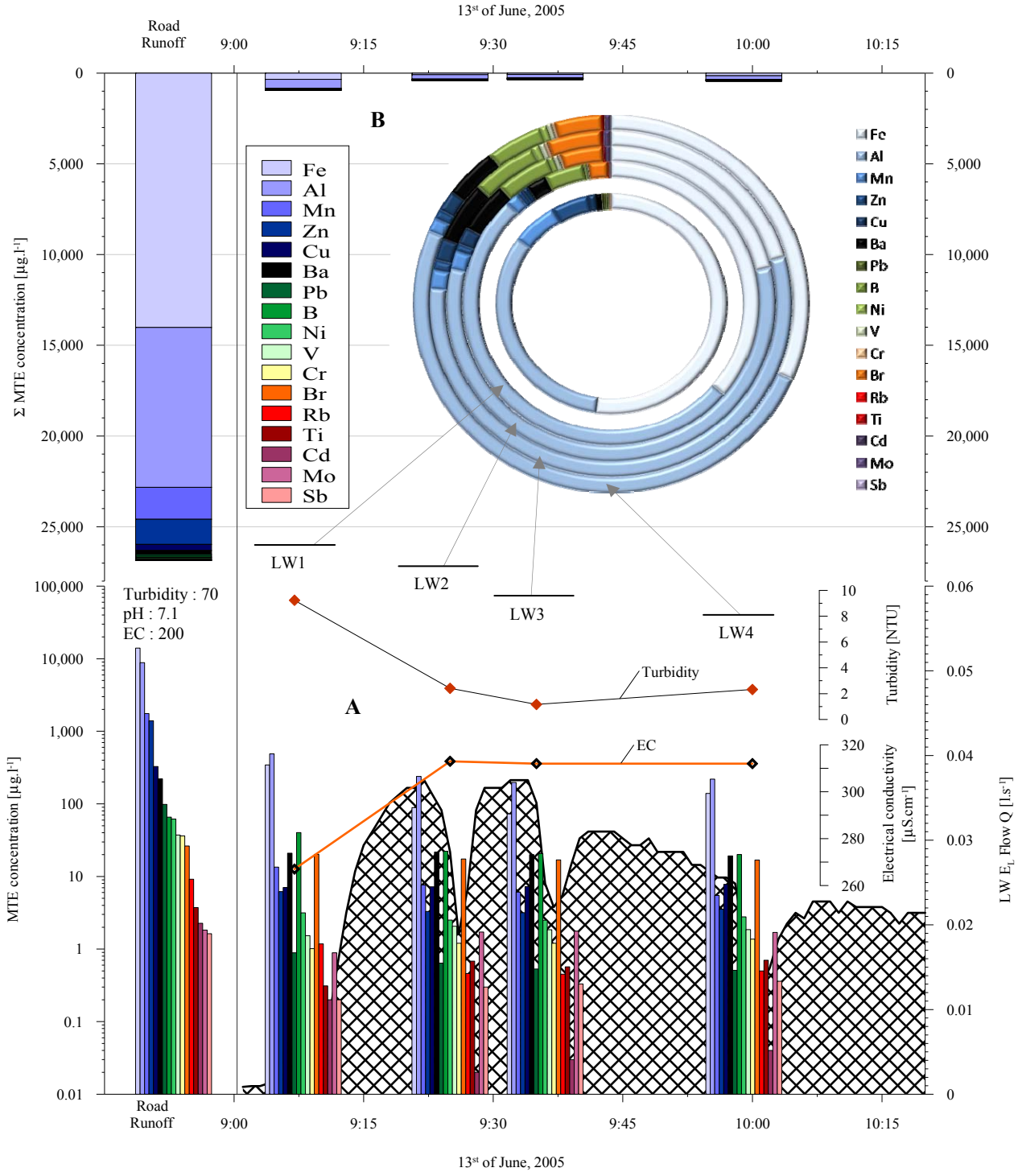

*Figure 4.21: Evolution of MTE concentration in the exfiltration water from LW. **A)** MTE concentration in the 4 samples (+road runoff; far left, for comparison purpose). Note the logarithmic scale. All MTE species are represented. MTE species are sorted out from their highest to their lowest concentration in the road runoff. The proportionality of all MTE stays roughly constant in all four samples. Some elements are relatively more concentrated than in the road runoff (B, Br, Mo). They indeed make recognizable peaks. Those elements are highly mobile. **B)** Sum of all MTE concentrations. This bar chart shows that Fe, Al, Mn, Zn and Cu constitute the fundamental part of the road runoff first flush MTE content. The total MTE concentration in the first flush shifted from 27'000 µg·l^{-1} in the road runoff to less than 1'000 µg·l^{-1} in the LW exfiltration water. **C)** MTE fractionation rings. The inner ring represents the road runoff. Outer circles represent the four road runoff samples, from the first one (inside) to the last sample (outside). The fractionation concerns especially the very mobile elements. Indeed, B, Ba, Br and Mo are proportionally much more present in the LW exfiltration water than in the road runoff. This emphasized the retention of elements with low mobility. MTE fractionation ring without Al and Fe is shown in appendix X.*

	Road runoff b Coefficient	LW b Coefficient	LH b Coefficient
Ti	1.18	1.07	0.61
Mo	0.90	1.12	0.84
B	0.86	0.95	0.78
Br	0.75	1.02	0.75
Rb	0.68	0.91	0.80
Zn	0.66	0.96	0.68
Cd	0.64	0.71	0.38
Pb	0.60	0.93	0.78
Sb	0.53	1.15	0.93
Cu	0.52	1.07	0.88
Ni	0.51	1.04	0.84
V	0.49	1.04	0.80
Al	0.48	0.89	0.80
Cr	0.47	1.09	0.83
Ba	0.46	1.02	0.78
Fe	0.41	0.83	0.82
Mn	0.39	0.88	0.72

Table 4.14: MTE b coefficients in the road runoff, LW and LH exfiltration waters. MTE are sorted out from negative to positive MTE pollutogram in the road runoff. Overall, MTE in the LW exfiltration water have neutral pollutogram Indeed, b coefficients are distributed around 1. Those with the higher concentration have the more positive pollutograms (Fe, Al, Mn). Sb, which has the lowest concentration, has the more negative pollutogram. In the LH exfiltration water, all MTE showed light to strong first flush pollutograms (0.38 < b < 0.93). No specific relationship exists between the road runoff and lysimeters b coefficients.

Overall, the total MTE concentration shifted from 27'000 $\mu g \cdot l^{-1}$ in the road runoff to less than 1000 $\mu g \cdot l^{-1}$ in the LW exfiltration water. Those 1'000 $\mu g \cdot l^{-1}$ are almost completely composed of Fe and Al (85%), which also showed the strongest first flush effect (figure 4.21B). The total concentration in the first sample LW1 is about twice as loaded as LW2, whereas LW4 is more concentrated that LW2 and 3. This correlation between the MTE total concentration and the turbidity demonstrates that the MTE total concentration is mainly caused by particles transport and not by solute transport. This is of course untrue for mobile MTE Effects of EC and/or pH are indiscernible. Because the flow Q curve was so buffered (flatten aspect), all the samples were plus or minus taken during the flow "maximum" (difference of 0.03 $l \cdot s^{-1}$ from the LW1 to LW2). The effect of the flow on concentrations is thus uncertain. The sample LW1 is the only one that had been taken during flow acceleration, though.

MTE that may cause problem to the environment or health (Pb, Cr, Cd, V) have very low concentrations; those concentrations concur with Swiss regulations maximum limits (see chapter 6).

LH showed total concentration in the LH exfiltration water similar to LW (1'000 $\mu g \cdot l^{-1}$; 78% of Al + Fe). However, as presented in table 4.14, MTE pollutograms were significantly different. They indeed presented light to strong first flush effect: contaminants peak were not buffered by the soil. The corresponding b coefficients are a bit superior to the road runoff values (but for Ti, Br, B, Mo, and Cd). The first flush is weaker. Environmentally dangerous MTE have concentration in the LH exfiltration water overall 1/3 superior to LW concentrations.

It is also interesting to assess the total MTE mass transmitted from the surface to the bottom of the lysimeter (figure 4.22). This gives a global view of how much MTE mass reached the lysimeter basis. The total contaminant mass transmitted from the surface to the lysimeter bottom was computed by integrating the massic flux along the duration of the exfiltration. Generally, MTE are very well retained.

To summarize, the overall trend of the total MTE concentration is correlated with the turbidity. Indeed, the greatest proportion of MTE is constituted by elements with low mobility (Al, Fe, Mn) that lead the total MTE concentration curve. Very mobile MTE (B, Br, Mo) are slightly more retarded and follow the EC curve trend. They are not concentrated enough to influence the total MTE concentration trend. Mobile elements keep the same concentration between the road runoff and LW exfiltration water. This means that low mobility elements are easily trapped in soils. This is certainly related to the alkaline pH.

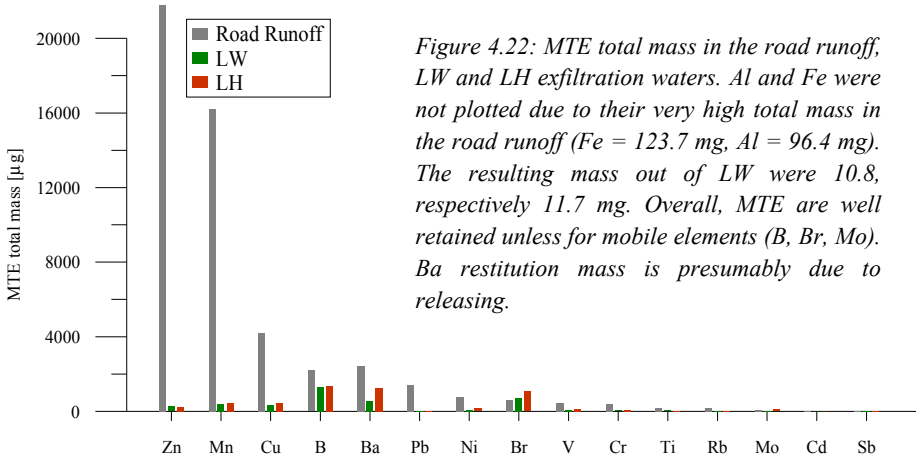

Figure 4.22: MTE total mass in the road runoff, LW and LH exfiltration waters. Al and Fe were not plotted due to their very high total mass in the road runoff (Fe = 123.7 mg, Al = 96.4 mg). The resulting mass out of LW were 10.8, respectively 11.7 mg. Overall, MTE are well retained unless for mobile elements (B, Br, Mo). Ba restitution mass is presumably due to releasing.

4.5.1.3 PAH

PAH concentrations in the LW exfiltration water are very low (figure 4.23A). All species have concentrations between 0 and 20 $ng \cdot l^{-1}$, which is at least 1000 times lower than the road runoff concentration. PAH have four concentration trends:

- Two peaks: pyrene, fluoranthene, chrysene, benzo(b)fluoranthene, benzo(g,h,i)perylene, and naphthalene have two recognizable peaks. Theirs concentrations were higher in the first and last samples. All those PAH have very low mobility ($K_d \approx 200$ and more). This enlightens a relationship between the PAH concentration and turbidity which had two also peaks. Naphthalene is however highly mobile ($K_d = 19$). Its first peak is certainly due to the high soil release during the stock mobilisation, while the second is caused by the infiltrating water.

- Decreasing trend: some species are present only in the first sample (Benzo(e)pyrene and benzo(a)anthracene). They are not detected afterward. Those PAH have therefore pollutograms presenting strong first flush effects (b = 0.27, table 4.15). They have low mobility ($K_d \approx 170$). Benzo(a)pyrene and benzo(k)fluoranthene have concentrations that decreased along the time. According to other PAH behaviours (see below), a second peak might exist. It is either strongly retarded either masked; it is not apparent in figure 4.23A. It is probable that their mobility was sufficient to stay in the liquid phase long enough; while species with $K_d = 200$ were sorbed and thus coincide with the turbidity second peak. Those two PAH have thus a first flush effect (b = 0.72 and 0.77 respectively). They also have low mobility ($K_d \approx 160$).

- Increasing trend: acenaphtene is detected in similar concentrations only in the two last samples LW3 and LW4. It thus has a pollutogram which is highly retarded (b = 1.38). Phenanthrene, anthracene, and fluorene had increasing concentrations. They are also retarded to strongly retarded (Phen b = 1.23; Anth b = 1.22; Fluo b = 1.38). Those PAH have very low K_d (between 30 and 60). They present their lowest concentrations in the first sample: they were not sorbed to particles. Results exposed here and in §4.3.2.3 suggest that phenanthrene is more mobile than what was calculated in batch tests. Phenanthrene indeed behaves as a very mobile PAH. It also had the second highest global restitution mass (see below).

- No peak: dibenz(a,h)anthracene is not detectable in any of the samples.

Table 4.15: PAH Pollutogram trends for the road runoff and LW exfiltration water compared to the K_d distribution coefficient. Species are sorted out as function of the LW b coefficients. Overall, the more mobile the PAH, the more negative the pollutogram is (b > 1). It is postulated that phenanthrene is more mobile than what was calculated during the batch tests.

PAH	Road runoff b coefficient	LW b coefficient	Batch K_d
Benzo(a)anthracene	0.61	0.27	177.8
Benzo(e)pyrene	0.61	0.27	187.9
Pyrene	0.65	0.31	256.4
Fluoranthene	0.66	0.52	247.2
Benzo(a)pyrene	0.61	0.72	181.1
Chrysene	0.62	0.74	193.6
Benzo(g,h,i)perylene	0.58	0.76	238.8
Benzo(k)fluoranthene	0.59	0.77	114.0
Indeno(1,2,3,d,d)pyrene	0.71	0.8	
Benzo(b)fluoranthene	0.61	0.93	199.5
Naphthalene	0.92	1.14	19.8
Anthracene	0.67	1.22	57.7
Phenanthrene	0.67	1.23	175.8
Fluorene	0.82	1.38	65.6
Acenaphtene	0.46	1.38	39.3
Dibenz(a,h)anthracene	0.67		73.3

The total PAH concentration shifted from 10'000 $ng \cdot l^{-1}$ to 60 $ng \cdot l^{-1}$ in the first sample. The other samples total concentrations are respectively 30, 35 and 50 $ng \cdot l^{-1}$. They well fit the turbidity trend (figure 4.23B). However, because the PAH total concentration is constituted by naphthalene and phenanthrene species, the transport mean cannot be assessed with precision. Indeed, naphthalene (1/3 to 1/2 of the total concentration) is soluble while phenanthrene (~1/3 of the total concentration) has a medium mobility (figure 4.23C). Based on the phenanthrene behaviour in the road runoff and LW exfiltration waters, as well as on its high restitution mass, it can however well

be postulated that phenanthrene is indeed mobile (with an estimated $K_d \approx 60$, based on comparison with other PAH). Besides the first peak clearly caused by turbidity, the PAH total concentration trend would therefore be due to mobile species at 80%. This would imply that PAH are overall less mobile than MTE.

The total mass that reached the bottom of the lysimeter is shown in figure 4.24. Besides naphthalene and phenanthrene, all species have total masses cut off to 1/2000 of their initial masses in the road runoff. This depicts a good PAH retention in soils.

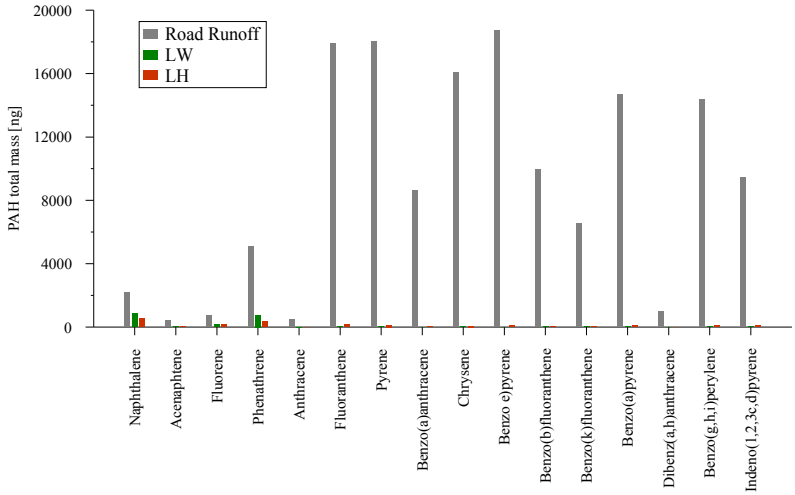

Figure 4.24: PAH total masses restitution in the LW and LH exfiltration waters. The road runoff mass is also given. Beside naphthalene and phenanthrene, all PAH have restitution masses about 2000 times smaller.

To summarize, PAH behaves like MTE do: mobile compounds stay in the solute form and only participate lightly to the first peak content, while compounds with low mobility easily complex to colloids and particles and thus participate greatly to the first peak concentration. PAH with low mobility then constitute the essential of the PAH total concentration. PAH with low mobility are well retained in soils.

Like for MTE, PAH pollutograms out of the LH lysimeter have stronger first flush, thus depicting a larger amount of particles being transported from the surface to the lysimeter bottom. The most significant fact is that the mobile PAH (naphthalene and phenanthrene) proportionally constitutes only 1/3 to 1/2 of the total PAH concentration, as opposed to the 80% in the LW exfiltration water. Particles do transit through LH more easily.

4.5.1.4 Aliphatic hydrocarbons

C_X are found in the LW exfiltration water in concentration sometimes higher than in the road runoff. For example, the triplet C_{16}-C_{18}-C_{20} is always showing high concentrations. This triplet is always found in the lysimeter exfiltration water and constitutes a great road tracer (appendix X). Their concentration is correlated to the exfiltration flow Q. It appears that there is not retention at all for those three C_X: they are completely mobile. Their pollutograms are lightly retarded ($b \approx 1.2$, table 4.16). Although they were already present in the rainwater used for the road watering, their presence on the road is confirmed by analysis of other natural precipitation runoff (§4.5.3). They therefore might infiltrate the aquifer. Their total cumulated mass reaching the lysimeter bottom is equal or superior to the road runoff total mass (unit in µg. R_R: $C_{16} = 28$; $C_{18} = 70$; $C_{20} = 33$. LW: $C_{16} = 27$; $C_{18} = 130$; $C_{20} = 47$). Leaching therefore occurred.

Lighter and heavier C_X, which constituted 85% of the road runoff concentration, quickly disappeared from the exfiltration water. They were not detected after LW2. It is supposedly due to their correlation with the turbidity (some species reappeared in the last sample LW4 which also showed a second turbidity peak). However, no data concerning C_X mobility is available. Their pollutograms present strong first flush effects ($b \approx 0.4$). Although present in very high concentration in the road runoff, those species are easily retained in the soils. They are rarely detected during other natural event.

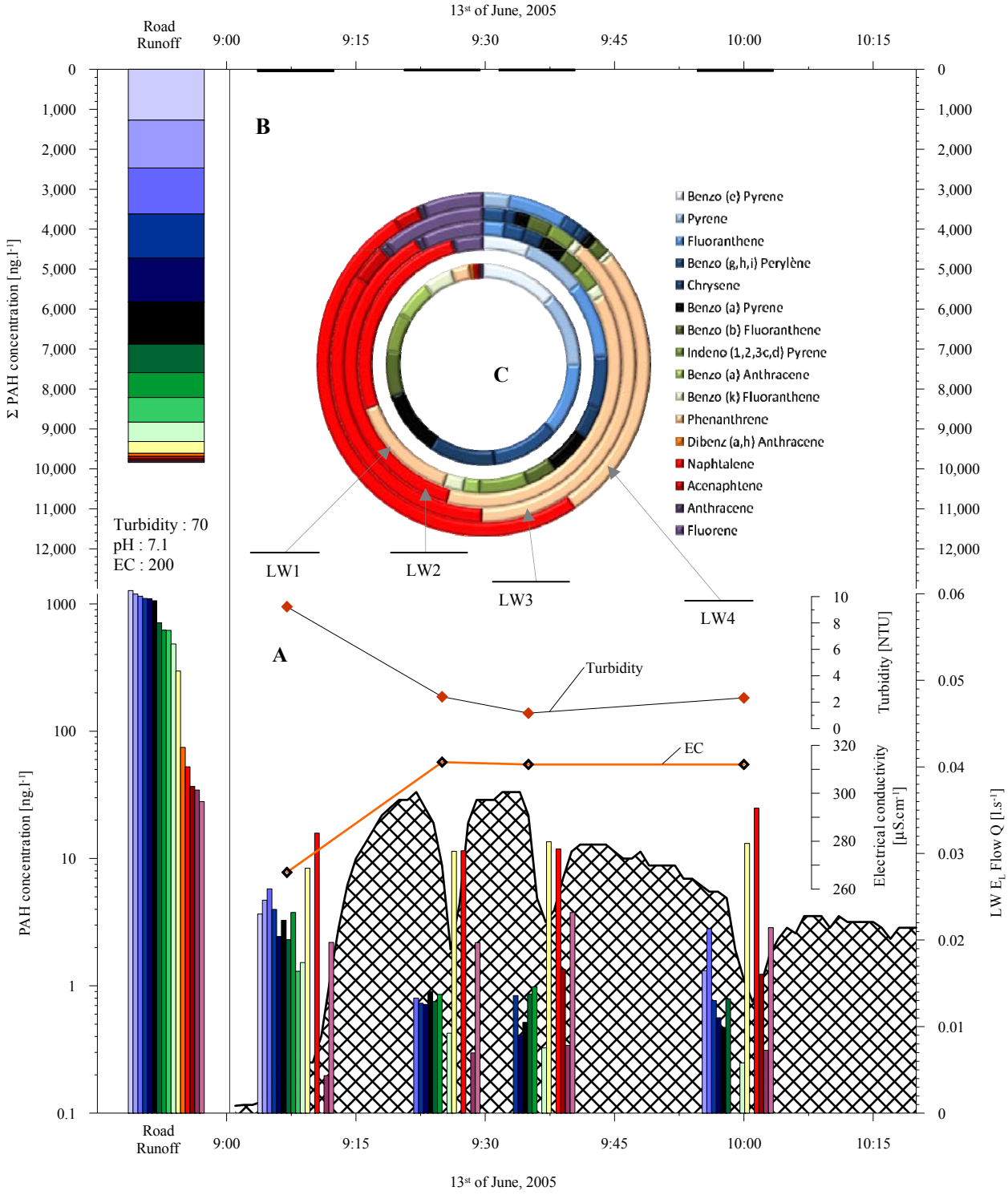

*Figure 4.23: Evolution of PAH concentration in the LW exfiltration water. **A)** PAH concentration in the 4 samples (+ road runoff on the far left). Note the logarithmic scale. PAH species are sorted out from their highest to their lowest concentration in the road runoff first flush. The proportionality of all PAH strongly varied along the time. Some PAH completely disappeared from the exfiltration water (BeP, BaA, DiB(ah)A, Acen) whereas other PAH are more concentrated at the beginning and end of the event. Phenanthrene, Naphthalene and fluorine conserve high concentrations. **B)** The total PAH concentration shifted from 9830 ng·l^{-1} in the road runoff first flush to 59 ng·l^{-1} in the first samples taken out from LW. This enlightens a great PAH retention. **C)** PAH fractionation in the four samples. The road runoff content (inner circle) was widely distributed between all PAH species, whereas naphthalene and phenanthrene constituted 80% of the LW samples. Only LW1 had a more homogeneous distribution.*

C_X concentrations measured in the LH exfiltration water have strangely lower concentrations than for LW. However, the pollutogram trends once again confirm a stronger first flush effect due to the by-pass infiltration path.

C_X	Road runoff b coefficient	LW b coefficient	LH b coefficient	PCB species	Road runoff b coefficient	LW b coefficient	LH b coefficient
C10		0.32		PCB 105	0.75	1.17	0.36
C11	0.92	0.33		PCB 128	0.8	8	0.53
C12	0.94	0.67	0.57	PCB 118	0.83	1.35	0.72
C14	0.95	1.23	0.75	PCB 138	0.86	1.5	0.76
C16	0.92	1.26	0.67	PCB 156	0.87		
C18	0.87	1.27	0.77	PCB 28	0.89	1.29	0.99
C20	1.04	1.27	0.78	PCB 52	0.89	1.56	0.91
C24	1.22	1.25		PCB 153	0.89	1.84	0.78
C28	0.99	1.06		PCB 180	0.89	1.87	5.18
C32	0.93	1		PCB 149	0.92	1.54	0.98
C36	1.25	0.92		PCB 101	0.99	1.45	0.77
C40	0.95	0.36		PCB 170	1.09	1.86	0.7

*Table 4.16: Pollutogram trends for C_X and PCB in the LW exfiltration water. **C_X**: C_X are sorted out according to their molecular weight. LW exfiltration water have retarded pollutograms for the triplet C_{16}-C_{18}-C_{20} (also for C_{14} and C_{24}, but their concentration are negligible); strong first flush effects for other species. In LH, the order is respected but absolute b values are far smaller. **PCB**: PCB species are sorted out as function of the road runoff b coefficient. LW exfiltration water b coefficients respect the general trend. Retardation is due to the piston effect. In LH, neither the order nor the absolute values are comparable.*

4.5.1.5 BTEX and MTBE

BTEX and MTBE were not detected in the LW exfiltration water during the artificial test n°2. Although the BTEX concentration was very high in the rainwater, all compounds were retained and presumably degraded in the soils. Indeed, BTEX are sufficiently volatile not to stay in the stock and sufficiently weak to be easily degraded by biomass. Stock remobilization never created a BTEX first flush. BTEX compounds are therefore not dangerous for the aquifer.

MTBE, although not detected in this particular case, was often detected. It is therefore not possible to cross it out of the major contaminant list. See §4.5.3 for natural events.

Only benzene, toluene and MTBE were detected in the LH exfiltration water. Total restitution masses were 10 to 5 times lower out of the lysimeter. Since the retention of those species in the soil was so good (at least for BTEX), it emphasizes not only preferential flow paths in LH but also water path running away from the soil material (along the geomembrane for example).

4.5.1.6 PCB

PCB concentrations in the LW exfiltration water are very low. The maximum concentration is found in the sample LW3 (sum of the 209 species is 5 $ng \cdot l^{-1}$; appendix X). This coincides with the flow Q maximum. Species 128 and 156 are not found in any sample. All other PCB are found in all samples. The fractionation is nearly inexistent: all PCB behave similarly. They are not correlated with the turbidity and are thus presumably very mobile in soils. Their pollutograms are retarded, of course influenced by the late arrival of the infiltration water (as opposed to the stock water).

PCB in the LH exfiltration water showed similar behaviour. Their relative concentration is similar in every sample and in the road runoff. However, their pollutograms show stronger first flush effects. Same causes inducing same effects: the water ran along preferential water paths and its content was not slowed down.

4.5.2 COMPARISON WITH NATURAL EVENTS

4.5.2.1 Estimation of the aerial deposition influence

A natural event very similar to test n°2 has been monitored on the 18th of July 2005. The preceding drought, the precipitation mean and maximum intensities as well as the total rain volume are very similar (9 days, 30 mm·h^{-1}, 7.6 mm, see appendix X for flow curve). The most fundamental difference is that the whole compartment, including the lysimeter, was watered during this natural event. It thus includes substances deposited on the lysimeter surface. As only the road was watered during the test n°2, substances transported downward come from the road only. The difference thus gives a good estimation of the aerial deposition in the surface comprised between 0 and 7 metres from the road (lysimeter surface). Four samples were taken from the LW exfiltration pipe during that event which allowed calculating the massic flux, and thus the total substance mass that comes from the lysimeter surface and the road runoff. Note that the road runoff was unknown for the natural event. However, the total masses measured in the LW exfiltration water are so similar that it is highly probable that the road runoff content were also similar. Moreover, only 1 month separate the two events. The lysimeter structure has thus not evolved.

MTE do not present a strong difference in total mass (figure 4.25). Total masses are similar whichever event is considered. Whether MTE come from the road runoff only or from the road runoff and the surface of the lysimeter has no influence on the final total mass. This demonstrates a strong relationship between the MTE transportation and the road runoff. MTE are predominantly carried by the road runoff, either sorbed to particles, either under solute form. Those similar results do not allow estimating the MTE aerial dissemination.

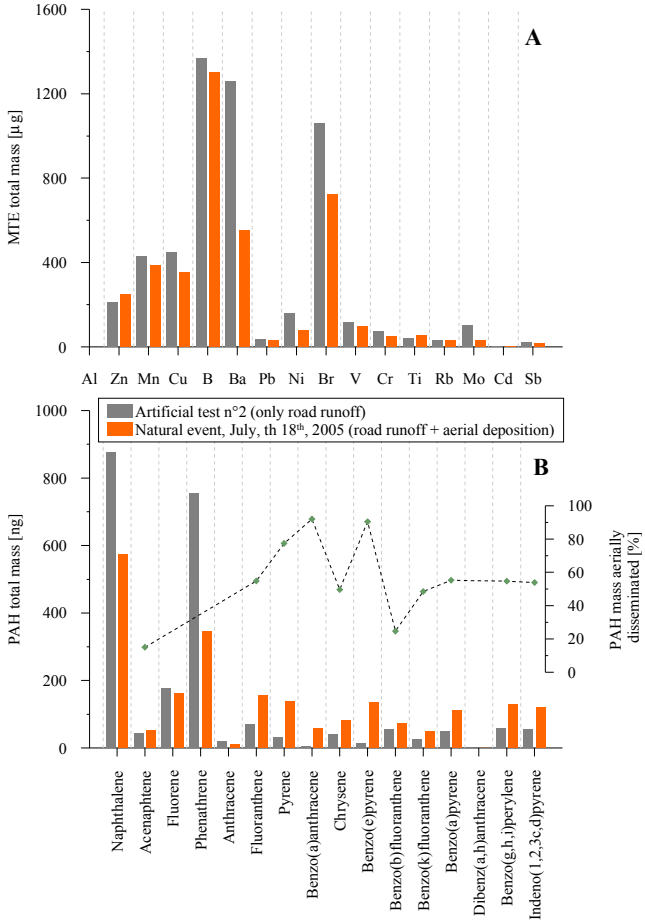

Figure 4.25: Comparison between the artificial event n°2 and a similar natural event. During the former, only the road was watered, while the road and the lysimeter were both rained upon during the latter. The difference allows estimating the influence of the aerial deposition on the lysimeter surface. ***A)*** *MTE have similar total mass whichever event is considered. This means that MTE are preferentially carried by the road runoff, either sorbed to particles, either in solute form. Al and Fe are not represented to allow a linear scale.* ***B)*** *On the contrary, PAH show a significant fractionation between the two events. The road runoff carries mostly light and mobile PAH whereas the aerial dissemination mostly concerns the heavier less mobile PAH. Acenaphtene and fluorene have similar total mass in both events. The percentage of PAH mass transported aerially is ranging from 20 to 90% (Acenaphtene is not considered because it is highly mobile; its lower total mass in the road runoff only might be a coincidence).*

On the opposite, PAH present very interesting results. Mobile, lighter PAH are evidently more present in the road runoff (naphthalene, phenanthrene), while less mobile, heavier PAH are predominantly found in the samples that also include the influence of the lysimeter surface. This implies that heavy PAH are predominantly deposited aerially. This concurs with the literature (Stotz (1987) demonstrated that only 14% of PAH are found in the road runoff). Total masses coming from the natural event are between 2 (fluoranthene) and 10 (benzo(e)pyrene) times higher than those

coming from the artificial test n°2. This means that heavy PAH are transported aerially at 20 to 90%, depending on the PAH species. Those percentages are however underestimated because the soil volume treating the infiltrating PAH, which origin is aerial, is far greater than the soil volume treating the road runoff (chapter 3). The retention is thus better; and the resulting PAH massic fluxes lower.

4.5.2.2 Concentrations during natural events

As it has been demonstrated in §4.3, the artificial watering test n°2 is highly representative of a similar natural event. Conclusions brought by the study of the substances behaviours during this test are thus of upmost importance. However, to assess the dimension of the potential pollution transmitted to the aquifer, chemical analysis of the LW exfiltration water have been carried out and compared to data coming from the test n°2.

MTE are widely found in the lysimeter exfiltration water. Figure 4.26A shows the MTE concentration in the first water collected. Note that the highest values recorded in the road runoff come from a natural event which is not always the event having induced the highest concentration in the LW or LH exfiltration water. It depends on the soil moisture and thus on soil fluxes (if the soil is wet, the stock have an influence). Concentrations of the first water collected is often the more loaded, although very mobile elements might have a later increase. Those are however not very dangerous for the environment and health. Mobile MTE have always concentrations similar to the road runoff concentrations (B, Br, Mo, Ba). Less mobile elements have lower restitution concentrations (Cr, Mn, Cu, Zn). Concentrations measured out of both lysimeters are comparable. No significant differences are emphasized. Results provided by natural events therefore confirm that the artificial test n°2 is representative of the MTE behaviour.

According to §4.5.3.1, the road runoff is not the only transportation vector regarding the PAH. The aerial (either dry or wet) deposition is also very significant. This means that the direct comparison between the road runoff and lysimeter exfiltrated concentrations is useless: the retention is far underestimated. The PAH road runoff concentration has thus been increased according to the aerial mass percentage calculated in §4.5.3.1. Results show that the retention is pretty good (figure 4.26B). Heavy PAH concentrations in the LW and LH exfiltration water are 100 times lower than in the road runoff. Light PAH (from naphthalene to anthracene) have concentrations 10 times lower. However light PAH did not show their highest concentrations in the first water collected during the artificial test n°2. It is thus probable that the light mobile PAH concentration in the lysimeter exfiltration water is equal to the road runoff concentration (like for mobile MTE and naphthalene).

4.5.3 SOIL CONTAMINATION AFTER 2 YEARS

In November 2006, the LB infiltration slope A and B horizons have been sampled. The purpose was to assess the soil contamination due to the road after 2 years of service. Indeed, comparison with data provided by the initial soil assessment (§4.2.1.2, September 2004) and the soil sampling (December 2007) allow determining the substance (MTE and PAH) concentration rate C(t)[22] in the soil, i.e. the substance mass retained during those 2 years. See §4.1.2 for methodology. To assess the substance repartition in the soil, samples have been collected in three different positions, at three different depths. To assure a sufficient mass for analysis, samples were 25cm long (auger was only 4.5 cm width to avoid destroying the infiltration slope). Sample locations are shown in figure 4.28A.

[22] C(t): concentration rate [$mg \cdot kg^{-1} \cdot month^{-1}$]. The concentration rate describes the increase of soil concentration per unit of time; calculated for the soil sample which has the highest variation. For MTE, it is the sample taken at 50cm depth, in the middle of the slope. For PAH, it is the surface sample also located in the middle of the slope.

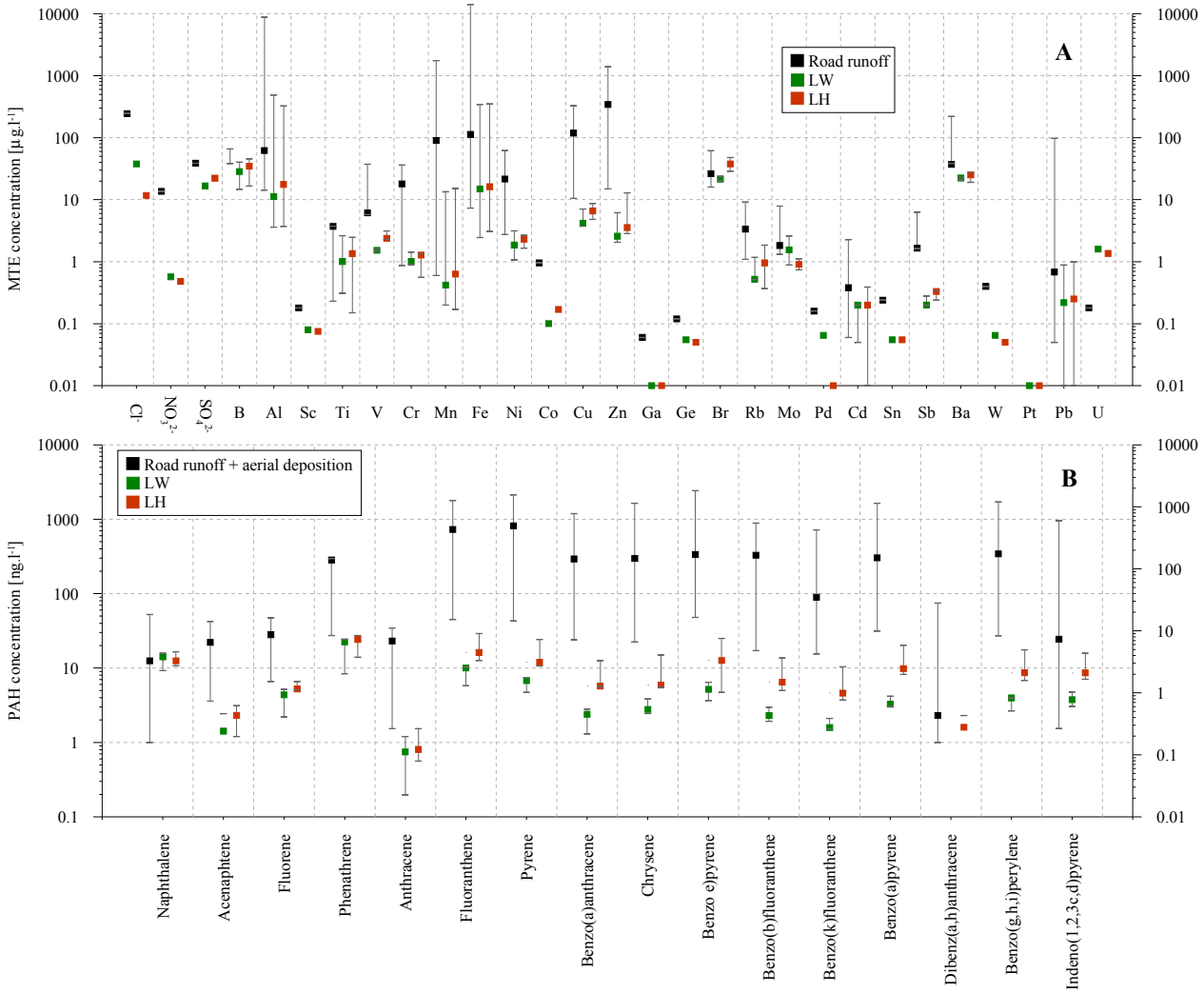

*Figure 4.26: Contaminant concentrations in the road runoff, LW, and LH exfiltration waters. Concentrations were measured in the first collected water. **A)** MTE concentrations. Mobile elements have concentrations similar to the road runoff concentration, whereas less mobile elements are better retained. Paragraph 4.5.3.1 demonstrated that MTE were predominantly carried by the road runoff; the comparison is thus pertinent. **B)** PAH concentrations. Road runoff concentrations were increased according to the percentage of mass aerially deposited on the soil surface (20 to 90% increases). Low mobility PAH are very well retained in both lysimeter; LH constantly has higher concentrations than LW, though. Even mobile PAH have concentrations lower in the road runoff and lysimeter waters (except naphthalene).*

The difference between the initial soil concentration and the concentration 2 years later is depicted in figure 4.27. Concerning MTE (fig. 4.27A), the difference is nearly inexistent. Only Rb shows concentration a bit higher after those 2 years, while other MTE have similar, even smaller, concentrations. This is presumably due to local variations: the location is not exactly the same (2006 sampling was conducted on the slope, while 2004 sampling was conducted on the opposite small ridge (figure 4.4). Ba concentration is surely very high in the grave I. The bottom samples have indeed been contaminated (bottom samples were drilled until the embankment was reached; a very small amount of grave material was therefore included to the sample). The distribution coefficient K_d is logically correlated with the concentration of MTE in soils, the correlation is not excellent, though. Concentration rates range from 0.005 (Mo) to 200 $mg \cdot kg^{-1} \cdot month^{-1}$ (Al, Fe). The concentration rate is correlated with the K_d. The more mobile the element is, the higher its concentration rate is. Again, Ti concentration and concentration rate suggest a lower K_d than what have been calculated in batch tests.

Figure 4.28B presents the ∑MTE distribution of concentrations. The highest concentrations are located in the middle of the slope, at the A-B horizon interface, whereas the lowest concentrations are at the surface, from the middle to the

end of the slope. Those places are correlated with the places where the water fluxes were the highest, respectively the lowest (§3.5.2.2). Therefore, the distribution of MTE concentrations enlightens the flow paths. MTE are preferentially transported in the runoff, either by solute transport, either by particle transport. The aerial dissemination is far less important. Those results confirm the §4.5.3.1 conclusions.

Figure 4.27B displays the PAH concentration in the soil. The difference between the 2004 and 2006 sampling campaigns is much more emphasized than for MTE. Indeed, PAH concentration at the soil surface is much higher 2 years after the road commissioning. Light PAH (from naphthalene to anthracene) have higher concentrations near the shoulder edge, whereas heavier PAH present their higher concentration in the middle of the slope. Light PAH were not detected in 2004. Absolute concentrations are low regarding the literature (0.3-3 $mg \cdot kg^{-1}$ in Grandson, 1-25 $mg \cdot kg^{-1}$ in Burgdorf; Boller, 2006). The correlation between PAH concentration and K_d is undeniable: the more mobile, the less concentrated. Also, a nearly perfect correlation exists between the concentration rate and the K_d. Concentration rates are very low for mobile PAH (~1 $\mu g \cdot kg^{-1} \cdot month^{-1}$ for naphthalene), while concentration rates range from 7 to 14 $\mu g \cdot kg^{-1} \cdot month^{-1}$ for heavier PAH. Phyto- and bioremediation are not taken into account.

PAH distribution in soil shows higher concentrations at the surface, while low concentrations are found at the bottom of soils (figure 4.28C). This enlightens the presence of aerial deposition (dry and wet) along the infiltration slope surface. As opposed to MTE, the flow paths do not carry the majority of PAH. This concurs with §4.5.3.1. The small difference in humus content between the A and B horizons is not sufficient to create such a difference in PAH content. The localisation of PAH deposition is certainly due to the air circulation around the slope (depression effect like a plane wing).

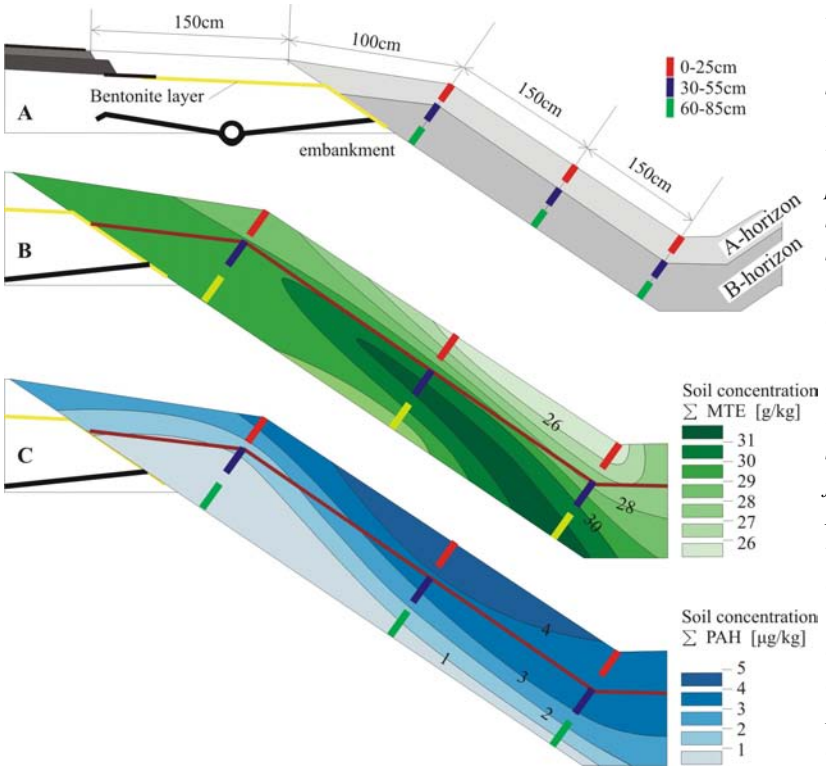

*Figure 4.28: **A)** soil sampling locations (2006) in the LB infiltration slope. The soil was sampled until the embankment was reached. Top samples were at the soil surface, middle samples were at the B horizon surface, and the bottom samples were at the B horizon bottom. Sampling profiles were perpendicular to the soil surface, at 1, 2.5 and 4 metres from the shoulder edge limit. **B)** ∑MTE concentrations in the LB profile. The higher concentration at the A – B horizons interface is not only due to the higher initial concentration demonstrated in §4.2.1.2. The blue sample in the middle of the slope also showed the higher concentration increase, followed by the yellow sample downward. Also, the place where the weakest water flux were noted (§3.5.2.2) has the lowest concentration increase. Main flow paths are thus enlightened by the higher concentrations. This concurs with chapter 3 conclusions. **C)** ∑PAH concentrations in the LB profile. As opposed to MTE, the highest concentrations are met in the middle of the slope, at the surface. The concentration decreases as function of the depth. This shows that PAH are mainly aerially deposited on the soil surface (dry and wet deposition) and then migrate through the soils. Turbulent depression caused by the slope explains why the highest concentration is met in the middle of the slope.*

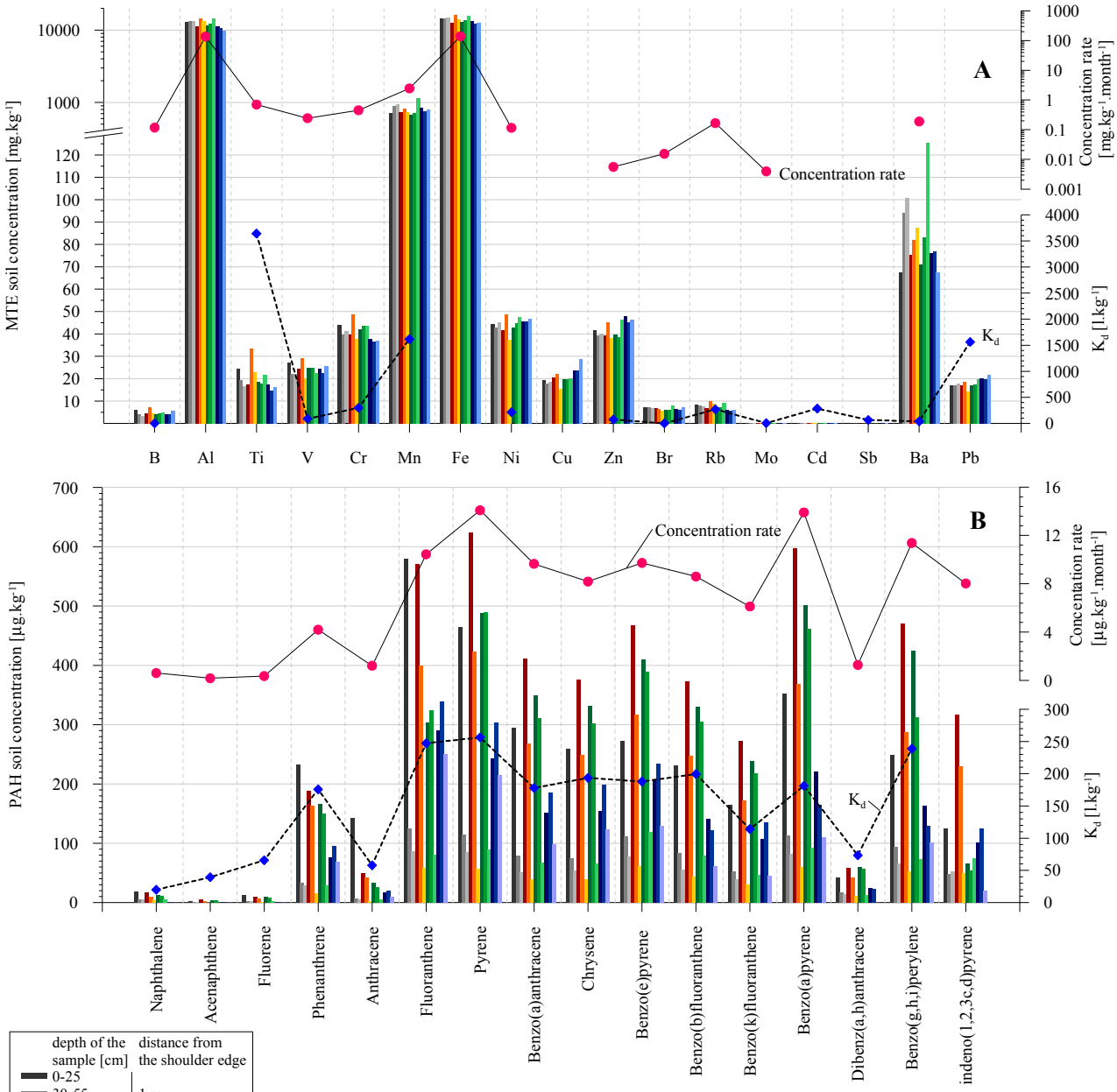

*Figure 4.27: MTE and PAH concentrations in soils. **A**) MTE concentrations during the 2004 (blue) and 2006 sampling campaigns. K_d are also mentioned. Values are very high for Fe and Al (10 mg·kg^{-1}). Overall, a single element shows similar concentrations whichever sample is considered. This allows considering the ∑MTE only and not the species (figure 4.28B). Only Ba has significant change along the profile. It is far more concentrated at the bottom, indicating a possible contamination by the Grave I. K_d distribution coefficient is more or less correlated with the concentrations found in soils. The moderate correlation is presumably due to soil leaching. For example, Fe, Al, and Ba are also geogenic and might be released by soil leaching. Ti, as previously postulated, should have a higher mobility. There is no significant difference between 2004 and 2006. The concentration rate is < 1 mg·kg^{-1}·month^{-1} for every elements but Al, Fe, and Mn. **B**) PAH concentrations and K_d. This time, the correlation between the concentration and distribution coefficient is nearly perfect. Mobile species have very low concentrations in soils, whereas PAH with low mobility present high concentrations. Generally, the surface samples (2006) have concentration much higher than bottom samples (2 to 5 times), whereas the difference between surface and bottom sample in 2004 was smaller. This clearly indicates a PAH contamination coming from the soil surface. Concentrations in the bottom sample (60-80 cm) show a smaller evolution, thus depicting a smaller influence. PAH are deposited on the surface. Highest concentrations are met near the road for light PAH (naphthalene to fluoranthene), and in the middle of the slope for heavier PAH (pyrene to indeno(1,2,3c,d)pyrene). However, because the light PAH concentrations are very low, only the ∑PAH is considered in figure 4.28C. Deposition rates are around 1µg·month^{-1} for mobile PAH and increasing up to 14 µg·kg^{-1}·month^{-1} for heavier PAH.*

4.6 AQUIFER CONTENT

After the artificial test n°2 and different natural precipitations, the aquifer has been sampled up- and downstream. See §4.1.1 for sampling methods. Differences between contaminant concentrations measured up- and downstream allow monitoring the impact of the road runoff on the aquifer. Remember that the road is entirely dipping eastward (walking path included), which is also the downstream side of the aquifer (§3.6.3). Contaminant already present in the aquifer upstream can therefore not be caused by the road runoff. However, for some types of contaminant (PAH for example), the aerial deposition might have a significant influence as well up- as downstream, depending on the wind conditions. The Arnon River quality is also of great importance. Indeed, the river infiltrates the aquifer and thus influences its quality. The Arnon River has also been sampled. The SB – LB compartment was not watered during the artificial test n°2 due to the lack of rainwater. Indeed, the test n°1 showed that the amount of water to be used was too significant.

4.6.1 AQUIFER QUALITY AFTER THE HYDRAULIC TEST N°1

As mentioned in §3.6.4, the aquifer was sampled after the artificial hydraulic test n°1. Remember that the water used for the road watering was pumped in the Arnon River (6 m^3). The river water was also sampled. Like during the Cl^- tracer test, the MTE concentration in the aquifer remained constant (figure 4.29A). No variation can be attributed to the road runoff specifically. The aquifer MTE concentration is similar up- and downstream. All small variations can easily be explained by the elements behaviours or the aquifer dynamic. Indeed, mobile elements show a small concentration increase from the river to the aquifer. Elements with low mobility, to the contrary, are rather depleted. Particles are slowed and retained as soon as the river water infiltrates the aquifer, upstream from the experimental site. Br and Ba have much higher concentration than other MTE in the aquifer (note the axis break). They can however come from geogenic origin; they are also widely found in the river. Note that Al, V, Cr, and Rb have also high concentrations in the river; they are however depleted in the aquifer because they certainly were carried sorbed to particles. Al, Zn, Cu, Ni, and Rb are more concentrated upstream than downstream (difference are negligible, though). Cr concentration is remarkably high and constant in the river water (~3µg·l^{-1}). The upstream piezometer S02_3 is less active (smaller fluxes) than the downstream piezometer S02_4 (§3.6). Pb, Cd and Ti were generally inexistent in the aquifer. Therefore, the hydraulic test n°1 did not emphasize the aquifer contamination by the road runoff.

4.6.2 AQUIFER QUALITY AFTER NATURAL EVENTS

The aquifer was also sampled in different rainfall and water height conditions. Samples were always taken at an estimated time, extrapolated from the LW lag time (LW lag time + ~1 hour). Presumably, the impact on the aquifer should have been higher when the aquifer showed its lowest level. However, this situation also implied that the soils were very dry. The rainwater maybe did not reach the aquifer but moisturized the soils and reconstituted the stock. The difference between high and low water level was never enlightened. Overall, the aquifer contaminant content was always corroborated with the river content. The content was also often (if not always) higher upstream than downstream. This could be explained by the use of the field overlaying the upstream compartment which is a crop field. Tractors and agricultural machines often turned over the soil surface, evidently favouring the infiltration and particles percolation.

Results concerning different events are presented in figure 4.29B. No significant difference is observable. On the contrary, whatever the precipitation, the water table height, or the Arnon Flow rate is, the aquifer MTE concentration remained remarkably stable. The Arnon concentration was not surprisingly higher during the peak flow and smaller during minimal flow. The repercussion on the aquifer water concentration is negligible. PAH results are presented in appendix X. The PAH concentration in the aquifer is fairly low (1 ng·l^{-1}, mobile PAH). Heavier PAH were not all detected. As described in the previous §4.5.3.1 and §4.5.4, PAH are also aerially deposited. However, the maximum distance is unknown. PAH are thus possibly from road origin (which road is the main issue) or from river origin. C_X

are also present. The triplet C_{16}-C_{18}-C_{20} is found in low concentration (maximum 0.3 $\mu g \cdot l^{-1}$, C_{18}), whereas other aliphatic hydrocarbons were not detected. BTEX were never detected. PCB28 and PCB52 species only have been detected in the aquifer (near the detection limit, 0.5 $ng \cdot l^{-1}$). The mobility of those contaminants is the key property leading the contaminant behaviour in the aquifer. Indeed, their global behaviour is the same as in the unsaturated zone. Mobile compounds showed concentration similar or even higher than the river concentration, while compounds with low mobility are depleted.

Overall, the aquifer contaminant concentrations are similarly distributed up- and downstream. Therefore, the influence of the road runoff could not be enlightened. The aquifer contamination provenance could be the river, the aerial deposition or the aquifer porous media leaching. However, whichever the provenance is, the concentrations are very low. They are mostly below the values of the Swiss regulation for drinkable water (MSDA), always below the limit values given by the Ordinance on contaminated sites.

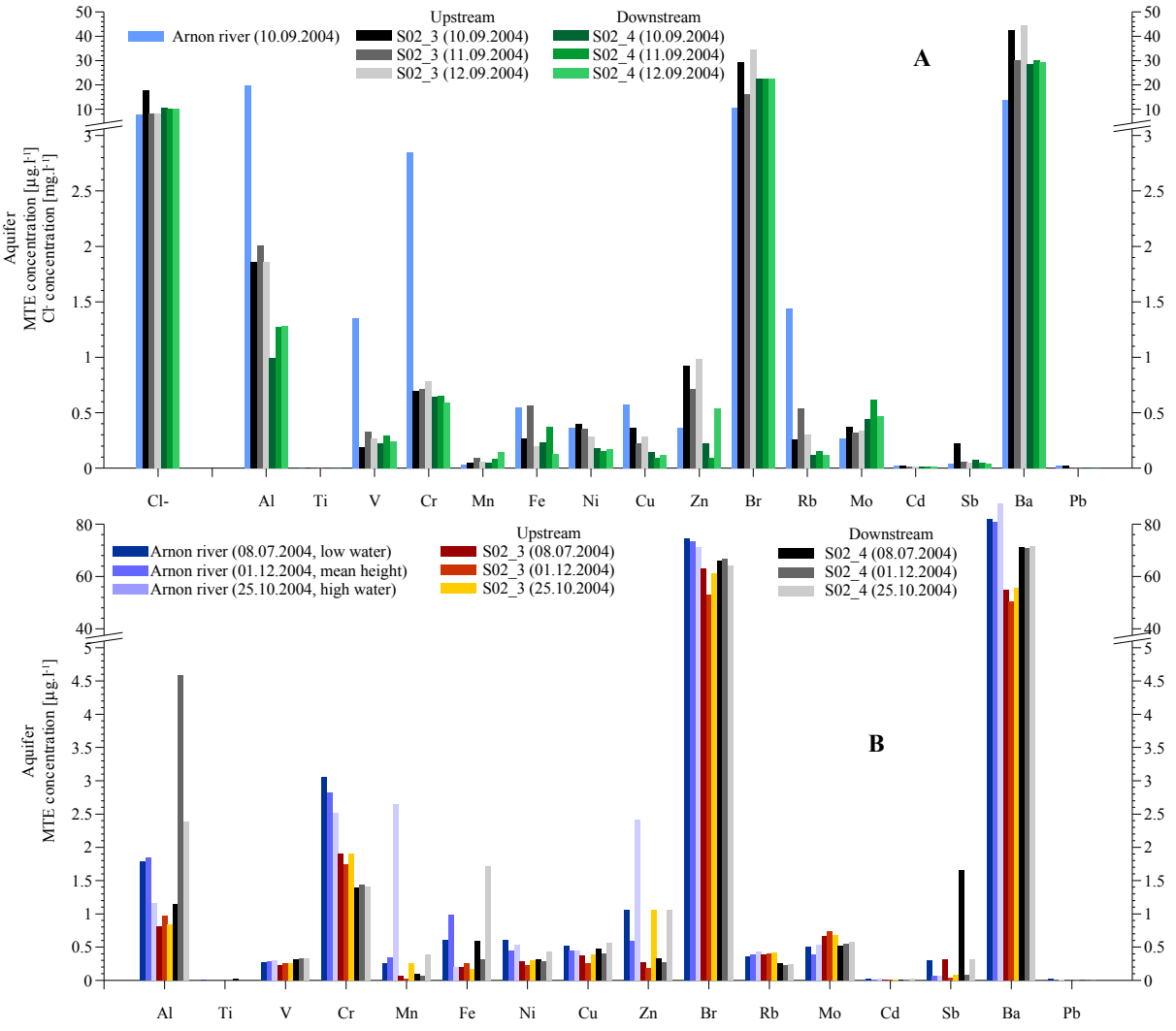

*Figure 4.29: MTE concentration in the aquifer up- and downstream of the road. **A)** Artificial hydraulic test n°1. The MTE concentration was not influenced by the road runoff. The variations observed are due to the elements behaviours themselves. Some elements have higher concentrations in the river (Al, V, Cr, Rb) and some have higher concentrations in the aquifer (Zn, Br, Ba). The fractionation is function of the element mobility. Some elements have higher concentration upstream than downstream (Al, Zn), whereas the reverse is inexistent. Note that Cl-, Br, and Ba have much higher concentration (axis break). **B)** MTE concentrations in the aquifer in three different conditions: low water (8.7.04), average water height (1.12.04) and high water (25.10.04). Despite few differences, the aquifer MTE content is fairly stable in every condition. No significant difference occurred: the MTE concentration in the aquifer is pretty stable whatever the event or the water table height is. Note the axis break.*

4.7 SUMMARY

In this chapter has been presented the results concerning the geochemical behaviour of the road runoff, unsaturated zone, and saturated zone. In a lesser way, the geochemical behaviour of shoulders has also been shown. The results provided concerned six families of contaminant: MTE, PAH, C_X, BTEX, MTBE, and PCB. MTE and PAH are two major families that have also been studied from a chemical point of view. Batch and column tests allowed calculating their sorption distribution in the Grandson soils. Comparisons were made with other typical Swiss soils. To especially emphasize the geochemical behaviour, an artificial precipitation test was created to control every aspect of the rainfall. It indeed allowed sampling and measuring physicochemical parameters in every sampling point, from the falling point to the lysimeter bottom. The water used was rainwater collected at the EPFL. Main results are summarized below.

4.7.1 BATCH AND COLUMN TESTS

- Batch tests performed with Grandson soils gave the MTE mobility (distribution coefficient K_d). Mobile elements are B, Br, Mo, Ba, Sb, Zn, and V ($0 < K_d < 90$). Less mobile elements are Ni, Cd, Cr, and Rb ($200 < K_d < 300$). Elements with very low mobility are Pb, Mn, and Ti ($1500 < K_d < 3500$). Ti was however depicted as mobile in the dynamic experimentation (test n°2, $K_d < 100$). Cu, Fe, and Al K_d were not calculated; they had however low mobility in dynamic tests.
- PAH mobility was high for the light PAH (Naphthalene, Acenaphtene, Fluorene, Anthracene; $K_d < 75$). Phenanthrene mobility was calculated as average but its behaviour during dynamic test was lower (it is indeed a light PAH). Heavy PAH had lower mobility ($K_d > 175$).
- Comparisons with other typical soils enlightened the predominant influence of the pH. Batch test performed with acidic soils (pH = 5.5) produced lower K_d. MTE are more mobile in acidic soils. Other physicochemical parameters have a smaller influence.
- The column test performed with a synthetically loaded solution (MTE and PAH) infiltrating the Grandson soils provided good results. MTE are more mobile in dynamic conditions. This is easily explained by the reduced contact time between the contaminant and the soil aggregates. PAH were not detected at the column outlet, thus showing a very good retention in the column soil.
- Soil layers analyses demonstrated that PAH were mostly retained in the surface layers. Also, MTE with low mobility show the same behaviour. Mobile elements showed no preferential retention layer.

4.7.2 ROAD RUNOFF

- Comparison between the particular and solute form confirmed that mobile elements are measured in similar concentrations whether the sample was filtered at 0.45 µm, at 1 µm, or not filtered at all prior to acidification. On the contrary, less mobile elements are easily sorbed to particles. The MTE concentration of the sorbed form range from 5% (Rb, Sb) to 98% (Pb) of the total concentration.
- The artificial test performed with rainwater as well as natural events confirmed the direct relationship between the hyetogram and road runoff flow. Any reactivation of the rain induces a road runoff flow peak.
- The EC has a first peak coinciding with the road runoff first flush. Any reactivation of the rainfall also induced a second EC peak. However, EC, which describes the total dissolved solid TDS, does not show a strong first flush effect. The global TDS pollutogram is neutral. Dissolved solids are continuously leached from the road, thus carried as function of the flow.
- The turbidity, on the contrary, is clearly correlated with the road runoff reactivation. Turbidity peaks are always present when the road runoff flow increases. It shows a strong first flush behaviour due to the mobilization of the particles lying on the road.
- TOC also shows a strong peak in the first collected water. It emphasized the strong first flush effect.

- To simplify, MTE and PAH contaminants have two different behaviours: mobile elements move mainly in solute and have concentration correlated with EC. They have neutral pollutograms. Elements with low mobility have higher concentrations correlated with the turbidity peaks. They are transported sorbed to particles. They have strong first flush effects.
- B, V, Cr, Mn, Ni, CU, Zn, Br, Mo, Cd, Sb, and Pb were identified as road tracers. Fe and Al represent 80% of the road runoff.
- C_X are well represented in the road runoff. However, only heavy species are commonly found. C_{32} is the most common specie. They all have neutral pollutograms showing a strong relation between the road runoff flow and concentrations.
- PCB are well correlated with the LW exfiltration water flow. They all have neutral pollutograms. All species are present.
- Overall, the road runoff is biphasic: the first wave mobilizes all particles deposited on the road. Small particles remain in the flow while larger ones might redeposit further away. All particles might be remobilized by a later road runoff flow reactivation. The solute part is continuously transported as long as there is some contaminant on the road. This is why the global concentration decreases along the time.

4.7.3 SHOULDERS

- SGH, which was specifically designed to retain pollutant (especially organic compounds) do not fulfil its role. The PAH concentration, for example, is similar to the one found out of SGL. Moreover, its humic acid content prevents the MTE retention.
- SGC, despite its high clay content that could supposedly help retaining MTE, also do not show a convincing behaviour. It especially let organic compounds through.
- SGL has globally the best retention potential. However, it strangely let the greatest BTEX concentration of all shoulders.
- SH seems to produce more than retain organic compounds. This is due to its very material composition. The contaminant pollutograms are similar to those from the road runoff. This demonstrates a direct circulation from the road to the shoulder bottom. Other shoulders have more buffered pollutograms.
- Interceptions of the shoulder runoff allowed demonstrating the road runoff first flush behaviour on the shoulder. The road runoff already fractionates on the shoulder surface. Indeed, the proportionality of one MTE concentration (regarding the total MTE concentration) was more similar to the shoulder exfiltration water than to the road runoff proportional concentrations.
- EC measurements of the shoulder runoff are highly representative of the road runoff first flush. If the conductivity is high, it depicts that the first flush is passing over the shoulder (SGC); if EC is low, the first flush has infiltrated the shoulder (SGH).

4.7.4 INFILTRATION SLOPES (INFILTRATION TEST N°2)

- The artificial precipitation test n°2 was representative of a thunderstorm. The LW exfiltration flow was also representative, very similar to natural events.
- EC measurements illustrated two different types of water. The stock S was pushed downward (piston effect) and preceded the infiltration water. The stock EC was lower. This illustrates the difference of element mobility as function of the contact time, already described by batch and column tests: the longer the contact time, the lower the mobility.
- The turbidity showed two peaks. The first one coincided with the stock water. Particles come from either the soil (around the pipe holes), either from the pipe itself (previous deposition). Particles deposited in the pipe

would have anyway reached the lysimeter bottom, collecting pipe or not. The second peak is caused by the infiltration particle. Those particles must however be smaller to percolate through one meter of soil.

- The pH was completely buffered by the soil high carbonate content. It thus shifted from 6.5 in the rainwater to 8 in the LW exfiltration water.
- Overall, the total MTE concentration in the LW first water collected decreased to $1/30^{th}$ of the road runoff first flush concentration. The LW concentration is mainly constituted by Al and Fe (75%). Mobile MTE are proportionally more concentrated than in the road runoff; this enlightens the soil retention for elements with low mobility. The MTE total mass decreased from 280 mg in the road runoff to 2.6 mg in the LW exfiltration water (1.6 mg of Al and Fe).
- The PAH total concentration in the LW first collected water was about 1'000 times lower than in the road runoff first flush. The PAH concentration was mainly constituted by mobile PAH naphthalene and phenanthrene. Heavy PAH were easily retained in the soil. The PAH total mass decreased from 0.144 mg in the road runoff to 0.002 mg in the LW exfiltration water (0.0015 mg of naphthalene and phenanthrene).
- The triplet C_{16}-C_{18}-C_{20} is always shows high concentration in the LW exfiltration water. This triplet is a great road tracer. It indeed is always present in the road runoff and exfiltration water. Their total mass was even greater than the total mass recorded in the roar runoff.
- PCB have very low concentrations in the LW first collected water. The total concentration for all 209 PCB is 5 $ng \cdot l^{-1}$. They are presumably very mobile, showing neutral pollutograms.
- BTEX were not detected in the LW exfiltration water.
- The comparison between the artificial test n°2 and a very similar natural event allowed estimating the aerial deposition. Indeed, the test n°2 concerned only the road surface, whereas the natural event also implicated the lysimeter surface. Results demonstrated no significant difference concerning MTE, while PAH are aerially transported (20 to 90%). This is an estimation.
- Studying the soil after two years of road service allowed calculating the concentration rate for MTE and PAH. MTE soil concentration did not change much. The concentration rate range from 0.005 (mobile elements) to 200 $mg \cdot kg^{-1} \cdot month^{-1}$ (Al, Fe). The PAH concentration rate is lower due to the emission rate: it ranges from 1 (mobile PAH) to 14 $\mu g \cdot kg^{-1} \cdot month^{-1}$ (PAH with low mobility).
- The soil extraction also allowed identifying the presence of preferential water paths (MTE deposition) along the A – B horizon boundary, while PAH were mostly deposited on the surface.

4.7.5 THE AQUIFER

- All families of contaminant are presented in the aquifer. However, the provenance of those contaminants remains uncertain. The aquifer was indeed as concentrated upstream as downstream. Moreover, the river concentrations had similar values. The contamination provenance is thus either the aerial deposition (equally distributed up- and downstream), either the Arnon River infiltrating the aquifer.
- Contaminants were often seen in higher concentration upstream. This is due to the crop field overlaying the aquifer there.
- The contaminant behaviours in the aquifer could be described. It confirmed the contaminant mobility previously noted during the batch, column and test n°2 experiments. Mobile substances are seen in higher concentrations, whereas substances with low mobility are sparsely found.

CHAPTER 5

GEOTECHNICAL BEHAVIOUR

5.1 CONCEPT AND METHODS

5.1.1 INTRODUCTION

The new concept, i.e. diffuse infiltration of the road runoff over the shoulder, needs verification from a geotechnical point of view. The water that infiltrates through shoulders or infiltration slopes might indeed move to the road foundation or embankment and reduce the bearing capacity of the foundation. From a practical point of view, the water lowers the internal friction angle φ and the apparent elastic modulus E; the bearing capacity is diminished and the initial pavement design appeared insufficient[1]. The road structure deformation initiates and develops a fast increasing degradation. The LAVOC (Traffic facilities laboratory, EPFL) has thus been mandated by the GEOLEP to monitor the mechanical behaviour of the Grandson experimental site road structure. FWD measurements were executed by Infralab SA; *in situ* measurements and calculations by Dr. Ould-Henia (LAVOC), with the collaboration of MM. Bueche and Hefti. Levelling campaigns were performed by the cantonal geometrician. Interpretations were made conjointly by the LAVOC and GEOLEP.

The goals of this monitoring were to:

- Verify the bearing capacity of all six compartments (figure 5.1) which are subject to shoulder infiltration.
- Compare the behaviours of the five compartments which shoulders have geomembranes with the reference compartment behaviour, i.e. the behaviour of the compartment where the shoulder has no geomembrane collecting the infiltrating water (SGL REF, 20 m, km 430-450, figure 5.1, in light blue). The road runoff may indeed infiltrate the road foundation in that compartment, whereas it cannot do so in other compartments. This appellation SGL REF is uniquely used in the present chapter 5 because this compartment is the reference one for geotechnical considerations only.

5.1.2 ROAD MONITORING

For reminder, the probes locations and monitoring campaigns are presented in the following boxed text. Calculation methods and probes installation are presented in appendix XI.

The road has been equipped with various instruments whose positions are shown in figure 5.1. Six PT100 temperature probes have been positioned during the construction along the km 435 profile at 6, 12 and 26 cm depths, right and left of the northbound traffic lane (Grandson direction). They are at the basis of the AB11s, HMT22s and HMF respectively. Those are used for the FWD data exploitation and freezing – thaw cycles monitoring.

Three deflectometers have been placed in the SGL (20 m), SH and SB road profiles. Temperature and deflection gauges are linked to a datalogger sited in the km475 collecting chamber. Acquiring time step for these instruments is 30 minutes.

Six points have been selected for the Falling Weight Deflectometry (FWD) campaigns. All emplacements are 1m away from the shoulder. The campaigns have been conducted in November 2004, April and September 2005. Those campaigns occurred during well different hydraulic conditions. In September 2005, the road bearing capacity was monitored after the artificial road watering test n°3 (§3.1.1.2).

[1] The lower the elastic modulus E, the sooner deteriorations may appear in the road structure.

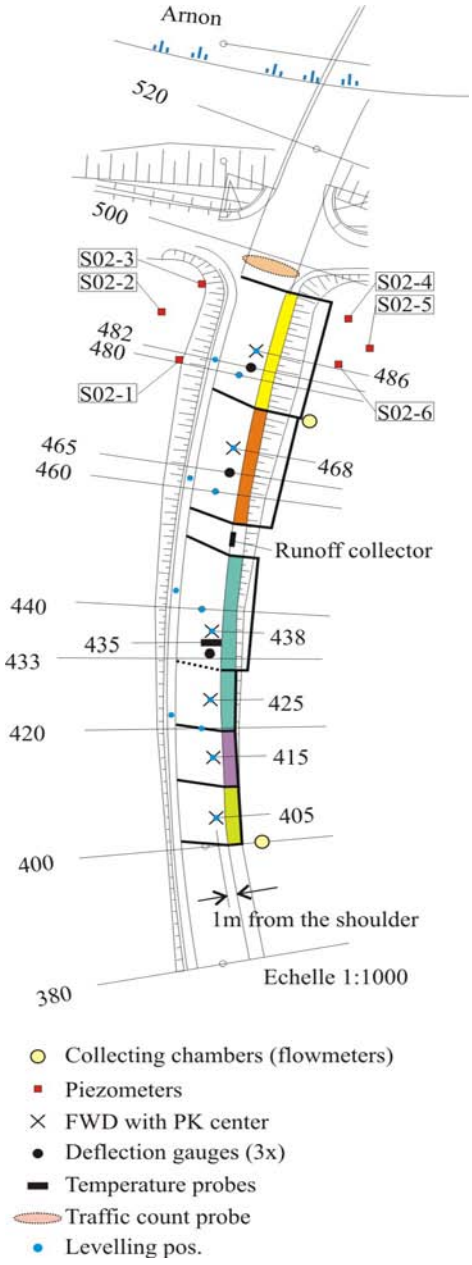

Levelling campaigns have been synchronously conducted with the FWD campaigns. Fourteen control points are positioned on the western walking path, on the road axis, and on the FWD control points (1 m from the shoulders). Two points (not shown on the figure 5.1) are reference points (km 69 and 201).

Road traffic rates are recorded in both south- and northbound directions. Inductive reels have been buried in the road pavement just south of the bridge over the Arnon River. A datalogger records the traffic rate [vehicles·hour^{-1}].

Figure 5.1: Road instrumentation localisation. Shoulders colours correspond to the figure 2.2. Piezometers positions and nomenclature, reference distances and compartment delimitations are also shown.

5.2 RESULTS

5.2.1 FWD CAMPAIGNS

5.2.1.1 Principle

The FWD measurement is based on the following principle: a mass (m = 50 to 300 kg) is liberated from a height varying from 2 to 40 cm. The resulting force is ranging from 7 to 105 kN (equ. XI.1, appendix XI). The mass falls on a rubber plate that distributes the resulting force. The plate spring constant is designed to assure a 28 ms (34 Hz) impulsion. This is equivalent to the passage of a heavy truck at 70 km/h. Deflexion are measured with 9 geophones (from D1 to D9), located from 0 to 1800 mm from the falling mass. The farther from the mass, the deeper is the inquisitive depth. All geophones thus measure the deflexion basin (illustration of the deflexion basin is presented in appendix XI). The geophone D1 (under the falling mass) thus measures the contribution of the road superstructure, embankment and soil; whereas D9 (1800 mm from the impact point) is mainly influenced by the underlying soil. The FWD apparatus used was a Dynatest 8000.

The constraint, deformation and displacement states are calculated using the Boussinesq equations (equ. XI.2, appendix XI). This implies that the road structure is considered homogenous, elastic and isotropic. To model multiple layers, the Odemark (equ. XI.3, appendix XI) method is used: the structure is divided in multiple different layers still concurring with the Boussinesq postulate (homogenous, elastic, isotropic).

The measured deflexion basin is modelled with a regression curve created by varying the elastic modulus E of the material constituting the different layers (asphalt, foundation, embankment, soil). In this project, all three constitutive bituminous layers (AB, HMT, HMF) are considered as one 26 cm thick layer. Embankment and foundation are made of the same material and are therefore also considered as on unit. Its thickness varies along the road longitudinal profile, though. The last unit is the soil; it has an infinite thickness. In the first FWD assessment, the soil and embankment + foundation were grouped in one unit. The recorded deflection amplitude is modelled using the simplified Boussinesq equation (XI.4, appendix XI). The equation is function of the geophone distance from the falling weight; it thus gives a curve which is horizontally asymptotic the farther from the mass. E moduli are function of the temperature; results are thus normalized to 15°C.

5.2.1.2 Measurements

Three campaigns have been performed. The first one during pretty dry conditions (18.11.2004), the second in wet conditions (05.04.2005) and the third in very wet conditions (test n°3, 07.11.2005). Points of measurements are shown in figure 5.1. The temperature is measured at the surface (infrared sensor) and in small drill holes (by the FWD operator). Temperatures measured by PT100 are also used (extrapolation along the road profile for all FWD testing points). The repeatability of the measurements was verified for D1 and D9. The variance was maximum 6.4% for D1 and maximum 9.1% for D9. The repeatability is considered as good.

5.2.1.3 Elastic modulus – regression fit for a bi-layer model

This bi-layer model considered only the 26 cm thick asphalt layer and the soil + embankment + foundation unit. Figure 5.2A shows the soil E modulus recorded during the three campaigns. The variability between campaigns is very small. The elastic modulus is increasing along the embankment thickness. For the AB + HMT + HMF elastic modulus calculation, a layer with E = 30'000 MPa has been introduced at 6m depth to avoid non linear irregularities. The calculated elastic modulus is the mean E; it considers the AB, HMT, and HMF E modulus. It is corrected to 15°C (LAVOC, equ. XI.5, appendix XI). Results are concurring with the kind of bituminous material usually used for road construction (figure 5.2B). Fluctuations between campaigns are acceptable; they are due to the thermal gradient, and to the regression fit itself which postulated a linear behaviour (which is only an approximation). Also, local differences in the material structure might cause small discrepancies. Overall, variations are negligible.

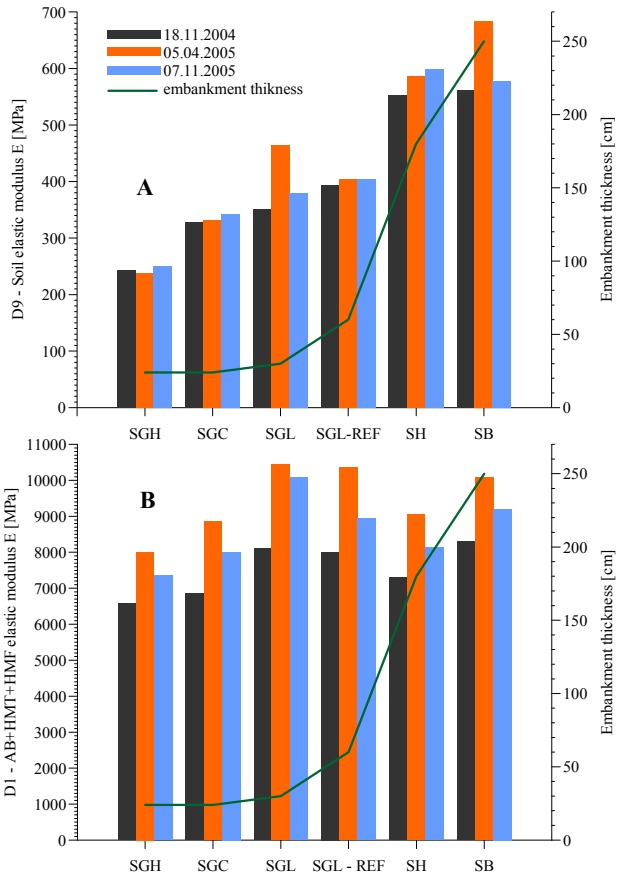

Figure 5.2: Elastic modulus E. **A**) Soil elastic modulus. E is function of the embankment thickness. The reference compartment (SGL REF), which is the only one there the road runoff could fully infiltrate the shoulder, presents no difference between the three campaigns whatsoever. **B**) AB + HMT + HMF elastic modulus E. Values are concurring with those of a typical bituminous material (Swiss norm B70/100) with conventional penetration binder. E moduli are comprised between 7'000 and 10'000MPa. The E variations between campaigns presented by the reference shoulder SGL REF is also shown by all other shoulders.

5.2.1.4 Regression fit taking the embankment thickening into account

The regression fit is based on a three - layers model. The first layer is the 26 cm AB + HMT + HMF layer, the second is the embankment layer with a variable thickness, and the third is the infinitely thick soil layer. This model also has a rigid layer with E = 30'000 Mpa at six metres depth. Results are shown in table 5.1. They are not significantly different from the §5.2.1.3. The embankment thickness still plays a significant role.

	18.11.2004	E modulus [MPa]		05.04.2005	E modulus [MPa]		07.11.2005	E modulus [MPa]	
	AB+HMT+HMF	Embankment	Soil	AB+HMT+HMF	Embankment	Soil	AB+HMT+HMF	Embankment	Soil
SGH	12869	821	171	13998	941	169	11669	1225	176
SGC	14385	663	242	15018	1040	242	12786	1115	247
SGL	14438	712	256	16459	885	259	11996	1277	269
SGL - REF	13035	527	300	15234	595	303	12407	660	288
SH	11376	463	630	12704	559	528	10846	585	513
SB	12147	507	649	14109	544	560	12507	546	576

Table 5.1: Elastic modulus E; calculated for the three different layers. This calculation takes the real embankment thickness into account. However, results are very similar to those proposed by the bi-layer model. Embankment E modulus increased along the time and not as function of the hydrometeorological conditions, whilst E modulus from AB + HMT + HMF and soils are greater during the dry event (5.4.05).Those variations are however negligible.

5.2.1.5 ELMOD Software

A classical exploitation of the data was provided by Infralab SA, using the ELMOD software. This software allowed making the same regression fit: the software considered the two same layers as in §5.2.1.3. Results are similar in every point. No difference is emphasized. The software also gives an estimation of the residual road lifetime. It is calculated in equivalent standard axles load [-]. The calculated road residual lifetime is ranging from $5 \cdot 10^8$ (SGH) to $3 \cdot 10^9$ residual axles load (SB). This is considered as very high (> 50 years).

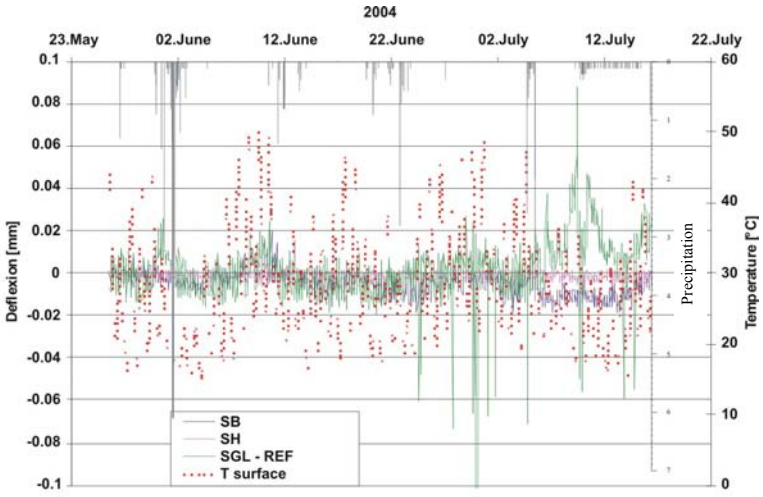

Figure 5.3: Deflection measurements in SGL – REF, SH and SB compartments. The greatest deflection is shown by SGL – REF, while SH and SB are very stable. Note that the absolute values are very small. Measurements for SH and SB are practically at the detection limit. The correlation between deflection and rainfall is not straightforward: large precipitations do not systematically induced deflection, whereas some deflection has been measured when no rain occurred.

5.2.2 DEFLECTION MEASUREMENTS

Deflection was recorded for the SGL (REF), SH and SB compartment. Records cover only 3 months (starting June 2004) because probes failed. The maximal deflexion recorded was in SGL REF (0.09 mm, figure 5.3). SH and SB showed practically no vertical movements. However, the deflection absolute values were very small. For comparison, a significant subsidence would be a few mm, while the passage of a heavy truck would cause a 0.1-0.2 mm deflection. Results presented in figure 5.3 are therefore to consider with precautions. Moreover, the relation between the rain and deflection is still to discover: no effective correlation existed between the precipitation events and the deflection measured in SGL – REF.

5.2.3 LEVELLING CAMPAIGNS

Levelling campaigns were systematically performed a few days after the FWD campaigns. See figure 5.1 for levelling location. They are located on the western lane, on the road axis, and on the eastern lane (FWD locations; 1 m from the shoulder). Table 5.2 presents the measured results. Elevation differences are calculated for the 2 last campaigns by comparison with the first one. The levelling measurements on the various points revealed the following results (the measurement precision is ± 1 mm):

- All points located on the western lane showed no subsidence at all
- All points located on the eastern lane, i.e. on the shoulder side, had subsidence between 2 and 4 mm.
- All points in between, i.e. on the road axis, showed intermediary subsidence (1-2 mm).

The small subsidence observed on the shoulder side was not increasing: it happened between the first and second campaign. Between the second and third campaign, some points showed lower subsidence value. For example, SB compartment evolved from -4 to -2 mm. This indicates that the initial subsidence measurement was not permanent. The difference between the western and eastern lanes is certainly due to the traffic distribution: as mentioned in §2.6.3, the traffic charge toward Champagnes, i.e. on the eastern lane, represents 85% of the total traffic recorded on the road segment. The traffic on the other western lane was only 15%. This was due to important work performed in Champagne that dissuaded the traffic toward Grandson.

Location	Shoulders	24.09.2004	12.11.2004	03.05.2005		09.11.2005	
		Elevation [m]		Elevation [m]	Δ elev.	Elevation [m]	Δ elev.
Reference							
69		447.957		447.957	+0	447.957	+0
201		448.143		448.143	+0	448.142	-1
Western lane							
422		449.167		449.167	+0	449.167	+0
442		449.382		449.381	-1	449.382	+0
462		449.607		449.607	+0	449.607	+0
482		449.793		449.793	+0	449.793	+0
Road axis							
420		448.861		448.861	+0	448.861	+0
440		449.080		449.079	-1	449.080	+0
460		449.296		449.295	-1	449.296	+0
480		449.485		449.483	-2	449.484	-1
Eastern lane							
405	**SGH**		448.576	448.574	-2	448.574	-2
415	**SGC**		448.686	448.685	-1	448.684	-2
425	**SGL**		448.795	448.793	-2	448.792	-3
438	**SGL REF**		448.930	448.928	-2	448.928	-2
468	**SH**		449.252	449.250	-2	449.251	-1
486	**SB**		449.395	449.391	-4	449.393	-2

Table 5.2: levelling campaigns results. No subsidence was noted on the western side, while the eastern side showed a ~2 mm subsidence. Points on the road axis have subsidence in-between. Differences between compartments are negligible: they all have subsidence similar to the reference compartment SGL REF (-2 mm).

Figure 5.4: Elevation variation on the shoulder (eastern) side of the road. Those are measured during the second and third levelling campaigns, regarding the first campaign measurements as reference. Compartment SGL REF showed a -2 mm settlement between the first and second campaign; and a 0 mm settlement between the second and third campaign. All other compartments showed the same behaviour (still on the shoulder side): the subsidence between the 1st and 2nd campaigns is significant, while the subsidence between the 2nd and 3rd campaigns is negligible. Thus, the subsidence stabilized after the initial settlement. Overall, the resulting total subsidence is very small.

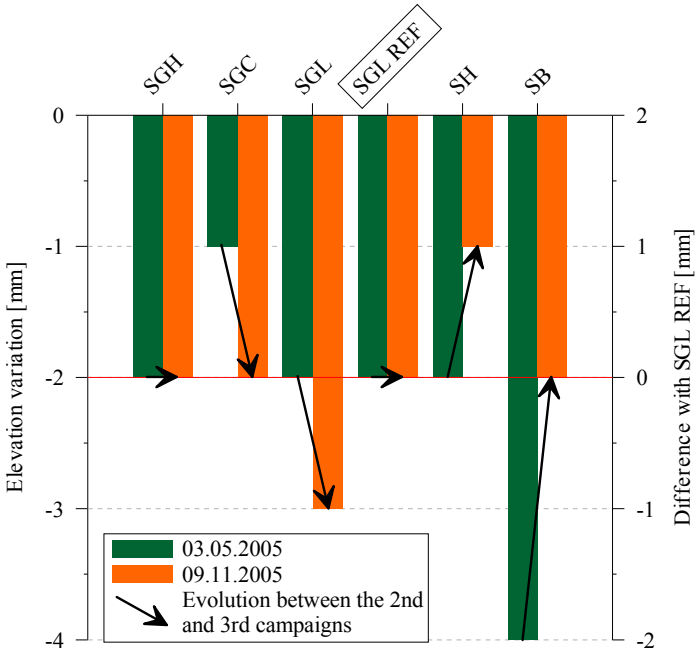

Figure 5.4 shows the evolution of the elevation. All shoulders have final subsidence (orange) similar to the SGL REF subsidence. They also have an intermediary subsidence (green) similar to

the final one (remember that the error is ± 1 mm). The greatest permanent settlement thus occurred between the first and second campaigns. This means that the subsidence was more or less stabilized between the second and third campaigns. The significant subsidence between the two first campaigns, showed by SB was reversible: it was not a permanent change. The particular case of the shoulder SGL – REF, which has no basal geomembrane and thus should have received the greatest part of water in its foundation, presented no evolution of the elevation between the second and third campaign (which was the massive infiltration test n°3). Overall, all shoulders show negligible settlements.

5.3 SYNTHESIS

The road structure particularities have to be taken into account when interpreting the results. Those properties clearly influence the road behaviour:

- the embankment is made of a very good quality gravel; it has geotechnical properties similar to the foundation grave I
- the road pavement is largely dimensioned: it is 26 cm thick[2] (HMF + HMT + AB22) whilst the requirements for such a road are only 17 cm

FWD tests enlightened the effect of the embankment thickness on the road structure elastic modulus E. The measurements repeatability was good. The apparent soil E value is higher for SH and SB, mainly because of the embankment thickness and compression. Compartments SH and SB have similar soil E modulus. Regarding the embankment thickness, SH is even more stable. Its basis is however larger and far more rigid than SB; this particular behaviour thus cannot be attributed to a good tightening of the shoulder. Anyway, the soil moduli are good for all shoulders. No specific variation was noted between the three campaigns. The bituminous layer E moduli are also good. The short period of observation, however, did not allow enlightening significant E changes that may further lead to the road degradation. Also, the traffic is particularly light (~2000 vehicles per day).

Deflection measurements enlightened the more severe variations in the shoulder having no tightening (SGL REF). This shoulder indeed showed the greatest deflection variation, while SH and SB presented practically no deflection. The absolute deflection values, however, were very low. Again, this is caused by the road particular dimensioning.

Levelling campaigns revealed that the subsidence was low on the shoulder side (~2 mm). Measurements on the opposite side showed no settlement at all (0 mm). This subsidence difference between the walking path and shoulder sides is clearly related to the traffic charge partition: the shoulder side, which settled a bit, welcomed 85% of the total traffic charge, whereas the other side, which did not settle at all, was only receiving 15% of the total traffic charge. The major settlement occurred between the first and second campaign. It did not significantly evolve after that. No specific difference was noted between the SGL REF and other shoulders. Beside the settlement induced by the traffic charge, no indication of further settlement was noted.

Overall, the bearing capacity of the road is very good. The road lifetime was evaluated to more than 20 years ($1 \cdot 10^9$ residual standard axle load). As conclusion, the Grandson experimental site could not conclusively demonstrate a worsening of the geotechnical behaviour of the SGL – REF compartment. This is due to the particularly good material and road pavement thickness used for this road. Infiltrating flux in the SGL – REF are high enough and would have doubtless caused a loss of bearing capacity in case the road would have been more modestly dimensioned; degradation would have occurred rapidly. It is therefore clear that the infiltration through the shoulder must be cut down to a minimum, for geotechnical reasons but environmental reasons as well. The shoulder must be tightened.

[2] Using the Swiss norm SN 640 394a and considering the light traffic (inferior limit of the T3 class) and the good material used (bearing capacity: S2 class), the structure thickness should be 17 cm. The road is thus largely dimensioned.

CHAPTER 6

SYNTHESIS

6.1 CONCEPT

The promotion of a new management concept concerning the road runoff was proposed by the Swiss federal office for the environment (directive 2002, OFEV). This new concept is based on diffuse infiltration over the shoulder. Infiltration slopes bordering the road play the role of filters retaining the road contaminants. This new concept has three main goals:

- To preserve the environment. Presently, road runoffs are collected in sewers and treating installations (particle and oil separators). The collected water, which is still polluted, is then simply and directly directed in the surface water (rivers and lakes). The new concept is based on substance retention in the soil; only clean water is released in the environment.
- To restore the natural water cycle. The rainwater should infiltrate soils as close as possible to the place where it has fallen onto. In Switzerland, roughly 1 km^2 per year of permeable soil is lost due to new constructions. This is thus a major issue.
- To reduce costs and land use. The particles and oil separators are expensive and invasive; they must be maintained and cleaned periodically, which add to the global cost.

While very promising, this new concept needed strong scientific justifications. Moreover, those justifications must clearly show that the concept is implementable, usable on a large scale, and really improve the road runoff environmental management. One real-scale experimental site has thus been designed and constructed to verify those points. Verifications have concerned:

- The road, shoulders and infiltration slopes construction. Those are very important to effectively reduce costs and ensure a good viability of the road and adjoining slopes. Road engineers must fully understand and agree with the concept to properly implement it.
- Shoulders tightening. If the road runoff mostly infiltrate through shoulders and not through infiltration slopes, it would not be properly filtered and cleaned. It would moreover endanger the road stability by introducing significant amount of water in the road foundation and embankment. This could cause major damage by reducing the bearing capacity.
- The road runoff filtering and cleaning. Once the road runoff infiltrates the infiltration slopes, it must be appropriately cleaned and deliver safe water to the underlying aquifer. Substances are either sorbed, either degraded.

Because all of those verifications were successfully and positively answered, the new OFEV concept can safely be implemented by road engineers to build new roads, or to modify existing roads.

6.2 SHOULDERS AND INFILTRATION SLOPES IMPLEMENTATION

Keeping in mind that shoulders should be as tightened as possible to avoid road runoff infiltration in the road foundation, shoulders were designed with those requirements:

- being 1.5 m width to accept a footway in the future
- being stabilized to bear to bear the charge of a vehicle (i.e. “banquette stabilisée”)
- being easy to build

All those requirements were successfully fulfilled. One issue was about the thickness of the gravel and humus/clay/lawn layer. Engineers of the road board of canton VD (SR) asked for 5 cm at maximum. New tests should however be performed to see if thicker layers really worsen the bearing capacity of the shoulder. This problem is further discussed below (§6.3.2 SGC). HMF lateral prolongation did not cause any trouble. The asphalting machine simply had to make one more run. The coating bituminous mixture was however tedious. The bentonitic geotextile cannot be put in contact with hot asphalt; a piece of geomembrane was thus set to link it to the road base (HMF). Discussions with road engineers (SR) lead to positive conclusions: it is nevertheless simple to implement.

Infiltration slopes were constructed according to the OFEV specifications. The construction of infiltration slopes was successful and satisfying. No visual indication of soil movements has been reported. Soils managed large amount of water without creating basal floods or earth flows. Soils were taken from a nearby construction site because the in situ soil volume was insufficient. Their contaminant content was measured. Soils were composed of 30 cm A-horizon and 50 cm B-horizon. Soil pH was about 8.2. The clay content was ~30% and the humus content was decreasing along the depth: 3.9 to 3%. Some OFEV optimal requirements were not reached: the optimal B-horizon would have been 70 cm, while the optimal humus content would be at least 4%. The infiltration, according to OFEV, was however admissible. The average vertical hydraulic conductivity was $1 \cdot 10^{-5}$ $m \cdot s^{-1}$.

One matter was about the infiltration slope stability. Due to its large volume and basal geomembrane, LH was judged unstable. Remember that infiltration slopes must cope with large amount of water coming from the road. A specific 3D-net (Geoweb, figure 6.1A) was used to stabilize the LH slope. However, this 3D-net is suspected to have partially contributed to the bad hydraulic behaviour encountered in that lysimeter (by-pass). Indeed, hydraulic analysis, tracer test, and substance qualification and quantification showed that the lysimeter LH structure had some defects causing preferential flows. For that matter, it was sufficient to compare the SH lag time and LH lag time that were roughly equal (sometimes the lysimeter lag time was even shorter). The preferential flow path was supposedly along the geomembrane surface (figure 6.1B). The effect of the 3D-net is unclear, but could be caused by the ineffective and incomplete filling of the net alveolus. What is sure is that the alveolus vertical walls prevented a good compaction of the basis of the B-horizon; the macroporosity was certainly well developed in that zone. Also, this preferential flow path that by-passes the main soil volume could have been avoided if the modification proposed in figure 6.3B, i.e. prolongation of the tightening layer over the B-horizon, could have been implemented for SH. Therefore, the infiltration slope design must take into account that no invasive comforting measure should be used. This could be a major issue, especially if the catchment surface is bigger (larger road). One way to solve the problem is to decrease the slope angle. This, however, enlarge the infiltration slope. A step slope could be considered. Carefully dimensioning the infiltration slope would solve this problem before encountered.

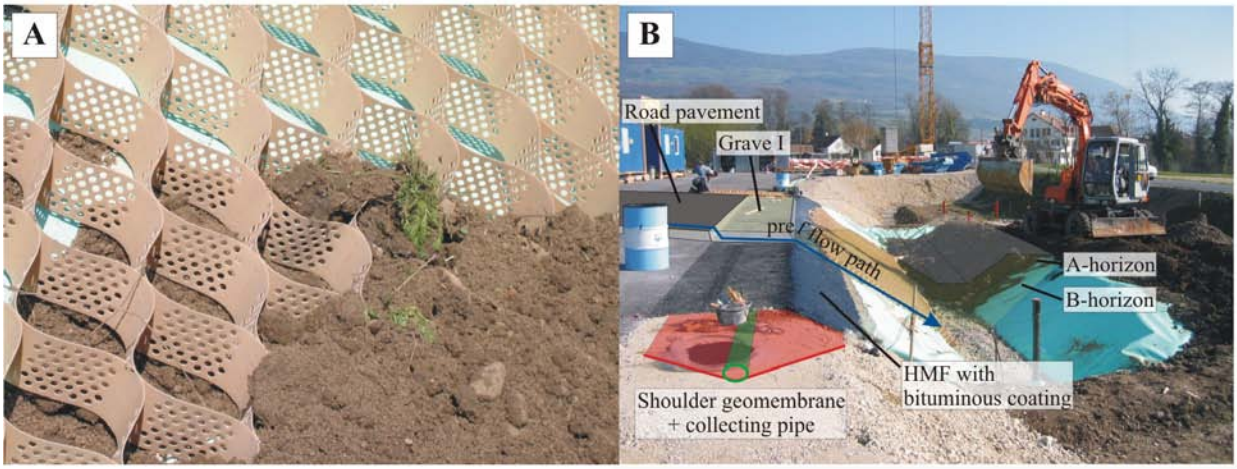

*Figure 6.1: **A)** Detail of the Geoweb structure reposing on the geomembrane (light blue). The B-horizon filled the alveolus. **B)** Illustration of the preferential flow path as function of structural conditions. The lysimeter and road pavements are graphically superposed to illustrate their location (not constructed yet). The preferential flow path runs over the HMF and geomembrane tops. The 3D-net favours its course. Most of the soil volume is not implicated. Note the bituminous coating.*

Another problem met was the soil permeability under the infiltration slope. It is evidently useless and even dangerous to overlay permeable soils on soils with lower permeability: it may create a perched groundwater between the infiltration slope bottom and the unsaturated zone; thus endangering the infiltration slope stability and, furthermore, the embankment. In the case of the Grandson experimental site, the LB infiltration slope was overlaying very impervious palustrine gleys. The problem was solved digging and filling 9 holes with gravel (100 cm Ø; 50 cm depth) along the infiltration slope bottom. This was however made for experimentation purpose; it cannot be implemented on a large scale. If it facilitated the infiltration toward the aquifer, it also surely lessened the substances retention in the unsaturated zone. A good permeable underlying unsaturated zone is thus a key issue; should it be absent, the diffuse infiltration concept could not be implemented.

Finally, the method used to install and compact the soil horizons could have an influence on the flow paths. Indeed, the hydraulic conductivity tensor ∇K (K ellipsoid, figure 6.2B) is conditioned by the compaction direction (the greatest hydraulic conductivity is met perpendicularly to the compacting direction; this is due to mineral orientation). In Grandson, the compaction was performed perpendicularly to the slope and offered satisfaction (figure 6.2A). No comparison data were available, though. Further experimentations about the effective influence of the K ellipsoid should be carried out if another compaction method is chosen (figure 6.2C). Compaction must, however, remain light to avoid obstructing the porosity. The resulting effective K ratio between the minimum and maximum values is unknown (literature values are between 0.5 and 1; Leroueil 2002, Richard 2001). This, however, must be nuanced regarding the porosity created by animals and plants: preferential flows along roots are vertical, while porosity induced by animals is chaotic. The infiltrating water widely uses those paths, though. The effect of ∇K must therefore be minimal, especially close to the surface. At a longer term, the soil settlement induces a horizontal K_{max} at the soil base.

Overall, the infiltration slope construction was satisfying and successful. If the preliminary hydrogeological assessment is performed with care, no particular issue are expected. The stability of the slope must be verified, particularly regarding the chosen shoulder type (see below). The shoulder design indeed influences the slope stability.

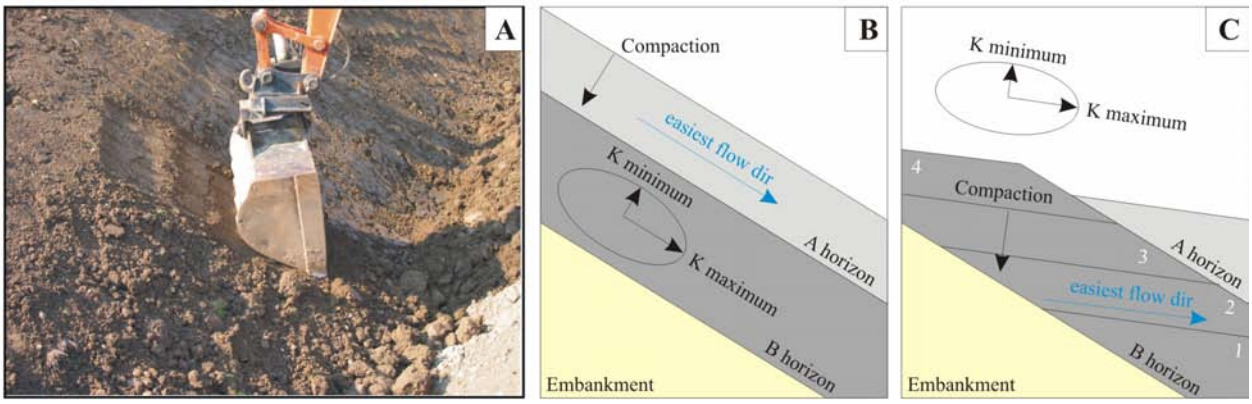

*Figure 6.2: Compaction influence on the easiest flow direction. **A)** Compaction is Grandson. **B)** The resulting K ellipsoid influenced the easiest flow direction; it was parallel to the dip slope. **C)** A different construction method might change the K ellipsoid. The example provided here is favourable: the easiest flow direction may keep the road runoff longer in the infiltration slope; it would therefore be more efficiently filtered and cleaned. The soil volume concerned by the road runoff infiltration would also be more important. However, the construction method might be longer and tedious; the effect of the K ellipsoid is furthermore not clearly demonstrated. This scheme is therefore not recommended without further verification.*

6.3 SHOULDERS TIGHTENING

To answer the first questions, i.e. "are the shoulders impervious?" and "which one has the best hydraulic behaviour?[1]", 112 natural rainfalls have been monitored. The resulting road runoff and infiltration flows were recorded. Moreover, because the shoulder responses were hard to assess all at once, two artificial watering experiments have been carried out. Those two tests were performed with water pumped from the Arnon River and watered onto the road. Their equivalent rainfall volumes were 30 mm for 100 $mm \cdot h^{-1}$.

Principally, results showed that large amount of water infiltrated the shoulders; only the artificial tightening with bentonite (bentonitic geotextile SB) offered a significant retention. Moreover, water exfiltrating the shoulders were heavily loaded with contaminant: no efficient retention occurs in shoulders. The evident conclusion is that shoulders must be artificially tightened to ensure that most of the road runoff reaches the infiltration slope. This stands for environmental as well as for geotechnical reasons. The 5 cm thick gravel and humus/clay/lawn mixture was far too insufficient to guarantee a good tightening. Shoulders particularities are presented below; shoulders are sorted out from the best to the worst hydraulic efficiency.

SB: Results showed that the shoulder SB was never challenged as the most efficient shoulder (runoff coefficient of 1). Water rarely exfiltrated this shoulder (only during the artificial experiments which had a ca. return period of 5 years). This shoulder is thus highly recommended and should be preferred to any other shoulder:

- The bentonitic geotextile has self-healing capacities when perforated, i.e. perforation fills in. It thus allows installing road signs and appliances[2].
- Its very design (two flexible textile mats surrounding the granular sodic bentonite) avoids deteriorations, migration of the bentonite, and leaching of the material.
- It is relatively cheap (14CHF/10€ per m^2, additional costs are negligible regarding the road and infiltration slope construction costs) and its installation is easy to implement on long distance (geomembrane and geotextile reels to unwind; width cut out at factory level).
- It fulfilled the road engineers' requirements about stability.

The bentonitic geotextile in Grandson is located at the foundation top. It notably follows the foundation edge to avoid backflows from the soils. While this situation did not create any specific problem during the 2 years of study, it is however not the most favourable situation from a chemical point of view: the road runoff infiltrates soils directly in the B-horizon; the A-horizon less participates to the substance filtration (figure 6.3A). An optimization would be to extend the geomembrane between the A and B-horizons: this would force the road runoff to infiltrate the A horizon and thus notably enhance the contaminant retention (figure 6.3B). This situation, however, is less favourable from the hydraulic point of view: a smaller thickness of soil is implicated; this could cause instabilities in the infiltration slope, i.e. the soil overlaying the geotextile might be washed away and destabilize the rest of the infiltration slope. Anyway, the road runoff passage between the shoulder and the infiltration slope is a major issue: one must take any disposition to avoid infiltration in the foundation and also try to increase the volume of soil implicated in the diffuse infiltration. The best solution is to drive the road runoff further away from the shoulder, if possible at shallow depth, to ensure that the A-horizon participates more to the road contaminant retention (humus-rich layer). Moreover, if the road runoff is directed to superior soil layers, it would take longer to percolate downward: the contact time between the loaded water and soil would increase and so the retention as well. Finally, it would enhance the phyto- and biodegradation (that take mainly place in the subsurface layer). Driving the road runoff further away would be the major improvement of the system.

Also, the bentonitic geotextile is compatible with new roads (figure 6.3C) as well as with ancient roads that must be refurbished (in case the asphalt is not concerned by the refurbishing; figure 6.3D). Even if the geomembrane piece cannot be fitted under the base course (HMF), an edge made of pressed bentonitic powder should well do the job.

[1] Which one let the smallest amount of water penetrate its body?
[2] As long as the stake has a diameter < 10 cm.

This material is well-known, easy to handle and costless. It can however migrate like clays. Applying some pressure during the installation would reduce this process.

The biggest issue concerning SB is the installation of crash barrier or other road appliances which stakes are profiled (H-shape for example) or have diameters large than 10 cm. Indeed, discussions with road engineers enlightened the fact that the geotextile could hardly be driven in without tearing the textile. The self-healing property of the geotextile would be insufficient in that case. The surface layer should therefore be made of gravel and clay overlaying the bentonitic geotextile. This would render the shoulder completely tightened even in case of casual or regular piercing.

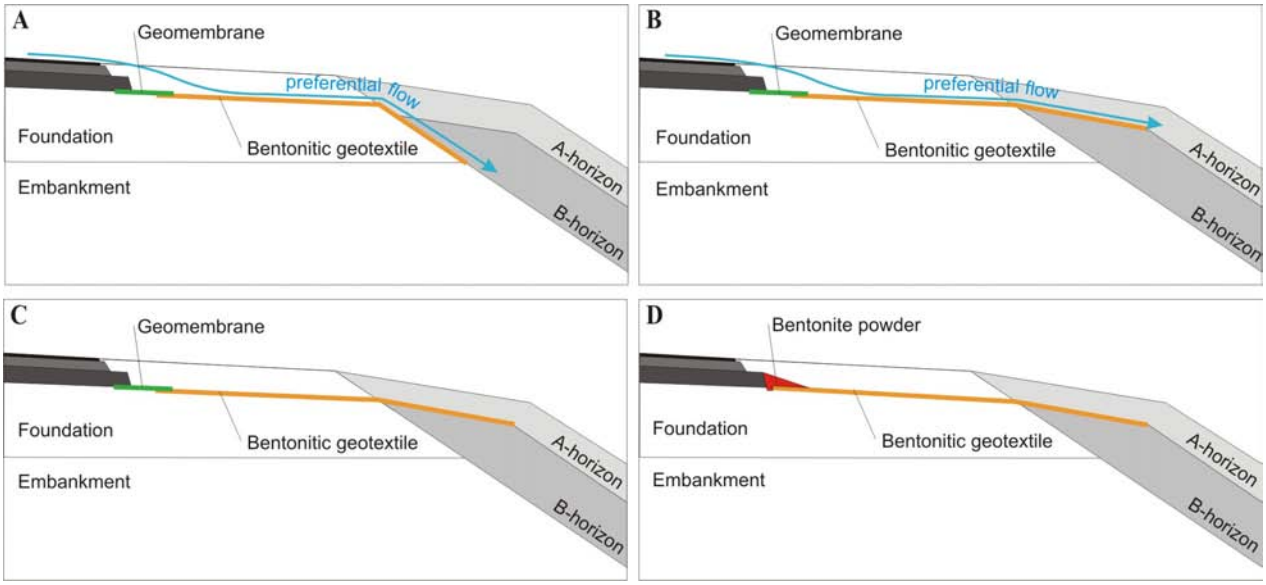

*Figure 6.3: **A)** SB profile in Grandson. The geotextile wraps the foundation; the road runoff may directly enter the B-horizon. This is less favourable from a chemical point of view. **B)** Modification proposed about the geotextile location. It is overlaying the B-horizon and thus forces the road runoff to infiltrate the A-horizon first. The implicated soil thickness is function of the asphalt thickness. Any intermediary situations between A) and B) are possible but more complicated to construct. **C)** Situation proposed for a new road. The geomembrane overlapping the geotextile really guarantees a perfect tightening. **D)** In case of an ancient road being refurbished, the edge between the geotextile and the road may be tightened with compressed bentonitic powder.*

SGC: This shoulder was constructed on the same design basis as SGH and SGL shoulders, i.e. 5 cm of tightening layer. SGC results however showed a better tightening (runoff coefficient of 0.6). This was not surprising considering the material used (clay). It also drove most of the first flush to the infiltration slope. Its bare surface let the runoff freely flow. Its design fully complied with the engineers' needs and methods (figure 6.4A). The wet mixing of clay was not a matter. Its material homogeneity allows using every kind of road appliances. The stake location surrounding can easily and effectively be tightened with bentonitic powder. For this reason, SGC can be constructed wherever SB is not applicable. Particularly, when crash barriers must be implemented, this shoulder presents a better acceptance. To improve SGC tightening capacity, the clay content should however be increased, as well as the thickness of the mixed gravel + clay layer. Moreover, the bentonitic geotextile should be used as well (figure 6.4B). Yet, this optimization should be tested, particularly from a stability point of view. The mixing of the material (clay + gravel) must be very well performed to avoid creating aggregates which could lead to increasing the macroporosity and thus the preferential flow paths. Higher clay content would indeed favour the aggregate formation and swelling. One must keep in mind that in spite of the amelioration, SGC would never have similar tightening properties as SB.

The greatest issue about SGC was its durability and persistence. SGC indeed showed some evidences of clay migration. The higher clay content was measured at the lower end of the shoulder, i.e. to the downstream side at the S-E. It proved a surface migration of clays. Also, the average clay content was lower than what have been used for

the gravel + clay mixture. However, this migration supposedly especially concerns the surface. Deeper clay migration must be lower, even inexistent. A thicker clay material layer would make this problem negligible.

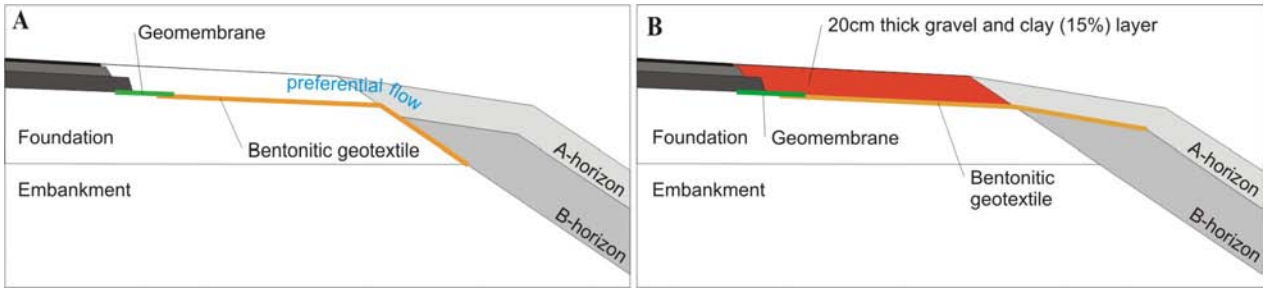

*Figure 6.4: **A)** SB such as built in Grandson. See figure 6.3 for explanation. **B)** Modification recommended for the SB design. The new gravel + clay layer would be 20 cm thick (or until the bentonitic geotextile top) and would contain more clay (15-20%%). Those values are arbitrarily proposed and would need scientific verifications. The bearing capacity also would have to be controlled. This new shoulder would have a great tightening in every situation, even in case of piercing.*

SH: Considering the particular care taken over the construction of this shoulder, its hydraulic tightening proved to be completely ineffective (runoff coefficient of 0.5). Indeed, large amount of water infiltrated that shoulder. The water paths were unclear: whether the water got through the HMF itself or skirted around and infiltrated the foundation from the soil is uncertain. Tracer tests suggested that both processes occurred. This is explained by the HMF itself which has a significant hydraulic conductivity ($1 \cdot 10^{-6}$ $m \cdot s^{-1}$, Hassan & White; 1996), and by the complete ineffectiveness of the coating made of bituminous mixture which should have tightened the shoulder. However, the road runoff proportion that infiltrated the shoulder is still lower than for SGH and SGL. SGC showed similar proportion or better, depending on the precipitation. What really disqualifies this shoulder as competitive is its particular material composition. Indeed, the HMF layer released large amounts of contaminant, especially PAH. As the underlying gravel has no confirmed retention potential, the massic fluxes reaching the aquifer are richer, and thus more dangerous for the environment. Finally, installations of road signs and appliances would durably alter the HMF tightening by creating preferential flow paths along the stakes.

SGL: This shoulder, however good its enhanced stability was, procured bad hydraulic results. Its runoff coefficient was 0.15, which is terrible. Reasons are multifaceted: the lawn intercepting the runoff, the higher vertical hydraulic conductivity, preferential flow paths along roots, dead plants leaving root voids, etc. This shoulder should not be considered for the specific purpose studied here, i.e. to drive the road runoff to the infiltration slope. This shoulder provided the best contaminant retention potential. It by the way validates the choice of gravel and lawn for infiltrating car park. It is far from perfect, though.

SGH: This shoulder showed a higher runoff coefficient than SGL (0.6). This coefficient has been calculated with limited number of data, though. Moreover, tracer tests and chemical analyses proved that the road runoff first flush infiltrates the shoulder first; the water running over the shoulder is not the more loaded water. This is why this shoulder has been put in last position. The contaminant retention postulated during its design is negligible. Moreover, its humus content lower the pH, which is a key parameter leading the MTE retention. In conclusion, this shoulder must not be considered for any use.

6.4 SUBSTANCE RETENTION IN SOILS AND UNSATURATED ZONE

To achieve a good understanding of the substance retention in the infiltration slope, the substances concentrations in the road runoff and exfiltration water were compared. Also, the aquifer quality was systematically assessed after major infiltration events. To efficiently pinpoint the substance retention in controlled conditions, an artificial precipitation event was performed with rainwater collected on PE sheets. When applicable, the measured massic flux

allowed calculating the global substance mass transmitted from the road to the lysimeter bottom. Overall, the substance retention was excellent; no chemical interaction between the road runoff and aquifer could be enlightened. It of course does not mean that there is none, but the effect of the road runoff on the aquifer was either null, either so small that its effect was impossible to perceive. Indeed, substances concentrations in the aquifer were always similar up- and downstream; no difference was noted. The concentration in the river was also of the same order of magnitude. Consequently, the origin of the aquifer specific and low substance concentration was not identified and could not conclusively be attributed to the road runoff.

Regarding the Swiss legislation, this main conclusion (above underlined) is absolutely favourable and allows the diffuse infiltration; it validates the "over the shoulder diffuse infiltration" concept. Swiss particularities are emphasized in the text box further below (§6.7).

So, the infiltration slopes fulfilled their jobs, although their humus content was a bit less than what was recommended. Humus and carbonate contents modifies the soil pH, which was highly favourable in Grandson (pH = 8.2; MTE are more easily retained in alkaline soils). In less favourable conditions (for example in Vevey, pH = 5.5), the MTE mobility is increased. Thus, the soil pH must be thoroughly controlled: it is a key parameter leading the infiltration slope efficiency, and thus leading the applicability of the concept as function of the location (in Switzerland or elsewhere). Indeed, in places where the soil is really acidic, the retention of mineral trace element could be compromised. This would need further real-scale verifications. Other contaminant should not be influenced. Slightly lower humus content than recommended (3.5% instead of minimum 4%) did not jeopardize the organic compound retention and also increased the pH a bit.

Modification which effects are still to assess concerns the clay content. Indeed, recommendations specifically insist on high clay content, whereas one must not forget that high clay content also has unfavourable side effects: dwelling and soil creeping are two example of what may be caused by too much clay. It causes preferential flow paths (filter by-pass) and instabilities. The latter was never observed, while the former might have occurred. It was not emphasized, though. The preferential flow path observed in LH was caused by structural and design origin, whereas LW did not procure evidence of preferential infiltration. Overall, a slightly smaller clay content than what is recommended would not endanger the substance retention, but on the other hand would ensure a better soil structure and stability. The soil granulometry should however be kept on the thinner side (silt) to guarantee the particles and colloids retention (those transport the higher concentration of contaminant). The new proposed clay content is 10-15%.

The lysimeter LW showed overall lower concentrations than LH, but of the same order of magnitude nevertheless. See the text box below for concentration values and comparison with Swiss legal limits. This concentration difference must be nuanced regarding the adjoining shoulder: LW is associated to SGL, whereas LH is bordering SH. SH transmitted greater amount of water to the infiltrations slopes and thus, supposedly so, larger concentrations of contaminant. However, the bad behaviour of LH (structurally induced), and the lysimeter volume difference camouflaged the real behaviour difference between LW and LH. Anyway, the small concentration difference noted in both LW and LH exfiltration waters enlightens more pertinently and durably the good retention occurring in soils: contaminants were well retained whatever lysimeter is considered. Mobile substances not surprisingly ran more easily through the soils. They were measured in proportionally higher concentration in the lysimeter exfiltration waters than in the road runoff. Substances that are less mobile readily sorbed to particles and colloids on the road surface. Those particles (*lato sensu*, Ø>0.45µm) were washed away by the precipitation, thus forming the greatest part of the road runoff first flush. Particles were then retained by the soil that played the role of filters. Only the thinnest fraction might, in certain hydraulic conditions, percolate through the soil and reach the lysimeter bottom during the same event. Other particles slowly migrate along time. This was emphasized by the turbidity found in the collecting pipes. The particles migration put the emphasis on the filtering role of soils. For this reason, one must absolutely avoid the creation of macroporosity: particles may by-pass the soil filters. Once again, lowering the soil clay content and driving the road runoff inside the soil structure (fig.6.3B) would guarantee good filtering properties. Implementing the new modification proposed in §6.3, i.e. prolongation of the tightening layer (fig 6.3B), would

overall considerably improve the soil retention capacity by simply increasing the flow path length: higher volume of soil would be implicated and the contact time would be longer. This would also increase the soil lifetime, although it is already considered as very high.

Comparisons between artificial and natural event enlightened the aerial dissemination of road-related substances. MTE are in a great majority participating to the road runoff, whereas PAH were aerially disseminated (estimat. 20 to 90% depending on the specie). The surface concerned, i.e. the distance from the road, is however unknown. Literature is fairly opened on this subject (distances provided are ranging from a few meters to hundreds of meters). The fraction deposited aerially is slowly carried downward by precipitations in the best conditions: no interference of the shoulder design or composition is altering its infiltration; no concentrating effect occurs (as opposed to the road runoff first flush). The area considered is also larger: a higher volume of soil is receiving the massic flux. All considered, the aerial dissemination of the road substance was not an issue in the case of Grandson. Yet, it would be a problem to seriously consider if the road is situated in a fragile environment, i.e. cropping field, very shallow groundwater, etc.

The soil contaminant content was assessed at the beginning and end of this study. This allowed calculating the concentration change along the time. MTE greatest change was observed in the middle of the slope at the A – B-horizon interface. The concentration rate was about 200 $mg \cdot kg^{-1}$ per month but mostly concerned Al and Fe, which origins are not clearly related to the road. Dangerous substance have much lower concentration rate (Cr for example: 0.5 $mg \cdot kg^{-1} \cdot month^{-1}$). Concerning PAH, the concentration rate was lower: it ranges from 1 (mobile PAH) to 14 $\mu g \cdot kg^{-1} \cdot month^{-1}$ (PAH with low mobility) and was recorded at the surface and in the middle of the slope. The location of the deposition (in the middle of the slope) emphasized the importance of the road profile subjected to the wind: the situation and topography of the road clearly influence the substance dissemination. In the case of Grandson, the high banks[3] supposedly created perturbation and whirlwinds that pinned down aerial contamination to the slope. Ballistic deposition would have differently accumulated contaminants.

MTE and PAH were well retained. MTE concentration in the first collected water were cut down to $1/30^{th}$ of the road first flush (which was Al and Fe at 75%; MTE total mass decreased from 280 mg to 2.6 mg (Fe + Al: 1.6 mg)); PAH concentrations were cut down to $1/100^{th}$ of their initial concentration; only the very mobile compounds were detected in higher concentration. Those values did not stand for LH which shoulder composition greatly altered the water infiltrating the lysimeter. Once again, the shoulder SH is discarded for this very reason. The PAH total mass decreased from 0.144 mg in the road runoff to 0.002 mg in the LW exfiltration water (0.0015 mg of naphthalene and phenanthrene which are the mobile species). The triplet C_{16}-C_{18}-C_{20} represents the only C_X species that were widely found in the lysimeter exfiltration. Others were almost completely retained. This constituted a great road tracer. BTEX, MTBE and PCB were also detected in low concentrations. See the text box below for comparison with indicative concentration limits.

6.5 ROAD INTEGRITY

During all the real-scale experimentation, the road integrity was never compromised. The only significant variation that has been observed was a 2 mm subsidence; it occurred on the road side were 85% of the traffic was recorded. The relation between the traffic and subsidence is undeniable. The effect of the road runoff infiltration on the road bearing capacity was never emphasized. Particularly, the massive infiltration test n°3 performed to moisturize the foundation caused no variation at all, either considering the bearing capacity (FWD) or the road settlement[4]. However, those results must be nuanced: the Grandson road pavement was especially thick, and the foundation and embankment were made of very good quality material. In case the road would have been less well dimensioned, it

[3] At the northern end of the experimental site, the infiltration slope foot is at least two metres below the asphalt elevation.
[4] It was of course not the goal of this test to provoke a permanent settlement of the road. The amount of water use for this artificial test was calculated in agreement with road engineers from LAVOC.

would probably have shown some indications of deflection or higher settlement, maybe further leading to damage or at least signs of conditions worsening.

Nevertheless, if the chosen shoulder is SB, those problems would never be an issue any more. No water would infiltrate the foundation, and thus no risk of bearing capacity modification would occur in the road pavement. Moreover, forcing the road runoff further away (fig. 6.3B) would also guarantee that it does not infiltrate the embankment (in case the embankment is very thick, which is the case in Grandson, the soil partly overlay the embankment).

6.6 Swiss specificities

Swiss legislation is very specific regarding the infiltration of polluted water: according to the ordinance on water (OEaux[5]), polluted water coming from communication ways are considered as polluted water *lato sensu*. They are therefore submitted to special conditions regarding the infiltration. It is notably specified that "the authorities may allow the diffuse infiltration (...) if the receptive underground water respects, after infiltration of the polluted water, OEaux quality specifications[6]. The second main goal of the present study is thus to verify that the substances concentrations in the underground water is not increased by the road runoff infiltration. For this purpose, measured concentrations in the aquifer were compared to various limit concentrations edited by the Swiss confederation[7]. *In extenso*, the new OFEV concept is valid for all countries who wish to apply it.

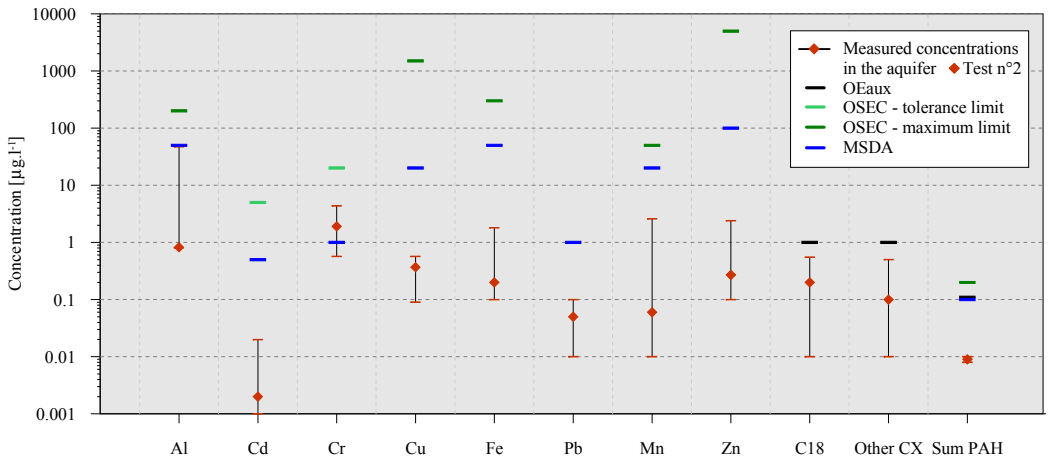

Figure 6.5: OEaux, OSEC, and MSDA limit concentrations. The measured concentrations were recorded in the aquifer (red lozenges = test n°2 concentrations). Those were thus concentrations after imission. Overall, only Cd and Cr overtake the MSDA maximum limits. All other pollutants which concentrations are regulated presented lower values. The aquifer water was almost of drinkable quality. It above all respected OEaux and OSEC quality standards. Note the logarithmic scale in $\mu g \cdot l^{-1}$ for all contaminants.

Specification about the concentrations limits are shown in the following figure 6.5. They all concern the aquifer concentration after imission. Overall, all concentrations recorded in the aquifer respected the OEaux limits. Other concentrations limits were respected unless for Cr which concentrations were 2 to 4 times higher than MSDA limit (Cr VI^{+}). This limit was thus only slightly overtaken. Moreover, the analysed Cr concentration was postulated to be

[5] Appendix 3.3, chapter 1, al. 2.
[6] Appendix 2 of OEaux, art. 22.
[7] OEaux, OSEC (Ordinance on alien substances and compounds), MSDA (Swiss manual on foodstuffs), and OSol (Ordinance on soils). Those regulations are listed in appendix I.

entirely Cr VI which is undoubtedly not the case. This was postulated because of the oxidizing environment, and to stay on the safety side. Cr VI is highly toxic.

The fact that pollutant concentrations were similar up- and downstream of the road implied that the road runoff was not the cause of the aquifer contamination. However, some pollutants are clearly related to the road (Cr, V, PAH, MTBE, and C_{18}); they must be related to either the river content, either the aerial dissemination that caused diffuse infiltration in the surroundings. Other substances are obviously present (mobile substances) but are not exhaustively considered as pollutants.

Also, as the influence of the road runoff could not be measured in the aquifer, the experimental site emissions (at the base of the lysimeter) are compared to emission limits, i.e. the OSite values (Ordinance on contaminated sites). Comparison about the substances considered as pollutants are shown in figure 6.6. Note that the emission concentrations are those measured out of the LH lysimeter, which had higher concentrations than LW. All concentrations were well below the OSite limitations (many orders of magnitude). Road runoff infiltration can therefore not be considered as a contaminated site. Closest concentrations concern highly toxic pollutants: they have lower legal limits (Cr, Sb, Benzo(a)pyrene, the sum of PCB).

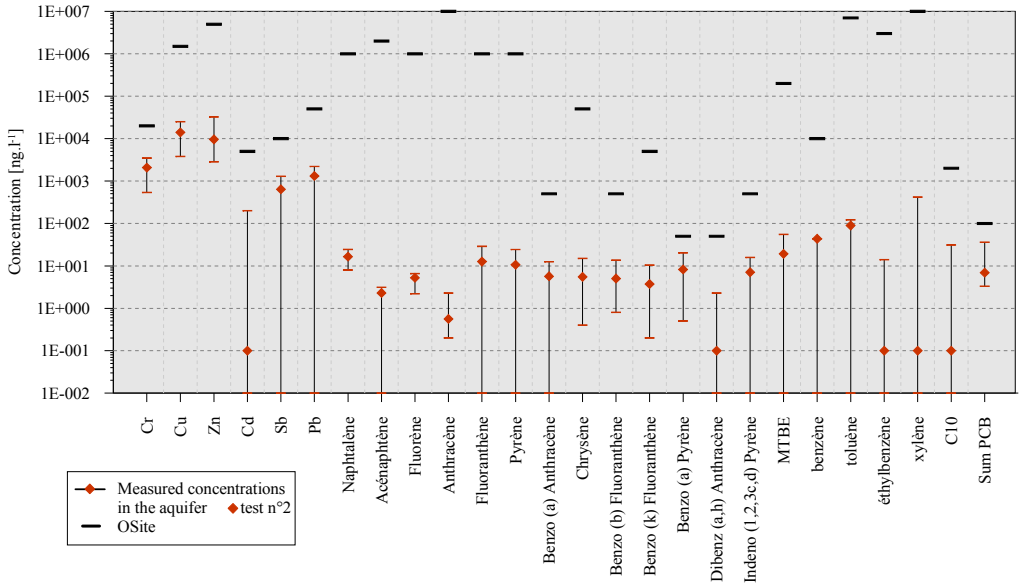

Figure 6.6: Comparison between the emission (measured at the bottom of the LH lysimeter which had the worst substance retention) and the OSite limit values. There not a single pollutant concentration that went beyond the OSite limit values. Note the logarithmic scale. Red lozenges are artificial test n°2 concentrations. The sum of PCB is calculated as follow (CEOCOX): ∑PCB = 4.3·(PCB28+PCB52+PCB101+PCB138+PCB153+PCB180).

CHAPTER 7

CONCLUSIONS

This project made the concept "over the shoulder diffuse infiltration" evolve to a real feasibility. It can be easily and fruitfully implemented, either for a new road construction, either for a road refurbished. The real-scale experimentation performed during this project proved to be a powerful and excellent tool to assess the strengths and weaknesses of this concept. The strengths are:

- It is now readily possible, without further research, to build at low cost a really good shoulder (shoulder tightened with bentonitic geotextile - SB) that would drive all of the road runoff to the infiltration slope. Soils are available where the road must be constructed. This concept is thus easily implementable.
- Alternative shoulder (shoulder tightened with clay and gravel mixture - SGC) could be considered in particular conditions, i.e. where the shoulder must welcome numerous road appliances. SGC must be enhanced. This concept is thus flexible.
- The road runoff is well purified in the infiltration slope; all contaminant concentrations are either greatly decreasing, either not detectable any more (under detection limit). The environmental impact is very positive: pollutants are no longer dumped in the surface water, while precipitations are recharging the aquifer. The legal requirements were completely fulfilled. This concept is thus environmentally conclusive.
- The road emissions are concentrated in one place only, i.e. the infiltration slope, which can accumulate pollutant for a very long time (> 50years, Boller 2006). This concept is thus robust and durable.
- The structural stability of the road is preserved: driving the road runoff far from the foundation guarantees that no water infiltrate the superstructure; the road conserves its bearing capacity. This concept is thus technically safe.

Identified weaknesses of the concept are:

- The particular issue of the aerial dissemination is not addressed by this new concept. Only the aerial deposition in the first few meters from the road is taken care of. However, this particular issue is already well attended by road engineers: barriers designed to reduce the traffic noise also stop the contaminant dissemination. Those barriers are more and more considered within cities as well as for motorways.
- The particular cases of traffic accident and their consequences on the groundwater were not studied. Still, the infiltration slopes have shown a notable tolerance about the contaminant concentration.

Implementing the new "over the shoulder diffuse infiltration" will greatly reduce the environmental impact roads. This concept combines the advantages of smoothing the discharges of surface water, low hydrogeological incidences without diminishing the road stability if the shoulder is built to be watertight. It will also lower the maintenance costs.

As the results of the present study are very conclusive, there is no specific need of a surveillance network once the concept is implemented. However, the good environmental performance of this concept does not free the authorities (cantonal water board, for example) to continuously assess the groundwater quality. Also, the road engineers must think differently about the road maintenance. From now on, it will concern the bearing capacity and road degradation assessments but the environmental impact as well.

However, some points about the concept are still to precise. Those are linked to the long term evolution of the soil structure and composition like porosity obstruction, paedogenesis, soil creeping, etc. Therefore, a 5-years observation program of the experimental station of Grandson has begun in spring 2007. Goals of this monitoring are:

- To observe the slope stability; particularly to detect slope movements, landslides, cracks opening, etc. caused by the large amount of water issued from the road.
- To monitor the soil composition evolution, particularly the increase of humus content in the A-horizon, the clay migration, the compaction, and the pores obstruction.
- To check the tightening of the bentonitic shoulder during ageing of the material in real road conditions
- To measure the evolution of the soil sorption capacity through the monitoring of some natural events and regular tests (artificial precipitation), and particularly the increase of the releasing processes. Those are indeed considered as insight of the soil lifetime.

Those points will be studied by the GEOLEP thanks to a joint funding of two cantonal administrations (roads and water protection).

At present, the new environmental issue widely considered is the global warming. This is already influencing the consumers' choice about car and motorisation. Also, major players like car makers, municipalities, or even countries promote the use of greener cars. The main point is to minimize the CO_2 emission by using alternative e-fuels (bio-ethanol, natural gas, etc.), hybrids, electric, or hydrogen cell-fuel cars. Although politicians and public have a real consideration about the environment and wish to improve the situation, it is doubtful that the transition would occur rapidly. Economic and strategic issues are still very influent. The only sure point is that the fuel used in Europe will no longer be only fossil fuels. The petrol peak is behind us: the use of petrol is on the verge. This, however, is largely compensated by the strong traffic increase. Therefore, the emission of pollutants specifically caused by petrol combustion is more likely to remain constant for years. The experimental station in Grandson will be working for the next 5 years at least; maybe some change will appear during this period. It is improbable, though, due to the short period of observation. It would however cover eight years of traffic evolution.

Yet, the fuel evolution will not turn the "over the shoulder diffuse infiltration" concept useless. To the contrary, it will be the most powerful line of defence against the road pollution. Indeed, cars will always need and use lubricating motor and gearbox oils, tyres, and a great variety of metals. Also, the road pavement will release organic and inorganic compounds for years. The traffic charge is constantly increasing: the concentrations emitted will also be greater. This concept is thus more contemporary than ever. All the more, the changes implied by this new concept will improve the perception of the road by the society: the road which was once a dirty and soiled milieu will now be more environmental-friendly.

This new concept is consequently robust, durable, and a considerable improvement in the road system management for the 21st century. It goes above and beyond the simple road runoff management: it is a new environmental philosophy which is highly innovative, forthcoming and decisive.

REFERENCES

Acres G. J. K. 1991. *The development of emission control technology for motor vehicles*. R. S. Hamilton & R. M. Harrison (Eds), Highway Pollution, p. 376-396. Amsterdam, Elsevier Science.

Alloway B. J. 1995. *Heavy metals in soils*. Second ed. Glasgow [etc.]: Blackie Academic & Professional.

Amellal N., Portal J.-M., Vogel T., Berthelin J. 2001. *Distribution and location of polycyclic aromatic hydrocarbons (PAHs) and PAH-degrading bacteria within polluted soil aggregates*. Biodegradation. Volume 12, Number 1, pp. 49-57(9)

Baize D., Jabiol B. 1995. *Guide pour la description des sols*. Paris : Institut National de la Recherche Agronomique, 1995.

Baize D., Tercé M. 2002. *Les éléments traces métalliques dans les sols : approches fonctionnelles et spatiales*. Paris : Institut national de la recherche agronomique

Baladès J.-D., Legret M., Madiec H. 1995. *Permeable pavements: pollution management tools*. Water Science and Technology, 32(1), p. 49-56.

Ball, D.J.; R.S. Hamilton; and R.M. Harrison. 1991. *The Influence of Highway-Related Pollutants on Environmental Quality*. In Highway Pollution, ed. R.S. Hamilton and R.M. Harrison. Amsterdam: Elsevier, p. 1-47.

Ballschmitter K., Zell M. 1980. *Analysis of polychlorinated biphenyls (PCBs) by glass capilliary chromography. Composition of technical Aroclor and Clophen PCB mixtures*. Z Analyt Chem 302:20–31

Benfenatti E., Valzacchi S., Mariani G., Airoldi L., Fanelli R. 1992. *PCDD, PCDF, PCB, PAH, cadmium and lead in roadside soils: relationship between road distance and concentrations*. Chemosphere, vol. 24, p. 1077-1083.

Bensimon M., Gabus J. H., Parriaux A. 1991. *Characterization of natural waters using trace elements analysis obtained in a plasma source mass spectrometer*. J. Trace Microprobe Techn. 9(2&3), 81-93.

Bensimon M., Looser M. O., Parriaux A., Reed N. 1994. *Characterisation of groundwater and polluted water by ultra trace element analysis, using High Resolution Plasma Source Mass Spectrometry*. Eclogae geol. Helv. 87/2: 325-334.

Bensimon, M., Parriaux A. 1990. *Application of inductively coupled plasma mass spectrometry (ICP-MS) to the determination of trace elements in water resources*. Memoires of the XXIInd Congress of IAH, EPFL, Lausanne, Part 1, 314-319.

Berbee R., Rijis, G., de Brouwer, R., van Velzen, L. 1999. *Characterization and treatment of runoff from highways in the Netherlands paved with impervious and pervious asphalt*. Water Environment Research 71(2) (March-April): 183-190.

Bertrand-Krajewski J. L. 1991. *Modélisation des débits et du transport solide en réseau d'assainissement. Etude bibliographique.* Rapport ENITRS, Lyonnaise des Eaux, université louis pasteur Strasbourg. 207p.

Bertrand-Krajewski J. L. 1992. *Modélisation conceptuelle du transport solide en réseau d'assainissement unitaire.* Thèse de doctorat, Université Louis Pasteur de Strasbourg, Lyonnaise des Eaux Dumez, 165p. + annexes.

Bertrand-Krajewski J. L., Chebbo G., Saget A. 1997. *Répartition des masses de polluants en fonction du volume dans les rejets urbains de temps de pluie. Conséquences pour la notion de premier flot.* TSM, 92 ème année, n°2, p. 53-67.

Bertrand-Krajewski J. L., Chebbo G., Saget A. 1998. *Distribution of pollutant mass versus volume in stormwater discharges and the first flush phenomenon.* Water Research, vol.32, n°8, p. 2341-2356.

Boivin P. Work under progress. *Filtration des pollutants routiers dans les sols, example de l'A9 en Valais*.

Boller M. 2002. *Charakterisung von Strassenabwasser – Emissionen und Immissionen*, VSA – Fortbildungskurs.

Boller M. 2002. *Stoffflüsse und Massenbilanzen von Strassenabschnitten*, VSA – Fortbildungskurs.

Boller M., Haefliger M. 1996. *Verbleib von Schwermetallen bei unterschiedlicher Meteorwasserentsorgung (Fate of heavy metals in alternative sewer systems)*. GWA: Gas, Wasser, Abwasser, vol. 76, n°1, pp. 3-15 (48 ref.)

Boller M., Kaufmann P., Ochsenbein U. 2006. *Bankette bestehender Strassen, Untersuchung des versickerung von Strassenabwasser über Strassenrandstreifen an einer bestehender Strasse*, rapport final, Burgdorf.

Bouchard D. C., Mravik S. C., Smith G. B. 1990. *Benzene and naphthalene sorption on soils contaminated with high molecular weight residual hydrocarbons from unleaded gasoline*. Chemosphere, vol. 12, no. 8, p. 975-989.

Bouwer H. 1978. *Groundwater Hydrology*. Ed. New York; McGraw-Hill.

Bradford S. A., Bettahar M., Simunek J., Van Genuchten M. T. 2004. *Straining and attachment of colloids in physically heterogeneous porous media*. VZJ, no. 3, p. 384-394.

Bradshaw N., Hall E. F. H., Sanderson N. E. 1989. *Inductively coupled plasma as an ion-source for high-resolution mass-spectrometry*. J. Anal. At. Spectrom., no. 4, p. 801−803.

Braudeau E., Zidi C., Mtimet A. 2002. *La rétractométrie : mesure de référence des paramètres physiques du sol. Vers une maîtrise des impacts environnementaux de l'irrigation*. Actes de l'atelier du PCSI, 28-29 mai, Montpellier, France. CEMAGREF, CIRAD, IRD. Serge Marletet PierreRuelle (éditeursscientifiques)

Brooks, R. H., Corey A. T. 1966. *Properties of porous media affecting fluid flow*. Journal of Irrigation and Drainage Div., ASCE IR 2, 92: 61-88.

Brusseau M. L., Rao P. S. C. 1989. *The influence of sorbate-organic matter interaction on sorption nonequilibrium*. Chemosphere, no. 18, p. 1691-1706.

Butler J. D., Butterworth V., Kellow S. C., Robinson H. C. 1984. *Some observations on the polycyclic aromatic hydrocarbon (PAH) content of surface soils in urban areas*. Science of the total environment. 1984, vol. 33, pp. 75-85 (11 ref.). Elsevier Science.

Cerniglia, C. E. 1993. *Biodegradation of polycyclic aromatic hydrocarbons*. Current Opinion in Biotechnology, vol. 4, no. 3, p. 331-338.

Chiou C. T. 2002. *Partition and adsorption of organic contaminant in environmental systems*. Wiley-Interscience. J. Wiley and Sons, NJ.

Chiou C. T., Shoup T. D. 1985. *Soil sorption of organic vapours and effects of humidity on sorptive mechanism and capacity*. Environmental science & technology. 1985, vol. 19, n°12, pp. 1196-1200 (19 ref.)

Choi H., Corapcioglu M. Y. 1997. *Transport of non-volatile contaminant in unsaturated porous media in the presence of colloids*. J. of Contaminant Hydrology, no. 25, p. 299-324.

Church P., Friesz P. 1993. *Effectiveness of highway drainage system in preventing road-salt contamination in groundwater*. Trasnportation Research Records 1420, p. 56-64.

Clément F. E. 1916. *Plant succession: an analysis of the development of vegetation*. Carnegie Institute of Washington Publication. 242. Climax theory.

Contat F., Shariat-Madari H., Stadelmann F. X. 1991. *Déposition et accumulation de plomb de long de quatre secteurs autoroutiers de 1978 a 1988. 1. Evolution en fonction des années, des saisons et de la météorologie* (Deposition and accumulation of lead at four sites near the highway from 1978 to 1988. 1. Trends in relationship to year, season, and meteorology). Schweizerische landwirtschaftliche Forschung (Switzerland), v. 30(1-2) p. 29-43.

Corapcioglu M. Y., Kim S. 1995. *Modeling facilitated contaminant transport by mobile bacteria*. Water Resources research, vol. 31, no 11, p 2639-2648.

Cristina C., Sansalone J. J. 2003. *First flush, power law model and process selection diagram for urban storm-water particulates*. ASCE J. of Environmental Engineering, vol. 129, no. 4, p. 298-307.

Cyr R.Y., Chiasson P. 1999. *Modelling subsoil drainage systems for urban roadways*. Canadian Journal of Civil Engineering, Vol. 26, pp. 799-809.

Dahan O., McDonald E., Young M. 2003. *Development of a flexible TDR probe for deep vadose zone monitoring*. Vadose Zone J., vol. 2, p. 270-275.

Dakhel N., Pasteris G., Werner D., Höhener P. 2003. *Small-volume releases of gasoline in the vadose zone : impact of the additives MTBE and ethanol on groundwater quality*. Environmental science & technology; 37(10): p. 2127-2133.

Dakhel N., Pasteris G., Werner D., Höhener P. 2003. *Small-volume releases of gasoline in the vadose zone: impact of the additives MTBE and ethanol on groundwater quality*. Environ. Sci. Technol., no. 37, p. 2127-2133.

Daub J., Hermann R., Forster J., Striebel T. 1994. *Chemodynamics of trace pollutants during roof and street runoff*. Water Science and Technology, vol. 29, no 1-2, p. 73-82.

De Coulon Herzog S., Parriaux A., Bensimon M., Tarradelas J., Vedy J. C. 1994. *Interaction entre les routes et l'environnement souterrain.* 7ème congres de l'Association Internationale de Geologie de l'Ingénieur, actes du congrès de Lisbonne, 5-9 sept. 1994

De Jonge L. W., Kjaergaard C., Moldrup P. 2004. *Colloids and colloid-facilitated transport of contaminants in soils: An introduction*. VZJ 3:321-325.

De Vlieger L., Lenaers G., Craps R. 1994. *Vehicle emissions estimations and measurements in Belgium*. The Sci. of the Total Environ., no. 146/147, p. 217-223.

Dean, C. M., Sansalone, J. J., Cartledge, F. K., Pardue, J. H. 2005. *Influence of hydrology on storm water metal element speciation at the upper end of the urban watershed*. ASCE J. of Environmental Engineering, vol. 131, no 4.

Delmas-Gadras C. 2000. *Influence des conditions physico-chimiques sur la mobilité du plomb et du zinc dans un sol et un sédiment en milieu routier*. PhD, thesis. U. de Pau et du Pays de Ladour.

DeNovio N. M., Saiers J. E., Ryan J. N., 2004. *Colloid movement in unsaturated porous media: Recent advances and future directions*. Vadose Zone Journal 3, 338-351.

Docourt M. 2005. *Mobilité des polluants routiers dans les sols. Exemple des hydrocarbures aromatiques polycycliques et des éléments traces minéraux*, Mémoire de recherche postgrade, GEOLEP, EPFL.

Dogan S., Haerdi W. 1981. *High-speed analysis for acid-rain anions by Single-Column Ion Chromatography (SCIC)*. Chromatographia Journal, Vieweg Verlag, vol 16, no 1, p. 312-316.

Dogan S., Haerdi W. 1981. *Séparation et dosage d'anions dans les eaux naturelles par chromatographie ionique et detection conductivimétrique*. Chimia no. 35.

Driscoll J. N. 1992. *Review of field screening mehodology for analysis of hydrocarbons in soils and groundwater*. International Labmate, 27-32.

Driss M. R., Bouguerra L. 1991. *Analysis of volatile organic compounds in water by purge-and-trap and gas chromatography techniques*. International J. of Environ. Analytical Chemistry, vol. 45, p. 193-204.

Duchaufour P. 2001. *Introduction à la science du sol - Sol, végétation, environnement*. Ed Dunod.

Dunnivant F. M., Jardine P. M., Taylor D. L., McCarthy J. F. 1992. *Cotransport of cadmium and hexachlorobiphenyl by dissolved organic carbon through columns containing aquifer material*. Environmental science & technology, vol. 26, n°2, pp. 360-368 (34 ref.)

Dzombak D. A., Luthy R. G. 1984. *Estimating adsorption of polycyclic aromatic hydrocarbons on soils*. Soil science (Soil sci.), vol. 137, n°5, p. 292-308 (2 p.)

Enfield C. G., Bengtsson G., Lindquist R. 1989. *Influence of macromolecules on chemical transport*. Environ. Sci. Technol., 23:1278--1286, 1989.

Förstner U. 1985. *Chemicals forms and reactivities of metals in sediments in "chemical methods for assessing bio-available metals in sludges and soil"*, Leschber R., Davis R.D., L'Hermite P., CEC, Elsevier Applied Science publishers, p. 1-30.

Gardner W. R. 1958. *Some steady state solutions of the unsaturated moisture flow equation with application to evaporation from a Water-Table*. Soil Science, no 85, p. 228-232.

Geiger W. F. 1987. *Flushing effect in combined sewer systems*. Proceedings de la 4eme conference international "Urban Storm Drainage", Lausanne, Switzerland, 31 août – 4 sept., p. 40-46.

GEOLEP 2004. *Rétention des polluants des eaux de chausses: "infiltration sur les banquettes". Vérification In Situ et optimisation*, Rapport 1.

Gjessing E., Lygren E., Andersen S., Berglind L., Carlberg G., Efraimsen H., Källqvist T., Martinsen K. 1984. *Acute toxicity and chemical characteristics of moderately polluted runoff from highways*. The Science of the Total Environ., vol. 33.

Glenn D.W., Liu D., Sansalone J.J. 2001. *Influence of highway runoff chemistry, hydrology and residence Time on non-equilibrium partitioning of heavy metals – Implications for treatment at the highway shoulder*. J. of Transportation Research Record, 1775, p. 129-140.

Gobat J.-M., Aragno M., Matthey W. 1998. *Le sol vivant*. Presse Polytechniques et Universitaires Romandes, Lausanne.

Golwer A. 1995. *Verkehrswege und ihr Grundwasserrisiko*. Eclogae Geologicae Helvetiae 88/2.

Gottker M., Schilling W. 1991. *Hydrological and pollutional aspect of stormwater infiltration*. EAWAG. Proceedings of the second European junior scientist workshop, Luzern, Switzerland, 4-7.

Green W. H., Ampt A. A. 1911. *Studies in soil physics. 1) The flow of water and air through soils*. J. Agric. *Sci., 4*: *l-24.*

Grolimund, D., Borkovec M., Barmettler K., Sticher H. 1996. *Colloid-facilitated transport of strongly sorbing contaminants in natural porous media: a laboratory column study*. Environ. Sci. Technol., vol. 30, p. 3118–3123.

Grottker M. 1987. *Runoff quality from a street with medium traffic loading.* The Science of the Total Environment, no 59, p. 457-466.

Hamilton R. S., Revitt D. M., Warren R. S. 1984. *Levels of physico-chemical associations of Cd, Cu, Pb and Zn in road sediment.* The Science of the Total Envionment, no 33, p. 59-74.

Hansson K. 2005. Water and heat transport in road structures: development of mechanistic models. PhD thesis.

Harrison R. M., Johnston W. R. 1985. *Deposition fluxes of lead, cadmium, copper and polynuclear aromatic hydrocarbons (PAH) on the verges of a major highway*. Sci. Total Environ., no 46, p. 121.

Hartmann D., Michel P. 1992. *Protection des eaux souterraines en Suisse*. Gas, Wasser, Abwasser, vol. 7, p. 9-16.

Hassan H. F., White T. D. 1996. *Locating the drainage layer for flwxible pavements*. Final report no. FHWA/INDOT/JTRP-96/14. Federal Highway Administration, Wachington D.C.

Hasset J.J., Banwart W.L. 1989. *The sorption of nonpolar organics by soils and sediments*. *In* B.L. Sawhney and K. Brown (ed.) Reactions and movements of organic chemicals in soils. SSSA Spec. Publ., no 22, p. 31.. SSSA, Madison, WI.

Hautala E.-L., Rekilä R., Tarhanen J., Ruuskanen J. 1995. *Deposition of motor vehichle emissions and winter maintenance along roadside assessed by snow analyses*. Environ. Pollut., no. 87, p. 45-49.

Helsel D. R., Hirsch R. M. 1992. *Statistical methods in water resources*. Studies in Environmental Sciences, no. 49.

Helsel D. R., Kim J. I., Grizzard T. J., Randall C. W., Höhn R. C. 1979. *Land Use Influences on Metals in Storm Drainage*. Journal of the Water Pollution. Control Federal. Vol. 51, no. 4, p. 709-717.

Hermann R. 1981. *Transport of polycyclic aromatic hydrocarbons through a partly urbanized river basin*. Water, Air, and Soil Pollut. 16, 445.

Hermann R., Daub J., Förster J., Striebel T. 1994. *Chemodynamics of trace pollutants during roof and street runoff*. Wat. Sci. Tech., vol. 29, no. 1-2, p. 73-82.

Hermann R., Daub J., Striebel T. 1992. *Qualitative Beurteilung der Niederschlagabflüsse*. Schadstoffe im Regenabfluss II. Presses de l'Institut für Siedlungswasserwirtschaft, Université de Karlsruhe, vol. 64, p. 113-145.

Hewitt C. N., Rashed M. B. 1990. *An integrated budget for selected pollutants for a major rural highway*. Science of the total environment, vol. 93, p. 375-384. International symposium on highway pollution, Munich, 18-22 September 1989.

Hewitt C. N., Rashed, M. B. 1992. *Removal rates of selected pollutants in the runoff waters from a major rural highway*, Water Resources, vol.

Hewitt C.N., Rashed M.B. 1992. *Removal rates of selected pollutants in the runoff waters from a major rural highway*. Water Res., no 26, p. 311–319.

Hildeman L. M., Markowski G. R., Cass G. R. 1991. *Chemical composition of emissions from urban sources of fine organic aerosol.* Environ. Sci. Technol., col. 25, p. 744.

Hoffman E. J., Mills G. L., Latimer J. S., Quinn J. G. 1984. *Urban runoff as a source of polycyclic hydrocarbons to coastal waters*. Environ. Sci. Techol., vol. 18, p. 580-587.

Hoffman E. J., Latimer J. S., Hunt C. D., Mills G. L., Quinn J. G. 1985. *Stormwater runoff from highways*. Water, Air, & Soil Pollution, vol. 25, no 4, p. 249-264.

Höhener P., Dakhel N., Pasteris G., Werner D. 2002. *Biodegradation of volatile organic compounds in the unsaturated zone*. In: D. Halm & P. Grathwohl (Eds), proccedings of the first International Workshop on Groundwater risk assessment at contaminated sites. Tübinger Geowissenschaftliche Arbeiten, Heft, no. 61, p. 88-93.

Hvitved-Jacobson T., Yousef Y. 1991. *Highway runoff quality, environmental impacts and control*. In: R.S. Hamilton, R.M. Harrison (Eds.), Highway Pollution, pp. 165-208. Elsevier London.

International norm ISO 1438/1-1980. *Mesure de débit de l'eau dans les canaux découverts au moyen de déversoirs et de canaux Venturi -- Partie 1: Déversoirs en mince paroi.*

Johnston W. *R., Harrison R. M. 1984*. *Deposition of metallic and organic pollutants alongside the M6 motorway.* The Sci. of the Total Environ., vol. 33, Special Issue: Highway pollution, p. 119-127.

Kanazawa J. 1989. *Relationship between the soil sorption constants for pesticides and their physicochemical properties*. Environmental toxicology and chemistry, vol. 8, no 6, p. 477-484.

Karickhoff S.W. 1984. *Organic pollutant sorption in aquatic systems*. J. Hydraul. Eng. Div. Am. Soc. Civ. Eng., no 110, p. 707–735.

Kelly C. A., Law R. J., Emerson H. S. 2000. *Methods of analysing hydrocarbons and polycyclic aromatic hydrocarbons in marine samples*. Aquatic Environment Protection: analytical methods, no. 12, p. 1-18.

Kjaergaard C., De Jonge L. W., Moldrup P., Schjønning P. 2004. *Water-dispersible colloids: effects of measurement method, clay content, initial soil matrix potential and wetting rate*. VZJ 3:403-412.

Kjaergaard, C., Moldrup P., De Jonge L. W., Jacobsen O. H. 2004. *Colloid mobilization and transport in undisturbed soil columns. II) The role of colloid dispersibility and preferential flow*. VZJ 3:424-433.

Kjaergaard, C., Poulsen T.G., Moldrup P., De Jonge L. W. 2004. *Colloid mobilization and transport in undisturbed soil columns. I) Pore structure characterization and tritium transport*. VZJ 3:413-423.

Kördel W., Stutte J., Kotthof G. 1993. *HPLC screening method for the determination of the adsorption coefficient on soil comparison of different stationary phases*. Chemosphere, vol. 27, p. 2341-2352.

Krauth H., Klein H. 1982. *Untersuchungen über die Beschaffenheit des Oberflächenwassers von Bundesautobahnen*. Forsch-. Straßenbau und Straßenverkehrstechnik H.363, Bonn.

Krein A., Schorer M. 2000. *Road runoff pollution by polycyclic aromatic hydrocarbons and its contribution to river sediments*. Water Research, vol. 34, p. 4110-4115.

Labadia C. F., Buttle J. M. 1996. *Road salt accumulation in highway snow banks and transport through the unsaturated zone of the Oak Ridges Moraine, southern Ontario*. Hydrological Processes, vol. 10, p. 1575-1589.

Lacas J.-G. 2005. *Processus de dissipation des produits phytosanitaires dans les zones tampons enherbées. Etude expérimentale et modélisation en vue de limiter la contamination des eaux de surface*. PhD thesis.

Lange G. 1990. *The design and construction of treatment processes for highway runoff in the FRG.* The Sci. of the Total Environ., vol. 93.

Latimer J. S., Hoffman E. J., Hoffman G., Fasching J. L., Quinn J, 1990. *Sources of petroleum hydrocarbons in urban runoff*. Water, Air and soil pollution, vol. 52, p. 1-21.

Ledieu J. P., Ridder D., Dautrebande A. 1986. *A Method for Measuring Soil Moisture Content by Time Domain Reflectometry*. Journal of Hydrology, no. 88, p. 319-328.

Lee G. F., Jones-Lee G. F. 1994. *Water quality aspects of groundwater recharge: chemical characteristics of recharge waters and long term liabilities of recharge projects*. Proceedings of the second international symposium on artificial recharge of groundwater, p. 402-511, Florida.

Lee J.-Y., Lee K.-K. 2003. *Viability of natural attenuation in a petroleum-contaminated shallow sandy aquifer*. Environ. Pollution, no. 126, p. 201-212.

Legret M. 1998. *Simulation of heavy metal pollution from stormwater infiltration through a porous pavement with reservoir structure.* Novatech 1998 (3ème Conférence internationale sur les nouvelles technologies en assainissement pluvial), Lyon, France, 4-6 mai 1998.

Legret M., Colandini V. 1999. *Effects of a pavement with structure on runoff water: Water quality and fate of heavy metals.* Water Science and Technologies, vol. 39, no 2, p. 111-117.

Legret M., Colandini V., Le Marc C. 1995. *Impact d'une chaussée à structure réservoir sur la qualité des eaux pluviales et du sol*. Bulletin de liaison des Laboratoires des Ponts et Chaussées, n°197.

Legret M., Colandini V., Le Marc C. 1996. *Effects of a porous pavement with reservoir structure on the quality of runoff water and soil*. The Science of the Total Environment. 189/190 p. 335-340.

Legret M., Le Marc C., Demare D. 1997. *Pollution des eaux de ruissellement de chaussées autoroutières : L'autoroute A11 près de Nantes*. Bulletin des Laboratoires des Ponts et Chaussées, n° 211, septembre-octobre 1997.

Legret M., Paggoto C. 1999. *Evaluation of pollutant loadings in the runoff waters from a major rural highway.* The Science of the Total Environment, no 235, p. 143-150.

Legret M., Paggoto C. 2006. *Heavy metal deposition and soil pollution along two major rural highways.* Environmental Technology, vol. 27, p. 247-254.

Leroueil S., Le Bihan J.-P., Sebaihi S., Alicescu V. 2002. *Hydraulic conductivity of compacted tills from northern Quebec*. Canadian geotechnical J., vol. 39, no. 5, p. 1039-1049.

Li X., Poon C.-S., Liu P. S. 2001. *Heavy contamination of urban soil and street dust in Hong-Kong*. Applied Geochemistry, no. 16, p. 1361-1368.

Lin, C.-P. 2003. *Frequency Domain versus Traveltime analyses of TDR Waveforms for Soil Moisture Measurements*. Soil Sci. Soc. Am. J., 67: 720-729.

Lind Bo B., Karro E. 1995. *Stormwater infiltration and accumulation of heavy metals in roadside green areas in Goteborg, Sweden*. Ecological Engineering, vol. 5, p. 533-539.

Lindgren A. 1996. *Asphalt wear and pollution transport*. The Sci. of the Total Environ., no. 189/190, p. 281-286.

Lindgren, Å. 1996. *Asphalt wear and pollution transport*. Sci. Total Environ., vol. 189/190, p. 281–286.

Looser M. 1997. *Méthode de detection et de characterisation de pollutions du sous-sol par les sites contaminés, à l'aide des traceurs inorganiques*. PhD thesis.

Lozet J., Mathieu C. 1997. *Dictionnaire de science du sol*. Coll. Tec et Doc, Lavoisier, Paris.

Lygren E., Gjessing E., Berglind L. 1984. *Pollution transport from a highway*. The Science of the Total Environment, vol. 33, p. 147-159.

Maeght J.-L., Hammecker C. 2002. Dispositif expérimental pour le suivi de l'évolution physico-chimique des sols et la détermination de leurs paramètres hydrodynamiques au laboratoire. Actes de l'atelier du PCSI, CEMAGREF, CIRAD, IRD, Montpellier, France.

Maloszewski P., Zuber A. 1985. *On the theory of tracer experiments in fissured rocks with a porous matrix*. Journal of Hydrology, vol. 79, p. 333-358.

Mason Y., Ammann A. A., Ulrich A., Sigg L. 1999. *Behaviour of heavy metals, nutrients, and major components during roof runoff infiltration*. Environmental Science and Technology, vol. 33, p. 1588-1597.

Mathieu C., Pieltain F. 1998. *Analyse physique des sols: méthodes choisies*. Lavoisier, Paris.

McCarthy J. F. 1989. *Role of colloidal particles on subsurface transport of contaminants: five-year subprogram plan for U.S. Department of Energy Subsurface Transport Program*. DOE/ER-0384. U.S. Department of Energy, Washington, D.C. 48pp.

McCarthy J. F., McKay L .D. 2004. *Colloid transport in the subsurface: past, present and future challenges*. VZJ, no. 3, p. 326-337.

McCarthy J. F. 1989. *Mobility of colloidal particles in the subsurface: Chemistry and hydrology of colloid-aquifer interactions*. DOE/ER-0425. U.S. Department of Energy, Washington, D.C. 111pp.

Memon F. A., Butler D. 2005. *Characterisation of pollutants washed off from road surfaces during wet weather.* Urban Water Journal, vol. 2, issue 3, p. 171-182.

Mermoud, A. 1999. *Eléments de physique du sol*. Ed. H. G. A., Bucarest.

Mikkelsen P. S., Häfliger M. 1994. *Pollution from two infiltration systems for road runoff in Switzerland*. EAWAG.

Mikkelsen P. S., Häfliger M., Ochs M., Tjell J. C., Jacobsen P., Boller M. 1996. *Experimental assessment of soil and groundwater contamination from two old infiltration systems for road runoff in Switzerland*. The Sci. of the Total Environ., no. 189/190, p. 341-347.

Morgenthaler S. 1997. *Introduction à la statistique*. Presses Polytechniques et Universitaires Romandes Lausanne, 1997, Suisse.

Mualem Y. 1976. *A new model for predicting the hydraulic conductivity of unsaturated porous media*, Water Resour. Res., vol. 12(3), p. 513–521.

Mueller C., Boivin P. 2004. *Caractérisation physico-chimique des sols des talus d'infiltration du site de Corcelettes, Canton de Vaud*. VSS 2001/203, LPE, EPFL.

Muschack W. 1989. *Pollution of street Run-off by traffic and local conditions*. Science of the total environment. International symposium on highway pollution. 3, Munich , Germany, vol. 93, p. 419-431.

Muschack W. 1990. *Pollution of street-runoff by traffic and local conditions*, The Science of the Total Environment, vol. 93, p. 419-431.

Musy A., Soutter M. 1991. *Physique du sol*. Lausanne, Pr. polytechniques et universitaires romandes.

OCDE/OECD 1981 - 2000. *Guideline for the testing of chemicals – adsorption desorption using a batch equilibrium method*, 106.

OFEFP 1992. *Bodenverschmutzung durch des Strassen und Schienenverkehr in der Schweiz*.

OFEFP 2002. *Directive « Protection des eaux lors de l'évacuation des eaux des voies de communication »*. Collection l'environnement pratique. VU-2310-F.

OFEFP. *Gewässerschutzmassnahmen beim Strassenbau*, Grundlagenbericht, Schriftenreihe Umwelt N°263.

OFEG 2002. *Utilisation des traceurs artificiels en hydrogeologie.* Guide pratique. Rapports de l'OFEG, Série géologie, no. 3.

OFROU 1990. *Anteil des Fahrzeugkategorien in Abhängigkeit von Strassentyp*. Forschungauftrag 35/88.

Ould-Henia M., Hefti J.-J., Dumont A.-G. 2006. *Comportement mécanique des structure routières; cas de Grandson*. Rapport d'étude, LAVOC, EPFL.

Pagotto C. 1999. *Emission et transfert dans les eaux et les sols des elements traces métalliques et hydrocarbures dans le domaine routier*. PhD thesis.

Pagotto C., Legret M., Le Cloirec P. 2000. *Comparison of the hydraulic behaviour and the quality of highway runoff water according to the type of pavement*. Water Research, 34(18), p. 4446-4454.

Pagotto C., Legret M., Le Cloirec P. 2000. *Comparison of the hydraulic behaviour and the quality of highway runoff water according to the type of pavement*. Water Resources 34(18), p. 4446-4454.

Pagotto C., Remy N., Legret M., Le Cloirec P. 2001. *Heavy metal pollution of road dist and roadside soil near a major rural highway*. Environmental Technology, vol. 22, p. 307-319.

Parmentier C., Garrec J.-P. 1994. *Impact de la pollution atmosphérique le long des routes et autoroutes sur la végétation environnante : utilisation de la bio-indication végétale : synthèse bibliographique*. Ed. INRA.

Parriaux A., Bensimon M., Looser M. 1996. *Contribution and use of the high resolution plasma source mass spectrometry tecnique in environmental geology*. Analusis Magazine, vol. 24, no. 9/10, p. 16-18.

Parriaux A., Tarradellas J., Spack L., Bensimmon M. 1999. *Interaction entre les routes et l'environnement souterrain*, cahier OFROU N°426.

Penmann-Monteigh Food and Agriculture Organisation FAO equations. 1998.

Perrono P. 1999. *Les micropolluants métalliques des boues de stations d'épuration urbaine et l'épandage agricole*. Mém. D.U.E.S.S., D.E.P., Univ. Picardie, Amiens.

Petruzzelli L., Celi L., Cignetti A., Ajmone Marsan F. 2002. *Influence of soil organic matter on the leaching of polycyclic aromatic hydrocarbons in soils*. J. of Environ. Sci. And Health.

Pfister R. 1998. *L'évacuation des eaux de chaussées par infiltration dans le sol selon la législation suisse*. Mémoires du symposium international de l'Association mondiale de la route (AIPCR) sur le drainage interne des chaussées et couches de forme, Granada.

Price M. 1994. *Drainage from roads and airfields to soakways : groundwater pollutants or valuable recharge ?* J. Of the institute of Wat. and Environ. Management, no. 8, p. 468-479.

Ranchet J., Penaud F., Le Grand R., Constant A., Obry P., Soudieu B. 1995. *Comparing a block paving and a porous pavement from a hydraulic behaviour standpoint and their impact on stormwater pollution control*. International conference on innovative technologies in the domain of urban storm water drainage, no. 2, p. 635-639.

Reinirkens P. 1996. A*nalysis of emissions through traffic volume in roadside soils and their effects on seepage water*. The Science of the Total Environment, no. 189/190, p. 361-369.

Richard G., Cousin I., Sillon J. F., Bruand A., Guérif J. 2001. *Effect of compaction on the porosity of a silty soil: influence on unsaturated hydraulic properties*. European J. of soil Science, vol. 52 (1), p. 49-58.

Richter J. 1990. *Models for processes in the soil*. Catena paperback.

Rogge W. F., Hildemann L. M., Mazurek M. A., Cass G. R., Simoneit B. R. T. 1993. *Sources of fine organic aerosol. 2) Noncatalyst and catalyst-equipped automobiles and heavy-duty diesel trucks*. Environ. Sci. Technol, no. 27, p. 636-651.

Roseen M., Thomas P., Ballestero J., Houle J. 2006. *The UNH Stormwater Center: measuring the effectiveness of stormwater best management practices and technologies*. Proceeding NNECAPA annual meeting.

Roth C. H., Malicki M. A., Plagge R. 1992. *Empirical evaluation of the relationship between soil dielectric constant and volumetric water content as the basis for calibrating soil moisture measurements by TDR*. J. Soil Sci., no. 43, p. 1-13.

Rousseau M., Di Pietro L., Angulo-Jaramillo R., Tessier D., Cabibel B. 2004. *Preferential transport of soil colloidal particles, physicochemical effects on particle mobilization* . VZJ, no. 3, p. 247-261.

Ryan J. N., Gschwend P.M. 1990. *Groundwater colloids in two Atlantic Coastal Plain aquifers: Field studies*. Water Resources Research, no. 26, p. 307-322.

Saget A., Chebbo G., Desbordes M. 1995. *Urban discharges during wet weather: what volumes have to be treated?* Water Science and Technology, vol. 32, no. 1, p. 225-232.

Sansalone J. J., Buchberger S. G. 1996. *Characterization of metals and solids in urban highway snow and rainfall-runoff*. Transportation Research Record, 1523, p. 147-159.

Sansalone J. J., Buchberger S. G. 1997. *Characterization of particulate loading in the urban storm water first flush*. Water Science and Technology, vol. 36, no. 9, p. 155-160.

Sansalone J. J., Buchberger S. G. 1997. *Partitioning and first flush of metals in urban storm water*. ASCE J. of Environmental Engineering, vol. 123, no. 2, p. 134-143.

Sansalone J. J., Buchberger S. G. and Al-Abed S. 1996. *Fractionation of heavy metals in pavement runoff first-flush*. The Science of the Total Environment, 189-190, p. 175-183.

Sansalone J. J., Buchberger S. G., Koechling M. 1995. *Correlations between metals and suspended solids in runoff*. Transportation Research Record, 1483, p. 112-119.

Sansalone J. J., Buchberger S. G., Koran J., Smithson J. 1997. *Relationship between particle size and surface area of roadway solids*. Transportation Research Record, 1601, p. 95-98.

Sansalone J. J., Cristina, C. M. 2004. *First flush concepts for suspended and dissolved solids in small impervious watersheds*. ASCE J. of Environmental Engineering, vol. 130, no. 11.

Sansalone J. J., Glenn D. W. 2000. *Temporal variation in heavy metal partitioning and loading in urban highway pavement sheet flow – Implications of in-situ treatment design*. J. of Transportation Research Record, 1720, p. 100-111.

Sansalone J. J., Smithson J., Koran J. 1998. *Development and testing of a partial exfiltration trench for treatment of urban runoff*. Transportation Research Record, 1647, p. 34-42.

Schlaepfer D., Hugi C., Zysset A. 1996. *Gewässerschutzmassnahmen beim Strassenbau*. Basler and Partner AG, OFEFP, Schriftnereihe Umwelt no. 263.

Schnegg P.-A. 2003. *A new field fluorometer for multi-tracer tests and turbidity measurement applied to hydrogeological problems*. Proc. of the 8th International Congress of the Brazilian Geophysical Society, Rio de Janeiro, Brazil

Schnegg P.-A., Costa R. 2003. *Tracer tests made easier with field fluorometers*. Technical note. Bull. Hydrogeol. No. 20.

Schraps S., Opperhuizen A. 1989. *Quantifying the sorption of organic chemicals on sediments*. Chemosphere, no. 18, p. 1883-1893.

Simoneit B. R. T. 1986. *Characterization of organic constituents in aerosols in relation to their origin and transport: a review*. International J. of Environ. Analystical Chemistry, vol. 23, p. 207-237.

Simunek J., Jarvis N. T., Van Genuchten M. T., Gärdened A. 2003. *Review and comparison of models for describing non-equilibrium and preferential flow and transport in the vadose zone*. J. Hydrol., no. 272, p. 14-35.

Smith J., Sievers K. 2000. *Occurrence and phase distribution of polycyclic aromatic hydrocarbons in urban storm-water runoff*. Water Science & Technology, vol 42, no 3-4, p. 383–388.

Spangberg A. 1994. *Storm water quality measured by turbidity*. Rep. no. 3179, Dept. of Water Resources Eng, Lund Inst. of Tech./ U. of Lund. 84 p.

Spangberg A., Niemczynowicz J. 1993. *Measurements of pollution wash-off from an asphalt surface*. Dept. of Water Resources Eng., Univ. of Lund, Sweden. p. 423-428.

Squillace P. J., Pankow J. F., Korte N. E., Zogorski J. S. 1997. *A review of the environmental behaviour and fate of MTBE*. Journal of Environmental Toxicology and Chemistry, vol. 16, no. 9, p. 1836-1844.

Stahre P., Urbonas B. 1990. *Stormwater detention for drainage, water quality, and CSO management*. Prentice Hall, Englewood Cliffs, NJ.

Startin J., Landsdown R. 1994. *Drainage from highway and other paved areas: methods of collection, disposal and treatment*. J. of the institute of Wat. And Environ. Management, no. 8, p. 518-526.

Stotz G. 1987. *Investigations of the properties of the surface water run-off from federal highways in the FRG*. Sci. Total Environ., vol. 59, p. 329–337.

Stotz G., Krauth K. 1994. *The pollution of effluents from pervious pavements of an experimental highway section: first results*. The Sci. of the Total Environ., vol. 146/147, p. 465-470.

Strecker E., Driscoll E., Shelley P., Gaboury D. 1987. *Characterization of pollutants loadings from highway runoff in the USA*. Fourth international conference on urban storm drainage, Lausanne, p. 85-90.

Tebaay R. H. 1994. *Untersuchungen zu Gehalten, zur mikrobiellen Toxizität und zurm Adsorption und Löslichkeit von PAKs und PCBs in verschiedenen Böden Nordrhein-Westfa- lens*. Bonner Bodenkundl. Abhandlungen Bd., no. 14, p. 262.

Topp G. C., Davis J. L., Annan A. P. 1980. *Electromagnetic determination of soil water content: measurements in coaxial transmission lines*. Water Resources Research, no. 16, p. 574-582.

Topp G. C., Davis J. L., Bailey W. G., Zebchuk W. D. 1984. *The measurement of soil water content using a portable TDR hand probe*. Can. J. Soil Sci., vol. 64, p. 313–321.

Totsche K. U., Kögel-Knaber I. 2004. *Mobile organic sorbent affected contaminant transport in soil: numerical case studies for enhanced and reduced mobility*. VZJ, no. 3, p. 352-367.

Turer D., Maynard B. J., Sansalone J.J. 2001. *Heavy metal contamination in soils of urban highways: comparison between runoff and soil concentrations*. J. of Water, Air and Soil Pollution, vol. 132, no.3, p 214 – 230.

Van Genuchten M. T. 1980. *A closed-form equation for predicting the hydraulic conductivity of unsaturated soils*. Soil Sci. Soc Am. J., vol. 44, p. 892–898.

Van Genuchten M. T., Wierenga P. J. 1976. *Mass transfer studies in sorbing porous media: I) Analytical solutions*. Soil Science Society of America Journal, vol. 40, p. 473-480.

Van Genuchten M.T. 1980. *A closed-form equation for predicting the hydraulic conductivity of unsaturated soils*. Soil Sci. Soc. Am. J., vol. 44, p. 892–898.

VSA 2002. *Richtlinie zur Versickerung, Retention und Ableitung von Niederachlagswasser in Siedlungsgebieten*.

VSS. *Evacuation des eaux de chausses – intensité des pluies*, SN 640 350

Walter T., Ederer H. J., Forst C., Stieglitz L. 2000. *Sorption of selected polycyclic aromatic hydrocarbons on soils in oil-contaminated systems*. Chemosphere, vol. 41, p.387-397.

Wan J., Wilson J. L. 1994. *Visualization of the role of the gas-water interface on the fate and transport of colloids in porous media*. Water Resour., vol. 30, p. 11-23.

Wanielista M.P., Yousef Y.A. 1993. *Stormwater management*, Eds J.Wiley and Sons, New York.

Wiedemeier T. H., Rifai H. S., Newell C. J., Wilson J. T. 1999. *Natural attenuation of fuels and chlorinated solvents in the subsurface. Eds* J. Wiley & Sons, New York.

Wild S. R., Berrow M. L., Jones C. K. 1991. *The persistence of polycyclic aromatic hydrocarbons in sewage sludge amended agricultural soils*. Environ Pollut, vol. 72, p. 141-157.

Wood A. L., Bouchard D. C., Brusseau M. L. Rao P. S. C. 1990. *Cosolvent effects on sorption and mobility of organic contaminants in soils*. Chemosphere, vol 21, p. 575-587.

Xanthopoulos C., Hahn H. H. 1994. *Priority pollutants from urban runoff into the environment*. European Water Pollution Control, vol. 4, no. 5.

Zhou Y. M., Liu R. X., Tang H. X. 2004. *Kinetics study of aqueous sorption of phenanthrene to humic acids and sediments*. Journal of Environmental Sciences, vol. 16, no. 3, p. 408-413.

Zysset A., Basler E. 1996. *Nouvelles directives concernant l'assainissement des eaux sur les routes*. Résumé de l'étude « Strassenentwässerung ». OFEFP.

LIST OF FIGURES

LIST OF TABLES

APPENDICES

APPENDIX I LEGISLATION: SWISS LAWS, ORDINANCES AND DIRECTIVES

Swiss legislation specifies that surface waters that are not polluted must be infiltrated wherever it is possible (Hartmann & Michel 1992) (see appendix II for conditions), while polluted waters must be treated (LEaux 1991, art.7, OEaux 1998). The application of this general concept to road runoff (Pfister 1998) leaded to the redaction of a directive project written by the Swiss Confederation (OFEFP, now OFEV, 1996). Road runoff was therefore considered as not polluted and handled in the following priority:

- Diffuse over the shoulder infiltration,
- Centralized infiltration (bio-active ponds, retaining lakes, etc)
- Centralized infiltration (wells or trenches cutting the unsaturated zone)
- Retention and distribution in the surface water network

Although nowadays the resulting handling process is the same, road runoff is considered polluted. Soil plays the filtering role (OFEFP 2002, appendix II). Criteria for infiltration admissibility are thoroughly described in appendix II. Surrounding soils used as filters will not be submitted to the OSol regulation.

I.1 Here are the main legal bases of the present research:

- Federal laws
  - Federal law on Water protection, January 24th 1991, LEaux, RS 814.20
  - Federal law on Environment protection, October 7th 1983, LPE, RS 814.01
  - Federal law on National road, March 8th 1960, RS 725.11

- Federal Ordinances
  - Ordinance on Main roads, April 8th 1987, RS 725.116.23
  - Ordinance on Water protection, October 28th 1998, OEaux, RS 814.201
  - Ordinance on Polluted water distribution, December 8th 1975, ODEU
  - Ordinance on Water protection against alien products, September 28th 1981, OPEL, RS 814.226.21
  - Ordinance on Pollutants in soil, June 9th 1986, OSOL, RS 814.12
  - Ordinance on Protection against major accidents, February 27th 1991, OPAM, RS 814.012
  - Ordinance on Dangerous compounds for the environment, June 9th 1986, rev. January 1st 1996, OSUBST

- Directives
  - Directives on the preventive treatment and distribution of residual waters coming from automobile sector buildings, December 1987, OFEFP.
  - Practical instructions for the delimitation of underground water protection sectors, zones and perimeter, October 1977, rev. 1982, OFEFP.
  - Directive for water protection during evacuation of communication ways runoffs, OFEFP 2002.

I.2 Underground water protection sectors, zones and perimeter:

Water protection zones
OEaux appendix 4 ch.

221 Distal protection zone S3
[1]Are not authorized in the S3 zone:
c. infiltration of runoffs, excepting unpolluted water coming from the roofs. Infiltration must be conducted through a vegetation covered layer.

222 Proximal protection zone S2
[1]Exigences from 221 are applicable. Moreover are forbidden:
c. infiltration of runoffs

223 Catchment facility S1
In this zone only construction and works related to exploitation of the aquifer is authorized. (…)

23 Underground water protection perimeter
[1]Construction and other activities executed in the underground water protection perimeter must satisfy the exigencies fixed in 222.

A_U protection zone: designated to protect exploitable groundwater
A_0 protection zone: designated to protect surface water, if it is necessary to guarantee a particular use of that water
Z_U alimentation area is designated to protect the water quality alimenting the public catchment area, existing or forecasted, if the water quality is contaminated by substances which degradation or retention are insufficient, or if those substances represent a real pollution danger.
Z_0 alimentation area is designated to protect superficial water, if that water is contaminated by phytosanitarian (...) or fertilizing products, carried by the runoff.

APPENDIX II OFEV DIRECTIVE

OFEV Directive 2002 – Main frame – Water Protection during evacuation of communication ways runoffs.
"Protection des eaux lors de l'évacuation des eaux des voies de communication", OFEV, 2002

Translation could have somewhat altered the original German text. Here are presented only the specific simplified paragraphs helping the comprehension of the present study. For an extensive comprehension of the Swiss Legislation, please see the original text.

II.1 Objectives:

The 2002 directive main goal is to offer a legal frame to choose the best suitable runoff evacuation system for each particular case. The following must be considered: legal context, local feasibility and principle of proportionality. The directive must apply to all existing and future communication ways.

II.2 Definitions:

Communication ways implies railways, roadways, runways and parking lots. Runoff means free water flowing over the communication ways and able to mobilize the pollutants and compounds deposited by the usual traffic.

II.3 Limitations:

1) National airports
2) Land, bush and forest ways
3) Places with frequent transportation, loading and unloading of dangerous substances
4) Construction site runoffs
5) Underground site runoffs
6) Major accidents

II.4 Legal basis:

1) LEaux 1991
2) LPE 1983
3) OEaux 1998
4) OPAM 1991
5) OSol 1998

Legal basis texts are presented in appendix I.

II.5 Pollutants:

Important substances identified in the basic report "Gewässerschutzmassnahmen beim Strassenbau" (Water protection means during road construction).

Substance	Origin / properties	railways	runways (airport)	roadways	limit values [mg/l]
Cadmium Cd	Tyres and brake wearing. Most dangerous heavy metal for public health; toxic action on Human, plants and animals.	1Δ	1	1	ES: 0.0002 (total) ET: p/e LT: 0.005
Chlorine Cl	Found in all common anti freezing products, salts etc; very soluble, low toxicity. Corrosion effects.	0	0	1	ES: p/e ET: 40
Chromium Cr	Brake wearing and lubricating products; toxic action on Human and animals.	1Δ	1	1	ES: 0.005 (total) ET: p/e LT: 0.02
Copper Cu	Brakes and contact lines; toxic at high concentration for Human, animals and plants.	1	1Δ	1	ES: 0.005 (total) ET: p/e LT: 1.5 (tolerated)
Zinc Zn	Gasoline, road wearing and leaks. Most commonly found in road runoff. Toxic action on plants.	1Δ	1	1	ES: 0.02 (total) ET: p/e LT: 5 (tolerated)
Lead Pb	Tyres wearing. Tends to disappear in the past few years but is very persistent in soils.	0	1Δ	1Δ	ES: 0.01 (total) ET: p/e LT: 0.01
Ammonium (sum of NH_4-N and NH_3-N)	Anti freezing products. Could transform in nitrites and become very toxic for Human, animals and plants.	0	1	0	ES: 0.2-0.4 depending on T°C ET: 0.08 (oxidant) 0.4 (reducting)

Substance	Origin / properties	railways	runways (airport)	roadways	limit values [mg/l]
Gasoline additives	Gasoline additives to enhance the combustion process. Variation in toxicity depending on the type.	0	0	1Δ	
Dissolved organic carbon (DOC)	Global index of nocive substances coming from the gasoline, leaks and wearing course.	1	1	1	ES: 1-4 depending on natural pollution ET: 2
Herbicides	Possible utilisation in specific road segment.	1Δ	0	1Δ	ES: 0.0001 ES: 0.0001 depending on substance
PAH	Gasoline rests, leaks; toxic and carcinogenous effect on Human and animals.	1	1	1	ES: p/e ET: 0.0001

Table II.1: Main substances found in the "Gewässerschutzmassnahmen beim strassebau" study.
(1): Presence in the communication ways runoff. Possible effect on water quality
(0): Non significant presence
Δ: increasing or decreasing tendency
ES: Quantitative requirements for superficial water; OEaux annexe 2 Ch. 12
ET: Quantitative requirements for underground water, OEaux annexe 2 Ch. 22
LT: Limit values for drinkable water; Alien substances and compounds Ordinance OSEC
p/e: no specific quantitative requirement; OEaux annexe 2

II.6 Special frame for the present study:

The present study concerns only the simplest case described in the OFEV directive, i.e. over the shoulder diffuse infiltration. Are not concerned:

1) infiltration with specific treatment installation
2) runoff conducted to superficial water streams
3) runoff conducted to superficial water streams after retention
4) runoff conducted to superficial water streams after retention and treatment
5) runoff conducted to public treatment plants

II.7 Feasibility examination:

The feasibility examination concerns the following:

1) Hydrogeological factors (water quantity, infiltration capacity, layer thickness, alluvial aquifer level during wet season)
2) Geographic and topographic factors (surface availability, communication way conception, legislation (neighbourhood rights))

II.8 Water evacuation admissibility:

1) Level of pollution; ranking based on evaluation points EP. See table 2.

Appreciation factor	Evaluation criterium	Points EP
Traffic charge		
Daily traffic	Roads: EP = number of vehicles per day /1000	[+EP]
Traffic composition		
Traffic part > 2.5t	Roads: EP = 2 if part > 8%; EP = 1 if part > 4%	[+EP]
Segment slope	Road slope > 8%	[+1]
Communication ways maintenance		
Plants treatment	Products for plant treatment used once a year on segment	[+1]
Usual road/runway wiping/ cleaning	Number of mechanical cleaning per month	[-EP]
	SUM	…

Table II.2: EP for traffic charge.

Ranking of total level of pollution	
low	< 5
average	5 to 14
high	> 14

Table II.2 (continuing): Traffic charges and corresponding evaluation points.

2) Underground water vulnerability

Vulnerability of underground water is a measure of the sensibility to qualitative risk from surface influence. Underground water vulnerability is determined by soil thickness, nature and extension and by the unsaturated zone. Generally, infiltrated water is purified by the soil during infiltration. The better the filtration and purification is, the lower the vulnerability is. Three types of aquifers are considered:

a. Unstable rock aquifer: vulnerability is low to high. Vulnerability is low in case the soil thickness is great and made of fine particles with humus. Vulnerability is high if the soil thickness is small and made of coarse material.
b. Karstic aquifer: vulnerability is generally average to high due to the low evolution of overlaying soils. Vulnerability is very high when a direct connection exists between the surface and the aquifer.
c. Fissured aquifer: vulnerability ranges from low to high depending on the overlaying soils.

The optimal soil structure for pollution retention depends on:

a. Thickness of A and B horizons. The filtering capacity is proportional to the soil thickness
b. Clay content. A high content may fix the heavy metals but also may reduce the infiltration capacity.
c. Humus content. Humus plays a crucial role in fixing and degrading the organic compounds like PAH.
d. pH values. High values help to fix the heavy metals in soils.

An optimal soil is therefore 1m thick, has a clay content of 10 to 35%, a humus content of >4% and high pH >6.5. Table 3 summarizes the important factors and associated values. Insufficient optimal

Structure	A horizon								B horizon				
	Thickness [cm]		pH		Humus content [%]		Clay content A [%]		Thickness [cm]		Humus content [%]		Clay content [%]
Optimal	≥ 30	*and*	≥ 6.5	*and*	≥ 4	*and*	10 < A < 35	*and*	≥ 70	*and*	≥ 1	*and*	10 < A < 35
Average	≥ 20	*and*	≥ 5.5	*and*	≥ 2	*and*	10 < A < 35	*and*	≥ 30	*and*	≥ 1	*and*	10 < A < 35
Minimal	≥ 10	*and*	≥ 5.5	*and*	≥ 2	*and*	10 < A < 35	*and*	≥ 20	*and*	≥ 1	*and*	10 < A < 35
Insufficient	In case of non respect of the minimal condition												

Table II.3: Optimal, average and minimal soil requirements in case of runoff infiltration.

3) Unsaturated zone consideration

The unsaturated zone also influences the vulnerability of underground water. It has its own filtering and retentive capacity. While simplifying, 3 classes are discerned:

a. Unsaturated zone with high infiltration and absorption capacities, i.e. unstable rock with fine granulometry like clay, silts, or fine sand (lacustrine deposit, alluvial deposit, basement till, etc.)
b. unsaturated zone with average infiltration and absorption capacities, i.e. unstable rock with coarse granulometry like sandy gravel (alluvial gravel, gravel moraines) and solid fissured rock.
c. Unsaturated zone with low or null infiltration an absorption capacities, i.e. cristallin and metamorphic rock (granit, gneiss etc.).

4) Global evaluation of underground water vulnerability

Table 4 summarizes the global underground water vulnerability. The minimal basic requirement is a cumulative soil and unsaturated zone thickness of one meter. In case this thickness is not reached, vulnerability must be raised of one degree at least. On the other hand, if the unsaturated zone thickness reach many meters, further investigations must be conducted in order to lower the vulnerability degree.

Underground water vulnerability				
Structure of the unsaturated zone (thickness > 1m)	**Soil structure** (see table 3)			
	Optimal	Average	minimal	Unsufficient
unsaturated zone type a.	**low**	**low**	**average**	**high**
unsaturated zone type b.	**low**	**average**	**high**	**high**
unsaturated zone type c.	**average**	**high**	**high**	**very high**

Table II.4: Underground water vulnerability

5) Global infiltration admissibility integrating pollution level and underground water vulnerability.

The global admissibility in based on the different factors previously mentioned. Table 5 presents the final considerations.

Infiltration				
Water protection zone/sector	**Underground water vulnerability** (see table 4)	**Pollution level ranking** (see table 2)		
		low	**average**	**high**
Other sector	low	admissible	admissible	admissible
	average	admissible	admissible	admissible
	high	admissible	with treatment	with treatment
	very high	with treatment	with treatment	with treatment
Protection sector A_u	low	admissible	admissible	admissible
	average	admissible	admissible	with treatment
	high	with treatment	with treatment	with treatment
	very high	with treatment	with treatment	with treatment
Protection zone and perimeter		not admissible	not admissible	not admissible

Table II.5: Global infiltration admissibility. Note that in protection zone and perimeter no infiltration at all is tolerated.

APPENDIX III INFILTRATION TEST, TRENCHES AND BOREHOLES LOGS

III.1 Infiltration tests

Porchet infiltration tests 11.02.2002

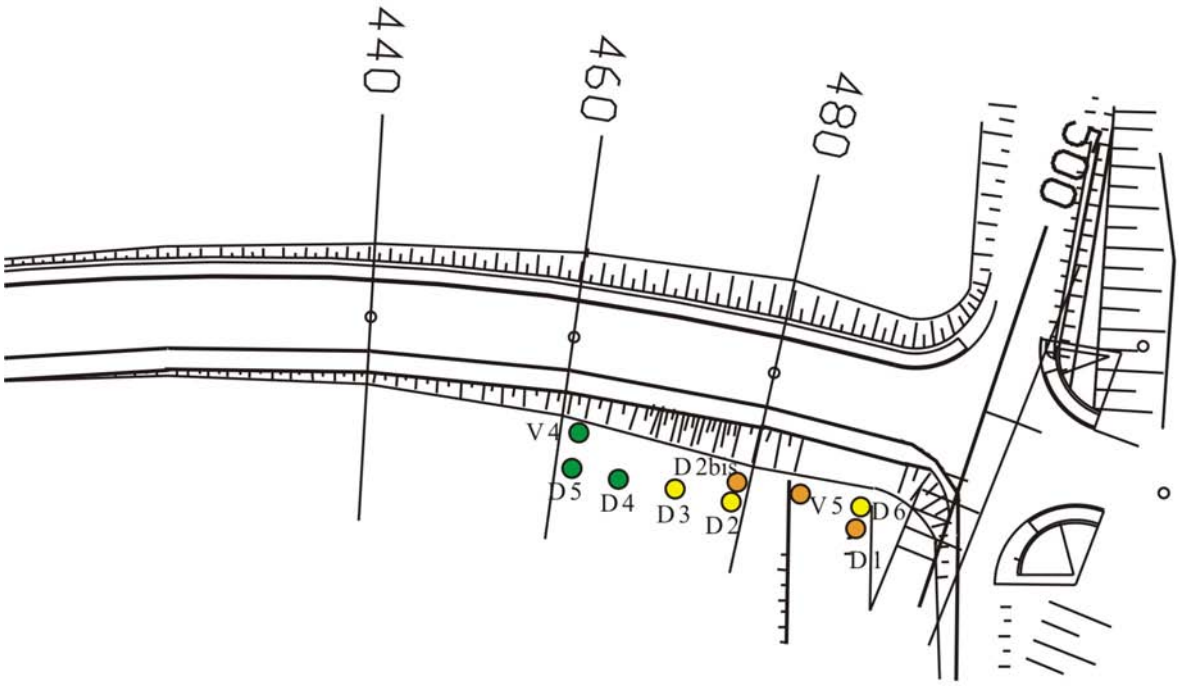

Drawdown [cm]	D1	D2	D2bis	D3	D4	D5	D6	V4	V5
0-1 h	27	41.5	20	35	25	18	16	14.5	92
20 mn – 1 h	9.5	11.5	5.5	7.5	3	4	4.5	2	Vide à 45 mn
K Porchet $m.s^{-1}$	2.10^{-6}	$1{,}73.10^{-6}$	$1{,}38.10^{-6}$	7.10^{-7}	$2{,}7.10^{-7}$	$6{,}9.10^{-7}$	$1{,}38.10^{-6}$	$1{,}07.10^{-7}$	$1{,}04.10^{-5}$

Mean drawdown
Average ranging from 20 to 60 minutes

> 4 cm
= 8 cm
< 8 cm

III.2 Trenches logs

OFROU Service des routes	Ecole Polytecnique Fédérale de Lausanne GEOLEP-Laboratoire de géologie de l'ingénieur et de l'environnement	
Date : 23.10.2002		Fouille : 1

Fouille 1 : Sol Brun Calcaire alluvial à Gley
Aquifère dans les graviers jurassiens

Visualisation

	Profil	Description lithologique	Formation
0,35		horizon A, limon sableux carbonaté	alluvion fine
0,75		horizon B, limon sableux carbonaté	
0,95		lentille de graviers à galets jurassiens mal classés	alluvion
1,35		argile limoneuse gris-noire globalement réduite localement oxydée dans les fentes à morceaux de bois et inclusions noires de charbon et à galets jurassiens : horizon décarbonaté	gley palustre
		traces rouilles d'oxydo-réduction du fer dans la zone de battement de la nappe	
2		gravier calcaire gris bien calibré dans matrice argilo-sableuse gris foncée de plus en plus humide : gravier jurassien	alluvion
2,10		gravier calcaire orangé bien classé, saturé en eau : gravier jurassien	
2,50			

Localisation

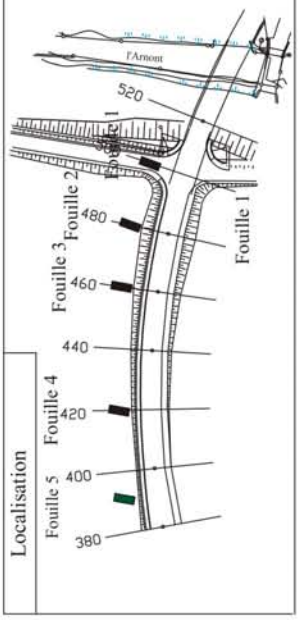

OFROU Service des Routes	Ecole Polytecnique Fédérale de Lausanne GEOLEP-Laboratoire de géologie de l'ingénieur et de l'environnement	
Date : 23.10.2002		Fouille 2

Fouille 2: Sol Brun Calcaire alluvial
Aquifère dans les graviers jurassiens

Visualisation

	Profil	Description lithologique	formation
0,30		horizon A, limon sableux carbonaté	alluvion fine
1 1,00		horizon B, limon sableux peu carbonaté, en partie colluvionné, peu d'hydromorphie	
1,20		horizon Br : argile grise faiblement carbonatée contenant quelques graviers, restes de matière organique diffus, traces de charbon, un peu d'hydromorphie	gley palustre
1,60		gravier calcaire gris bien calibré dans matrice argilo-sableuse gris foncée de plus en plus humide : gravier jurassien	graviers aquifères
1,70		évolution progressive vers des gros galets	
2 2,10		gravier calcaire orangé bien classé, à matrice plus grossière sableuse à traces de rouille : gravier jurassien zone en partie saturée	
2,50		moraine de fond compacte rhodanienne ou alpine	moraine de fond
3			

Localisation

OFROU Service des Routes	Ecole Polytecnique Fédérale de Lausanne GEOLEP-Laboratoire de géologie de l'ingénieur et de l'environnement	
Date : 23.10.2002		Fouille 3

Fouille 3 : Sol Brun, terre végétale labourée pas d'arrivée d'eau

Visualisation

Moraine de fond

Profil	Description lithologique	formation
0,30	horizon A, limon sableux, terre végétale labourée	alluvion fine
0,35	zone de transition, loess	moraine de fond décom-primée
0,75	sable limono graveleux à galets	
1		
2	sable limono graveleux à galets de plus en plus compact 20 à 30 % de carbonates	moraine de fond
0,7		
3		

Localisation

OFROU Service des Routes	Ecole Polytecnique Fédérale de Lausanne GEOLEP-Laboratoire de géologie de l'ingénieur et de l'environnement	
Date : 23.10.2002		Fouille 4

Fouille 4 : Sol Brun, terre végétale labourée

Visualisation

	Profil	Description lithologique	formation
0,30		horizon A, limon sableux, terre végétale labourée	alluvion fine
1,20		loess éolien d'origine géologique ayant subi une pédogénèse endohydromorphie et formation de chenaux avec des recarbonatations dans les chenaux épaisseur variable	loess éolien
2		sable limono graveleux à galets compact	moraine de fond
3,00			

Localisation

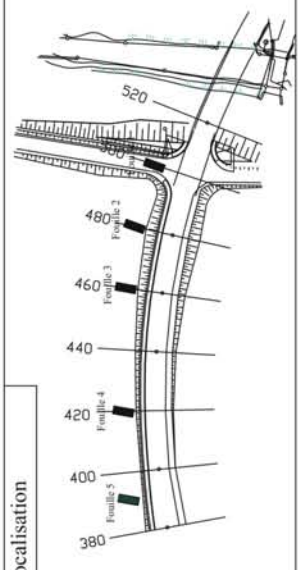

OFROU Service des Routes	Ecole Polytecnique Fédérale de Lausanne GEOLEP-Laboratoire de géologie de l'ingénieur et de l'environnement	
Date : 23.10.2002		Fouille 5

Fouille 5 : Sol Brun, terre végétale labourée
Pas de nappe

Visualisation

Profil	Description lithologique	formation
0,30	horizon A, limon sableux, terre végétale labourée	alluvion fine
0,60	horizon B : sable limoneux à concrétions rouilles d'hydromorphie	
1	sable limono graveleux grossier à galets compact	moraine de fond
1,60	drain en terre cuite	
2		
3		

Localisation

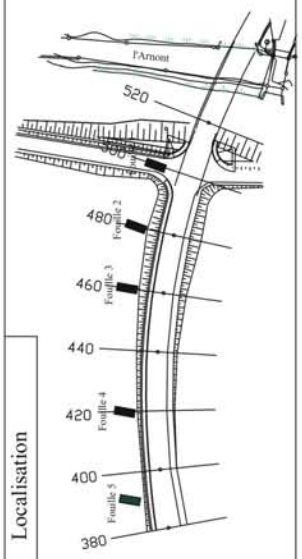

III.3 Drillholes logs

Sondage carotté	Ecole Polytechnique Fédérale de Lausanne GEOLEP - Laboratoire de géologie de l'ingénieur et de l'environnement	
Service des Routes - Routes Nationales Date : 10.09.2002		Sondage : S02-1
Entreprise : Fortini SA Sondeur : M. Carlos	Equipement : Piézomètre 4"1/2	

Profondeur (m)	Profil	Visualisation	Description lithologique	Formation géologique	Carottie	Méthode de sondage	Revêtement	Niveau d'eau	Equipement
0,45			Limon sableux carbonaté brun clair, horizon A	sol					bouchon d'argile
0,83			Limon sableuxcarbonaté brun beige à éléments grossiers: horizon B						
0,96			Limon argileux à galets						
1			Galet calcaire jurassien						
1,06			Limon argileux brun foncé peu compact à nombreux graviers jurassiens		180				1,20
1,43									
2			Gravier calcaire jurassien bien calibrés dans matrice argilo sableuse à galet	alluvion		Rot			
			Limon gris clair localement beige à lits sableux gris						
			Sable fin limoneux marron à lits plus limono-argileux						
3			Sable limoneux gris clair peu compact	moraine décom-primée					
3,10									3,20
4			Sable limono-graveleux compact à galets	moraine de fond	160				
4,20									
5									

Sondage semi-destructif	Ecole Polytechnique Fédérale de Lausanne GEOLEP - Laboratoire de géologie de l'ingénieur et de l'environnement	
Service des Routes - Routes Nationales Date : 10.09.2002		Sondage : S02-2
Entreprise : Fortini SA Sondeur : M. Carlos	Equipement : Piézomètre 4"1/2	

Profondeur (m)	Profil	Visualisation	Description lithologique	Formation géologique	Carotti	Méthode de sondage	Revêtement	Niveau d'eau	Equipement
0,15			Limon sableux carbonaté brun, horizon A						bouchon d'argile
			Limon sableux carbonaté brun beige peu hydromorphe à concrétions blanches, horizon B	sol					
0,64			Argile limoneuse brun à foncée noire à traces de charbon et galets jurassiens de diamètre centimétrique	gley palustre					
1			Gravier calcaire jurassien gris, bien classé, arrondi (diamètre centimétrique) dans matrice sablo argileuse gris foncée, non cohésif	alluvion	180				1,36
2									
2,08			Gravier calcaire jurassien gris orangé bien classé dans matrice plus argileuse brun beige, non cohésif			Rot			
2,23			Gravier et galet bien classés dans matrice sableuse peu limoneuse beige, non cohésif						
2,87									
3			Sable limoneux gris clair peu compact	moraine décom-primée					
3,10									3,36
			Limon gris beige compact à graviers, cohésif	moraine de fond	160				
4									
4,36									
5									

Sondage carotté	Ecole Polytechnique Fédérale de Lausanne GEOLEP - Laboratoire de géologie de l'ingénieur et de l'environnement	
Service des Routes - Routes Nationales Date : 10.09.2002		Sondage : S02-3
Entreprise : Fortini SA Sondeur : M. Carlos	Equipement : Piézomètre 4"1/2	

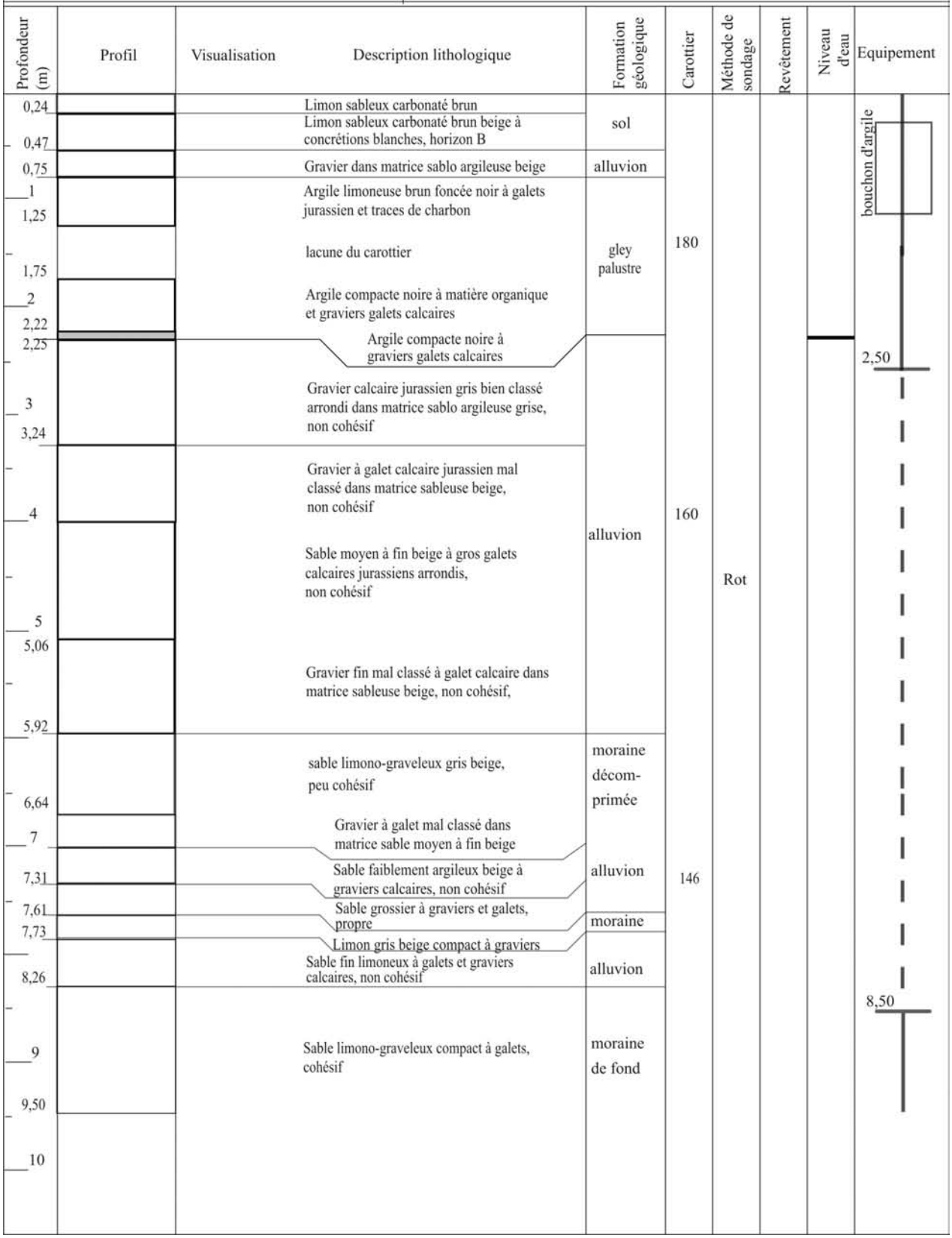

Sondage carotté	Ecole Polytechnique Fédérale de Lausanne GEOLEP - Laboratoire de géologie de l'ingénieur et de l'environnement	
Service des Routes - Routes Nationales Date : 10.09.2002		Sondage : S02-4
Entreprise : Fortini SA Sondeur : M. Carlos	Equipement : Piézomètre 4"1/2	

Profondeur (m)	Profil	Visualisation	Description lithologique	Formation géologique	Carottier	Méthode sondage	Revêtement	Niveau d'eau	Equipement
0,29			Limon sableux carbonaté brun, horizon A						
0,58			Limon sableux carbonaté brun beige peu hydromorphe, horizon B	sol					
1			Limon sableux beige à galets jurassiens arrondis	alluvion					
1,45			Argile limoneuse brun foncée compacte à traces de charbon et galets jurassiens	gley	180				bouchon d'argile 1,30
2			Sable grossier gris beige à graviers calcaires jurassiens gris (diamètre centimétrique), non cohésif						
2,38			Galet calcaire jurassien gris bien classé arrondi (diamètre 5 cm) dans matrice sablo argileuse beige, peu cohésif	alluvion					
2,66			Gravier galet bien classé dans matrice sableuse peu limoneuse, saturé d'eau						
3			Gravier à galet bien classé dans matrice sableuse peu limoneuse beige						
3,19			Gravier calcaire dans matrice sableuse gris noire, non cohésif						3,30
3,67					160	Rot			
4			Sable limono-graveleux compact gris beige à graviers	moraine					4,50
4,77			Sable moyen beige à gros galets						
5				alluvion					
5,02			Gravier à galet dans matrice sablo argileuse, non cohésif						
5,16									5,30
7			Sable limono-graveleux compact à galets, cohésif	moraine de fond	146				
7,30									
9									
10									

Sondage semi destructif	Ecole Polytechnique Fédérale de Lausanne GEOLEP - Laboratoire de géologie de l'ingénieur et de l'environnement	
Service des Routes - Route Nationale Date : 10.09.2002		Sondage : S02-5
Entreprise : Fortini SA Sondeur : M. Carlos	Equipement : Piézomètre 4"1/2	

Profondeur (m)	Profil	Visualisation	Description lithologique	Formation géologique	Carottier	Méthode de sondage	Revêtement	Niveau d'eau	Equipement
0,23			Limon sableux carbonaté brun, horizon A						
			Limon sableux carbonaté brun beige peu hydromorphe, horizon B	sol					
0,63			Gravier galet calcaire dans matrice sablo argileuse beige	alluvion					
0,81									
1			Argile limoneuse brun foncée noir à traces de charbon et galets jurassien	gley palustre	180				
1,05			Argile sableuse compacte à traces d'oxydation						
1,37			Gravier calcaire jurassien gris dans matrice sablo limoneuse beige, non cohésif						
2				alluvion		Rot			
2,20			Gravier à galet calcaire jurassien dans matrice sablo argileuse brune, non cohésif						
2,64									
2,91			Gravier calcaire gris bien classé dans matrice sablo argileuse beige						
3			Limon argileux gris beige à graviers, peu compact	moraine décompri-mée					
3,10					160				
			Galet calcaire dans matrice sablo argileuse, non cohésif	alluvion					
3,67									
4			Sable limono-graveleux compact à galets, cohésif	moraine de fond					
4,57									
5									

Sondage carotté	Ecole Polytechnique Fédérale de Lausanne GEOLEP - Laboratoire de géologie de l'ingénieur et de l'environnement	
Service des Routes - Routes Nationales Date : 10.09.2002		Sondage : S02-6
Entreprise : Fortini SA Sondeur : M. Carlos	Equipement : Piézomètre 4"1/2	

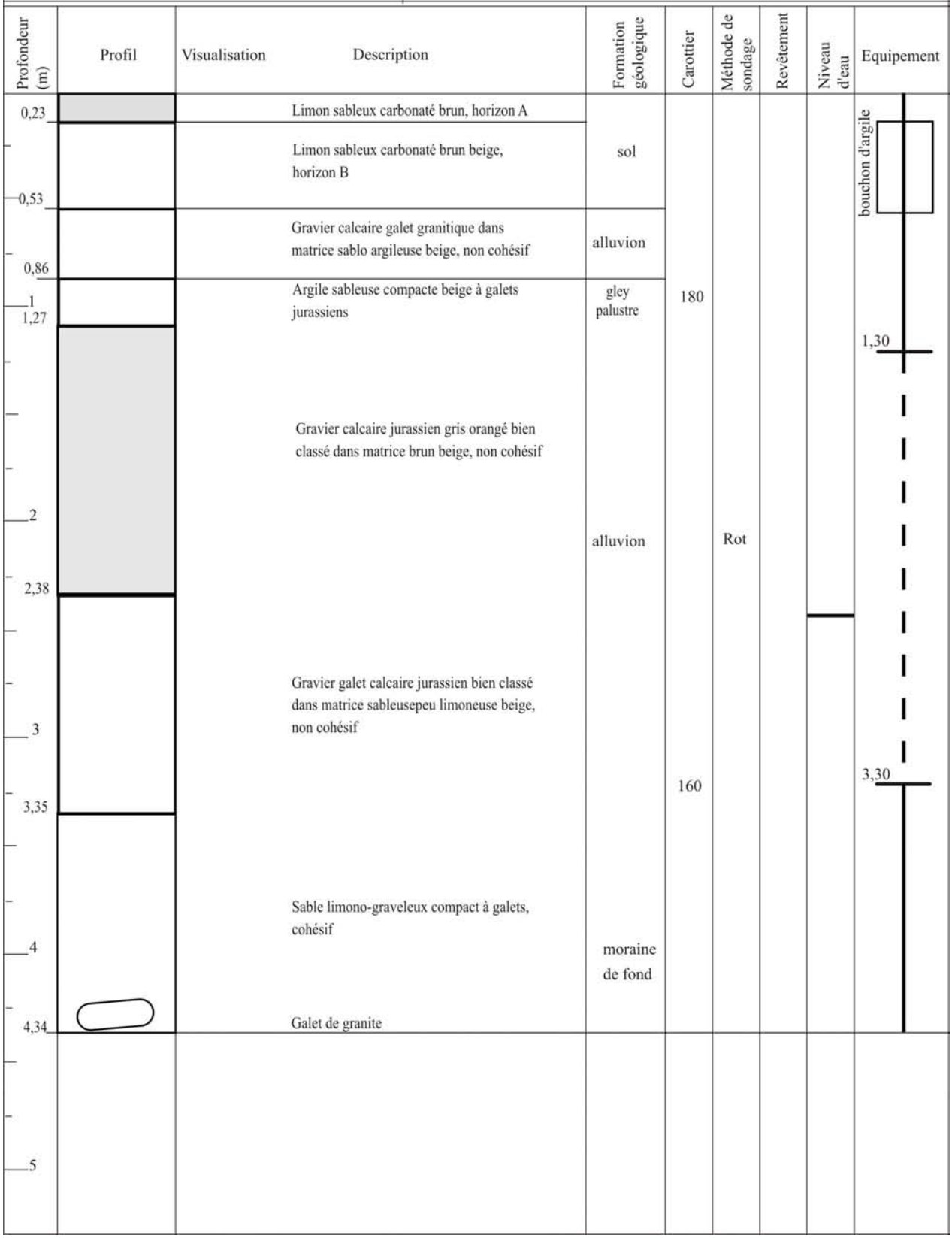

APPENDIX IV FLUX AND FLOWS; BASIC EQUATIONS FOR THE MATHEMATICAL SOLVING

IV.1 Fluxes balance equations

Darcy's Law, general formulation:

Equ. IV.a) $$q = -K(\theta) \cdot grad(H)$$ [m·s^{-1}]

Darcy's Law, unidimensional vertical:

Equ. IV.b) $$q = -K(\theta) \cdot (-\frac{\partial \Psi(\theta)}{\delta z} - 1)$$ [m·s^{-1}]

Continuity Law, general formulation:

Equ. IV.c) $$\frac{\delta \theta}{\delta t} = -div \cdot q$$ [s^{-1}]

(the Continuity Law says that the variation of the water content θ over the time is equal to the spatial variation of the fluxes q)

Continuity Law, unidimensional vertical:

Equ. IV.d) $$\frac{\delta \theta}{\delta t} = -\frac{\delta q}{\delta z}$$ [s^{-1}]

IV.2 Artificial test n°1, results for other shoulder than SGH, presented in the main text.

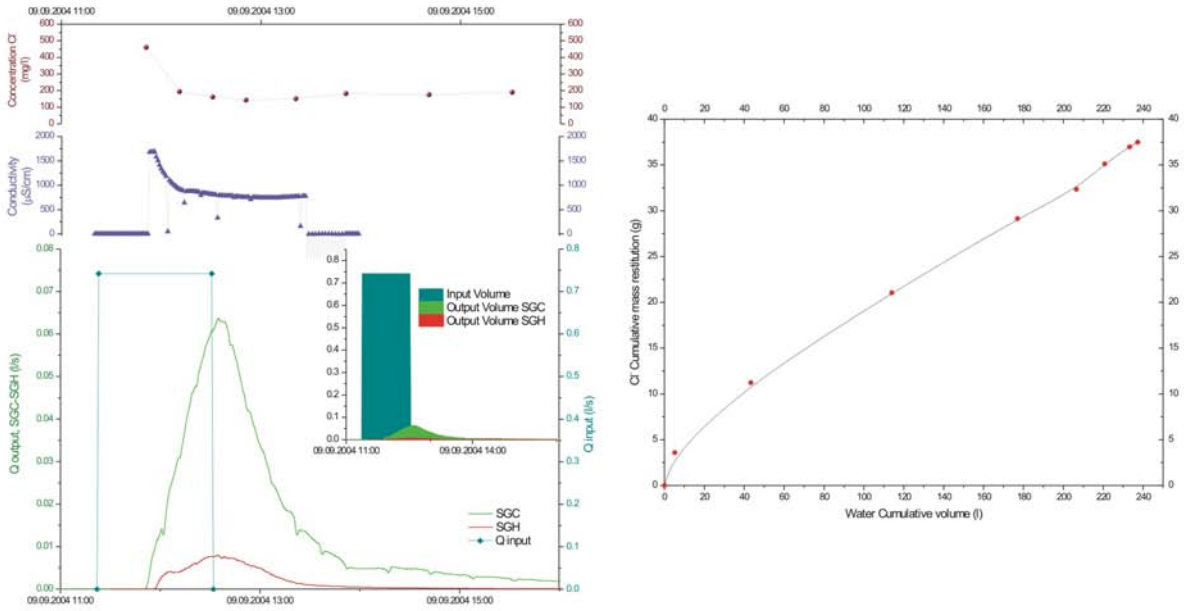

Figure IV.1: SGC. Note the trend is the same as SGH. The decreasing curve is however less pronounced. The Cl^- concentration shows a first peak in the first water exfiltrating the shoulder and a second rise later. The pollutogram is not frankly presenting a first flush. Note also the exfiltrating curve of SGH (red) due to the lateral runoff along the road.

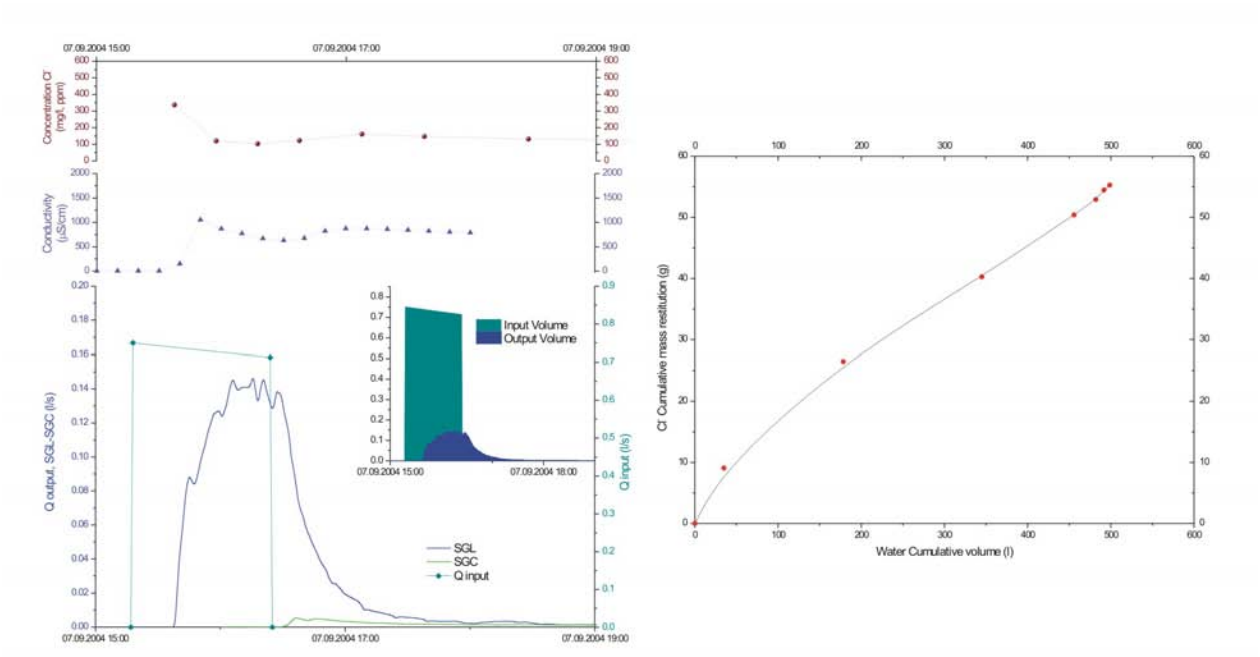

Figure IV.2: SGL. The linear progression of Q is the least distinct. Note the constant Q output during the watering. The concentration of Cl⁻ shows two distinct peaks. The SGL pollutogram is positive but not strongly so.

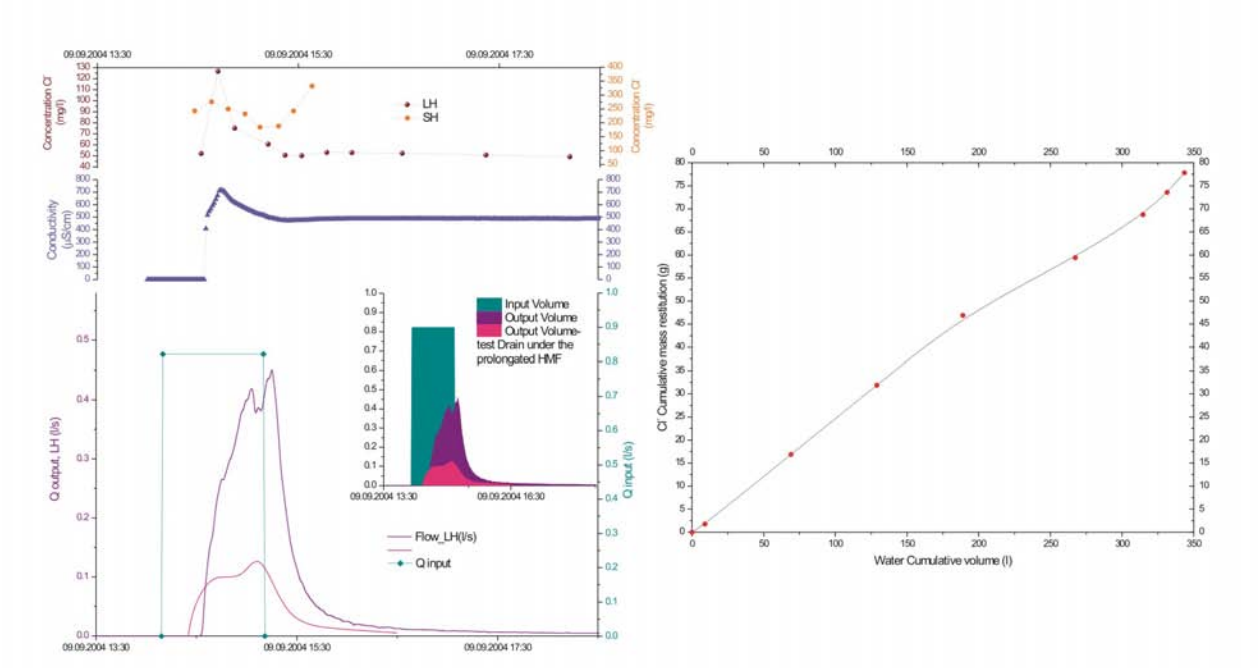

Figure IV.3: SH. The output flow (pink) is less pronounced than for other shoulders. The output flow of the associated lysimeter is also shown (violet). The Cl⁻ concentration presents a large second peak at the end of the event. The pollutogram (right) is neutral. The chlorine concentration for LH is more similar to the shoulder in its behaviour than to LW. It indeed shows one peak and a later augmentation. The pollutogram (here below) is always positive and has a first-flush effect similar to the SGH.

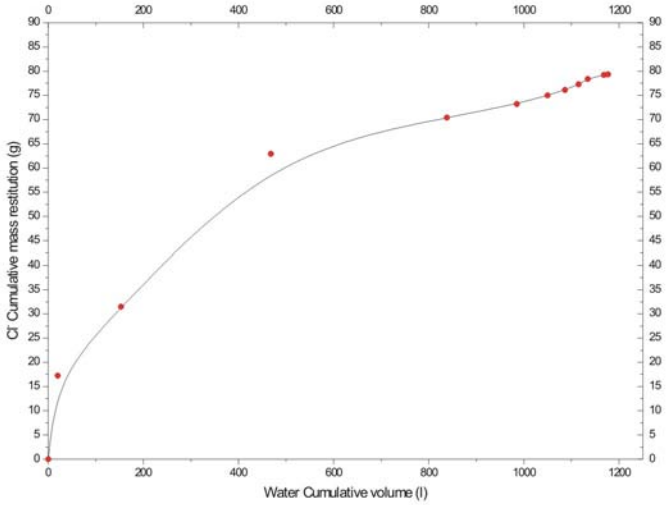

Figure IV.4: LH pollutogram. The pollutogram is always positive and has a first-flush effect similar to the SGH. Hydraulic curves for LH are presented in the previous figure.

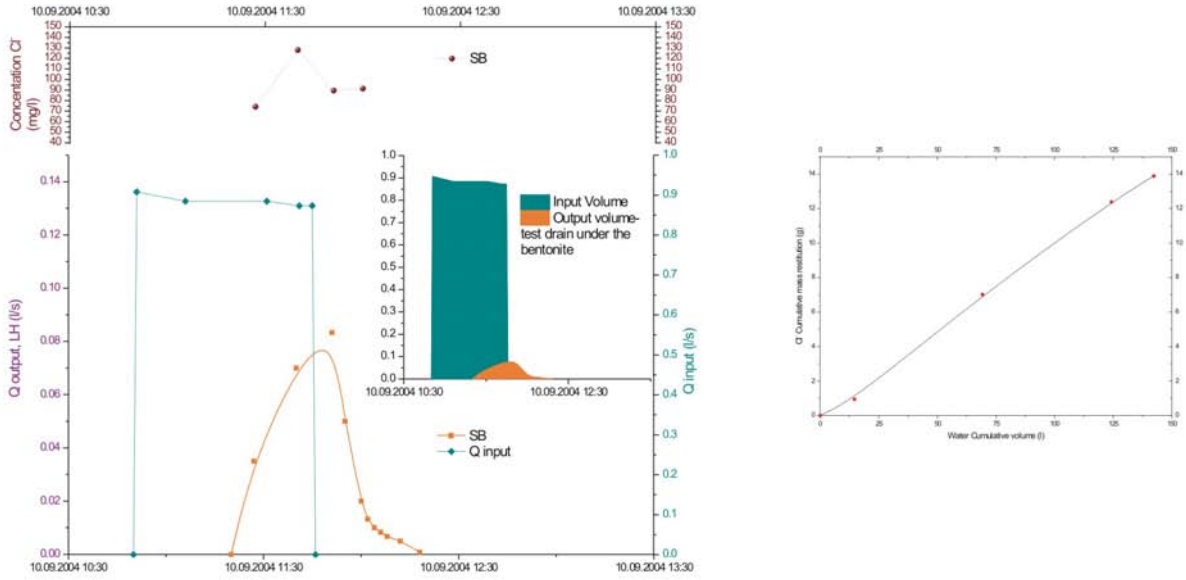

Figure IV.5: SB illustration. The output flow is similar to SH. It is well retarded. The Cl- concentration shows also a retarded peak. The pollutogram is neutral.

APPENDIX V FLOWS CALCULATION, ERROR, AND CALIBRATION CURVES

V.1 Flow measurement and calculation

The flow calculation is a very important step and thus shall be performed thoroughly. It comprehends 4 main points that are 1) the raw data verification, 2) the data transformation into flows, 3) the flow transformation into volumes and 4) the synthesis. All the calculations have been performed in an ACCESS database with homemade macros. Only the fundamental equations will be described here.
The flowmeters used are ISCO 4230 bubble flowmeter. The principle is to release small bubbles at the bottom of the weir. The pressure needed to push the bubble from the small vertical pipe equals the pressure at that depth. The apparatus releases 1 bubble per second and records 1 average depth per minute. The precision is down to 0.1mm depth. Due to its complexity, those apparatus have sometimes malfunctioned (pump failure).

Step 1: Data verification
Data are recorded with the software ISCO FLOWLINK v4.15. The verification consists in pinpointing the malfunctioning apparatus (erratic signal) and locating the erroneous data (clearly out of the main trend due to a specific apparatus error, often due to purging, electrical failure, pump failure, etc.). Electrical parasites also occurred.

Step 2: Data transformation into flows
Kindersvater-Shen equation (international norm ISO 1438/1-1980, Equation 2.1):

Equ.V.1)
$$Q = C * \frac{8}{15} * tg(\frac{\alpha}{2}) * \sqrt{2g} * (h^a)^{\frac{5}{2}} \qquad [m^3s^{-1}]$$

With:

$$h^a = h + k \qquad [m]$$

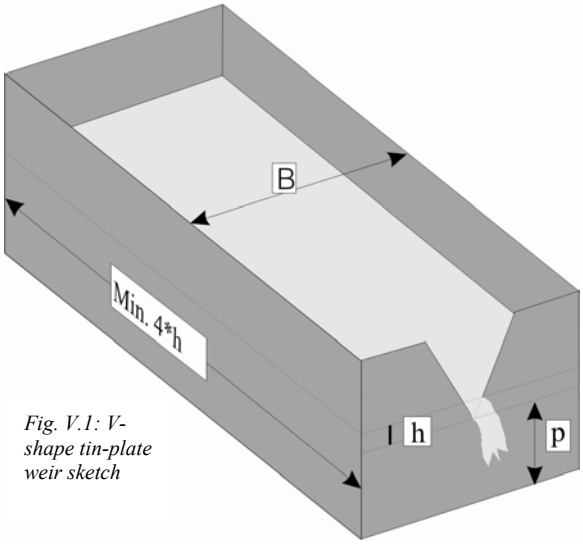

Fig. V.1: V-shape tin-plate weir sketch

(Q: flow [m^3s^{-1}]; C: flow coefficient f (h/p; p/B; α) [no unit]; α: v-shape weir opening angle [°]; g: gravity constant g = 9.81 [m^2s^{-1}]; h: water level [m]; k: experimental correction value [m]; see figure V.1)

The instrument measures the level p + h. The water level previous to a rainfall event is p (steady state, no rain). The overflow height h is then deducted by subtracting p for each event. As p may vary (evaporation, instrumental deviance), this solution is more convenient than measuring P only once and gives the best results.
Empirical curves for C determinations are shown in ISO1438-1975, p.202. C depends on the constant p (weir depth) and B (weir width). Factor k was determined in laboratory.
Machine and weir error on the flow calculation is 1.3%. The global error on the water flow is:

Equ. V.2)
$$E(Q) = \pm\sqrt{E^2(C_E) + 2.5^2 E(h^a)} \qquad [\%]$$

With:

Equ. V.3)
$$E(h^a) = \pm\frac{\sqrt{E^2(h) + E^2(k)}}{h} \qquad [\%]$$

(E(Q): global error; $E(C_E)$: error on the flow coefficient; $E(h^a)$: error on the effective hydraulic head; E(h): error on the measured hydraulic head; E(k): error on the hydraulic head correction factor)

Limit errors on the flow coefficient $E(C_E)$ and on the hydraulic head correction factor E(k) are respectively ±1% and 0.3mm (ISO 1438/1-1980). Limit error on h is more complicated to calculate. It must include: the hysteresis error

(±0.1% of h), the temperature effect error (±0.6% of h), the resolution error (0.1mm), the h=0 adjustment error (±1mm). The error E(h) is then:

Equ. V.4) $$E^2(h) = 4.10^{-6} \cdot h^2 + (\frac{0.1}{\sqrt{3}})^2 + (\frac{1}{3})^2 = 4.10^{-6} \cdot h^2 + 0.11\overline{4} \quad [mm^2]$$

(division by 3: normal distribution; divided by √3: rectangle distribution)

The error on the effective hydraulic head $E(h^a)$ is:

Equ. V.5) $$E(h^a) = \pm 100 \cdot \frac{\sqrt{4.10^{-6} \cdot h^2 + 0.71\overline{4}}}{h} \quad [\%]$$

Therefore, the global error is a function of h^a:

Equ. V.6) $$E(Q) = \pm\sqrt{1 + 6.25 \cdot E(h^a)^2} \quad [\%]$$

The figure V.2 shows the error curve on the calculated flows. Note that the lower the flow, the greater the error.

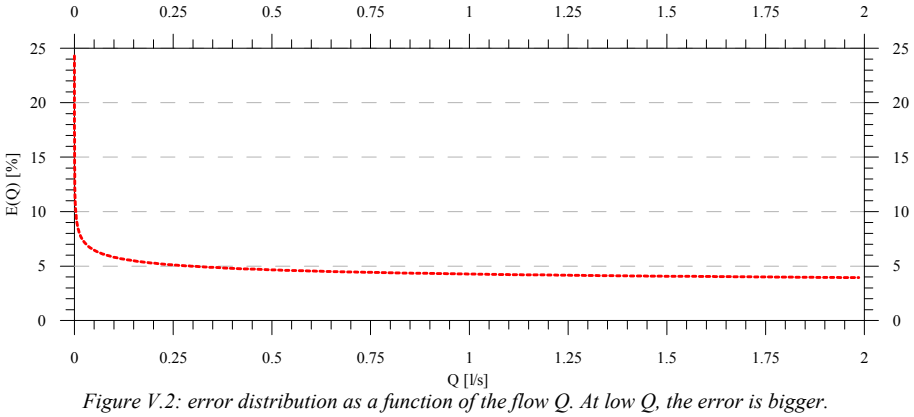

Figure V.2: error distribution as a function of the flow Q. At low Q, the error is bigger.

Main characteristics including opening angles for the 6 main weirs are shown in table A. Weirs and flowmeters were gauged conjointly in laboratory (figure b)

Compartiment	Surface s [m²]						volume [m³]						Weir angle [°]	Flow Coef. C [-]	Cor. factor k [m]
	Road	E(s_R)	Shoulder	E(s_S)	Lysimeter	E(s_L)	Shoulder	E(v_S)	Lyimeter						
	s_R	[%]	s_S	[%]	s_L	[%]	v_S	[%]	A-hor. v_{LA}	E(v_{LA}) [%]	B-Hor. v_{LB}	E(v_{LB}) [%]			
RUN	13.6	±3.2											20.8	0.58	0.002
SGH	76.3	±1.3	18.1	±3.3			9.8	±13					30.3	0.6	2E-04
SGC	83.0	±1.3	18.5	±3.3			9.9	±13					31.1	0.65	0.002
SGL	78.0	±1.3	17.5	±3.3			9.6	±13					30.9	0.65	0.004
SGL - LW	178.1	±1.3	38.0	±3.3	89.3	±11	20.6	±13	21.0	±18	36.0	±15	49.5	0.58	0.002
SH - LH	167.9	±1.3	39.9	±3.3	114.7	±10	12.3[1]	±13	35.6	±17	59.9	±14	54.9	0.55	1E-04
SB - LB	160.2	±1.3	39.2	±3.3	120.1	±10	28.9[2]	±13	39.2	±17	66.7	±14			

Table V.1: Compartment main Characteristics: surfaces s and volumes v with corresponding respective errors, weir angles, flow coefficient C and the correction factor k.

[1] the volume of the HMF is deducted. Only the volume of the grave I is considered
[2] the volume of the bentonitic layer is neglected

V.2 Step 3: Flow transformation into volumes

Water volume are calculated by integrating the flow Q along the time t.

Equ. V.7a)

$$V_{EXFILTRATION} = \int_{t_0}^{t_{end}} Q dt \qquad \text{[litres]}$$

Due to the complexity of the water flow curves, a good approximation is made:

Equ. V.7b)

$$V_{EXFILTRATION} = \sum_{t=0}^{t_{end}} Q(t) * 60 \qquad \text{[litres]}$$

The minimal time step (1 min) and slow Q variation guarantees small difference between equ. V.7a and b. To facilitate comparisons between flows coming from the different shoulders, lysimeters and rain gauge, the preceding result is then normalized on the catchment's surface s from each compartment.

Equ. V.8a)

$$V_{normalized} = \frac{V_{EXFILTRATION}}{s} \qquad \text{[mm]}$$

Catchment's surfaces s are shown in table V.1. Table V.2 shows values of the road runoff R_R and exfiltration E_S and E_L for all precipitations. The error on the volume calculation is (as it is an addition, error must be calculated in absolute value and not in percent):

Equ. V.8b)

$$E(V) = \sum_{t=0}^{t_{end}} E(Q_t) \qquad \text{[mm]}$$

which correspond to the sum of the error on the flow. The error due to the rectangular approximation is assumed to be zero, because the error on the increasing curve ≈ -error on the decreasing curve. Experience shows that the error on the volume is always close to 10%. The reason is that the error on the flow is close to 10% as well (unless for very low Q values which have little influence). For simplification purpose, this value has been used: E(V)=10%. The calculation of the error has been systematically made. They are shown in the table below.

Figure V.3: illustration of the collecting pipes and weirs. From left to right are visible the LW, road runoff (note the water colour!) and SH pipes and weirs. Far bottom right is discernable the LH collecting pipe. Grey boxes are the flowmeters. Note that the air pipes are placed in tubes to avoid the effect of waves forming at the surface of the weirs. Are also visible the funnels and bottles collecting the first-flush. At last, in the runoff funnel is placed the EC probe (black cable).

V.3 Calibration curves for the weirs

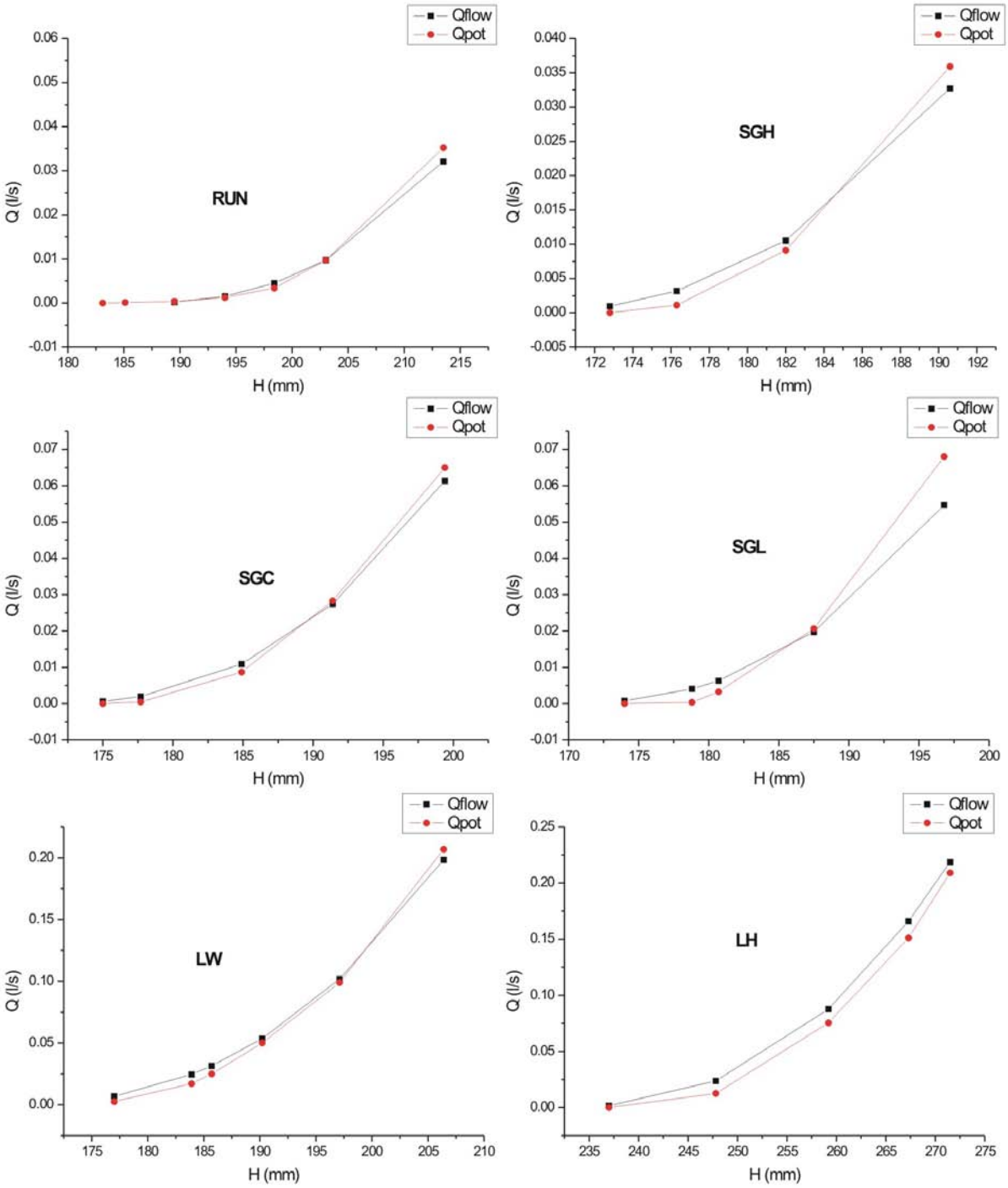

Fig. V.4: Weirs calibration curves. Qflow means the data was recorded by the flowmeter. Qpot means the data has been collected using a pot and a chronometer.

Date	R_R	E_S				E_L	
	RUN ± E(R_R)	SGH ± E(E_S)	SGC ± E(E_S)	SGL ± E(E_S)	SH± E(E_S)	LW± E(E_L)	LH± E(E_L)
(2004)	[mm]						
05.03.2004	1.2 ± 0.12	4.3 ± 0.43	4.6 ± 0.46	2.3 ± 0.23		0.0 ± 0.00	0.0 ± 0.00
12.03.2004	1.2 ± 0.12	0.2 ± 0.02	0.1 ± 0.01	0.0 ± 0.00		0.0 ± 0.00	0.0 ± 0.00
13.03.2004	21.3 ± 2.13	55.7 ± 5.57	57.1 ± 5.71	89.9 ± 8.99		23.9 ± 2.39	40.2 ± 4.02
20.03.2004	0.4 ± 0.04	0.1 ± 0.01	0.1 ± 0.01	0.0 ± 0.00		0.0 ± 0.00	0.0 ± 0.00
21.03.2004	3.9 ± 0.39	1.9 ± 0.19	0.4 ± 0.04	1.2 ± 0.12		0.0 ± 0.00	0.1 ± 0.01
05.04.2004	0.1 ± 0.01	0.2 ± 0.02	0.1 ± 0.01	0.0 ± 0.00			0.0 ± 0.00
06.04.2004	2.7 ± 0.27	11.3 ± 1.13	2.7 ± 0.27	3.4 ± 0.34		0.4 ± 0.04	1.8 ± 0.18
18.04.2004	0.6 ± 0.06	1.3 ± 0.13	0.5 ± 0.05	0.2 ± 0.02		0.0 ± 0.00	0.0 ± 0.00
23.04.2004	0.7 ± 0.07	1.7 ± 0.17	0.3 ± 0.03	0.2 ± 0.02		0.0 ± 0.00	0.0 ± 0.00
02.05.2004	0.1 ± 0.01	0.0 ± 0.00	0.0 ± 0.00	0.0 ± 0.00		0.0 ± 0.00	0.0 ± 0.00
05.05.2004	6.5 ± 0.65	12.5 ± 1.25	1.9 ± 0.19	7.9 ± 0.79			0.9 ± 0.09
07.05.2004	0.4 ± 0.04	0.5 ± 0.05	0.0 ± 0.00	0.0 ± 0.00			0.0 ± 0.00
08.05.2004	13.7 ± 1.37	69.4 ± 6.94	17.7 ± 1.77	45.2 ± 4.52			6.9 ± 0.69
27.05.2004	1.0 ± 0.10	0.5 ± 0.05	0.0 ± 0.00	0.0 ± 0.00			0.0 ± 0.00
30.05.2004	24.6 ± 2.46	127.0 ± 12.70	39.0 ± 3.90	96.5 ± 9.65		20.2 ± 2.02	29.0 ± 2.90
11.06.2004	1.2 ± 0.12	5.3 ± 0.53	0.0 ± 0.00	0.1 ± 0.01		0.0 ± 0.00	0.0 ± 0.00
20.06.2004	0.6 ± 0.06	0.9 ± 0.09	0.0 ± 0.00	0.0 ± 0.00		0.0 ± 0.00	0.0 ± 0.00
21.06.2004	0.5 ± 0.05	2.5 ± 0.25	0.0 ± 0.00	0.0 ± 0.00		0.0 ± 0.00	0.0 ± 0.00
23.06.2004	2.1 ± 0.21	17.9 ± 1.79	4.8 ± 0.48	2.7 ± 0.27		0.0 ± 0.00	0.2 ± 0.02
05.07.2004	4.4 ± 0.44	15.0 ± 1.50	1.3 ± 0.13	3.1 ± 0.31		0.1 ± 0.01	0.9 ± 0.09
08.07.2004	3.1 ± 0.31	18.3 ± 1.83	4.4 ± 0.44	3.8 ± 0.38		1.5 ± 0.15	3.0 ± 0.30
17.07.2004		15.7 ± 1.57	3.7 ± 0.37	7.9 ± 0.79		7.2 ± 0.72	5.7 ± 0.57
14.08.2004	4.5 ± 0.45	2.7 ± 0.27	0.5 ± 0.05	2.6 ± 0.26		0.0 ± 0.00	0.0 ± 0.00
16.08.2004	0.6 ± 0.06	0.0 ± 0.00	0.0 ± 0.00	0.0 ± 0.00		0.0 ± 0.00	0.0 ± 0.00
17.08.2004	15.7 ± 1.57	20.8 ± 2.08	48.6 ± 4.86	70.2 ± 7.02		12.2 ± 1.22	15.9 ± 1.59
19.08.2004	26.0 ± 2.60	52.2 ± 5.22	88.0 ± 8.80	197.9 ± 19.79		14.5 ± 1.45	42.9 ± 4.29
24.08.2004	16.1 ± 1.61	19.3 ± 1.93	34.5 ± 3.45	83.1 ± 8.31		23.3 ± 2.33	21.2 ± 2.12
30.08.2004	1.3 ± 0.13	0.3 ± 0.03	0.9 ± 0.09	4.1 ± 0.41		0.0 ± 0.00	0.0 ± 0.00
11.09.2004	18.1 ± 1.81		15.0 ± 1.50	36.6 ± 3.66		7.1 ± 0.71	4.6 ± 0.46
14.09.2004	1.3 ± 0.13		0.8 ± 0.08	2.0 ± 0.20		0.0 ± 0.00	0.0 ± 0.00
15.09.2004	5.9 ± 0.59		5.3 ± 0.53	12.0 ± 1.20		5.2 ± 0.52	2.8 ± 0.28
23.09.2004	31.1 ± 3.11		6.6 ± 0.66	27.4 ± 2.74		3.5 ± 0.35	
06.10.2004	16.7 ± 1.67		2.7 ± 0.27	9.4 ± 0.94		0.0 ± 0.00	1.0 ± 0.10
08.10.2004	10.2 ± 1.02		1.1 ± 0.11	6.1 ± 0.61		1.3 ± 0.13	1.1 ± 0.11
10.10.2004	44.1 ± 4.41		6.0 ± 0.60	23.9 ± 2.39		2.3 ± 0.23	2.3 ± 0.23
14.10.2004	16.3 ± 1.63		1.2 ± 0.12	3.3 ± 0.33		0.1 ± 0.01	0.5 ± 0.05
15.10.2004	38.4 ± 3.84		16.9 ± 1.69	41.9 ± 4.19		6.5 ± 0.65	5.4 ± 0.54
16.10.2004	5.6 ± 0.56		0.5 ± 0.05	2.3 ± 0.23		0.2 ± 0.02	0.0 ± 0.00
17.10.2004	13.9 ± 1.39		1.2 ± 0.12	4.3 ± 0.43		0.3 ± 0.03	0.3 ± 0.03
18.10.2004	114.0 ± 11.40		39.5 ± 3.95	90.5 ± 9.05		18.8 ± 1.88	9.8 ± 0.98
21.10.2004	2.3 ± 0.23		2.6 ± 0.26	6.6 ± 0.66		0.8 ± 0.08	0.5 ± 0.05
25.10.2004	95.1 ± 9.51					117.9 ± 11.79	62.9 ± 6.29
27.10.2004	5.2 ± 0.52		8.7 ± 0.87	22.9 ± 2.29		4.4 ± 0.44	2.1 ± 0.21
28.10.2004	4.0 ± 0.40		7.9 ± 0.79	23.0 ± 2.30		3.5 ± 0.35	2.7 ± 0.27
29.10.2004	0.7 ± 0.07		0.1 ± 0.01	0.8 ± 0.08		0.1 ± 0.01	0.1 ± 0.01
30.10.2004	1.1 ± 0.11		1.5 ± 0.15	5.7 ± 0.57		0.4 ± 0.04	0.5 ± 0.05
01.11.2004	2.2 ± 0.22		0.6 ± 0.06	4.1 ± 0.41			0.1 ± 0.01
29.11.2004	17.5 ± 1.75		10.0 ± 1.00	20.3 ± 2.03			1.0 ± 0.10
01.12.2004	7.6 ± 0.76		5.6 ± 0.56	10.0 ± 1.00			0.8 ± 0.08
03.12.2004	4.6 ± 0.46		4.0 ± 0.40	10.3 ± 1.03		1.9 ± 0.19	0.7 ± 0.07
16.12.2004	3.5 ± 0.35		2.4 ± 0.24	6.2 ± 0.62		0.0 ± 0.00	
17.12.2004	5.3 ± 0.53		6.0 ± 0.60	15.2 ± 1.52		3.4 ± 0.34	
19.12.2004	19.7 ± 1.97		56.3 ± 5.63	166.2 ± 16.62		52.6 ± 5.26	
25.12.2004	7.2 ± 0.72	12.1 ± 1.21	19.0 ± 1.90	35.1 ± 3.51		4.5 ± 0.45	0.8 ± 0.08

Table V.2:. R_R and E_S values and the corresponding errors. See text for calculation procedures. This page: year 2004; next page Year 2005.

Date	R_R	E_S				E_L	
	RUN ± E(R_R)	SGH ± E(E_S)	SGC ± E(E_S)	SGL ± E(E_S)	SH± E(E_S)	LW± E(E_L)	LH± E(E_L)
(2005)	[mm]						
01.01.2005	4.7 ± 0.47	5.7 ± 0.57	6.3 ± 0.63	12.6 ± 1.26		1.8 ± 0.18	0.5 ± 0.05
02.01.2005	1.7 ± 0.17	1.6 ± 0.16	1.8 ± 0.18	6.5 ± 0.65			0.2 ± 0.02
05.01.2005	3.6 ± 0.36	4.5 ± 0.45	7.4 ± 0.74	3.4 ± 0.34			0.0 ± 0.00
12.01.2005	3.3 ± 0.33	2.3 ± 0.23	5.6 ± 0.56	9.0 ± 0.90			0.0 ± 0.00
18.01.2005	13.9 ± 1.39	23.4 ± 2.34	15.0 ± 1.50	46.6 ± 4.66		8.1 ± 0.81	3.1 ± 0.31
22.03.2005	11.2 ± 1.12	7.2 ± 0.72	8.8 ± 0.88			0.0 ± 0.00	0.3 ± 0.03
24.03.2005	24.3 ± 2.43	15.0 ± 1.50				3.1 ± 0.31	1.4 ± 0.14
26.03.2005	26.0 ± 2.60	39.3 ± 3.93	46.4 ± 4.64	103.9 ± 10.39			8.5 ± 0.85
16.04.2005	43.3 ± 4.33	110.9 ± 11.09	156.3 ± 15.63			90.3 ± 9.03	29.9 ± 2.99
22.04.2005	54.9 ± 5.49	0.7 ± 0.07	1.4 ± 0.14	1.7 ± 0.17			0.0 ± 0.00
23.04.2005	1.5 ± 0.15	0.2 ± 0.02	0.3 ± 0.03	0.7 ± 0.07			0.0 ± 0.00
24.04.2005	60.2 ± 6.02	14.8 ± 1.48	60.0 ± 6.00	115.9 ± 11.59		9.5 ± 0.95	11.6 ± 1.16
14.05.2005	2.0 ± 0.20	2.9 ± 0.29		4.4 ± 0.44		0.0 ± 0.00	0.2 ± 0.02
15.05.2005	0.5 ± 0.05	0.4 ± 0.04		2.7 ± 0.27		0.0 ± 0.00	0.0 ± 0.00
16.05.2005	7.1 ± 0.71	14.3 ± 1.43		34.7 ± 3.47		3.3 ± 0.33	3.1 ± 0.31
21.05.2005	5.6 ± 0.56	0.6 ± 0.06				0.0 ± 0.00	0.0 ± 0.00
22.05.2005	5.8 ± 0.58	1.3 ± 0.13		4.7 ± 0.47		0.0 ± 0.00	0.2 ± 0.02
23.05.2005	16.5 ± 1.65	15.1 ± 1.51		44.2 ± 4.42		1.7 ± 0.17	3.0 ± 0.30
29.05.2005	2.3 ± 0.23	0.7 ± 0.07		2.2 ± 0.22	3.44 ± 0.34	0.0 ± 0.00	0.0 ± 0.00
30.05.2005	3.0 ± 0.30	2.7 ± 0.27		6.6 ± 0.66	8.53 ± 0.85	0.1 ± 0.01	0.1 ± 0.01
04.06.2005	1.4 ± 0.14			6.4 ± 0.64	2.75 ± 0.28	0.0 ± 0.00	0.0 ± 0.00
06.06.2005	1.0 ± 0.10	2.4 ± 0.24		5.6 ± 0.56	1.95 ± 0.19	0.0 ± 0.00	0.0 ± 0.00
12.06.2005	1.7 ± 0.17	0.4 ± 0.04	0.4 ± 0.04	1.3 ± 0.13		0.0 ± 0.00	0.0 ± 0.00
13.06.2005	48.4 ± 4.84	26.9 ± 2.69	28.7 ± 2.87	51.7 ± 5.17		2.9 ± 0.29	6.7 ± 0.67
24.06.2005	1.1 ± 0.11	1.5 ± 0.15		7.6 ± 0.76		0.0 ± 0.00	0.0 ± 0.00
25.06.2005	5.2 ± 0.52	5.5 ± 0.55		19.2 ± 1.92	12.3 ± 1.23	0.0 ± 0.00	1.6 ± 0.16
27.06.2005	8.5 ± 0.85			20.9 ± 2.09	19.5 ± 1.95	3.2 ± 0.32	3.5 ± 0.35
29.06.2005	13.8 ± 1.38			72.0 ± 7.20	34.4 ± 3.44	11.9 ± 1.19	9.2 ± 0.92
04.07.2005	7.5 ± 0.75	11.5 ± 1.15		30.8 ± 3.08	26.7 ± 2.67	3.5 ± 0.35	2.7 ± 0.27
06.07.2005	19.4 ± 1.94	17.0 ± 1.70		98.9 ± 9.89	42.3 ± 4.23	11.0 ± 1.10	7.6 ± 0.76
09.07.2005	3.4 ± 0.34	2.2 ± 0.22			7.63 ± 0.76	0.6 ± 0.06	0.6 ± 0.06
10.07.2005	1.7 ± 0.17	1.2 ± 0.12			4.16 ± 0.42	0.2 ± 0.02	0.0 ± 0.00
16.07.2005	1.3 ± 0.13	0.1 ± 0.01		2.6 ± 0.26	1.78 ± 0.18	0.0 ± 0.00	
17.07.2005	3.2 ± 0.32	4.2 ± 0.42		8.4 ± 0.84	3.84 ± 0.38	0.0 ± 0.00	
18.07.2005	5.3 ± 0.53	8.8 ± 0.88		16.0 ± 1.60	15.9 ± 1.59	0.4 ± 0.04	0.8 ± 0.08
25.07.2005	0.4 ± 0.04	0.2 ± 0.02		0.0 ± 0.00	1.19 ± 0.12	0.0 ± 0.00	0.0 ± 0.00
29.07.2005	4.2 ± 0.42	7.0 ± 0.70		8.7 ± 0.87	19.4 ± 1.94	0.0 ± 0.00	0.3 ± 0.03
02.08.2005	13.7 ± 1.37	32.7 ± 3.27		50.9 ± 5.09	78.3 ± 7.83	5.1 ± 0.51	3.8 ± 0.38
13.08.2005	0.4 ± 0.04	0.0 ± 0.00		0.0 ± 0.00		0.0 ± 0.00	0.0 ± 0.00
14.08.2005	11.1 ± 1.11	6.0 ± 0.60		12.9 ± 1.29		0.0 ± 0.00	0.4 ± 0.04
19.08.2005	1.1 ± 0.11	0.7 ± 0.07		1.5 ± 0.15		0.0 ± 0.00	0.0 ± 0.00
20.08.2005	1.8 ± 0.18	4.3 ± 0.43	3.7 ± 0.37	5.7 ± 0.57	5.81 ± 0.58	0.0 ± 0.00	0.3 ± 0.03
21.08.2005	2.0 ± 0.20	1.5 ± 0.15	2.1 ± 0.21	3.4 ± 0.34	3.7 ± 0.37	0.0 ± 0.00	0.3 ± 0.03
22.08.2005	11.3 ± 1.13	15.2 ± 1.52	21.8 ± 2.18	36.0 ± 3.60	24.3 ± 2.43	5.4 ± 0.54	4.8 ± 0.48
23.08.2005	3.6 ± 0.36	3.1 ± 0.31	3.7 ± 0.37	10.0 ± 1.00	5.57 ± 0.56	1.3 ± 0.13	1.4 ± 0.14
25.08.2005	4.2 ± 0.42	5.2 ± 0.52	7.6 ± 0.76	14.6 ± 1.46	10.1 ± 1.01	2.1 ± 0.21	1.6 ± 0.16
27.08.2005	1.2 ± 0.12	1.4 ± 0.14	2.4 ± 0.24	6.3 ± 0.63	4.84 ± 0.48	0.0 ± 0.00	0.0 ± 0.00
05.09.2005	0.3 ± 0.03	0.3 ± 0.03	0.0 ± 0.00	0.0 ± 0.00	0.69 ± 0.07	0.0 ± 0.00	
06.09.2005	27.9 ± 2.79	3.7 ± 0.37	3.8 ± 0.38	12.5 ± 1.25	6.54 ± 0.65	0.5 ± 0.05	0.0 ± 0.00
09.09.2005	3.0 ± 0.30	9.5 ± 0.95	6.0 ± 0.60	18.8 ± 1.88	9.82 ± 0.98	1.1 ± 0.11	1.0 ± 0.10
10.09.2005	7.4 ± 0.74		25.6 ± 2.56	72.9 ± 7.29		12.2 ± 1.22	7.8 ± 0.78
16.09.2005		31.2 ± 3.12	29.9 ± 2.99	65.9 ± 6.59	29.6 ± 2.96	4.7 ± 0.47	4.1 ± 0.41
26.09.2005	0.8 ± 0.08	2.3 ± 0.23	2.4 ± 0.24		3.49 ± 0.35		0.0 ± 0.00
01.10.2005	8.9 ± 0.89	55.1 ± 5.51	53.2 ± 5.32	97.4 ± 9.74	53.4 ± 5.34	6.1 ± 0.61	5.8 ± 0.58
18.10.2005	4.1 ± 0.41	8.1 ± 0.81	8.0 ± 0.80	12.2 ± 1.22	9.63 ± 0.96		0.5 ± 0.05
21.10.2005	28.5 ± 2.85	57.2 ± 5.72	77.2 ± 7.72	195.9 ± 19.59	74.3 ± 7.43	33.3 ± 3.33	17.2 ± 1.72
01.11.2005	0.6 ± 0.06		1.9 ± 0.19	2.7 ± 0.27		0.0 ± 0.00	0.0 ± 0.00
04.11.2005	3.5 ± 0.35	20.0 ± 2.00	27.9 ± 2.79	45.0 ± 4.50	27.2 ± 2.72	14.8 ± 1.48	6.1 ± 0.61

APPENDIX VI ETP AND API CALCULATION

VI.1 ETP calculation

The evaporation and transpiration are governed by the PMFAO (Penmann-Monteith Food and Agriculture Organisation, simplified version of the Penmann-Monteigh):

Equ. VI.1)

$$ETP = \frac{0.408 \cdot \Delta \cdot (Rn - G) + \gamma \cdot (\frac{890}{T + 273}) \cdot U \cdot (Ea - Ed)}{\Delta + \gamma \cdot (1 + 0.34 \cdot U)} \quad \text{[mm]}$$

(Δ: vapour pressure slope [kPa.°C^{-1}]; Rn: net solar heat flux [kJ.m^2.s^{-1}]; G: soil heat flux [kJ.m^2.s^{-1}]; γ: psychometric constant [kPa.°C^{-1}]; T: mean temperature [°C]; U: wind speed [m.s^{-1}]; Ea: saturating vapour pressure [kPa]; Ed: effective vapour pressure [kPa])

As it is an empirical equation, the unit of the variables must be respected. Needed data have been supplied by Meteoswiss; they were recorded in the Mathod meteorological station (10km West from Yverdon-les-Bains). Results of ETP are shown in the table below. ETP results are mean daily values.

VI.2 API calculation

API is calculated with the help of the ETP. The initial moisture condition of the shoulder/soil is calculated for each rainfall event. API formulation is as follow:

Equ. VI.2)

$$API = API_0 * K_{API} + P \quad \text{[mm]}$$

(API: antecedent precipitation index [mm]; API_0: API on day d-1 [mm]; K_{API}: recession constant [no unit]; P: precipitation [mm])

K_{API} depends on the evapotranspiration ETP and exploitable water reserve ("*réserve utile"* RU):

Equ. VI.3)

$$K_{API} = e^{-ETP/RU} \quad \text{[-]}$$

(K_{API}: recession constant [-]; ETP: Evapotranspiration [mm]; P: precipitation [mm])

RU is defined as follow:

Equ. VI.4)

$$RU = (\theta_{cr} - \theta_{dp}) \cdot h \quad \text{[m]}$$

(θ_{cr}: volumetric water content at retention capacity [%]; θ_{fp}: volumetric water content at permanent plant dying point (suction ψ ≈ 15 bars) [%]; h: roots depth [m])

As the different volumetric water contents were unknown, standard values of RU have been calculated using estimation of the roots depth and water contents (estimated values for the shoulder are θ_{cr} = 15%; θ_{dp} = 5%; h= 0.05 m. Estimated values for the lysimeter are: θ_{cr} =35%; θ_{dp} = 20 %; h=0.15 m). Values of RU are thus 5 and 23 [mm] for the shoulders and lysimeters respectively. Values of API are listed in the table below.

Date	Rainfall	Duration	Max intensity	Mean intensity	Preceding drought	Mean T	Humidity	QFF-P	Sunlight	Solar heat flux	Wind	ETP	IPA		ΔS	
													S	L	S	L
(2004)	[mm]	[hours]	[mm/h]	[mm/h]	[day]	[°C]	[%]	[hPa]	[min]	[W/m^2]	[m/s]	[mm]	[mm]		[mm]	
05.03.2004	4.1	13.84	0.6	0.3	10	2.7	86.8	1021	0	33.2	0.5	0.054	11.37	28.90	3.98	4.03
12.03.2004	1.4	8.9	0.3	0.15	6	0.5	82.6	1019	33	44.1	0.9	0.099	13.56	34.00	1.13	1.25
13.03.2004	27.2	25.33	2.7	1.1	0.375	3.8	90.7	1024	0	25	0.7	0.055	14.70	35.25	27.04	27.12
20.03.2004	0.9	1.1	0.4	0.81	6	11.9	74.3	1025	3	51.7	7.2	0.945	26.28	59.02	-3.62	-1.48
21.03.2004	3.6	17.84	0.9	0.2	1.75	10	64.8	1019	20	45.4	6.9	1.132	21.76	56.64	-0.81	0.88
05.04.2004	0.9	10.6	0.2	0.09	0.54	10.1	55.2	1022	393	174	6.7	1.437	7.77	45.13	-1.04	-1.83
06.04.2004	8.1	47.66	1.6	0.17	0.9	6.8	72.3	1012	15	77.6	6.6	0.713	5.83	42.40	7.32	6.81
18.04.2004	1.6	8.25	0.5	0.2	8	9.9	67.5	1000	317	148	5.4	0.959	3.97	37.07	0.91	0.09
23.04.2004	1.9	4.25	1.1	0.45	4	14.6	72.3	1019	246	173.7	3.3	0.899	4.54	35.12	1.15	0.55
02.05.2004	0.4	0.16	0.3	0.24	5	12.1	68.6	1011	313	191.8	1.7	0.605	0.88	24.39	0.30	-0.23
05.05.2004	9.3	29.8	2.1	0.3	2.7	8.5	77.4	993	27	108.7	2.8	0.459	2.69	24.81	9.06	8.81
07.05.2004	0.7	1.35	0.4	0.52	0.75	8.4	67.4	1006	190	173.4	4.1	0.785	11.51	33.71	-0.97	-0.43
08.05.2004	17.3	26.55	2.4	0.065	1.17	7	78.2	1009	0	96	7.2	0.584	9.94	32.67	16.20	16.48
27.05.2004	1.5	0.55	1.4	3	6	13.2	74.9	1021	120	101.3	1.4	0.456	0.99	21.07	1.41	1.09
30.05.2004	38	72	6.2	0.53	3	15.2	58.4	1022	558	231.1	2.1	1.105	0.76	18.95	37.85	37.11
11.06.2004	3.8	4.5	1.4	0.85	3	17.4	79	1022	23	82.4	1.3	0.470	6.31	32.07	3.23	3.15
20.06.2004	2.2	0.5	0.9	4.4	6	12.7	74.6	1011	137	152.1	1.5	0.469	3.27	27.68	1.91	1.64
21.06.2004	1.5	13	0.4	0.11	1	15.1	69.7	1015	249	187.8	1.4	0.620	3.58	27.73	1.08	0.76
23.06.2004	5.6	3.15	2.7	1.75	1	17.6	79.9	1015	34	100.1	4.6	0.904	10.45	34.02	3.87	4.29
05.07.2004	11.2	18.15	4.1	1.24	12	18.8	71.5	1020	89	112.1	2.5	1.038	3.91	20.92	10.47	10.28
08.07.2004		9			3	17.4	79	1013	175	123	2.2	0.655	12.49	30.63	-1.53	-0.86
17.07.2004	12	0.24	7.9	48	3	20.8	71.2	1018	585	231.7	1.6	0.909	13.50	41.61	9.76	10.39
14.08.2004	2.4	0.5	2	4.8	0	17.8	62.8	1022	143	139.3	2.9	1.379	21.89	60.84	-2.87	-1.14
16.08.2004	1.4	0.25	1.2	5.6	2	17.3	79.4	1015	231	117.1	1	0.380	14.70	55.80	0.32	0.49
17.08.2004	21	5.85	3.2	2.15	1	18.2	86.7	1012	24	90	1.3	0.313	23.43	64.69	19.58	20.13
19.08.2004	40.3	23	2.5	1.75	1	18.2	86.8	1015	12	43.2	1.1	0.275	42.11	87.05	38.05	39.27
24.08.2004	26.9	19.61	2.65	1.38	2	18.2	81	1019	198	111.5	3.6	0.800	49.16	118.72	19.63	22.84
30.08.2004	1.9	3.6	0.9	0.54	2	17.2	71.5	1018	168	112.6	4	1.182	28.79	112.01	-4.16	-3.71
11.09.2004	14.5	10	3	1.45	3	19.4	67.3	1022	325	147.5	1.7	0.985	5.17	76.88	13.58	11.28
14.09.2004	1.7	4.35	0.7	0.4	4	17.2	82.9	1016	0	64.3	1.9	0.483	15.58	83.70	0.26	-0.04
15.09.2004	8.9	0.41	8.5	21.36	0.25	14.9	70.8	1021	168	115.1	1.7	0.669	20.74	88.56	6.30	6.36
23.09.2004	11.5	7	4	1.65	9	15.6	71.7	1018	66	74.3	5.6	1.211	6.37	68.49	10.13	7.99
06.10.2004	6.6	23.8	1.5	0.28	12	15.5	83.2	1020	11	35.3	1.5	0.368	2.82	54.41	6.40	5.74
08.10.2004	4.6	0.25	4.5	18	1.9	17	83.9	1016	217	90.3	0.9	0.269	10.25	61.07	4.06	3.89
10.10.2004	6.6	10.33	1.8	0.64	1	14.2	86.4	1011	73	46.7	1.9	0.320	11.99	62.36	5.86	5.74
14.10.2004	3.3	2.73	2.9	1.2	3.8	11.1	85.1	1011	43	52	2.3	0.322	13.92	64.25	2.43	2.41
15.10.2004	10.1	13.95	2.9	0.72	0.83	8.9	81.4	1005	8	38.2	4.4	0.476	26.45	76.75	7.70	8.53
16.10.2004	1.5	3.35	1.1	0.45	0.45	7.8	76.2	1006	303	116.5	3.6	0.521	30.05	81.18	-1.47	-0.32
17.10.2004	2.5	3.3	0.8	0.75	0.54	7.8	80.2	1012	98	56.1	4.7	0.484	29.38	81.66	-0.21	0.80
18.10.2004	20.7	24.66	2.3	0.84	0.58	10.4	75.9	1015	170	99.3	3	0.573	28.86	82.16	17.57	18.68
21.10.2004	2.4	0.3	1.7	7.28	0.29	14.5	77.1	1017	290	95.5	1.8	0.531	51.51	106.52	-2.79	-0.03
25.10.2004	78.1	33.5	7.2	2.34	4.2	12.8	86.7	1016	59	44	1.1	0.199	43.81	103.65	76.39	77.21
27.10.2004	8.1	15.67	1.5	0.52	1.1	9.3	83	1008	0	47.5	1.2	0.216	114.32	176.37	3.26	6.45
28.10.2004	5.2	6.34	2.5	0.82	0.125	10.5	87.7	1004	100	53	1.1	0.159	112.68	177.92	1.67	3.97
29.10.2004	0.9	0.1	0.9	9	0.71	11.3	88.5	1003	43	57.9	1.2	0.167	118.35	185.90	-2.98	-0.44
30.10.2004	1.6	1.5	0.8	1.05	0.125	10.4	77.4	1010	565	101	1.7	0.390	118.77	188.85	-7.32	-1.58
01.11.2004	2.9	1.84	1.3	1.57	2.7	11.2	85.6	1016	5	44	1.1	0.194	99.22	181.61	-0.88	1.37
29.11.2004	8	9.9	1.2	0.81	9.5	6.7	84.9	1014	0	20	2.5	0.256	32.40	145.29	6.38	6.39
01.12.2004	4.4	3.5	1.7	1.25	1.5	1.6	89.2	1013	64	31	0.5	0.041	31.28	144.20	4.14	4.14
03.12.2004	3.2	5.9	1.7	0.54	1.5	5.4	88.4	1022	50	37	0.6	0.067	37.90	150.86	2.70	2.76
16.12.2004	3.3	7.67	0.9	0.43	13.2	1.1	90.8	1022	0	20	0.9	0.055	27.86	141.11	3.00	2.97
17.12.2004	5.6	9.4	1.1	0.73	0.33	5.5	78.7	1011	0	16	7.4	0.520	28.86	142.08	2.75	2.42
19.12.2004	30.7	11.65	5.8	2.61	1.4	4	84.7	1007	0	14	6.7	0.328	30.25	142.79	28.78	28.68
25.12.2004	9.2	26.45	0.9	0.35	1.2	4.3	79.2	1004	187	47	3.1	0.336	28.36	141.25	7.36	7.15

Table VI.1: summary of all meteorological data recorded in the field, as well as the resulting calculated ETP, API and stock variation ΔS. Year 2004 is presented on this page, whereas year 2005 s presented on next page.

Date	Rainfall	Duration	Max intensity	Mean intensity	Preceding drought	Mean T	Humidity	QFF-P	Sunlight	Sunbeam	Wind	ETP	IPA		ΔS	
													S	L	S	L
(2005)	[mm]	[hours]	[mm/h]	[mm/h]	[day]	[°C]	[%]	[hPa]	[min]	[W/m^2]	[m/s]	[mm]	[mm]		[mm]	
01.01.2005	5.1	12.3	0.9	0.41	0.92	3.3	82.4	1033	77	44	1.6	0.183	30.52	143.34	4.01	3.97
02.01.2005	0.8	4.25	0.3	0.19	0.45	4.9	76.8	1032	6	20	4.1	0.443	30.73	143.50	-1.80	-1.94
05.01.2005	2.7	8.4	0.5	0.32	2	2.6	76	1036	307	60	2.4	0.303	28.25	140.81	1.04	0.86
12.01.2005	1.9	6.18	0.8	0.31	6.3	1.6	84.1	1032	96	44	0.8	0.089	21.03	131.99	1.53	1.39
18.01.2005	11	9.5	7.2	1.16	5.3	2.9	77.8	1012	0	15	5.4	0.411	20.76	131.13	9.36	8.68
22.03.2005	4.7	11.42	1.7	0.41	7.1	8.7	86.2	1018	0	33	1.6	0.205	5.01	86.67	4.50	3.93
24.03.2005	8.8	19.78	1.3	0.45	1.3	11.3	86.4	1020	32	74	1.7	0.249	10.27	90.74	8.30	7.82
26.03.2005	18.7	21.67	2.7	0.87	1.8	11	77.3	1011	183	119	1.8	0.422	19.40	99.27	17.13	16.89
16.04.2005	35.1	62.89	6.5	0.57	0.6	6.2	82.2	1002	0	30	3.1	0.327	8.31	78.65	34.57	33.99
22.04.2005	3	2.84	1.6	1.03	4.1	8.5	64	1017	720	249	1.3	0.461	36.70	115.17	-0.23	0.71
23.04.2005	1	1.35	0.9	0.74	0.1	9.9	82.1	1015	58	83	1.1	0.223	33.47	112.89	-0.46	-0.09
24.04.2005	28.4	32.25	3.4	0.88	0.19	10.8	89.6	1012	0	49	1.8	0.191	39.01	118.80	26.94	27.42
14.05.2005	4.8	5.18	2	0.93		12.8	84.7	1016	28	86	3.7	0.468	6.91	81.76	4.18	3.15
15.05.2005	0.5	0.44	0.5	1.25	0.51	14.2	69	1017	329	203	1.8	0.706	11.49	85.32	-1.01	-2.08
16.05.2005	10.6	7.9	2.1	1.34	1	10.2	85	1015	0	63	1	0.177	9.98	82.74	10.25	9.96
21.05.2005	2.1	2.4	1.3	0.85	4.1	16.2	73.3	1017	179	145	1.4	0.584	14.99	86.54	0.45	-0.07
22.05.2005	3.3	7.6	1.1	0.43	0.47	14.9	76.1	1016	191	158	1.4	0.483	17.34	88.37	1.70	1.46
23.05.2005	12.9	14.9	1.8	0.87	0.425	11.5	81.4	1023	105	112	1.7	0.345	27.04	97.83	11.10	11.44
29.05.2005	2.8	0.2	2.8	14	6.4	22.1	69.4	1017	527	218	1	0.752	30.74	101.87	-1.49	-0.47
30.05.2005	1.2	1.44	0.7	0.85	0.64	17	73	1022	23	72	2.6	0.901	14.98	87.13	-1.27	-2.15
04.06.2005	0.7	3.09	0.3	0.23	4.3	17.3	59.9	1019	419	240	4.8	1.801	8.45	74.40	-1.86	-4.90
06.06.2005	1.2	0.95	0.9	1.26	2.6	15	71.4	1022	25	134	1.3	0.552	4.81	65.80	0.70	-0.36
12.06.2005	1.2	0.19	1.2	6.67	5.5	17.5	63.8	1010	384	203	2	1.075	1.30	47.12	0.95	-0.95
13.06.2005	18.2	37.05	7.7	0.49	1	16.8	76	1010	217	164	2.4	0.759	1.05	44.97	18.05	16.74
24.06.2005	4.2	6.38	1.3	0.66	3.4	22.6	73.1	1017	496	224	1.7	0.980	2.56	40.38	3.74	2.52
25.06.2005	8.6	4.02	3.4	2.15	0.5	20.3	84.3	1020	394	185	1.4	0.441	12.10	48.69	7.58	7.67
27.06.2005	10.8	0.55	10.7	19.64	2	23.3	70.8	1020	621	260	1.1	0.826	19.29	57.19	7.86	8.78
29.06.2005	8.8	1.98	5.3	4.4	1.8	20.9	76.2	1012	337	178	1.9	0.841	14.07	53.40	6.62	6.88
04.07.2005	7.5	4.44		1.69	3	17.3	77	1014	266	108	2.3	0.731	15.97	60.24	5.33	5.61
06.07.2005	21.2	28.46		0.75	1.9	14.3	78	1016	34	108	2.6	0.622	14.95	60.02	19.45	19.60
09.07.2005	3.4	0.5		6.82	2.3	14.4	75.4	1019	556	245	1.6	0.527	20.06	67.50	1.39	1.87
10.07.2005	1.7	2.05		0.83	1	17.4	75.5	1021	575	265	3.7	0.996	23.46	71.37	-2.54	-1.32
16.07.2005	1.3	1.9		0.66	5.2	23.7	64.3	1017	542	239	2.9	1.876	5.80	51.39	-0.52	-2.73
17.07.2005	3.2	0.24		13.46	1.6	23.8	63.5	1015	660	262	1.1	1.061	6.09	49.47	2.04	0.97
18.07.2005	5.35	1.66		3.22	0.9	20.4	74.4	1013	259	138	2.7	1.069	4.92	47.24	4.40	3.20
25.07.2005	0.7	0.16	0.2	4.2	0.05	21.1	76	1011	106	129	2.3	0.958	2.68	36.37	0.23	-0.78
29.07.2005	9.1	9.7	0.3	0.94	4.1	23	64.8	1014	435	201	2.2	1.531	1.58	30.01	8.68	7.17
02.08.2005	18	12.16	3.8	1.48	2.9	17.3	83.1	1018	0	52	1.3	0.375	7.68	34.26	17.44	17.45
13.08.2005	0.5	0.2	0.4	2.27	10	18.8	60.9	1020	496	215	1.7	1.137	2.77	26.54	-0.06	-0.78
14.08.2005	8.4	7.47	1.9	1.48	1.2	15.4	71.5	1019	82	80	3.4	0.985	2.21	25.26	8.01	7.34
19.08.2005	1.7	0.18	1.7	9.45	0.9	17.5	75.4	1018	240	129	1.3	0.554	4.69	26.00	1.21	1.08
20.08.2005	3.8	1.47	2.5	2.58	1	15.9	78.5	1019	2	68	1.4	0.461	10.70	31.88	2.86	3.17
21.08.2005	2	2.26	1.1	0.8	0.4	15.8	81.6	1015	0	38	2	0.492	19.36	40.84	0.19	1.14
22.08.2005	11	16.2	1.5	0.4	0.6	17	82.1	1015	0	32	1.8	0.483	37.84	60.28	7.51	9.75
23.08.2005	4.5	0.71	0.7	6.08	1.5	17.7	76.4	1017	134	116	1.6	0.618	41.76	66.43	-0.35	2.74
25.08.2005	6.1	3.76	3.1	1.63	1.6	17.9	75.2	1014	76	82	3.6	1.025	36.50	66.80	-0.66	3.19
27.08.2005	2.8	4.9	0.5	0.57	1.8	15.9	79	1019	185	147	1	0.356	30.20	67.32	0.72	1.77
05.09.2005	1	0.4	1	2.5	8.6	19	79	1017	347	140	1.3	0.518	11.16	55.73	-0.10	-0.24
06.09.2005	6.3	1.6	4.5	3.94	0.2	19.6	78.7	1013	393	172	1.7	0.651	22.16	66.59	3.60	4.44
09.09.2005	6.5	6.93	3.2	0.92	0.4	19.1	80.4	1013	304	130	1.6	0.559	15.22	61.44	4.89	5.03
10.09.2005	15.6	3.8	4.5	4.11	1	18.1	81.3	1013	96	113	1	0.362	21.41	67.77	14.10	14.54
16.09.2005					5.9	17	75.4	1011	387	139	2.9	0.869	18.78	69.64	-3.00	-2.58
26.09.2005	0.9	1.4	0.5	0.64	8.4	16.2	83.3	1023	189	98	1.1	0.309	12.18	66.12	0.17	0.02
01.10.2005	19.5	61.7	1.5	0.32	1.5	11.4	84.4	1021	0	38	2.4	0.352	7.53	59.45	18.99	18.60
18.10.2005	5.9	11.89	1.8	0.5	13.7	9.9	81.6	1022	3	56	1.5	0.283	19.80	76.35	4.81	4.96
21.10.2005	29.7	44.15	5.2	0.67	2.4	14	82.8	1012	149	63	1.5	0.344	24.55	81.55	28.07	28.49
01.11.2005	1.9	1.25	1.5	1.52	8.4	12	87.3	1021	97	59	1.3	0.203	36.58	98.62	0.44	1.03
04.11.2005	14.5	14.44	2.7	1.01	3.3	11.8	91.6	1020	28	41	1.2	0.126	34.03	97.12	13.66	13.97

APPENDIX VII TIME DOMAIN REFLECTOMETRY TDR

VII.1 TDR – principle and calculation

The TDR method is used to assess the soil moisture. Results are given in volumetric water content θ [$m^3.m^{-3}$]. The principle is to deduce the soil moisture from the soil dielectric constant ε, using a fitting calibration equation. The dielectric constant is obtained by measuring the time needed to an electromagnetic wave to propagate along the two metallic rods put in the soil. Every now and then, the electromagnetic wave encounters a discontinuity that reflects the wave. At the end of the rods, practically all the electromagnetic impulse is reflected. The time t needed for the impulsion to go and bounce back from the rod ends (length L) is measured. The soil dielectric constant is then deduced:

Equ. VII.1) $$v = \frac{L}{t} = \frac{c}{\sqrt{\varepsilon}}$$ [$m.s^{-1}$]

Equ. VII.2) $$\varepsilon = \frac{c^2}{v^2}$$ [-]

(ε: soil dielectric constant ; c: light speed ; L: length of the rods ; t: time needed for the impulsion to go and come back)

Many calibration equations exist and are readily found in the literature. The equation established by Topp et al. has been chosen. Mermoud (1999) indeed assumed that this calibration equation is unaffected by the soil nature, the temperature and the salt contents. Because substance content in the runoff water is very high, a calibration equation that is not influenced by salt contents is appropriate. The Topp equation has a disadvantage, though: it is not as linear as other calibration equations (for example Roth or Ledieu). It nevertheless has little influence on field measurements because θ is never bigger than 0.35 – 0.4. Figure VII.1 (right) shows the equation trends for various values of ε. The Topp equation is:

Equ. VII.3) $$\theta = (0.043 \cdot \varepsilon^3 - 5.5 \cdot \varepsilon^2 - 292 \cdot \varepsilon - 530) \cdot 10^{-4}$$ [$m^3.m^{-3}$]

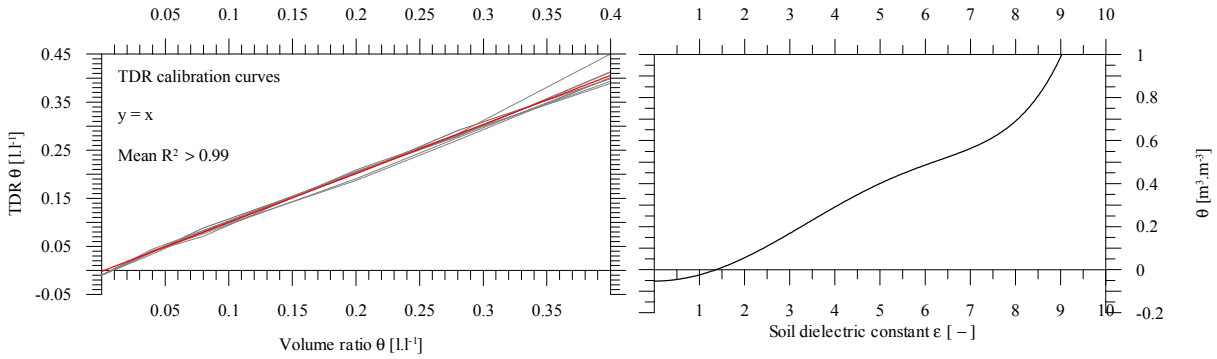

*Figure VII.1: **Left**: TDR calibration curves. The mean R2 depicts a very good correlation between the TDR θ and the handmade θ. See text for discussion. **Right**: Topp et al. calibration curve.*

As ε highly depends on the L and t values, the rod and cable length (the time t being a function of the cable length) are the most influent input values. The calibration of the probes consists in finding the L and cable length values that give the best moisture result. In practice, the software routine is modified, new L and cable length values being entered. See the software routine below for details.
The calibration of each probe has been made in laboratory. Each probe have been put in a known volume of sand ("sable de Fontainebleau") to assess the zero value, then the sand is moisturized with a known volume of water (so the θ is known). This operation is repeated for different amount of water and for each probe. Calibration curves are shown in figure VII.1 (left). Best L and cable length values are respectively 0.149 and 18.6 meters. Probe offset is 0.015 meters. The probe offset is the rod length that is pinned into the probe.

VII.2 Probes locations

The positions of the 8 TDR probes are shown in figure VII.2. Because the probes measure the moisture between the two rods, they needed to be placed as horizontal as possible. In that case only, the moisture measurement corresponds to a precise depth. In case the probe is vertical, it measures the average moisture on 15cm. For practical reasons, the probes at maximum depth have dip of 45 ° (it was hard enough to implement it at 45cm depth, inserting them through a 10cm diameter hole). The probe located in the shoulder body was inserted in a "Fontainebleau" sand bag to ensure a good soil – water – probe contact. The shoulder gravel was indeed far too coarse to ensure such a good contact. This has some effects on the moisturizing – draining curve hysteresis. The cross section is located on the 440 LW profile.

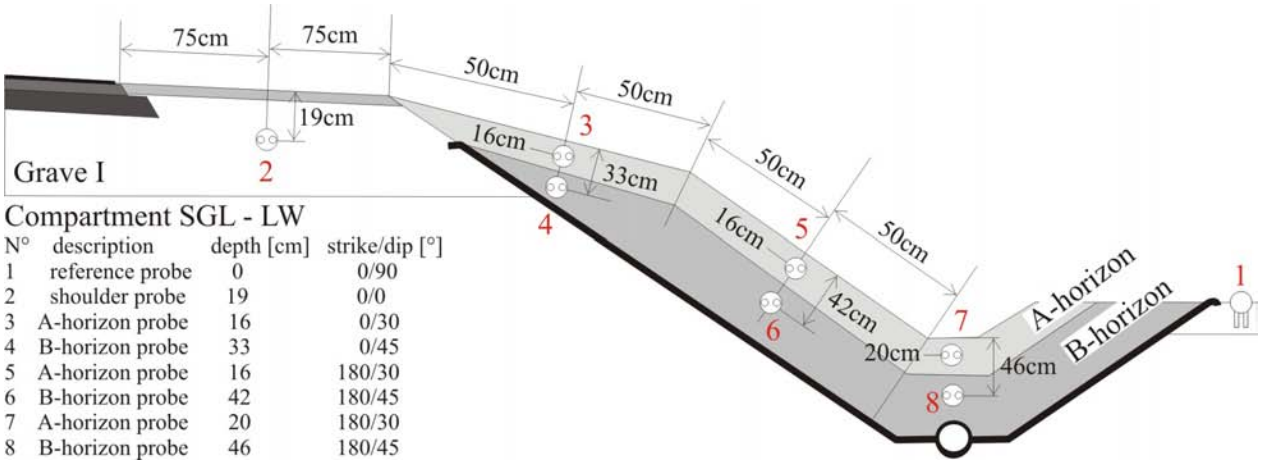

Compartment SGL - LW

N°	description	depth [cm]	strike/dip [°]
1	reference probe	0	0/90
2	shoulder probe	19	0/0
3	A-horizon probe	16	0/30
4	B-horizon probe	33	0/45
5	A-horizon probe	16	180/30
6	B-horizon probe	42	180/45
7	A-horizon probe	20	180/30
8	B-horizon probe	46	180/45

Figure VII.2: TDR probes positions, depths, strike and dip. Note that the probe n°2 is placed in a sand ("Fontainebleau") socket because the grave I is too coarse grained.

APPENDIX VIII STATISTICAL ANALYSIS, 3D PLOTS, AND GRAPHICAL ANALYSIS

VIII.1 Linear correlation

Reminder: the linear correlation method gives insights on the eventual linear correlation bounding two parameters. It has three steps:

1) Parameters are standardized. Standard value are calculated this way:

Equ. VIII.1)
$$V°1_i = \frac{(V1_i - \overline{V}1)}{\sigma 1}$$

($V°1_i$: Standard value, parameter 1, data I; $V1_i$: parameter 1, data i; $\overline{V}$ 1: mean V1; σ1: standard deviation)

2) Parameters are correlated using the covariance:

Equ. VIII.2)
$$R = Cov(V1;V2) \qquad R \in [0;1]$$

(R: Linear correlation coefficient)

R^2 is often used instead of R because the R value is linearly distributed, while the confidence is not. Thus R=0.5 becomes R^2=0.25 for example. High R2 means a very good correlation.

3) Linear correlation coefficient R is tested using the student T-test:

Equ. VIII.3)
$$T_{Student} = |R| \cdot \sqrt{\frac{N-2}{1-R^2}} \qquad R \in [0;1]$$

($T_{Student}$: student T-test; N: number of data)

The higher $T_{Student}$ is, the better the correlation is. Tables exist in the literature presenting the relationship between the $T_{Student}$ number and the interval of confidence (in the present case, if $T_{Student}$ > 10.5 with N=80, then the interval of confidence is >95%). The table VIII.1 below shows the final results ($T_{Student}$, R^2); N=80.

			Student T-test											
		Date	Rainfall	Duration	Max I	Mean I	Preceding drought	Temp.	Humidity	Atmos. Pressure	Sunning	Solar heat flux	Wind	IPA
	Date		0.43	1.23	0.12	0.04	0.44	4.27	0.80	0.99	2.10	1.87	3.44	0.66
R^2-Covariance	Rainfall	0.00		9.35	6.92	0.15	1.33	0.44	2.69	1.16	1.94	2.26	0.19	0.51
	Duration	0.01	0.45		3.27	2.57	0.78	2.71	1.26	1.41	2.49	2.56	1.41	0.95
	Max intensity	0.00	0.32	0.10		5.31	1.10	1.23	0.97	1.17	0.23	0.07	0.45	0.26
	Mean intensity	0.00	0.00	0.06	0.21		0.73	3.64	1.63	0.34	4.08	3.58	2.02	0.32
	Preceding drought	0.00	0.02	0.01	0.01	0.00		0.62	0.25	2.05	0.01	0.30	1.12	2.45
	T°C moy	0.14	0.00	0.06	0.01	0.11	0.00		4.42	0.03	5.67	8.30	2.08	3.33
	Humidity	0.01	0.06	0.01	0.01	0.02	0.00	0.15		0.62	8.46	11.01	3.73	3.67
	Atmos. Pressure	0.01	0.01	0.02	0.01	0.00	0.04	0.00	0.00		0.42	0.05	1.95	1.38
	Sunning	0.04	0.03	0.05	0.00	0.13	0.00	0.23	0.39	0.00		19.41	1.27	1.04
	Solar heat flux	0.03	0.04	0.06	0.00	0.10	0.00	0.38	0.52	0.00	0.77		0.90	3.22
	Wind	0.10	0.00	0.02	0.00	0.04	0.01	0.04	0.11	0.03	0.01	0.01		0.64
	IPA	0.00	0.00	0.01	0.00	0.00	0.05	0.09	0.11	0.02	0.01	0.09	0.00	

*Table VIII.1: Results of the linear correlation tests. **Lower left**: R^2 covariance. The highest value is 0.77 (good correlation, "Introduction à la Statistique", op. cit.) and correlates the solar heat flux with the sunning. This is not surprising. More interesting is the correlation between the rainfall and the maximum intensity that does not exist between rainfall and mean intensity. **Upper right**: Student T-test. The higher the value is, the better the correlation is. For example, consider the correlation between the solar heat flux and the sunning: R^2=0.77 and $T_{Student}$ = 19.41. This means the correlation is good (R^2) and that the interval of confidence is >95% ($T_{Student}$).*

VIII.2 Principal components analysis PCA

PCA are very useful and powerful tools to assess the eventual relationships that exist between the different parameter governing the infiltration. PCA have been plotted for all data recorded in 2004 and 2005. PCA have been computed using the extension macro XLStat with excel. Data are available in appendix VI. Tables below are the results provided by the computation.

Variables	Date	Rainfall	Duration	I Max	I Mean	Preceding	Mean T	Humidity	QFF-P	Sunning	Solar heat	Wind	ETP	IPA Shoulder	IPA lysimeter	ΔS Shoulder	ΔS Lysimeter
Date	**1.00**	-0.03	-0.09	0.09	-0.02	-0.04	**0.35**	0.13	0.10	0.12	0.10	**-0.34**	-0.06	-0.02	0.08	-0.02	-0.03
Rainfall	-0.03	**1.00**	**0.66**	**0.57**	-0.01	-0.13	-0.01	**0.24**	-0.12	-0.14	-0.18	-0.01	-0.15	0.04	0.03	**0.99**	**1.00**
Duration	-0.09	**0.66**	**1.00**	**0.30**	**-0.24**	-0.08	**-0.22**	0.10	-0.14	-0.18	**-0.20**	0.14	-0.10	-0.11	-0.08	**0.68**	**0.67**
Max	0.09	**0.57**	**0.30**	**1.00**	**0.50**	-0.12	**0.21**	0.05	-0.13	0.14	0.10	-0.04	0.01	-0.06	-0.05	**0.57**	**0.57**
Mean	-0.02	-0.01	**-0.24**	**0.50**	**1.00**	-0.06	**0.33**	-0.13	0.03	**0.37**	**0.33**	-0.17	0.12	0.00	-0.08	-0.03	-0.02
Preceding	-0.04	-0.13	-0.08	-0.12	-0.06	**1.00**	-0.06	-0.02	**0.21**	0.00	-0.02	-0.10	0.00	**-0.23**	-0.14	-0.08	-0.11
Mean T	**0.35**	-0.01	**-0.22**	**0.21**	**0.33**	-0.06	**1.00**	**-0.35**	0.01	**0.43**	**0.60**	**-0.21**	**0.54**	**-0.20**	**-0.45**	-0.02	-0.03
Humidity	0.13	**0.24**	0.10	0.05	-0.13	-0.02	**-0.35**	**1.00**	-0.06	**-0.62**	**-0.73**	**-0.36**	**-0.86**	**0.35**	**0.41**	**0.25**	**0.28**
QFF-P	0.10	-0.12	-0.14	-0.13	0.03	**0.21**	0.01	-0.06	**1.00**	0.04	-0.02	-0.19	0.02	-0.18	0.00	-0.10	-0.12
Sunlight	0.12	-0.14	-0.18	0.14	**0.37**	0.00	**0.43**	**-0.62**	0.04	**1.00**	**0.86**	-0.13	**0.47**	-0.09	-0.15	-0.16	-0.17
Solar heat	0.10	-0.18	**-0.20**	0.10	**0.33**	-0.02	**0.60**	**-0.73**	-0.02	**0.86**	**1.00**	-0.09	**0.62**	**-0.30**	**-0.42**	-0.18	**-0.20**
Wind	**-0.34**	-0.01	0.14	-0.04	-0.17	-0.10	**-0.21**	**-0.36**	-0.19	-0.13	-0.09	**1.00**	**0.48**	-0.14	-0.07	-0.05	-0.06
ETP	-0.06	-0.15	-0.10	0.01	0.12	0.00	**0.54**	**-0.86**	0.02	**0.47**	**0.62**	**0.48**	**1.00**	**-0.35**	**-0.44**	-0.18	**-0.21**
IPA Shoulder	-0.02	0.04	-0.11	-0.06	0.00	**-0.23**	**-0.20**	**0.35**	-0.18	-0.09	**-0.30**	-0.14	**-0.35**	**1.00**	**0.78**	-0.06	0.02
IPA lysimeter	0.08	0.03	-0.08	-0.05	-0.08	-0.14	**-0.45**	**0.41**	0.00	-0.15	**-0.42**	-0.07	**-0.44**	**0.78**	**1.00**	-0.04	0.00
ΔS Shoulder	-0.02	**0.99**	**0.68**	**0.57**	-0.03	-0.08	-0.02	**0.25**	-0.10	-0.16	-0.18	-0.05	-0.18	-0.06	-0.04	**1.00**	**0.99**
ΔS Lysimeter	-0.03	**1.00**	**0.67**	**0.57**	-0.02	-0.11	-0.03	**0.28**	-0.12	-0.17	**-0.20**	-0.06	**-0.21**	0.02	0.00	**0.99**	**1.00**

Table VIII.2: Correlation matrix. Data in bold are values significantly different from zero. Differences that occurred between this correlation matrix and the one made for the linear correlation are mainly due to the standardization process. In the present case, the parameters are standardized in respect to all other parameters. In the previous table, they were standardized in respect to only one other parameter.

	F1	F2	F3	F4	F5	F6	F7	F8	F9	F10	F11	F12	F13	F14	F15	F16	F17
Date	-0.03	0.02	-0.37	-0.23	0.58	0.03	0.22	0.39	-0.41	-0.02	-0.24	-0.08	-0.21	0.03	0.04	0.00	0.00
Rainfall	0.33	0.35	0.00	0.02	0.03	0.14	0.01	0.02	0.18	-0.17	-0.16	-0.04	-0.02	-0.02	-0.01	-0.62	-0.52
Duration	0.27	0.25	0.24	-0.02	0.14	0.17	-0.12	-0.12	-0.33	0.76	0.03	0.14	0.12	0.06	-0.01	-0.01	0.00
Max	0.13	0.36	-0.22	0.11	-0.28	-0.16	0.17	0.25	-0.29	-0.06	0.71	-0.05	-0.09	-0.01	0.02	0.00	0.00
Mean	-0.11	0.17	-0.36	0.14	-0.56	-0.26	0.17	0.02	-0.12	0.27	-0.55	-0.06	0.02	0.04	0.02	0.00	0.00
Preceding	-0.05	-0.05	0.09	-0.45	-0.35	0.25	-0.42	0.63	0.10	0.08	-0.02	0.03	-0.03	0.07	-0.02	-0.01	0.00
Mean T	-0.23	0.27	-0.26	-0.08	0.25	-0.21	0.11	0.15	0.53	0.23	0.12	0.27	0.27	0.04	-0.40	0.03	0.01
Humidity	0.35	-0.21	-0.21	-0.16	0.00	-0.26	-0.02	0.01	0.05	-0.05	0.01	0.60	0.20	-0.01	0.54	-0.02	0.00
QFF-P	-0.07	-0.06	-0.06	-0.41	-0.22	0.52	0.62	-0.24	0.09	0.05	0.09	0.15	-0.09	0.10	0.02	0.01	0.00
Sunlight	-0.29	0.22	-0.23	0.16	-0.03	0.37	-0.28	-0.12	-0.22	-0.17	-0.05	0.46	-0.05	-0.51	-0.09	0.03	0.00
Solar heat	-0.35	0.27	-0.13	0.07	0.06	0.15	-0.26	-0.17	-0.07	-0.14	0.04	0.05	0.09	0.74	0.28	-0.04	0.00
Wind	-0.04	0.04	0.51	0.34	-0.03	-0.03	0.32	0.36	-0.12	-0.16	-0.16	0.48	-0.09	0.23	-0.16	0.03	0.00
ETP	-0.32	0.24	0.23	0.15	0.10	0.11	0.20	0.24	0.23	0.14	0.00	-0.20	0.14	-0.32	0.64	0.00	0.04
IPA Shoulder	0.15	-0.22	-0.28	0.46	0.04	0.24	-0.08	0.12	0.35	0.28	0.07	0.05	-0.56	0.11	0.10	0.09	-0.04
IPA lysimeter	0.19	-0.27	-0.23	0.35	-0.01	0.41	0.09	0.21	-0.08	-0.06	0.01	-0.14	0.67	0.06	-0.11	-0.01	0.06
ΔS Shoulder	0.33	0.36	0.01	-0.05	0.02	0.10	-0.02	-0.01	0.12	-0.20	-0.16	-0.08	0.05	0.02	0.02	0.77	-0.27
ΔS Lysimeter	0.34	0.34	-0.01	-0.02	0.02	0.10	-0.02	-0.01	0.17	-0.17	-0.16	-0.03	-0.09	0.01	-0.01	-0.14	0.80

Table VIII.3: Eigenvectors. They describe the weight of the projection vectors and are the basis to the building of the bi-axis plot shown below. F1 and F2 are used are the principal projection vectors.

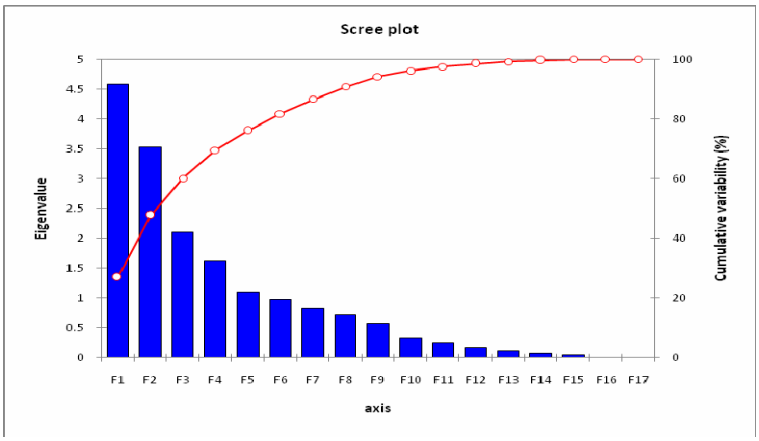

Figure VIII.1: Eigenvectors of each F vector. The cumulative variability represents the variance weight for each vector F. The 2 chosen vectors for the projection are F1 and F2. They both cumulate up to 50% of the overall variability.

The building of PCA is thoroughly explained in “Introduction à la statistique”, Stephan Morgenthaler, 1997. The principle is to build parameter vectors as a function of the main direction of variance. Main directions of variance (called component) build projection axes. Vectors are then weighted and correlated in that new coordinate system. The resulting PCA plot is shown in the text.

VIII.3 3D plots axes resulting from ACP

The 3D plots needs 3 axes. They are the precipitation P, the mean intensity I_{mean} and the IPA. The distribution of the events along those three axes is determinant for the visualisation. The figure below shows the log-normal distribution of the events along the three 3 axes. The distribution responds to the equation:

Equ. VIII.4)

$$F(x) = \frac{e^{-((\ln((x-\theta)/m))^2/2\sigma^2))}}{(x-\theta)\sigma\sqrt{2\pi}}$$

(θ: location parameter; σ: shape parameter; m: scale parameter)

Parameters were fitted using a fitting software (Datafit 8.2; Oakdale Engineering). The quartiles were also computed (XLStat).

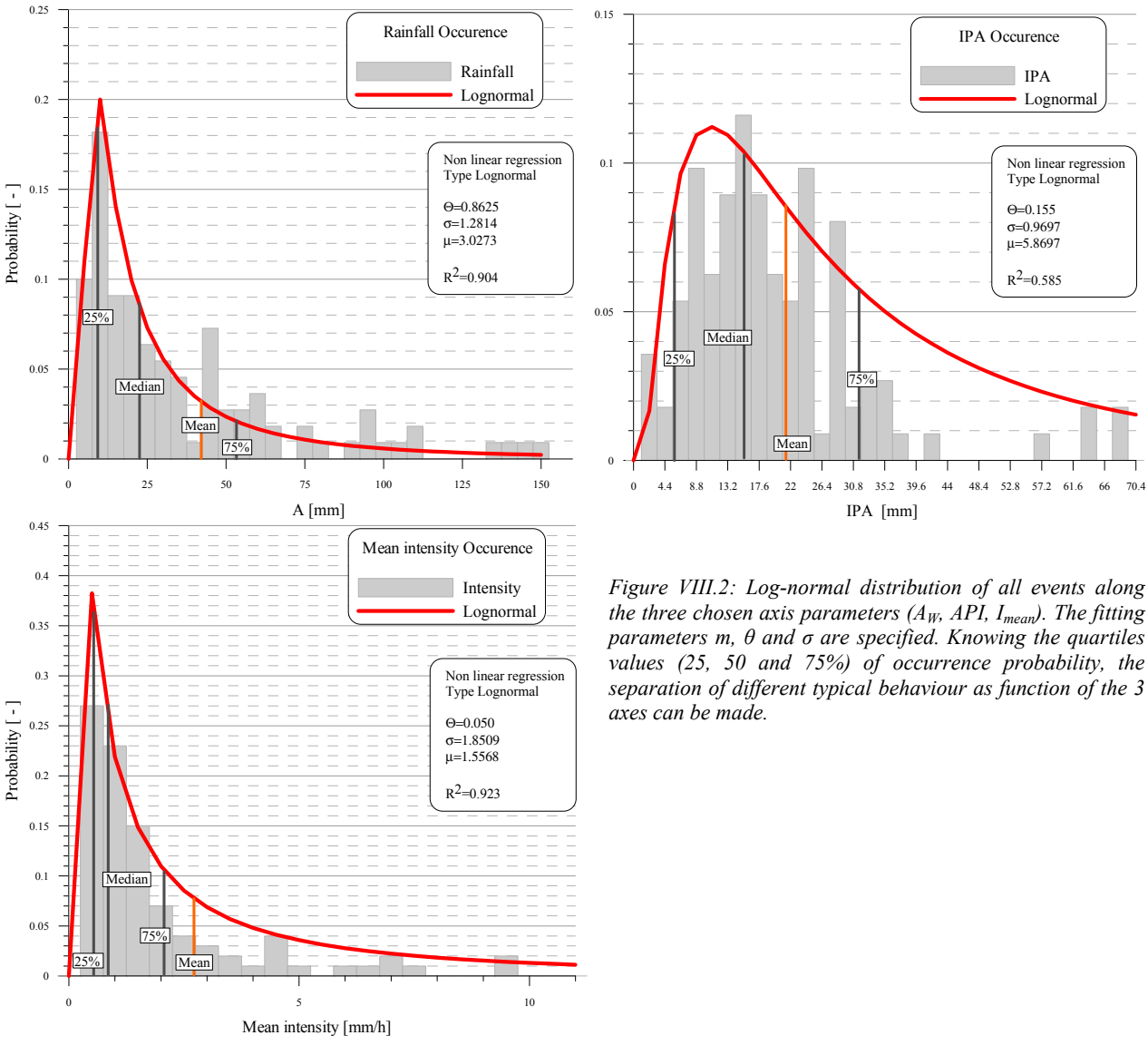

Figure VIII.2: Log-normal distribution of all events along the three chosen axis parameters (A_W, API, I_{mean}). The fitting parameters m, θ and σ are specified. Knowing the quartiles values (25, 50 and 75%) of occurrence probability, the separation of different typical behaviour as function of the 3 axes can be made.

VIII.4 3D-plots

A) Discrimination as function of the exfiltrated water

To avoid repetition, extensive results are not presented in the thesis. The resulting 3D diagrams are hereby presented. Remarks about the shoulder SGC, SGL and SH are (SGH is presented in the text):

SGC: the C_G of the first interval (0; 5mm) is just above the 25% A_W quartile, on the 50% API and 50% I_{mean} quartiles. The last C_G (70; 145mm) is well beyond the 75% A_W quartile and pretty much on the same 50% API and I_{mean} quartiles. The evolution of E_S along the A_W axis is again flagrant: the more it rains the more the shoulder exfiltrates. E_S behaves along the API axis the same way as it does for SGH but augments only very little: the shift is far smaller. Finally, the evolution of ES along the I_{mean} axis is more or less unreadable. No specific behaviour is relevant. Finally, the coloured areas are pretty much the same as for SGH. The A_W shift is neat, the API shift is questionable and the I_{mean} shift is inexistent.

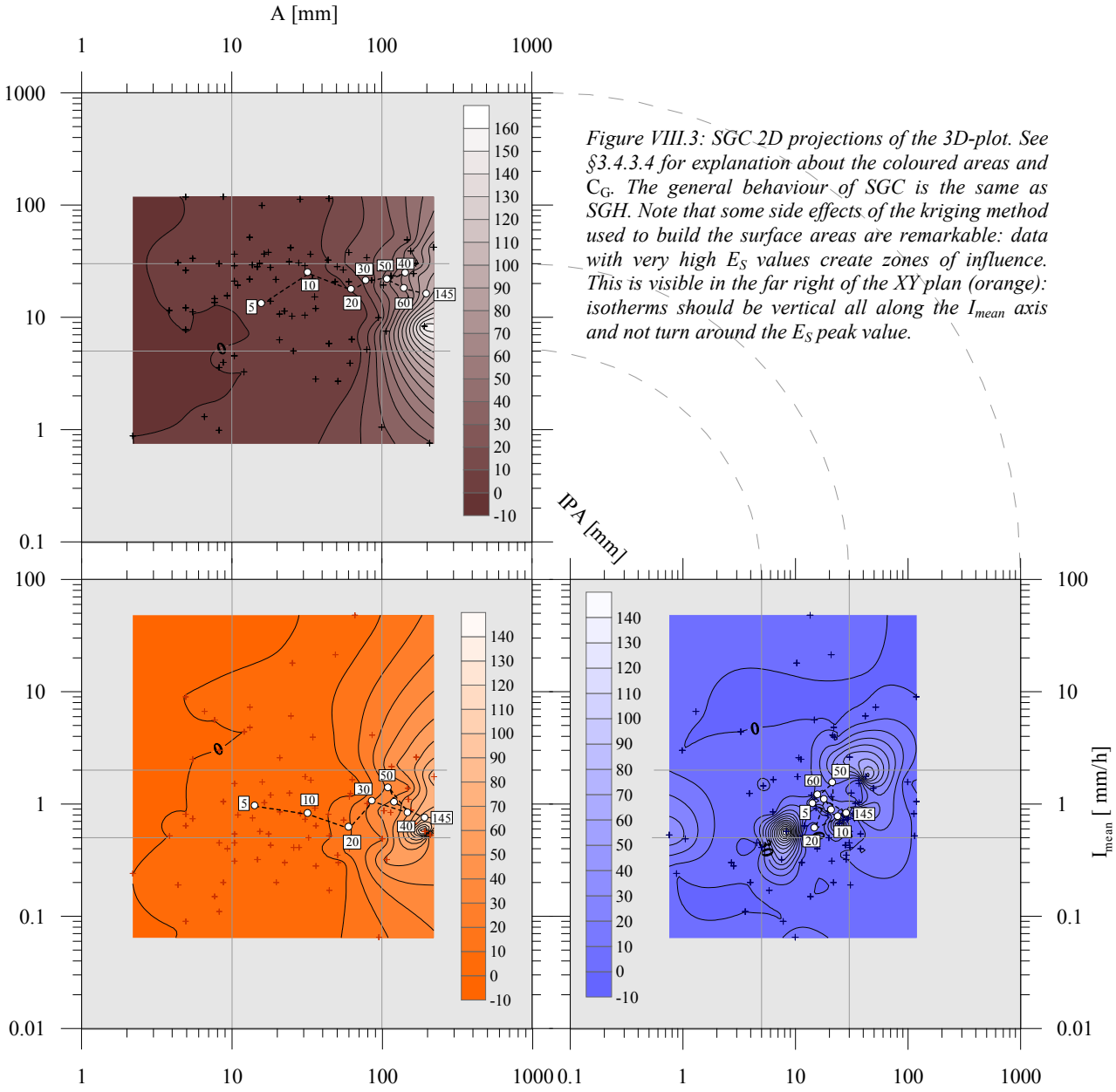

Figure VIII.3: SGC 2D projections of the 3D-plot. See §3.4.3.4 for explanation about the coloured areas and C_G. The general behaviour of SGC is the same as SGH. Note that some side effects of the kriging method used to build the surface areas are remarkable: data with very high E_S values create zones of influence. This is visible in the far right of the XY plan (orange): isotherms should be vertical all along the I_{mean} axis and not turn around the E_S peak value.

SGL: the C_G of the first interval (0; 5mm) is placed on the 25% A_W quartile, and nearly on the 50% API and I_{mean} quartiles. The C_G of the last interval (70; 200) is well beyond the 75% A_W quartiles and still on the 50% API and I_{mean} quartiles. The E_S augmentation along the A_W axis is regular and neat. It again means that the shoulder exfiltrates more water when more water is available. The E_S augmentation is linked to API, although this is not clear regarding the C_G. The coloured area is more explicative. Again, the distribution of E_S along the I_{mean} axis is random. IPA and I_{mean} C_G remain close to the 50% quartiles. Coloured areas show the same pattern as before.

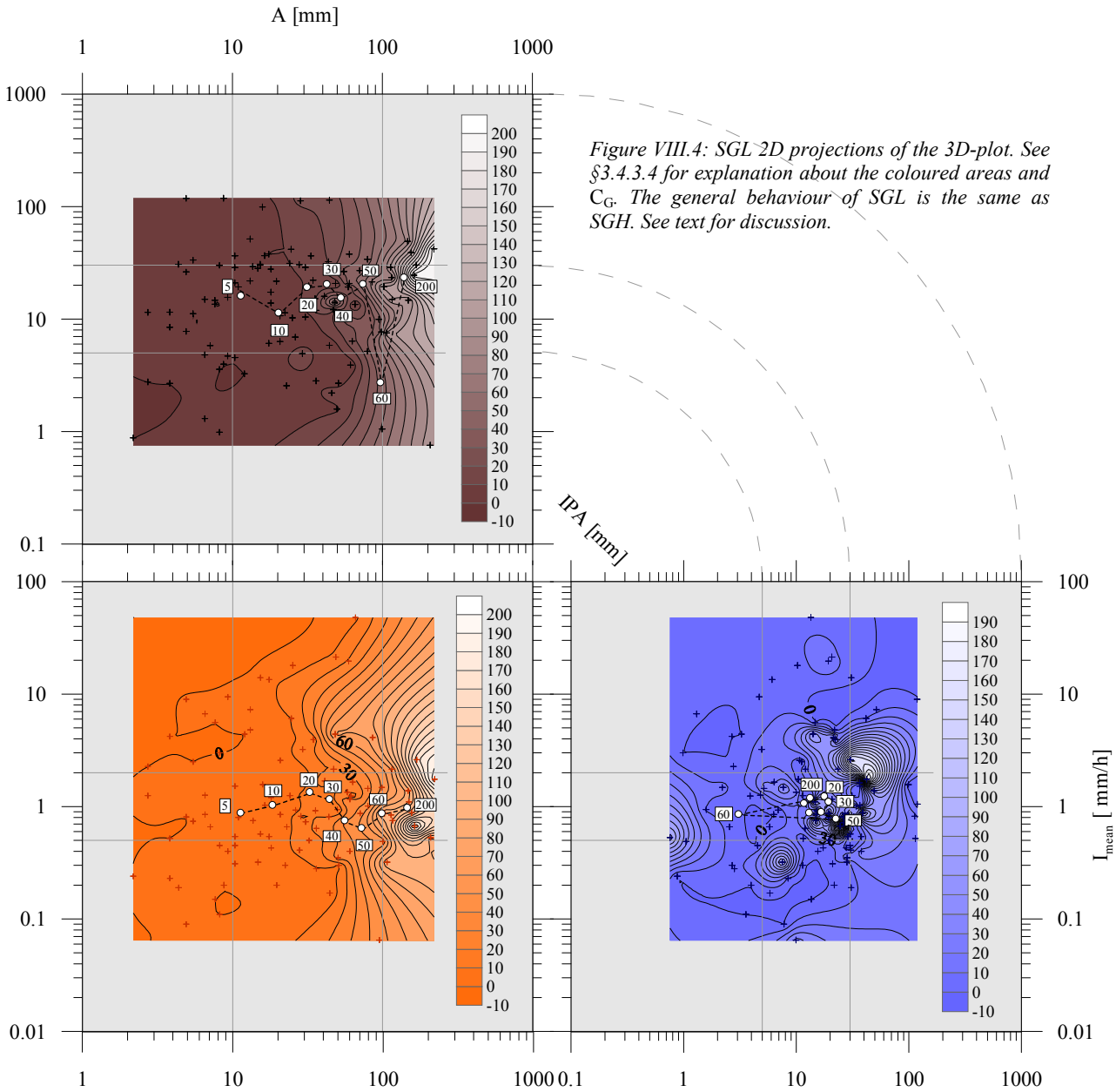

Figure VIII.4: SGL 2D projections of the 3D-plot. See §3.4.3.4 for explanation about the coloured areas and C_G. The general behaviour of SGL is the same as SGH. See text for discussion.

SH: C_G of the first interval (0; 5mm) is similarly positioned as for the other shoulders (25% A_W, 50% API, 50% I_{mean} quartiles). The last C_G (60; 80) is also placed like for the other shoulders. The repartition of the C_G along the A_W axis is less straightforward: it indeed has a back-loop between the C_G 30 and 40. Nevertheless, the general trend is the same: the greater A_W is the bigger the exfiltration is. The influence of API is more sensible than for the other shoulders. E_S varies from 50 to 75% quartiles and back. The fact that all the shoulders show a similar though weaker trend might be due to a link between the available water A_W and the API (rainfall volumes and API as well are dependant of the season). However, no particular link appears when plotting the API versus A_W: it shows an erratic behaviour. Finally, the E_S variation along the I_{mean} axis as erratic as for the other shoulder but the amplitude of variation is far greater. The C_G moves from the 25% to beyond the 75% quartiles. Coloured areas show exactly the same trend as for the other shoulders.

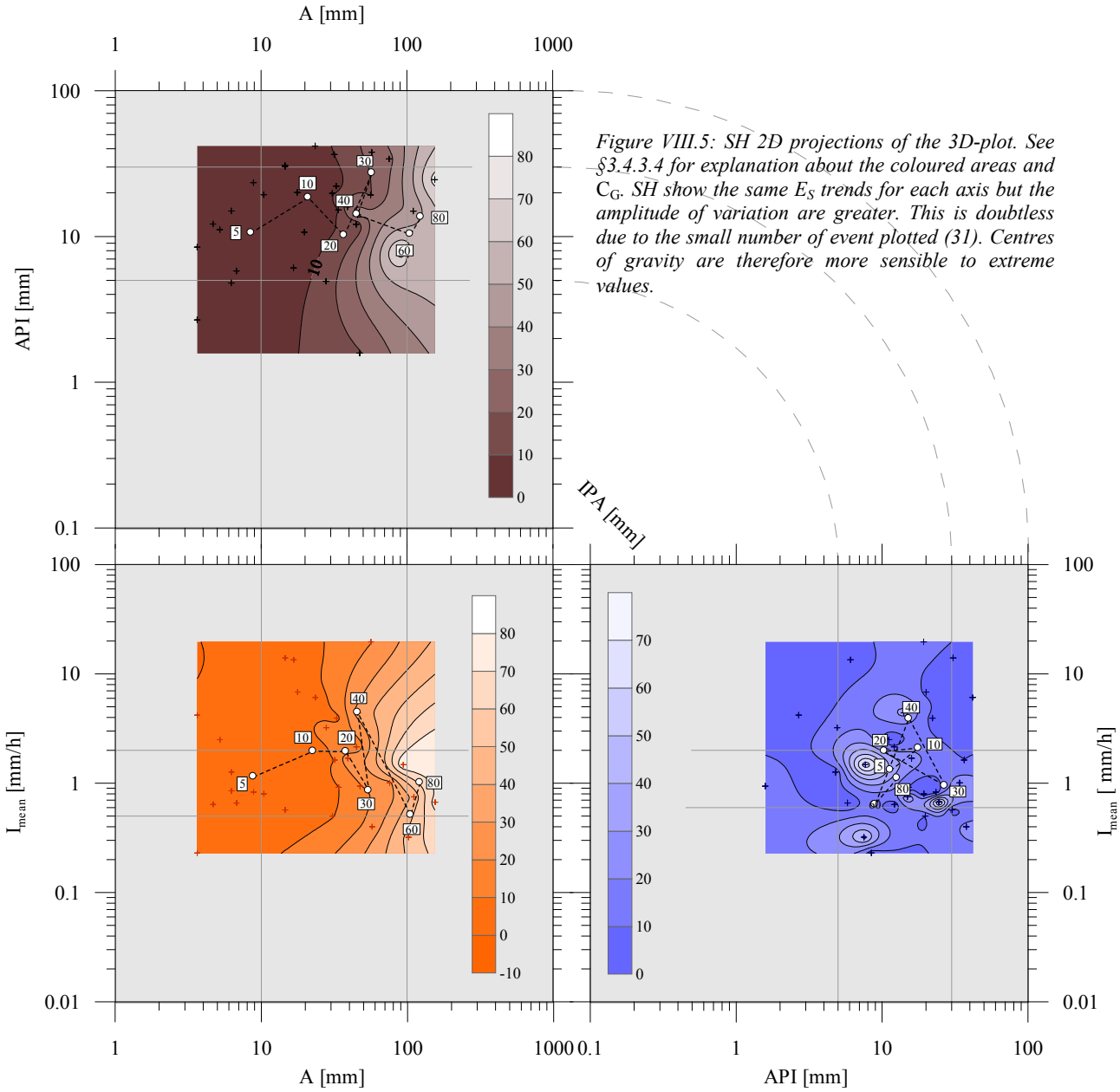

Figure VIII.5: SH 2D projections of the 3D-plot. See §3.4.3.4 for explanation about the coloured areas and C_G. SH show the same E_S trends for each axis but the amplitude of variation are greater. This is doubtless due to the small number of event plotted (31). Centres of gravity are therefore more sensible to extreme values.

Conclusions about the results provided are discussed in the text.

B) Discrimination as function of the lag time

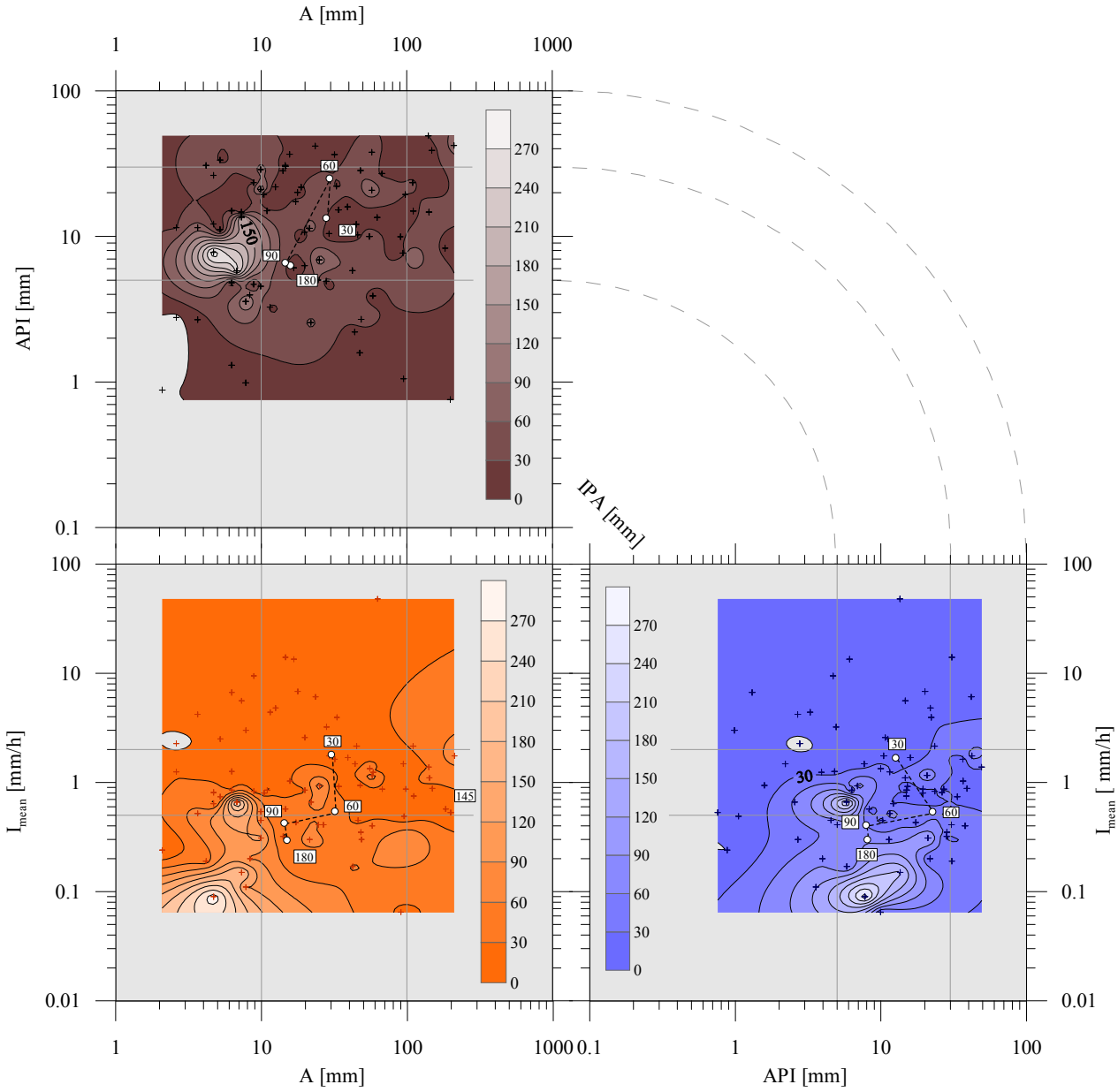

SGH Lag time discrimination. The maximum lag time is only 127 minutes. Lag times are correlated with the mean rainfall intensity. The correlation with API is hard to assess.

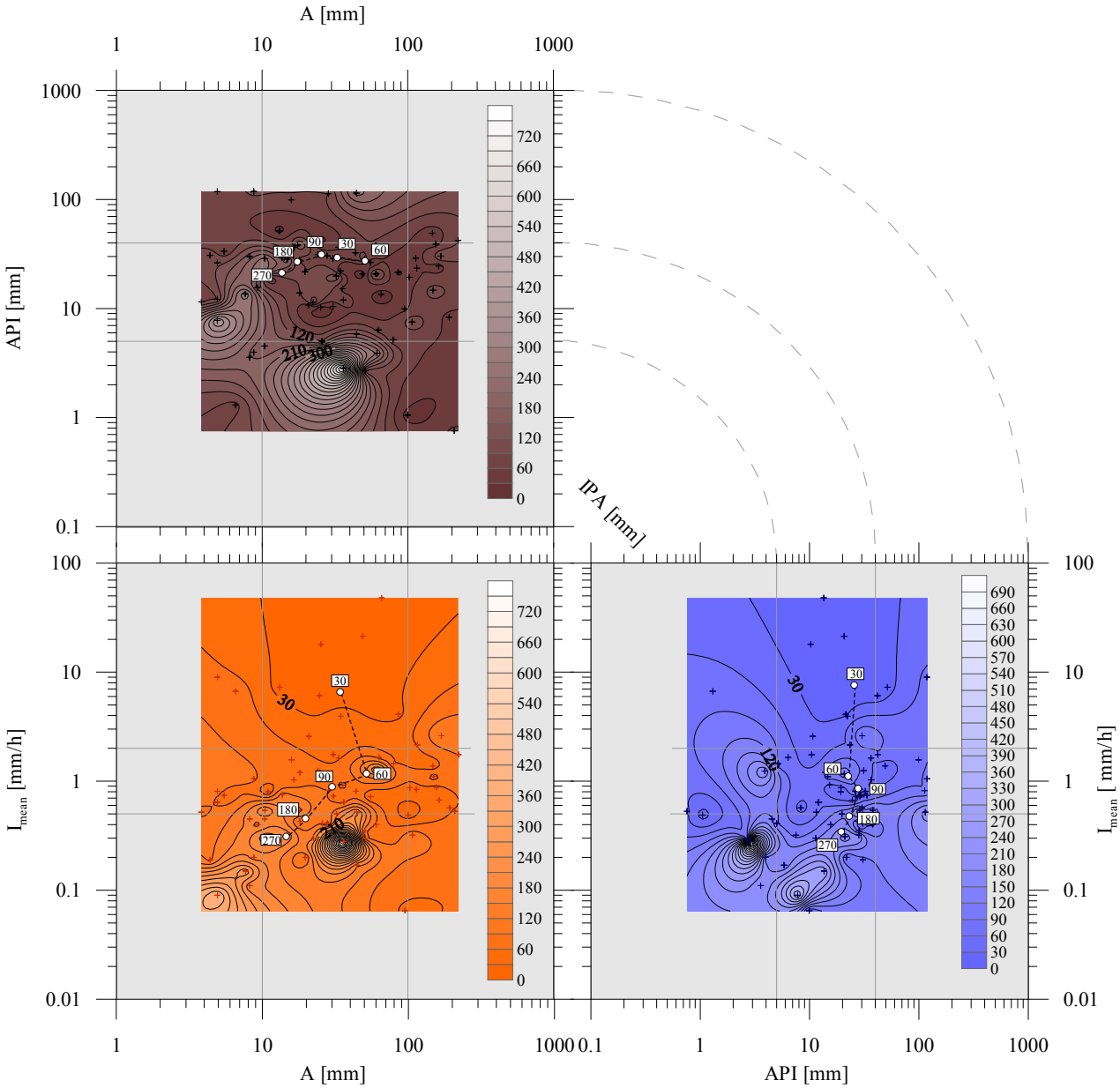

SGC lag time discrimination. Again, lag times correlation with the rainfall intensity is obvious. There is almost no correlation at all between lag times and API. The available water A_W on the shoulder surface has also an influence on the exfiltration volume: the higher the volume, the shorted the lag time. Nevertheless, the mean intensity is the leading process.

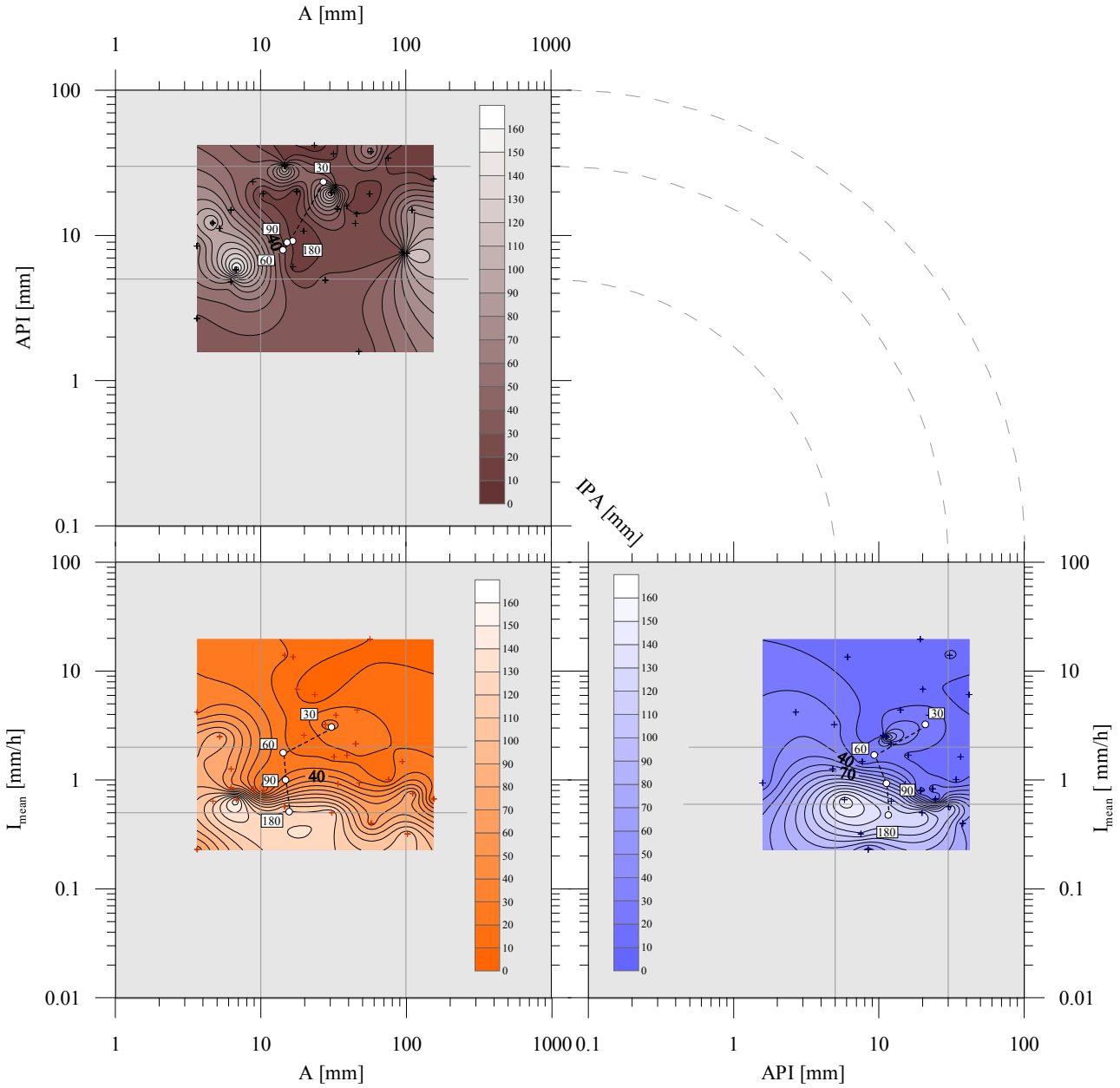

SH lag times discrimination. The influence of the I_{mean} on the lag time is again obvious. The available water on the surface A_W has also a slight influence for heavy rainfalls (>20 mm). This was not observed for other shoulders

VIII.5 Graphical analyses

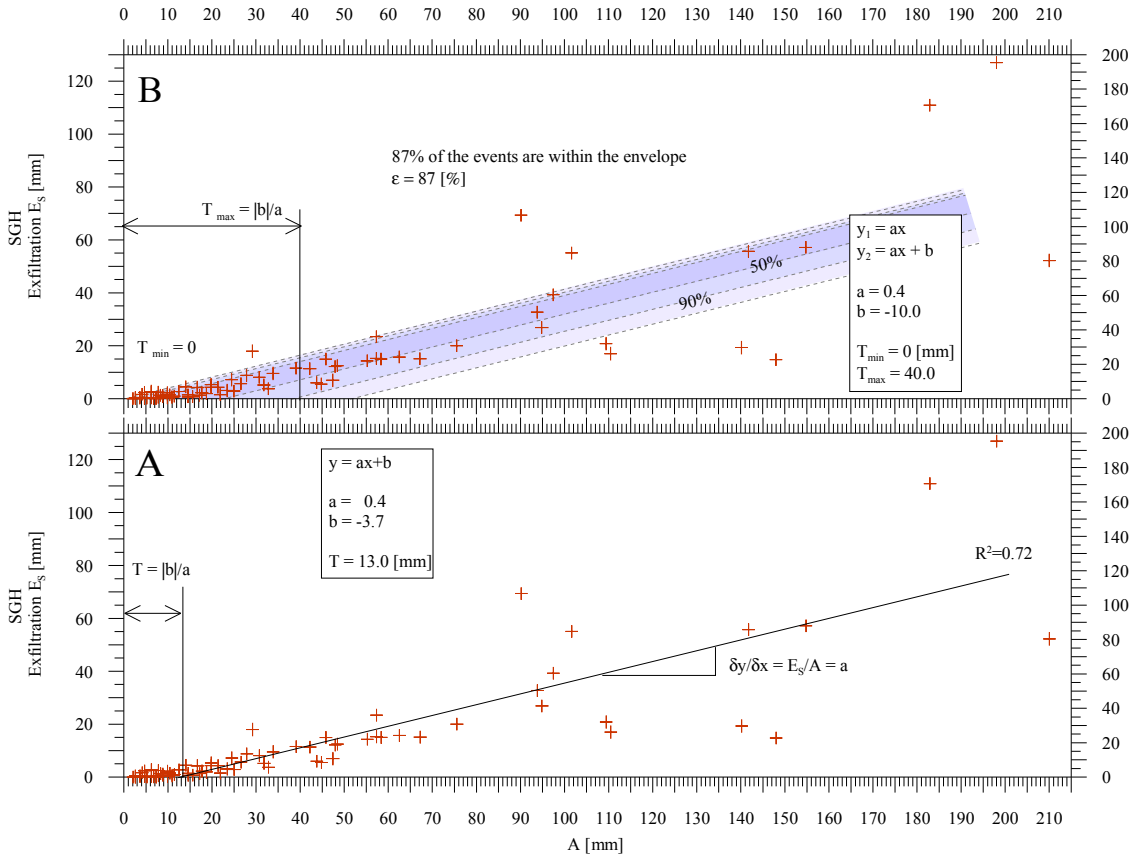

Graphical resolutions Above: SGH; Below: SGC

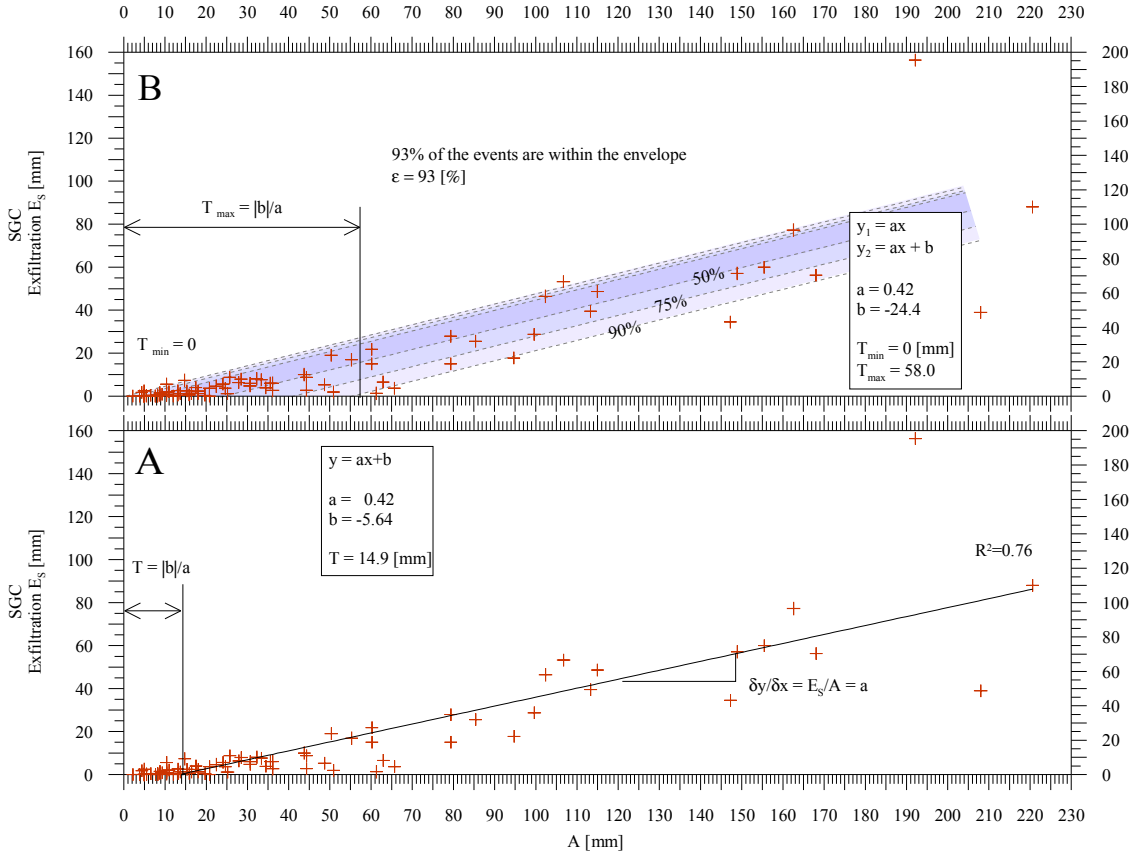

Graphical resolutions Shoulder SH.

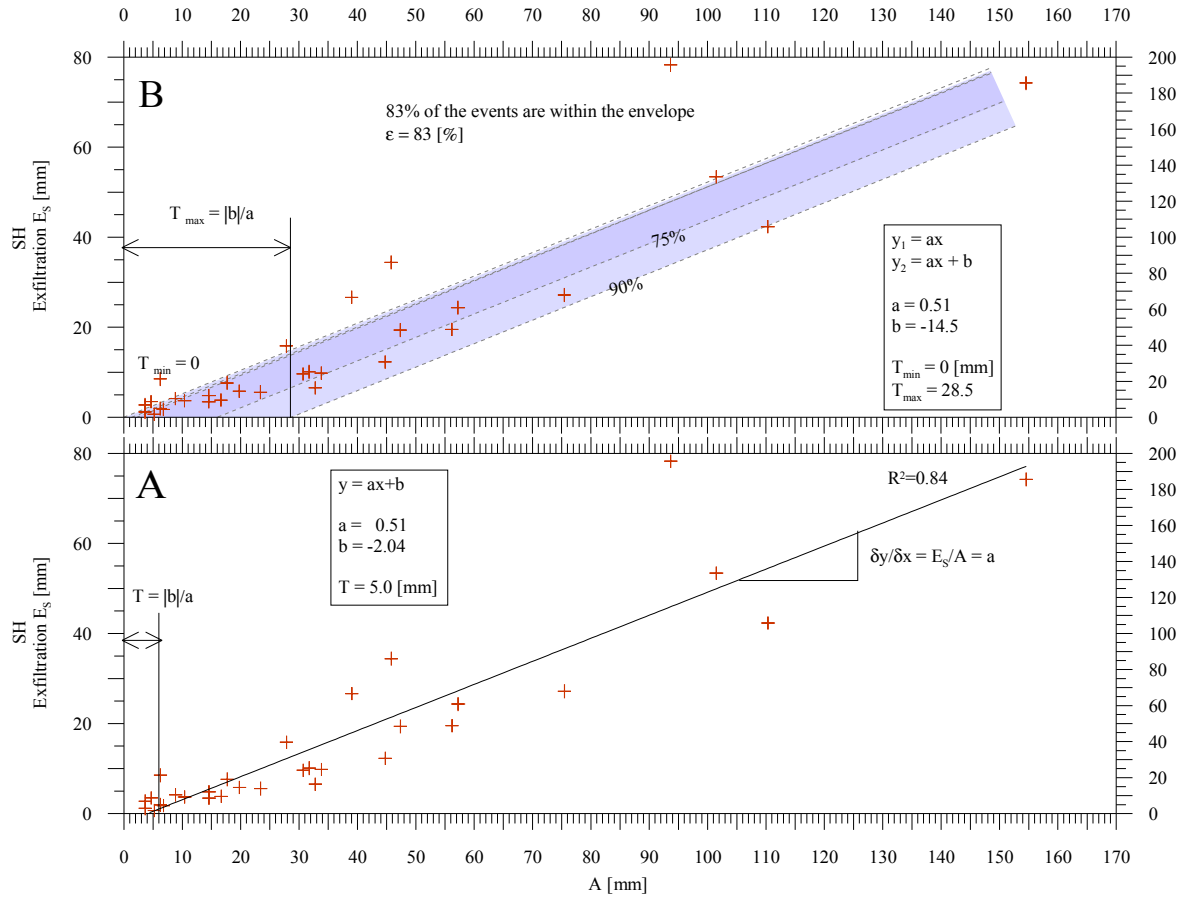

APPENDIX IX ANALYTIC METHODOLOGY; BATCH AND COLUMN TESTS PROTOCOLS

IX.1 MTE

Instrument and experimental conditions

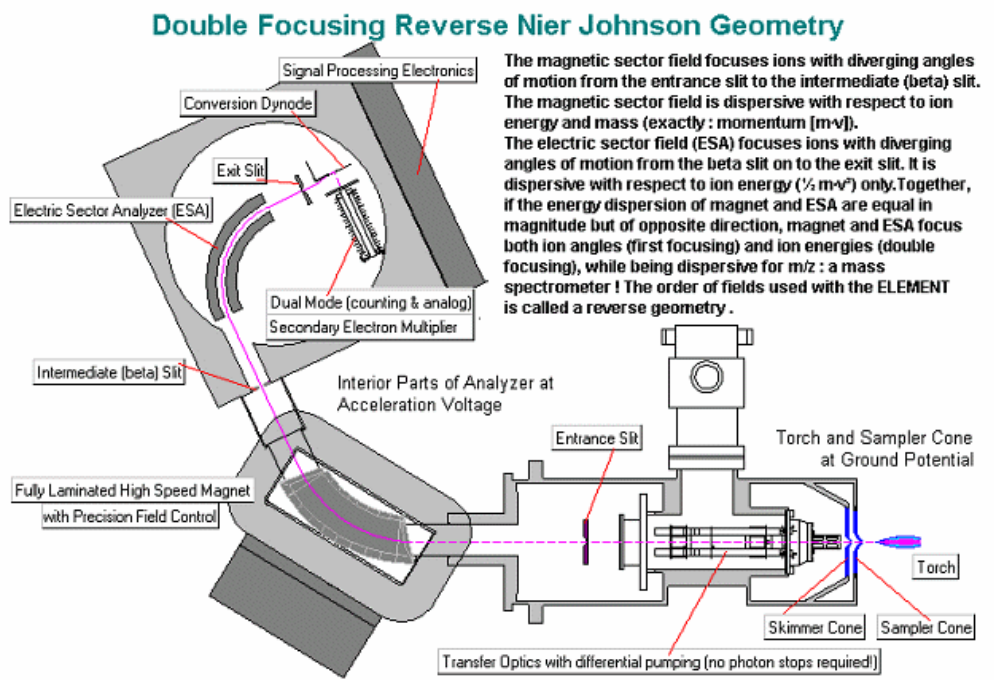

The mass resolution was set to 4000 in order to use the ability of the high resolution technique to resolve most spectral interferences from the analyte ions observed for transition metals. The high resolution mode is also useful for samples having unexpected or unknown interferences, because the quantification is obtained by integrating only the area of the analyte peak, without the influence of an unexpected interference peak.

Operating conditions

The Element2 instrument was used with a standard glass spray chamber and Meinhard nebulizer, under operating conditions shown in the adjoining table.

ICP-SFMS conditions	
Incident Rf power	1.2 kW
Plasma gas flow rate	15 l min-1
Nebulizer gas flow rate	0.8 l min-1
Cool gas flow rate	1.2 l min-1
Accelerating voltage	5 kV
Mass resolution (10% valley)	500 , 4000 and 10000

Sensitivity

The sensitivity was better than $1.2x10^5$ cps/ppb of ^{115}In at a mass resolution of 4000, which corresponds to $1.2x10^6$ cps/ppb at low resolution mode of 500.

Repeatability

Measurement repeatability expressed in terms of RSD was better than 5%, depending on the element.

Accuracy

The accuracy of the method was tested using certified riverine water reference materials SLRS-3. Accuracy was better than 5%.

Detection limits

The detection limits obtained for trace metals in the Medium resolution mode (R=4000) without the influence of signal interferences were in routine mode less than 0.2 $ng \cdot l^{-1}$ for all elements.

Standards and sampling

Calibration standards were prepared through successive dilutions in cleaned Teflon bottles, of $1g \cdot l^{-1}$ ICPMS stock solutions (Bernd Kraft). Suprapur® grade nitric acid (65% Merck) was used for the acidification of samples and for

the preparation of standards (2+1000). Ultrapure water was produced using Milli-Q® Ultrapure Water System (Millipore, Bedford, USA). New low density polyethylene (LDPE) bottles used for sampling and Teflon bottles were cleaned several times with diluted ultrapure HNO3 solution (10+1000) and rinsed with ultrapure water.

Tuning
Standard solution containing 1 µg l^{-1} of Li, Be, Co, In, La and U was used for tuning and testing the stability of the instrument.
Riverine water certified reference material for trace metals used for accuracy measurements was SLRS-3 from National Research Council Canada, Ottawa, Ontario.
Typical stability test repeatability was better than 2% Relative Standard Deviation (RSD).

Samples treatment and storage
Samples were acidified (2+1000) with suprapur® grade nitric acid (65% Merck). If necessary, the samples were then filtrated and stored at low temperature. Membranes, 0.45µm filters, type HAWP04700, from Millipore™, were used for sample filtration.

IX.2 PAH, PCB and CX

EXTRACTION LIQUID – LIQUID

Extraction
800ml (or 200ml for batch tests) of sample are placed in a glass can. Fifty ml (30ml for batch tests) of pentane are added to extract the organic compounds by agitation. The process is repeated three times. The solute was set to rest for 15min between each extraction. The fraction is then dried on a sodium sulphate funnel. If the decantation is insufficient, it is centrifuged at 2500t for ten minutes. The rest is evaporated at Rotavapor (780mbar; 30°C) at 1ml. It is then concentrated under nitrogen flux until 0.5ml and purified.

Protocol
A 40cm length, 10mm diameter column equipped with a tap and fitted with a woolglass piece is prepared under "slurry" conditions, i.e. with 6g of deactivated silicagel 60 and 6g of deactivated alumina. Two g of sodium sulphate are added at the column top. The solvent at the column top is eluated drop by drop (1ml/min) until the top of the sodium sulphate layer is without solvent. The sample is added with a micropipette. The glass can is rinsed 3 times with 1ml hexane. Before each adding on the column, the sodium sulphate surface must be without solvent. The sample is then eluated with a) 20ml hexane (for C_X), b) hexane:dichloromethane 95:5 (for PAH+PCB) and c) 40ml hexane:dichloromethane 80:20 (for PAH). b)+c) are combined in the the same 100ml glass canister and concentrated at 1ml. The canister is then rinsed with isopropanol and concentrated under nitrogen flux to 0.5ml. It is then injected in the HPLC.

Detection limit
The detection limits are shown below. Detection limits depend on the specific considered test. Overall, the detection is minimal for samples coming from the field and then increase for column test samples, batch test samples and soil extraction.

EXTRACTION SOLID – LIQUID

Extraction
Ten grams of soil are introduced in a glass container with 100ml of methanol. 2N of KOH was prior dissolved in the methanol. This mixture is boiled for two hours and then cooled. The liquid part is then put in a decanting canister. 50ml of pentane are added in the glass container which contains the solid part. Agitating the can extracts the pollutants from the solid matter. The pentane is next poured in the liquid part to extract (agitation) the pollutants from

the solute. The operation is repeated three times. Organic compounds are then collected in another glass can by filtration/drying on a filter containing sodium sulphate. Evaporate the rest at Rotavapor (780mbar; 30°C) at 1ml.

Preparation of the adsorbent

Aluminium oxide (70-230mesh) is activated at 400°C for 12 hours. It is then deactivated with adding 5% of its weight of water MQ and agitated for 20 minutes. It then rest for 4 hours at minimum.

Purification

A n-pentane-DCM 1:1 solution is prepared. One g of aluminium oxide in a micropipette is then added and rinsed with the n-pentane solution. The extract and is added and solved with 2x1ml of n-pentane. It is then placed in a centrifugal tube and concentrated. Finally, it is set in solution by isopropanol at 0.5 or 1 ml.

PAH Detection limit

Detection limit are calculated as function of the manipulation. The following table 4.3 shows the detection limit for four different types of analysis. The water sample coming from the field, the column tests (sample of 800ml for HPLC volume of 0.5ml), the batch tests (sample of 200ml for HPLC volume of 0.5ml) and soil tests (sample of 10g for HPLC volume of 1ml).

PAH	**1 litre glass bottle analysis**	**Column tests***	**Batch tests**	**Soil analyses**
	[$ng \cdot l^{-1}$]	[$\mu g \cdot l^{-1}$]	[$\mu g \cdot l^{-1}$]	[$\mu g \cdot kg^{-1}$]
Napthalene	0.14	0.011	0.026	1.121
Acenaphtene	0.23	0.020	0.098	1.967
Fluorene	0.24	0.020	0.102	2.042
Phenanthrene	0.08	0.007	0.034	0.686
Anthracene	0.03	0.003	0.015	0.302
Fluoranthene	0.09	0.010	0.049	0.971
Pyrene	0.04	0.005	0.024	0.471
Benzo(a)anthracene	0.10	0.011	0.053	1.068
Chrysene	0.04	0.006	0.031	0.629
Benzo(e)pyrene	0.24	0.028	0.141	2.812
Benzo(b)fluoranthene	0.06	0.006	0.029	0.578
Benzo(k)fluoranthene	0.01	0.001	0.006	0.114
Benzo(a)pyrene	0.02	0.002	0.008	0.160
Dibenz(a,h)anthracene	0.05	0.003	0.017	0.331
Benzo(g,h,i)perylene	0.04	0.005	0.023	0.462
Indeno(1,2,3c,d)pyrene	0.08	0.008	0.043	0.854

Table IX.1: PAH detection limit according to the considered test. Note that the detection limit in the water samples coming from the field are far lower (scale is in $ng \cdot l^{-1}$). This is because samples are punctual and volume calibrated. (*) those values do not concern the lixiviation test.

IX.3 BTEX

Due to their high volatility, BTEX were analysed as soon as back from the field with the samples. 15ml of sample are put in a purge and trap analytical system. The principle is as follow: a 25ml tank is purged with He. He thus sucks the sample to analyse to a special silicate column. After 10 minutes, the column is heated and desorbed with the chromatograph gas. This method has no preparatory manipulation; it avoids losses and contamination.

APPENDIX X SUBSTANCES CONCENTRATIONS IN THE ROAD RUNOFF AND EXFILTRATION WATERS

X.1 Aliphatic hydrocarbons in the road runoff, artificial precipitation test n°2

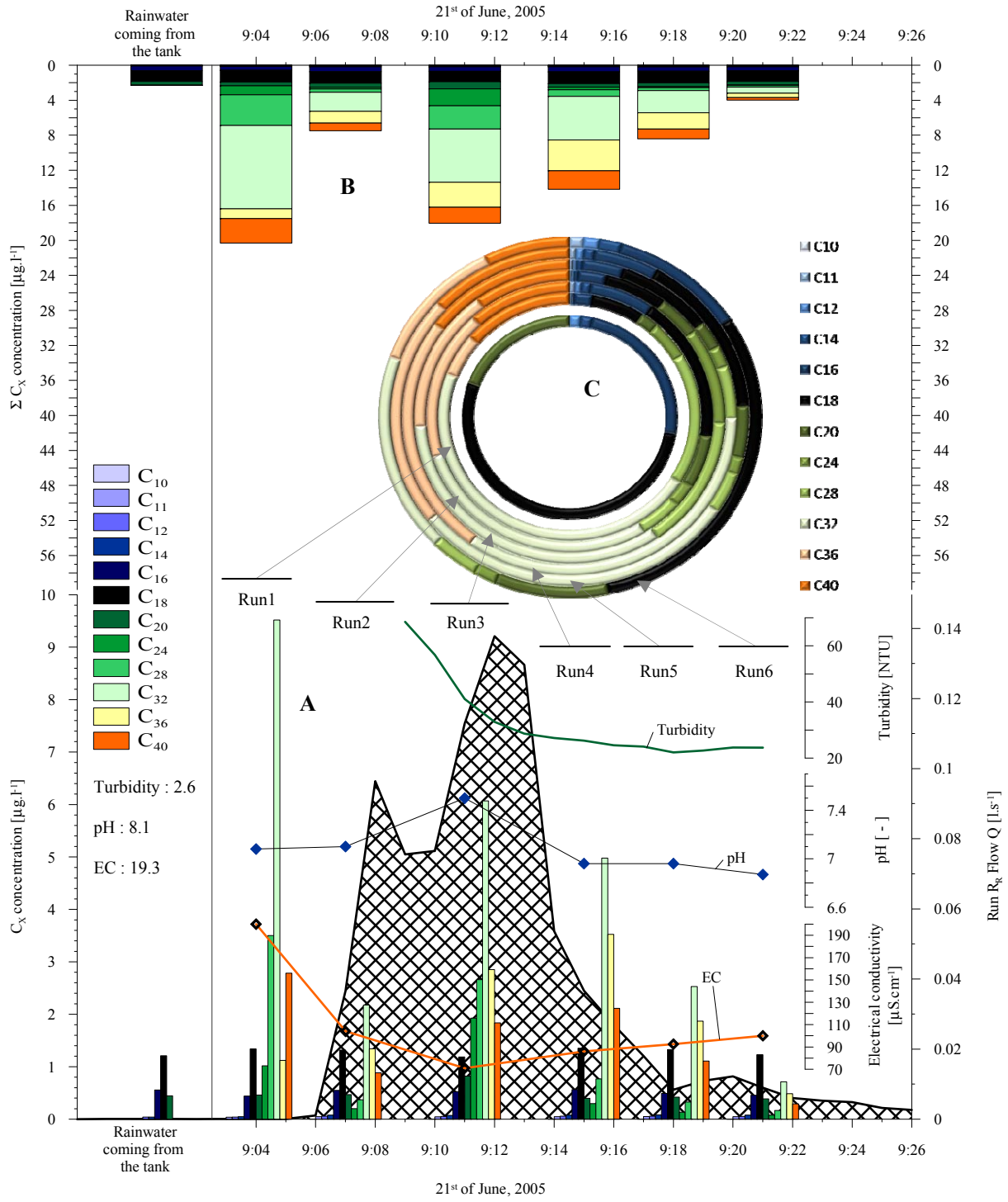

Figure X.1: Evolution of C_X concentration in the road runoff. ***A)*** *C_X concentration in the seven samples. The sample on the left hand is the reference sample (rainwater). All C_X species but C_{10} are represented. C_X species are sorted out from their lowest to their highest weight. Lighter C_X are present in all samples; they come from the rainwater. C_X which are more concentrated at the end of the event are the heavier ones. They indeed make recognizable peaks.* ***B)*** *Sum of all C_X concentrations. This bar chart shows that C_{28} and C_{32} constitute an important part of the road runoff C_X content. A second peak of C_X is discernable, coinciding with the flow peak.* ***C)*** *C_X fractionation rings. The inner ring represents the rainwater sample. Outer circles represent the six road runoff samples, from the first flush (inside) to the last sample (outside). The fractionation is nearly inexistent if the light compounds C_{10} to C_{20} are not considered (because they come from the watering).*

X.2 BTEX concentrations in the road runoff, artificial precipitation test n°2.

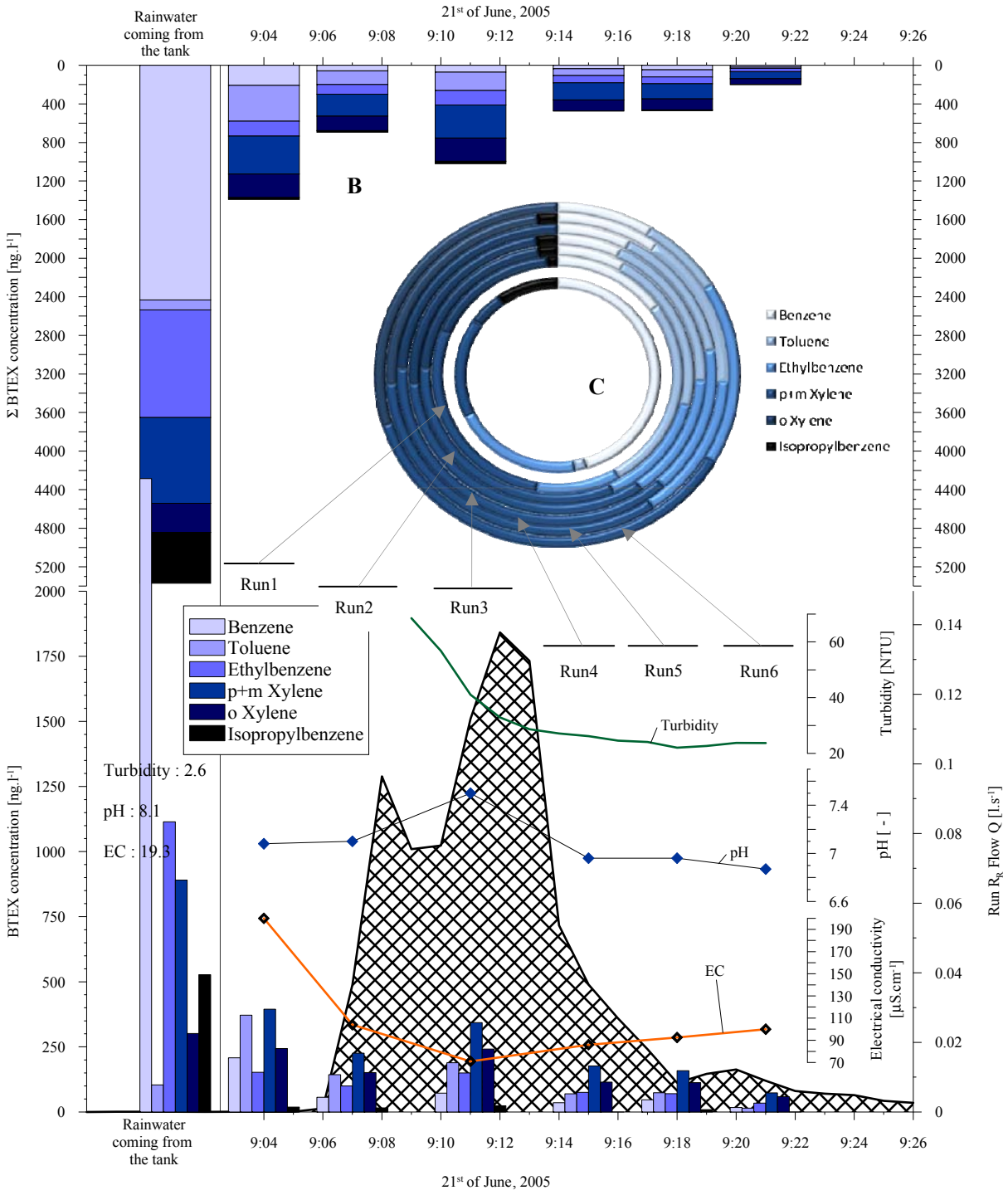

*Figure X.2: Evolution of BTEX concentration in the road runoff. **A)** BTEX concentration in the seven samples. The sample on the left hand is the reference sample (rainwater). Concentrations in the reference sample were much too high to assess the BTEX concentration deposited on the road. The only valid information given by the BTEX dynamic is that most of the BTEX evaporate from the road. Indeed, the concentration found in the first flush sample is much lower than the rainwater sample. Benzene is especially lowered. The toluene is the only BTEX that is slightly higher in the first flush than in the rainwater. **B)** Sum of all BTEX concentrations. This bar chart shows that the rainwater sample had five times higher concentration that the first flush. The second BTEX peak is surely due to the flow peak. **C)** BTEX fractionation rings. The inner ring represents the rainwater sample. Outer circles represent the six road runoff samples, from the first flush (inside) to the last sample (outside). The fractionation is heavy between the rainwater and the first flush. Light, highly volatile BTEX like benzene easily evaporate from the road. The benzene represents 50% of the BTEX in the rainwater, but only 5-10% in the other samples.*

X.3 PCB concentrations in the road runoff, artificial precipitation test n°2.

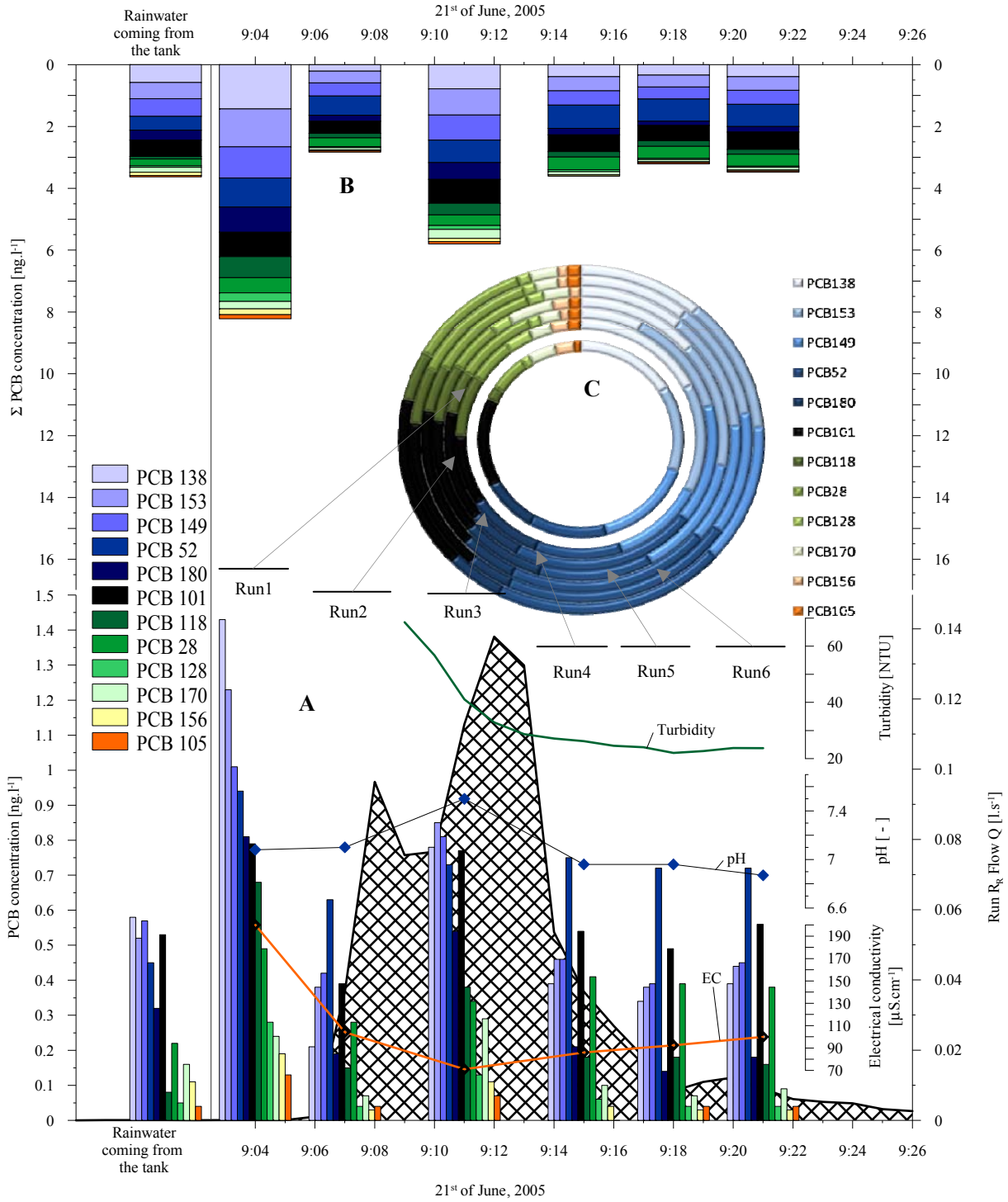

*Figure X.3: Evolution of PCB concentration in the road runoff. **A**) PCB concentration in the seven samples. The sample on the left hand is the reference sample (rainwater). Note the scale is in ng·l^{-1}; the absolute concentrations are thus relatively low. Overall, even if the reference sample did contain some PCB, Some species clearly come from the road pavement (PCB138, 153, 149, etc). Run 4, 5, and 6 have the same proportional concentrations. PCB 138,153 and 149 have clearly higher concentration in the first flush and in the flow Q peak. PCB 28, 52 and 101 kept a constant concentration in all samples. **B**) Sum of all PCB concentrations. This bar chart shows that the rainwater sample had concentrations similar to the Run 2, 4, 5 and 6 samples. The second PCB peak is surely due to the flow peak. **C**) PCB fractionation rings. The fractionation is almost null between the rainwater sample and road runoff sample. The notable difference concerns the PCB 118. It indeed constitutes a greater part in the road runoff than in the rainwater. PCB 28, 52 and 101 also proportionally increased along the time. This is because their absolute concentrations did not vary much.*

X.4 **Synthesis and generalisation** (related to §4.3.4.4)

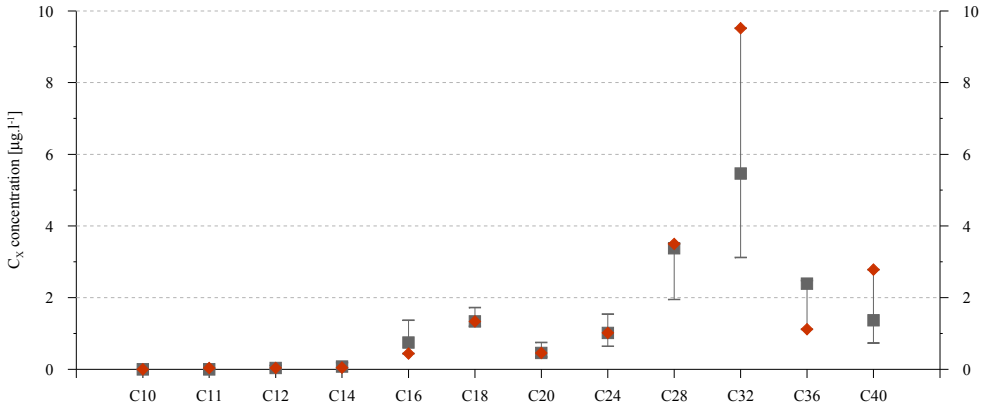

Figure X.4: Aliphatic hydrocarbons concentration in the road runoff. Squares represent the arithmetic averages of the most concentrated sample (3 of them), while error bars represent the maximum and minimum values. Note that those concentrations were not measured in the first flush because the C_X pollutograms are neutral (b coef. ≈1): the first flush is not inevitably the most concentrated. C_X are sorted out according to their molecular weights. Artificial test n°2 values are noted in red. Concentrations recorded during the artificial test n°2 are well representative of concentrations recorded in natural conditions. Only species from C_{16} are found in the road runoff, with high concentrations for C_{32}.

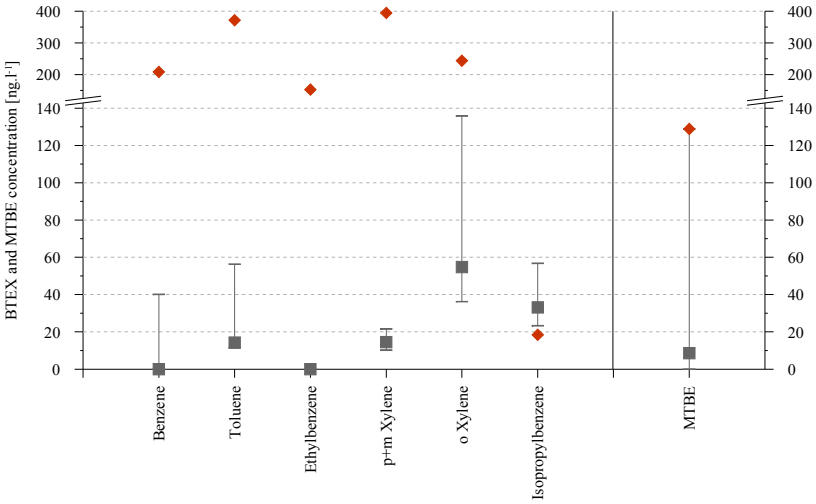

Figure X.5: BTEX and MTBE concentration in the road runoff. Squares represent the arithmetic averages of the first flush (4 of them), while error bars represent the maximum and minimum values. BTEX are sorted out according to their molecular weights. Artificial test n°2 values are noted in red. Note that those very high concentrations were caused by a strong contamination of the watering rainwater. Usually, BTEX and MTBE are present in very low concentrations.

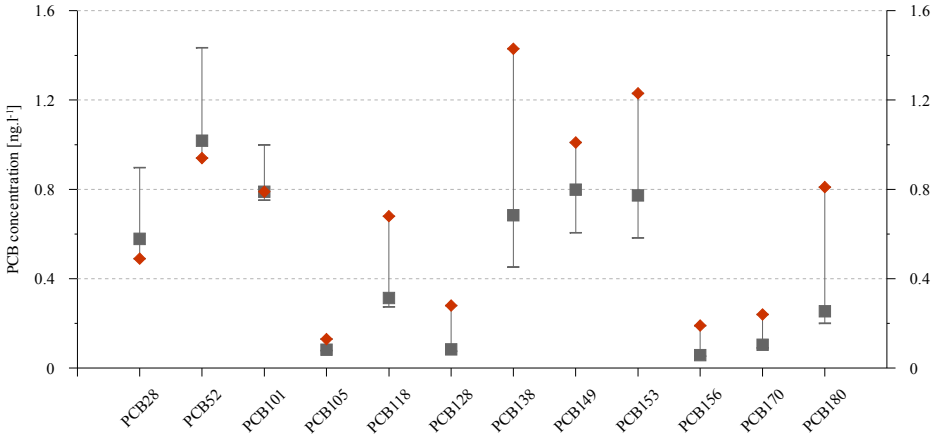

Figure X.6: PCB concentration in the road runoff. Squares represent the arithmetic averages of the most concentrated sample (4 of them), while error bars represent the maximum and minimum values. Note that those concentrations were not measured in the first flush because the PCB pollutograms are neutral (b coef. ≈1): the first flush is not inevitably the most concentrated. Artificial test n°2 values are noted in red. Concentrations are however notably higher for PCB >118. Species with the lowest concentration and lowest chlorine content (PCB 105, 118, 128) also have the highest b coefficient.

X.5 Substances in the shoulder exfiltration waters

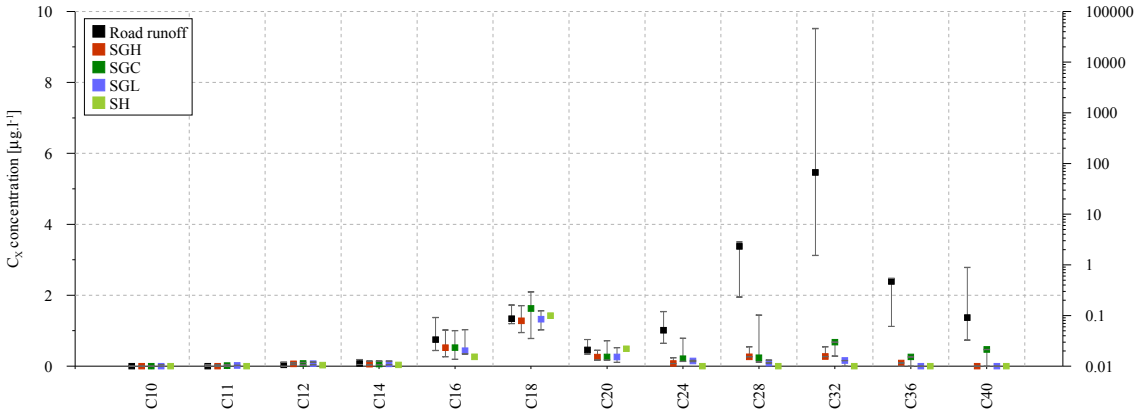

*Figure X.7: **C_X** concentrations in the first flush. Squares represent the average of the first flush concentrations; minima and maxima are the extreme first flush concentration values. Overall, C_X have low concentrations in the shoulder exfiltration water. All Cx have neutral pollutogram (0.8<b<1.2). However, species which have the lowest b coef. (C16, C18, C20) are the most mobile: they are not retained at all in the shoulders. Heavier C_X which have more neutral b coefficient are almost completely retained in all shoulders.*

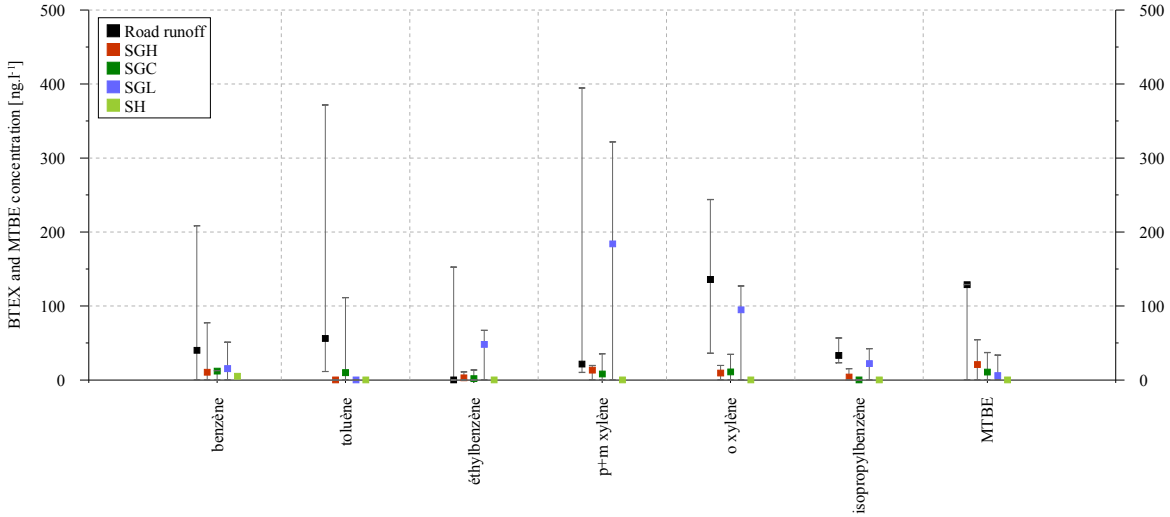

*Figure X.8: **BTEX** and **MTBE** concentrations in the first flush. Squares represent the average of the first flush concentrations; minima and maxima are the extreme first flush concentration values. Overall, BTEX have low concentrations in the shoulder exfiltration water. This is not true for SGL which exfiltration water is almost as loaded as the road runoff.*

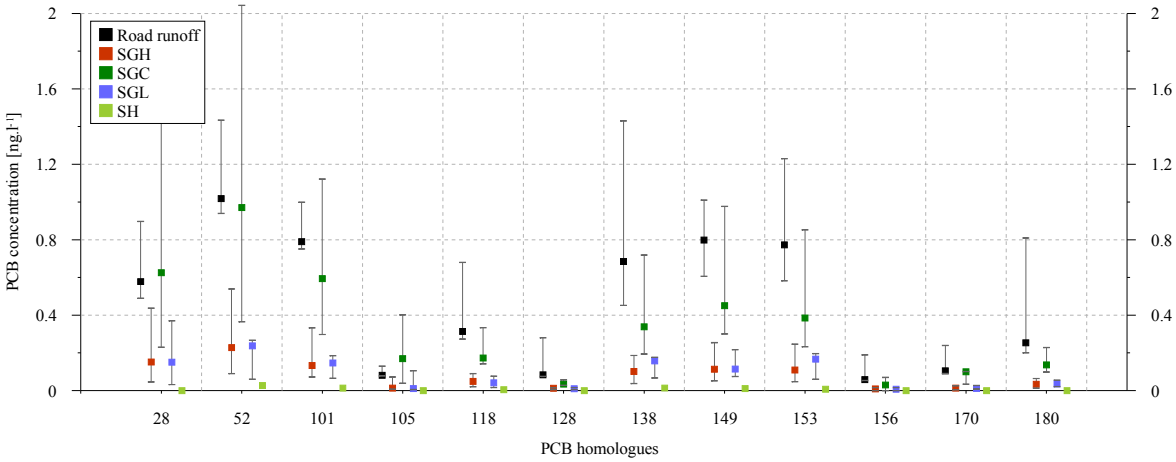

*Figure X.9: **PCB** concentrations in the first flush. Squares represent the average of the first flush concentrations; minima and maxima are the extreme first flush concentration values. Overall, PCB have very low concentrations in the shoulder exfiltration water. This is not true for SGC which exfiltration water is almost as loaded as the road runoff. Other shoulders retain PCB in the same way.*

X.6 First flush coefficients b; substances coming out of the shoulders; comparison with the road runoff first flush

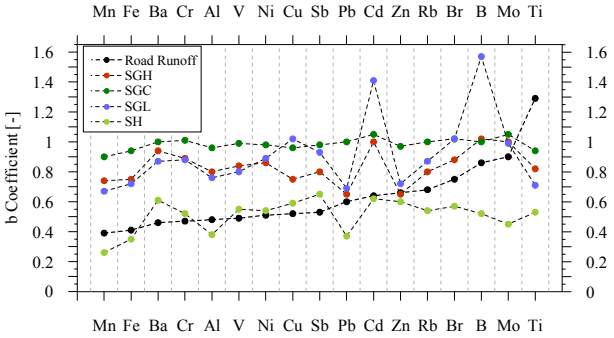

Figure X.10:
***A)** MTE b coefficient in the shoulders. The strongest first flush effects are met for immobile MTE. All shoulders show higher b coefficients, thus stronger retardation, than the road runoff. Only SH showed similar values.*

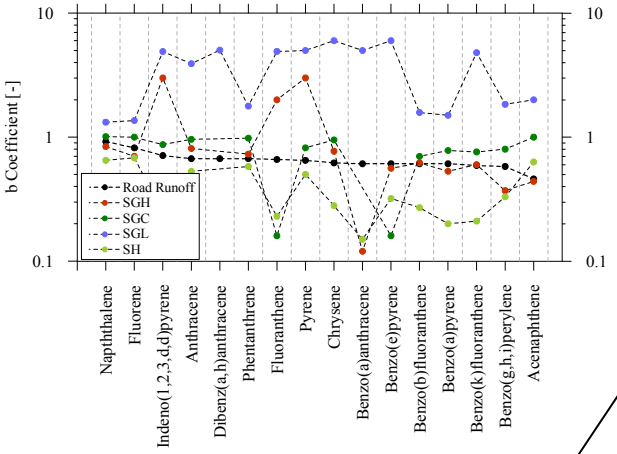

***B)** PAH b coefficient in the shoulders. The shoulders fractionate the compounds behaviour. The black line is the reference Road runoff. Note the strong retardation in SGL. SGH and SGC have sometimes higher, sometimes lower b coefficient, depending on the compounds mobility. SH always has stronger first flush effect than the road runoff.*

***C)** CX b coefficient for all shoulders.*

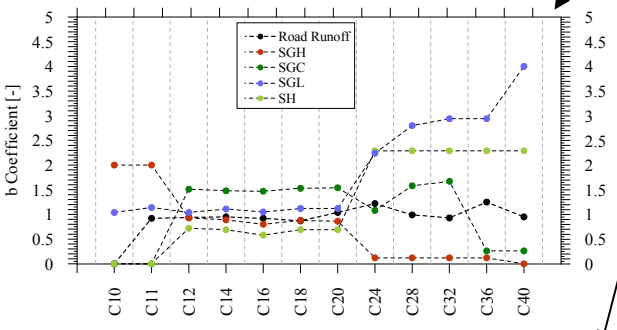

***D)** BTEX and MTBE b coefficient for all shoulders.*

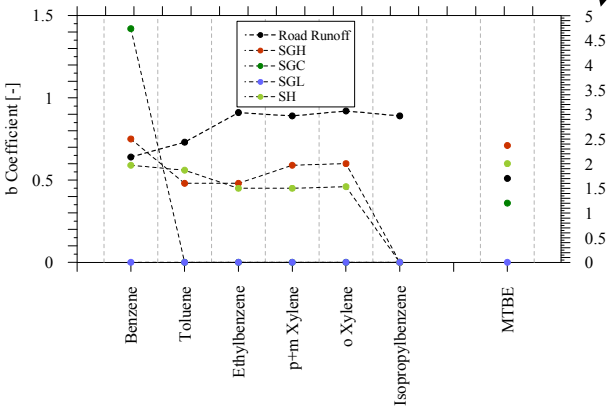

***E)** PCB b coefficient for all shoulders.*

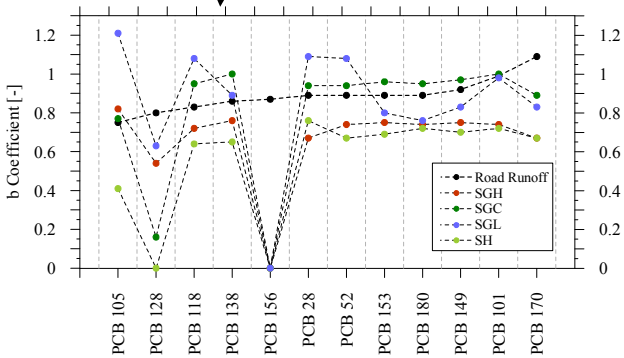

X.7 Shoulders exfiltration: artificial test n°2, flow, EC, turbidity and pH measurements

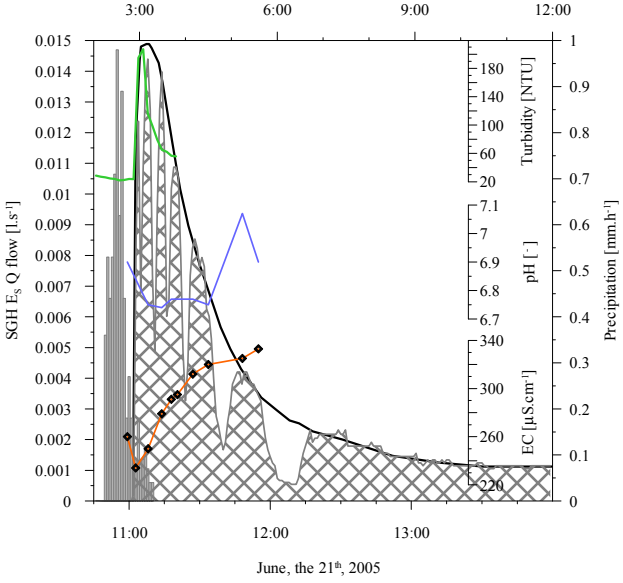

No results are provided for SH because all the probes were put in the LH weir during this compartment watering. See text for comparison with the road runoff.

Figure X.11

A) *SGH*

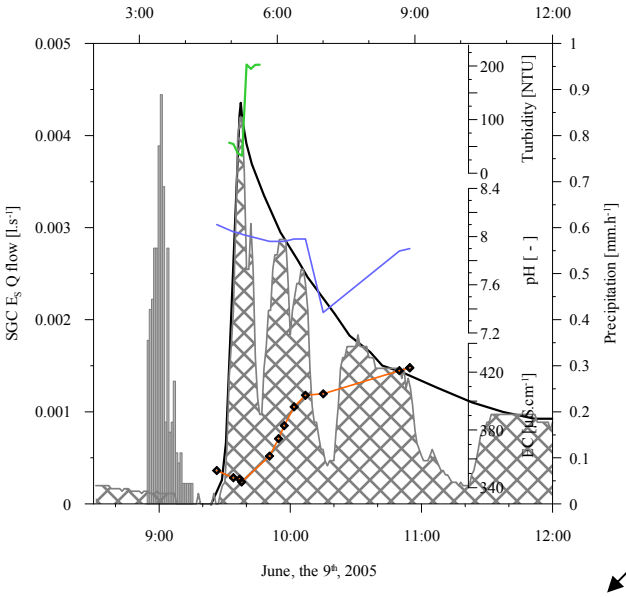

B) *SGC*

C) *SGL*

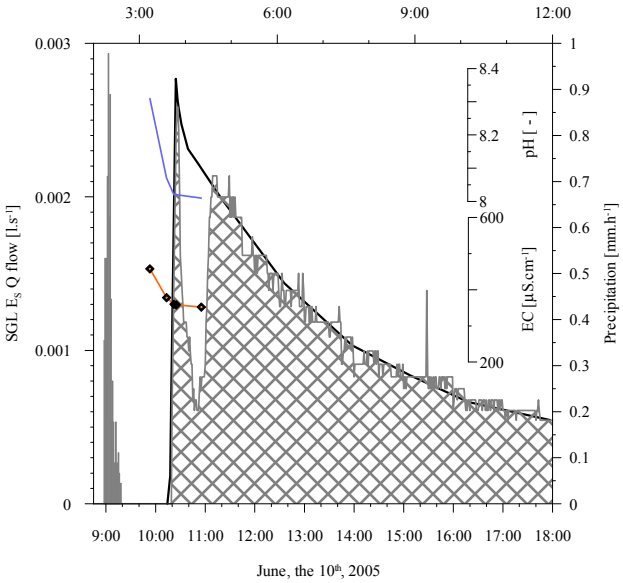

D) *SH*

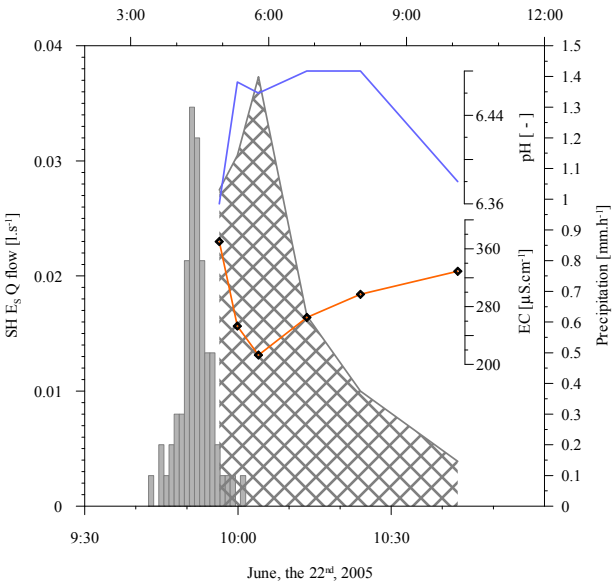

X.8 Shoulder exfiltration: substances concentrations in the exfiltrated water

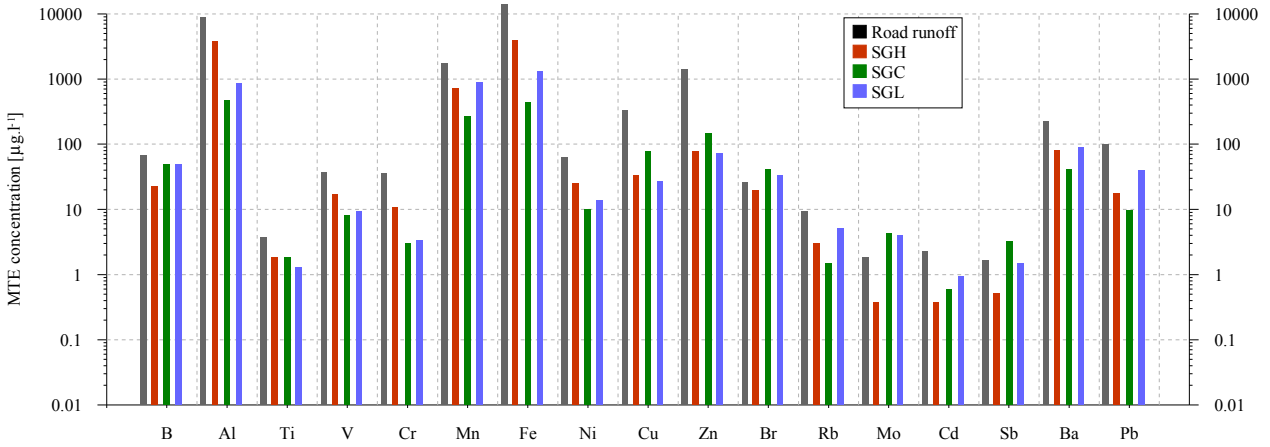

Figure X.12: MTE concentrations in the exfiltrated water.

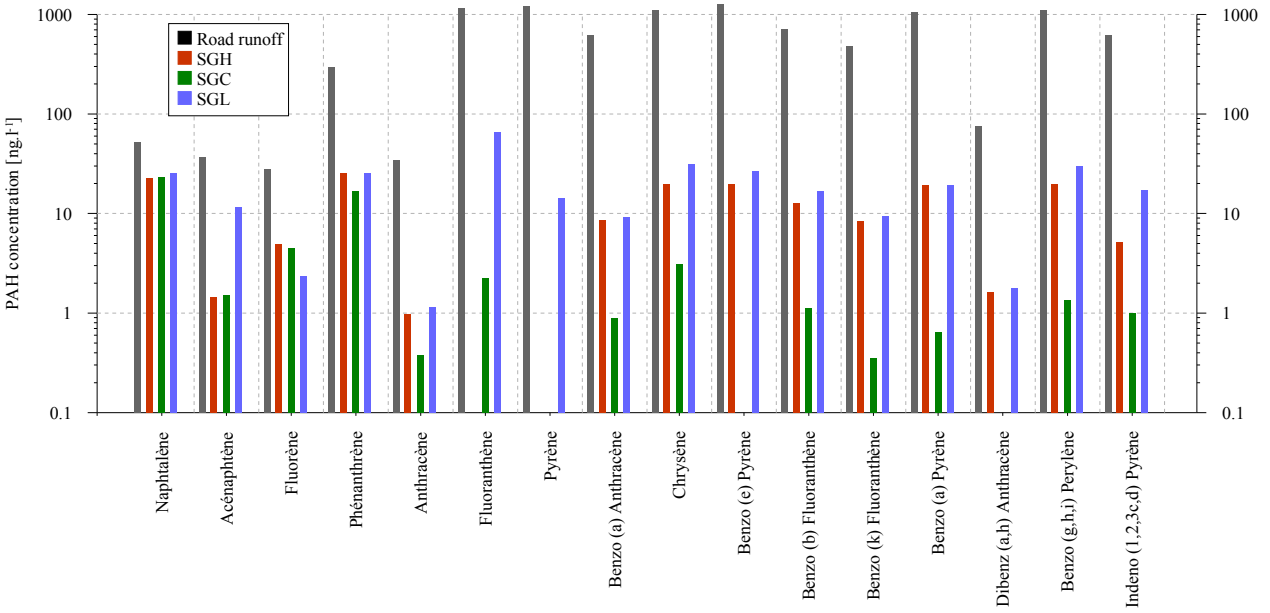

Figure X.13: PAH concentrations in the exfiltrated water.

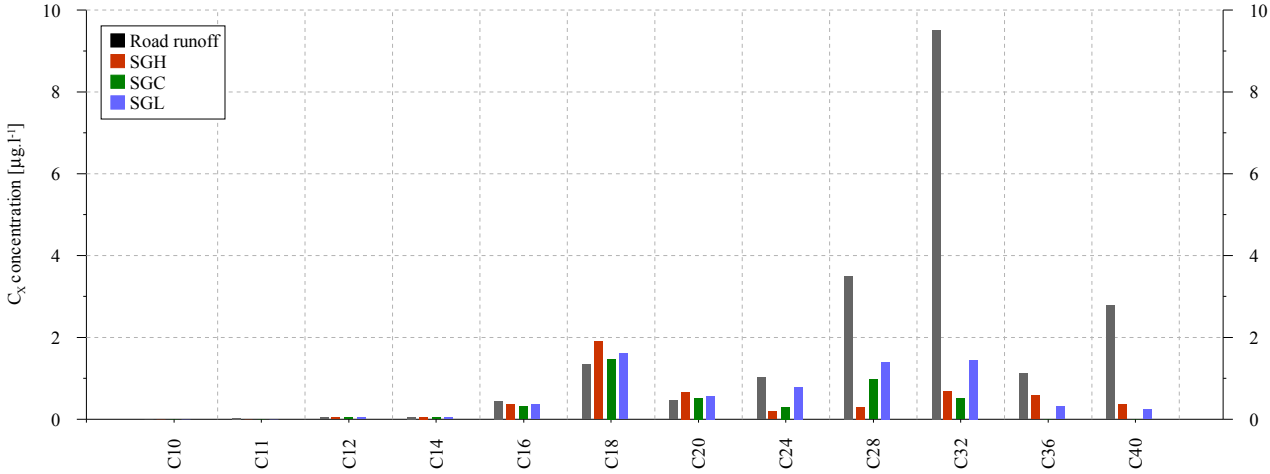

Figure X.14: C_X concentrations in the exfiltrated water.

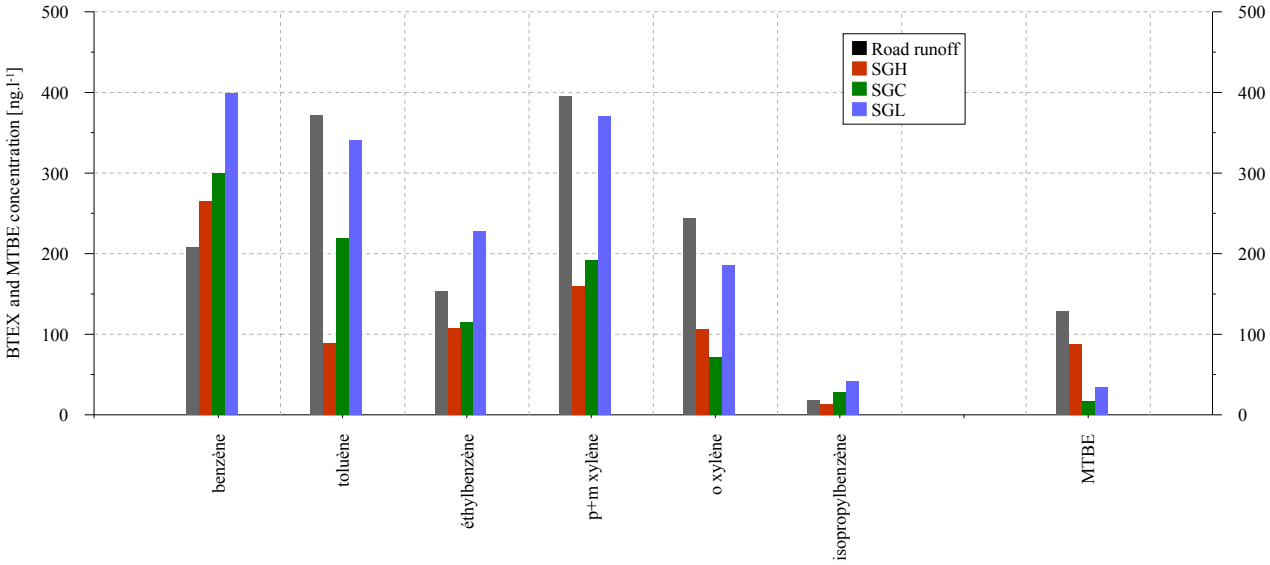

Figure X.15: BTEX and MTBE concentrations in the exfiltrated water.

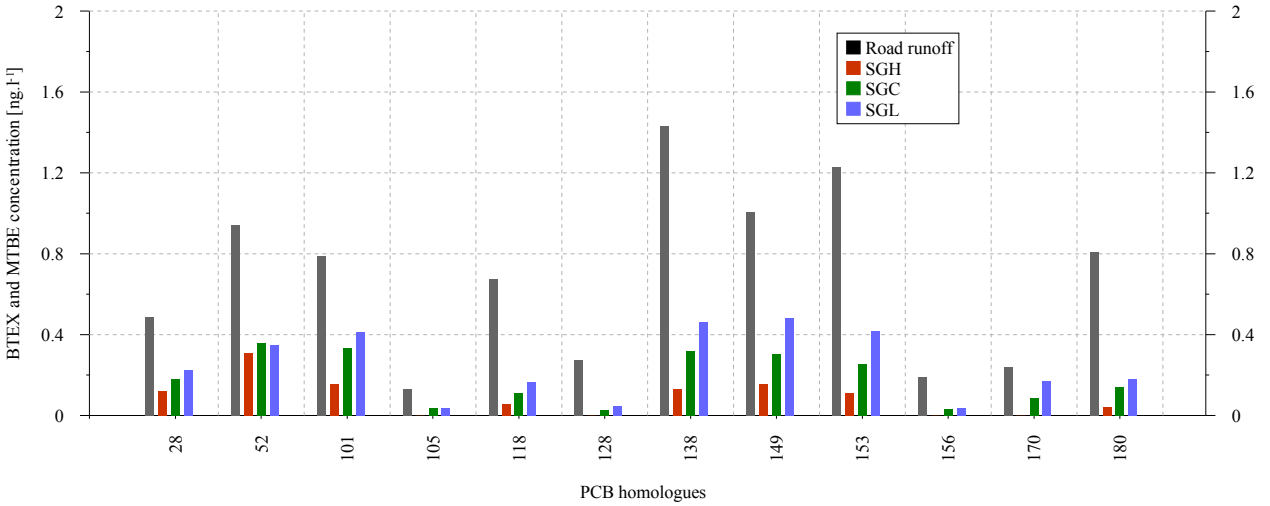

Figure X.16: PCB concentrations in the exfiltrated water.

X.9 Substances concentrations in the lysimeter LW exfiltration water

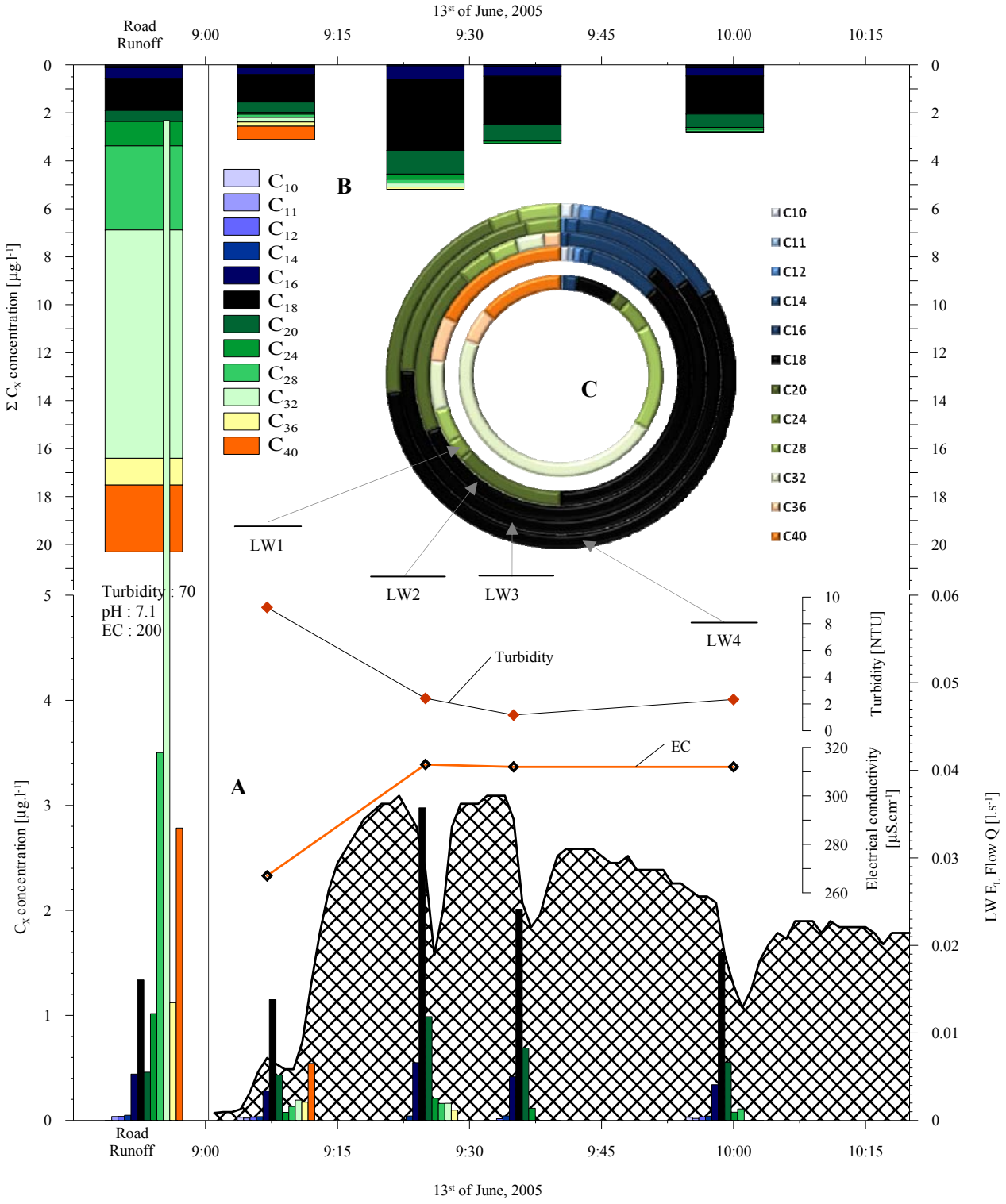

*Figure X.17: Evolution of C_X concentration in the LW exfiltration water. **A)** C_X concentration in the four samples. The sample on the left hand is the reference sample (road runoff). All C_X species are represented. C_X species are sorted out from their lowest to their highest weight. Lighter C_X are present only in the first sample; they come from the rainwater. C_X which are more concentrated at the end of the event are the C_{16}-C_{18}-C_{20}. They indeed make recognizable peaks. **B)** Sum of all C_X concentrations. This bar chart shows that C_{28} and C_{32} constitute an important part of the road runoff C_X content. In the LW exfiltration water, the concentration is mainly constituted by C_{16}-C_{18}-C_{20}. Only one peak of C_X is visible. It does coincide with the flow peak. **C)** C_X fractionation rings. The inner ring represents the road runoff first flush. C_{16}-C_{18}-C_{20} proportionally represent the greatest part of the C_X concentration.*

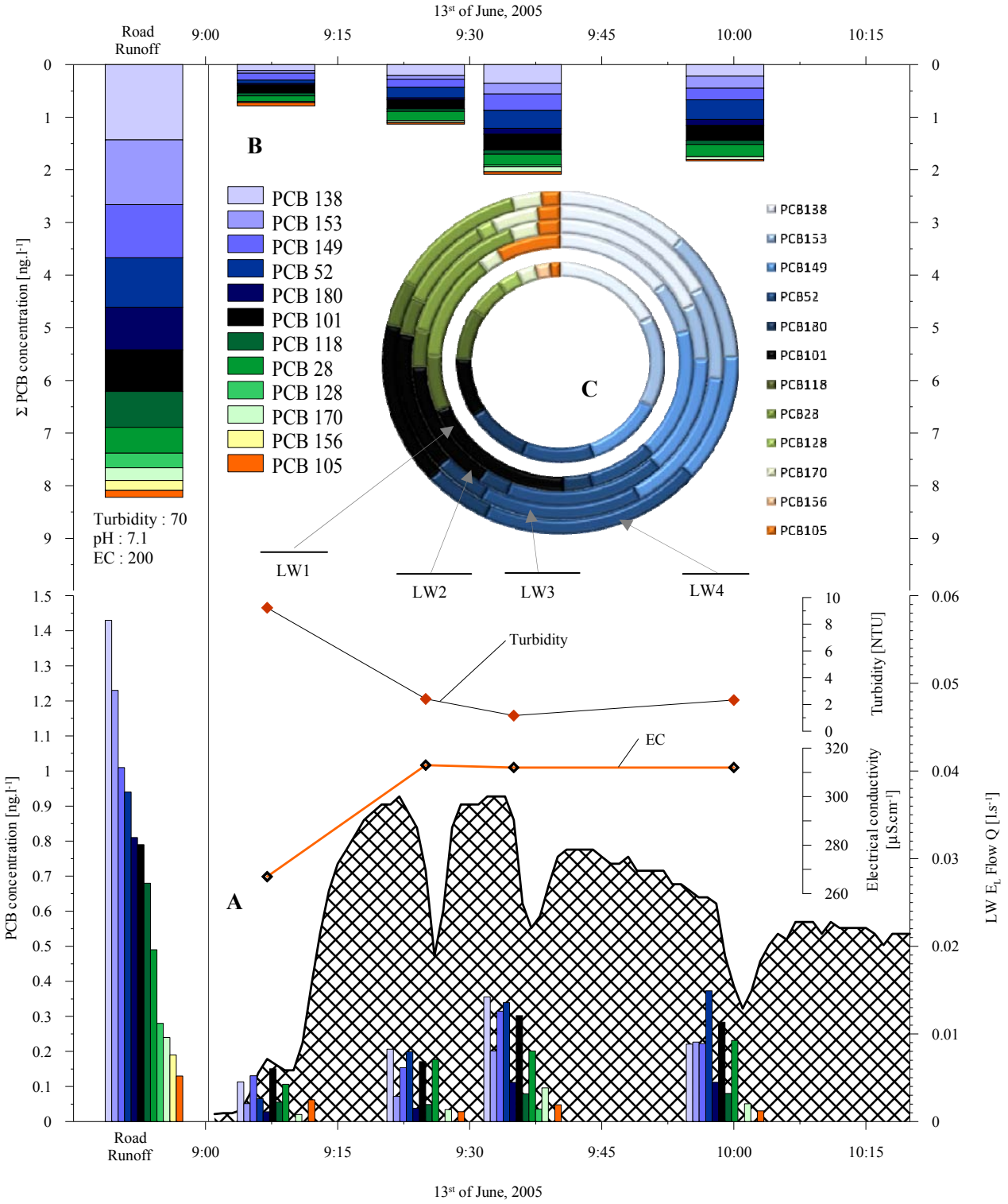

*Figure X.18: Evolution of PCB concentration in the LW exfiltration water. **A)** PCB concentration in the four samples. The sample on the left hand is the reference sample (runoff water). Species are sorted out according to their relative concentration in the road runoff. Note the scale is in ng·l^{-1}; the absolute concentrations are thus very low (total PCB concentration in the first sample is 1 ng·l^{-1}). Some species are not detected in the LW exfiltration water: 128 and 156. Other PCB are all present in all samples. For most of them, their maximum concentration is reached correlated with the turbidity minimum, which more or less corresponds to the flow peak. **B)** PCB total concentrations. The maximum total concentration is reached in sample LW3. This does correlate with other substances types. **C)** PCB fractionation rings. Overall, the fractionation is weak: the proportionality found in the road runoff is the same as the proportionality found in the LW exfiltration water.*

APPENDIX XI GEOTECHNICAL PROBES; EQUATIONS

XI.I PROBES

Temperature probes PT100 at -26cm. ***Left****: detail of the probe.* ***Right****: HMF laying. Probes were protected with a fine bituminous layer.*

Temperature probes located at the HMF – HMT interface (-12cm). Probes were fitted with silicon.

LVDT deflection sensor

2m depth drillhole

LVDT placed in the hole

Repartition plate and levelling

XI.II EQUATIONS

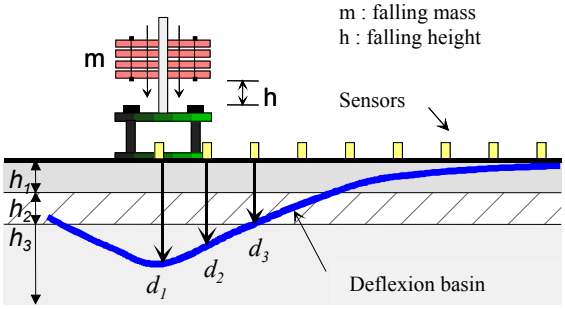

Equ. XI.1)

$$F = \sqrt{2 \cdot m \cdot h \cdot k} \qquad \text{[kN]}$$

(F: force transmitted on the road; m: mass [kg]; h: height [m]; k: spring constant of the plate (30cm Ø) the mass fall onto)

Equ. XI.2)

$$d_z = \frac{(1+\nu)\cdot\sigma_0\cdot a}{E}\cdot\left[\frac{1}{\sqrt{1+\left(\frac{z}{a}\right)^2}}+(1-2\cdot\nu)\cdot\left(\sqrt{1+\left(\frac{z}{a}\right)^2}-\frac{z}{a}\right)\right]$$

(z: depth [m]; ν: poisson coefficient; σ_0: uniform pressure; a: plate radius; E: elastic modulus)

Equ. XI.3)

$$\frac{h_1\ E_1\ \nu_1}{E_2\ \nu_2} \Rightarrow \frac{h_e\ E_2\ \nu_2}{E_2\ \nu_2} \qquad h_e = h_1\sqrt[3]{\frac{E_1}{E_2}\cdot\frac{1-\nu_2^2}{1-\nu_1^2}}$$

(h_i: thickness; E_i: elastic moduli; ν_i: poisson coefficients)

Equ. XI.4)

$$E_i = \frac{(1-\nu_i)\cdot\sigma\cdot a^2}{r_i\cdot d_i} \qquad \text{[MPa]}$$

(E_i: elastic moduli; ν_i: poisson coefficients; σ: uniform pressure; a: mass radius; d_i: deflection amplitude; r_i: distance from the geophone to the mass)

Equ. XI.5)

$$E(\theta_{ref}) = \frac{E(\theta)}{\left(0.985-1.94\cdot\log\left(\frac{\theta}{\theta_{ref}}\right)\right)} \qquad \text{[MPa]}$$

(θ: measurement temperature; θ_{ref}: reference temperature 15°C; E(θ): E modulus at measurement temperature; $E(\theta_{ref})$: E modulus at 15°C)

Pascal PIGUET
Date of birth: 14/07/1979
Gender: male
Marital status: single
Nationality: Swiss
pascal.piguet@epfl.ch

EDUCATION

2007	WATSAN (Water and Sanitation engineering) specialization. Courses conjointly given by the ICRC (International Committee of the Red Cross) and CHYN (centre of hydrogeology, University of Neuchâtel UNINE).
2004-2007	PhD thesis entitled: "Road runoff over the shoulder diffuse infiltration. Real-scale experimentation and optimization", GEOLEP, EPFL
2004-2007	Doctoral school in environment. Specialization in natural hazards, from mitigation toward development (preparedness, relief, rehabilitation). Other points of interest were underground water modelling and urban sewage system optimization
1997-2002	Diploma in Earth and environmental sciences (MSc equivalent) "Structures and petrology of the intrusion-related rocks, SW of the granito-dioritic Ticka pluton, High-Atlas, Morocco", University of Neuchâtel, Earth and Environmental Sciences Institute.
1994-1997	"Maturité fédérale", C-type (scientific) with mention "très bien", Gymnase cantonal de Neuchâtel

AWARDS

Diploma of Earth and Environmental sciences obtained with the highest mention delivered by the Faculty of Sciences, i.e. "très bien" (very good, overall band 5.8 out of 6).

The diploma thesis obtained the "Prix Jean Landry" for its excellence.

EMPLOYMENT HISTORY

2004-2007	Assistant/researcher at GEOLEP, EPFL. Executive chief of a 4-years federal mandate on which the PhD study was based.
2003 (8 months)	Junior scientist, Structural geology group, ETHZ. Development and implementation of new methods; Laboratory work
2002 (6 months)	Invited as a "visiting scholar" by the CRC*pmd (Co-operative Research Center for Predictive Mineral Discovery), James Cook University (JCU), Townsville, Australia. Specialization in environmental problems relative to mining operations
2002 (4 months)	Coordinator/developer (80%) for the SVC (Swiss Virtual Campus). Responsible for the coordination and liaison with the SVC main office.
2002 (4 months)	Webmaster (20%) of the students'association ANEG, voluntary help

MEMBERSHIPS AND OTHER EXPERIENCES

Secretary of ANEG (Association Neuchâteloise des Etudiants en Géologie) from 1999 to 2000. Webmaster since April 2002.

Active member of ANES (Association Neuchâteloise des Etudiants en Science) and FEN (Fédération des Etudiants Neuchâtelois)

Voluntary help, rising fund for building schools in Mali, summer 1997 to 2001.

LANGUAGES

French:	Mother language
English:	Fluent both written and oral: IELTS (International English Language Training System) overall band 7.5 out of 9, JCU language centre, Australia, 2002
German:	Good skills
Spanish:	Beginner

OTHER USEFUL SKILLS

PC power-user, Unix user
Good skills in standard software (Office suite, graphic suite)
GIS (Geographic Information System) Arcview & Arcinfo user (specialization course, UNINE 2000)
Underground water modelling software (Modflow, FeFlow)
Field operations in many different circumstances and area

HOBBIES

Sports (windsurf, snowboard, scuba diving)
Photography
Trekking (numerous field trips as backpacker in Africa, Latin America, and Asia)